Summer 7-9-2014

Coupled Thermo-Poro-Mechanical Axisymmetric Finite Element Modeling of Soil-Structure Interaction in Partially Saturated Soils

Wei Wang
University of Colorado Boulder, wei.wang-2@colorado.edu

Coupled thermo-poro-mechanical axisymmetric finite element modeling of soil-structure interaction in partially saturated soils

by

Wei Wang

B.A., Dalian University of Technology, 2006

M.S., Dalian University of Technology, 2009

A thesis submitted to the

Faculty of the Graduate School of the

University of Colorado in partial fulfillment

of the requirements for the degree of

Doctor of Philosophy

Department of Civil, Environmental and Architectural Engineering

2014

This thesis entitled:
Coupled thermo-poro-mechanical axisymmetric finite element modeling of soil-structure interaction in partially saturated soils
written by Wei Wang
has been approved for the Department of Civil, Environmental and Architectural Engineering

Associate Professor Richard A. Regueiro

Associate Professor John S. McCartney

Professor Shemin Ge

Professor Ronald Y.S. Pak

Professor Harihar Rajaram

Date

The final copy of this thesis has been examined by the signatories, and we find that both the content and the form meet acceptable presentation standards of scholarly work in the above mentioned discipline.

Wang, Wei (Ph.D., Civil, Enviromental and Architectural Engineering)

Coupled thermo-poro-mechanical axisymmetric finite element modeling of soil-structure interaction in partially saturated soils

Thesis directed by Associate Professor Richard A. Regueiro

Energy foundations (or geothermal foundations) are becoming more popular as an energy-saving and environmentally-friendly technology. By fully utilizing the steady ground temperature and the thermal properties of concrete, buildings can be heated and cooled through energy foundations with heat pumps at very low cost. Although some observations have been obtained from full-scale field tests and centrifuge-scale tests, there are still issues that are not well understood with respect to the complex interactions among temperature change, induced effective stress, and pore fluid flow in partially saturated soils.

In order to investigate soil-structure interaction between energy foundations and partially saturated soil under non-isothermal condition, the thesis develops a fully coupled thermo-poro-mechanical (TPM) finite element (FE) model with both nonlinear elastic, and temperature- and suction-dependent elasto-plastic solid skeleton constitutive models implemented. Based on the mixture theory of porous media and fundamental laws of continuum mechanics, governing equations are formulated to account for the coupled processes involving the mechanical response, multiphase pore fluid flow, and heat transfer. Constitutive relations consist of the effective stress concept, Fourier's law, as well as Darcy's law and Fick's law for pore liquid and gas flow. The elasto-plastic constitutive model for the soil solid skeleton is based on a critical state soil mechanics framework. The constitutive parameters are mostly fitted with experimental data. The TPM model is formulated under small strain and axisymmetric condition, and implemented within the finite element method (FEM). We then simulate a series of energy foundation centrifuge experiments conducted at the University of Colorado, Boulder. Good agreement is obtained between the experimental observations and modeling results.

Another novelty and challenge of the thesis is to develop a double-noded zero-thickness TPM cohesive interface element (CIE) model with elastoplasticity for fractured geomaterials under saturated or partially saturated condition. The advantage of TPM CIE is to take account of various jumps within the fracture with respect to tangential and normal displacements, pore liquid and gas pressure, as well as temperature. Both pre-existing fracture and developing fracture can be analyzed by choosing appropriate constitutive models. With CIE implemented at the soil-foundation interface, we are able to capture the plastic failure process of energy foundations due to the loss of side shear resistance. We can also apply the TPM CIE to better understand the generation of fractures involving coupled processes in other applications involving mudstone/shale, such as hydraulic fracturing, and reservoir storage of CO_2 or nuclear waste.

Dedication

To my parents and my husband,

Acknowledgements

I would like to express my deepest gratitude to my advisor, Professor Richard A. Regueiro. It has been an honor and a joy to be his Ph.D student. His guidance, encouragement, and patience help me to build up confidence in myself and accumulate enthusiasm in research during the tough pursuit of Ph.D degree. I am also grateful for the excellent role model he has provided as a modest, diligent, and successful scholar and professor.

Besides my advisor, I would like to thank the rest of my committee members for their contribution of time, academic advice and guidance. First, I would like to thank Professor John S. McCartney for his funding on geothermal foundation, which was the initial reason for me to start in this fresh and promising field. I would also like to thank Professor Ronald Y.S. Pak and Professor Harihar Rajaram for helping me to develop my background and guiding my research for the past several years. Last but not least, I would like to acknowledge the guidance and encouragement from Professor Shemin Ge when I encountered difficulties during the development of interface element.

I would also like to thank Professor Hon-Yim Ko, who has been a great friend and mentor. My sincere thanks also goes to Professor Carlos A. Felippa for his genuine help. Many thanks to my friends who have been supportive and make my lonely life colorful.

In addition, I sincerely thank my parents for their unconditional love and support, which is great treasure throughout my life. I am grateful of them for educating me well, and for making all the efforts and sacrifices in my behalf.

I want to thank my husband Yuming Sun, for sharing every moment of my joy and sorrow as a soulmate. His love, patience, and encouragement make me a better person.

Finally, funding for this research was provided by National Science Foundation grant CMMI-0928159. This funding is gratefully acknowledged.

Contents

Chapter

Tables

Table

Figures

Figure

Chapter 1

Introduction

1.1 Motivation

Energy foundations, which involve heat exchange loops attached to the reinforcing cage within a drifted-shuft, are a fast-growing geothermal heat-exchange system. With adequate design and installation, energy foundations can fulfill not only the geotechnical but also the thermal requirements of buildings without relying solely on conventional heating and cooling systems; hence, energy consumption can be reduced, as well as carbon dioxide emissions (Preene and Powrie, 2009). Typically, heat carrier fluid is pumped through heat exchange pipes to exchange energy between a building and energy foundations. In summer, the ground operates as a heat sink by storing thermal energy, meanwhile, the infrastructure is cooled. While in winter, the energy is extracted for heating purposes, thus making the ground act as a heat source (Pahud and Matthey, 2001; Brandl, 2006; De Moel et al., 2010).

Relevant studies in the past decade have indicated the feasibility of energy foundations both technologically and economically (Hepbasli, 2002; Hepbasli et al., 2003). By using the good thermal conductivity and thermal storage capacity of concrete, energy foundations can be applied for heating and cooling of buildings of any size, as well as road pavements, bridge decks, etc (Brandl, 2006). Given an investment-return period of 5-10 years, this innovative technology can provide significant long-term cost savings for heating and cooling, compared with conventional systems. And this investment-return period may vary depending on various effects including ground strata, geotechnical, geothermal and hydrogeological properties, etc.(Doherty et al., 2004; Brandl, 2006; De Moel

et al., 2010). As an energy-saving and environmentally-friendly technology, energy foundations have been widely used for both residential and commercial buildings (Hepbasli, 2003; Hamada et al., 2007; Omer, 2008). A total of 80 countries have been reported to use certain forms of geothermal energy as of 2000 (Hepbasli, 2003). According to Yari and Javani (2007), the installations of shallow energy systems have covered 33 countries as of 2007 in North America and Europe, compared to 26 countries as of 2000. Brandl (2006) reports there is an exponential increase of energy foundations in Austria; the number of energy foundations installed has grown to $\approx 23,000$ as of 2004 since the beginning of the 1980's.

Observations of energy foundation performance have been conducted in order to investigate geotechnical and thermal issues. Hepbasli (2002) reports that heat and moisture flow induced by the operation of energy foundation systems occurs in the surrounding soil. Rees et al. (2000) explain that conduction, convection, and latent heat of vaporization and condensation are the main mechanisms of heat transfer in porous media, however, radiation is usually negligible. Hepbasli (2002); Hepbasli et al. (2003) explain that the efficiency of heat transfer greatly depends on soil type, temperature and moisture gradients. Thomas and Rees (2009) report that heat conduction mainly depends on the degree of saturation of the soil. Brandl (2006) indicates that freezing and thawing may also transfer significant heat.

Notwithstanding the large amount of research and promising investigations hitherto, a diverse range of research activity has proved necessary in order to provide thorough guidance on the design and installation of energy foundation systems. Furthermore, it is nontrivial to adequately describe the varied and sometimes complex interactions among temperature change, induced stress and pore fluid flow in partially saturated soils, together with soil-structure interaction (SSI). For example, concurrent with shrinkage or expansion of foundations might be the loss of soil-foundation friction; thermally induced stress or deformations of foundations may affect structural performance; furthermore, thermally-induced fluid flow may occur due to high temperature in the soil close to foundations, which can cause malfunctions of energy foundation systems. Although the focus of the research is on modeling thermo-poro-mechanical (TPM) soil-structure interaction (SSI) in

energy foundation centrifuge experiments, other applications for thermo-poro-mechanical modeling, including use of a cohesive interface element, include hydraulic fracturing in shale, and storage of CO_2 and nuclear waste with shale cap rock features.

1.2 Background on coupled thermo-poro-mechanical processes

1.2.1 Experimental investigations on TPM responses

Thermal effects on the mechanical behavior of soils have been investigated through a number of experiments, e.g. temperature dependence of elastic modulus and failure criterion, of soils. Graham et al. (2001, 2004); Cekerevac and Laloui (2004) stated that there was no significant change of M (the slope of critical state line in the $p' - q$ plane) with temperature variation, while Hueckel and Pellegrini (1989); Hueckel and Baldi (1990); Burghignoli et al. (2000) observed a small reduction of M. Plum and Esrig (1969) observed that heating a cohesive soil increased compressibility when low mean effective stress was applied; in contrast, cooling the soil changed stress-strain characteristics and made the soil behave like an over-consolidated soil. Blatz and Graham (2003) tested the influence of suction on yield stress and shear strength regarding unsaturated highly plastic clay materials. Uchaipichat and Khalili (2009) performed temperature-controlled soaking, suction-controlled thermal loading and unloading, and temperature-suction-controlled isotropic consolidation tests using modified traditional triaxial equipments to investigate the thermo-hydro-mechanical behavior of partially saturated soils under elevated temperature. Experiments by Ghabezloo and Sulem (2009) indicated that temperature increase in saturated soils under undrained conditions led to a reduction of the effective mean stress and might cause shear failure or hydraulic fracturing. Many attempts have been made to explore the thermal effects on the soils with different overconsolidation ratios (OCRs). (Campanella and Mitchell, 1968; Hueckel and Baldi, 1990; Hueckel and Borsetto, 1990; Towhata et al., 1993; Cekerevac and Laloui, 2004; Cui et al., 2000). Paaswell (1967); Tidfors and Sallfors (1989); Cui et al. (2000) observed that volumetric strains due to heating of the soil had a strong dependence on over-consolidation ratio (OCR). Kuntiwattanakul et al. (1995) investigated

the effects of high temperature (90 ^oC) on the undrained shear characteristics of both normally consolidated (NC) and overconsolidated (OC) clays, and observed that increasing temperature caused an increase of the initial secant modulus of both NC and OC clays, but only normally consolidated clay showed an increase of shear strength under heating.

Research work (Grant and Salehzadeh, 1996; Delage et al., 2000; Romero et al., 2001)has also been conducted regarding the thermal effects on the hydraulic properties of soils, e.g. permeability, water retention curve (SWRC), etc. Grant and Salehzadeh (1996) investigate temperature effects on wetting coefficients, and concluded that wetting coefficients affected the temperature sensitivity of the capillary pressure function significantly; a general expression that related capillary pressure and temperature was proposed as follows

$$p_c|_{\theta=\theta_f} = p_c|_{\theta=\theta_r} \times \left(\frac{\beta_0 + \theta_f}{\beta_0 + \theta_r}\right) \tag{1.1}$$

where $p_c|_{\theta=\theta_f}$ and $p_c|_{\theta=\theta_r}$ are the capillary pressures at an observational temperature θ_f and a reference temperature θ_r, respectively; β_0 is fitting parameter. Thus, the van Genuchten soil water retention model was accordingly modified as:

$$\theta(p_c, \theta_f) = \theta_\mathrm{r} + \frac{\theta_\mathrm{s} - \theta_\mathrm{r}}{[1 + (ap_c(\theta_f))^n]^m} \tag{1.2}$$

where θ_r is the residual water content, θ_s is saturated water content, and α $\left[cm^{-1}\right]$, n and m are empirical fitting parameters. Romero et al. (2001) studied temperature on water retention and permeability of partially saturated clays. It was investigated that the total suction tended to decrease as temperature increased at constant water content, and this dependence became weaker at a lower suction (see Figure 1.1). As for the apparent permeability for water phase, the temperature influence was shown to be more significant under near-saturated conditions, and this effect became hardly noticeable when the degree of saturation is below 75 % (see Figure 1.2 bottom). In addition, the experimental data showed that no significant temperature dependence was detected for relative permeability (Figure 1.3). An extrapolated interpretation for temperature effects on water permeability under saturated condition was formulated at constant void ratio e and water content

w as follows (Romero et al., 2001),

$$\frac{k_w(e,\theta,T_f)}{k_w(e,\theta,T_r)} \mid_{e,\theta} = \frac{\rho_w(T_f)\mu_w(T_r)}{\rho_w(\theta_r)\mu_w(\theta)} \approx 1 + \beta_T(T_f - T_r) \tag{1.3}$$

where β_T is an empirical coefficient that fits relative viscosity data over a temperature range of $22^oC \leq \theta \leq 80^oC$. Many experimental investigations has been carried out for different types of soils to estimate the value of β_T under saturated condition (Volckaert et al., 1996; Cho et al., 1999) and unsaturated conditions with low suction (Haridasan and Jensen, 1972; Hopmans and Dane, 1986).

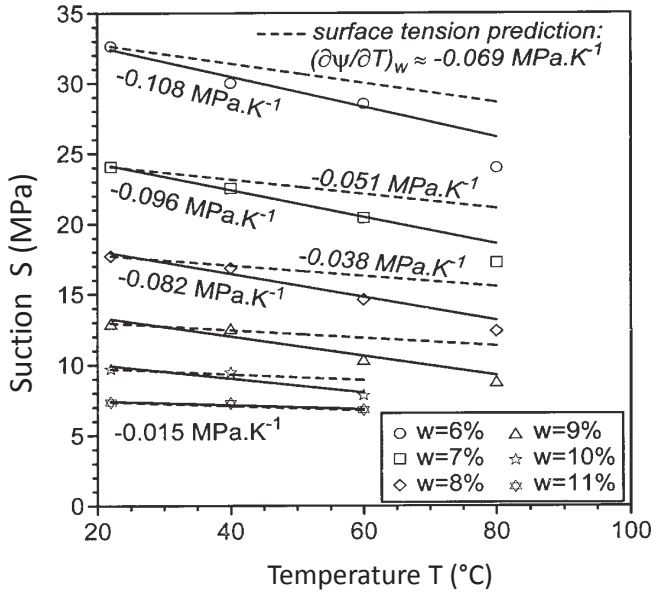

Figure 1.1: Total suction-temperature plots at constant water content (Romero et al., 2001).

Wu et al. (2004) presented an extended constitutive TPM models for partially saturated soils based on the work by Hueckel and Baldi (1990); Hueckel and Borsetto (1990); Hueckel and Pellegrini (1989) and Cui et al. (2000), and explored the coupling behavior between suction and temperature. Tong et al. (2009) and Tong et al. (2012) proposed an effective thermal conductivity model and a new water retention curve (SWRC) model, which included the effect of porosity and temperature on suction.

Dumont et al. (2011) introduced capillary stress defined as the summed capillary forces

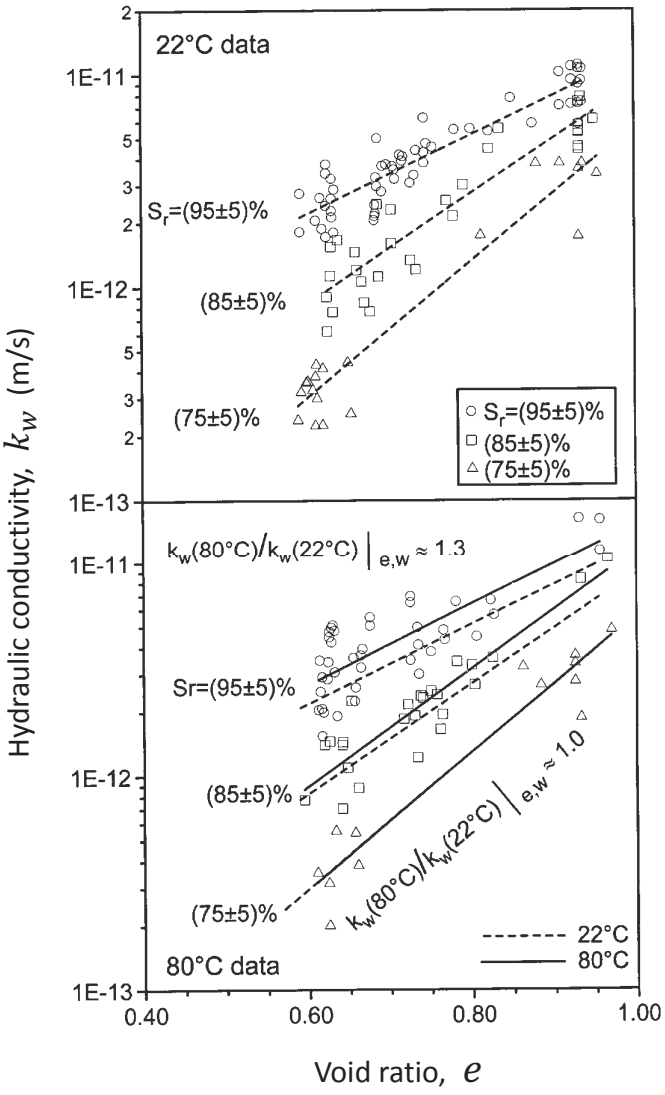

Figure 1.2: Hydraulic conductivity (k_w) vs.void ratio for different degrees of saturation at 22 ^oC and 80 ^oC (Romero et al., 2001).

divided by the cross-section area of the REV (representative elementary volume) to the effective stress concept based on microstructural model and modeled the effect of desaturation and thermal softening phenomenon. Laloui and Cekerevac (2003) present an isotropic thermo-plastic mechanism of clay based on considerations of the thermal effect on void ratio. Figure 1.4 and Figure 1.5 show an example of T-p_c-θ relationship of a silt soil.

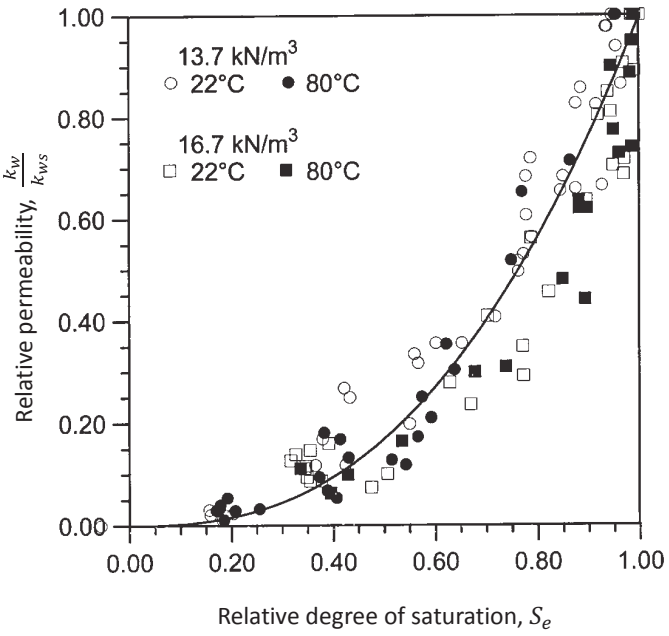

Figure 1.3: Relative permeability ($k_{rw} = \frac{k_w}{k_{ws}}$) versus relative degree of saturation S_e at 22 ^oC and 80 ^oC (Romero et al., 2001).

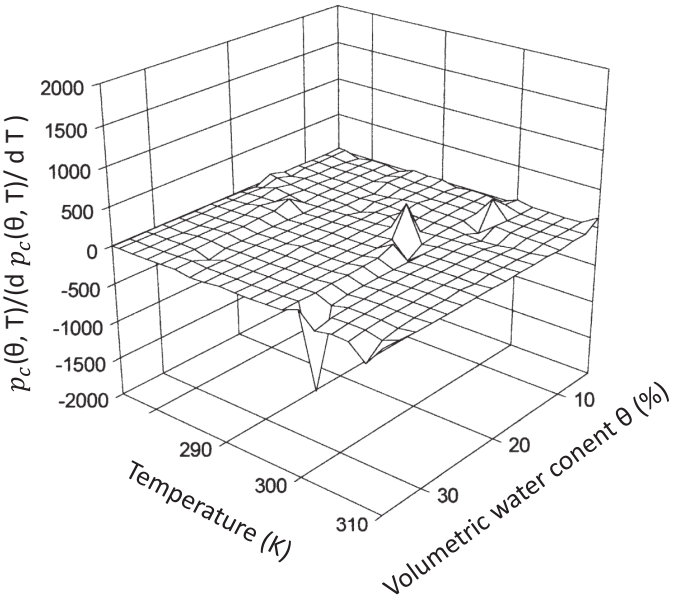

Figure 1.4: Plot of function $\Psi/(\partial\Psi/\partial T)$ vs. absolute volumetric temperature vs. water content for silt. (Bachmann and van der Ploeg, 2002).

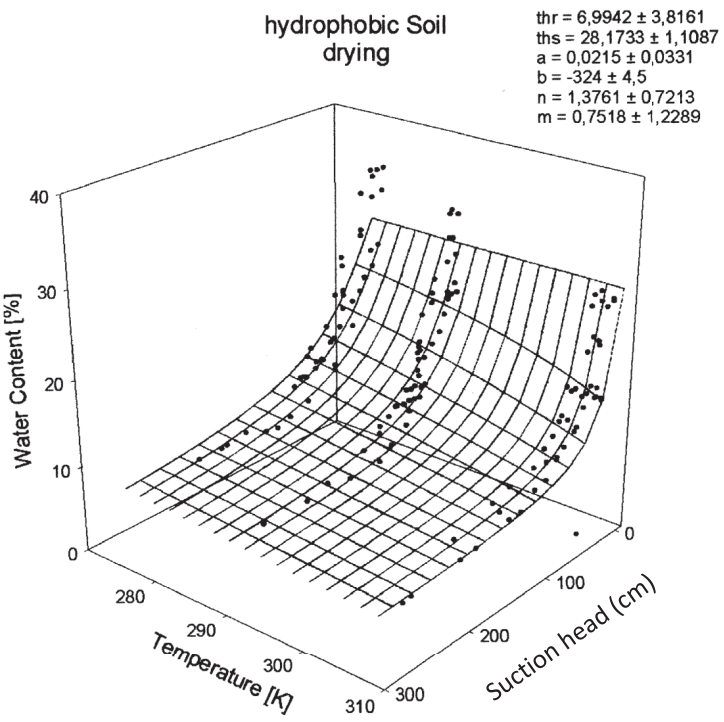

Figure 1.5: Global fit of the temperature-dependent van Genuchten function for a drying humid sand (Bachmann and van der Ploeg, 2002).

1.2.2 Thermo-poro-mechanical model

Porous media theory has a long tradition (de Boer, 2005). Research has been done on poro-mechanics based on the mixture theory restricted by the volume fraction concept Bear and Bachmat (1990); Bowen (1980, 1982) Some authors studied porous media from nano or micro scales (Brochard et al., 2012; Dormieux et al., 2006). Alonso et al. (1990); Toll (1990); Gens and Alonso (1992) have made great contribution to the development of constitutive models for partially saturated soils under isothermal condition. From the aspect of numerical modeling, Borja (1991); Borja et al. (1997); Borja and Tamagnini (1998); Borja (2004a) developed the algorithms of numerically implementing modified Cam-Clay plasticity model for both saturated and partially saturated soils at small strain and finite strain. In the last 50 years, coupled thermo-poro-mechanical processes has aroused great interest in different fields, such as the nuclear waste repository (Tsang et al., 2012; Rutqvist et al., 2014), carbon dioxide injection and sequestration (Hou et al., 2012; Fang et al., 2013; Soltanzadeh and Jafari, 2013), geothermal systems (Gelet et al., 2012; Wang et al., 2012; Jiang et al., 2013), reservoir simulation and borehole stability (Pao et al., 2001; Longuemare et al., 2002; Zhai et al., 2009; Lee and Ghassemi, 2010). Hassanizadeh and Gray (1980, 1990); Gray and Schrefler (2001); Schrefler (2002); Coussy (2004) introduced macroscale thermodynamics to describe the multiphase flow in porous media. Philip and de Vries (1957); de Vries (1958) proposed a model for the movement of liquid water and water vapor in rigid porous media under the combined gradients of temperature and moisture content. This model later was modified by Milly (1982); Bear et al. (1991); Thomas and King (1991), which replaced volumetric moisture content with matric suction as a primary variable. However, these models all assumed a rigid solid skeleton. Deformation of solid skeleton was considered to obtain coupled thermo-poro-mechanical model Thomas and He (1995); Schrefler et al. (1995); Thomas and He (1997); Zhou et al. (1998), and finite element method is mainly used to solve the initial-boundary-value-problem (IBVP) (Noorishad et al., 1982, 1984; Thomas and Missoum, 1999; Korsawe et al., 2006). Some research considered elastic constitutive model for soil (Aboustit et al., 1985a,b; Korsawe et al., 2006); others introduced Coussy (1989); Khalili and

Loret (2001); Laloui and Cekerevac (2003) considered thermo-plasticity with dependence on suction and temperature in the finite element element. Aboustit et al. (1985a) presented a thermoelastic consolidation model with general variational principles and finite element method, and ignored heat convection and the coupling term between the temperature and pressure. Coussy (1989) proposed a general theory of thermo-poro-elasto-plasticity for saturated porous materials derived from thermodynamics of open systems and irreversible processes. Wheeler (1996) proposed an elasto-plastic model by introducing variation of specific water volume taken into account, which could predict the specific water volume during wetting and drying, loading and unloading as well as shearing by only adding two additional suction-dependent soil parameters. It also could predict the variation of suction during undrained loading. Khalili and Loret (2001) proposed an elasto-plastic THM model to account for the suction and temperature effects on the yield function based on the works by Alonso et al. (1990); Hueckel and Baldi (1990). Laloui and Cekerevac (2003) presented a thermo-plastic model for saturated soil. Lewis et al. (1986); Lewis and Schrefler (1998); Coussy (2004); de Boer (2005) have proposed finite element models of elastic and elastoplastic thermo-poro-mechanical model for both saturated and partially saturated porous media. Yang et al. (1998) proposed an elastoplastic three-dimensional finite element model to analyze the transient coupled heat and fluid flow as well as the stress and strain of partially saturated soil skeleton. Lee and Ghassemi (2011) presented the stress-dependent permeability in a three-dimensional THM finite element model with damage mechanics. Bluhm (2002) and Niessner and Hassanizadeh (2009) relaxed the assumption of local thermal equilibrium by considering different phase temperatures and interphase heat transfer, respectively. Schrefler et al. (1995) simulated the soil skeleton deformation, heat and fluid (water and air) flow in porous media, considering both conduction and convection but latent heat. Olivella and Gens (2000) discussed the phase change (from water to vapor) and vapor transport under temperature gradients in partially saturated soils. Research on the multiphase flow and transport in porous media has been conducted (Spalding, 1980; Miller et al., 1998; Tryggvason et al., 2001; Shin and Juric, 2002; Blunt et al., 2002), and several simulators have been developed for the flow and heat analysis in porous media (Pruess, 1991; Olivella et al., 1996; Kolditz et al., 2012).

Rutqvist et al. (2001) compared four finite element simulators (ROCMAS, THAMES, FRACON and AQCLAY) with respect to governing equations and constitutive relations. Modaressi and Laloui (1997); Oka et al. (2004) extended for thermo-viscoplastic model. Thermo-poro-mechanical model under quasi-static condition have been extended to analyze dynamic problems, such as seismic triggering and evolution of catastrophic landslides (Vardoulakis, 2002; Sulem et al., 2004; Rice, 2006; Sulem et al., 2007).

Some research focused on solving the coupled thermo-poro-elastic problems analytically: Booker and Savvidou (1985) developed an analytical solution for the consolidation around a point and a spherical heat source in saturated thermoelastic soil. The mechanical contribution to the energy conservation equation is neglected to uncouple the temperature field from the calculation of displacement and pressure. Bai and Abousleiman (1997) presented an analytical solution of a 1-D linear, quasi-static elastic, saturated system. Various coupling cases are compared to discover the influence of each coupling term. For partially saturated porous media, close form solutions of two-dimensional and three-dimensional transient quasi-static thermo-poro-mechanical problems are developed (Jabbari and Gatmiri, 2007; Gatmiri et al., 2010; Maghoul et al., 2010). Suction and temperature effect on soil skeleton deformation and the inverse effects are incorporated.

1.2.2.1 Hydraulic properties of soils

The soil-water characteristic curve (SWCC) for soil is defined as the relationship between water content and suction of soil. The suction can be either the matric suction (also known as capillary pressure) that equals $s = p_g - p_w$ or total suction (i.e. matric suction plus osmotic suction), where p_g and p_w are the pore gas and pore water pressures, respectively. At high suction (greater than about 1500 kPa), it can be assumed that matric suction approximately equals total suction, according to Fredlund and Xing (1994). A great number of experiments have been done to obtain the SWCC, which is usually plotted on a logarithmic (base 10) scale. A typical plot of SWCC for a silty soil (see Figure 1.6) shows the information about the air-entry value or the bubbling pressure (i.e., the matric suction where air begins to enter the biggest pores in the soil

upon drying), the residual water content θ_r and the residual air content. The difference between the absorption (wetting) and desorption (drying) is the result of hysteresis. The SWCC for soils with different plasticity (Figure 1.7) shows the air-entry value increases with increasing cohesion of soil.

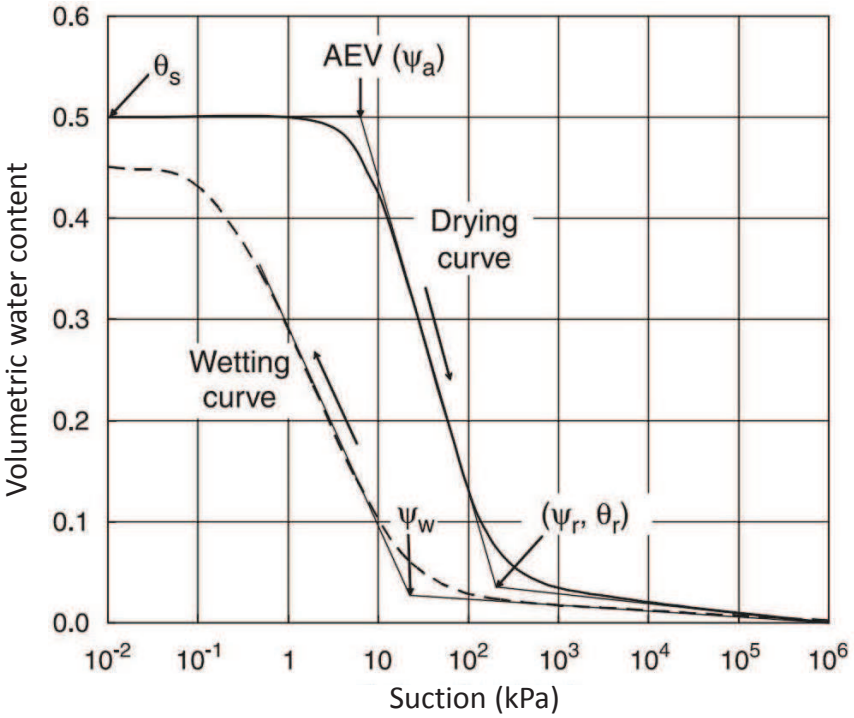

Figure 1.6: Typical soil-water characteristic for a silty soil (Fredlund and Xing, 1994).

Among many empirical equations which have been developed to simulate the soil-water characteristic curve, two most frequently used forms are respectively proposed by Brooks and Corey (1964) and van Genuchten (1980) as shown in (1.4) and (1.5), respectively.

$$\Theta = \left(\frac{s_{ae}}{s}\right)^{\lambda} \tag{1.4}$$

where $\Theta = (\theta - \theta_r)/(\theta_s - \theta_r)$, with θ_s and θ_r the saturated and residual volumetric water contents respectively, s_{ae} the air-entry value, λ the pore size distribution index, and

$$\Theta = \left[\frac{1}{1 + (p\,s)^n}\right]^m \tag{1.5}$$

where p, n, and m are fitting parameters, and $m = 1 - 1/n$.

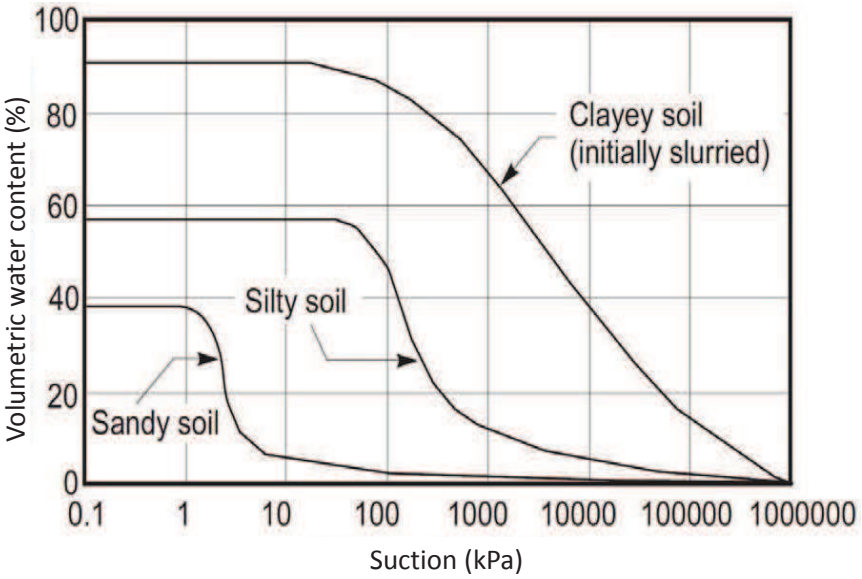

Figure 1.7: Soil-water characteristic curves for a sandy soil, silty soil and clayey soil (Fredlund and Xing, 1994).

The model by Brooks and Corey (1964) has been proved to work well for suction higher than the air-entry value, while the model by van Genuchten (1980) provides more flexibility. Another valid form (1.6) was proposed by McKee and Bumb (1987) to deal with conditions in low suction range, while this relationship would fail in the high suction range.

$$\Theta = \frac{1}{1 + e^{(s-a)/b}} \tag{1.6}$$

where a and b are fitting parameters.

The coefficient of permeability of a partially saturated soil depends on the volumetric water content n^w or the soil suction s. The relative permeability k_r is defined as:

$$k_r = \frac{k}{k_s} \tag{1.7}$$

where k_s is saturated permeability, according to Coussy (2004) it is related to fluid viscosity η_f and the intrinsic permeability ($\kappa = l^2\delta(n)$, l is a geometric length scale associated with the pore space), which depends on the geometry of the porous media irrespective of the fluid, such that

$$k_s = \frac{\kappa}{\eta_f} = \frac{l^2\delta(n)}{\eta_f} \tag{1.8}$$

$$\delta(n) = \frac{n^3}{1-n^2} \tag{1.9}$$

where n is the porosity of soil. (1.9) is the often used Kozeny-Carman's formula (Coussy, 2004). Some empirical equations are proposed to estimate the permeability of partially saturated soils. Based on a large number of experimental data, Brooks and Corey (1964) gave the expression of relative permeability as,

$$k_{rw} = (S_e)^{\frac{2+3\,\lambda}{\lambda}} \tag{1.10}$$

$$k_{rnw} = (1-S_e)^2 \left(1 - S_e^{\frac{2+\lambda}{\lambda}}\right) \tag{1.11}$$

$$S_e = \frac{S_w - S_{wr}}{1 - S_{wr}} \tag{1.12}$$

where k_{rw} and k_{rnw} are relative permeability of wetting (e.g. water) and non-wetting (e.g. air) phases respectively, λ is the same as that in (1.4), S_e is the effective (or relative) degree of saturation, and $k = k_s$ is used when $s < s_b$. van Genuchten (1980) proposed an expression to relate relative permeability to suction as follows

$$k_{rw}(S_e) = \sqrt{S_e}\left(1 - \left(1 - S_e^{1/m}\right)^m\right)^2 \tag{1.13}$$

$$k_{rnw}(S_e) = \sqrt{1-S_e}\left(1 - S_e^{1/m}\right)^{2m} \tag{1.14}$$

where S_e is the effective (or relative) degree of saturation as defined in (1.12), and m is fitting parameter as that in (1.5).

1.2.2.2 Effective stress theory of partially saturated soils

For saturated and partially saturated soils, the effective stress principle is necessary to distinguish between pore air and water pressures and the solid skeleton constitutive response, involving elastic or elastoplastic constitutive models. Terzaghi (1936) proposed the expression of effective stress for saturated soils:

$$\sigma'_{ij} = \sigma_{ij} + \alpha p_w\, \delta_{ij} \tag{1.15}$$

where σ'_{ij} and σ_{ij} are respectively effective stress and total stress, and the sign convention follows solid mechanics, i.e. positive in tension; p_w is pore water pressure, which is positive in compression;

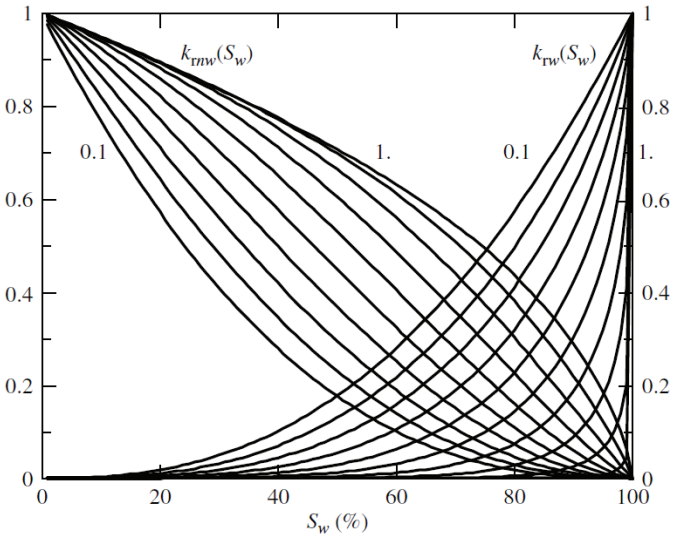

Figure 1.8: Relative permeability k_{rw} and k_{rnw} plotted against S_w when varying m from 0.1 to 1 (Coussy, 2004).

The Biot's coefficient α is introduced to account for the volumetric deformability of the solid particles as follows (Biot, 1941; Skempton, 1984; Gawin et al., 1996): $\alpha = 1 - \frac{K_T}{K_S} \leq 1$, where K_T and K_S denote the bulk moduli of the porous medium and the solid particle, respectively.

For partially saturated soils, it is demonstrated that the capillary effect from the format of water menisci at the pore air-water and solid interfaces should be incorporated. The capillary forces are complex in that it is dependent upon soil properties, degree of saturation, matric suction and the properties of the multiphase fluid interface (air-water surface tension, contact angle) (Lu and Likos, 2006). The effective stress for partially saturated soil is usually written as (Gawin et al., 1996)

$$\sigma'_{ij} = \sigma_{ij} + \alpha \bar{p} \delta_{ij} \tag{1.16}$$

where α is Biot's coefficient as defined before, and $\bar{p}$ is an average pressure of the mixture, and is shown as follows (Gray and Hassanizadeh, 1991):

$$\bar{p} = S_w \, p_w + (1 - S_w) \, P_g \tag{1.17}$$

Bishop (1959) gives the effective stress formula in the following:

$$\boldsymbol{\sigma}' = \boldsymbol{\sigma}^{net} + \chi \, s \mathbf{1} \tag{1.18}$$

where $\boldsymbol{\sigma}^{net} = \boldsymbol{\sigma} - p_g \mathbf{1}$ is the net stress, $s = p_g - p_w$ is matric suction, p_g is pore gas pressure, χ is the effective stress parameter,related to the degree of saturation S_w of soils. Bishop proposed that χ equals 1 for saturated soils and 0 for dry soils. Despite experimental validation by Bishop and Donald (1961), and Bishop and Blight (1963), the validity of Bishop's effective stress principle for partially saturated soils has been criticized by many researchers through a series of consolidation tests. Among these arguments (Kohgo et al., 1993; Bolzon et al., 1996; Loret and Khalili, 2000; Khalili and Loret, 2001), some researchers investigated the effect of plastic deformation on the effective stress expression by defining the yield surface as a function of suction. Others pointed out through experiments that the relationship between χ and S_w is not unique, it also depends on the soil structure (Coleman, 1962), drying and wetting cycles, and stress history. Khalili and Khabbaz (1998) presented a plot of χ versus suction ratio (the ratio of matrix suction over the air entry value). Fredlund and Morgenstern (1977) proposed two independent stresses variables, $\sigma_{ij} - p_g \delta_{ij}$ and $p_g - p_w$ respectively from a macroscopic view and pore scale to express the stress state in partially saturated soils.

Recently, the relationship between the deviatoric stress and effective mean stress for both saturated and partially saturated soils has been extensively studied. Data from the triaxial shear tests (Figure 1.9 and Figure 1.10) show the uniqueness of the critical state line (CSL) for both saturated and partially saturated soils under different suction values (Maatouk et al., 1995; Cui and Delage, 1996; Wheeler and Sivakumar, 1995a).

Khalili et al. (2004) analyzed these literature and validated this relationship experimentally, and also demonstrated the incremental form of effective stress equation used in path-dependent processes. For saturated soils, the incremental effective stress equals the total counterpart:

$$\delta \sigma'_{ij} = \delta \sigma_{ij} - \delta p_w \delta_{ij} \tag{1.19}$$

For partially saturated soils,

$$\delta \sigma'_{ij} = \delta \sigma^{net}_{ij} - \delta (\chi s) \delta_{ij} \tag{1.20}$$

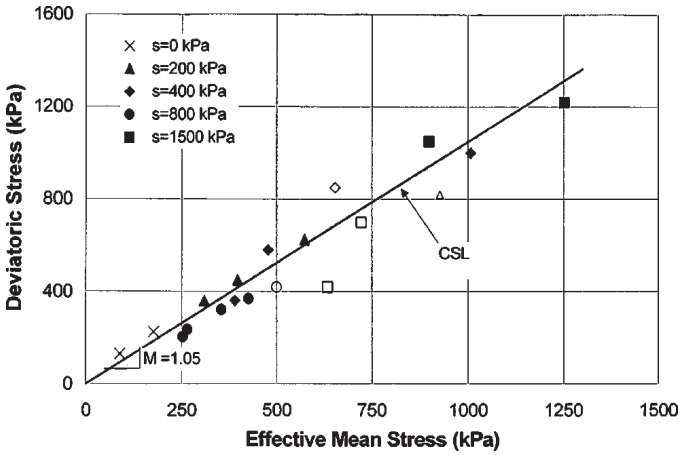

Figure 1.9: Evolution of critical state with suction in p'-q plane for Jossigny silt (Cui and Delage, 1996).

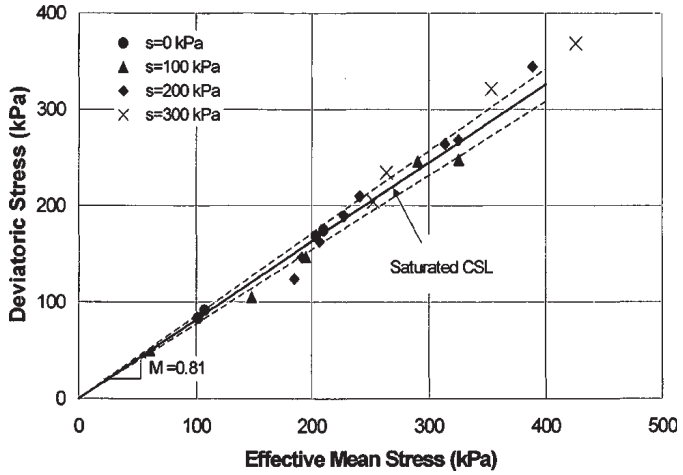

Figure 1.10: Evolution of critical state with suction in p'-q plane for kaolin clay (Wheeler and Sivakumar, 1995a).

where χ is defined by Khalili and Khabbaz (1998) as

$$\chi = \begin{cases} \left(\frac{s}{s_e}\right)^{-0.55} & \text{if } s > s_e \\ 1 & \text{if } s \leq s_e \end{cases} \tag{1.21}$$

where s_e is the suction value marking the transition between saturated and partially saturated states. For wetting processes, s_e is equal to the air expulsion value, while for drying processes, s_e is equal to the air entry value, which can be obtained from the soil water characteristic curve (SWCC) (e.g. figure 1.6).

For the stress state variables, three possible combinations of stress variables to define the stress state are as follows: (1) $(\sigma_{ii} - p_w)$ and $(p_g - p_w)$; (2) $(\sigma_{ii} - p_g)$ and $(p_g - p_w)$; (3) $(\sigma_{ii} - p_g)$ and $(\sigma_{ii} - p_w)$, where σ_{ii} is the total normal stress component, were proposed and verified by experiments (Fredlund and Morgenstern, 1977). Lately the stress state variable theory has been modified to add soil properties to the constitutive model of partially saturated soils (Gallipoli et al., 2003b; Khalili et al., 2008; Kohgo et al., 1993; Tamagnini, 2004; Wheeler et al., 2003) . Wheeler et al. (2003) argued that Bishop's stress failed to consider the influence of meniscus water. He proposed to employ two new stress variables σ^*_{ij} and s^* defined as:

$$\sigma^*_{ij} = \sigma_{ij} - [S_w p_w + (1 - S_w) p_g]\delta_{ij} \tag{1.22}$$

$$s^* = ns = n(p_g - p_w) \tag{1.23}$$

where σ_{ij} is the total stress tensor, S_w is degree of saturation, p_w and p_g are pore water and pore gas pressure, s is suction, n is porosity. Bishop's stress tensor can be attained if we replace S_w by χ. Similar conclusion is made by Houlsby (1997),who suggested to add the porosity n to the stress variables in the principle of work conjugacy. Wheeler et al. (2003) also presented the simplified incremental form of input work dW (see (1.24)) of triaxial test as

$$dW = p^* d\epsilon_v + q d\epsilon_s - s^* dS_r \tag{1.24}$$

where q is the deviatoric stress, p^* is the mean Bishop's stress, defined by

$$p^* = p - S_w\, p_w - (1 - S_w)\, p_g \tag{1.25}$$

The stresses p^*,q and s^* are chosen to be the three stress variables for triaxial test; ϵ_v and ϵ_s are respectively volumetric strain and deviotoric strains. Compared to the traditional variables which are net stress and suction, the approach of using new stress variables is more complex, and thus makes the development of corresponding constitutive models more difficult. Lu et al. (2010) extended the theory of Bishop's stress, and gave a modified form of effective stress for all saturations,

$$\sigma'_{ij} = (\sigma_{ij} - p_g) - \sigma^s \delta_{ij} \tag{1.26}$$

where σ^s is defined as suction stress, and the closed form solution is attained with SWCC model by van Genuchten (1980) :

$$\sigma^s = \begin{cases} -(p_g - p_w) & \text{if } p_g - p_w \leq 0 \\ -\frac{p_g - p_w}{\{1+[\alpha(p_g - p_w)]^n\}^{(n-1)/n}} & \text{if } p_g - p_w \geq 0 \end{cases} \tag{1.27}$$

Lu and Likos (2006) developed the concept of suction stress characteristic curve (SSCC) to describe the stress state of partially saturated soil. And this concept is verified experimentally in terms of Mohr-Coulomb failure and critical state failure.

1.3 Background on soil-structure interaction

1.3.1 Background on interface element models

Cohesive interface elements have been widely used to model nucleation or propagation of cracks in composite materials (e.g. delamination of fiber-reinforced composite laminates (Balzani and Wagner, 2008), cross-ply composite laminates (Aymerich et al., 2008, 2009), and polymer matrix composite (Corigliano and Ricci, 2001)), rock failure (e.g. fault slip (Aagaard et al., 2013)), soil-structure interaction (e.g. soil-wall and soil-pile) (Cai et al., 2000; Hu and Pu, 2004), and soil-reinforcement analysis (Gens et al., 1989). Desai et al. (1984) proposed a thin-layer interface element for soil-structure interaction with special constitutive law to model cracks under opening and shearing modes. Given the same constitutive parameters, the performance of the interface element can be affected by the thickness of the thin-layer. This effect was discussed by Sharma and Desai (1992) through an extensive parametric study; certain guidelines were provided to empirically determine the element thickness under various conditions. Different approaches have been proposed for the constitutive model of discontinuity including penalty method (Papadopoulos and Taylor, 1992; Xie and Waas, 2006), Lagrange multipliers (Aagaard et al., 2013). Numerical performance of different interface laws (or stress-displacement curves), e.g.bilinear, linear-parabolic, exponential, and trapezoidal, for debonding problems was studied using pure-mode problems (Alfano, 2006); it was reported that the choice of softening curve depended greatly on ratio between

the interface toughness and the stiffness of the bulk material. In geomechanics, several categories of finite elements that have been proposed to model the soil-structure interaction, soil-reinforcement interaction, and rock joints (Goodman et al., 1968; Beer, 1985; Griffiths, 1985; Pande and Sharma, 1979; Gens et al., 1989). Some examples are: Gens et al. (1989) used zero-thickness solid interface elements to analyze the soil-reinforcement interaction in a pull-out test; softening behavior of the interface was observed. Carol et al. (1997) proposed a general normal/shear cracking model for quasi-brittle materials, which was used for discrete crack analysis. Katona (1983) introduced a contact-friction interface element to simulate the frictional slippage, separation and re-bonding between two bodies along the interface and the subsequent deformation due to an arbitrary static loading. Zong-Ze et al. (1995) explored the constitutive law using a direct shear test and proposed an interface element model with small thickness. Day and Potts (1994) numerically investigated the effects of stiffness matrix and stress gradients on the stability of zero-thickness interface elements in practical applications. Some research work related to mesh free method (Dolbow and Belytschko, 1999; Sukumar and Belytschko, 2000; Wells and Sluys, 2001; Remmers et al., 2003) have been developed based on partition-of-unity property of finite element shape functions Melenk and Babuška (1996). The key feature is to capture the crack initiation/propagation in an arbitrary direction independent of mesh structure. Therefore, mesh bias can be avoided and remeshing is not necessary during the crack propagation.

1.3.2 Multiphase flow and heat transfer in fractured porous media

Fluid flow in saturated fracture has been studied by many researchers. Fractures saturated with liquid in geomaterials act as main flow paths. Noorishad et al. (1982) studied the coupled stress and fluid flow in a fracture-closing problem due to fluid withdraw in a saturated fractured medium. Ge (1997) proposed a generalized equation to predict fluid flow behavior in a saturated fracture with nonparallel and nonsmooth geometry surfaces under steady state conditions. Segura and Carol (2004) presented a double-noded zero-thickness flow interface model to account for both longitudinal and transversal fluid flows in a single discontinuity. The model was further extended

to a coupled hydro-mechanical interface model for geomaterials with existing or developing fractures by Segura and Carol (2007a,b, 2010). In contrast to saturated fractures, multiphase flow and transport processes in partially saturated fractures are theoretically more complex and practically more significant. For partially saturated fractures with two phases (gas and liquid) coexisting, and the presence of one phase produces various degrees of resistance to the flow of the other phase, depending on phase saturation. With the flow paths distorted, the fractures may act as barriers for the phase under low saturation. Several mathematical models have been proposed to describe the multiphase flow in fractured porous media under partially saturated condition (Therrien and Sudicky, 1996; Pruess and Tsang, 1990; Persoff and Pruess, 1995). Recently, coupling between flow and mechanical response in cracks of geomaterials has gained increasing attention. A typical application is related to geomechanical analysis of geological sequestration of CO_2, which is broadly considered as a challenging but promising technology to mitigate climate change. Reservoir failure or fault slip may happen due to increased fluid pressure during geological sequestration of CO_2, and earthquake may be induced by the fault-instability processes (Rutqvist et al., 2007, 2008, 2010; Cappa and Rutqvist, 2011a,b). Fluid flow and chemical transport in fractured porous media under non-isothermal conditions have received increasing attention due to various geotechnical applications. A number of numerical simulations have been reported to predict the more complex interaction between multiphase flow, chemical transport, and heat transfer processes (Pruess et al., 1990; Xu and Pruess, 2001). Rutqvist et al. (2002) developed a coupled thermo-hydrologic-mechanical-chemical simulator by combining two existing computer codes TOUGH2 and FLAC^{3D}. The so-called "coupling" between flow and mechanical responses in the analysis are based on linking the multiphase flow simulator TOUGH2 (Pruess et al., 1999) and commercial geomechanical code FLAC^{3D}.

1.4 Interaction of soil-atmosphere surfaces

Evaluation of evaporative fluxes at the soil surface is necessary in many geotechnical applications when temperature and partially saturated conditions are considered. Research dealing with

evaporation from the surface of either saturated or partially saturated soil can not avoid the concept of potential evaporation (PE), which is considered to be an upper limit or maximum rate of evaporation (Wilson et al., 1997). The International Glossary of Hydrology (World Meteorological Organization gives the definition of potential evaporation as "The quantity of water vapor which could be emitted by a surface of pure water per unit surface area and unit time under the existing atmospheric conditions." Gray (1970) gave the evaporation rate E from a free water surface:

$$E = f(u)(e_s - e_a) \tag{1.28}$$

Where, e_s and e_a are, relatively, the saturation vapor pressure of the water surface and the vapor pressure in the atmosphere above the water surface (kPa), and $f(u)$ is a transmission function that may be evaluated empirically with the characteristics of the air above the evaporation surface. The actual rate of evaporation from vegetated and bare soil surface can only be approximated using the theory of PE under the condition of unlimited supply or availability of water to the soil surface (Penman, 1948). However, the prediction by traditional methods may overestimate the evaporation rate for partially saturated soil surfaces (Granger, 1989). For a few decades, many researchers have been investigating how to measure or compute the actual evaporation (AE) rate for partially saturated soils. Most of them attempted to find a relationship between PE and AE (Gray, 1970; Holmes, 1961). A few empirical methods have been developed due to the difficulties in evaluating the soil properties that determine evaporation from partially saturated soil surfaces (Hillel, 1980; Yanful et al., 1993). Some efforts have been made to define certain functions of evaporation with dependent variables, e.g., humidity and water content of near surface soil (Barton, 1979), moisture and temperature gradients (Hammel et al., 1981). Wilson et al. (1994) developed a coupled soil-atmosphere model for soil evaporation. This model calculated the vapor pressure at the soil surface with the assistance of coupled heat and mass balance equations for the soil profile under the surface. Although the comparison was good between the model prediction and the experimental results with ideal cohesionless uniform sand, this model is not ready for wide application due to the lack of generality, i.e. for fine silt and cohesive clay. Wilson et al. (1997) carried out experiments

on three different soil samples to study the evaporative fluxes from nonvegetated soil surfaces. A unique relationship was discovered between the actual evaporation rate and total suction for all three soil samples independent of soil texture, drying time and water content. The normalized soil evaporation was found to be unity approximately until the total suction at the soil surface exceeded $3000kPa$.

1.5 Objectives

Numerical modeling of the thermo-poro-mechanical behavior of partially saturated soils is a significant issue in the analysis of geothermal structures. It can be also applied to solve other problems such as nuclear waste isolation and CO_2 storage. Based on extensive study of existing models, the author proposes a general coupled finite element model which incorporates different coupling physics of partially saturated soils, mainly, thermo-poro-mechanics (TPM). A new research code is written to understand how all the coupled physics fit together in a monolithically-coupled finite element (FE) framework in which to insert our constitutive model for certain type of soil (e.g. silt, sand, clay, or some mix). A partially saturated porous media can be treated as three-phase (solid,liquid water, and gas) or four constituent (solid (s), liquid water (w), water vapor (gv), and dry air (ga)) mixture. The gas phase is considered to be a combination of dry air and water vapor. The governing equations are developed according to mixture theory Goodman and Cowin (1972); Bowen (1980, 1982); de Boer (2005), and satisfy the balance of mass, momentum and energy conservation (first law of thermodynamics). Heat transfer is considered through conduction and convection. Thermal effects are taken into account in fluid flow, viscosity and density variation. Constitutive equations are adopted, such as Fick's law of diffusion, Newton's law of viscosity, Fourier's law for heat flux, and other relations about relative permeability of wetting and non-wetting phases. Entropy inequality is used to assure that the second law of thermodynamics is not violated, and some constitutive relations are obtained following the procedure proposed by Coleman and Noll (1963). Local continuum thermal equilibrium is assumed throughout, where mixture temperature θ equals that of the constituents, i.e. $\theta = \theta_s = \theta_w = \theta_{gv}\theta_{ga}$. The solid and liquid water

are both assumed to be mechanically incompressible for now (bulk moduli $K_s \to \infty$, $K_w \to \infty$). They can easily be modified to be compressible if needed. The solid skeleton is compressible. Solid skeleton displacement vector, pore water pressure, pore gas pressure and temperature are the primary field variables.

In general, the main research objectives of the thesis include:

(1) Develop thermo-poro-mechanical (TPM) model for saturated and partially saturated soils with linear and nonlinear elastic constitutive model for solid skeleton;

(2) Extend for temperature- and suction- dependent elastoplastic solid skeleton constitutive model for partially saturated soils;

(3) Fit the material parameters of soil used in the energy centrifuge experiments;

(4) Develop thermo-poro-mechanical cohesive interface element, and implement it at the soil foundation interface;

(5) Simulate the energy foundation centrifuge tests with partially saturated soil, and compare the numerical modeling results and centrifuge modeling observations.

Chapter 2

Thermoelasticity

2.1 Introduction

First, let us start from the theory of thermo-elasticity for solid. In this chapter, governing equations in terms of balance of linear momentum and conservation of energy are derived for solid, which are supplemented with the second law of thermodynamics. Finite element formulations in axisymmetric coordinate are presented; several numerical examples regarding thermal expansion are analyzed.

2.2 Governing equations

2.2.1 Balance of linear momentum

The balance of linear momentum of a solid is given as:

$$\frac{D}{Dt}\int_{\Omega}(\rho \boldsymbol{v})dv = \int_{\Omega}\rho \boldsymbol{b}dv + \int_{\partial\Omega}\boldsymbol{T}da \tag{2.1}$$

where, $D(\bullet)/D\,t$ is the material time derivative, ρ is the mass density, $\boldsymbol{v}$ the velocity vector, $\boldsymbol{b}$ the body force vector per unit mass, and $\boldsymbol{T}$ the surface traction vector, which is defined as

$$\boldsymbol{T} = \boldsymbol{\sigma}\cdot\boldsymbol{n} \tag{2.2}$$

where, $\boldsymbol{\sigma}$ is the symmetric Cauchy stress tensor, and $\boldsymbol{n}$ is the unit normal to the surface $\partial\Omega$. Assuming constant ρ and small strains,

$$\frac{D}{D\,t}\int_{\Omega}(\rho \boldsymbol{v})dv = \int_{\Omega}\frac{D}{D\,t}(\rho \boldsymbol{v})dv = \int_{\Omega}\rho \boldsymbol{a}\,dv \tag{2.3}$$

where, $\boldsymbol{a}$ is the acceleration vector, which will be ignored for quasi-static condition. Using the divergence theorem,

$$\int_{\partial\Omega} \boldsymbol{T} da = \int_{\partial\Omega} \boldsymbol{\sigma} \cdot \boldsymbol{n} da = \int_{\Omega} \mathrm{div}\boldsymbol{\sigma} dv \tag{2.4}$$

Ignoring the inertia term, the local form of the balance of linear momentum equation (2.1) is then:

$$\mathrm{div}(\boldsymbol{\sigma}) + \rho \boldsymbol{b} = \boldsymbol{0} \tag{2.5}$$

2.2.2 Balance of energy

2.2.2.1 The first law of thermodynamics

The first law of thermodynamics, (or the energy conservation) states that the rate of internal energy and kinetic energy equals the rate of the mechanical work and the heat. The first law is expressed as:

$$\dot{E} + \dot{K} = P + \dot{Q} \tag{2.6}$$

where, E, K, P and Q are, respectively the internal energy, the kinetic energy, the rate of mechanical work caused by the external forces (body force and surface traction in this thesis), and the heat supplied to the system by the surroundings. And they are given by

$$\begin{aligned} \dot{E} + \dot{K} &= \frac{D}{D\,t} \int_{\Omega} (\rho e + \frac{1}{2} \rho \boldsymbol{v} \cdot \boldsymbol{v}) dv \\ &= \int_{\Omega} \left[\frac{D(\rho e)}{D\,t} + \rho \boldsymbol{v} \cdot \boldsymbol{a} \right] dv \end{aligned} \tag{2.7}$$

where, e is the internal energy per unit mass, and the inertia term will be ignored later. The external power is

$$P = \int_{\Omega} \rho \boldsymbol{b} \cdot \boldsymbol{v} dv + \int_{\partial\Omega} \boldsymbol{T} \cdot \boldsymbol{v}\, da \tag{2.8}$$

Using the divergence theorem and (2.2),

$$\begin{aligned}\int_{\partial\Omega} \boldsymbol{T}\cdot\boldsymbol{v}\,da = \int_{\partial\Omega}(T_i\,v_i)\,da &= \int_{\partial\Omega}(\sigma_{ij}\,n_j\,v_i)\,da \\ &= \int_{\partial\Omega}(\sigma_{ji}\,v_i\,n_j)\,da \\ &= \int_{\partial\Omega}(\boldsymbol{\sigma}\cdot\boldsymbol{v})\cdot\boldsymbol{n}\,da \\ &= \int_{\Omega}\mathrm{div}(\boldsymbol{\sigma}\cdot\boldsymbol{v})\,dv \\ &= \int_{\Omega}\mathrm{div}(\boldsymbol{\sigma})\cdot\boldsymbol{v}\,dv + \int_{\Omega}\boldsymbol{\sigma}:\mathrm{grad}(\boldsymbol{v})\,dv \end{aligned} \tag{2.9}$$

Using (2.9), we get:

$$P = \int_{\Omega}\left[\left(\underbrace{\rho\boldsymbol{b}+\mathrm{div}\,\boldsymbol{\sigma}}_{R1}\right)\cdot\boldsymbol{v} + \boldsymbol{\sigma}:\mathrm{grad}\,\boldsymbol{v}\right]dv \tag{2.10}$$

The terms $R1 = 0$ according to (2.5).

$$\mathrm{grad}(\boldsymbol{v}) = \dot{u}_{i,j} = \underbrace{\frac{1}{2}(\dot{u}_{i,j}+\dot{u}_{j,i})}_{\dot{\boldsymbol{\epsilon}}} + \underbrace{\frac{1}{2}(\dot{u}_{i,j}-\dot{u}_{j,i})}_{\dot{\boldsymbol{\Omega}}} = \dot{\boldsymbol{\epsilon}}+\dot{\boldsymbol{\Omega}} \tag{2.11}$$

where a comma stands for spatial differentiation (i.e., $u_{i,j} = du_i/dx_j$), and $\dot{\boldsymbol{u}}$ stands for material time derivative of the displacement (i.e., $\dot{\boldsymbol{u}} = D\boldsymbol{u}/D\,t$). $\dot{\boldsymbol{\epsilon}}$ is the symmetric strain rate tensor for small strain theory, and $\dot{\boldsymbol{\Omega}}$ is defined as rotation rate tensor, which is a skew symmetric tensor, thus

$$\boldsymbol{\sigma}:\mathrm{grad}\,\boldsymbol{v} = \boldsymbol{\sigma}:\dot{\boldsymbol{\epsilon}} + \underbrace{\boldsymbol{\sigma}:\dot{\boldsymbol{\Omega}}}_{R2} \tag{2.12}$$

where $R2 = 0$. Substitution of (2.12) leads to the internal stress power

$$P = \int_{\Omega}\boldsymbol{\sigma}:\dot{\boldsymbol{\epsilon}}\,dv \tag{2.13}$$

The rate of heat supply is expressed in the form:

$$\begin{aligned}\dot{Q} &= \int_{\Omega}\rho r dv - \int_{\partial\Omega}\boldsymbol{q}\cdot\boldsymbol{n}da \\ &= \int_{\Omega}\rho r dv - \int_{\Omega}\mathrm{div}\boldsymbol{q}dv\end{aligned} \tag{2.14}$$

where, r is the heat source or heat supply per unit mass, and $\boldsymbol{q}$ the heat flux vector, which is positive when entering the body. Let us assume the heat flux vector is defined in terms of the

temperature gradient by the generalized Fourier's law:

$$q_i = -K^{\theta}_{ij}\theta_{,j}, \quad K^{\theta}_{ij} = K^{\theta}_{ji} \quad \text{(symmetric)} \tag{2.15}$$

where $\boldsymbol{K}^{\theta}$ is referred to as the thermal conductivity matrix, and the components K^{θ}_{ij} are constants throughout Ω for a homogeneous body, but homogeneity can be accounted for through a finite element mesh where different elements have different material properties. The most common situation is the isotropic case in which $K^{\theta}_{ij} = K^{\theta}\delta_{ij}$, where δ_{ij} is the Kronecker delta (Hughes, 2000). Substitution of (2.7), (2.13) and (2.14) into (2.6) gives the balance of energy equation in the form:

$$\frac{D(\rho e)}{D\,t} = \boldsymbol{\sigma} : \dot{\boldsymbol{\epsilon}} + \rho r - \operatorname{div} \boldsymbol{q} \tag{2.16}$$

2.2.2.2 The second law of thermodynamics

The conservation laws must be supplemented with the second law of thermodynamics. According to this law, the rate of net entropy production of the system must be non-negative. The second law of thermodynamics is expressed as:

$$\frac{D}{D\,t}\int_{\Omega} \rho\eta dv \geq \int_{\Omega} \frac{\rho r}{\theta} dv - \int_{\partial\Omega} \frac{\boldsymbol{q}\cdot\boldsymbol{n}}{\theta} da \tag{2.17}$$

where, η is the entropy per unit mass; θ is the temperature. Considering the divergence theorem, we get:

$$\int_{\partial\Omega} \frac{\boldsymbol{q}\cdot\boldsymbol{n}}{\theta} da = \int_{\Omega} \operatorname{div}\left(\frac{\boldsymbol{q}}{\theta}\right) dv = \int_{\Omega} \left(\frac{\operatorname{div}(\boldsymbol{q})}{\theta} - \frac{\boldsymbol{q}\cdot\operatorname{grad}\theta}{\theta^2}\right) dv \tag{2.18}$$

Using (2.18) and localizing the integral leads to an expression for the second law of thermodynamics:

$$\theta\frac{D(\rho\eta)}{D\,t} \geq \rho r - \operatorname{div}(\boldsymbol{q}) + \frac{\boldsymbol{q}\operatorname{grad}(\theta)}{\theta} \tag{2.19}$$

To relate the first law and second law of thermodynamics, we consider the Helmholtz free energy function per unit mass ψ :

$$\psi = e - \eta\,\theta \tag{2.20}$$

Multiplying by ρ and applying the material time derivative on both sides of (2.20) yield:

$$\frac{D(\rho\psi)}{D\,t} = \frac{D(\rho e)}{D\,t} - \theta\frac{D(\rho\eta)}{D\,t} - \rho\eta\frac{D\theta}{D\,t} \tag{2.21}$$

The Helmholtz free energy per unit mass is hypothesized to be a function of strain and temperature:

$$\psi = \psi(\boldsymbol{\epsilon}, \theta) \tag{2.22}$$

so that,

$$\frac{D(\rho\psi)}{D\,t} = \frac{\partial(\rho\psi)}{\partial\boldsymbol{\epsilon}} : \frac{D\boldsymbol{\epsilon}}{D\,t} + \frac{\partial(\rho\psi)}{\partial\theta} : \frac{D\theta}{D\,t} \tag{2.23}$$

Using (2.23) and (2.21), we can rewrite (2.16) in the form:

$$\frac{\partial(\rho\psi)}{\partial\boldsymbol{\epsilon}} : \frac{D\boldsymbol{\epsilon}}{Dt} + \frac{\partial(\rho\psi)}{\partial\theta} : \frac{D\theta}{Dt} + \theta\frac{D(\rho\eta)}{Dt} + \rho\eta\frac{D\theta}{Dt} = \boldsymbol{\sigma} : \frac{D\boldsymbol{\epsilon}}{Dt} + \rho r - \mathrm{div}(\boldsymbol{q}) \tag{2.24}$$

Combining (2.19) and (2.24), and regrouping terms lead to:

$$\left[\boldsymbol{\sigma} - \frac{\partial(\rho\psi)}{\partial\boldsymbol{\epsilon}}\right] : \dot{\boldsymbol{\epsilon}} - \left[\rho\eta + \frac{\partial(\rho\psi)}{\partial\theta}\right]\dot{\theta} - \frac{\boldsymbol{q}\cdot\mathrm{grad}(\theta)}{\theta} \geq 0 \tag{2.25}$$

Following the thermodynamic arguments explored by Coleman and Noll (1963) that the rate processes $\dot{\boldsymbol{\epsilon}}$ and $\dot{\theta}$ can be varied independently, we derive the constitutive equations in the form:

$$\boldsymbol{\sigma} = \frac{\partial(\rho\psi)}{\partial\boldsymbol{\epsilon}} \tag{2.26}$$

$$\rho\eta = -\frac{\partial(\rho\psi)}{\partial\theta} \tag{2.27}$$

such that the second law (2.25) is always satisfied.

Thus, the reduced energy dissipation inequality becomes:

$$-\frac{\boldsymbol{q}\cdot\mathrm{grad}\,\theta}{\theta} \geq 0 \tag{2.28}$$

The above inequality states that heat flows spontaneously from high temperature to low temperature, and therefore justifies the form of the Fourier's law in (2.15). Substitution of (2.26) and (2.27) into (2.24) leads to the expression of energy conservation:

$$\theta\frac{D(\rho\eta)}{Dt} = \rho r - \mathrm{div}\boldsymbol{q} \tag{2.29}$$

2.2.2.3 The entropy of an elastic solid system

In this part, I follow the procedure in Biot (1956) to identify the relation linking the entropy and elastic strain; we need to revisit the first law. Ignoring the kinetic energy, the first law is written in differential form as:

$$dE = dW + dQ \tag{2.30}$$

where, dE, dW, dQ respectively, are the infinitesimal amount of internal energy, the infinitesimal amount of external work done on the system, and the infinitesimal amount of heat supplied to the system, note that $dW = P\,dt$ According to (2.13), over dv we have

$$dW = \boldsymbol{\sigma} : d\boldsymbol{\epsilon} \tag{2.31}$$

$$dQ = dE - \boldsymbol{\sigma} : d\boldsymbol{\epsilon} \tag{2.32}$$

Introducing entropy per unit volume S (same as $\rho\eta$) and using (2.32):

$$dS = \frac{dQ}{\theta} = \frac{dE}{\theta} - \frac{1}{\theta}\boldsymbol{\sigma} : d\boldsymbol{\epsilon} \tag{2.33}$$

The internal energy $E(\boldsymbol{\epsilon}, \theta)$ is assumed to depend on total strain $\boldsymbol{\epsilon}$ and temperature θ. (2.33) can be written as:

$$dS = \frac{1}{\theta}\frac{\partial E}{\partial \theta}d\theta + \frac{1}{\theta}\left[\frac{\partial E}{\partial \boldsymbol{\epsilon}} - \boldsymbol{\sigma}\right] : d\boldsymbol{\epsilon} \tag{2.34}$$

According to the second law, dS is required to be an exact differential in θ and $\boldsymbol{\epsilon}$. This implies:

$$\frac{\partial\left[\frac{1}{\theta}\left(\frac{\partial E}{\partial \boldsymbol{\epsilon}} - \boldsymbol{\sigma}\right)\right]}{\partial \theta} = 0 \tag{2.35}$$

with the assumption:

$$\frac{\partial^2 E}{\partial \boldsymbol{\epsilon}\partial\theta} = 0 \tag{2.36}$$

we get:

$$\frac{\partial E}{\partial \boldsymbol{\epsilon}} = \boldsymbol{\sigma} - \frac{\partial \boldsymbol{\sigma}}{\partial \theta}\theta \tag{2.37}$$

For linear isotropic thermoelasticity, the Cauchy stress tensor is written as:

$$\boldsymbol{\sigma} = \boldsymbol{c}^e : \boldsymbol{\epsilon}^e \tag{2.38}$$

where, $\boldsymbol{c}^e(\theta)$ is the isotropic elastic modulus tensor, which is defined as:

$$c^e_{ijkl}(\theta) = \lambda(\theta)\delta_{ij}\delta_{kl} + 2\mu(\theta)I_{ijkl} \tag{2.39}$$

and where, $\lambda(\theta)$ and $\mu(\theta)$ are the temperature-dependent *Lamé* parameters, $\boldsymbol{I}$ is the fourth order identity tensor, and is defined as:

$$I_{ijkl} = \frac{1}{2}(\delta_{ik}\delta_{jl} + \delta_{il}\delta_{jk}) \tag{2.40}$$

The small strain is defined as:

$$\epsilon_{ij} = \frac{1}{2}(u_{i,j} + u_{j,i}) \tag{2.41}$$

In small strain thermo-elasticity, the total strain is additively-decomposed into the mechanical (elastic for thermoelasticity) strain $\boldsymbol{\epsilon}^e$ and the thermal strain $\boldsymbol{\epsilon}^\theta$:

$$\boldsymbol{\epsilon} = \boldsymbol{\epsilon}^e + \boldsymbol{\epsilon}^\theta \tag{2.42}$$

in which,

$$\boldsymbol{\epsilon}^\theta = \alpha^\theta(\theta - \theta_0)\mathbf{1} \tag{2.43}$$

and where, α^θ is the linear thermal expansion coefficient; $\theta - \theta_0$ the increment of temperature; θ_0 the reference temperature, with the unit of Kelvin; $\mathbf{1}$ the second order identity tensor. Substitution of (2.39), (2.40), (2.42), (2.43) into (2.38) yields:

$$\boldsymbol{\sigma} = \boldsymbol{c}^e : \boldsymbol{\epsilon} - \underbrace{(3\lambda + 2\mu)\alpha^\theta}_{\beta}(\theta - \theta_0)\mathbf{1} \tag{2.44}$$

where, $\beta = (3\lambda + 2\mu)\alpha^\theta$. From (2.44) we can derive

$$\frac{\partial \boldsymbol{\sigma}}{\partial \theta} = -\beta\mathbf{1} \tag{2.45}$$

Substitution of (2.45) into (2.37) yields:

$$\frac{\partial E}{\partial \boldsymbol{\epsilon}} = \boldsymbol{\sigma} + \beta\theta\mathbf{1} \tag{2.46}$$

Combining (2.34) and (2.46), we get

$$dS = \frac{1}{\theta}\frac{\partial E}{\partial \theta}d\theta + \beta d\epsilon_{kk} \tag{2.47}$$

where ϵ_{kk} is the volumetric strain. From (2.32),we have

$$\frac{dQ}{d\theta} = \frac{\partial E}{\partial \theta} = \rho C \tag{2.48}$$

where C is the heat capacity per unit mass. Substitution of (2.48) into (2.47) yields the differential of entropy:

$$dS = \frac{\rho C}{\theta} d\theta + \beta d\epsilon_{kk} \tag{2.49}$$

With the definition $S = \rho\eta$, where η is the entropy per unit mass, (2.29) can be expressed as

$$\rho C\dot{\theta} + \beta\theta \mathrm{tr}(\dot{\boldsymbol{\epsilon}}) - \rho r + \mathrm{div}\boldsymbol{q} = 0 \tag{2.50}$$

2.2.2.4 An alternative way of choosing independent variables for ψ

In this section, I will introduce an alternative way of choosing independent variables for the Helmholtz free energy per unit mass ψ. Instead of using the total strain $\boldsymbol{\epsilon}$, we will use the elastic strain $\boldsymbol{\epsilon}^e$ as one of two independent variables in the form:

$$\psi = \psi(\boldsymbol{\epsilon}^e, \theta) \tag{2.51}$$

such that,

$$\frac{D(\rho\psi)}{Dt} = \frac{\partial(\rho\psi)}{\partial \boldsymbol{\epsilon}^e} : \frac{D\boldsymbol{\epsilon}^e}{Dt} + \frac{\partial(\rho\psi)}{\partial\theta} : \frac{D\theta}{Dt} \tag{2.52}$$

Using (2.42) and (2.43), we can express $\boldsymbol{\sigma} : \dot{\boldsymbol{\epsilon}}$ in the form:

$$\begin{aligned} \boldsymbol{\sigma} : \frac{D\boldsymbol{\epsilon}}{D\,t} &= \boldsymbol{\sigma} : \frac{D\boldsymbol{\epsilon}^e}{D\,t} + \boldsymbol{\sigma} : \frac{D\boldsymbol{\epsilon}^\theta}{D\,t} \\ &= \boldsymbol{\sigma} : \frac{D\boldsymbol{\epsilon}^e}{D\,t} + \left[(\theta - \theta_0)\frac{d\alpha^\theta}{D\,t} + \alpha^\theta \frac{D\theta}{D\,t}\right] \mathrm{tr}(\boldsymbol{\sigma}) \end{aligned} \tag{2.53}$$

where, $\mathrm{tr}(\boldsymbol{\sigma})$ is the trace of the stress tensor, and $\mathrm{tr}(\boldsymbol{\sigma}) = \sigma_{kk}$. We assume the linear thermal expansion coefficient does not dependent on temperature, that is,

$$\frac{D\alpha^\theta}{D\,t} = 0 \tag{2.54}$$

thus, we have:

$$\boldsymbol{\sigma} : \frac{D\boldsymbol{\epsilon}}{D\,t} = \boldsymbol{\sigma} : \frac{D\boldsymbol{\epsilon}^e}{D\,t} + \alpha^\theta \frac{D\theta}{D\,t} \mathrm{tr}(\boldsymbol{\sigma}) \tag{2.55}$$

Comparing to (2.24), we will write instead,

$$\frac{\partial(\rho\psi)}{\partial\boldsymbol{\epsilon}^e} : \frac{D\boldsymbol{\epsilon}^e}{Dt} + \frac{\partial(\rho\psi)}{\partial\theta} : \frac{D\theta}{Dt} + \theta\frac{D(\rho\eta)}{Dt} + \rho\eta\frac{D\theta}{Dt} = \boldsymbol{\sigma} : \frac{D\,\boldsymbol{\epsilon}^e}{D\,t} + \alpha^\theta\frac{D\theta}{D\,t}\mathrm{tr}(\boldsymbol{\sigma}) + \rho\,r - \mathrm{div}(\boldsymbol{q}) \tag{2.56}$$

Combining (2.56) and (2.19) , and regrouping terms lead to:

$$\left[\boldsymbol{\sigma} - \frac{\partial(\rho\psi)}{\partial\boldsymbol{\epsilon}^e}\right] : \frac{D\boldsymbol{\epsilon}^e}{Dt} - \left[\rho\eta + \frac{\partial(\rho\psi)}{\partial\theta} - \alpha^\theta\mathrm{tr}(\boldsymbol{\sigma})\right]\frac{D\theta}{Dt} - \frac{\boldsymbol{q}\cdot\mathrm{grad}(\theta)}{\theta} \geq 0 \tag{2.57}$$

Now with the thermodynamics arguments in Coleman and Noll (1963), we will get:

$$\boldsymbol{\sigma} = \frac{\partial(\rho\psi)}{\partial\boldsymbol{\epsilon}^e} \tag{2.58}$$

$$\rho\eta = -\frac{\partial(\rho\psi)}{\partial\theta} + \alpha^\theta\mathrm{tr}(\boldsymbol{\sigma}) \tag{2.59}$$

with (2.59), and together with the definition:

$$-\frac{\partial^2(\rho\psi)}{\partial\theta^2} = \frac{\rho C}{\theta} \tag{2.60}$$

we get:

$$\frac{D(\rho\eta)}{Dt} = -\frac{\partial^2(\rho\psi)}{\partial\theta^2}\dot{\theta} + \alpha^\theta\mathrm{tr}(\dot{\boldsymbol{\sigma}}) \tag{2.61}$$

Substitution of (2.61) into (2.29) provides the general form (with nonlinear constitutive model) of the balance of energy equation

$$\rho\,C\,\dot{\theta} + \alpha^\theta\,\theta\,\mathrm{tr}(\dot{\boldsymbol{\sigma}}) - \rho\,r + \mathrm{div}(\boldsymbol{q}) = 0 \tag{2.62}$$

A combination of (2.39) and (2.40) gives an expression of the elastic modulus tensor in the form:

$$c^e_{ijkl}(\theta) = \lambda(\theta)\delta_{ij}\delta_{kl} + \mu(\theta)(\delta_{ik}\delta_{jl} + \delta_{il}\delta_{jk}) \tag{2.63}$$

Therefore, (2.44) is written as:

$$\begin{aligned}\sigma_{ij} &= c^e_{ijkl}\,\epsilon_{kl} - \beta(\theta-\theta_0)\delta_{ij} \\ &= \lambda\delta_{ij}\delta_{kl}\epsilon_{kl} + \mu(\delta_{ik}\delta_{jl} + \delta_{il}\delta_{jk})\epsilon_{kl} - \beta(\theta-\theta_0)\delta_{ij} \\ &= \lambda\delta_{ij}\epsilon_{kk} + 2\mu\epsilon_{ij} - \beta(\theta-\theta_0)\delta_{ij}\end{aligned} \tag{2.64}$$

and the trace of $\boldsymbol{\sigma}$ is:

$$\mathrm{tr}(\boldsymbol{\sigma}) = \sigma_{mm} = \underbrace{(3\lambda + 2\mu)}_{3K}\,\epsilon_{mm} - 3\beta(\theta - \theta_0) \tag{2.65}$$

thus,

$$\mathrm{tr}(\dot{\boldsymbol{\sigma}}) = 3K\,\mathrm{tr}(\dot{\boldsymbol{\epsilon}}) - 3\beta\dot{\theta} \tag{2.66}$$

where K is the bulk modulus. Thus, the balance of energy equation with linear constitutive model is then written as

$$\left[\rho\, C - 9(\alpha^{\theta})^2\theta K\right]\,\dot{\theta} + \beta\,\theta\,\mathrm{tr}(\dot{\boldsymbol{\epsilon}}) - \rho\, r + \mathrm{div}(\boldsymbol{q}) = 0 \tag{2.67}$$

2.3 Finite element analysis

In this section, by consulting Hughes (2000), I develop the weak form based upon the strong form of the thermoelastic boundary value problem. Galerkin's method is then adopted to seek the approximate solution to the weak form. Displacement $\boldsymbol{u}$ and temperature θ are chosen to be the two primary variables. The governing equations used here are stated as (2.5) and (2.62).

2.3.1 Strong and Weak forms

The strong form of thermoelastic problem involving the governing equations (2.5) and (2.62), as well as the boundary conditions imposed on the primary variables $\boldsymbol{u}$ and θ is as follows:

$$(S)\left\{\begin{array}{rcll}
\text{Find } \boldsymbol{u}(\boldsymbol{x},t) \in \mathscr{S}^u, \text{ and } \theta(\boldsymbol{x},t) \in \mathscr{S}^{\theta}, \text{ with} \quad t & \in [0,T], & \text{such that} & \\
\sigma_{ij,j} + \rho b_i & = & 0 & \in \Omega \\
u_i & = & g_i^u & \text{on } \Gamma_u \\
\sigma_{ij} n_j & = & t_i^{\sigma} & \text{on } \Gamma_t \\
u_i(\boldsymbol{x},0) & = & u_{0i}(\boldsymbol{x}) & \in\ \Omega \\
\rho\, C\,\dot{\theta} + \alpha^{\theta}\,\theta\,\mathrm{tr}(\dot{\boldsymbol{\sigma}}) - \rho\, r + \mathrm{div}(\boldsymbol{q}) & = & 0 & \in \Omega \\
\theta & = & g^{\theta} & \text{on } \Gamma_{\theta} \\
-n_i q_i & = & q & \text{on } \Gamma_q \\
\theta(\boldsymbol{x},0) & = & \theta_0(\boldsymbol{x}) & \in\ \Omega
\end{array}\right. \tag{2.68}$$

where $\mathscr{S}^u$ and $\mathscr{S}^\theta$ are the trial solution spaces,

$$\begin{aligned}\mathscr{S}^u &= \{u_i : \Omega \times [0,T] \mapsto \mathbb{R}^2, u_i \in H^1, u_i(t) = g_i^u(t) \,\text{on}\, \Gamma_u, u_i(\boldsymbol{x},0) = u_{i0}(\boldsymbol{x})\} \\ \mathscr{S}^\theta &= \{\theta : \Omega \times [0,T] \mapsto \mathbb{R}, \theta \in H^1, \theta(t) = g^\theta(t) \,\text{on}\, \Gamma_\theta, \theta(\boldsymbol{x},0) = \theta_0(\boldsymbol{x})\}\end{aligned} \tag{2.69}$$

where $\boldsymbol{x}$ is the coordinate vector; Ω stands for the domain of the body, Γ stands for the boundary of the Ω, respectively; Γ_u and Γ_t denote respectively the boundary where displacement is prescribed and the boundary with surface traction; Γ_θ and Γ_q denote the boundary where temperature is prescribed and the boundary with heat flux; $\boldsymbol{u}_0$ and θ_0 are the initial displacement vector and temperature, respectively. H^1 is the first Sobolev space (Hughes, 2000).

To define the weak or variational form of the strong form (2.68), we choose the weighting functions (also called variations) of the primary variables as follows:

$$\begin{aligned}\boldsymbol{w}(\boldsymbol{x},t) &= \delta\boldsymbol{u}(\boldsymbol{x},t) \\ \omega(\boldsymbol{x},t) &= \delta\theta(\boldsymbol{x},t)\end{aligned} \tag{2.70}$$

where $w_i \in \mathscr{V}^u$, $\omega \in \mathscr{V}^\theta$, with variation spaces

$$\begin{aligned}\mathscr{V}^u &= \{w_i : \Omega \mapsto \mathbb{R}^2, w_i \in H^1, w_i = 0 \quad \text{on}\, \Gamma_u\} \\ \mathscr{V}^\theta &= \{\omega : \Omega \mapsto \mathbb{R}, \omega \in H^1, \omega = 0 \quad \text{on}\, \Gamma_\theta\}\end{aligned} \tag{2.71}$$

Using the weighting function $\boldsymbol{w}(\boldsymbol{x},t)$, we get the weak form of balance of linear momentum as follows:

$$\int_\Omega w_i \left(\sigma_{ij,j} + \rho b_i\right) dv = 0 \tag{2.72}$$

Making use of the chain rule, the derivative of $\boldsymbol{w}\,\boldsymbol{\sigma}$ can be written as

$$\left(w_i \sigma_{ij}\right)_{,j} = w_{i,j}\sigma_{ij} + w_i \sigma_{ij,j} \tag{2.73}$$

and with the divergence theorem:

$$\begin{aligned}\int_\Omega (w_i\sigma_{ij})_{,j}\,dv &= \int_{\Gamma_t} (w_i\sigma_{ij})n_j\,da + \underbrace{\int_{\Gamma_u} (w_i\sigma_{ij})n_j\,da}_{=0} \\ &= \int_{\Gamma_t} (w_i\sigma_{ji})n_j da \\ &= \int_{\Gamma_t} w_i(\sigma_{ij}n_j)da \\ &= \int_{\Gamma_t} w_i\, t_i^\sigma\, da \end{aligned} \tag{2.74}$$

result in

$$\int_\Omega w_{i,j}\sigma_{ij}dv = \int_\Omega \rho w_i b_i da + \int_{\Gamma_t} w_i t_i^\sigma da \tag{2.75}$$

For linear thermoelasticity specifically, use (2.64) to yield:

$$w_{i,j}\sigma_{ij} = c^e_{ijkl}\,\epsilon_{kl} - \beta(\theta-\theta_0)\,w_{i,i} \tag{2.76}$$

Therefore (2.75) becomes:

$$\int_\Omega \left[w_{i,j}c^e_{ijkl}\,\epsilon_{kl} - \beta(\theta-\theta_0)\,w_{i,i}\right] dv = \int_\Omega \rho w_i b_i da + \int_{\Gamma_t} w_i t_i^\sigma da \tag{2.77}$$

With the weighting function $\omega(\boldsymbol{x},t)$, we get the weak form of the balance of energy as follows:

$$\int_\Omega \omega\,\left\{\left[\rho\,C - 9(\alpha^\theta)^2\theta K\right]\,\dot\theta + \beta\,\theta\,\mathrm{tr}(\dot{\boldsymbol{\epsilon}}) + \mathrm{div}(\boldsymbol{q}) - \rho\,r\right\}\,dv = 0 \tag{2.78}$$

Using the chain rule,

$$(\omega\boldsymbol{q}_i)_{,i} = \omega_{,i}\,q_i + \omega\,q_{i,i} \tag{2.79}$$

and the divergence theorem again,

$$\begin{aligned}\int_\Omega (\omega\boldsymbol{q}_i)_{,i}dv &= \int_{\Gamma_q} (\omega\boldsymbol{q}_i)n_i\,da + \underbrace{\int_{\Gamma_\theta} (\omega\boldsymbol{q}_i)n_i\,da}_{=0} \\ &= -\int_{\Gamma_q} \omega q\,da \end{aligned} \tag{2.80}$$

The weak form of the balance of energy is:

$$\begin{aligned}&\int_\Omega \omega\left[\rho\,C - 9(\alpha^\theta)^2\theta K\right]\dot\theta dv + \int_\Omega \omega\beta\,\theta\,\mathrm{tr}(\dot{\boldsymbol{\epsilon}})dv \\ &+ \int_\Omega \omega_{,i}K^\theta_{ij}\theta_{,j}dv = \int_{\Gamma_q}\omega q da + \int_\Omega \omega\rho\,r dv\end{aligned} \tag{2.81}$$

where, q is the surface heat flux scalar on boundary Γ_q, and q_i is defined by (2.15).

To summarize, the weak form of the nonlinear thermoelastic problem goes as follows:

$$
(W)\begin{cases}
\text{Find } u_i(\boldsymbol{x},t)\in\mathscr{S}^u \text{ and } \theta(\boldsymbol{x},t)\in\mathscr{S}^\theta \text{ such that}\\
\displaystyle\int_\Omega w_{i,j}\, sigma_{ij}\, dv=\int_\Omega \rho w_i b_i da+\int_{\Gamma_t} w_i t_i^\sigma\, da\\
\displaystyle\int_\Omega \omega\rho\, C\dot\theta\, dv+\int_\Omega \omega\alpha^\theta\,\theta\,\mathrm{tr}(\dot{\boldsymbol{\sigma}})\, dv\\
\quad\displaystyle+\int_\Omega \omega_{,i}K_{ij}^\theta\theta_{,j}\, dv=\int_{\Gamma_q}\omega q da+\int_\Omega \omega\rho\, r\, dv\\
\text{holds } \forall w_i(\boldsymbol{x})\in\mathscr{V}^u \text{ and } \forall\omega(\boldsymbol{x})\in\mathscr{V}^\theta\\
\mathscr{S}^u=\{u_i:\Omega\times[0,T]\mapsto\mathbb{R}^2, u_i\in H^1, u_i(t)=g_i^u(t)\,\text{on}\,\Gamma_u, u_i(\boldsymbol{x},0)=u_{i0}(\boldsymbol{x})\}\\
\mathscr{S}^\theta=\{\theta:\Omega\times[0,T]\mapsto\mathbb{R}, \theta\in H^1, \theta(t)=g^\theta(t)\,\text{on}\,\Gamma_\theta, \theta(\boldsymbol{x},0)=\theta_0(\boldsymbol{x})\}\\
\mathscr{V}^u=\{w_i:\Omega\mapsto\mathbb{R}^2, w_i\in H^1, w_i=0\,\text{on}\,\Gamma_u\}\\
\mathscr{V}^\theta=\{\omega:\Omega\mapsto\mathbb{R}, \omega\in H^1, \omega=0\,\text{on}\,\Gamma_\theta\}
\end{cases}
\tag{2.82}
$$

For linear thermoelastic problem, the second equation in (2.82) will then be written as

$$
\int_\Omega \left[w_{i,j}c_{ijkl}^e\,\epsilon_{kl}-\beta(\theta-\theta_0)\,w_{i,i}\right]\, dv=\int_\Omega \rho w_i b_i da+\int_{\Gamma_t} w_i t_i^\sigma\, da \tag{2.83}
$$

$$
\begin{aligned}
&\int_\Omega \omega\left[\rho\, C-9(\alpha^\theta)^2\theta K\right]\dot\theta\, dv+\int_\Omega \omega\beta\,\theta\,\mathrm{tr}(\dot{\boldsymbol{\epsilon}})\, dv\\
&\quad+\int_\Omega \omega_{,i}K_{ij}^\theta\theta_{,j}\, dv=\int_{\Gamma_q}\omega q da+\int_\Omega \omega\rho\, r\, dv
\end{aligned}
\tag{2.84}
$$

2.3.2 Axisymmetric formulations

In this section, I refer to Felippa (2010) and Hughes (2000) regarding the axisymmetric formulation. To simplify the governing equations of axisymmetric problem, we adopt the cylindrical coordinate system (r,z,θ),

$$
\begin{aligned}
r &= \text{the radial coordinate}\\
z &= \text{the axial coordinate}\\
\theta &= \text{ the circumferential coordinate}
\end{aligned}
\tag{2.85}
$$

The basic postulation of torsionless axisymmetry is that all functions under consideration are only functions of r and z, i.e., they are independent of the angle θ. Therefore three-dimensional problems

are reduced to two-dimensional ones. Another basic assumption of axisymmetry is that $u_\theta = 0$ based on the rotational symmetry. Thus the displacement field is defined by two components, which are functions of r and z:

$$\boldsymbol{u}(r,z) = \begin{bmatrix} u_r(r,z) \\ u_z(r,z) \end{bmatrix}$$

where, u_r is called the radial displacement, and u_z is the axial displacement. Due to the assumption of axisymmetry, we have:

$$\begin{aligned} \epsilon_{r\theta} = \epsilon_{z\theta} = 0 \\ \sigma_{r\theta} = \sigma_{r\theta} = 0 \end{aligned} \tag{2.86}$$

The nonvanishing components of stress and strain vectors are:

$$\boldsymbol{\sigma} = \begin{Bmatrix} \sigma_{rr} \\ \sigma_{zz} \\ \sigma_{rz} \\ \sigma_{\theta\theta} \end{Bmatrix}; \qquad \boldsymbol{\epsilon} = \begin{Bmatrix} \epsilon_{rr} \\ \epsilon_{zz} \\ 2\epsilon_{rz} \\ \epsilon_{\theta\theta} \end{Bmatrix} \tag{2.87}$$

The strain-displacement equations for small strain axisymmetric problem are:

$$\epsilon_{rr} = \frac{\partial u_r}{\partial r}, \quad \epsilon_{zz} = \frac{\partial u_z}{\partial z}, \quad \epsilon_{\theta\theta} = \frac{u_r}{r}, \quad \epsilon_{rz} = \frac{1}{2}\left(\frac{\partial u_r}{\partial z} + \frac{\partial u_z}{\partial r}\right) \tag{2.88}$$

In matrix form:

$$\boldsymbol{\epsilon} = \begin{bmatrix} \dfrac{\partial}{\partial r} & 0 \\ 0 & \dfrac{\partial}{\partial z} \\ \dfrac{1}{r} & 0 \\ \dfrac{\partial}{\partial z} & \dfrac{\partial}{\partial r} \end{bmatrix} \begin{bmatrix} u_r \\ u_z \end{bmatrix} \tag{2.89}$$

2.3.2.1 Dimensionality reduction

The element of volume dv can be expressed as

$$dv = 2\pi r da = 2\pi r dr dz \tag{2.90}$$

where da is the element of area in the generating cross section in $r-z$ plane, such that the volume integral over the volume element Ω^e can be expressed as

$$\int_{\Omega^e}(\bullet)dv = 2\pi\int_{\Omega^e}(\bullet)rdrdz = 2\pi\int_{-1}^{1}\int_{-1}^{1}(\hat{\bullet})\,r(\boldsymbol{\xi})j^e\,d\xi\,d\eta \tag{2.91}$$

where $(\bullet)$ denotes a function that depends on $\boldsymbol{r}$; $(\hat{\bullet})$ is the function estimation in natural coordinate $\boldsymbol{\xi}$. $j^e = det(\boldsymbol{J}^e)$, and $\boldsymbol{J}^e$ is referred to as Jacobian of coordinate transformation,

$$\boldsymbol{J}^e = d\boldsymbol{r}/d\boldsymbol{\xi}, \quad \boldsymbol{r} = [r,z], \quad \boldsymbol{\xi} = [\xi,\eta]. \tag{2.92}$$

Similarly, the element of surface dS can be expressed as

$$dS = 2\pi r ds \tag{2.93}$$

where ds is an arclength element, and can be expressed as

$$ds = \sqrt{(dr)^2 + (dz)^2} \tag{2.94}$$

Thus, the surface integral over the surface element S^e can be expressed as

$$\int_{S^e}(\bullet)dS = 2\pi\int_{S^e}(\bullet)rds = 2\pi\int_{-1}^{1}(\hat{\bullet})r(\xi)\sqrt{\left(\frac{\partial r}{\partial\xi}\right)^2 + \left(\frac{\partial z}{\partial\xi}\right)^2}\,d\xi \tag{2.95}$$

where it is assumed that $(\bullet)$ is evaluated at $\eta = \pm 1$ depending on which element surface S^e the boundary condition acts (traction or heat flux).

2.3.3 Coupled finite element formulation

We adopt Galerkin's method to obtain solutions to the weak form. $\mathscr{S}^h$ and $\mathscr{V}^h$ are introduced to denote the finite -dimensional approximations to $\mathscr{S}$ and $\mathscr{V}$, respectively. "The superscript refers to the association of $\mathscr{S}^h$ and $\mathscr{V}^h$ with a mesh, or discretization, of the domain Ω, which is parameterized by a characteristic length scale h" (Hughes, 2000). It is assumed that:

$$\begin{aligned}
&\boldsymbol{u}^h \in (\mathscr{S}^u)^h; \quad (\mathscr{S}^u)^h \subset \mathscr{S}^u;\\
&\boldsymbol{w}^h \in (\mathscr{V}^u)^h; \quad (\mathscr{V}^u)^h \subset \mathscr{V}^u;\\
&\theta^h \in (\mathscr{S}^\theta)^h; \quad (\mathscr{S}^\theta)^h \subset \mathscr{S}^\theta;\\
&\omega^h \in (\mathscr{V}^\theta)^h; \quad (\mathscr{V}^\theta)^h \subset \mathscr{V}^\theta;
\end{aligned} \tag{2.96}$$

We assume that all members of $(\mathscr{V}^u)^h$ and $(\mathscr{V}^\theta)^h$ vanish, or approximately vanish on Γ_u and Γ_θ, respectively, i.e.,

$$\begin{aligned} w_i^h &= 0 \text{ on } \Gamma_u,\ \forall w_i^h(\boldsymbol{x}) \in (\mathscr{V}^u)^h \\ \omega^h &= 0 \text{ on } \Gamma_\theta,\ \forall \omega^h(\boldsymbol{x}) \in (\mathscr{V}^\theta)^h \end{aligned} \tag{2.97}$$

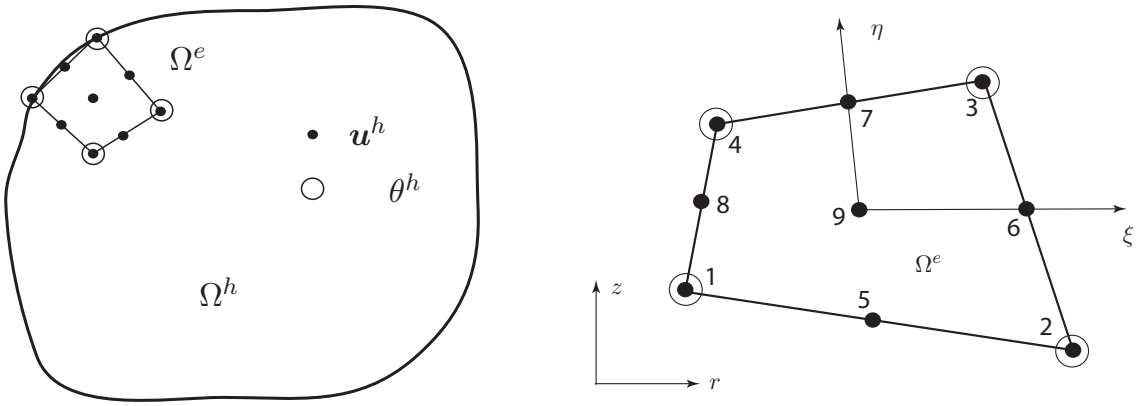

Figure 2.1: Discretization into thermoelastic mixed quadrilateral elements .

Figure 2.1 shows the element, i.e. biquadratic in displacement, and bilinear in temperature. We discretize the domain Ω^h into element domains Ω^e, $1 \le e \le n_{el}$, see Figure 2.1. For this two dimensional thermoelastic problem, we introduce the mixed quadrilateral elements, i.e. biquadratic interpolation in displacement and bilinear interpolation in temperature. Using interpolation functions, we write $\boldsymbol{u}^h$, $\boldsymbol{w}^h$, θ^h and ω^h in natural coordinates as follows:

(1) Displacement $\boldsymbol{u}$:

$$\begin{aligned} \boldsymbol{u}^h(\boldsymbol{\xi}, t) &= \sum_{a=1}^{9} N_a^u(\boldsymbol{\xi})\, \boldsymbol{d}_a^e(t) = \boldsymbol{N}^{e,u} \cdot \boldsymbol{d}^e \\ &= \begin{bmatrix} \boldsymbol{N}_1^u & \dots & \boldsymbol{N}_9^u \end{bmatrix} \begin{bmatrix} \boldsymbol{d}_1^e \\ \vdots \\ \boldsymbol{d}_9^e \end{bmatrix} \end{aligned} \tag{2.98}$$

$$\boldsymbol{N}_a^u = \begin{bmatrix} N_a^u & 0 \\ 0 & N_a^u \end{bmatrix}, \quad \boldsymbol{d}_a^e = \begin{bmatrix} d_{r(a)}^e \\ d_{z(a)}^e \end{bmatrix} \tag{2.99}$$

$$\boldsymbol{w}^h(\boldsymbol{\xi}) = \boldsymbol{N}^{e,u} \cdot \boldsymbol{c}^e \tag{2.100}$$

where, $\boldsymbol{d}_a^e$ and N_a^u, $a = 1, 2, ..., 9$ are nodal displacement and shape functions for displacement, respectively. Superscript e denotes element. The components of vector $\boldsymbol{c}^e$ are the nodal values of the weighting function $\boldsymbol{w}^h$.

(2) Temperature θ:

$$\begin{aligned}\theta^h(\boldsymbol{\xi}, t) &= \sum_{a=1}^{4} N_a^\theta(\boldsymbol{\xi})\, \theta_a^e(t) = \boldsymbol{N}^{e,\theta} \cdot \boldsymbol{\theta}^e \\ &= \begin{bmatrix} N_1^\theta & N_2^\theta & N_3^\theta & N_4^\theta \end{bmatrix} \begin{bmatrix} \theta_1^e \\ \theta_2^e \\ \theta_3^e \\ \theta_4^e \end{bmatrix}\end{aligned} \tag{2.101}$$

$$\omega^h(\boldsymbol{\xi}, t) = \boldsymbol{N}^{e,\theta} \cdot \boldsymbol{\alpha}^e \tag{2.102}$$

where, θ_a^e and N_a^θ, $a = 1, 2, 3, 4$ are nodal temperature and shape functions for temperature, respectively. The components of vector $\boldsymbol{\alpha}^e$ are the nodal values of the weighting function ω^h.

The gradient of temperature is calculated as,

$$\begin{aligned}\text{grad}(\theta^h) = \theta^h_{,i} = & \quad \boldsymbol{B}^{e,\theta} \cdot \boldsymbol{\theta}^e \\ \text{where,} \boldsymbol{B}^{e,\theta} = & \quad \begin{bmatrix} \boldsymbol{B}_1^\theta & \boldsymbol{B}_2^\theta & \boldsymbol{B}_3^\theta & \boldsymbol{B}_4^\theta \end{bmatrix} \\ \boldsymbol{B}_a^\theta = & \quad \begin{bmatrix} \dfrac{\partial N_a^\theta}{\partial r} \\ \dfrac{\partial N_a^\theta}{\partial z} \end{bmatrix}, \quad (a = 1, ..., 4)\end{aligned} \tag{2.103}$$

(3) Strain: According to (2.89), the total strain is written as

$$\boldsymbol{\epsilon} = \boldsymbol{B}^{e,u} \cdot \boldsymbol{d}^e \tag{2.104}$$

where

$$\begin{aligned}\boldsymbol{B}^{e,u} &= \begin{bmatrix} \boldsymbol{B}_1^u & \dots & \boldsymbol{B}_9^u \end{bmatrix} \\ \boldsymbol{B}_a^u &= \begin{bmatrix} \dfrac{\partial N_a^u}{\partial r} & 0 \\ 0 & \dfrac{\partial N_a^u}{\partial z} \\ \dfrac{N_a^u}{r} & 0 \\ \dfrac{\partial N_a^u}{\partial z} & \dfrac{\partial N_a^u}{\partial r} \end{bmatrix}, \quad (a = 1, \dots, 9)\end{aligned} \tag{2.105}$$

$$\nabla \boldsymbol{w}^h(\xi) = \boldsymbol{B}^{e,u} \cdot \boldsymbol{c}^e \tag{2.106}$$

The term $\dot{\epsilon}_{mm}$ in (2.67) is written as:

$$\begin{aligned} \mathrm{tr}(\dot{\boldsymbol{\epsilon}}) = \dot{u}^h_{m,m} &= \sum_{a=1}^{9} \left[\begin{array}{cc} \left(\dfrac{\partial N^u_a}{\partial r} + \dfrac{N^u_a}{r}\right) & \dfrac{\partial N^u_a}{\partial z} \end{array} \right] \left[\begin{array}{c} \dot{d}_r \\ \dot{d}_z \end{array} \right] \\ &= \left[\begin{array}{ccc} \boldsymbol{B}^u_1 & \dots & \boldsymbol{B}^u_9 \end{array} \right] \left[\begin{array}{c} \dot{\boldsymbol{d}}^e_1 \\ \vdots \\ \dot{\boldsymbol{d}}^e_9 \end{array} \right] = \tilde{\boldsymbol{B}}^{e,u} \cdot \dot{d}^e \\ \text{where,} \quad \tilde{\boldsymbol{B}}^u_a &= \left[\begin{array}{cc} \left(\dfrac{\partial N^u_a}{\partial r} + \dfrac{N^u_a}{r}\right) & \dfrac{\partial N^u_a}{\partial z} \end{array} \right], \quad (a = 1, \dots, 9) \end{aligned} \tag{2.107}$$

The coupled FE equations for this thermoelastic problem are written as:

(1) Balance of linear momentum:

$$\begin{aligned} \mathop{\mathbf{A}}_{e=1}^{n_{\mathrm{el}}} (\boldsymbol{c}^e)^T \Bigg\{ & \underbrace{\left[\int_{\Omega^e} (\boldsymbol{B}^{e,u})^T \cdot \boldsymbol{D} \cdot \boldsymbol{B}^{e,u}\, dv\right]}_{\boldsymbol{k}^{dd}_e} \cdot \boldsymbol{d}^e - \underbrace{\left[\int_{\Omega^e} 3K\alpha^\theta (\tilde{\boldsymbol{B}}^{e,u})^T \cdot \boldsymbol{N}^{e,\theta}\, dv\right]}_{\boldsymbol{k}^{d\theta}_e} \cdot (\boldsymbol{\theta}^e - \boldsymbol{\theta}^e_0) \\ & = \underbrace{\int_{\Omega^e} \rho (\boldsymbol{N}^{e,u})^T \boldsymbol{b}\, dv}_{\boldsymbol{f}^{df,ext}_e} + \underbrace{\int_{\Gamma^e_t} (\boldsymbol{N}^{e,u})^T \boldsymbol{t}^\sigma\, da}_{\boldsymbol{f}^{dt,ext}_e} \Bigg\} \end{aligned} \tag{2.108}$$

(2) Balance of energy:

$$\begin{aligned} \mathop{\mathbf{A}}_{e=1}^{n_{\mathrm{el}}} (\boldsymbol{\alpha}^e)^T \Bigg\{ & \underbrace{\left[\int_{\Omega^e} \rho C (\boldsymbol{N}^{e,\theta})^T \cdot \boldsymbol{N}^{e,\theta} dv\right]}_{\boldsymbol{k}^{\theta\theta,1}_e} \cdot \dot{\boldsymbol{\theta}}^e \\ & + \underbrace{\left(\int_{\Omega^e} \alpha^\theta_{skel} (\boldsymbol{N}^{e,\theta})^T (\boldsymbol{N}^{e,\theta} \boldsymbol{\theta}^e) \cdot \mathrm{tr}(\boldsymbol{\sigma}')dv\right)}_{\boldsymbol{f}^{\theta d}_e} + \underbrace{\left[\int_{\Omega^e} K^\theta (\boldsymbol{B}^{e,\theta})^T \cdot \boldsymbol{B}^{e,\theta}\, dv\right]}_{\boldsymbol{k}^{\theta\theta,2}_e} \cdot \boldsymbol{\theta}^e \\ & = \underbrace{\int_{\Omega^e} \rho (\boldsymbol{N}^{e,\theta})^T r dv}_{\boldsymbol{f}^{\theta r,ext}_e} + \underbrace{\int_{\Gamma^e_q} (\boldsymbol{N}^{e,\theta})^T q\, da}_{\boldsymbol{f}^{\theta q,ext}_e} \Bigg\} \end{aligned} \tag{2.109}$$

For the linear isotropic elastic problem, we then have

$$\begin{aligned}\mathop{\mathsf{A}}_{e=1}^{n_{\mathrm{el}}}(\boldsymbol{\alpha}^e)^T \Bigg\{ & \underbrace{\left\{\int_{\Omega^e}\left[\rho C - 9K(\alpha^\theta)^2(\boldsymbol{N}^{e,\theta}\cdot\boldsymbol{\theta}^e)\right](\boldsymbol{N}^{e,\theta})^T\cdot\boldsymbol{N}^{e,\theta}dv\right\}}_{\boldsymbol{k}_e^{\theta\theta,1}}\cdot\dot{\boldsymbol{\theta}}^e \\ & + \underbrace{\left[\int_{\Omega^e} 3K\alpha^\theta(\boldsymbol{N}^{e,\theta})^T(\boldsymbol{N}^{e,\theta}\cdot\boldsymbol{\theta}^e)\tilde{\boldsymbol{B}}^{e,u}dv\right]}_{\boldsymbol{k}_e^{\theta d}}\cdot\dot{\boldsymbol{d}}^e + \underbrace{\left[\int_{\Omega^e} K^\theta(\boldsymbol{B}^{e,\theta})^T\cdot\boldsymbol{B}^{e,\theta}\,dv\right]}_{\boldsymbol{k}_e^{\theta\theta,2}}\cdot\boldsymbol{\theta}^e \\ & = \underbrace{\int_{\Omega^e}\rho(\boldsymbol{N}^{e,\theta})^T r dv}_{\boldsymbol{f}_e^{\theta r,ext}} + \underbrace{\int_{\Gamma_q^e}(\boldsymbol{N}^{e,\theta})^T q\,da}_{\boldsymbol{f}_e^{\theta q,ext}}\Bigg\}\end{aligned} \tag{2.110}$$

We can write the coupled FE equations in the form:

$$\begin{aligned}&\mathop{\mathsf{A}}_{e=1}^{n_{\mathrm{el}}}(\boldsymbol{c}^e)^T\cdot\left[\boldsymbol{f}_e^{dd,int} - \boldsymbol{f}_e^{d\theta,int} = \boldsymbol{f}_e^{df,ext} + \boldsymbol{f}_e^{dt,ext}\right] \\ &\mathop{\mathsf{A}}_{e=1}^{n_{\mathrm{el}}}(\boldsymbol{\alpha}^e)^T\cdot\left[\boldsymbol{k}_e^{\theta d}\cdot\dot{\boldsymbol{d}}^e + \boldsymbol{k}_e^{\theta\theta}\cdot\dot{\boldsymbol{\theta}}^e + \boldsymbol{f}_e^{\theta,int} = \boldsymbol{f}_e^{\theta,ext}\right]\end{aligned} \tag{2.111}$$

in which,

$$\begin{aligned}&\boldsymbol{f}_e^{dd,int} = \boldsymbol{k}_e^{dd}\cdot\boldsymbol{d}^e; \quad \boldsymbol{f}_e^{d\theta,int} = \boldsymbol{k}_e^{d\theta}\cdot(\boldsymbol{\theta}^e - \boldsymbol{\theta}_0^e) \\ &\boldsymbol{f}_e^{\theta,int} = \boldsymbol{k}_e^{\theta\theta,2}\cdot\boldsymbol{\theta}; \quad \boldsymbol{f}_e^{\theta,ext} = \boldsymbol{f}_e^{\theta r,ext} + \boldsymbol{f}_e^{\theta q,ext}\end{aligned} \tag{2.112}$$

After element assembly, we arrive at the coupled FE equations in matrix form:

$$\underbrace{\begin{bmatrix}0 & 0\\ \boldsymbol{K}^{\theta d} & \boldsymbol{K}^{\theta\theta}\end{bmatrix}}_{\boldsymbol{C}(\boldsymbol{D})}\cdot\underbrace{\begin{Bmatrix}\dot{\boldsymbol{d}}\\ \dot{\boldsymbol{\theta}}\end{Bmatrix}}_{\boldsymbol{V}} + \underbrace{\begin{bmatrix}\boldsymbol{F}^{dd,INT} - \boldsymbol{F}^{d\theta,INT}\\ \boldsymbol{F}^{\theta,INT}\end{bmatrix}}_{\boldsymbol{F}^{INT}(\boldsymbol{D})} = \underbrace{\begin{bmatrix}\boldsymbol{F}^{df,EXT} + \boldsymbol{F}^{dt,EXT}\\ \boldsymbol{F}^{\theta,EXT}\end{bmatrix}}_{\boldsymbol{F}^{EXT}(\boldsymbol{D})} \tag{2.113}$$

We evaluate the coupled equations at time t_{n+1}, and introduce difference formulas for $\boldsymbol{D}_{n+1}$ and $\boldsymbol{V}_{n+1}$, where α is the time integration parameter for the generalized trapezoidal rule (Hughes, 2000)

$$\boldsymbol{D}_{n+1} = \boldsymbol{D}_n + \Delta t\boldsymbol{V}_{n+\alpha} \tag{2.114}$$

$$\boldsymbol{V}_{n+\alpha} = (1-\alpha)\boldsymbol{V}_n + \alpha\boldsymbol{V}_{n+1} \tag{2.115}$$

so that,

$$\boldsymbol{D}_{n+1} = \underbrace{\boldsymbol{D}_n + \Delta t(1-\alpha)\boldsymbol{V}_n}_{\widetilde{\boldsymbol{D}}_{n+1}} + \Delta t\alpha\boldsymbol{V}_{n+1} \tag{2.116}$$

α	method	type
0	forward Euler	explicit (if $\boldsymbol{C}$ diagonal, which it is not)
1/2	trapezoidal rule	implicit
1	backward Euler	implicit

Apply the generalized trapezoidal rule to (2.113) to get:

$$\boldsymbol{C}(\boldsymbol{D}_{n+1}) \cdot \boldsymbol{V}_{n+1} + \boldsymbol{F}^{INT}(\boldsymbol{D}_{n+1}) = \boldsymbol{F}^{EXT}(\boldsymbol{D}_{n+1}) \tag{2.117}$$

The Newton-Raphson iteration algorithm will be used to solve for $\boldsymbol{V}_{n+1}^{k+1}$ with the current iteration value $\boldsymbol{V}_{n+1}^{k}$ as follows:

$$\begin{aligned}
\boldsymbol{R}(\boldsymbol{V}_{n+1}^{k+1}) = \boldsymbol{C}(\boldsymbol{D}_{n+1}^{k+1}) \cdot \boldsymbol{V}_{n+1}^{k+1} + \boldsymbol{F}^{INT}(\boldsymbol{D}_{n+1}^{k+1}) - \boldsymbol{F}^{EXT}(\boldsymbol{D}_{n+1}^{k+1}) &= \boldsymbol{0} \\
\approx \boldsymbol{R}^k + \frac{\partial \boldsymbol{R}^k}{\partial \boldsymbol{V}} \cdot \delta \boldsymbol{V} & \\
\implies \delta \boldsymbol{V} = -\left(\frac{\partial \boldsymbol{R}^k}{\partial \boldsymbol{V}}\right)^{-1} \cdot \boldsymbol{R}^k & \\
\boldsymbol{V}_{n+1}^{k+1} = \boldsymbol{V}_{n+1}^{k} + \delta \boldsymbol{V} & \\
\boldsymbol{D}_{n+1}^{k+1} = \tilde{\boldsymbol{D}}_{n+1} + \alpha \Delta t \boldsymbol{V}_{n+1}^{k+1} &
\end{aligned} \tag{2.118}$$

Consistent tangent used can be written as:

$$\begin{aligned}
\frac{\partial \boldsymbol{R}}{\partial \boldsymbol{V}} &= \left(\frac{\partial \boldsymbol{C}}{\partial \boldsymbol{D}} \cdot \frac{\partial \boldsymbol{D}}{\partial \boldsymbol{V}}\right) \cdot \boldsymbol{V} + \boldsymbol{C} + \frac{\partial \boldsymbol{F}^{INT}}{\partial \boldsymbol{D}} \cdot \frac{\partial \boldsymbol{D}}{\partial \boldsymbol{V}} - \frac{\partial \boldsymbol{F}^{EXT}}{\partial \boldsymbol{D}} \cdot \frac{\partial \boldsymbol{D}}{\partial \boldsymbol{V}} \\
&= \boldsymbol{C} + \left(\frac{\partial \boldsymbol{C}}{\partial \boldsymbol{D}} \cdot \boldsymbol{V} + \frac{\partial \boldsymbol{F}^{INT}}{\partial \boldsymbol{D}} - \frac{\partial \boldsymbol{F}^{EXT}}{\partial \boldsymbol{D}}\right) \cdot \frac{\partial \boldsymbol{D}}{\partial \boldsymbol{V}}
\end{aligned} \tag{2.119}$$

where,

$$\frac{\partial \boldsymbol{D}}{\partial \boldsymbol{V}} = \alpha \Delta t \tag{2.120}$$

$$\boldsymbol{C} \cdot \boldsymbol{V} = \begin{bmatrix} \boldsymbol{0} \\ \boldsymbol{K}^{\theta d} \cdot \dot{\boldsymbol{d}} + \boldsymbol{K}^{\theta\theta} \cdot \dot{\boldsymbol{\theta}} \end{bmatrix} \tag{2.121}$$

$$\frac{\partial \boldsymbol{C}}{\partial \boldsymbol{D}} \cdot \boldsymbol{V} = \begin{bmatrix} \boldsymbol{0} & \boldsymbol{0} \\ \left(\frac{\partial \boldsymbol{K}^{\theta d}}{\partial \boldsymbol{d}} \cdot \dot{\boldsymbol{d}} + \frac{\partial \boldsymbol{K}^{\theta\theta}}{\partial \boldsymbol{d}} \cdot \dot{\boldsymbol{\theta}}\right) & \left(\frac{\partial \boldsymbol{K}^{\theta d}}{\partial \boldsymbol{\theta}} \cdot \dot{\boldsymbol{d}} + \frac{\partial \boldsymbol{K}^{\theta\theta}}{\partial \boldsymbol{\theta}} \cdot \dot{\boldsymbol{\theta}}\right) \end{bmatrix} \tag{2.122}$$

$$\begin{aligned}
\frac{\partial \boldsymbol{F}^{INT}}{\partial \boldsymbol{D}} &= \left[\begin{array}{cc} \dfrac{\partial \boldsymbol{F}^{INT}}{\partial \boldsymbol{d}} & \dfrac{\partial \boldsymbol{F}^{INT}}{\partial \boldsymbol{\theta}} \end{array} \right] \\
&= \left[\begin{array}{cc} \left(\dfrac{\partial \boldsymbol{F}^{dd,INT}}{\partial \boldsymbol{d}} - \dfrac{\partial \boldsymbol{F}^{d\theta,INT}}{\partial \boldsymbol{d}} \right) & \left(\dfrac{\partial \boldsymbol{F}^{dd,INT}}{\partial \boldsymbol{\theta}} - \dfrac{\boldsymbol{F}^{d\theta,INT}}{\partial \boldsymbol{\theta}} \right) \\ \dfrac{\partial \boldsymbol{F}^{\theta,INT}}{\partial \boldsymbol{d}} & \dfrac{\partial \boldsymbol{F}^{\theta,INT}}{\partial \boldsymbol{\theta}} \end{array} \right] \\
&= \left[\begin{array}{cc} \boldsymbol{K}^{dd} & -\boldsymbol{K}^{d\theta} \\ \boldsymbol{0} & \boldsymbol{K}^{\theta\theta,2} \end{array} \right]
\end{aligned} \tag{2.123}$$

$$\begin{aligned}
\frac{\partial \boldsymbol{F}^{EXT}}{\partial \boldsymbol{D}} &= \left[\begin{array}{cc} \dfrac{\partial \boldsymbol{F}^{EXT}}{\partial \boldsymbol{d}} & \dfrac{\partial \boldsymbol{F}^{EXT}}{\partial \boldsymbol{\theta}} \end{array} \right] \\
&= \left[\begin{array}{cc} \boldsymbol{0} & \boldsymbol{0} \\ \boldsymbol{0} & \boldsymbol{0} \end{array} \right]
\end{aligned} \tag{2.124}$$

2.4 Numerical examples

2.4.1 Free thermal expansion

First, to test the FE model for thermoelasticity, let us look at a simple example of free thermal expansion. As Figure 2.2 shows, the bottom of the column is fixed in vertical direction, and the surface is free to expand. Due to the axisymmetry, the central axis is fixed in the horizontal direction. The height and radius of the column are 0.3 m and 0.1 m, respectively. The column is discretized into 10 elements. The initial temperature is uniform 20 ^oC. The bottom and the side surface are adiabatic. The temperature is prescribed at the top surface to be 40 ^oC. The top and the side surfaces are free of traction. Table 2.1 lists the parameters used in the example.

Table 2.1: Constant parameters used in the FEA of thermo-elastic modeling

Parameter	Symbol	Value	Units
Thermal expansion coefficient	α^θ	11.7×10^{-4}	$m/(m \cdot K)$
Specific heat capacity	C	855	$J/(K \cdot kg)$
Thermal conductivity	K^θ	0.817	$W/(m \cdot K)$
Mass density	ρ	2000	kg/m^3
Lame parameter	λ	1.35×10^6	Pa
Lame parameter	μ	5.4×10^6	Pa

Figure 2.3 (a) shows that the temperature becomes uniform after 100 hours. Figure 2.3 (c) shows that the total strain (can be additively decomposed to the thermal strain and the elastic strain) arrives at 0.0234 when the temperature becomes uniform eventually. This value is equal to $\alpha^\theta \times (\theta - \theta_0) = 11.7 \times 10^{-4} \times 20 = 0.0234$. Since the example models the free thermal expansion, we can also observe from Figure 2.3 (c) that the total strain is equal to the thermal strain, i.e., the elastic strain is almost equal to zero. Figure 2.3 (d) illustrates the stress distribution arrives at zero eventually inside the column when temperature is uniform and thus strain is uniform.

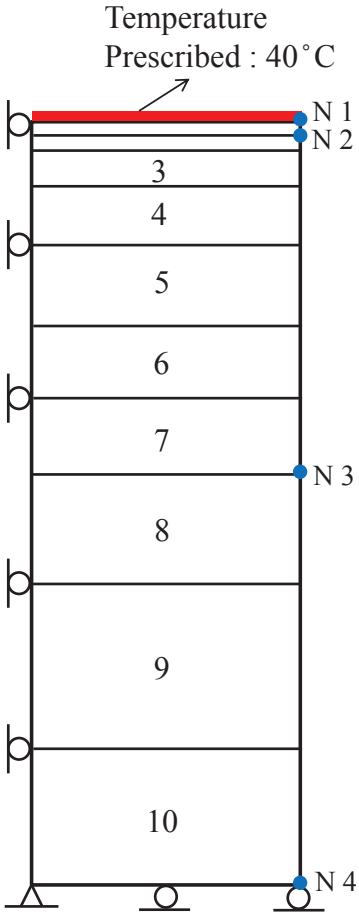

Figure 2.2: 10 element mesh for axisymmetric free thermal expansion example

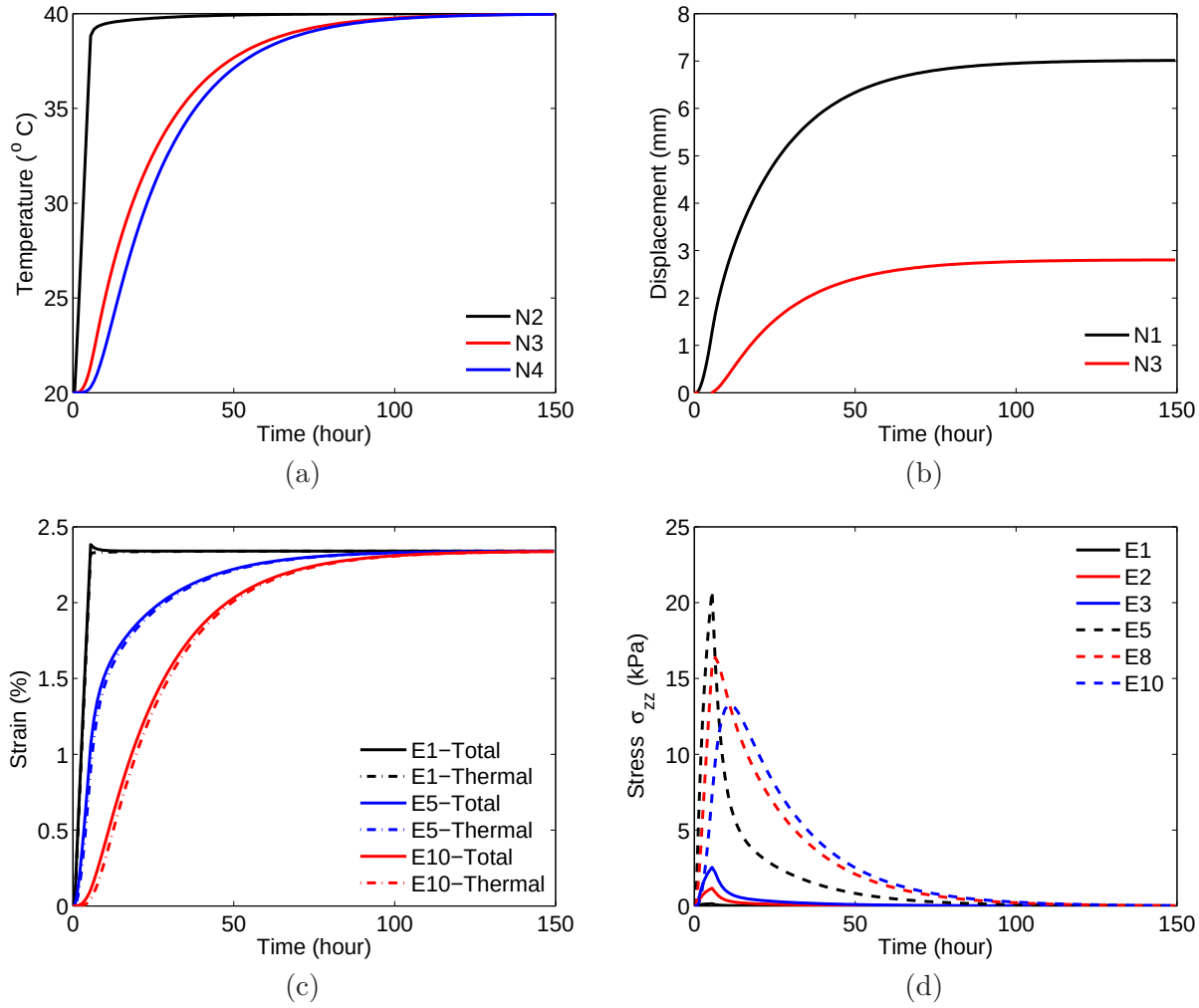

Figure 2.3: (a) Temperature variation at nodes 2, 3 and 4 (N2, N3, N4 in Figure 2.2). (b) Vertical displacement at nodes 1 and 3. (c) Variation of total strain and thermal strain at the top Gauss integration points of elements 1, 5 and 10. (d) Variation of stress at the top Gauss integration points of elements 1, 2, 3, 5, 8, 10.

2.4.2 Comparison between the fully coupled and the decoupled TE models

The comparative analysis is designed to illustrate the influence of the coupling term. Here let us call the method we elaborated in Section (2.3.3) the fully coupled TE model. On the other hand, we ignore the thermal expansion coefficient in the balance of energy equation to obtain the decoupled TE model, in which we solve the temperature separately, instead of solving the displacement and the temperature monolithically. We use the same geometry and the mesh as shown in Figure 2.2, as well as the same material parameters (see Table 2.1) in this example. The initial and boundary conditions are the same except that the gravity acceleration is applied as the body force and the vertical traction ($t^{\sigma} = 9 \times 10^{4} Pa$) are exerted on the top.

The compared results, as shown in Figure 2.4 (a)-(d) indicate that the coupled model and decoupled model match each other well. Compared to the fully coupled model, the decoupled model, which is a simpler method, can also achieve reasonably accurate results for the thermo-elastic analysis.

Figure 2.4: Comparison between fully coupled and decoupled thermo-elastic models. (a) Temperature variation at the bottom nodes of elements 1, 3, 5 and 10. (b) Vertical displacement at the top nodes of elements 1, 5 and 10. (c) Variation of total strain ϵ_{zz} at the top Gauss integration points of elements 1, 5 and 10. (d) Variation of stress σ_{zz} at the top Gauss integration points of elements 1, 5 and 10.

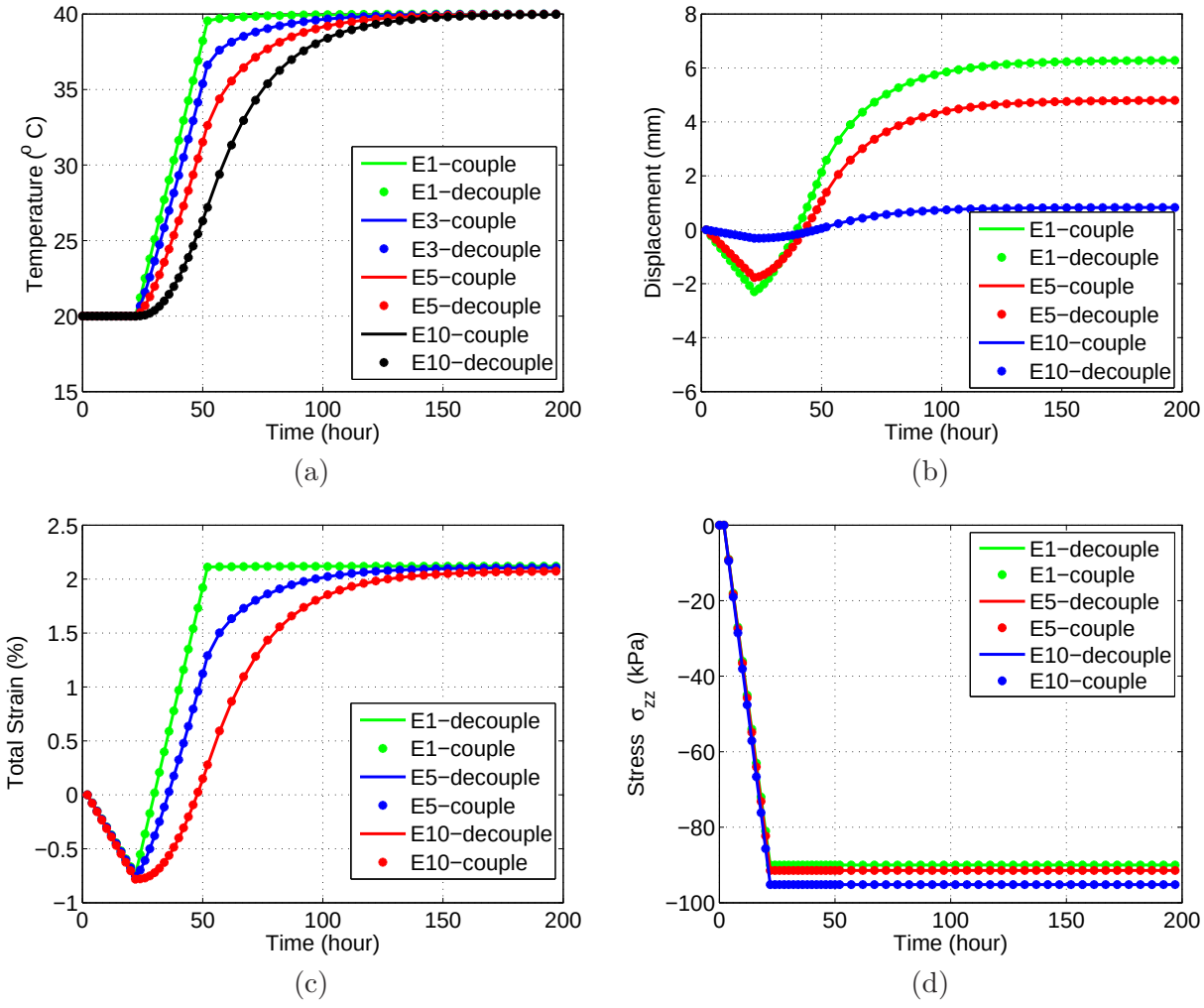

Chapter 3

Saturated thermoporomechanics

The mixture theory is used to formulate balance equations for porous media Coussy (2004). Governing equations, including balance of mass, balance of linear momentum and balance of energy are developed for each constituent. The pore fluid pressure p_f, the displacement of solid skeleton u_i and the temperature of the mixture θ are selected as three primary variables.

3.1 Governing equations

3.1.1 Balance of mass

Saturated soil is usually treated as a two-phase mixture, i.e., solid phase (s) and fluid phase (f) (de Boer, 2005; Coussy, 2004). The volume of the mixture, solid phase and fluid phase are respectively noted as v, v_s, and v_f. The corresponding masses are m, m_s and m_f. And for $\alpha(\alpha = s, f)$ phase, $m_\alpha = \rho^{\alpha R} v_\alpha$, where $\rho^{\alpha R}$ is the real mass density of α phase. The partial mass density of α phase is defined as $\rho^\alpha = n^\alpha \rho^{\alpha R}$, where n^α is the volumetric fraction occupied by α phase, i.e. $n^\alpha = v_\alpha / v$ for a homogeneous soil, or $n^\alpha = dv_\alpha / dv$ for heterogeneous case, and $n^f + n^s = 1$. The density of a soil mixture is $\rho = m/v = \rho^f + \rho^s$. And for saturated soil, the porosity $n = n^f$.

Recall the material time derivative of a scalar field $\psi(\boldsymbol{x}, t)$ following the α phase motion is (de Boer, 2005; Coussy, 2004):

$$\frac{D^\alpha \psi(\boldsymbol{\chi}_\alpha(\boldsymbol{X}_\alpha, t), t)}{Dt} = \frac{\partial \psi(\boldsymbol{x}, t)}{\partial t} + \frac{\partial \psi(\boldsymbol{x}, t)}{\partial \boldsymbol{x}} \frac{\partial \boldsymbol{\chi}_\alpha}{\partial t} = \frac{\partial \psi}{\partial t} + \mathrm{grad}\psi \cdot \boldsymbol{v}_\alpha \tag{3.1}$$

where $\boldsymbol{\chi}_\alpha$ denotes the motion of phase α, $\boldsymbol{X}_\alpha$ is reference position of phase α, $\boldsymbol{x}$ is the current position of all phases smeared together at time t, and $\boldsymbol{v}_\alpha$ is the velocity of phase α. These notations imply a finite strain formulation, but we will simply eventually to assume small strain on the material. Thus the relationship between the material time derivative $D^\alpha(\bullet)/Dt$ and partial derivative for fluid and solid phases are:

$$\frac{D^{\mathrm{f}}\psi(\boldsymbol{\chi}_{\mathrm{f}}(\boldsymbol{X}_{\mathrm{f}},t),t)}{Dt} = \frac{\partial\psi(\boldsymbol{x},t)}{\partial t} + \frac{\partial\psi(\boldsymbol{x},t)}{\partial \boldsymbol{x}}\frac{\partial \boldsymbol{\chi}_{\mathrm{f}}}{\partial t} = \frac{\partial\psi}{\partial t} + \mathrm{grad}\psi\cdot\boldsymbol{v}_{\mathrm{f}} \tag{3.2}$$

$$\frac{D^{\mathrm{s}}\psi(\boldsymbol{\chi}_{\mathrm{s}}(\boldsymbol{X}_{\mathrm{s}},t),t)}{Dt} = \frac{\partial\psi(\boldsymbol{x},t)}{\partial t} + \frac{\partial\psi(\boldsymbol{x},t)}{\partial \boldsymbol{x}}\frac{\partial \boldsymbol{\chi}_{\mathrm{s}}}{\partial t} = \frac{\partial\psi}{\partial t} + \mathrm{grad}\psi\cdot\boldsymbol{v}_{\mathrm{s}} \tag{3.3}$$

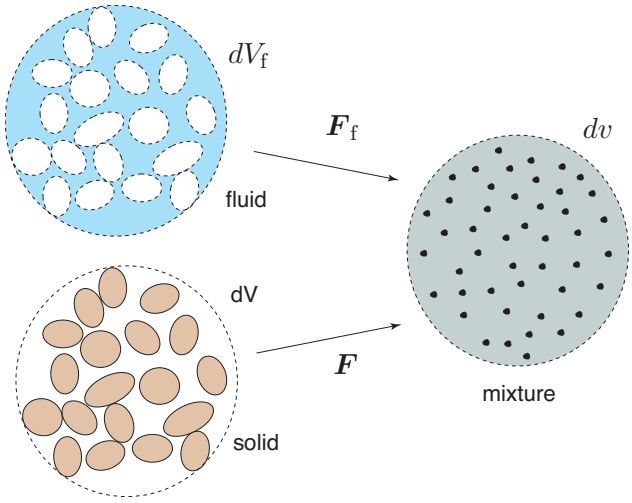

Figure 3.1: The transformation of material volume.

In Figure (3.1), dV_α is the initial material volume of α phase, and dv is the current material volume of the mixture, such that

$$dv = J_\alpha dV_\alpha \tag{3.4}$$

$$dv_\alpha = n^\alpha dv = n^\alpha J_\alpha dV_\alpha \tag{3.5}$$

where, dv_α is the current material volume of α phase. J_α is the Jacobian of deformation of α phase, and $J_\alpha = \det \boldsymbol{F}_\alpha$ with $\boldsymbol{F}_\alpha$ the deformation gradient of phase α. The material time derivatives of

the integral over the current volume needs to be converted to be that over initial material volume:

$$\begin{aligned}\frac{D^\alpha}{D\,t}\int_\Omega (\bullet)dv &= \frac{D^\alpha}{D\,t}\int_{\Omega_0^\alpha}(\bullet)J_\alpha dV_\alpha \\ &= \int_{\Omega_0^\alpha}\frac{D^\alpha}{D\,t}\left[(\bullet)J_\alpha\right]dV_\alpha \\ &= \int_{\Omega_0^\alpha}J_\alpha\frac{D^\alpha(\bullet)}{Dt}dV_\alpha + \int_{\Omega_0^\alpha}(\bullet)\frac{D^\alpha J_\alpha}{Dt}dV_\alpha \end{aligned} \tag{3.6}$$

The material time derivative of J_α is defined as:

$$\frac{D^\alpha}{Dt}J_\alpha = J_\alpha\,\mathrm{div}\boldsymbol{v}_\alpha \tag{3.7}$$

where $\boldsymbol{v}_\alpha$ is the velocity of α constituent, $\boldsymbol{v}_\alpha = \frac{D^\alpha \boldsymbol{u}_\alpha}{Dt}$, and where, $\boldsymbol{u}_\alpha$ is the displacement of α phase. Thus,

$$\frac{D^\alpha}{D\,t}\int_\Omega(\bullet)dv = \int_{\Omega_0^\alpha}\left[\frac{D^\alpha(\bullet)}{Dt} + (\bullet)\mathrm{div}(\boldsymbol{v}_\alpha)\right]J_\alpha dV_\alpha = \int_\Omega\left[\frac{D^\alpha(\bullet)}{Dt} + (\bullet)\mathrm{div}(\boldsymbol{v}_\alpha)\right]dv \tag{3.8}$$

The total mass of the α phase in Ω is written as:

$$m_\alpha = \int_{\Omega_\alpha}\rho^{\alpha R}dv_\alpha = \int_\Omega \rho^\alpha dv \tag{3.9}$$

Ignoring sources and sinks and chemical reaction between phases for now, the balance of mass equation for the α phase is written as:

$$\frac{D^\alpha m_\alpha}{Dt} = \int_\Omega \hat{\rho}^\alpha dv \tag{3.10}$$

where $\hat{\rho}^\alpha$ is the mass supply rate per volume. For saturated condition, it is assumed that there is no mass exchange between solid and fluid phases, and no separate source of mass, i.e. $\hat{\rho}^\alpha = 0$. Substitution of (3.8) and (3.9) into (3.10) provides:

$$\int_\Omega\left[\frac{D^\alpha\rho^\alpha}{D\,t} + (\rho^\alpha)\mathrm{div}\boldsymbol{v}_\alpha\right]dv = \int_\Omega\hat{\rho}^\alpha dv \tag{3.11}$$

Thus the local form of the balance of mass equation for the α phase is:

$$\frac{D^\alpha\rho^\alpha}{D\,t} + \rho^\alpha\,\mathrm{div}\boldsymbol{v}_\alpha = 0 \tag{3.12}$$

Now we write the balance of mass for solid and fluid separately

$$\frac{D^s \rho^s}{D\, t} + \rho^s \, \mathrm{div} \boldsymbol{v}_s = 0 \tag{3.13}$$

$$\frac{D^f \rho^f}{D\, t} + \rho^f \, \mathrm{div} \boldsymbol{v}_f = 0 \tag{3.14}$$

We would like to express the derivatives solely in terms of the motion of the solid phase for eventual Lagrangian FEA. A combination of (3.2) and (3.3) yields:

$$\frac{D^f(\bullet)}{Dt} = \frac{D^s(\bullet)}{Dt} + \mathrm{grad}(\bullet) \cdot \tilde{\boldsymbol{v}}_f \tag{3.15}$$

where, $(\bullet)$ indicates any variable, $\tilde{\boldsymbol{v}}_f = \boldsymbol{v}_f - \boldsymbol{v}_s$ is relative velocity vector of fluid phase with respect to the solid phase motion. Use of (3.15) in (3.14) allows us to express the balance of mass of fluid phase in the form:

$$\frac{D^f \rho^f}{D\, t} + \rho^f \, \mathrm{div} \boldsymbol{v}_f = -\mathrm{div}(\rho^f \tilde{\boldsymbol{v}}_f) \tag{3.16}$$

Combining (3.13) and (3.16), we get the balance of mass equation for the mixture:

$$\frac{D^s \rho}{Dt} + \rho \, \mathrm{div} \boldsymbol{v}_s = -\mathrm{div}(\rho^f \tilde{\boldsymbol{v}}_f) \tag{3.17}$$

In addition, the densities of solid and fluid constituents are expressed as (Lewis and Schrefler, 1998):

$$\frac{1}{\rho^{sR}} \frac{D^s \rho^{sR}}{Dt} = \left(\frac{1}{K^s} \frac{D^s p^s}{Dt} - \beta_s^\theta \frac{D^s \theta}{Dt} \right) \tag{3.18}$$

$$\frac{1}{\rho^{fR}} \frac{D^f \rho^{fR}}{Dt} = \left(\frac{1}{K^f} \frac{D^f p^f}{Dt} - \beta_f^\theta \frac{D^f \theta}{Dt} \right) \tag{3.19}$$

where K^α is the bulk modulus, β_α^θ is the volumetric thermal expansion coefficient of $\alpha(\alpha = s, f)$ constituent, and $\beta_\alpha^\theta = 3\alpha_\alpha^\theta$, where α_α^θ is the linear thermal expansion coefficient of $\alpha(\alpha = s, f)$ phase. The first terms of the bracket in (3.18) and (3.19) are ignored, owing to the fact that solid and fluid phases (water for saturated condition) are nearly mechanically incompressible compared to the skeleton. Thus the densities of solid and fluid are only functions of temperature:

$$\frac{1}{\rho^{sR}} \frac{D^s \rho^{sR}}{Dt} = -\beta_s^\theta \frac{D^s \theta}{Dt} \tag{3.20}$$

$$\frac{1}{\rho^{fR}} \frac{D^f \rho^{fR}}{Dt} = -\beta_f^\theta \frac{D^f \theta}{Dt} \tag{3.21}$$

Using $\rho^\alpha = \rho^{\alpha R}\, n^\alpha$, together with (3.20) and (3.21), we can alternatively write (3.13) and (3.14) as:

$$\frac{D^s n^s}{D\, t} + n^s \,\mathrm{div}\boldsymbol{v}_s = \beta_s^\theta \, n^s \frac{D^s \theta}{Dt} \tag{3.22}$$

$$\frac{D^f n^f}{D\, t} + n^f \,\mathrm{div}\boldsymbol{v}_f = \beta_f^\theta \, n^f \frac{D^f \theta}{Dt} \tag{3.23}$$

Use of (3.15) in (3.23), and together with (3.22), allows us to express the balance of mass for the mixture, accounting for thermal expansion of the solid and fluid constituents,

$$\mathrm{div}\boldsymbol{v}_s + \mathrm{div}\tilde{\boldsymbol{v}}_f^D - \left(\beta_s^\theta n^s + \beta_f^\theta n^f\right) \frac{D^s \theta}{Dt} - \beta_f^\theta \tilde{\boldsymbol{v}}_f^D \cdot \mathrm{grad}\theta = 0 \tag{3.24}$$

where $\tilde{\boldsymbol{v}}_f^D = n^f \tilde{\boldsymbol{v}}_f$ is the superficial Darcy velocity.

3.1.2 Balance of linear momentum

The balance of linear momentum for the $\alpha\,(\alpha = s, f)$ phase is written in global form:

$$\frac{D^\alpha}{Dt} \int_\Omega \rho^\alpha \boldsymbol{v}_\alpha dv = \int_\Omega \left(\rho^\alpha \, \boldsymbol{b}^\alpha + \hat{\boldsymbol{h}}^\alpha\right) dv + \int_{\partial\Omega} \boldsymbol{T}^\alpha da \tag{3.25}$$

where $\boldsymbol{\sigma}^\alpha$ is the partial stress of phase α, $\boldsymbol{\sigma}^\alpha = n^\alpha \boldsymbol{\sigma}$; and the total stress is: $\boldsymbol{\sigma} = \boldsymbol{\sigma}^s + \boldsymbol{\sigma}^f$. $\boldsymbol{b}^\alpha$ is the body force vector per unit mass of α phase, we assume it equals to acceleration of gravity: $\boldsymbol{b}^\alpha = \boldsymbol{b} = \boldsymbol{g}$, where g is the acceleration vector of gravity. $\hat{\boldsymbol{h}}^\alpha$ is internal body force drag on constituent α caused by the other constituents, and

$$\sum_{\alpha=s,f} \hat{\boldsymbol{h}^\alpha} = \boldsymbol{0} \tag{3.26}$$

Using (3.8), we rewrite the LHS of (3.25):

$$\begin{aligned}
\frac{D^\alpha}{Dt} \int_\Omega \rho^\alpha \boldsymbol{v}_\alpha dv &= \int_\Omega \left[\frac{D^\alpha}{Dt}(\rho^\alpha \boldsymbol{v}_\alpha) + \rho^\alpha \boldsymbol{v}_\alpha \mathrm{div}(\boldsymbol{v}_\alpha)\right] dv \\
&= \int_\Omega \left[\boldsymbol{v}_\alpha \frac{D^\alpha \rho^\alpha}{Dt} + \rho^\alpha \boldsymbol{a}_\alpha + \rho^\alpha \boldsymbol{v}_\alpha \mathrm{div}(\boldsymbol{v}_\alpha)\right] dv \\
&= \int_\Omega \boldsymbol{v}_\alpha \left[\frac{D^\alpha \rho^\alpha}{Dt} + \rho^\alpha \mathrm{div}(\boldsymbol{v}_\alpha)\right] dv + \int_\Omega \rho^\alpha \boldsymbol{a}_\alpha dv
\end{aligned} \tag{3.27}$$

where, $\boldsymbol{a}_\alpha$ is the acceleration of α phase:

$$\boldsymbol{a}_\alpha = \frac{D^\alpha \boldsymbol{v}_\alpha}{Dt} \tag{3.28}$$

Using the balance of mass equation (3.12), and ignoring the inertia term, we obtain:

$$\frac{D^{\alpha}}{Dt}\int_{\Omega}\rho^{\alpha}\boldsymbol{v}_{\alpha}=0 \tag{3.29}$$

The traction on α constituent is:

$$\boldsymbol{T}^{\alpha}=\boldsymbol{\sigma}^{\alpha}\cdot\boldsymbol{n} \tag{3.30}$$

where, $\boldsymbol{\sigma}^{\alpha}$ and $\boldsymbol{n}$ are respectively the partial Cauchy stress tensor and the unit normal at the surface of α constituent. Using divergence theorem to obtain:

$$\int_{\partial\Omega}\boldsymbol{T}^{\alpha}da=\int_{\Omega}\mathrm{div}(\boldsymbol{\sigma}^{\alpha})dv \tag{3.31}$$

If we substitute (3.27) and (3.31) into (3.25), and localize the integral, we will obtain:

$$\mathrm{div}\boldsymbol{\sigma}^{\alpha}+\rho^{\alpha}\boldsymbol{b}^{\alpha}+\hat{\boldsymbol{h}}^{\alpha}=\boldsymbol{0} \tag{3.32}$$

By summing up the individual balance of linear momentum equations for solid and fluid phases and using (3.26), we have the balance equation for the mixture

$$\mathrm{div}\boldsymbol{\sigma}+\rho\boldsymbol{b}=\boldsymbol{0} \tag{3.33}$$

The balance of angular momentum for non-polar constituents states that the respective partial stresses (and, in turn, the total stress) are symmetric:

$$\boldsymbol{\sigma}^{\alpha}=(\boldsymbol{\sigma}^{\alpha})^{T} \tag{3.34}$$

3.1.3 Balance of energy

3.1.3.1 The first law of thermodynamics

The first law of thermodynamics (or energy conservation) is written for each constituent (de Boer, 2005):

$$\dot{E}^{\alpha}+\dot{K}^{\alpha}=P^{\alpha}+\dot{Q}^{\alpha}+\int_{\Omega}\hat{e}^{\alpha}dv \tag{3.35}$$

where E^α, K^α, P, Q^α and $\hat{e}^\alpha$ are respectively the internal energy, the kinetic energy, the rate of mechanical work rate caused by external forces (i.e. body force and surface forces), the input heat to α constituent, and the energy supply rate to α constituent caused by all other constituents.

$$\dot{E}^\alpha = \frac{D^\alpha}{Dt}\int_\Omega \rho^\alpha e^\alpha dv \tag{3.36}$$

$$\dot{K}^\alpha = \frac{D^\alpha}{Dt}\int_\Omega \frac{1}{2}\rho^\alpha \boldsymbol{v}_\alpha \cdot \boldsymbol{v}_\alpha dv \tag{3.37}$$

$$P^\alpha = \int_\Omega \rho^\alpha \boldsymbol{b}^\alpha \cdot \boldsymbol{v}_\alpha dv + \int_{\partial\Omega} \boldsymbol{T}^\alpha \cdot \boldsymbol{v}_\alpha da \tag{3.38}$$

$$\dot{Q}^\alpha = \int_\Omega \rho^\alpha r^\alpha dv - \int_{\partial\Omega} \boldsymbol{q}^\alpha \cdot \boldsymbol{n}^\alpha da \tag{3.39}$$

where, e^α is the internal energy per unit mass, $\boldsymbol{T}^\alpha$ is the traction on α phase, r^α and $\boldsymbol{q}^\alpha$ are respectively heat source per unit mass and heat flux vector at surface of α phase.

Using (3.8) in (3.36) and (3.37) allows us to write:

$$\begin{aligned}\dot{E}^\alpha + \dot{K}^\alpha = &\int_\Omega \left[\frac{D^\alpha}{Dt}\left(\frac{1}{2}\rho^\alpha \boldsymbol{v}_\alpha \cdot \boldsymbol{v}_\alpha\right) + \frac{1}{2}\rho^\alpha \boldsymbol{v}_\alpha \cdot \boldsymbol{v}_\alpha \mathrm{div}\boldsymbol{v}_\alpha\right] dv \\ &+ \int_\Omega \left[\frac{D^\alpha}{Dt}\left(\rho^\alpha e^\alpha\right) + \rho^\alpha e^\alpha \,\mathrm{div}\boldsymbol{v}_\alpha\right] dv\end{aligned} \tag{3.40}$$

Using the chain rule, we have

$$\frac{D^\alpha}{Dt}\left(\frac{1}{2}\rho^\alpha \boldsymbol{v}_\alpha \cdot \boldsymbol{v}_\alpha\right) = \frac{1}{2}\boldsymbol{v}_\alpha \cdot \boldsymbol{v}_\alpha \frac{D^\alpha \rho^\alpha}{Dt} + \rho^\alpha \boldsymbol{v}_\alpha \cdot \boldsymbol{a}^\alpha \tag{3.41}$$

$$\frac{D^\alpha}{Dt}\left(\rho^\alpha e^\alpha\right) = e^\alpha \frac{D^\alpha \rho^\alpha}{Dt} + \rho^\alpha \frac{D^\alpha e^\alpha}{Dt} \tag{3.42}$$

Combining (3.40 - 3.42), and ignoring the inertia term $\rho^\alpha \boldsymbol{a}^\alpha$, we get:

$$\dot{E}^\alpha + \dot{K}^\alpha = \int_\Omega \left[\left(\frac{\boldsymbol{v}_\alpha^2}{2} + e^\alpha\right)\left(\frac{D^\alpha \rho^\alpha}{Dt} + \rho^\alpha \mathrm{div}\boldsymbol{v}_\alpha\right) + \rho^\alpha \frac{D^\alpha e^\alpha}{Dt}\right] dv \tag{3.43}$$

Substitution of the balance of mass equation (3.12) into (3.43) yields:

$$\dot{E}^\alpha + \dot{K}^\alpha = \int_\Omega \rho^\alpha \frac{D^\alpha e^\alpha}{D\,t} dv \tag{3.44}$$

We express the power done on α constituent in the form:

$$P^\alpha = \int_\Omega \left(\rho^\alpha \boldsymbol{b}^\alpha \cdot \boldsymbol{v}_\alpha + \mathrm{div}\,\boldsymbol{\sigma}^\alpha \cdot \boldsymbol{v}_\alpha + \boldsymbol{\sigma}^\alpha : \frac{D^\alpha \boldsymbol{\epsilon}^\alpha}{Dt}\right) dv \tag{3.45}$$

Using the balance of linear momentum (3.32), we obtain:

$$P^\alpha = \int_\Omega \left(\boldsymbol{\sigma}^\alpha : \frac{D^\alpha \boldsymbol{\epsilon}^\alpha}{Dt} - \hat{\boldsymbol{h}}^\alpha \cdot \boldsymbol{v}_\alpha \right) dv \tag{3.46}$$

Substitution of (3.39), (3.44) and (3.46) into (3.35), and use of divergence theorem lead to the local form of balance of energy equation for α constituent:

$$\rho^\alpha \frac{D^\alpha e^\alpha}{Dt} - \boldsymbol{\sigma}^\alpha : \frac{D^\alpha \boldsymbol{\epsilon}^\alpha}{Dt} + \hat{\boldsymbol{h}}^\alpha \cdot \boldsymbol{v}_\alpha - \rho^\alpha r^\alpha + \mathrm{div}\boldsymbol{q}^\alpha - \hat{e}^\alpha = 0 \tag{3.47}$$

3.1.3.2 The second law of thermodynamics

The second law of thermodynamics (or entropy inequality) has to be adopted in order to obtain restrictions for constitutive equations. The procedure was described in Coleman and Noll (1963). The postulate is that it is necessary and sufficient to apply the entropy inequality principle to all constituents for the existence of dissipation mechanisms within the mixture (de Boer, 2005):

$$\frac{D^\alpha}{D\,t} \int_\Omega \rho^\alpha \eta^\alpha dv \geq \int_\Omega \frac{\rho^\alpha r^\alpha}{\theta^\alpha} dv - \int_{\partial\Omega} \frac{\boldsymbol{q}^\alpha \cdot \boldsymbol{n}}{\theta^\alpha} da \tag{3.48}$$

Again, use of (3.8) provides:

$$\begin{aligned} \frac{D^\alpha}{D\,t} \int_\Omega \rho^\alpha \eta^\alpha dv &= \int_\Omega \left[\frac{D^\alpha}{D\,t}(\rho^\alpha \eta^\alpha) + \rho^\alpha \eta^\alpha \,\mathrm{div}\boldsymbol{v}_\alpha \right] dv \\ &= \int_\Omega \left[\rho^\alpha \frac{D^\alpha \eta^\alpha}{D\,t} + \eta^\alpha \left(\underbrace{\frac{D^\alpha \rho^\alpha}{Dt} + \rho^\alpha \mathrm{div}\boldsymbol{v}_\alpha}_{=0} \right) \right] \end{aligned} \tag{3.49}$$

Using the balance of mass (3.12), we get:

$$\frac{D^\alpha}{D\,t} \int_\Omega \rho^\alpha \eta^\alpha dv = \int_\Omega \rho^\alpha \frac{D^\alpha \eta^\alpha}{D\,t} dv \tag{3.50}$$

Applying the divergence theorem, we derive:

$$\begin{aligned} \int_{\partial\Omega} \frac{\boldsymbol{q}^\alpha \cdot \boldsymbol{n}}{\theta^\alpha} da &= \int_\Omega \mathrm{div}\left(\frac{\boldsymbol{q}^\alpha}{\theta^\alpha} \right) dv \\ &= \int_\Omega \left[\frac{\mathrm{div}\boldsymbol{q}^\alpha}{\theta^\alpha} - \frac{\boldsymbol{q}^\alpha \cdot \mathrm{grad}\,\theta^\alpha}{(\theta^\alpha)^2} \right] dv \end{aligned} \tag{3.51}$$

The local form of the entropy inequality is gained as:

$$\rho^\alpha \theta^\alpha \frac{D^\alpha \eta^\alpha}{D\,t} - \rho^\alpha r^\alpha + \mathrm{div}\boldsymbol{q}^\alpha - \frac{\boldsymbol{q}^\alpha \cdot \mathrm{grad}\,\theta^\alpha}{\theta^\alpha} \geq 0 \tag{3.52}$$

To relate the first and the second laws of thermodynamics, we introducing the Helmholtz free energy per unit mass:

$$\psi^\alpha = e^\alpha - \theta^\alpha \eta^\alpha \tag{3.53}$$

Thus, the material time derivative following the motion of α phase is:

$$\frac{D^\alpha \psi^\alpha}{Dt} = \frac{D^\alpha e^\alpha}{Dt} - \theta^\alpha \frac{D^\alpha \eta^\alpha}{Dt} - \eta^\alpha \frac{D^\alpha \theta^\alpha}{Dt} \tag{3.54}$$

Combining (3.54) and (3.52), and canceling the term $\theta^\alpha \frac{D^\alpha \eta^\alpha}{Dt}$, we arrive at:

$$\rho^\alpha \frac{D^\alpha e^\alpha}{D\,t} - \rho^\alpha \eta^\alpha \frac{D^\alpha \theta^\alpha}{Dt} - \rho^\alpha \frac{D^\alpha \psi^\alpha}{Dt} - \rho^\alpha r^\alpha + \mathrm{div}\boldsymbol{q}^\alpha - \frac{\boldsymbol{q}^\alpha \cdot \mathrm{grad}\,\theta^\alpha}{\theta^\alpha} \geq 0 \tag{3.55}$$

Combining (3.55) and (3.47), together with the assumption (de Boer, 2005):

$$\sum_{\alpha=s,f} \hat{e}^\alpha = 0 \tag{3.56}$$

we obtain the entropy inequality for the mixture:

$$\sum_{\alpha=s,f} \left[\boldsymbol{\sigma}^\alpha : \frac{D^\alpha \boldsymbol{\epsilon}^\alpha}{Dt} - \rho^\alpha \eta^\alpha \frac{D^\alpha \theta}{Dt} - \rho^\alpha \frac{D^\alpha \psi^\alpha}{Dt} - \frac{\boldsymbol{q}^\alpha \cdot \mathrm{grad}\,\theta}{\theta} - \hat{\boldsymbol{h}}^\alpha \cdot \boldsymbol{v}_\alpha \right] \geq 0 \tag{3.57}$$

Let us recall the partial stress tensors $\boldsymbol{\sigma}^\alpha$ (Terzaghi, 1936), invoking the effective stress principle and assuming an inviscid fluid,

$$\boldsymbol{\sigma}^s = \boldsymbol{\sigma}' - p_f(1-n)\mathbf{1} \tag{3.58}$$

$$\boldsymbol{\sigma}^f = -n\,p_f \mathbf{1} \tag{3.59}$$

$$\boldsymbol{\sigma} = \boldsymbol{\sigma}^s + \boldsymbol{\sigma}^f \tag{3.60}$$

where, p_f is the pore fluid pressure, n is the porosity ($=n^f$ in the saturated condition), $\boldsymbol{\sigma}$ and $\boldsymbol{\sigma}'$ are respectively the total and effective stress tensors. Now let us go back to (3.57), and look at the terms $\boldsymbol{\sigma}^\alpha : \frac{D^\alpha \boldsymbol{\epsilon}^\alpha}{Dt}$ for each constituent separately. For the solid skeleton, use of (3.58) provides:

$$\boldsymbol{\sigma}^s : \frac{D^s\boldsymbol{\epsilon}^s}{Dt} = \boldsymbol{\sigma}' : \frac{D^s\boldsymbol{\epsilon}^s}{Dt} - (1-n)p_f\,\mathbf{1} : \frac{D^s\boldsymbol{\epsilon}^s}{Dt} \tag{3.61}$$

Using small strain theory, we write:

$$\begin{aligned} \mathbf{1} : \boldsymbol{\epsilon}^\alpha &= \delta_{ij}\,\frac{1}{2}[(u_\alpha)_{i,j} + (u_\alpha)_{j,i}] \\ &= \frac{1}{2}[(u_\alpha)_{i,i} + (u_\alpha)_{i,i}] \\ &= \operatorname{div}(\boldsymbol{u}_\alpha) \end{aligned} \tag{3.62}$$

Thus,

$$\mathbf{1} : \frac{D^\alpha\boldsymbol{\epsilon}^\alpha}{Dt} = \operatorname{div}\left(\frac{D^\alpha\boldsymbol{u}_\alpha}{D\,t}\right) = \operatorname{div}\boldsymbol{v}_\alpha \tag{3.63}$$

With (3.63), (3.61) is written as:

$$\boldsymbol{\sigma}^s : \frac{D^s\boldsymbol{\epsilon}^s}{Dt} = \boldsymbol{\sigma}' : \frac{D^s\boldsymbol{\epsilon}^s}{Dt} - (1-n)\,p_f\operatorname{div}(\boldsymbol{v}_s) \tag{3.64}$$

The total strain of the solid skeleton is defined as:

$$\boldsymbol{\epsilon}^s = \boldsymbol{\epsilon}^{skel,e} + \boldsymbol{\epsilon}^{skel,\theta} \tag{3.65}$$

where $\boldsymbol{\epsilon}^{skel,e}$ is the strain caused by mechanical loading (elastic currently), and $\boldsymbol{\epsilon}^{skel,\theta}$ is the strain caused by thermal loading, which is defined as

$$\boldsymbol{\epsilon}^{skel,\theta} = \alpha^\theta_{skel}(\theta^s - \theta^s_0)\mathbf{1} \tag{3.66}$$

where θ^s and θ^s_0 refer to the current and initial temperatures of the solid phase. α^θ_{skel} is the linear thermal expansion coefficient of the solid skeleton. Palciauskas and Domenico (1982) proposed an expression of α^θ_{skel} in the form:

$$\alpha^\theta_{skel} = (1-n)\alpha^\theta_s + n\alpha^\theta_p \tag{3.67}$$

where n is the porosity of porous media. α^θ_s and α^θ_p are the linear thermal expansion coefficients of the solid and pores.

Some literature suggested that α^θ_{skel} is equal to α^θ_s approximately if all the solid grains are in contact (Walsh, 1973; Campanella and Mitchell, 1968). Khalili et al. (2010) showed experimentally that

the thermal expansion coefficient of the porous media is equal to that of the solid constituent, and is independent of the porosity or void ratio. Thus $\alpha_{skel} = \alpha_s^\theta$ will be used in the FEA.

Substitution of (3.65) and (3.66) into (3.64) gives:

$$\boldsymbol{\sigma}^s : \frac{D^s \boldsymbol{\epsilon}^s}{Dt} = \boldsymbol{\sigma}' : \frac{D^s \boldsymbol{\epsilon}^{skel,e}}{Dt} + \alpha_{skel}^\theta \mathrm{tr}(\boldsymbol{\sigma}') \frac{D^s \theta^s}{Dt} - (1-n) p_f \mathrm{div} \boldsymbol{v}_s \tag{3.68}$$

where, $\mathrm{tr}(\boldsymbol{\sigma}') = \sigma'_{kk}$ is the trace of the Cauchy effective stress tensor. With (3.59), we have,

$$\boldsymbol{\sigma}^f : \frac{D^f \boldsymbol{\epsilon}^f}{Dt} = -n^f p_f \mathrm{div}\left(\boldsymbol{v}_f\right) \tag{3.69}$$

Now let us derive the term $\hat{\boldsymbol{h}}^\alpha \cdot \boldsymbol{v}_\alpha$ in (3.57). Recall the balance of linear momentum equation (3.32):

$$\hat{\boldsymbol{h}}^f = -\mathrm{div}\boldsymbol{\sigma}^f - \rho^f \boldsymbol{b}^f \tag{3.70}$$

Considering (3.26), we get:

$$\hat{\boldsymbol{h}}^s = -\hat{\boldsymbol{h}}^f = \mathrm{div}\boldsymbol{\sigma}^f + \rho^f \boldsymbol{b}^f \tag{3.71}$$

According to (3.59),

$$\begin{aligned} \mathrm{div}(\boldsymbol{\sigma}^f) &= \mathrm{div}\left(-n^f p_f\right)\mathbf{1} \\ &= -\mathrm{grad}(n^f p_f) \\ &= -p_f \,\mathrm{grad}(n^f) - n^f \,\mathrm{grad}(p_f) \end{aligned} \tag{3.72}$$

Combining (3.70), (3.71) and (3.72) gives:

$$\sum_{\alpha=s,f} \hat{\boldsymbol{h}}^\alpha \cdot \boldsymbol{v}_\alpha = \tilde{\boldsymbol{v}}_f^D \cdot (\mathrm{grad} p_f - \rho^{fR} \boldsymbol{b}) + p_f \tilde{\boldsymbol{v}}_f \cdot \mathrm{grad} n \tag{3.73}$$

in which, $\tilde{\boldsymbol{v}}_f = \boldsymbol{v}_f - \boldsymbol{v}_s$ is the relative velocity of fluid, $\tilde{\boldsymbol{v}}_f^D = n\tilde{\boldsymbol{v}}_f$ is Darcy's velocity, and $n = n^f$ for saturated case. We will assume body force per unit mass $\boldsymbol{b}^s = \boldsymbol{b}^f = \boldsymbol{b} = \boldsymbol{g}$ is the acceleration due to gravity for soils. Substitution of (3.64), (3.69) and (3.73) into (3.57) yields:

$$\begin{aligned} &\boldsymbol{\sigma}' : \frac{D^s \boldsymbol{\epsilon}^{skel,e}}{Dt} + \alpha_{skel}^\theta \frac{D^s \theta}{Dt} \mathrm{tr}(\boldsymbol{\sigma}') \underbrace{-(1-n) p_f \mathrm{div}\, \boldsymbol{v}_s - n p_f \mathrm{div}\, \boldsymbol{v}_f - p_f \tilde{\boldsymbol{v}}_f \cdot \mathrm{grad} n}_{Term1} \\ &- \tilde{\boldsymbol{v}}_f^s \cdot \left(\mathrm{grad} p_f - \rho^{fR} \boldsymbol{g}\right) - \frac{\boldsymbol{q} \cdot \mathrm{grad}\, \theta}{\theta} - \sum_{\alpha=s,f} \left(\rho^\alpha \eta^\alpha \frac{D^\alpha \theta}{Dt} + \rho^\alpha \frac{D^\alpha \psi^\alpha}{Dt}\right) \geq 0 \end{aligned} \tag{3.74}$$

where $\boldsymbol{q} = \boldsymbol{q}^s + \boldsymbol{q}^f$ is the heat flux of the mixture, and local thermal equilibrium is assumed, i.e., $\theta^s = \theta^f = \theta$. Term 1 in (3.74) can be rewritten in the form:

$$\begin{aligned} \text{Term 1} &= -p_f \,\mathrm{div}\boldsymbol{v}_s - n\, p_f \,\mathrm{div}\tilde{\boldsymbol{v}}_f - p_f \tilde{\boldsymbol{v}}_f \cdot \mathrm{grad} n \\ &= -p_f \,\mathrm{div}\boldsymbol{v}_s - p_f \,\mathrm{div}(n\tilde{\boldsymbol{v}}_f) \end{aligned} \tag{3.75}$$

Use of (3.24) and (3.15) in (3.75) allows us to rewrite $Term1$ in (3.74) in the form:

$$\text{Term 1} = -p_f \left(\beta_s^\theta n^s \frac{D^s\theta}{Dt} + \beta_f^\theta n^f \frac{D^f\theta}{Dt} \right) \tag{3.76}$$

where, n^s and n^f are the volume fraction of solid and fluid, and $n^s = 1 - n$, $n^f = n$.

According to de Boer (2005); Hassanizadeh and Gray (1990), the Helmholtz free energy can depend on the combination of certain independent variables, e.g., $\rho^{\alpha R}$, $\boldsymbol{\epsilon}^\alpha$, n^α, S_w, θ, gradθ etc. In the thesis, a simpler functional dependence of free energies is postulated:

$$\psi^s = \psi^s(\boldsymbol{\epsilon}^{skel,e}, \theta); \quad \psi^f = \psi^f(\theta) \tag{3.77}$$

Thus,

$$\sum_{\alpha=s,f} \rho^\alpha \frac{D^\alpha \psi^\alpha}{Dt} = \rho^s \frac{\partial \psi^s}{\partial \boldsymbol{\epsilon}^{skel,e}} : \frac{D^s \boldsymbol{\epsilon}^{skel,e}}{Dt} + \rho^s \frac{\partial \psi^s}{\partial \theta} \frac{D^s\theta}{Dt} + \rho^f \frac{\partial \psi^f}{\partial \theta} \frac{D^f\theta}{Dt} \tag{3.78}$$

Substituting (3.78) into (3.74) and regrouping terms, we get:

$$\begin{aligned} &\left(\boldsymbol{\sigma}' - \rho^s \frac{\partial \psi^s}{\partial \boldsymbol{\epsilon}^{skel,e}} \right) : \frac{D^s \boldsymbol{\epsilon}^{skel,e}}{Dt} - \left[\rho^s \frac{\partial \psi^s}{\partial \theta} + \rho^s \eta^s + p_f \beta_s^\theta n^s - \alpha_{skel}^\theta \mathrm{tr}(\boldsymbol{\sigma}') \right] \frac{D^s\theta}{Dt} \\ &- \left(\rho^f \frac{\partial \psi^f}{\partial \theta} + p_f \beta_f^\theta n^f + \rho^f \eta^f \right) \frac{D^f\theta}{Dt} + \tilde{\boldsymbol{v}}_f^s \left[-\mathrm{grad}\, p_f + \rho^{fR} \boldsymbol{g} \right] - \frac{\boldsymbol{q} \cdot \mathrm{grad}\theta}{\theta} \geq 0 \end{aligned} \tag{3.79}$$

The entropy inequality must remain valid for all possible thermodynamic states. This requirement restricts the constitutive assumptions in certain ways (Hassanizadeh and Gray, 1990), and can be interpreted as: the rates can be controlled independently (Coleman and Noll, 1963), such that for (3.79) to hold,

$$\boldsymbol{\sigma}' = \rho^s \frac{\partial \psi^s}{\partial\, \boldsymbol{\epsilon}^{skel,e}} \tag{3.80}$$

$$\rho^s \eta^s = -\rho^s \frac{\partial \psi^s}{\partial \theta} - p_f \beta_s^\theta n^s + \alpha_{skel}^\theta \mathrm{tr}(\boldsymbol{\sigma}') \tag{3.81}$$

$$\rho^f \eta^f = -\rho^f \frac{\partial \psi^f}{\partial \theta} - p_f \beta_f^\theta n^f \tag{3.82}$$

Thus, (3.79) reduces to:

$$\tilde{\boldsymbol{v}}_f^s \left(-\text{grad}\, p_f + \rho^{fR}\boldsymbol{g}\right) - \frac{\boldsymbol{q}\cdot\text{grad}\theta}{\theta} \geq 0 \tag{3.83}$$

Due to the distinct nature of dissipations, the inequality (3.83) can be decoupled to two inequalities (Coussy, 2004):

$$\begin{cases} -\dfrac{\boldsymbol{q}\cdot\text{grad}\theta}{\theta} \geq 0 \\ \tilde{\boldsymbol{v}}_f^s \left(-\text{grad}\, p_f + \rho^{fR}\boldsymbol{g}\right) \geq 0 \end{cases} \tag{3.84}$$

The first inequality in (3.84) states that heat spontaneously flows from high temperature to low temperature, and the second inequality in (3.84) states that the velocity $\tilde{\boldsymbol{v}}_f^s$ and the force producing the velocity $\mathcal{L} = -\text{grad}\, p_f + \rho^{fR}\boldsymbol{b}^f$ have the same sign. Darcy's law is the simplest constitutive relation which linearly relates $\tilde{\boldsymbol{v}}_f^s$ and $\mathcal{L}$ (Coussy, 2004) in the form:

$$\tilde{\boldsymbol{v}}_f^s = k\left(-\text{grad}\, p_f + \rho^{fR}\boldsymbol{g}\right) \tag{3.85}$$

where the body force $\boldsymbol{b}^f$ is assumed to equal gravity $\boldsymbol{g}$, k is the isotropic permeability of the fluid, which must be positive. Let us go back to the first law written for the mixture:

$$\sum_{\alpha=s,f}\left(\rho^\alpha \frac{D^\alpha e^\alpha}{Dt} - \boldsymbol{\sigma}^\alpha : \frac{D^\alpha \boldsymbol{\epsilon}^\alpha}{Dt} + \hat{\boldsymbol{h}}^\alpha \cdot \boldsymbol{v}_\alpha - \rho^\alpha r^\alpha + \text{div}\boldsymbol{q}^\alpha\right) = 0 \tag{3.86}$$

Combining (3.54) and (3.86), we derive:

$$\sum_{\alpha=s,f}\left(\rho^\alpha\theta\frac{D^\alpha\eta^\alpha}{Dt} + \underbrace{\rho^\alpha\frac{D^\alpha\psi^\alpha}{Dt} + \rho^\alpha\eta^\alpha\frac{D^\alpha\theta}{Dt} - \boldsymbol{\sigma}^\alpha : \frac{D^\alpha\boldsymbol{\epsilon}^\alpha}{Dt} + \hat{\boldsymbol{h}}^\alpha\cdot\boldsymbol{v}_\alpha}_{R} - \rho^\alpha r^\alpha + \text{div}\boldsymbol{q}^\alpha\right) = 0 \tag{3.87}$$

A comparison between (3.87) and (3.57) shows that the same terms (term R in (3.87)) appear in both equations with opposite signs, together with the dissipation inequality (3.83), we can derive:

$$\sum_{\alpha=s,f}\left(\rho^\alpha\frac{D^\alpha\psi^\alpha}{Dt} + \rho^\alpha\eta^\alpha\frac{D^\alpha\theta}{Dt} - \boldsymbol{\sigma}^\alpha : \frac{D^\alpha\boldsymbol{\epsilon}^\alpha}{Dt} + \hat{\boldsymbol{h}}^\alpha\cdot\boldsymbol{v}_\alpha\right) = -\tilde{\boldsymbol{v}}_f^s\left(-\text{grad}\, p_f + \rho^{fR}\boldsymbol{g}\right) \tag{3.88}$$

Substitution of (3.88) into (3.87) provides the first law written in the form:

$$\sum_{\alpha=s,f}\left(\rho^\alpha\theta\frac{D^\alpha\eta^\alpha}{Dt} - \rho^\alpha r^\alpha + \text{div}\boldsymbol{q}^\alpha\right) - \tilde{\boldsymbol{v}}_f^s\left(-\text{grad}\, p_f + \rho^{fR}\boldsymbol{g}\right) = 0 \tag{3.89}$$

With the assumption

$$\frac{\partial^2 \psi^s}{\partial \theta \, \partial \epsilon^{skel,e}} = 0 \tag{3.90}$$

together with the definition:

$$-\frac{\partial^2 \psi^s}{\partial \theta^2} = \frac{C^s}{\theta} \tag{3.91}$$

we derive from (3.81):

$$\rho^s \frac{D^s \eta^s}{Dt} = \frac{\rho^s C^s}{\theta} \frac{D^s \theta}{Dt} - \beta_s^\theta n^s \frac{D^s p_f}{Dt} + \alpha_{skel}^\theta \frac{D^s \mathrm{tr}(\boldsymbol{\sigma}')}{Dt} \tag{3.92}$$

$$\rho^f \frac{D^f \eta^f}{Dt} = \frac{\rho^f C^f}{\theta} \frac{D^f \theta}{Dt} - \beta_f^\theta n^f \frac{D^f p_f}{Dt} \tag{3.93}$$

where, C^s and C^s are respectively the heat capacity per unit mass of solid and fluid phases. (3.93) is in agreement with the conclusion in (Coussy, 2004)(Chap.4, equation (4.53)). Substitution of (3.92) and (3.93) into (3.89), and use of (3.15) give the balance of energy for mixture in the form:

$$\begin{aligned} &(\rho C)_m \dot{\theta} + \rho^{fR} C_p^f \tilde{\boldsymbol{v}}_f^s \cdot \mathrm{grad}\, \theta - \tilde{\boldsymbol{v}}_f^s \cdot (-\mathrm{grad}\, p_f + \rho^{fR} \boldsymbol{g}) \\ &+ \alpha_{skel}^\theta \, \theta \, \mathrm{tr}(\dot{\boldsymbol{\sigma}}) + \mathrm{div}(\boldsymbol{q}) - \rho \, r - \left(\beta_s^\theta n^s + \beta_f^\theta n^f \right) \frac{D^s p_f}{Dt} - \beta_f^\theta \tilde{\boldsymbol{v}}_f^s \cdot \mathrm{grad}\, p_f = 0 \end{aligned} \tag{3.94}$$

For linear isotropic elasticity, (3.94) is then written as

$$\begin{aligned} &\left[(\rho C)_m - 9K^{skel} (\alpha_{skel}^\theta)^2 \theta \right] \dot{\theta} + \rho^{fR} C_p^f \tilde{\boldsymbol{v}}_f^s \cdot \mathrm{grad}\, \theta - \tilde{\boldsymbol{v}}_f^s \cdot (-\mathrm{grad}\, p_f + \rho^{fR} \boldsymbol{g}) \\ &+ 3K^{skel} \alpha_{skel}^\theta \, \theta \, \mathrm{tr}(\dot{\epsilon}) + \mathrm{div}(\boldsymbol{q}) - \rho \, r - \left(\beta_s^\theta n^s + \beta_f^\theta n^f \right) \frac{D^s p_f}{Dt} - \beta_f^\theta \tilde{\boldsymbol{v}}_f^s \cdot \mathrm{grad}\, p_f = 0 \end{aligned} \tag{3.95}$$

where K^{skel} is the bulk modulus of the solid skeleton. The heat capacity density of the mixture $(\rho\, C)_m = \rho^s C^s + \rho^f C^f$; the heat source term $\rho r = \rho^s r^s + \rho^f r^f$; heat flux vector $\boldsymbol{q} = \boldsymbol{q}^s + \boldsymbol{q}^f$; $\dot{f} = \frac{D^s f}{Dt}$, and where, f is any function.

3.2 Finite Element Analysis

3.2.1 Strong and Weak forms

The strong form of the coupled thermo-poro-elastic problem for saturated porous soils can be written as follows:

$$
(S)\begin{cases}
\text{Find } \boldsymbol{u}(\boldsymbol{x},t)\in\mathscr{S}^u,\ p_f(\boldsymbol{x},t)\in\mathscr{S}^p, & & & \\
\text{and } \theta(\boldsymbol{x},t)\in\mathscr{S}^\theta,\ \text{with } t\in[0,T], \quad \text{such that} & & & \\
\sigma_{ij,j}+\rho b_i = 0 & \in\Omega \\
u_i = g_i^u & \text{on }\Gamma_u \\
\sigma_{ij}n_j = t_i^\sigma & \text{on }\Gamma_t \\
u_i(\boldsymbol{x},0) = u_{0i} & \in\Omega \\
\dot{u}_{i,i}+(\tilde{v}_f^D)_{i,i}-(\beta_s^\theta\, n^s+\beta_f^\theta\, n^f)\dot{\theta}-\beta_f^\theta\,\tilde{\boldsymbol{v}}_f^D\cdot\operatorname{grad}\theta = 0 & \in\Omega_f \\
p_{\mathrm{f}} = g^f & \text{on }\Gamma_f \\
-n_i(\tilde{v}_f^D)_i = S^w & \text{on }\Gamma_s \\
p_{\mathrm{f}}(\boldsymbol{x},0) = p_{\mathrm{f0}} & \in\Omega_{\mathrm{f}} \\
\left[(\rho C)_m-9K^{skel}\,(\alpha_{skel}^\theta)^2\,\theta\right]\dot{\theta}+\rho^{fR}C_p^f\tilde{\boldsymbol{v}}_f^D\cdot\operatorname{grad}\theta & & & \\
-\tilde{\boldsymbol{v}}_f^D\cdot(-\operatorname{grad}p_f+\rho^{fR}\boldsymbol{g})+3K^{skel}\alpha_{skel}^\theta\,\theta\,\operatorname{tr}(\dot{\epsilon})+\operatorname{div}(\boldsymbol{q}) & & & \\
-\rho\, r-\left(\beta_s^\theta n^s+\beta_f^\theta n^f\right)\dot{p_f}-\beta_f^\theta\tilde{\boldsymbol{v}}_f^D\cdot\operatorname{grad}p_f = 0 & \in\Omega \\
\theta = g^\theta & \text{on }\Gamma_\theta \\
-n_iq_i = q & \text{on }\Gamma_q \\
\theta(\boldsymbol{x},0) = \theta_0 & \in\Omega
\end{cases}
\tag{3.96}
$$

where $\mathscr{S}^u$, $\mathscr{S}^p$ and $\mathscr{S}^\theta$ are the collections of trial solution,

$$
\begin{aligned}
\mathscr{S}^u &= \{u_i:\Omega\times[0,T]\mapsto\mathbb{R}^2, u_i\in H^1, u_i(t)=g_i^u(t)\,\text{on}\,\Gamma_u, u_i(\boldsymbol{x},0)=u_{i0}(\boldsymbol{x})\}\\
\mathscr{S}^\theta &= \{\theta:\Omega\times[0,T]\mapsto\mathbb{R}, \theta\in H^1, \theta(t)=g^\theta(t)\,\text{on}\,\Gamma_\theta, \theta(\boldsymbol{x},0)=\theta_0(\boldsymbol{x})\}\\
\mathscr{S}^p &= \{p_f:\Omega\times[0,T]\mapsto\mathbb{R}, p_f\in H^1, p_f(t)=g^f(t)\,\text{on}\,\Gamma_f, p_f(\boldsymbol{x},0)=p_{f0}(\boldsymbol{x})\}
\end{aligned}
\tag{3.97}
$$

The symbols Ω, Γ, Γ_u, Γ_t, Γ_θ, Γ_q, g_i^u, g^θ, $\boldsymbol{u}_0$ and θ_0 are the same as those in (2.68), and Ω_f stands for the domain of the pore fluid, Γ_f stands for the boundary where pore fluid pressure is prescribed, and Γ_s denotes the boundary of infiltration, and p_{f_0} denotes the initial pore fluid pressure. To obtain the weak form or variational form of the strong form (3.96), we choose the weighting functions as follows:

$$\begin{aligned} \boldsymbol{w}(\boldsymbol{x},t) &= \delta\,\boldsymbol{u}(\boldsymbol{x},t) \\ \omega(\boldsymbol{x},t) &= \delta\,p_f(\boldsymbol{x},t) \\ \varphi(\boldsymbol{x},t) &= \delta\,\theta(\boldsymbol{x},t) \end{aligned} \tag{3.98}$$

where $w_i \in \mathscr{V}^u$, $\varphi \in \mathscr{V}^p$ and $\omega \in \mathscr{V}^\theta$ for the variational spaces,

$$\begin{aligned} \mathscr{V}^u &= \{w_i : \Omega \mapsto \mathbb{R}^2, w_i \in H^1, w_i = 0 \quad \text{on}\,\Gamma_u\} \\ \mathscr{V}^p &= \{\omega : \Omega \mapsto \mathbb{R}, \omega \in H^1, \varphi = 0 \quad \text{on}\,\Gamma_f\} \\ \mathscr{V}^\theta &= \{\varphi : \Omega \mapsto \mathbb{R}, \varphi \in H^1, \omega = 0 \quad \text{on}\,\Gamma_\theta\} \end{aligned} \tag{3.99}$$

After applying the weighting functions $\boldsymbol{w}$, ω and φ to the coupled strong form of the balance equations respectively, we obtain the coupled weak form as follows:

$$
(W)\begin{cases}
\text{Find } u_i(\boldsymbol{x},t) \in \mathscr{S}^u,\ p_f(\boldsymbol{x},t) \in \mathscr{S}^p, \text{ and } \theta(\boldsymbol{x},t) \in \mathscr{S}^\theta \text{ such that} \\
\displaystyle\int_\Omega w_{i,j}\,\sigma'_{ij} - w_{i,i}\,p_f dv = \int_\Omega w_i\,\rho\,g_i da + \int_{\Gamma_t} w_i\,t_i^\sigma da \\
\displaystyle\int_{\Omega_f} \omega \dot{u}_{i,i}\,dv - \int_{\Omega_f} \omega_{,i}(\tilde{v}_f^D)_i\,dv - \int_{\Omega_f} \omega(\beta_s^\theta\,n^s + \beta_f^\theta\,n^f)\dot{\theta}\,dv \\
\quad \displaystyle - \int_{\Omega_f} \omega \beta_f^\theta\,(\tilde{\boldsymbol{v}}_f^D)_i \theta_{,i}\,dv = \int_{\Gamma_s} \omega\,s\,da \\
\displaystyle\int_\Omega \varphi(\rho C)_m \dot{\theta}\,dv + \int_\Omega \varphi \rho^{fR} c^f (\tilde{v}_f^D)_i \theta_{,i}\,dv + \int_\Omega \varphi_{,i} K_{ij}^\theta \theta_{,j}\,dv \\
\quad \displaystyle - \int_\Omega \varphi(\widetilde{v}_f^D)_i \left[-(p_f)_{,i} + \rho^{fR} g_i\right]\,dv + \int_\Omega \varphi(\alpha_{skel}^\theta\,\theta)\dot{\sigma}_{kk}\,dv \\
\quad \displaystyle - \int_\Omega \varphi \left(\beta_s^\theta n^s + \beta_f^\theta n^f\right) \dot{p_f}\,dv - \int_\Omega \varphi \beta_f^\theta (\tilde{\boldsymbol{v}}_f^D)_i (p_f)_{,i}\,dv = \int_{\Gamma_q} \varphi q\,da + \int_\Omega \varphi r\,dv \\
\text{holds } \forall w_i(\boldsymbol{x}) \in \mathscr{V}^u \text{ and } \eta(\boldsymbol{x}) \in \mathscr{V}^\theta \\
\mathscr{S}^u = \{u_i : \Omega \times [0,T] \mapsto \mathbb{R}^2, u_i \in H^1, u_i(t) = g_i^u(t) \text{ on } \Gamma_u, u_i(\boldsymbol{x},0) = u_{i0}(\boldsymbol{x})\} \\
\mathscr{S}^p = \{p_{\mathrm{f}} : \Omega_{\mathrm{f}} \times [0,T] \mapsto \mathbb{R}, p_{\mathrm{f}} \in H^1, p_{\mathrm{f}}(t) = r(t) \text{ on } \Gamma_r, p_{\mathrm{f}}(\boldsymbol{x},0) = p_{\mathrm{f}0}(\boldsymbol{x})\} \\
\mathscr{S}^\theta = \{\theta : \Omega \times [0,T] \mapsto \mathbb{R}, \theta \in H^1, \theta(t) = g^\theta(t) \text{ on } \Gamma_\theta, \theta(\boldsymbol{x},0) = \theta_0(\boldsymbol{x})\} \\
\mathscr{V}^u = \{w_i : \Omega \mapsto \mathbb{R}^2, w_i \in H^1, w_i = 0 \text{ on } \Gamma_u\} \\
\mathscr{V}^p = \{\omega : \Omega \mapsto \mathbb{R}, \eta \in H^1, \omega = 0 \text{ on } \Gamma_f\} \\
\mathscr{V}^\theta = \{\varphi : \Omega \mapsto \mathbb{R}, \xi \in H^1, \varphi = 0 \text{ on } \Gamma_\theta\}
\end{cases} \tag{3.100}
$$

3.2.2 Coupled finite element formulation

Following the same procedure we used for thermoelastic problems, we introduce the following symbols used in Galerkin's method:

$$\begin{aligned}
&\boldsymbol{u}^h \in (\mathscr{S}^u)^h; \quad (\mathscr{S}^u)^h \subset \mathscr{S}^u;\\
&\boldsymbol{w}^h \in (\mathscr{V}^u)^h; \quad (\mathscr{V}^u)^h \subset \mathscr{V}^u;\\
&p_f^h \in (\mathscr{S}^f)^h; \quad (\mathscr{S}^f)^h \subset \mathscr{S}^f;\\
&\omega^h \in (\mathscr{V}^f)^h; \quad (\mathscr{V}^f)^h \subset \mathscr{V}^f;\\
&\theta^h \in (\mathscr{S}^\theta)^h; \quad (\mathscr{S}^\theta)^h \subset \mathscr{S}^\theta;\\
&\varphi^h \in (\mathscr{V}^\theta)^h; \quad (\mathscr{V}^\theta)^h \subset \mathscr{V}^\theta;
\end{aligned} \tag{3.101}$$

We assume that all members of $(\mathscr{V}^u)^h$, $(\mathscr{V}^f)^h$ and $(\mathscr{V}^\theta)^h$ vanish, or approximately vanish on Γ_u, Γ_f and Γ_θ, respectively, i.e.,

$$\begin{aligned}
&w_i^h = 0 \text{ on } \Gamma_u, \ \forall w_i^h(\boldsymbol{x}) \in (\mathscr{V}^u)^h\\
&\omega^h = 0 \text{ on } \Gamma_f, \ \forall \omega^h(\boldsymbol{x}) \in (\mathscr{V}^f)^h\\
&\varphi^h = 0 \text{ on } \Gamma_\theta, \ \forall \varphi^h(\boldsymbol{x}) \in (\mathscr{V}^\theta)^h
\end{aligned} \tag{3.102}$$

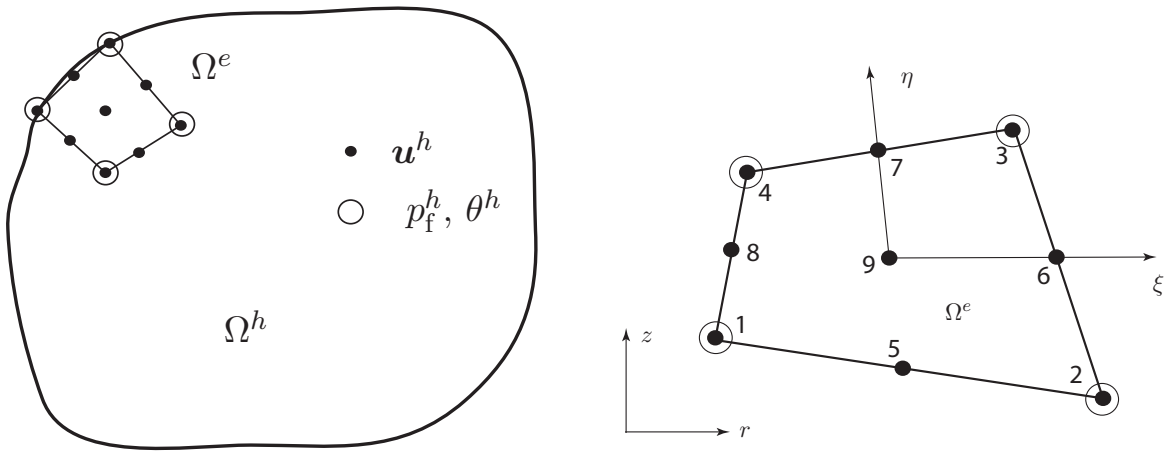

Figure 3.2: Discretization into therm-poro-elastic mixed quadrilateral elements.

Fig. (3.2) shows the mixed quadrilateral element, i.e. biquadratic in displacement, and bilinear in pore fluid pressure and temperature. Using interpolation functions, we can write the

functions $\boldsymbol{u}^h$, p_f^h, θ^h, $\boldsymbol{w}^h$,ω^h and φ^h in terms of nodal values and shape functions as follows:

$$\begin{aligned}
\boldsymbol{u}^h(\boldsymbol{\xi},t) &= \boldsymbol{N}^{e,u}\cdot\boldsymbol{d}^e \\
\boldsymbol{w}^h(\boldsymbol{\xi},t) &= \boldsymbol{N}^{e,u}\cdot\boldsymbol{c}^e \\
p_f^h(\boldsymbol{\xi},t) &= \boldsymbol{N}^{e,\theta}\cdot\boldsymbol{p}_f^e \\
\omega^h(\boldsymbol{\xi},t) &= \boldsymbol{N}^{e,\theta}\cdot\boldsymbol{\alpha}^e \\
\theta^h(\boldsymbol{\xi},t) &= \boldsymbol{N}^{e,\theta}\cdot\boldsymbol{\theta}^e \\
\varphi^h(\boldsymbol{\xi},t) &= \boldsymbol{N}^{e,\theta}\cdot\boldsymbol{\beta}^e
\end{aligned} \tag{3.103}$$

in which $\boldsymbol{N}^{e,u}$ and $\boldsymbol{N}^{e,\theta}$ are defined in (6.18) and (6.28). The gradients of temperature θ^h and pore water pressure p_f are written as,

$$\begin{aligned}
\operatorname{grad}\theta^h &= \boldsymbol{B}^{e,\theta}\cdot\boldsymbol{\theta}^e \\
\operatorname{grad}p_f^h &= \boldsymbol{B}^{e,\theta}\cdot\boldsymbol{p}_f^e
\end{aligned} \tag{3.104}$$

The coupled thermo-poro-elastic finite element equations are written as:

(1) Balance of linear momentum:

$$\begin{aligned}
\mathop{\mathbf{A}}_{e=1}^{n_{\mathrm{el}}}(\boldsymbol{c}^e)^T\cdot\Bigg[&\underbrace{\int_{\Omega^e}(\boldsymbol{B}^{e,u})^T\cdot\boldsymbol{\sigma}'\,dv}_{\boldsymbol{f}_e^{d,int}} - \underbrace{\int_{\Omega^e}(\tilde{\boldsymbol{B}}^{e,u})^T\cdot\boldsymbol{N}^{e,\theta}\cdot\boldsymbol{p}_f^e\,dv}_{\boldsymbol{f}_e^{dp,int}} \\
&= \underbrace{\int_{\Omega^e}\rho(\boldsymbol{N}^{e,u})^T\boldsymbol{b}\,dv}_{\boldsymbol{f}_e^{df,ext}} + \underbrace{\int_{\Gamma_t^e}(\boldsymbol{N}^{e,u})^T\boldsymbol{t}^\sigma da}_{\boldsymbol{f}_e^{dt,ext}}\Bigg]
\end{aligned} \tag{3.105}$$

For linear isotropic elasticity, (3.105) is then simplified as

$$\begin{aligned}
\mathop{\mathbf{A}}_{e=1}^{n_{\mathrm{el}}}(\boldsymbol{c}^e)^T\cdot\Bigg[&\underbrace{\int_{\Omega^e}(\boldsymbol{B}^{e,u})^T\cdot\boldsymbol{D}\cdot\boldsymbol{B}^{e,u}\cdot\boldsymbol{d}^e\,dv}_{\boldsymbol{f}_e^{dd,int}} - \underbrace{\int_{\Omega^e}3\boldsymbol{K}^{skel}\alpha_{skel}^{\theta}(\tilde{\boldsymbol{B}}^{e,u})^T\cdot\boldsymbol{N}^{e,\theta}\cdot(\boldsymbol{\theta}^e-\boldsymbol{\theta}_0^e)\,dv}_{\boldsymbol{f}_e^{d\theta,int}} \\
&- \underbrace{\int_{\Omega^e}(\tilde{\boldsymbol{B}}^{e,u})^T\cdot\boldsymbol{N}^{e,\theta}\cdot\boldsymbol{p}_f^e\,dv}_{\boldsymbol{f}_e^{dp,int}} = \underbrace{\int_{\Omega^e}\rho(\boldsymbol{N}^{e,u})^T\boldsymbol{b}\,dv}_{\boldsymbol{f}_e^{df,ext}} + \underbrace{\int_{\Gamma_t^e}(\boldsymbol{N}^{e,u})^T\boldsymbol{t}^\sigma da}_{\boldsymbol{f}_e^{dt,ext}}\Bigg]
\end{aligned} \tag{3.106}$$

(2) Balance of mass:

$$\begin{aligned}\mathop{\mathsf{A}}_{e=1}^{n_{\mathrm{el}}}(\boldsymbol{\alpha}^e)^T\cdot\Bigg[&\underbrace{\left(\int_{\Omega_{\mathrm{f}}^e}(\boldsymbol{N}^{e,\theta})^T\cdot\tilde{\boldsymbol{B}}^{e,u}dv\right)}_{\boldsymbol{k}_e^{pd}}\cdot\dot{\boldsymbol{d}}^e-\underbrace{\left[\int_{\Omega_{\mathrm{f}}^e}(\beta_s^\theta\,n^s+\beta_f^\theta\,n^f)(\boldsymbol{N}^{e,\theta})^T\cdot\boldsymbol{N}^{e,\theta}\,dv\right]}_{\boldsymbol{k}_e^{p\theta}}\cdot\dot{\boldsymbol{\theta}}^e\\&-\underbrace{\int_{\Omega_{\mathrm{f}}^e}(\boldsymbol{B}^{e,\theta})^T\cdot\tilde{\boldsymbol{v}}_f^D\,dv}_{\boldsymbol{f}_e^{pp,int}}-\underbrace{\int_{\Omega_{\mathrm{f}}^e}\beta_f^\theta(\boldsymbol{N}^{e,\theta})^T\cdot\left[(\tilde{\boldsymbol{v}}_f^D)^T\cdot\boldsymbol{B}^{e,\theta}\cdot\boldsymbol{\theta}^e\right]dv}_{\boldsymbol{f}_e^{p\theta,int}}=\underbrace{\int_{\Gamma_s^e}(\boldsymbol{N}^{e,\theta})^T s\,da}_{\boldsymbol{f}_e^{p,ext}}\Bigg]\end{aligned}\tag{3.107}$$

(3) Balance of energy

$$\begin{aligned}\mathop{\mathsf{A}}_{e=1}^{n_{\mathrm{el}}}(\boldsymbol{\beta}^e)^T\cdot\Bigg[&\underbrace{\int_{\Omega^e}\left((\rho C)_m(\boldsymbol{N}^{e,\theta})^T\cdot\boldsymbol{N}^{e,\theta}dv\right)}_{\boldsymbol{k}_e^{\theta\theta}}\cdot\dot{\boldsymbol{\theta}}^e\\&-\underbrace{\left(\int_{\Omega^e}(\beta_s^\theta\,n^s+\beta_f^\theta\,n^f)(\boldsymbol{N}^{e,\theta})^T\boldsymbol{N}^{e,\theta}\,dv\right)}_{\boldsymbol{k}_e^{\theta p}}\cdot\dot{\boldsymbol{p}}_f^e+\underbrace{\left(\int_{\Omega^e}\alpha_{skel}^\theta(\boldsymbol{N}^{e,\theta})^T(\boldsymbol{N}^{e,\theta}\boldsymbol{\theta}^e)\cdot\mathrm{tr}(\boldsymbol{\sigma}')dv\right)}_{\boldsymbol{f}_e^{\theta d}}\\&+\underbrace{\int_{\Omega^e}(\boldsymbol{B}^{e,\theta})^T\cdot\boldsymbol{K}_\theta\cdot\boldsymbol{B}^{e,\theta}\cdot\boldsymbol{\theta}^e dv}_{\boldsymbol{f}_e^{\theta 1,int}}+\underbrace{\int_{\Omega^e}\rho^{fR}C^f(\boldsymbol{N}^{e,\theta})^T\,(\tilde{\boldsymbol{v}}_f^D)^T\cdot\boldsymbol{B}^{e,\theta}\cdot\boldsymbol{\theta}^e\,dv}_{\boldsymbol{f}_e^{\theta 2,int}}\\&-\underbrace{\int_{\Omega^e}(\boldsymbol{N}^{e,\theta})^T\cdot(\tilde{\boldsymbol{v}}_f^D)^T\cdot(-\boldsymbol{B}^{e,\theta}\cdot\boldsymbol{p}_f^e+\rho^{fR}\boldsymbol{g})\,dv}_{\boldsymbol{f}_e^{\theta 3,int}}-\underbrace{\int_{\Omega^e}\beta_f^\theta(\boldsymbol{N}^{e,\theta})^T\cdot(\tilde{\boldsymbol{v}}_f^D)^T\cdot(\boldsymbol{B}^{e,\theta}\cdot\boldsymbol{p}_f^e)\,dv}_{\boldsymbol{f}_e^{\theta 4,int}}\\&=\underbrace{\int_{\Omega^e}\rho(\boldsymbol{N}^{e,\theta})^T r\,dv}_{\boldsymbol{f}_e^{\theta r,ext}}+\underbrace{\int_{\Gamma_q^e}(\boldsymbol{N}^{e,\theta})^T q\,da}_{\boldsymbol{f}_e^{\theta q,ext}}\Bigg]\end{aligned}\tag{3.108}$$

For the linear isotropic elastic problem, (3.108) is then written as

$$\begin{aligned}
&\mathop{\mathbf{A}}_{e=1}^{n_{\text{el}}}(\boldsymbol{\beta}^e)^T\cdot\Bigg[\underbrace{\left(\int_{\Omega^e}\left((\rho C)_m-9K^{skel}(\alpha^\theta_{skel})^2(\boldsymbol{N}^{e,\theta}\cdot\boldsymbol{\theta}^e)\right)(\boldsymbol{N}^{e,\theta})^T\cdot\boldsymbol{N}^{e,\theta}dv\right)}_{\boldsymbol{k}_e^{\theta\theta}}\cdot\dot{\boldsymbol{\theta}}^e+\\
&\underbrace{\left(\int_{\Omega^e}3K^{skel}\alpha^\theta_{skel}(\boldsymbol{N}^{e,\theta})^T(\boldsymbol{N}^{e,\theta}\boldsymbol{\theta}^e)\cdot\tilde{\boldsymbol{B}}^{e,u}dv\right)}_{\boldsymbol{k}_e^{\theta d}}\cdot\dot{\boldsymbol{d}}^e-\underbrace{\left(\int_{\Omega^e}(\beta^\theta_s\,n^s+\beta^\theta_f\,n^f)(\boldsymbol{N}^{e,\theta})^T\boldsymbol{N}^{e,\theta}\,dv\right)}_{\boldsymbol{k}_e^{\theta p}}\cdot\dot{\boldsymbol{p}}^e_f\\
&+\underbrace{\int_{\Omega^e}(\boldsymbol{B}^{e,\theta})^T\cdot\boldsymbol{K}_\theta\cdot\boldsymbol{B}^{e,\theta}\cdot\boldsymbol{\theta}^e dv}_{\boldsymbol{f}_e^{\theta1,int}}+\underbrace{\int_{\Omega^e}\rho^{fR}C^f(\boldsymbol{N}^{e,\theta})^T(\tilde{\boldsymbol{v}}^D_f)^T\cdot\boldsymbol{B}^{e,\theta}\cdot\boldsymbol{\theta}^e\,dv}_{\boldsymbol{f}_e^{\theta2,int}}\\
&-\underbrace{\int_{\Omega^e}(\boldsymbol{N}^{e,\theta})^T\cdot(\tilde{\boldsymbol{v}}^D_f)^T\cdot(-\boldsymbol{B}^{e,\theta}\cdot\boldsymbol{p}^e_f+\rho^{fR}\boldsymbol{g})\,dv}_{\boldsymbol{f}_e^{\theta3,int}}-\underbrace{\int_{\Omega^e}\beta^\theta_f(\boldsymbol{N}^{e,\theta})^T\cdot(\tilde{\boldsymbol{v}}^D_f)^T\cdot(\boldsymbol{B}^{e,\theta}\cdot\boldsymbol{p}^e_f)\,dv}_{\boldsymbol{f}_e^{\theta4,int}}\\
&=\underbrace{\int_{\Omega^e}\rho(\boldsymbol{N}^{e,\theta})^T r\,dv}_{\boldsymbol{f}_e^{\theta r,ext}}+\underbrace{\int_{\Gamma^e_q}(\boldsymbol{N}^{e,\theta})^T q\,da}_{\boldsymbol{f}_e^{\theta q,ext}}\Bigg]
\end{aligned}\tag{3.109}$$

After element assembly, we arrive at the coupled FE matrix equation in the form:

$$\begin{bmatrix}\mathbf{0}&\mathbf{0}&\mathbf{0}\\ \boldsymbol{K}^{pd}&\mathbf{0}&\boldsymbol{K}^{p\theta}\\ \boldsymbol{K}^{\theta d}&\boldsymbol{K}^{\theta p}&\boldsymbol{K}^{\theta\theta}\end{bmatrix}\begin{Bmatrix}\dot{\boldsymbol{d}}\\ \dot{\boldsymbol{p}}_f\\ \dot{\boldsymbol{\theta}}\end{Bmatrix}+\begin{bmatrix}\boldsymbol{F}^{d,INT}\\ \boldsymbol{F}^{p,INT}\\ \boldsymbol{F}^{\theta,INT}\end{bmatrix}=\begin{Bmatrix}\boldsymbol{F}^{d,EXT}\\ \boldsymbol{F}^{p,EXT}\\ \boldsymbol{F}^{\theta,EXT}\end{Bmatrix}\tag{3.110}$$

in which,

$$\begin{aligned}
\boldsymbol{F}^{d,INT}&=\boldsymbol{F}^{dd,INT}-\boldsymbol{F}^{dp,INT}-\boldsymbol{F}^{d\theta,INT}\\
\boldsymbol{F}^{p,INT}&=-\boldsymbol{F}^{pp,INT}-\boldsymbol{F}^{p\theta,INT}\\
\boldsymbol{F}^{\theta,INT}&=\boldsymbol{F}^{\theta1,INT}+\boldsymbol{F}^{\theta2,INT}-\boldsymbol{F}^{\theta3,INT}-\boldsymbol{F}^{\theta4,INT}\\
\boldsymbol{F}^{d,EXT}&=\boldsymbol{F}^{df,EXT}+\boldsymbol{F}^{dt,EXT}\\
\boldsymbol{F}^{\theta,EXT}&=\boldsymbol{F}^{\theta r,EXT}+\boldsymbol{F}^{\theta q,EXT}
\end{aligned}\tag{3.111}$$

The Newton-Raphson method is again adopted to solve for this nonlinear matrix equation, we need

to write the consistent tangent as is shown in (2.119) for the saturated THM problem.

$$\boldsymbol{C}\cdot\boldsymbol{V}=\begin{bmatrix}\mathbf{0}\\ \boldsymbol{K}^{pd}\cdot\dot{\boldsymbol{d}}-\boldsymbol{K}^{p\theta}\cdot\dot{\boldsymbol{\theta}}\\ \boldsymbol{K}^{\theta d}\cdot\dot{\boldsymbol{d}}-\boldsymbol{K}^{\theta p}\cdot\dot{\boldsymbol{p}}_f+\boldsymbol{K}^{\theta\theta}\cdot\dot{\boldsymbol{\theta}}\end{bmatrix} \tag{3.112}$$

$$\begin{aligned}\frac{\partial\boldsymbol{C}}{\partial\boldsymbol{D}}\cdot\boldsymbol{V}=&\begin{bmatrix}\mathbf{0}\\ \frac{\partial\boldsymbol{K}^{pd}}{\partial\boldsymbol{d}}\cdot\dot{\boldsymbol{d}}-\frac{\partial\boldsymbol{K}^{p\theta}}{\partial\boldsymbol{d}}\cdot\dot{\boldsymbol{\theta}}\\ \frac{\partial\boldsymbol{K}^{\theta d}}{\partial\boldsymbol{d}}\cdot\dot{\boldsymbol{d}}-\frac{\partial\boldsymbol{K}^{\theta p}}{\partial\boldsymbol{d}}\cdot\dot{\boldsymbol{p}}_f+\frac{\partial\boldsymbol{K}^{\theta\theta}}{\partial\boldsymbol{d}}\cdot\dot{\boldsymbol{\theta}}\end{bmatrix}\\ &\begin{bmatrix}\mathbf{0}\\ \frac{\partial\boldsymbol{K}^{pd}}{\partial\boldsymbol{p}_f}\cdot\dot{\boldsymbol{d}}-\frac{\partial\boldsymbol{K}^{p\theta}}{\partial\boldsymbol{p}_f}\cdot\dot{\boldsymbol{\theta}}\\ \frac{\partial\boldsymbol{K}^{\theta d}}{\partial\boldsymbol{p}_f}\cdot\dot{\boldsymbol{d}}-\frac{\partial\boldsymbol{K}^{\theta p}}{\partial\boldsymbol{p}_f}\cdot\dot{\boldsymbol{p}}_f+\frac{\partial\boldsymbol{K}^{\theta\theta}}{\partial\boldsymbol{p}_f}\cdot\dot{\boldsymbol{\theta}}\end{bmatrix}\\ &\begin{bmatrix}\mathbf{0}\\ \frac{\partial\boldsymbol{K}^{pd}}{\partial\boldsymbol{\theta}}\cdot\dot{\boldsymbol{d}}-\frac{\partial\boldsymbol{K}^{p\theta}}{\partial\boldsymbol{\theta}}\cdot\dot{\boldsymbol{\theta}}\\ \frac{\partial\boldsymbol{K}^{\theta d}}{\partial\boldsymbol{\theta}}\cdot\dot{\boldsymbol{d}}-\frac{\partial\boldsymbol{K}^{\theta p}}{\partial\boldsymbol{\theta}}\cdot\dot{\boldsymbol{p}}_f+\frac{\partial\boldsymbol{K}^{\theta\theta}}{\partial\boldsymbol{\theta}}\cdot\dot{\boldsymbol{\theta}}\end{bmatrix}\end{aligned} \tag{3.113}$$

$$\begin{aligned}\frac{\partial\boldsymbol{F}^{INT}}{\partial\boldsymbol{D}}&=\begin{bmatrix}\frac{\partial\boldsymbol{F}^{INT}}{\partial\boldsymbol{d}} & \frac{\partial\boldsymbol{F}^{INT}}{\partial\boldsymbol{p}_f} & \frac{\partial\boldsymbol{F}^{INT}}{\partial\boldsymbol{\theta}}\end{bmatrix}\\ &=\begin{bmatrix}\frac{\partial\boldsymbol{F}^{d,INT}}{\partial\boldsymbol{d}} & \frac{\partial\boldsymbol{F}^{d,INT}}{\partial\boldsymbol{p}_f} & \frac{\partial\boldsymbol{F}^{d,INT}}{\partial\boldsymbol{\theta}}\\ \frac{\partial\boldsymbol{F}^{p,INT}}{\partial\boldsymbol{d}} & \frac{\partial\boldsymbol{F}^{p,INT}}{\partial\boldsymbol{p}_f} & \frac{\partial\boldsymbol{F}^{p,INT}}{\partial\boldsymbol{\theta}}\\ \frac{\partial\boldsymbol{F}^{\theta,INT}}{\partial\boldsymbol{d}} & \frac{\partial\boldsymbol{F}^{\theta,INT}}{\partial\boldsymbol{p}_f} & \frac{\partial\boldsymbol{F}^{\theta,INT}}{\partial\boldsymbol{\theta}}\end{bmatrix}\end{aligned} \tag{3.114}$$

in which

$$
\begin{aligned}
&\frac{\partial \boldsymbol{K}^{pd}}{\partial \boldsymbol{d}} \cdot \dot{\boldsymbol{d}} = \boldsymbol{0} \\
&\frac{\partial \boldsymbol{K}^{p\theta}}{\partial \boldsymbol{d}} \cdot \dot{\boldsymbol{\theta}} = \int_{\Omega^e} (\beta_f^\theta - \beta_s^\theta)(\boldsymbol{N}^{e,\theta} \cdot \dot{\theta}^e)(\boldsymbol{N}^{e,\theta})^T \cdot \frac{\partial n}{\partial \boldsymbol{d}^e}\, dv \\
&\frac{\partial \boldsymbol{K}^{pd}}{\partial \boldsymbol{p}_f} \cdot \dot{\boldsymbol{d}} = \boldsymbol{0} \\
&\frac{\partial \boldsymbol{K}^{p\theta}}{\partial \boldsymbol{p}_f} \cdot \dot{\boldsymbol{\theta}} = \boldsymbol{0} \\
&\frac{\partial \boldsymbol{K}^{pd}}{\partial \boldsymbol{\theta}} \cdot \dot{\boldsymbol{d}} = \boldsymbol{0} \\
&\frac{\partial \boldsymbol{K}^{p\theta}}{\partial \boldsymbol{\theta}} \cdot \dot{\boldsymbol{\theta}} = \boldsymbol{0} \\
&\frac{\partial \boldsymbol{K}^{\theta d}}{\partial \boldsymbol{d}} \cdot \dot{\boldsymbol{d}} = \boldsymbol{0} \\
&\frac{\partial \boldsymbol{K}^{\theta p}}{\partial \boldsymbol{d}} \cdot \dot{\boldsymbol{p}}_f = \int_{\Omega^e} (\beta_f^\theta - \beta_s^\theta)(\boldsymbol{N}^{e,\theta} \cdot \dot{\boldsymbol{p}}_f^e)(\boldsymbol{N}^{e,\theta})^T \cdot \frac{\partial n}{\partial \boldsymbol{d}^e}\, dv \\
&\frac{\partial \boldsymbol{K}^{\theta\theta}}{\partial \boldsymbol{d}} \cdot \dot{\boldsymbol{\theta}} = \int_{\Omega^e} \frac{\partial (\rho C)_m}{\partial \boldsymbol{d}^e} (\boldsymbol{N}^{e,\theta} \cdot \dot{\boldsymbol{\theta}}^e)(\boldsymbol{N}^{e,\theta})^T\, dv \\
&\frac{\partial \boldsymbol{K}^{\theta d}}{\partial \boldsymbol{p}_f} \cdot \dot{\boldsymbol{d}} = \boldsymbol{0} \\
&\frac{\partial \boldsymbol{K}^{\theta p}}{\partial \boldsymbol{p}_f} \cdot \dot{\boldsymbol{p}}_f = \boldsymbol{0} \\
&\frac{\partial \boldsymbol{K}^{\theta\theta}}{\partial \boldsymbol{p}_f} \cdot \dot{\boldsymbol{\theta}} = \boldsymbol{0} \\
&\frac{\partial \boldsymbol{K}^{\theta d}}{\partial \boldsymbol{\theta}} \cdot \dot{\boldsymbol{d}} = \int_{\Omega^e} 3K^{skel} \alpha_{skel}^\theta (\boldsymbol{N}^{e,\theta})^T \cdot (\tilde{\boldsymbol{B}}^{e,u} \cdot \dot{\boldsymbol{d}}^e) \boldsymbol{N}^{e,\theta}\, dv \\
&\frac{\partial \boldsymbol{K}^{\theta p}}{\partial \boldsymbol{\theta}} \cdot \dot{\boldsymbol{p}_f}_f = \boldsymbol{0} \\
&\frac{\partial \boldsymbol{K}^{\theta\theta}}{\partial \boldsymbol{\theta}} \cdot \dot{\boldsymbol{\theta}} = \int_{\Omega^e} (\boldsymbol{N}^{e,\theta} \cdot \dot{\boldsymbol{\theta}}^e)(\boldsymbol{N}^{e,\theta})^T \cdot \left[\frac{\partial (\rho C)_m}{\partial \boldsymbol{\theta}} - 9K^{skel} (\alpha_{skel}^\theta)^2 \boldsymbol{N}^{e,\theta} \right] dv
\end{aligned}
\tag{3.115}
$$

$$
\begin{aligned}
\frac{\partial \boldsymbol{F}^{d,int}}{\partial \boldsymbol{d}} &= \int_{\Omega^e} (\boldsymbol{B}^{e,u})^T \cdot \boldsymbol{D} \cdot \boldsymbol{B}^{e,u}\, dv \\
\frac{\partial \boldsymbol{F}^{d,int}}{\partial \boldsymbol{p}_f} &= \int_{\Omega^e} (\tilde{\boldsymbol{B}}^{e,u})^T \cdot \boldsymbol{N}^{e,\theta}\, dv \\
\frac{\partial \boldsymbol{F}^{d,int}}{\partial \boldsymbol{\theta}} &= \int_{\Omega^e} 3K^{skel}\alpha^{\theta}_{skel} (\tilde{\boldsymbol{B}}^{e,u})^T \cdot \boldsymbol{N}^{e,\theta}\, dv \\
\frac{\partial \boldsymbol{F}^{p,int}}{\partial \boldsymbol{d}} &= \int_{\Omega^e} \left[(\boldsymbol{B}^{e,\theta})^T + \beta^{\theta}_f (\boldsymbol{N}^{e,\theta})^T \cdot (\boldsymbol{B}^{e,\theta} \cdot \boldsymbol{\theta})^T \right] \cdot \frac{\partial \tilde{\boldsymbol{v}}^D_f}{\partial n} \cdot \frac{\partial n}{\partial \boldsymbol{d}}\, dv \\
\frac{\partial \boldsymbol{F}^{p,int}}{\partial \boldsymbol{p}_f} &= \int_{\Omega^e} \left[(\boldsymbol{B}^{e,\theta})^T + \beta^{\theta}_f (\boldsymbol{N}^{e,\theta})^T \cdot (\boldsymbol{B}^{e,\theta} \cdot \boldsymbol{\theta})^T \right] \cdot \frac{\partial \tilde{\boldsymbol{v}}^D_f}{\partial \boldsymbol{p}_f}\, dv \\
\frac{\partial \boldsymbol{F}^{p,int}}{\partial \boldsymbol{\theta}} &= \int_{\Omega^e} \left\{ \left[(\boldsymbol{B}^{e,\theta})^T + \beta^{\theta}_f (\boldsymbol{N}^{e,\theta})^T \cdot (\boldsymbol{B}^{e,\theta} \cdot \boldsymbol{\theta})^T \right] \cdot \frac{\partial \tilde{\boldsymbol{v}}^D_f}{\partial \boldsymbol{\theta}} + \beta^{\theta}_f (\boldsymbol{N}^{e,\theta})^T (\tilde{\boldsymbol{v}}^D_f)^T \cdot \boldsymbol{B}^{e,\theta} \right\} dv
\end{aligned}
\tag{3.116}
$$

$$
\begin{aligned}
\frac{\partial \boldsymbol{F}^{\theta,int}}{\partial \boldsymbol{d}} &= \int_{\Omega^e} \rho^{fR} C^f\, (\boldsymbol{N}^{e,\theta})^T \cdot (\boldsymbol{B}^{e,\theta} \cdot \boldsymbol{\theta})^T \cdot \frac{\partial \tilde{\boldsymbol{v}}^D_f}{\partial \boldsymbol{d}}\, dv \\
&\quad - \int_{\Omega^e} (\boldsymbol{N}^{e,\theta})^T \cdot \left[-\boldsymbol{B}^{e,\theta} \cdot \boldsymbol{p}^e_f + \rho^{fR}\boldsymbol{g} + \beta^{\theta}_f \boldsymbol{B}^{e,\theta} \cdot \boldsymbol{p}^e_f \right]^T \cdot \frac{\partial \tilde{\boldsymbol{v}}^D_f}{\partial \boldsymbol{d}}\, dv \\
\frac{\partial \boldsymbol{F}^{\theta,int}}{\partial \boldsymbol{p}_f} &= \int_{\Omega^e} \rho^{fR} C^f\, (\boldsymbol{N}^{e,\theta})^T \cdot (\boldsymbol{B}^{e,\theta} \cdot \boldsymbol{\theta})^T \cdot \frac{\partial \tilde{\boldsymbol{v}}^D_f}{\partial \boldsymbol{p}_f}\, dv \\
&\quad - \int_{\Omega^e} \left\{ (\beta^{\theta}_f - 1)(\boldsymbol{N}^{e,\theta})^T (\tilde{\boldsymbol{v}}^D_f)^T \cdot \boldsymbol{B}^{e,\theta} + (\boldsymbol{N}^{e,\theta})^T \left[\rho^{fR}\boldsymbol{g} + (\beta^{\theta}_f - 1)\boldsymbol{B}^{e,\theta} \cdot \boldsymbol{p}^e_f \right]^T \frac{\partial \tilde{\boldsymbol{v}}^D_f}{\partial \boldsymbol{p}_f} \right\} dv \\
\frac{\partial \boldsymbol{F}^{\theta,int}}{\partial \boldsymbol{\theta}} &= \int_{\Omega^e} \left[K_\theta (\boldsymbol{B}^{e,\theta})^T + \rho^{fR} C^f (\boldsymbol{N}^{e,\theta})^T (\tilde{\boldsymbol{v}}^D_f)^T \right] \cdot \boldsymbol{B}^{e,\theta}\, dv \\
&\quad + \int_{\Omega^e} C^f (\boldsymbol{N}^{e,\theta})^T (\tilde{\boldsymbol{v}^s_f})^T \cdot (\boldsymbol{B}^{e,\theta} \cdot \boldsymbol{\theta}) \cdot \frac{\partial \rho^{fR}}{\partial \theta} + \rho^{fR} C^f (\boldsymbol{N}^{e,\theta})^T \cdot (\boldsymbol{B}^{e,\theta} \cdot \boldsymbol{\theta})^T \cdot \frac{\partial \tilde{\boldsymbol{v}}^D_f}{\partial \boldsymbol{\theta}}\, dv \\
&\quad - \int_{\Omega^e} \left[(\boldsymbol{N}^{e,\theta})^T \left[\rho^{fR}\boldsymbol{g} + (\beta^{\theta}_f - 1)\boldsymbol{B}^{e,\theta} \cdot \boldsymbol{p}^e_f \right]^T \cdot \frac{\partial \tilde{\boldsymbol{v}}^D_f}{\partial \boldsymbol{\theta}} + (\boldsymbol{N}^{e,\theta})^T (\tilde{\boldsymbol{v}}^D_f)^T \boldsymbol{g} \cdot \frac{\partial \rho^{fR}}{\partial \boldsymbol{\theta}} \right] dv
\end{aligned}
\tag{3.117}
$$

3.3 Numerical examples

3.3.1 Analytical verification

3.3.1.1 Verification against the analytical solution by Bai and Abousleiman (1997)

To verify the saturated coupled TPM FE model, results are compared with the analytical solution provided by Bai and Abousleiman (1997). The height of the column is 0.3 m and the radius is 0.1 m as shown in Figure 3.3. Initially, the homogeneous temperature is 50 ^oC. The boundary conditions are: the lateral surface at $r = 0.1m$ is fixed in u_r, and the bottom surface is fixed in u_z; the top of the column is drained boundary ($p_w = 0$); the other surfaces are impermeable and adiabatic; the temperature is prescribed to be 0 ^oC at the top; traction ($\boldsymbol{t}^\sigma$) is applied on the top surface. To compare with the analytical solution (Bai and Abousleiman, 1997), the gravity acceleration is turned off in the TPM model. The selected parameters, with respect to the mechanical, thermal and hydraulic categories are listed in Table 3.1. Figure 3.4 illustrates the response of temperature, pore fluid pressure and displacement during the thermal consolidation of the column. The comparison shows a good match. The temperature variation at the bottom of the column is identified as shown in Figure 3.4(a). Figure 3.4(b) illustrates a similar dimensionless pore fluid pressure (p_w/t^σ) distribution in both results. Since the gravity acceleration is turned off, the pore fluid pressure arrives at steady state with $p_w = 0$. The top displacement arrives at steady state ($d_z = 18mm$) after the consolidation is complete, as shown in Figure 3.4(c).

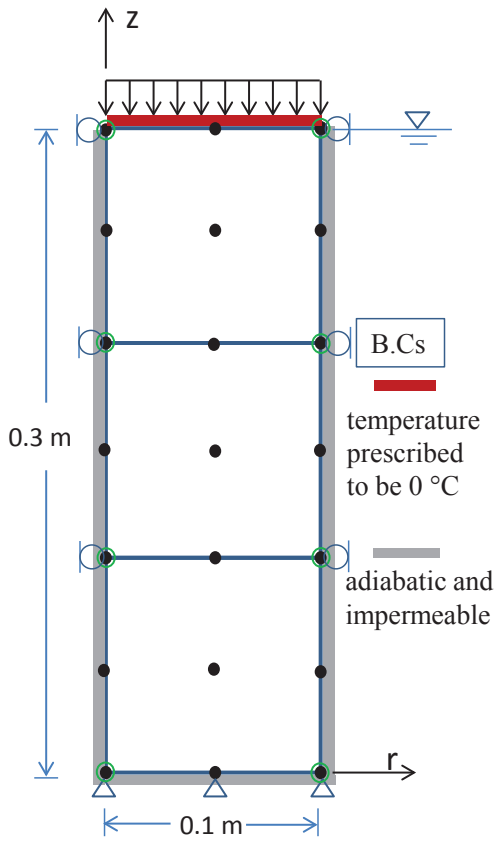

Figure 3.3: 3 element mesh for saturated non-isothermal consolidation

Table 3.1: Verification of saturated TPM model against an analytical solution by Bai and Abousleiman (1997)

Parameter	Symbol	Value	Units
Thermal expansion coefficient of solid	α_s^θ	1.65×10^{-6}	$m/(m \cdot K)$
Thermal expansion coefficient of fluid	α_f^θ	2.07×10^{-4}	$m/(m \cdot K)$
Specific heat capacity of solid	C_s	703	$J/(K \cdot kg)$
Specific heat capacity of fluid	C_f	4180	$J/(K \cdot kg)$
Thermal conductivity of solid	K_s^θ	1.38	$W/(m \cdot K)$
Thermal conductivity of fluid	K_f^θ	0.6	$W/(m \cdot K)$
Mass density of solid	ρ^{sR}	3696	kg/m^3
Mass density of fluid	ρ^{fR}	1000	kg/m^3
Intrinsic permeability	κ	1.0×10^{-14}	m^2
Lamé parameter	λ_{skel}	7.05×10^7	Pa
Lamé parameter	μ_{skel}	4.7×10^7	Pa
Traction on top	t^σ	1×10^7	Pa
Initial porosity	n_0	0.42	m^3/m^3
Viscosity of fluid (water)	μ_f	0.001	$Pa \cdot s$

Figure 3.4: (a) Temperature of the bottom. (b) Pore water pressure of the bottom. (c) Displacement of the top.

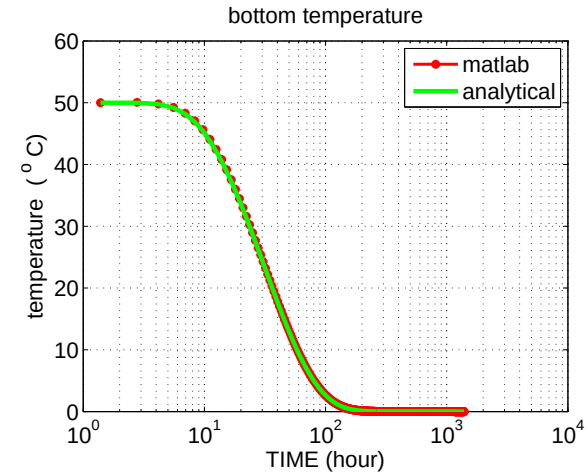

(a)

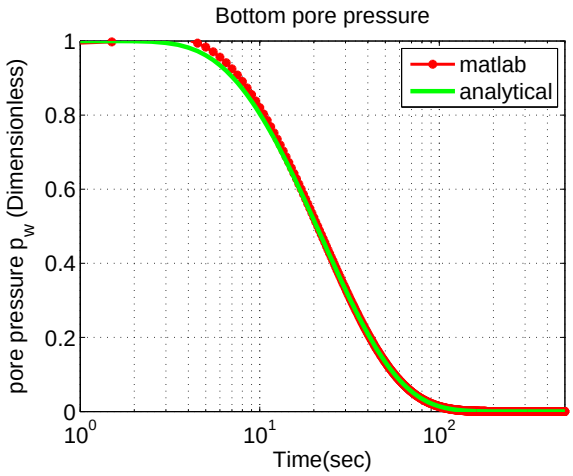

(b)

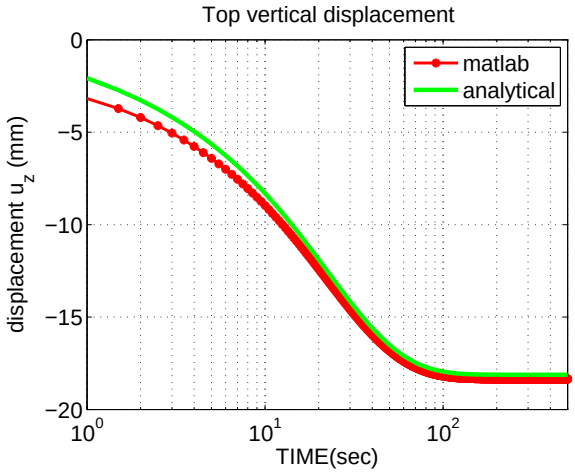

(c)

3.3.1.2 Verification against the analytical solution by Booker and Savvidou (1985)

The thermo-poro-elastic model is verified against another analytical solution by Booker and Savvidou (1985) regarding thermal consolidation of saturated soil due to a deep-buried cylindrical heat source. Figure 3.5(a) shows the geometry of the cylindrical heat source, which represents the orange part in the finite element mesh shown in figure 3.5(b). In the finite element analysis, initial temperature of the soil is uniform, i.e. $\theta_0 = 20^oC$; with gravity ignored, the initial pore water pressure is set to zero. Since the heat source is buried deep enough that the boundary effect at the soil top is negligible; in finite element analysis, Dirichlet boundary condition is assumed, i.e. prescribed temperature $\theta = 20^oC$ at the soil top. Traction is not applied at the soil top. All the surfaces except the top are fixed in normal directions. The comparisons between modeling results and analytical solutions are presented in figure 3.6 in terms of normalized temperature (θ/θ_N) and normalized pore water pressure (P_f/P_N) at three different radii, i.e. $r = r_0$, $r = 2r_0$, and $r = 5r_0$, and good agreement is obtained. Note that θ_N denotes a maximum value that temperature reaches at the midpoint on the surface of the cylinder; P_N denotes a maximum value that pore pressure could reach at the midpoint on the surface of the cylinder if the soil was impermeable; T denotes the dimensionless time given by $T = \kappa t/r_o^2$.

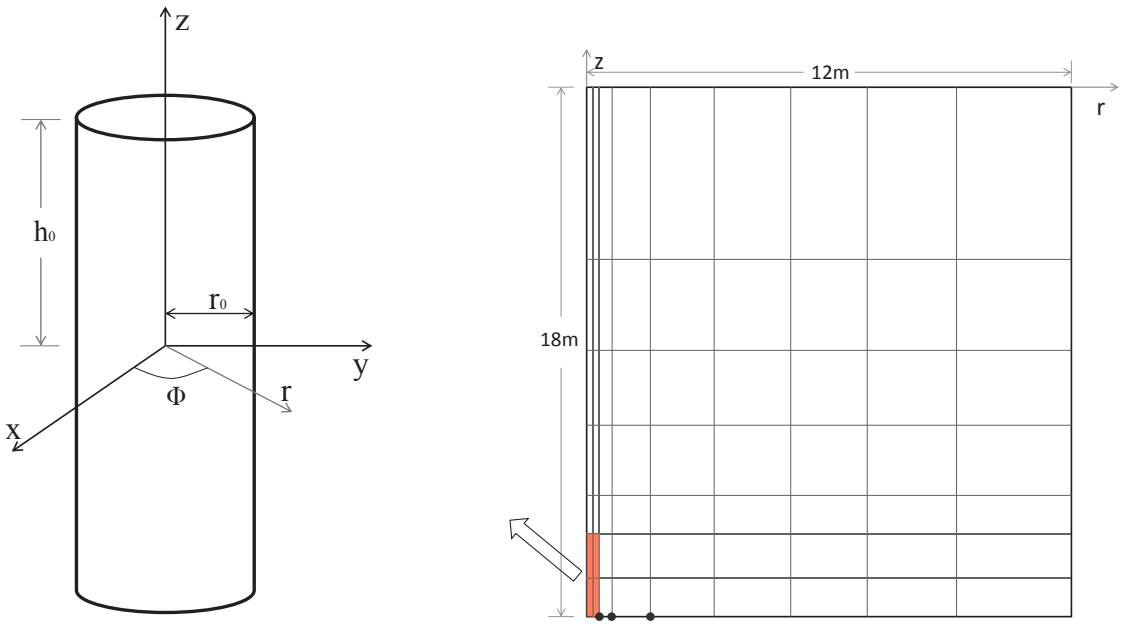

(a) (b)

Figure 3.5: Thermal consolidation of saturated soil around a cylinder heat source with analytical solution in Booker and Savvidou (1985): (a) schematic of the cylinder heat source. (b) FE mesh used in the axisymmetric coupled saturated TPM FEA.

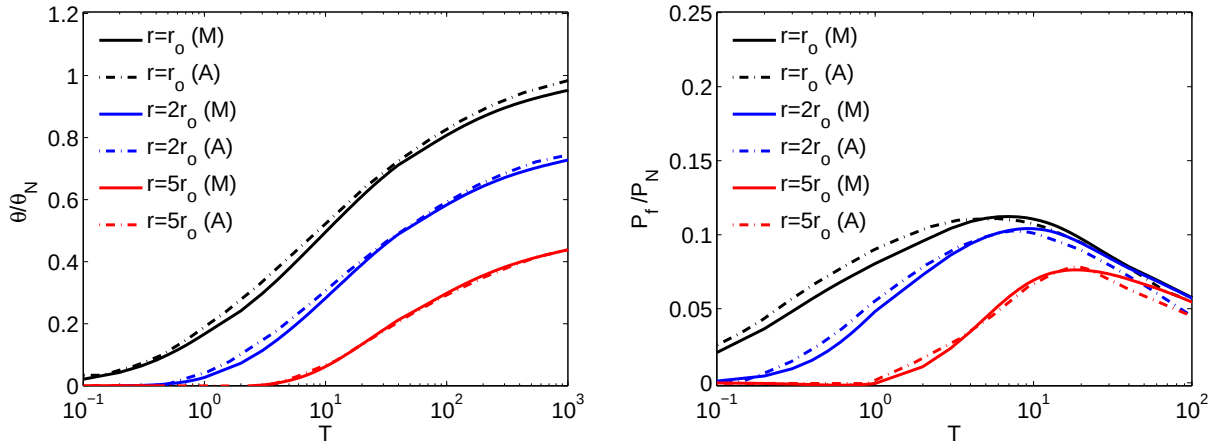

(a) (b)

Figure 3.6: (a) Variation of temperature with time. (b) Variation of pore pressure with time. In the legends, "A" represents the analytical solution from Booker and Savvidou (1985), and "M" represents the modeling results using the saturated TPM model.

3.3.2 Comparison between TPM model and poro-mechanical (PM) model

This section shows that the Thermo-poro-mechanical (TPM) model can be reduced to be a Poro-mechanical (PM) model by setting the temperature change prescribed on the top surface to zero. Figure 3.7 shows the geometry of the soil column, with the height of 3 m and the radius of 1 m. The domain is discretized to ten elements to analyze this axisymmetric problem. For two models, the initial homogeneous temperature is 20 ^oC. The boundary conditions are assumed to be: impermeable for the lateral and the bottom surfaces; the lateral surface has fixed displacement in r direction, and the bottom surface has fixed displacement in z direction; the pore fluid pressure is held at zero due to the saturated condition; traction is applied on the top. For the TPM model, all the lateral and bottom surfaces are adiabatic. All parameters adopted in the two models are the same except for the thermal parameters that are only used in the TPM model (see Table 3.2). The process is: first, ramp up the gravity acceleration from 0 to 9.18 m/s^2, and keep it constant for the rest of the time; second, ramp up the traction from 0 to 90 kPa, and keep it constant for the rest of the simulation time. The variations of displacement and pore fluid pressure with depth in Figure 3.8(a) and Figure 3.8(b) show a good agreement between the reduced TPM model and the PM model. Figure 3.8(c) shows that the final pore fluid pressure arrives at the hydrostatic distribution.

Table 3.2: Constant parameters used in the comparison between TPM model and PM model

Parameter	Symbol	Value	Units
Thermal expansion coefficient of solid	α_s^θ	3×10^{-5}	$m/(m \cdot K)$
Thermal expansion coefficient of fluid	α_f^θ	2.07×10^{-4}	$m/(m \cdot K)$
Thermal expansion coefficient of skeleton	α_{skel}^θ	8.7×10^{-6}	$m/(m \cdot K)$
Specific heat capacity of solid	C_s	870	$J/(K \cdot kg)$
Specific heat capacity of fluid	C_f	4180	$J/(K \cdot kg)$
Thermal conductivity of solid	K_s^θ	5	$W/(m \cdot K)$
Intrinsic permeability	κ	1.326×10^{-14}	m^2
Lamé parameter	λ_{skel}	2.9×10^7	Pa
Lamé parameter	μ_{skel}	7×10^6	Pa
Traction on top	t^σ	9×10^4	Pa
Initial porosity	n_0	0.38	m^3/m^3
Viscosity of fluid (water)	μ_f	0.001	$Pa \cdot s$

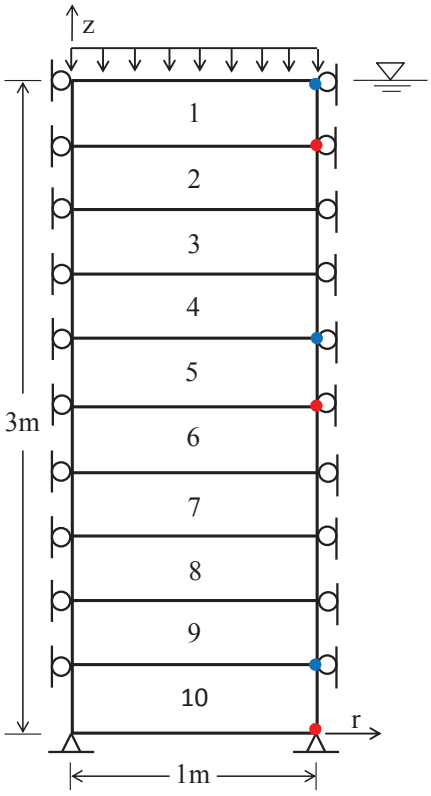

Figure 3.7: 10 element mesh

Figure 3.8: (a) Comparison of top displacement between TPM and PM models. (b) Comparison of pore fluid pressure at near top, middle and bottom between TPM and PM models. (c) Comparison of final pore fluid pressure distribution between TPM and PM models.

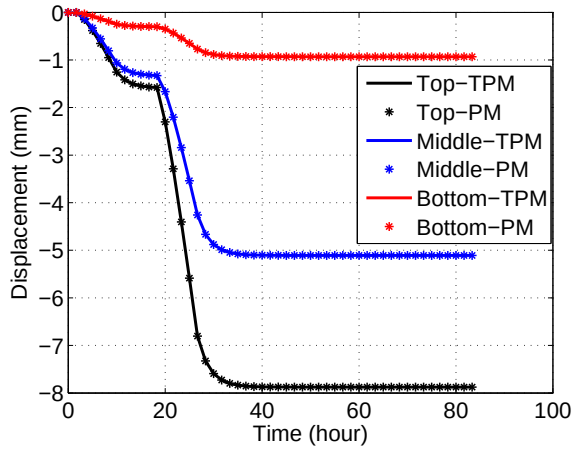

(a)

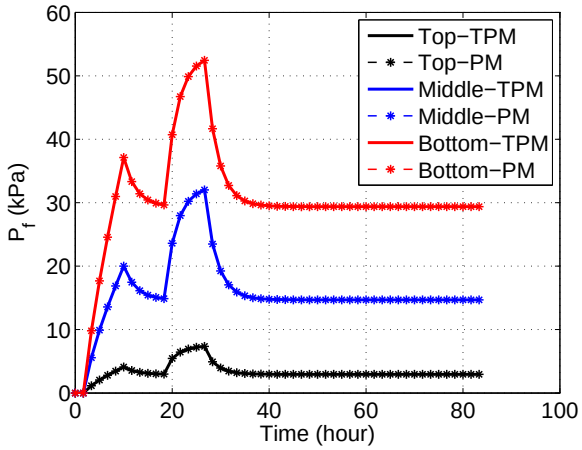

(b)

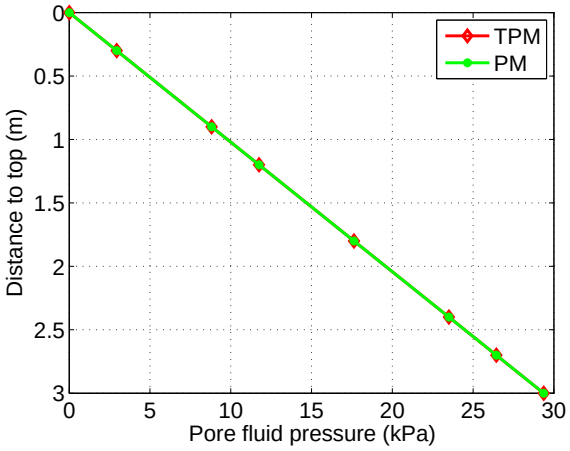

(c)

3.3.3 Comparison between TPM model and thermo-elastic (TE) model

This section shows that the Thermo-poro-mechanical (TPM) model can be reduced to be thermo-elastic (TE) model by setting the degree of freedoms (DOFs) of pore fluid pressure (p_f) to zero. Figure 3.9 shows the geometry, with the height of 0.3 m and radius of 0.1 m. The domain is discretized to ten elements to analyze this axisymmetric problem. For two models, the initial homogeneous temperature is 20 ^oC. The boundary conditions are assumed to be: no heat flux for the lateral and the bottom surfaces; the lateral surface is fixed in r direction, and the bottom surface is fixed in z direction; there is no traction on the top; and a temperature increase of 20 ^oC is prescribed on the top. For this case, the gravity is set to zero. For the TPM model, the pore water fluid pressure is set to zero initially, and all the lateral and bottom surfaces are impermeable. All parameters adopted in two models are the same (see Table 3.3) except for the hydraulic parameters only used in the TPM model. p_f will not be calculated in the reduced TPM model in which the DOFs of p_f are set to zero. The comparison of temperature and displacement of the chosen elements in Figure 3.10 shows a good agreement between the reduced TPM model and the TE model.

Table 3.3: Parameters used in the comparison between TPM model and TE model

Parameter	Symbol	Value	Units
Thermal expansion coefficient	α^{θ}_{skel}	11.7×10^{-4}	$m/(m \cdot K)$
Specific heat capacity	C_{mix}	1400	$J/(K \cdot kg)$
Thermal conductivity	K^{θ}_{mix}	0.817	$W/(m \cdot K)$
Mass density	ρ_{mix}	2500	kg/m^3
Lamé parameter	λ_{skel}	2.9×10^7	Pa
Lamé parameter	μ_{skel}	7×10^6	Pa

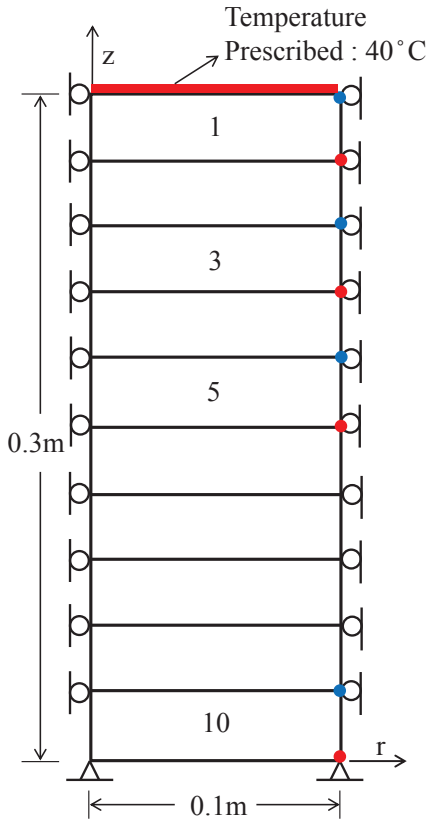

Figure 3.9: 10 element mesh

Figure 3.10: (a) Comparison of temperature between TPM and TE models. (b) Comparison of displacement between TPM and TE models.

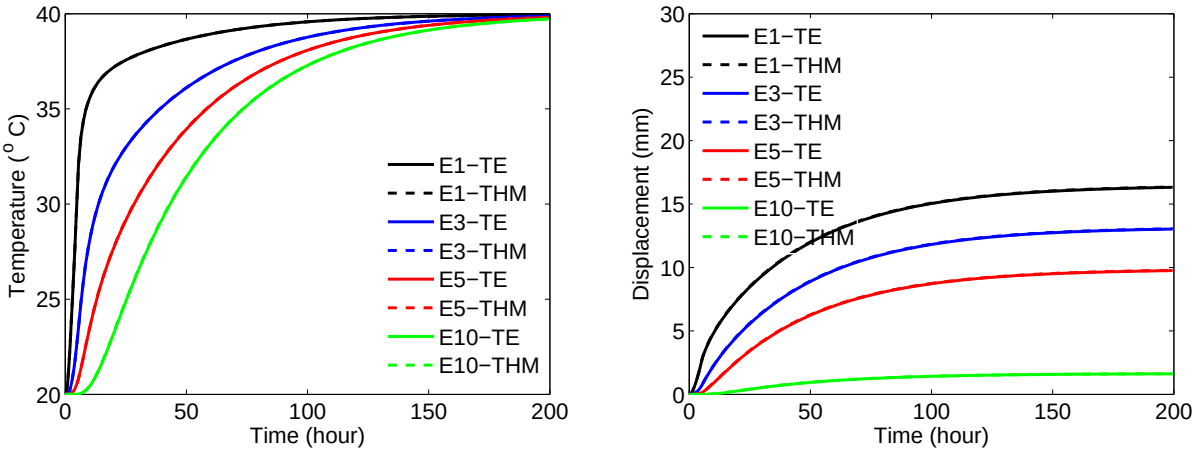

(a) (b)

Chapter 4

Partially saturated thermoporomechanics

In many processes, several fluids, such as two liquids or liquid and gas coexist in the pore space, so that the porous media is called partially saturated with respect to a reference fluid of main concern, usually chosen in liquid form (Coussy, 2004). This chapter introduces the thermo-poro-mechanical (TPM) coupling effects of partially saturated porous media, specially for soil.

4.1 Governing equations

Partially saturated porous media can be treated as a three-phase mixture, i.e. solid phase, liquid phase and gas phase. For soils, a water phase includes liquid water and air dissolved in water, while the latter is ignored in this thesis. The gas phase includes two constituents, which are water vapor (gv for "gas vapor") and dry air (ga for "gas air"). Therefore, the partially saturated soil is composed of four components, i.e., solid (s), liquid water (w), water vapor (gv), and dry air (ga). I refer to Coussy (2004); de Boer (2005); Lewis and Schrefler (1998) to formulate the governing equations using mixture theory at small strains of the solid skeleton ($skel$).

Similar to the saturated case, the governing equations include balance of mass, balance of linear momentum, and balance of energy, and are derived for each constituent. Phase change (vaporization) between liquid water and water vapor is considered through the latent heat. There are several possible combinations of primary variables that can be chosen (Lewis and Schrefler, 1998) for the partially saturated case. In my thesis, I choose the solid skeleton displacement $\boldsymbol{u}$, the temperature of the mixture θ, the pore water pressure p_w and pore gas pressure p_g as the four

primary variables to solve using nonlinear finite element analysis.

The notation used is as follows: the volume of the mixture is $v = v_s + v_w + v_g$, $v_g = v_{gv} + v_{ga}$ and the corresponding mass of the mixture is $m = m_s + m_w + m_g$. The differential mass of α $(\alpha = s, w, g)$ phase is written as $d\,m_\alpha = \rho^{\alpha R} dv_\alpha$, in which, $\rho^{\alpha R}$ is true mass density, and volume fraction of α phase $n^\alpha = dv_\alpha/dv$. Hence $m_\alpha = \rho^{\alpha R} n^\alpha dv$. $\rho^\alpha = n^\alpha \rho^{\alpha R}$ is defined to be partial mass density of α phase. One can show that,

$$\rho^s + \rho^w + \rho^g = \rho \tag{4.1}$$

$$n^s + n^w + n^g = n^s + n = 1 \tag{4.2}$$

$$n^w = \frac{dv_w}{dv};\ n^g = \frac{dv_g}{dv} \tag{4.3}$$

$$dv_{void} = dv_w + dv_g \tag{4.4}$$

$$S_w = \frac{n^w}{n} = \frac{n^w}{n^w + n^g} = \frac{dv_w}{dv_{void}} \tag{4.5}$$

$$n^w = nS_w\ , n^g = nS_g\ , S_w + S_g = 1 \tag{4.6}$$

$$S_w = \frac{dv_w}{dv_{void}};\ S_g = \frac{dv_g}{dv_{void}} \tag{4.7}$$

where n is porosity, S_w is the degree of water saturation, and S_g is the degree of gas saturation. ρ is the density of the soil mixture.

4.1.1 Balance of mass

The balance of mass for a partially saturated soil is similar to the balance of mass equation for the saturated condition, except that we need to consider the mass exchange term $\hat{\rho}^\alpha$ for partially saturated condition. The balance of mass for each constituent $\alpha(\alpha = s, w, ga, gv)$ is the same as (3.11), and the local form is:

$$\frac{D^\alpha \rho^\alpha}{D\,t} + \rho^\alpha \,\mathrm{div}\boldsymbol{v}_\alpha = \hat{\rho}^\alpha \tag{4.8}$$

where $\hat{\rho}^\alpha$ is the mass supply from the other phases per unit time per unit volume. Assuming $\hat{\rho}^s = \hat{\rho}^{ga} = 0$ (i.e., no dry air is convected from other constituents, and no solid is precipitated from other constituents), and $-\hat{\rho}^w = \hat{\rho}^g = \hat{\rho}^{gv}$, where, $\hat{\rho}^{gv}$ is the quantity of water lost through vaporization

per unit time per unit volume, which is positive. Writing the balance of mass equations for four constituents separately: for solid (s):

$$\frac{D^s\rho^s}{D\,t} + \rho^s \,\mathrm{div}\,\boldsymbol{v}_s = 0 \tag{4.9}$$

for water, (the air dissolved in water is ignored):

$$\frac{D^w\rho^w}{D\,t} + \rho^w \,\mathrm{div}\,\boldsymbol{v}_w = -\hat{\rho}^{gv} \tag{4.10}$$

for water vapor (gv):

$$\frac{D^{gv}\rho^{gv}}{Dt} + \rho^{gv} \,\mathrm{div}\,\boldsymbol{v}_{gv} = \hat{\rho}^{gv} \tag{4.11}$$

for dry air (ga):

$$\frac{D^{ga}\rho^{ga}}{Dt} + \rho^{ga} \,\mathrm{div}\,\boldsymbol{v}_{ga} = 0 \tag{4.12}$$

Using $\rho^\alpha = \rho^{\alpha R} n^\alpha$, and assuming the solid and water are mechanically incompressible (i.e., constant ρ^{sR} and ρ^{wR}), but allow thermal expansion (see (3.20) and (3.21)), we write (4.9) and (4.10) in the form:

$$\frac{D^s n^s}{D\,t} + n^s \mathrm{div}\boldsymbol{v}_s = \beta_s^\theta\, n^s \frac{D^s\theta}{D\,t} \tag{4.13}$$

$$\frac{D^w n^w}{D\,t} + n^w \mathrm{div}\boldsymbol{v}_w = \beta_w^\theta\, n^w \frac{D^w\theta}{D\,t} - \frac{\hat{\rho}^{gv}}{\rho^{wR}} \tag{4.14}$$

Use of (3.15) allows us to write (4.14) in the form:

$$\frac{D^s n^w}{D\,t} + n^w \mathrm{div}\boldsymbol{v}_w + \mathrm{grad} n^w \cdot \tilde{\boldsymbol{v}}_w = \beta_w^\theta\, n^w \frac{D^s\theta}{D\,t} + \beta_w^\theta n^w \mathrm{grad}\theta \cdot \tilde{\boldsymbol{v}}_w - \frac{\hat{\rho}^{gv}}{\rho^{wR}} \tag{4.15}$$

Substitution of $n^w = nS_w$ into (4.15) gives:

$$n\frac{D^s S_w}{D\,t} + S_w \frac{D^s n}{D\,t} + \mathrm{div}\,(n^w \tilde{\boldsymbol{v}}_w) + n^w \mathrm{div}\,\boldsymbol{v}_s = \beta_w^\theta\, nS_w \frac{D^s\theta}{D\,t} + \beta_w^\theta nS_w \mathrm{grad}\theta \cdot \tilde{\boldsymbol{v}}_w - \frac{\hat{\rho}^{gv}}{\rho^{wR}} \tag{4.16}$$

Use of $n^s = 1 - n$ in (4.13) gives the expression:

$$\frac{D^s n}{D\,t} = (1-n)\mathrm{div}\boldsymbol{v}_s - \beta_s^\theta\,(1-n)\frac{D^s\theta}{D\,t} \tag{4.17}$$

Substitution of (4.17) into (4.16) yields the balance of mass equation for liquid water:

$$S_w \mathrm{div}\, \boldsymbol{v}_s - S_w \left[(1-n)\beta_s^\theta + n\beta_w^\theta\right] \frac{D^s\theta}{D\,t} + n\frac{D^s S_w}{Dt} + \mathrm{div}\, \tilde{\boldsymbol{v}}_w^D - \beta_w^\theta \mathrm{grad}\,\theta \cdot \tilde{\boldsymbol{v}}_w^D = -\frac{\hat{\rho}^{gv}}{\rho^{wR}} \tag{4.18}$$

With the temperature dependent definition of real mass density of water,

$$\rho^{wR} = \rho^{wRo}\left[1 - \beta_w^\theta\,(\theta - \theta_0)\right] \tag{4.19}$$

one can derive,

$$\rho^{wR}\mathrm{div}\, \tilde{\boldsymbol{v}}_w^D - \rho^{wR}\beta_w^\theta \mathrm{grad}\,\theta \cdot \tilde{\boldsymbol{v}}_w^D = \rho^{wR}\mathrm{div}\, \tilde{\boldsymbol{v}}_w^D + \mathrm{grad}(\rho^{wR}) \cdot \tilde{\boldsymbol{v}}_w^D = \mathrm{div}(\rho^{wR}\, \tilde{\boldsymbol{v}}_w^D) \tag{4.20}$$

Thus, (4.18) becomes:

$$\rho^{wR} S_w \mathrm{div}\, \boldsymbol{v}_s - \rho^{wR} S_w \left[\beta_s^\theta(1-n) + n\beta_w^\theta\right] \frac{D^s\theta}{D\,t} + n\rho^{wR}\frac{D^s S_w}{Dt} + \mathrm{div}(\rho^{wR}\, \tilde{\boldsymbol{v}}_w^D) = -\hat{\rho}^{gv} \tag{4.21}$$

where $\tilde{\boldsymbol{v}}_\alpha^D = n^\alpha(\boldsymbol{v}_\alpha - \boldsymbol{v}_s)$ is the filtration vector associated with fluid constituent α ($\alpha = w, g$) (Coussy, 2004).

The gas phase is composed of two different species, which are dry air (ga) and water vapor (gv), which are miscible, so that they share the same volume fraction $n^g = nS_g$, where, $S_g = 1 - S_w$. Thus the partial mass densities of the water vapor and dry air are expressed in the form:

$$\rho^{gv} = n^g \rho^{gvR} \tag{4.22}$$

$$\rho^{ga} = n^g \rho^{gaR} \tag{4.23}$$

The ideal gas law is applied to the gas phase, such that the real mass density functions are written in the form:

$$\rho^{gvR} = \frac{p_{\mathrm{gv}} M_w}{\theta R} \tag{4.24}$$

$$\rho^{gaR} = \frac{p_{\mathrm{ga}} M_a}{\theta R} \tag{4.25}$$

where p_{gv} and p_{ga} are pore pressure of water vapor and dry air, respectively, M_w and M_a are molar mass of constituent water and air, and R is the universal gas constant. The real mass density of the gas phase is simply the superposition of its two components:

$$\rho^{gR} = \rho^{gaR} + \rho^{gvR} \tag{4.26}$$

According to (4.24) we have

$$\begin{aligned}\frac{D^{gv}\rho^{gvR}}{Dt} &= \frac{M_w}{R}\left(\frac{1}{\theta}\frac{D^{gv}p_{gv}}{Dt}-\frac{1}{\theta^2}\frac{D^{gv}\theta}{Dt}\right)\\ &= \frac{p_{gv}M_{\mathrm{w}}}{\theta R}\left(\frac{1}{p_{gv}}\frac{D^{gv}p_{gv}}{Dt}-\frac{1}{\theta}\frac{D^{gv}\theta}{Dt}\right)\\ &= \rho^{gvR}\left(\frac{1}{p_{gv}}\frac{D^{gv}p_{gv}}{Dt}-\frac{1}{\theta}\frac{D^{gv}\theta}{Dt}\right)\end{aligned} \tag{4.27}$$

Substitute (4.27) into (4.11), and divide ρ^{gvR} on both sides, we get:

$$\frac{D^{gv}n^g}{D\,t}+n^g\mathrm{div}\boldsymbol{v}_{gv}+n^g\left(\frac{1}{p_{gv}}\frac{D^{gv}p_{gv}}{Dt}-\frac{1}{\theta}\frac{D^{gv}\theta}{Dt}\right)=\frac{\hat{\rho}^{gv}}{\rho^{gvR}} \tag{4.28}$$

Use

$$\frac{D^{gv}(\bullet)}{Dt}=\frac{D^{s}(\bullet)}{Dt}+\mathrm{grad}(\bullet)\cdot\tilde{\boldsymbol{v}}_{gv} \tag{4.29}$$

and substitute $n^g = nS_g$ and (4.17) into (4.28), we can obtain the balance of mass equation for water vapor:

$$\begin{aligned}&S_g\mathrm{div}\,\boldsymbol{v}_s-S_g\left[\beta_s^{\theta}(1-n)+\frac{n}{\theta}\right]\frac{D^s\theta}{D\,t}+n\frac{D^sS_g}{Dt}+\mathrm{div}\,\tilde{\boldsymbol{v}}_{gv}^{D}\\ &-\frac{1}{\theta}\mathrm{grad}\,\theta\cdot\tilde{\boldsymbol{v}}_{gv}^{D}+\frac{n^g}{p_{gv}}\frac{D^sp_{gv}}{Dt}+\frac{1}{p_{gv}}\mathrm{grad}\,(p_{gv})\cdot\tilde{\boldsymbol{v}}_{gv}^{D}=\frac{\hat{\rho}^{gv}}{\rho^{gvR}}\end{aligned} \tag{4.30}$$

where $\tilde{\boldsymbol{v}}_{gv}^{D}=n^g\tilde{\boldsymbol{v}}_{gv}$. Use (4.24) to obtain:

$$-\rho^{gvR}S_g\frac{n}{\theta}\frac{D^s\theta}{D\,t}+\frac{\rho^{gvR}n^g}{p_{gv}}\frac{D^sp_{gv}}{Dt}=nS_g\frac{D^s\rho^{gvR}}{Dt} \tag{4.31}$$

and,

$$\begin{aligned}&\rho^{gvR}\mathrm{div}\,\tilde{\boldsymbol{v}}_{gv}^{D}-\frac{\rho^{gvR}}{\theta}\mathrm{grad}\,\theta\cdot\tilde{\boldsymbol{v}}_{gv}^{D}+\frac{\rho^{gvR}}{p_{gv}}\mathrm{grad}\,p_{gv}\cdot\tilde{\boldsymbol{v}}_{gv}^{D}\\ =&\rho^{gvR}\mathrm{div}\,\tilde{\boldsymbol{v}}_{gv}^{D}+\mathrm{grad}(\rho^{gvR})\cdot\tilde{\boldsymbol{v}}_{gv}^{D}=\mathrm{div}(\rho^{gvR}\,\tilde{\boldsymbol{v}}_{gv}^{D})\end{aligned} \tag{4.32}$$

Thus, (4.30) becomes:

$$\rho^{gvR}S_g\mathrm{div}\,\boldsymbol{v}_s-\rho^{gvR}S_g\beta_s^{\theta}(1-n)\frac{D^s\theta}{D\,t}+n\rho^{gvR}\frac{D^sS_g}{Dt}+nS_g\frac{D^s\rho^{gvR}}{Dt}+\mathrm{div}(\rho^{gvR}\,\tilde{\boldsymbol{v}}_{gv}^{D})=\hat{\rho}^{gv} \tag{4.33}$$

Combining (4.21) and (4.33) allows us to write the balance equation of mass for water species (liquid water + water vapor) as follows:

$$
\begin{aligned}
&(\rho^{wR}S_w + \rho^{gvR}S_g)\mathrm{div}\,\boldsymbol{v}_s - \left[(1-n)(\rho^{wR}S_w + \rho^{gvR}S_g)\beta_s^\theta + n\rho^{wR}S_w\beta_w^\theta\right]\frac{D^s\theta}{D\,t} \\
&+ n(\rho^{wR} - \rho^{gvR})\frac{D^sS_w}{Dt} + nS_g\frac{D^s\rho^{gvR}}{Dt} + \mathrm{div}(\rho^{gvR}\,\tilde{\boldsymbol{v}}_{gv}^D + \rho^{wR}\,\tilde{\boldsymbol{v}}_w^D) = 0
\end{aligned}
\tag{4.34}
$$

We follow the same procedure as we used to derive for water vapor to obtain the balance of mass equation for dry air:

$$
\begin{aligned}
&S_g\mathrm{div}\,\boldsymbol{v}_s - S_g\left[\beta_s^\theta(1-n) + \frac{n}{\theta}\right]\frac{D^s\theta}{D\,t} + n\frac{D^sS_g}{Dt} + \mathrm{div}\,\tilde{\boldsymbol{v}}_{ga}^D \\
&- \frac{\mathrm{grad}\,\theta}{\theta}\cdot\tilde{\boldsymbol{v}}_{ga}^D + \frac{n^g}{p_{ga}}\frac{D^sp_{ga}}{Dt} + \frac{1}{p_{ga}}\mathrm{grad}\,p_{ga}\cdot\tilde{\boldsymbol{v}}_{ga}^D = 0
\end{aligned}
\tag{4.35}
$$

Use (4.25) to obtain:

$$
-S_g\frac{n}{\theta}\frac{D^s\theta}{D\,t} + \frac{n^g}{p_{ga}}\frac{D^sp_{ga}}{Dt} = \frac{nS_g}{\rho^{gaR}}\frac{D^s\rho^{gaR}}{Dt}
\tag{4.36}
$$

and,

$$
\mathrm{div}\,\tilde{\boldsymbol{v}}_{ga}^D - \frac{\mathrm{grad}\,\theta}{\theta}\cdot\tilde{\boldsymbol{v}}_{ga}^D + \frac{1}{p_{ga}}\mathrm{grad}\,p_{ga}\cdot\tilde{\boldsymbol{v}}_{ga}^D = \frac{1}{\rho^{gaR}}\mathrm{div}(\rho^{gaR}\,\tilde{\boldsymbol{v}}_{ga}^D)
\tag{4.37}
$$

Substitute (4.36) and 4.37) into (4.35) and multiply by ρ^{gaR} on both sides to get the balance of mass equation for dry air as follows:

$$
\rho^{gaR}S_g\mathrm{div}\,\boldsymbol{v}_s - \rho^{gaR}S_g\beta_s^\theta(1-n)\frac{D^s\theta}{D\,t} + nS_g\frac{D^s\rho^{gaR}}{Dt} - n\rho^{gaR}\frac{D^sS_w}{Dt} + \mathrm{div}(\rho^{gaR}\,\tilde{\boldsymbol{v}}_{ga}^D) = 0
\tag{4.38}
$$

4.1.2 Balance of linear momentum

Let us follow the same procedure as the one we used for saturated condition. If we substitute (4.8) into (3.27), and ignore the acceleration of gravity $\boldsymbol{a}_\alpha$, we have:

$$
\frac{D^\alpha}{Dt}\int_\Omega \rho^\alpha\boldsymbol{v}_\alpha dv = \int_\Omega \hat{\rho}^\alpha\boldsymbol{v}_\alpha dv
\tag{4.39}
$$

Substitute (3.31) and (4.39) into (3.25), we arrive at the local form of the balance of linear momentum equation for constituent α:

$$
\nabla\cdot\boldsymbol{\sigma}^\alpha + \rho^\alpha\boldsymbol{b}^\alpha + \hat{\boldsymbol{h}}^\alpha = \hat{\rho}^\alpha\boldsymbol{v}_\alpha
\tag{4.40}
$$

where $\boldsymbol{\sigma}^\alpha$ is the partial stress of the α phase, $\boldsymbol{\sigma}^\alpha = n^\alpha\boldsymbol{\sigma}$; and the total stress is: $\boldsymbol{\sigma} = \boldsymbol{\sigma}^s + \boldsymbol{\sigma}^w + \boldsymbol{\sigma}^g$; $\boldsymbol{b}^\alpha$ is the body force vector per unit mass of α phase, which we assume is equal to acceleration of

gravity: $\boldsymbol{b}^\alpha = \boldsymbol{b} = \boldsymbol{g}$; $\hat{\rho}^\alpha \boldsymbol{v}_\alpha$ is the contribution to momentum of constituent α due to mass exchange with other constituents; $\hat{\boldsymbol{h}}^\alpha$ is the internal body force drag of other constituents on constituent α, where

$$\sum_{\alpha=s,w,g} \hat{\boldsymbol{h}}^\alpha = \boldsymbol{0} \tag{4.41}$$

According to de Boer (2005), $\sum(\hat{\rho}^\alpha \boldsymbol{v}_\alpha) \approx 0$. Thus, the balance of linear momentum equation for the partially saturated mixture looks the same as that for saturated condition, except that the effective stress equation is different, and mass density includes more terms.

$$\mathrm{div}(\boldsymbol{\sigma}) + \rho \boldsymbol{g} = \boldsymbol{0} \tag{4.42}$$

4.1.3 Energy conservation

4.1.3.1 1st law of thermodynamics

The first law of thermodynamics written for constituent α (de Boer, 2005)

$$\dot{E}^\alpha + \dot{K}^\alpha = P^\alpha + \dot{Q}^\alpha + \int_\Omega \hat{e}^\alpha dv \tag{4.43}$$

where $\dot{E}^\alpha$, $\dot{K}^\alpha$, P^α, $\dot{Q}^\alpha$ and $\hat{e}^\alpha$ are the same as those in (3.35). With the balance of mass equation (4.8), (3.43) is written for partially saturated condition in the form:

$$\dot{E}^\alpha + \dot{K}^\alpha = \int_\Omega \left[\hat{\rho}^\alpha \left(\frac{\boldsymbol{v}_\alpha \cdot \boldsymbol{v}_\alpha}{2} + e^\alpha \right) + \rho^\alpha \frac{D^\alpha e^\alpha}{D\, t} \right] dv \tag{4.44}$$

Substituting the balance of linear momentum (4.40) into (3.45), we get the expression of the input power on α constituent:

$$P^\alpha = \int_\Omega \left[\boldsymbol{\sigma}^\alpha : \frac{D^\alpha \boldsymbol{\epsilon}^\alpha}{Dt} + (\hat{\rho}^\alpha \boldsymbol{v}_\alpha - \hat{\boldsymbol{h}}^\alpha) \cdot \boldsymbol{v}_\alpha \right] dv \tag{4.45}$$

The rate of heat supply $\dot{Q}^\alpha$ is:

$$\dot{Q}^\alpha = \int_\Omega (\rho^\alpha r^\alpha - \mathrm{div} \boldsymbol{q}^\alpha)\, dv \tag{4.46}$$

Substitution of (4.44), (4.45), and (4.46) into(4.43) allows us to write the local form of the balance of energy equation for constituent α:

$$\rho^\alpha \frac{D^\alpha e^\alpha}{Dt} - \boldsymbol{\sigma}^\alpha : \frac{D^\alpha \boldsymbol{\epsilon}^\alpha}{Dt} + \hat{\boldsymbol{h}}^\alpha \cdot \boldsymbol{v}_\alpha - \frac{1}{2} \hat{\rho}^\alpha \boldsymbol{v}_\alpha \cdot \boldsymbol{v}_\alpha - \rho^\alpha r^\alpha + \mathrm{div} \boldsymbol{q}^\alpha + \hat{\rho}^\alpha e^\alpha - \hat{e}^\alpha = 0 \tag{4.47}$$

Summing up (4.47) over $\alpha = s, w, g$, and with the assumption (de Boer, 2005):

$$\sum_{\alpha=s,w,g} \hat{e}^{\alpha} = 0 \tag{4.48}$$

we get the balance of energy equation for the mixture in the form:

$$\sum_{\alpha=s,w,g} \left(\rho^{\alpha} \frac{D^{\alpha} e^{\alpha}}{Dt} - \boldsymbol{\sigma}^{\alpha} : \frac{D^{\alpha} \boldsymbol{\epsilon}^{\alpha}}{Dt} + \hat{\boldsymbol{h}}^{\alpha} \cdot \boldsymbol{v}_{\alpha} - \frac{1}{2} \hat{\rho}^{\alpha} \boldsymbol{v}_{\alpha} \cdot \boldsymbol{v}_{\alpha} - \rho^{\alpha} r^{\alpha} + \mathrm{div} \boldsymbol{q}^{\alpha} + \hat{\rho}^{\alpha} e^{\alpha} \right) = 0 \tag{4.49}$$

4.1.3.2 The second law of thermodynamics

The entropy inequality for constituent α of a partially saturated porous media is:

$$\frac{D^{\alpha}}{D\,t} \int_{\Omega} \rho^{\alpha} \eta^{\alpha} dv \geq \int_{\Omega} \frac{\rho^{\alpha} r^{\alpha}}{\theta^{\alpha}} dv - \int_{\partial\Omega} \frac{\boldsymbol{q}^{\alpha} \cdot \boldsymbol{n}}{\theta^{\alpha}} da \tag{4.50}$$

Using (3.8) and the balance of mass equation (4.8), we obtain:

$$\frac{D^{\alpha}}{D\,t} \int_{\Omega} \rho^{\alpha} \eta^{\alpha} dv = \int_{\Omega} \rho^{\alpha} \frac{D^{\alpha} \eta^{\alpha}}{D\,t}\, dv + \int_{\Omega} \hat{\rho}^{\alpha} \eta^{\alpha}\, dv \tag{4.51}$$

Applying the divergence theorem, we derive:

$$\int_{\partial\Omega} \frac{\boldsymbol{q}^{\alpha} \cdot \boldsymbol{n}}{\theta^{\alpha}} da = \int_{\Omega} \left[\frac{\mathrm{div} \boldsymbol{q}^{\alpha}}{\theta^{\alpha}} - \frac{\boldsymbol{q}^{\alpha} \cdot \mathrm{grad}\, \theta^{\alpha}}{(\theta^{\alpha})^2} \right] dv \tag{4.52}$$

Substitution of (4.51) and (4.52) into (4.50) gives an expression of the entropy inequality in the local form:

$$\rho^{\alpha} \theta^{\alpha} \frac{D^{\alpha} \eta^{\alpha}}{D\,t} + \hat{\rho}^{\alpha} \eta^{\alpha} \theta^{\alpha} - \rho^{\alpha} r^{\alpha} + \mathrm{div}(\boldsymbol{q}^{\alpha}) - \frac{\boldsymbol{q}^{\alpha} \cdot \mathrm{grad}\, \theta^{\alpha}}{\theta^{\alpha}} \geq 0 \tag{4.53}$$

In order to consider the liquid-vapor phase change, the Gibbs potential g^f is introduced for the fluid constituents:

$$g^f = \psi^f - \theta^f \eta^f, \quad f = w, gv, ga \tag{4.54}$$

The internal energy per unit mass is in turn expressed as:

$$e^f = \psi^f - \frac{p_f}{\rho^{fR}} \tag{4.55}$$

where ψ^f is the Helmholtz free energy per unit mass, and p_f is the pore fluid pressure. Combining (4.54) and (4.55), we can relate e^f and g^f in the form:

$$e^f = g^f + \theta^f \eta^f - \frac{p_f}{\rho^{fR}} \tag{4.56}$$

and the material time derivative of internal energy:

$$\frac{D^f e^f}{Dt} = \frac{D^f g^f}{Dt} + \theta^f \frac{D^f \eta^f}{Dt} + \eta^f \frac{D^f \theta^f}{Dt} - \frac{1}{\rho^{fR}} \frac{D^f p_f}{Dt} + \frac{p_f}{(\rho^{fR})^2} \frac{D^f \rho^{fR}}{Dt} \tag{4.57}$$

According to $\rho^f = n^f \rho^{fR}$, we get:

$$\frac{D^f \rho^f}{Dt} = n^f \frac{D^f \rho^{fR}}{Dt} + \rho^{fR} \frac{D^f n^f}{Dt} \tag{4.58}$$

Combining the balance of mass equation (4.8) and (4.58), we have:

$$\begin{aligned} \frac{D^f \rho^{fR}}{Dt} &= \frac{1}{n^f} \left(\frac{D^f \rho^f}{Dt} - \rho^{fR} \frac{D^f n^f}{Dt} \right) \\ &= \frac{1}{n^f} \left(-\rho^f \operatorname{div}(\boldsymbol{v}_f) + \hat{\rho}^f - \rho^{fR} \frac{D^f n^f}{Dt} \right) \\ &= -\rho^{fR} \operatorname{div}(\boldsymbol{v}_f) + \frac{\hat{\rho}^f}{n^f} - \frac{\rho^{fR}}{n^f} \frac{D^f n^f}{Dt} \end{aligned} \tag{4.59}$$

Substituting (4.59) into (4.57), we get:

$$\begin{aligned} \rho^f \theta^f \frac{D^f \eta^f}{Dt} &= \rho^f \frac{D^f e^f}{Dt} - \rho^f \frac{D^f g^f}{Dt} - \rho^f \eta^f \frac{D^f \theta^f}{Dt} + n^f \frac{D^f p_f}{Dt} \\ &\quad - \frac{\rho^f p_f}{(\rho^{fR})^2} \left(-\rho^{fR} \operatorname{div}(\boldsymbol{v}_f) + \frac{\hat{\rho}^f}{n^f} - \frac{\rho^{fR}}{n^f} \frac{D^f n^f}{Dt} \right) \\ &= \rho^f \frac{D^f e^f}{Dt} - \rho^f \frac{D^f g^f}{Dt} - \rho^f \eta^f \frac{D^f \theta^f}{Dt} + n^f \frac{D^f p_f}{Dt} \\ &\quad + n^f p_f \operatorname{div}(\boldsymbol{v}_f) - \frac{p_f}{\rho^{fR}} \hat{\rho}^f + p_f \frac{D^f n^f}{Dt} \end{aligned} \tag{4.60}$$

From the balance of energy (4.47) with $\alpha = f$, we get:

$$\rho^f \frac{D^f e_f}{Dt} = \boldsymbol{\sigma}^f : \frac{D^f \boldsymbol{\epsilon}^f}{Dt} - \hat{\rho}^f e^f + \frac{1}{2} \hat{\rho}^f \boldsymbol{v}_f \cdot \boldsymbol{v}_f - \hat{\boldsymbol{h}}^f \cdot \boldsymbol{v}_f - \operatorname{div}(\boldsymbol{q}^f) + \rho^f r^f + \hat{e}^f \tag{4.61}$$

Substitute (4.61) into (4.60), and then substitute the expression of $\rho^f \theta^f \frac{D^f \eta^f}{Dt}$ into the entropy inequality (4.53) with $\alpha = f$, we have:

$$\begin{aligned} &\left[\boldsymbol{\sigma}^f : \frac{D^f \boldsymbol{\epsilon}^f}{Dt} - \hat{\rho}^f e^f + \frac{1}{2} \hat{\rho}^f \boldsymbol{v}_f \cdot \boldsymbol{v}_f - \hat{\boldsymbol{h}}^f \cdot \boldsymbol{v}_f \cancel{- \operatorname{div}(\boldsymbol{q}^f) + \rho^f r^f} + \hat{e}^f \right] - \rho^f \frac{D^f g^f}{Dt} \\ &- \rho^f \eta^f \frac{D^f \theta^f}{Dt} + n^f \frac{D^f p_f}{Dt} + n^f p_f \operatorname{div}(\boldsymbol{v}_f) - \frac{p_f}{\rho^{fR}} \hat{\rho}^f + p_f \frac{D^f n^f}{Dt} + \hat{\rho}^f \eta^f \theta^f \\ &\cancel{+ \operatorname{div}(\boldsymbol{q}^f) - \rho^f r^f} - \frac{\boldsymbol{q}^f \cdot \operatorname{grad} \theta^f}{\theta^f} \geq 0 \end{aligned} \tag{4.62}$$

where terms in [ ] are from (4.61), and where, according to (3.69),

$$\boldsymbol{\sigma}^f : \frac{D^f \boldsymbol{\epsilon}^f}{Dt} = -n^f p_f \,\mathrm{div}\,(\boldsymbol{v}_f) \tag{4.63}$$

so that, $\boldsymbol{\sigma}^f : \frac{D^f \boldsymbol{\epsilon}^f}{Dt}$ and $n^f p_f \mathrm{div}(\boldsymbol{v}_f)$ in (4.62) will cancel each other out in (4.62). We introduce the definition of enthalpy per unit mass:

$$H^\alpha = e^\alpha + \frac{p_\alpha}{\rho^{\alpha R}} \tag{4.64}$$

Let us combine the following two terms in (4.62), and with (4.64), we derive:

$$-\hat{\rho}^f e^f - \frac{p_f}{\rho^{fR}}\hat{\rho}^f = -\hat{\rho}^f \left(e^f + \frac{p_f}{\rho^{fR}} \right) = -\hat{\rho}^f H^f \tag{4.65}$$

where H^f is the enthalpy of fluid constituent per unit mass, and is written in terms of the Gibbs potential g^f and the entropy of fluid in this way:

$$H^f = g^f + \eta^f \theta^f \tag{4.66}$$

With (4.66), the term $\hat{\rho}^f \eta^f \theta^f$ in (4.62) can be written as:

$$\hat{\rho}^f \eta^f \theta^f = \hat{\rho}^f (H^f - g^f) \tag{4.67}$$

Combining (4.65) and (4.67), we obtain:

$$\hat{\rho}^f \eta^f \theta^f - \hat{\rho}^f e^f - \frac{p_f}{\rho^{fR}}\hat{\rho}^f = -\hat{\rho}^f g^f \tag{4.68}$$

According to Coussy (2004)(chapter 6), the local thermodynamic equilibrium between the liquid water and water vapor requires their Gibbs potentials to be equal:

$$g^w = g^{gv} \tag{4.69}$$

Since $\hat{\rho}^w = -\hat{\rho}^{gv}$, we have

$$\hat{\rho}^w \, g^w + \hat{\rho}^{gv} \, g^{gv} = 0 \tag{4.70}$$

Let us apply (4.62) to the liquid water, water vapor, and dry air, and sum up the three inequalities to get the entropy inequality of the fluids:

$$\sum_{f=w,gv,ga}\left[-\hat{\boldsymbol{h}}^f\cdot\boldsymbol{v}_f+\frac{1}{2}\hat{\rho}^f\boldsymbol{v}_f\cdot\boldsymbol{v}_f+\hat{e}^f-\rho^f\frac{D^f g^f}{Dt}-\rho^f\eta^f\frac{D^f\theta^f}{Dt}\right.$$
$$\left.+n^f\frac{D^f p_f}{Dt}+p_f\frac{D^f n^f}{Dt}-\frac{\boldsymbol{q}^f\cdot\operatorname{grad}\theta^f}{\theta^f}\right]\geq 0 \tag{4.71}$$

According to Coussy (2004), the Gibbs potential of fluid $g^f(p_f,\theta^f)$ depends on the pore fluid pressure p_f and the temperature of the fluid θ^f, thus the material time derivative of g^f is written in the form:

$$\frac{D^f g^f}{Dt}=\frac{\partial g^f}{\partial p_f}\frac{D^f p_f}{Dt}+\frac{\partial g^f}{\partial\theta^f}\frac{D^f\theta^f}{Dt} \tag{4.72}$$

Substitution of (4.72) into (4.71) gives an alternative expression of the entropy inequality of the fluid phase in the form:

$$\sum_{f=w,g}\left[-\hat{\boldsymbol{h}}^f\cdot\boldsymbol{v}_f+\frac{1}{2}\hat{\rho}^f\boldsymbol{v}_f\cdot\boldsymbol{v}_f+\hat{e}^f-\rho^f\frac{\partial g^f}{\partial p_f}\frac{D^f p_f}{Dt}-\rho^f\frac{\partial g^f}{\partial\theta^f}\frac{D^f\theta^f}{Dt}\right.$$
$$\left.-\rho^f\eta^f\frac{D^f\theta^f}{Dt}+n^f\frac{D^f p_f}{Dt}+p_f\frac{D^f n^f}{Dt}-\frac{\boldsymbol{q}^f\cdot\operatorname{grad}\theta^f}{\theta^f}\right]\geq 0 \tag{4.73}$$

Similar to the saturated condition, we adopt the Helmholtz free energy per unit mass ψ^s for solid phase:

$$\psi^s=e^s-\theta^s\eta^s \tag{4.74}$$

Thus, the material time derivative of ψ^s is written in the form:

$$\frac{D^s\psi^s}{Dt}=\frac{D^s e^s}{Dt}-\theta^s\frac{D^s\eta^s}{Dt}-\eta^s\frac{D^s\theta^s}{Dt} \tag{4.75}$$

From the balance of energy (3.47) with $\alpha=s$, we get an expression of $\rho^s\frac{D^s e^s}{Dt}$ in the form:

$$\rho^s\frac{D^s e^s}{Dt}=\boldsymbol{\sigma}^s:\frac{D^s\boldsymbol{\epsilon}^s}{Dt}-\hat{\boldsymbol{h}}^s\cdot\boldsymbol{v}_s-\operatorname{div}(\boldsymbol{q}^s)+\rho^s r^s+\hat{e}^s \tag{4.76}$$

Combining (4.75) and (4.76), we have:

$$\rho^s\theta^s\frac{D^s\eta^s}{Dt}=\boldsymbol{\sigma}^s:\frac{D^s\boldsymbol{\epsilon}^s}{Dt}-\hat{\boldsymbol{h}}^s\cdot\boldsymbol{v}_s-\operatorname{div}(\boldsymbol{q}^s)+\rho^s r^s+\hat{e}^s-\rho^s\eta^s\frac{D^s\theta^s}{Dt}-\rho^s\frac{D^s\psi^s}{Dt} \tag{4.77}$$

The total stress tensor $\boldsymbol{\sigma}$ is written as the sum of the partial stress tensors of each phase: $\boldsymbol{\sigma}^w$, $\boldsymbol{\sigma}^g$, and $\boldsymbol{\sigma}^s$ (de Boer, 2005; Coussy, 2004) (ignoring viscosity for water and gas):

$$\boldsymbol{\sigma} = \boldsymbol{\sigma}^w + \boldsymbol{\sigma}^g + \boldsymbol{\sigma}^s \tag{4.78}$$

$$\boldsymbol{\sigma}^w = -n^w\, p_w \mathbf{1} \tag{4.79}$$

$$\boldsymbol{\sigma}^g = -n^g\, p_g \mathbf{1} \tag{4.80}$$

A combination of (4.78)-(4.80) provides:

$$\boldsymbol{\sigma}^s = \boldsymbol{\sigma} + (n^w p_w + n^g p_g)\, \mathbf{1} \tag{4.81}$$

The relationship between the total stress tensor and the effective stress tensor is written as (Bishop and Blight, 1963)

$$\boldsymbol{\sigma} = \boldsymbol{\sigma}' - \bar{p}\, \mathbf{1} \tag{4.82}$$

where $\boldsymbol{\sigma}'$ is the effective stress tensor, and $\bar{p}$ is called averaged pore pressure, which is defined as:

$$\bar{p} = (1-\chi) p_g + \chi p_w \tag{4.83}$$

where χ is the effective stress parameter ($\chi = 1$ for saturated condition with water; $\chi = 0$ for dry condition). Combining (4.81)-(4.83) gives:

$$\boldsymbol{\sigma}^s = \boldsymbol{\sigma}' + [n^g - (1-\chi)]\, p_g \mathbf{1} + (n^w - \chi) p_w \mathbf{1} \tag{4.84}$$

Therefore, substituting (3.63) and (4.84), we derive:

$$\boldsymbol{\sigma}^s : \frac{D^s \boldsymbol{\epsilon}^s}{Dt} = \boldsymbol{\sigma}' : \frac{D^s \boldsymbol{\epsilon}^s}{Dt} + \{[n^g - (1-\chi)]\, p_g + (n^w - \chi) p_w\} \operatorname{div} \boldsymbol{v}_s \tag{4.85}$$

Let us revisit the definition of the total strain of the solid skeleton (3.65), we have:

$$\boldsymbol{\sigma}^s : \frac{D^s \boldsymbol{\epsilon}^s}{Dt} = \boldsymbol{\sigma}' : \frac{D^s \boldsymbol{\epsilon}^{skel,e}}{Dt} + \alpha^{\theta}_{skel} \mathrm{tr}(\boldsymbol{\sigma}') \frac{D^s \theta^s}{Dt} + \{[n^g - (1-\chi)]\, p_g + (n^w - \chi) p_w\} \operatorname{div} \boldsymbol{v}_s \tag{4.86}$$

Setting $\alpha = s$, and $\hat{\rho}^s = 0$ in (4.53), we write the entropy inequality for the solid skeleton:

$$\rho^s \theta^s \frac{D^s \eta^s}{D\, t} - \rho^s r^s + \operatorname{div}(\boldsymbol{q}^s) - \frac{\boldsymbol{q}^s \cdot \operatorname{grad} \theta^s}{\theta^s} \geq 0 \tag{4.87}$$

Substitution of (4.86) into (4.77), and then (4.87) is written as:

$$\begin{aligned}&\boldsymbol{\sigma}' : \frac{D^s \boldsymbol{\epsilon}^{skel,e}}{Dt} + \alpha^{\theta}_{skel}\mathrm{tr}(\boldsymbol{\sigma}')\frac{D^s\theta^s}{Dt} + \{[n^g - (1-\chi)]\, p_g + (n^w - \chi)p_w\}\,\mathrm{div}\,\boldsymbol{v}_s - \hat{\boldsymbol{h}}^{s}\cdot\boldsymbol{v}_s \\ &\cancel{-\mathrm{div}(\boldsymbol{q}^s) + \rho^s r^s} + \hat{e}^s - \rho^s\eta^s\frac{D^s\theta^s}{Dt} - \rho^s\frac{D^s\psi^s}{Dt} \cancel{+\mathrm{div}(\boldsymbol{q}^s) - \rho^s r^s} - \frac{\boldsymbol{q}^s\cdot\mathrm{grad}\,\theta^s}{\theta^s} \geq \mathbf{0}\end{aligned} \tag{4.88}$$

Let us derive the internal force drag term $\hat{\boldsymbol{h}}^{\alpha}$, and recall

$$\hat{\boldsymbol{h}}^{s} + \hat{\boldsymbol{h}}^{w} + \hat{\boldsymbol{h}}^{g} = 0 \tag{4.89}$$

From the balance of linear momentum equation (4.40), we derive for water and gas phases:

$$\hat{\boldsymbol{h}}^{w} = -\mathrm{div}(\boldsymbol{\sigma}^w) - \rho^w\boldsymbol{b} + \hat{\rho}^w\boldsymbol{v}_w \tag{4.90}$$

$$\hat{\boldsymbol{h}}^{g} = -\mathrm{div}(\boldsymbol{\sigma}^g) - \rho^w\boldsymbol{b} + \hat{\rho}^g\boldsymbol{v}_g \tag{4.91}$$

in which, according to (3.72):

$$\mathrm{div}(\boldsymbol{\sigma}^w) = -p_w\,\mathrm{grad}(n^w) - n^w\,\mathrm{grad}(p_w) \tag{4.92}$$

$$\mathrm{div}(\boldsymbol{\sigma}^g) = -p_g\,\mathrm{grad}(n^g) - n^g\,\mathrm{grad}(p_g) \tag{4.93}$$

A combination of (4.89), (4.92) and (4.93) allows us to write:

$$\begin{aligned}&\hat{\boldsymbol{h}}^{w}\cdot\boldsymbol{v}_w + \hat{\boldsymbol{h}}^{g}\cdot\boldsymbol{v}_g + \hat{\boldsymbol{h}}^{s}\cdot\boldsymbol{v}_s \\ =&\hat{\boldsymbol{h}}^{w}\cdot\boldsymbol{v}_w + \hat{\boldsymbol{h}}^{g}\cdot\boldsymbol{v}_g - (\hat{\boldsymbol{h}}^{w} + \hat{\boldsymbol{h}}^{g})\cdot\boldsymbol{v}_s \\ =&\hat{\boldsymbol{h}}^{w}\cdot(\boldsymbol{v}_w - \boldsymbol{v}_s) + \hat{\boldsymbol{h}}^{g}\cdot(\boldsymbol{v}_g - \boldsymbol{v}_s) \\ =&\,[p_w\,\mathrm{grad}(n^w) + n^w\,\mathrm{grad}(p_w) - \rho^w\boldsymbol{b} + \hat{\rho}^w\boldsymbol{v}_w]\cdot\tilde{\boldsymbol{v}}_w \\ &+ [p_g\,\mathrm{grad}(n^g) + n^g\,\mathrm{grad}(p_g) - \rho^g\boldsymbol{b} + \hat{\rho}^g\boldsymbol{v}_g]\cdot\tilde{\boldsymbol{v}}_g \\ =&\tilde{\boldsymbol{v}}^D_w\cdot\left[\mathrm{grad}(p_w) - \rho^{wR}\boldsymbol{b}\right] + \tilde{\boldsymbol{v}}^D_g\cdot\left[\mathrm{grad}(p_g) - \rho^{gR}\boldsymbol{b}\right] \\ &+ p_w\tilde{\boldsymbol{v}}_w\cdot\mathrm{grad}(n^w) + p_g\tilde{\boldsymbol{v}}_g\cdot\mathrm{grad}(n^g) + \hat{\rho}^w\boldsymbol{v}_w\cdot\tilde{\boldsymbol{v}}_w + \hat{\rho}^g\boldsymbol{v}_g\cdot\tilde{\boldsymbol{v}}_g\end{aligned} \tag{4.94}$$

From the balance of mass equation for solid (4.13), we have:

$$\mathrm{div}(\boldsymbol{v}_s) = -\frac{1}{n^s}\frac{D^s n^s}{Dt} + \beta^{\theta}_s\frac{D^s\theta^s}{Dt} \tag{4.95}$$

According to Coussy (2004), a simpler functional dependence of the Helmholtz free energy per unit mass for the solid skeleton is postulated to be:

$$\psi^s = \psi^s(\boldsymbol{\epsilon}^{skel,e}, \theta, S_w) \tag{4.96}$$

so that,

$$\frac{D^s\psi^s}{Dt} = \frac{\partial\psi^s}{\partial\boldsymbol{\epsilon}^{skel,e}}\frac{D^s\boldsymbol{\epsilon}^{skel,e}}{Dt} + \frac{\partial\psi^s}{\partial\theta^s}\frac{D^s\theta^s}{Dt} + \frac{\partial\psi^s}{\partial S_w}\frac{D^sS_w}{Dt} \tag{4.97}$$

Substituting (4.95) and (4.97) into (4.88) to get entropy inequality for solid, and then combining that with (4.73) and using (4.94), we arrive at the entropy inequality for the mixture:

$$\begin{aligned}
&\left\{-\rho^s\frac{\partial\psi^s}{\partial\theta} + \alpha^\theta_{skel}\mathrm{tr}(\boldsymbol{\sigma'}) - \rho^s\eta^s + 3\alpha^\theta_s\left[(n^g+\chi-1)p_g + (n^w-\chi)p_w\right]\right\}\frac{D^s\theta}{Dt}\\
&+\left(\boldsymbol{\sigma'} - \rho^s\frac{\partial\psi^s}{\partial\boldsymbol{\epsilon}^{skel,e}}\right) : \frac{D^s\boldsymbol{\epsilon}^{skel,e}}{Dt} \underbrace{-\frac{1}{n^s}\left[(n^g+\chi-1)p_g + (n^w-\chi)p_w\right]\frac{D^sn^s}{Dt}}_{R1}\\
&-\rho^s\frac{\partial\psi^s}{\partial S_w}\frac{D^sS_w}{Dt} + \left(n^w - \rho^w\frac{\partial g^w}{\partial p_w}\right)\frac{D^wp_w}{Dt} - \left(\rho^w\frac{\partial g^w}{\partial\theta} + \rho^w\eta^w\right)\frac{D^w\theta}{Dt}\\
&+\left(n^g - \rho^g\frac{\partial g^g}{\partial p_g}\right)\frac{D^gp_g}{Dt} - \left(\rho^g\frac{\partial g^g}{\partial\theta} + \rho^g\eta^w\right)\frac{D^g\theta}{Dt}\\
&-\tilde{\boldsymbol{v}}^D_w\cdot\left[\mathrm{grad}(p_w) - \rho^{wR}\boldsymbol{b}\right] - \tilde{\boldsymbol{v}}^D_g\cdot\left[\mathrm{grad}(p_g) - \rho^{gR}\boldsymbol{b}\right] - \frac{\boldsymbol{q}\cdot\mathrm{grad}\,\theta}{\theta}\\
&\underbrace{-p_w\tilde{\boldsymbol{v}}_w\cdot\mathrm{grad}(n^w) - p_g\tilde{\boldsymbol{v}}_g\cdot\mathrm{grad}(n^g) + p_w\frac{D^wn^w}{Dt} + p_g\frac{D^gn^g}{Dt}}_{R2}\\
&-\hat{\rho}^w\boldsymbol{v}_w\cdot\tilde{\boldsymbol{v}}_w - \hat{\rho}^g\boldsymbol{v}_g\cdot\tilde{\boldsymbol{v}}_g + \frac{1}{2}\hat{\rho}^w\boldsymbol{v}_w\cdot\boldsymbol{v}_w + \frac{1}{2}\hat{\rho}^g\boldsymbol{v}_g\cdot\boldsymbol{v}_g \geq 0
\end{aligned} \tag{4.98}$$

where $\boldsymbol{q} = \boldsymbol{q}^s + \boldsymbol{q}^w + \boldsymbol{q}^g$, $\theta = \theta^s = \theta^f$. Use of (3.15), and $n^\alpha = nS_\alpha, \alpha = w, g$, allows us to write the terms called $R1$ in (4.102):

$$\begin{aligned}
R1 &= p_w\frac{D^sn^w}{Dt} + p_g\frac{D^sn^g}{Dt}\\
&= \left(p_wS_w + p_gS_g\right)\frac{D^sn}{Dt} - n(p_g - p_w)\frac{D^sS_w}{Dt}
\end{aligned} \tag{4.99}$$

We introduce the definition of suction s:

$$s = p_g - p_w \tag{4.100}$$

If we use $\chi = S_w$ (Bishop and Blight, 1963) and $n^s = 1 - n$, the terms called $R2$ in (4.102) is written as:

$$R2 = (-p_wS_w - p_gS_g)\frac{D^sn}{Dt} \tag{4.101}$$

It is straightforward to see that (4.101) will cancel the first term in (4.99). Substitution of (4.99) and (4.101) into (4.102), we obtain:

$$\begin{aligned}
&\left\{-\rho^s\frac{\partial\psi^s}{\partial\theta}+\alpha^\theta_{skel}\mathrm{tr}(\boldsymbol{\sigma}')-\rho^s\eta^s+\beta^\theta_s\left[(n^g+\chi-1)p_g+(n^w-\chi)p_w\right]\right\}\frac{D^s\theta}{Dt}\\
&+\left(\boldsymbol{\sigma}'-\rho^s\frac{\partial\psi^s}{\partial\boldsymbol{\epsilon}^{skel,e}}\right):\frac{D^s\boldsymbol{\epsilon}^{skel,e}}{Dt}-\left[ns+\rho^s\frac{\partial\psi^s}{\partial S_w}\right]\frac{D^sS_w}{Dt}\\
&+\left(n^w-\rho^w\frac{\partial g^w}{\partial p_w}\right)\frac{D^wp_w}{Dt}-\left(\rho^w\frac{\partial g^w}{\partial\theta}+\rho^w\eta^w\right)\frac{D^w\theta}{Dt}\\
&+\left(n^g-\rho^g\frac{\partial g^g}{\partial p_g}\right)\frac{D^gp_g}{Dt}-\left(\rho^g\frac{\partial g^g}{\partial\theta}+\rho^g\eta^w\right)\frac{D^g\theta}{Dt}\\
&-\tilde{\boldsymbol{v}}^D_w\cdot\left[\mathrm{grad}(p_w)-\rho^{wR}\boldsymbol{b}\right]-\tilde{\boldsymbol{v}}^D_g\cdot\left[\mathrm{grad}(p_g)-\rho^{gR}\boldsymbol{b}\right]-\frac{\boldsymbol{q}\cdot\mathrm{grad}\,\theta}{\theta}\\
&-\hat{\rho}^w\boldsymbol{v}_w\cdot\tilde{\boldsymbol{v}}_w-\hat{\rho}^g\boldsymbol{v}_g\cdot\tilde{\boldsymbol{v}}_g+\frac{1}{2}\hat{\rho}^w\boldsymbol{v}_w\cdot\boldsymbol{v}_w+\frac{1}{2}\hat{\rho}^g\boldsymbol{v}_g\cdot\boldsymbol{v}_g\geq 0
\end{aligned}\tag{4.102}$$

Again, the thermodynamic arguments (Coleman and Noll, 1963) are adopted to obtain the constitutive relations with respect to solid skeleton and fluids, respectively.

For solid skeleton:

$$\boldsymbol{\sigma}'=\rho^s\frac{\partial\psi^s}{\partial\,\boldsymbol{\epsilon}^{skel,e}}\tag{4.103}$$

$$\rho^s\eta^s=-\rho^s\frac{\partial\psi^s}{\partial\theta}+\alpha^\theta_{skel}\mathrm{tr}(\boldsymbol{\sigma}')+\beta^\theta_s\left[(n^g+\chi-1)p_g+(n^w-\chi)p_w\right]\tag{4.104}$$

$$ns=-\rho^s\frac{\partial\psi^s}{\partial S_w}\tag{4.105}$$

For fluids, $f=w,g$

$$\eta^f=-\frac{\partial g^f}{\partial\theta}\tag{4.106}$$

$$\frac{n^f}{\rho^f}=\frac{1}{\rho^{fR}}=\frac{\partial g^f}{\partial p_f}\tag{4.107}$$

Coussy (2004) arrives at the same conclusion as (4.105), (4.106) and (4.107). (See Chapter 6, Page 156 and Chapter 3, Page 39). Thus, the reduced form of entropy inequality of the mixture is expressed as:

$$\begin{aligned}
&\tilde{\boldsymbol{v}}^D_w\cdot\left[-\mathrm{grad}(p_w)+\rho^{wR}\boldsymbol{b}\right]+\tilde{\boldsymbol{v}}^D_g\cdot\left[-\mathrm{grad}(p_g)+\rho^{gR}\boldsymbol{b}\right]-\frac{\boldsymbol{q}\cdot\mathrm{grad}\,\theta}{\theta}\\
&-\hat{\rho}^w\boldsymbol{v}_w\cdot\tilde{\boldsymbol{v}}_w-\hat{\rho}^g\boldsymbol{v}_g\cdot\tilde{\boldsymbol{v}}_g+\frac{1}{2}\hat{\rho}^w\boldsymbol{v}_w\cdot\boldsymbol{v}_w+\frac{1}{2}\hat{\rho}^g\boldsymbol{v}_g\cdot\boldsymbol{v}_g\geq 0
\end{aligned}\tag{4.108}$$

According to the postulate by Coussy (2004), two inequalities can be derived from (4.108) as follows:

$$-\frac{\boldsymbol{q}\cdot \mathrm{grad}\theta}{\theta} \geq 0 \tag{4.109}$$

$$\tilde{\boldsymbol{v}}_w^D \cdot \left[-\mathrm{grad}\left(p_w\right) + \rho^{fR}\boldsymbol{b}\right] \geq 0 \tag{4.110}$$

$$\tilde{\boldsymbol{v}}_g^D \cdot \left[-\mathrm{grad}\left(p_g\right) + \rho^{fR}\boldsymbol{b}\right] \geq 0 \tag{4.111}$$

Combining (4.60) and (4.72), we get:

$$\begin{aligned}
\rho^f \frac{D^f\, e^f}{Dt} &= \rho^f \frac{\partial\, g^f}{\partial p_f}\frac{D^f p_f}{Dt} + \rho^f \frac{\partial\, g^f}{\partial \theta^f}\frac{D^f \theta^f}{Dt} + \rho^f \theta^f \frac{D^f\, \eta^f}{Dt} + \rho^f \eta^f \frac{D^f\, \theta^f}{Dt} \\
&\quad -n^f \frac{D^f\, p_f}{Dt} - n^f p_f \mathrm{div}(\boldsymbol{v}_f) + \frac{p_f}{\rho^{fR}}\hat{\rho}^f - p_f \frac{D^f\, n^f}{Dt} \\
&= \left(\rho^f \frac{\partial\, g^f}{\partial p_f} - n^f\right)\frac{D^f p_f}{Dt} + \rho^f \left(\frac{\partial\, g^f}{\partial \theta^f} + \eta^f\right)\frac{D^f \theta^f}{Dt} \\
&\quad +\rho^f \theta^f \frac{D^f\, \eta^f}{Dt} - n^f p_f \mathrm{div}(\boldsymbol{v}_f) + \frac{p_f}{\rho^{fR}}\hat{\rho}^f - p_f \frac{D^f\, n^f}{Dt}
\end{aligned} \tag{4.112}$$

Use of (4.106) and (4.107) allows us to reduce (4.112) to:

$$\rho^f \frac{D^f\, e^f}{Dt} = \rho^f \theta^f \frac{D^f\, \eta^f}{Dt} - n^f p_f \mathrm{div}(\boldsymbol{v}_f) + \frac{p_f}{\rho^{fR}}\hat{\rho}^f - p_f \frac{D^f\, n^f}{Dt} \tag{4.113}$$

Combining (4.75) and (4.97), we get:

$$\frac{D^s e^s}{Dt} = \frac{\partial \psi^s}{\partial \boldsymbol{\epsilon}^{skel,e}}\frac{D^s \boldsymbol{\epsilon}^{skel,e}}{Dt} + \frac{\partial \psi^s}{\partial \theta^s}\frac{D^s \theta^s}{Dt} + \frac{\partial \psi^s}{\partial S_w}\frac{D^s S_w}{Dt} + \theta^s \frac{D^s \eta^s}{Dt} + \eta^s \frac{D^s \theta^s}{Dt} \tag{4.114}$$

Substitution of (4.113) with $f = w, g$, (4.114), 4.63, (4.86) as well as (4.94) into (4.49), we arrive at:

$$
\begin{aligned}
&\rho^w\theta\frac{D^w\,\eta^w}{Dt} - n^w p_w \mathrm{div}(\boldsymbol{v}_w) + \frac{p_w}{\rho^{wR}}\hat{\rho}^w - p_w\frac{D^w\,n^w}{Dt}\\
&+\rho^g\theta\frac{D^g\,\eta^g}{Dt} - n^g p_g \mathrm{div}(\boldsymbol{v}_g) + \frac{p_g}{\rho^{gR}}\hat{\rho}^g - p_g\frac{D^g\,n^g}{Dt}\\
&+\rho^s\left(\frac{\partial\psi^s}{\partial\boldsymbol{\epsilon}^{skel,e}}\frac{D^s\boldsymbol{\epsilon}^{skel,e}}{Dt} + \frac{\partial\psi^s}{\partial\theta}\frac{D^s\theta}{Dt} + \frac{\partial\psi^s}{\partial S_w}\frac{D^s S_w}{Dt} + \theta\frac{D^s\eta^s}{Dt} + \eta^s\frac{D^s\theta}{Dt}\right)\\
&-\boldsymbol{\sigma}' : \frac{D^s\boldsymbol{\epsilon}^{skel,e}}{Dt} - \alpha^\theta_{skel}\mathrm{tr}(\boldsymbol{\sigma}')\frac{D^s\theta}{Dt} - \left\{\left[n^g-(1-\chi)\right]p_g + (n^w-\chi)p_w\right\}\mathrm{div}\,\boldsymbol{v}_s\\
&+n^w\,p_w\,\mathrm{div}\boldsymbol{v}_w + n^g\,p_g\,\mathrm{div}\boldsymbol{v}_g + \tilde{\boldsymbol{v}}^D_w\cdot\left[\mathrm{grad}(p_w) - \rho^{wR}\boldsymbol{b}\right] + \tilde{\boldsymbol{v}}^D_g\cdot\left[\mathrm{grad}(p_g) - \rho^{gR}\boldsymbol{b}\right]\\
&+p_w\tilde{\boldsymbol{v}}_w\cdot\mathrm{grad}(n^w) + p_g\tilde{\boldsymbol{v}}_g\cdot\mathrm{grad}(n^g) + \hat{\rho}^w\boldsymbol{v}_w\cdot\tilde{\boldsymbol{v}}_w + \hat{\rho}^g\boldsymbol{v}_g\cdot\tilde{\boldsymbol{v}}_g\\
&-\frac{1}{2}\hat{\rho}^w\boldsymbol{v}_w\cdot\boldsymbol{v}_w - \frac{1}{2}\hat{\rho}^g\boldsymbol{v}_g\cdot\boldsymbol{v}_g - \rho r + \mathrm{div}\,\boldsymbol{q} + \hat{\rho}^w e^w + \hat{\rho}^g e^g = 0
\end{aligned}
\tag{4.115}
$$

in the above equation, some terms cancel out in the following way:

$$
-n^w p_w\mathrm{div}(\boldsymbol{v}_w) - n^g p_g\mathrm{div}(\boldsymbol{v}_g) + n^w\,p_w\,\mathrm{div}\boldsymbol{v}_w + n^g\,p_g\,\mathrm{div}\boldsymbol{v}_g = 0 \tag{4.116}
$$

and use (4.64) gives

$$
\begin{aligned}
\frac{p_w}{\rho^{wR}}\hat{\rho}^w + \frac{p_g}{\rho^{gR}}\hat{\rho}^g + \hat{\rho}^w e^w + \hat{\rho}^g e^g &= \hat{\rho}^w\,H^w + \hat{\rho}^g\,H^g\\
&= \hat{\rho}^{gv}(H^g - H^w)\\
&= \hat{\rho}^{gv}H_{vap}
\end{aligned}
\tag{4.117}
$$

where, H_{vap} is called enthalpy of vaporization, or latent heat of vaporization, H_{vap} =2260 kJ/Kg. Comparing to (4.99), we get

$$
\begin{aligned}
&-p_w\frac{D^w\,n^w}{Dt} - p_g\frac{D^g\,n^g}{Dt} + p_w\tilde{\boldsymbol{v}}_w\cdot\mathrm{grad}(n^w) + p_g\tilde{\boldsymbol{v}}_g\cdot\mathrm{grad}(n^g)\\
=&\cancel{-\left(p_w S_w + p_g S_g\right)\frac{D^s n}{Dt}} + n(p_g - p_w)\frac{D^s S_w}{Dt}
\end{aligned}
\tag{4.118}
$$

using (4.95) and (4.101), we have

$$
\begin{aligned}
&-\left\{\left[n^g-(1-\chi)\right]p_g + (n^w-\chi)p_w\right\}\mathrm{div}\,\boldsymbol{v}_s\\
=&-\left\{\left[n^g-(1-\chi)\right]p_g + (n^w-\chi)p_w\right\}\left(-\frac{1}{n^s}\frac{D^s n^s}{Dt} + \beta^\theta_s\frac{D^s\theta}{Dt}\right)\\
=&\cancel{(p_w S_w + p_g S_g)\frac{D^s n}{Dt}} - \beta^\theta_s\left\{\left[n^g-(1-\chi)\right]p_g + (n^w-\chi)p_w\right\}\frac{D^s\theta}{Dt}
\end{aligned}
\tag{4.119}
$$

The first terms in (4.118) and (4.119) cancel out. Substituting (4.117) (4.119) into (4.115), we arrive at:

$$\begin{aligned}
&\rho^w\theta\frac{D^w\,\eta^w}{Dt}+\rho^w\theta\frac{D^w\eta^w}{Dt}+\rho^g\theta\frac{D^g\eta^g}{Dt}+\left[n\,s+\rho^s\frac{\partial\psi^s}{\partial S_w}\right]\frac{D^sS_w}{Dt}+\left(\rho^s\frac{\partial\psi^s}{\partial\boldsymbol{\epsilon}^{skel,e}}-\boldsymbol{\sigma}'\right):\frac{D^s\boldsymbol{\epsilon}^{skel,e}}{Dt}\\
&+\left\{\rho^s\frac{\partial\psi^s}{\partial\theta}-\alpha^\theta_{skel}\mathrm{tr}(\boldsymbol{\sigma}')+\rho^s\eta^s-\beta^\theta_s\left[(n^g+\chi-1)p_g+(n^w-\chi)p_w\right]\right\}\frac{D^s\theta}{Dt}\\
&+\tilde{\boldsymbol{v}}^D_w\cdot\left[\mathrm{grad}(p_w)-\rho^{wR}\boldsymbol{b}\right]+\tilde{\boldsymbol{v}}^D_g\cdot\left[\mathrm{grad}(p_g)-\rho^{gR}\boldsymbol{b}\right]+\hat{\rho}^w\boldsymbol{v}_w\cdot\tilde{\boldsymbol{v}}_w+\hat{\rho}^g\boldsymbol{v}_g\cdot\tilde{\boldsymbol{v}}_g\\
&-\frac{1}{2}\hat{\rho}^w\boldsymbol{v}_w\cdot\boldsymbol{v}_w-\frac{1}{2}\hat{\rho}^g\boldsymbol{v}_g\cdot\boldsymbol{v}_g-\rho r+\mathrm{div}\,\boldsymbol{q}+\hat{\rho}^{gv}H_{vap}=0
\end{aligned}\tag{4.120}$$

Use of the conclusions (4.103)-(4.105) provides:

$$\begin{aligned}
&\rho^s\theta\frac{D^s\eta^s}{Dt}+\rho^w\theta\frac{D^w\eta^w}{Dt}+\rho^g\theta\frac{D^g\eta^g}{Dt}-\rho\,r+\mathrm{div}\,\boldsymbol{q}+\hat{\rho}^{gv}H_{vap}\\
&-\frac{1}{2}\hat{\rho}^w\boldsymbol{v}_w\cdot\boldsymbol{v}_w-\frac{1}{2}\hat{\rho}^g\boldsymbol{v}_g\cdot\boldsymbol{v}_g+\hat{\rho}^w\boldsymbol{v}_w\cdot\tilde{\boldsymbol{v}}_w+\hat{\rho}^g\boldsymbol{v}_g\cdot\tilde{\boldsymbol{v}}_g\\
&+\tilde{\boldsymbol{v}}^D_w\cdot\left[\mathrm{grad}(p_w)-\rho^{wR}\boldsymbol{b}\right]+\tilde{\boldsymbol{v}}^D_g\cdot\left[\mathrm{grad}(p_g)-\rho^{gR}\boldsymbol{b}\right]=0
\end{aligned}\tag{4.121}$$

Introduce the definition of the heat capacity

$$\rho^s\theta^s\frac{D^s\eta^s}{Dt}=\rho^sC^s\frac{D^s\theta^s}{Dt};\quad \rho^w\theta^w\frac{D^w\eta^w}{Dt}=\rho^wC^w\frac{D^w\theta^w}{Dt};\quad \rho^g\theta^g\frac{D^g\eta^g}{Dt}=\rho^gC^g\frac{D^g\theta^g}{Dt}\tag{4.122}$$

where, C^s, C^w and C^g are the heat capacity per unit mass of solid, water and gas phases. Thus we can rewrite (4.121) with the derivatives expressed in terms of the motion of the solid phase:

$$\begin{aligned}
&(\rho\,C)_m\frac{D^s\theta}{Dt}+\rho^{wR}C^w\,\tilde{\boldsymbol{v}}^D_w\cdot\mathrm{grad}\,\theta+\rho^{gR}C^g\,\tilde{\boldsymbol{v}}^D_g\cdot\mathrm{grad}\,\theta-\rho r+\mathrm{div}\,\boldsymbol{q}\\
&+\hat{\rho}^{gv}H_{vap}-\frac{1}{2}\hat{\rho}^w\boldsymbol{v}_w\cdot\boldsymbol{v}_w-\frac{1}{2}\hat{\rho}^g\boldsymbol{v}_g\cdot\boldsymbol{v}_g+\hat{\rho}^w\boldsymbol{v}_w\cdot\tilde{\boldsymbol{v}}_w+\hat{\rho}^g\boldsymbol{v}_g\cdot\tilde{\boldsymbol{v}}_g\\
&+\tilde{\boldsymbol{v}}^D_w\cdot\left[\mathrm{grad}(p_w)-\rho^{wR}\boldsymbol{b}\right]+\tilde{\boldsymbol{v}}^D_g\cdot\left[\mathrm{grad}(p_g)-\rho^{gR}\boldsymbol{b}\right]=0
\end{aligned}\tag{4.123}$$

where $(\rho\,C)_m=\rho^s\,C^s+\rho^w\,C^w+\rho^g\,C^g$. It is easy to see the unit of each term in (4.123) is W/m^3. The expression of the term $\hat{\rho}^{gv}$ can be obtained from the balance equation of mass for liquid water (4.21).

4.1.4 Summary of governing equations

We summarize the four governing equations as follows: Balance of linear momentum:

$$\mathrm{div}\boldsymbol{\sigma}+\rho\boldsymbol{b}=\boldsymbol{0}\tag{4.124}$$

Balance of mass for water species (liquid water and water vapor):

$$\begin{aligned}&(\rho^{wR}S_w+\rho^{gvR}S_g)\mathrm{div}\,\boldsymbol{v}_s-\Big[(1-n)(\rho^{wR}S_w+\rho^{gvR}S_g)\beta_s^\theta+n\rho^{wR}S_w\beta_w^\theta\Big]\frac{D^s\theta}{D\,t}\\&+n(\rho^{wR}-\rho^{gvR})\frac{D^sS_w}{Dt}+nS_g\frac{D^s\rho^{gvR}}{Dt}+\mathrm{div}(\rho^{gvR}\,\tilde{\boldsymbol{v}}_{gv}^D+\rho^{wR}\,\tilde{\boldsymbol{v}}_w^D)=0\end{aligned}\tag{4.125}$$

Balance of mass for dry air:

$$\rho^{gaR}S_g\mathrm{div}\,\boldsymbol{v}_s-\rho^{gaR}S_g\beta_s^\theta(1-n)\frac{D^s\theta}{D\,t}+nS_g\frac{D^s\rho^{gaR}}{Dt}-n\rho^{gaR}\frac{D^sS_w}{Dt}+\mathrm{div}(\rho^{gaR}\,\tilde{\boldsymbol{v}}_{ga}^D)=0\tag{4.126}$$

Energy conservation of mixture:

$$\begin{aligned}&(\rho\,C)_m\frac{D^s\theta}{Dt}+\rho^{wR}C^w\,\tilde{\boldsymbol{v}}_w^D\cdot\mathrm{grad}\,\theta+\rho^{gR}C^g\,\tilde{\boldsymbol{v}}_g^D\cdot\mathrm{grad}\,\theta-\rho r+\mathrm{div}\,\boldsymbol{q}\\&+\hat{\rho}^{gv}H_{vap}-\frac{1}{2}\hat{\rho}^w\boldsymbol{v}_w\cdot\boldsymbol{v}_w-\frac{1}{2}\hat{\rho}^g\boldsymbol{v}_g\cdot\boldsymbol{v}_g+\hat{\rho}^w\boldsymbol{v}_w\cdot\tilde{\boldsymbol{v}}_w+\hat{\rho}^g\boldsymbol{v}_g\cdot\tilde{\boldsymbol{v}}_g\\&+\tilde{\boldsymbol{v}}_w^D\cdot\big[\mathrm{grad}(p_w)-\rho^{wR}\boldsymbol{b}\big]+\tilde{\boldsymbol{v}}_g^D\cdot\big[\mathrm{grad}(p_g)-\rho^{gR}\boldsymbol{b}\big]=0\end{aligned}\tag{4.127}$$

in which

$$\begin{aligned}\frac{D^s\rho^{gvR}}{Dt}&=\frac{\partial\rho^{gvR}}{\partial s}\frac{D^ss}{Dt}+\frac{\partial\rho^{gvR}}{\partial\theta}\frac{D^s\theta}{Dt}\\&=\frac{\partial\rho^{gvR}}{\partial s}\frac{D^sp_g}{Dt}-\frac{\partial\rho^{gvR}}{\partial s}\frac{D^sp_w}{Dt}+\frac{\partial\rho^{gvR}}{\partial\theta}\frac{D^s\theta}{Dt}\end{aligned}\tag{4.128}$$

and,

$$\frac{D^sS_w}{Dt}=\frac{\partial S_w}{\partial s}\frac{D^ss}{Dt}=\frac{\partial S_w}{\partial s}\frac{D^sp_g}{Dt}-\frac{\partial S_w}{\partial s}\frac{D^sp_w}{Dt}\tag{4.129}$$

$$q_i=-K_{ij}\,\theta_{,j}+\Delta H_{vap}(J_v)_i\tag{4.130}$$

where, $\boldsymbol{q}$ is the heat flux (W/m^2), and $\boldsymbol{J}_v$ is the mass flux of water vapor (kg/m^2s). ΔH_{vap} is the heat of vaporization of water.

4.2 Finite element formulations

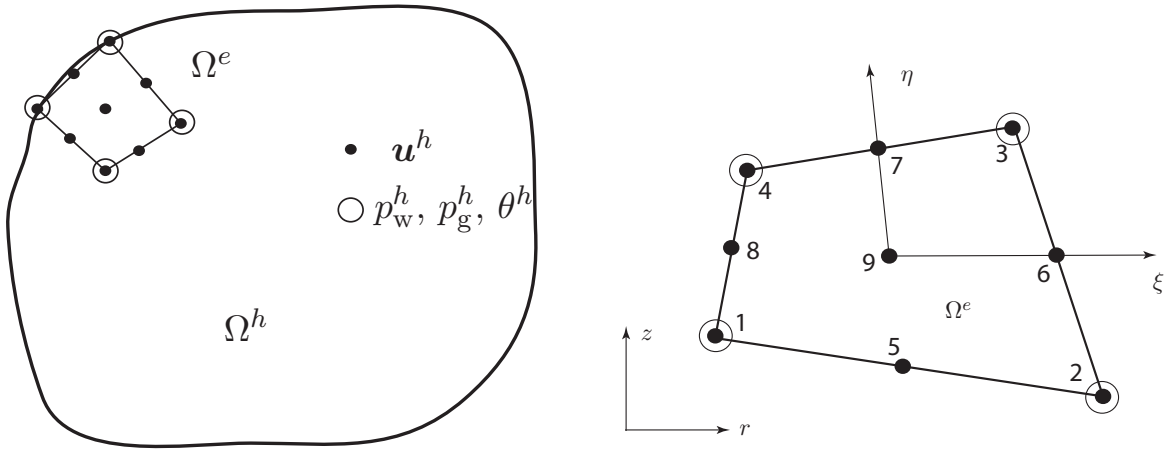

Figure 4.1: Discretization into mixed quadrilateral elements.

A weighted residual method is used to formulate the coupled variational equations from the governing differential equations, which are then discretized using finite elements. Quadrilateral finite elements with biquadratic interpolation in solid-skeleton displacement, bilinear in pore water and gas pressures and soil mixture temperature are employed to ensure numerical stability. Weighting functions $w_i(\boldsymbol{r})$, $\eta(\boldsymbol{r})$, $\omega(\boldsymbol{r})$ and $\varphi(\boldsymbol{r})$ are used for displacement, pore water pressure, pore gas pressure, and mixture temperature, respectively.

$$\boldsymbol{u}^h(\boldsymbol{r}) = \boldsymbol{N}^{e,u} \cdot \boldsymbol{d}^e \qquad \boldsymbol{w}^h(\boldsymbol{r}) = \boldsymbol{N}^{e,u} \cdot \boldsymbol{c}^e \tag{4.131}$$

$$p_w^h(\boldsymbol{r}) = \boldsymbol{N}^{e,p} \cdot \boldsymbol{p}_w^e \qquad \eta^h(\boldsymbol{r}) = \boldsymbol{N}^{e,p} \cdot \boldsymbol{\alpha}^e \tag{4.132}$$

$$p_g^h(\boldsymbol{r}) = \boldsymbol{N}^{e,p} \cdot \boldsymbol{p}_g^e \qquad \omega^h(\boldsymbol{r}) = \boldsymbol{N}^{e,p} \cdot \boldsymbol{\beta}^e \tag{4.133}$$

$$\theta^h(\boldsymbol{r}) = \boldsymbol{N}^{e,p} \cdot \boldsymbol{\theta}^e \qquad \varphi^h(\boldsymbol{r}) = \boldsymbol{N}^{e,p} \cdot \boldsymbol{\gamma}^e \tag{4.134}$$

in which $\boldsymbol{r} = [r, z]$ is the vector of coordinates, where, r is radial and z is axial coordinate.
The coupled thermo-poro-mechanical FE equations for partially saturated soils are written in the following form:

(1) Balance of linear momentum for the mixture

$$\begin{aligned}\mathop{\mathbf{A}}_{e=1}^{n_{\mathrm{el}}}(\boldsymbol{c}^e)^T\cdot\Bigg\{&\underbrace{\int_{\Omega^e}(\boldsymbol{B}^{e,u})^T\cdot\boldsymbol{\sigma}'\,dv}_{\boldsymbol{f}_e^{d,int}(\boldsymbol{d}^e)}-\underbrace{\int_{\Omega^e}(\tilde{\boldsymbol{B}}^{e,u})^T\cdot\boldsymbol{N}^{e,p}\cdot\left[\chi\boldsymbol{p}_w^e+(1-\chi)\boldsymbol{p}_g^e\right]\,dv}_{\boldsymbol{f}_e^{dp,int}(\boldsymbol{p}_w^e,\boldsymbol{p}_g^e)}\\&-\underbrace{\int_{\Omega^e}3K^{skel}\alpha_{skel}^{\theta}(\tilde{\boldsymbol{B}}^{e,u})^T\cdot\boldsymbol{N}^{e,\theta}\cdot(\boldsymbol{\theta}^e-\boldsymbol{\theta}_0^e)\,dv}_{\boldsymbol{f}_e^{d\theta,int}(\boldsymbol{\theta}^e)}=\underbrace{\int_{\Omega^e}\rho(\boldsymbol{N}^{e,u})^T\boldsymbol{b}\,dv}_{\boldsymbol{f}_e^{df,ext}(\boldsymbol{d}^e,\boldsymbol{p}_w^e,\boldsymbol{p}_g^e,\boldsymbol{\theta}^e)}+\underbrace{\int_{\Gamma_t^e}(\boldsymbol{N}^{e,u})^T\boldsymbol{t}^{\sigma}da}_{\boldsymbol{f}_e^{dt,ext}}\Bigg\}\end{aligned}\tag{4.135}$$

(2) Balance of mass for the water species

$$\begin{aligned}\mathop{\mathbf{A}}_{e=1}^{n_{\mathrm{el}}}(\boldsymbol{\alpha}^e)^T\cdot\Bigg\{&\underbrace{\int_{\Omega^e}(\rho^{wR}S_{\mathrm{w}}+\rho^{\mathrm{gv}R}S_{\mathrm{g}})(\boldsymbol{N}^{e,p})^T\tilde{\boldsymbol{B}}^{e,u}\,dv}_{\boldsymbol{k}_e^{wd}(\boldsymbol{p}_w^e,\boldsymbol{p}_g^e,\boldsymbol{\theta}^e)}\cdot\{\dot{\boldsymbol{d}}^e\}\\&-\underbrace{\int_{\Omega^e}\left[nS_g\frac{\partial\rho^{gvR}}{\partial s}+n(\rho^{wR}-\rho^{gvR})\frac{\partial S_w}{\partial s}\right](\boldsymbol{N}^{e,p})^T\boldsymbol{N}^{e,p}dv}_{\boldsymbol{k}_e^{wg}(\boldsymbol{d}^e,\boldsymbol{p}_w^e,\boldsymbol{p}_g^e,\boldsymbol{\theta}^e)}\cdot\{\dot{\boldsymbol{p}}_w^e-\dot{\boldsymbol{p}}_g^e\}\\&+\underbrace{\int_{\Omega^e}\left(nS_g\frac{\partial\rho^{gvR}}{\partial\theta}-\beta_{swg}\right)(\boldsymbol{N}^{e,p})^T\boldsymbol{N}^{e,\theta}dv}_{\boldsymbol{k}_e^{w\theta}(\boldsymbol{d}^e,\boldsymbol{p}_w^e,\boldsymbol{p}_g^e,\boldsymbol{\theta}^e)}\cdot\{\dot{\boldsymbol{\theta}}^e\}-\underbrace{\int_{\Omega^e}\rho^{wR}(\boldsymbol{B}^{e,p})^T\tilde{\boldsymbol{v}}_w^D\,dv}_{\boldsymbol{f}_e^{w1,int}(\boldsymbol{d}^e,\boldsymbol{p}_w^e,\boldsymbol{p}_g^e,\boldsymbol{\theta}^e)}\\&-\underbrace{\int_{\Omega^e}\rho^{gvR}(\boldsymbol{B}^{e,p})^T\tilde{\boldsymbol{v}}_{gv}^D\,dv}_{\boldsymbol{f}_e^{w2,int}(\boldsymbol{d}^e,\boldsymbol{p}_w^e,\boldsymbol{p}_g^e,\boldsymbol{\theta}^e)}=\underbrace{\int_{\Gamma^e}(\rho^{wR}S^w+\rho^{gvR}S^{gv})(\boldsymbol{N}^{e,p})^T da}_{\boldsymbol{f}_e^{w,ext}(\boldsymbol{p}_w^e,\boldsymbol{p}_g^e,\boldsymbol{\theta}^e)}\Bigg\}\end{aligned}\tag{4.136}$$

(3) Balance of mass for the gas

$$\begin{aligned}\mathop{\mathbf{A}}_{e=1}^{n_{\mathrm{el}}}(\boldsymbol{\beta}^e)^T\cdot\quad\Bigg\{&\underbrace{\int_{\Omega^e}\rho^{gaR}S_{\mathrm{g}}(\boldsymbol{N}^{e,p})^T\tilde{\boldsymbol{B}}^{e,u}\,dv}_{\boldsymbol{k}_e^{gd}(\boldsymbol{p}_w^e,\boldsymbol{p}_g^e,\boldsymbol{\theta}^e)}\cdot\dot{\boldsymbol{d}}^e\\&+\underbrace{\int_{\Omega^e}\left[nS_g\frac{\partial\rho^{gaR}}{\partial p_w}+n\rho^{gaR}\frac{\partial S_w}{\partial s}\right](\boldsymbol{N}^{e,p})^T\boldsymbol{N}^{e,p}dv}_{\boldsymbol{k}_e^{gw}(\boldsymbol{d}^e,\boldsymbol{p}_w^e,\boldsymbol{p}_g^e,\boldsymbol{\theta}^e)}\cdot\dot{\boldsymbol{p}}_w^e\end{aligned}$$

$$
\begin{aligned}
&+ \underbrace{\int_{\Omega^e} \left[nS_g \frac{\partial \rho^{gaR}}{\partial p_g} - n\rho^{gaR} \frac{\partial S_w}{\partial s} \right] (\boldsymbol{N}^{e,p})^T \boldsymbol{N}^{e,p} dv}_{\boldsymbol{k}_e^{gg}(\boldsymbol{d}^e, \boldsymbol{p}_w^e, \boldsymbol{p}_g^e, \boldsymbol{\theta}^e)} \cdot \dot{\boldsymbol{p}}_g^e \\
&+ \underbrace{\int_{\Omega^e} \left(nS_g \frac{\partial \rho^{gaR}}{\partial \theta} - \beta_s (1-n) \rho^{gaR} S_g \right) (\boldsymbol{N}^{e,p})^T \boldsymbol{N}^{e,\theta} dv}_{\boldsymbol{k}_e^{g\theta}(\boldsymbol{d}^e, \boldsymbol{p}_w^e, \boldsymbol{p}_g^e, \boldsymbol{\theta}^e)} \cdot \dot{\boldsymbol{\theta}}^e \\
&- \underbrace{\int_{\Omega^e} \rho^{gaR} (\boldsymbol{B}^{e,p})^T \tilde{\boldsymbol{v}}_{ga}^D dv}_{\boldsymbol{f}_e^{g,int}(\boldsymbol{d}^e, \boldsymbol{p}_w^e, \boldsymbol{p}_g^e, \boldsymbol{\theta}^e)} = \underbrace{\int_{\Gamma^e} \rho^{gaR} S^{ga} (\boldsymbol{N}^{e,p})^T da}_{\boldsymbol{f}_e^{g,ext}(\boldsymbol{p}_w^e, \boldsymbol{p}_g^e, \boldsymbol{\theta}^e)} \Bigg\}
\end{aligned} \tag{4.137}
$$

(4) Balance of energy for the mixture

$$
\begin{aligned}
\mathop{\mathbf{A}}_{e=1}^{n_{\mathrm{el}}} (\boldsymbol{\gamma}^e)^T \cdot \quad & \Bigg\{ \underbrace{\int_{\Omega^e} -\Delta H_{vap} \rho^{wR} S_w (\boldsymbol{N}^{e,\theta})^T \tilde{\boldsymbol{B}}^{e,u} \, dv}_{\boldsymbol{k}_e^{\theta d}(\boldsymbol{p}_w^e, \boldsymbol{p}_g^e, \boldsymbol{\theta}^e)} \cdot \dot{\boldsymbol{d}}^e \\
&+ \underbrace{\int_{\Omega^e} n\rho^{wR} \Delta H_{vap} \left(\frac{\partial S_w}{\partial s} \right) (\boldsymbol{N}^{e,\theta})^T \boldsymbol{N}^{e,p} dv}_{\boldsymbol{k}_e^{\theta w}(\boldsymbol{d}^e, \boldsymbol{p}_w^e, \boldsymbol{p}_g^e, \boldsymbol{\theta}^e)} \cdot \dot{\boldsymbol{p}}_w^e \\
&- \underbrace{\int_{\Omega^e} n\rho^{wR} \Delta H_{vap} \left(\frac{\partial S_w}{\partial s} \right) (\boldsymbol{N}^{e,\theta})^T \boldsymbol{N}^{e,p} dv}_{\boldsymbol{k}_e^{\theta g}(\boldsymbol{d}^e, \boldsymbol{p}_w^e, \boldsymbol{p}_g^e, \boldsymbol{\theta}^e)} \cdot \dot{\boldsymbol{p}}_g^e \\
&+ \underbrace{\int_{\Omega^e} \left\{ (\rho C)_{eff} + \Delta H_{vap} S_w \rho^{wR} [\beta_s^\theta (1-n) + \beta_w^\theta] \right\} (\boldsymbol{N}^{e,\theta})^T \boldsymbol{N}^{e,\theta} dv}_{\boldsymbol{k}_e^{\theta\theta}(\boldsymbol{d}^e, \boldsymbol{p}_w^e, \boldsymbol{p}_g^e, \boldsymbol{\theta}^e)} \cdot \dot{\boldsymbol{\theta}}^e \\
&+ \underbrace{\int_{\Omega^e} \left[(\boldsymbol{N}^{e,\theta})^T (\rho^{wR} C^w \tilde{v}_w^D + \rho^{gR} C^g \tilde{v}_g^D)^T + K_{eff}^\theta (\boldsymbol{B}^{e,\theta})^T \right] \cdot \boldsymbol{B}^{e,\theta} \cdot \boldsymbol{\theta} dv}_{\boldsymbol{f}_e^{\theta 1,int}(\boldsymbol{d}^e, \boldsymbol{p}_w^e, \boldsymbol{p}_g^e, \boldsymbol{\theta}^e)} \\
&+ \underbrace{\int_{\Omega^e} \Delta H_{vap} (\boldsymbol{B}^{e,\theta})^T (\rho^{wR} \tilde{v}_w^s - \rho^{gvR} \tilde{v}_{gv}^s) \, dv}_{\boldsymbol{f}_e^{\theta 2,int}(\boldsymbol{d}^e, \boldsymbol{p}_w^e, \boldsymbol{p}_g^e, \boldsymbol{\theta}^e)} = \underbrace{\int_{\Omega^e} (\boldsymbol{N}^{e,\theta})^T q \, dv}_{\boldsymbol{f}_e^{\theta 1,ext}} \\
&- \underbrace{\int_{\Gamma^e} \Delta H_{vap} \rho^{wR} s^w (\boldsymbol{N}^{e,\theta})^T da}_{\boldsymbol{f}_e^{\theta 2,ext}(\boldsymbol{\theta}^e)} + \underbrace{\int_{\Omega^e} \rho (\boldsymbol{N}^{e,\theta})^T r \, dv}_{\boldsymbol{f}_e^{\theta 3,ext}(\boldsymbol{d}^e, \boldsymbol{p}_w^e, \boldsymbol{p}_g^e, \theta)} \Bigg\}
\end{aligned} \tag{4.138}
$$

The above equations can be simply written as

$$\mathop{\mathbf{A}}_{e=1}^{n_{\text{el}}} (\boldsymbol{c}^e)^T \cdot \left[\boldsymbol{f}_e^{d,INT} - \boldsymbol{f}_e^{dp,INT} = \boldsymbol{f}_e^{df,EXT} + \boldsymbol{f}_e^{dt,EXT} \right] \tag{4.139}$$

$$\mathop{\mathbf{A}}_{e=1}^{n_{\text{el}}} (\boldsymbol{\alpha}^e)^T \cdot \left[\boldsymbol{k}_e^{wd} \cdot \dot{\boldsymbol{d}}^e - \boldsymbol{k}_e^{wg} \cdot \dot{\boldsymbol{p}}_w^e + \boldsymbol{k}_e^{wg} \cdot \dot{\boldsymbol{p}}_g^e + \boldsymbol{k}_e^{w\theta} \cdot \dot{\boldsymbol{\theta}}^e - \boldsymbol{f}_e^{w1,INT} - \boldsymbol{f}_e^{w2,INT} = \boldsymbol{f}_e^{w,EXT} \right] \tag{4.140}$$

$$\mathop{\mathbf{A}}_{e=1}^{n_{\text{el}}} (\boldsymbol{\beta}^e)^T \cdot \left[\boldsymbol{k}_e^{gd} \cdot \dot{\boldsymbol{d}}^e + \boldsymbol{k}_e^{gw} \cdot \dot{\boldsymbol{p}}_w^e + \boldsymbol{k}_e^{gg} \cdot \dot{\boldsymbol{p}}_g^e + \boldsymbol{k}_e^{g\theta} \cdot \dot{\boldsymbol{\theta}}^e - \boldsymbol{f}_e^{g,INT} = \boldsymbol{f}_e^{g,EXT} \right] \tag{4.141}$$

$$\mathop{\mathbf{A}}_{e=1}^{n_{\text{el}}} (\boldsymbol{\gamma}^e)^T \cdot \left[\boldsymbol{k}_e^{\theta d} \cdot \dot{\boldsymbol{d}}^e + \boldsymbol{k}_e^{\theta w} \cdot \dot{\boldsymbol{p}}_w^e - \boldsymbol{k}_e^{\theta g} \cdot \dot{\boldsymbol{p}}_g^e + \boldsymbol{k}_e^{\theta\theta} \cdot \dot{\boldsymbol{\theta}}^e + \boldsymbol{f}_e^{\theta 1,INT} + \boldsymbol{f}_e^{\theta 2,INT} = \boldsymbol{f}_e^{\theta 1,EXT} - \boldsymbol{f}_e^{\theta 2,EXT} + \boldsymbol{f}_e^{\theta 3,EXT} \right] \tag{4.142}$$

After element assembly, we have the coupled nonlinear PDEs to solve using generalized trapezoidal integration in time, and Newton-Raphson iteration.

$$\begin{cases} \boldsymbol{F}^{d,INT} - \boldsymbol{F}^{dp,INT} - \boldsymbol{F}^{d\theta,INT} = \boldsymbol{F}^{df,EXT} + \boldsymbol{F}^{dt,EXT} \\ \boldsymbol{K}^{wd} \cdot \dot{\boldsymbol{d}} - \boldsymbol{K}^{wg} \cdot \dot{\boldsymbol{p}}_w + \boldsymbol{K}^{wg} \cdot \dot{\boldsymbol{p}}_g + \boldsymbol{K}^{w\theta} \cdot \dot{\boldsymbol{\theta}} - \boldsymbol{F}^{w1,INT} - \boldsymbol{F}^{w2,INT} = \boldsymbol{F}^{w,EXT} \\ \boldsymbol{K}^{gd} \cdot \dot{\boldsymbol{d}} + \boldsymbol{K}^{gw} \cdot \dot{\boldsymbol{p}}_w + \boldsymbol{K}^{gg} \cdot \dot{\boldsymbol{p}}_g + \boldsymbol{K}^{g\theta} \cdot \dot{\boldsymbol{\theta}} - \boldsymbol{F}^{g,INT} = \boldsymbol{F}^{g,EXT} \\ \boldsymbol{K}^{\theta d} \cdot \dot{\boldsymbol{d}} + \boldsymbol{K}^{\theta w} \cdot \dot{\boldsymbol{p}}_w - \boldsymbol{K}^{\theta g} \cdot \dot{\boldsymbol{p}}_g + \boldsymbol{K}^{\theta\theta} \cdot \dot{\boldsymbol{\theta}} + \boldsymbol{F}^{\theta 1,INT} + \boldsymbol{F}^{\theta 2,INT} \\ = \boldsymbol{F}^{\theta 1,EXT} - \boldsymbol{F}^{\theta 2,EXT} + \boldsymbol{F}^{\theta 3,EXT} \end{cases} \tag{4.143}$$

Let us write the governing equations in matrix form:

$$\boldsymbol{C}(\boldsymbol{D}) \cdot \dot{\boldsymbol{D}} + \boldsymbol{F}^{INT}(\boldsymbol{D}) = \boldsymbol{F}^{EXT}(\boldsymbol{D}) \tag{4.144}$$

$$\dot{\boldsymbol{D}} = \begin{bmatrix} \dot{\boldsymbol{d}} \\ \dot{\boldsymbol{p}}_w \\ \dot{\boldsymbol{p}}_g \\ \dot{\boldsymbol{\theta}} \end{bmatrix}, \quad \boldsymbol{D} = \begin{bmatrix} \boldsymbol{d} \\ \boldsymbol{p}_w \\ \boldsymbol{p}_g \\ \boldsymbol{\theta} \end{bmatrix}, \quad \boldsymbol{C} = \begin{bmatrix} \boldsymbol{0} & \boldsymbol{0} & \boldsymbol{0} & \boldsymbol{0} \\ \boldsymbol{K}^{wd} & -\boldsymbol{K}^{wg} & \boldsymbol{K}^{wg} & \boldsymbol{K}^{w\theta} \\ \boldsymbol{K}^{gd} & \boldsymbol{K}^{gw} & \boldsymbol{K}^{gg} & \boldsymbol{K}^{g\theta} \\ \boldsymbol{K}^{\theta d} & \boldsymbol{K}^{\theta g} & -\boldsymbol{K}^{\theta g} & \boldsymbol{K}^{\theta\theta} \end{bmatrix}$$

$$\boldsymbol{F}^{INT} = \begin{bmatrix} \boldsymbol{F}^{d,INT} - \boldsymbol{F}^{dp,INT} - \boldsymbol{F}^{d\theta,INT} \\ -\boldsymbol{F}^{w1,INT} - \boldsymbol{F}^{w2,INT} \\ -\boldsymbol{F}^{g,INT} \\ \boldsymbol{F}^{\theta 1,INT} + \boldsymbol{F}^{\theta 2,INT} \end{bmatrix}, \boldsymbol{F}^{EXT} = \begin{bmatrix} \boldsymbol{F}^{df,EXT} + \boldsymbol{F}^{dt,EXT} \\ \boldsymbol{F}^{w,EXT} \\ \boldsymbol{F}^{g,EXT} \\ \boldsymbol{F}^{\theta 1,EXT} + \boldsymbol{F}^{\theta 2,EXT} + \boldsymbol{F}^{\theta 3,EXT} \end{bmatrix}$$

Recall the generalized trapezoidal integration:

$$\begin{gathered} \boldsymbol{C}(\boldsymbol{D}_{n+1}) \cdot \boldsymbol{V}_{n+1} + \boldsymbol{F}^{INT}(\boldsymbol{D}_{n+1}) = \boldsymbol{F}^{EXT}(\boldsymbol{D}_{n+1}) \\ \boldsymbol{D}_{n+1} = \tilde{\boldsymbol{D}}_{n+1} + \alpha \Delta t \boldsymbol{V}_{n+1},\ \tilde{\boldsymbol{D}}_{n+1} = \boldsymbol{D}_n + \Delta t(1-\alpha)\boldsymbol{V}_n \end{gathered} \tag{4.145}$$

Newton-Raphson iteration algorithm will be used to solve for $\boldsymbol{V}_{n+1}^{k+1}$ with the current value $\boldsymbol{V}_{n+1}^{k}$.

$$\begin{aligned} \boldsymbol{R}(\boldsymbol{V}_{n+1}^{k+1}) = \boldsymbol{C}(\boldsymbol{D}_{n+1}^{k+1}) \cdot \boldsymbol{V}_{n+1}^{k+1} + \boldsymbol{F}^{INT}(\boldsymbol{D}_{n+1}^{k+1}) - \boldsymbol{F}^{EXT}(\boldsymbol{D}_{n+1}^{k+1}) &= \boldsymbol{0} \\ = \boldsymbol{R}^k + \frac{\partial \boldsymbol{R}^k}{\partial \boldsymbol{V}} \cdot \delta \boldsymbol{V} & \\ \Longrightarrow \delta \boldsymbol{V} = -\left(\frac{\partial \boldsymbol{R}^k}{\partial \boldsymbol{V}}\right)^{-1} \cdot \boldsymbol{R}^k & \\ \boldsymbol{V}_{n+1}^{k+1} = \boldsymbol{V}_{n+1}^{k} + \delta \boldsymbol{V} & \\ \boldsymbol{D}_{n+1}^{k+1} = \tilde{\boldsymbol{D}}_{n+1} + \alpha \Delta t \boldsymbol{V}_{n+1}^{k+1} & \end{aligned} \tag{4.146}$$

The consistent tangent used can be written as:

$$\frac{\partial \boldsymbol{R}}{\partial \boldsymbol{V}} = \left(\frac{\partial \boldsymbol{C}}{\partial \boldsymbol{D}} \cdot \frac{\partial \boldsymbol{D}}{\partial \boldsymbol{V}}\right) \cdot \boldsymbol{V} + \boldsymbol{C} + \frac{\partial \boldsymbol{F}^{INT}}{\partial \boldsymbol{D}} \cdot \frac{\partial \boldsymbol{D}}{\partial \boldsymbol{V}} - \frac{\partial \boldsymbol{F}^{EXT}}{\partial \boldsymbol{D}} \cdot \frac{\partial \boldsymbol{D}}{\partial \boldsymbol{V}} \tag{4.147}$$

where,

$$\frac{\partial \boldsymbol{D}}{\partial \boldsymbol{V}} = \alpha \Delta t \tag{4.148}$$

$$\boldsymbol{C} \cdot \boldsymbol{V} = \begin{bmatrix} \boldsymbol{0} \\ \boldsymbol{K}^{wd} \cdot \dot{\boldsymbol{d}} - \boldsymbol{K}^{wg} \cdot \dot{\boldsymbol{p}}_w + \boldsymbol{K}^{wg} \cdot \dot{\boldsymbol{p}}_g + \boldsymbol{K}^{w\theta} \cdot \dot{\boldsymbol{\theta}} \\ \boldsymbol{K}^{gd} \cdot \dot{\boldsymbol{d}} + \boldsymbol{K}^{gw} \cdot \dot{\boldsymbol{p}}_w + \boldsymbol{K}^{gg} \cdot \dot{\boldsymbol{p}}_g + \boldsymbol{K}^{g\theta} \cdot \dot{\boldsymbol{\theta}} \\ \boldsymbol{K}^{\theta d} \cdot \dot{\boldsymbol{d}} + \boldsymbol{K}^{\theta g} \cdot \dot{\boldsymbol{p}}_w - \boldsymbol{K}^{\theta g} \cdot \dot{\boldsymbol{p}}_g v + \boldsymbol{K}^{\theta\theta} \cdot \dot{\boldsymbol{\theta}} \end{bmatrix} \tag{4.149}$$

then,

$$\frac{\partial \boldsymbol{C}}{\partial \boldsymbol{D}} \cdot \boldsymbol{V} = \begin{bmatrix} \mathbf{0} \\ \frac{\partial \boldsymbol{K}^{wd}}{\partial \boldsymbol{d}} \cdot \dot{\boldsymbol{d}} - \frac{\partial \boldsymbol{K}^{wg}}{\partial \boldsymbol{d}} \cdot \dot{\boldsymbol{p}}_w + \frac{\partial \boldsymbol{K}^{wg}}{\partial \boldsymbol{d}} \cdot \dot{\boldsymbol{p}}_g + \frac{\partial \boldsymbol{K}^{w\theta}}{\partial \boldsymbol{d}} \cdot \dot{\boldsymbol{\theta}} \\ \frac{\partial \boldsymbol{K}^{gd}}{\partial \boldsymbol{d}} \cdot \dot{\boldsymbol{d}} + \frac{\partial \boldsymbol{K}^{gw}}{\partial \boldsymbol{d}} \cdot \dot{\boldsymbol{p}}_w + \frac{\partial \boldsymbol{K}^{gg}}{\partial \boldsymbol{d}} \cdot \dot{\boldsymbol{p}}_g + \frac{\partial \boldsymbol{K}^{g\theta}}{\partial \boldsymbol{d}} \cdot \dot{\boldsymbol{\theta}} \\ \frac{\partial \boldsymbol{K}^{\theta d}}{\partial \boldsymbol{d}} \cdot \dot{\boldsymbol{d}} + \frac{\partial \boldsymbol{K}^{\theta g}}{\partial \boldsymbol{d}} \cdot \dot{\boldsymbol{p}}_w - \frac{\partial \boldsymbol{K}^{\theta g}}{\partial \boldsymbol{d}} \cdot \dot{\boldsymbol{p}}_g + \frac{\partial \boldsymbol{K}^{\theta\theta}}{\partial \boldsymbol{d}} \cdot \dot{\boldsymbol{\theta}} \end{bmatrix}$$

$$\begin{bmatrix} \mathbf{0} \\ \frac{\partial \boldsymbol{K}^{wd}}{\partial \boldsymbol{p}_w} \cdot \dot{\boldsymbol{d}} - \frac{\partial \boldsymbol{K}^{wg}}{\partial \boldsymbol{p}_w} \cdot \dot{\boldsymbol{p}}_w + \frac{\partial \boldsymbol{K}^{wg}}{\partial \boldsymbol{p}_w} \cdot \dot{\boldsymbol{p}}_g + \frac{\partial \boldsymbol{K}^{w\theta}}{\partial \boldsymbol{p}_w} \cdot \dot{\boldsymbol{\theta}} \\ \frac{\partial \boldsymbol{K}^{gd}}{\partial \boldsymbol{p}_w} \cdot \dot{\boldsymbol{d}} + \frac{\partial \boldsymbol{K}^{gw}}{\partial \boldsymbol{p}_w} \cdot \dot{\boldsymbol{p}}_w + \frac{\partial \boldsymbol{K}^{gg}}{\partial \boldsymbol{p}_w} \cdot \dot{\boldsymbol{p}}_g + \frac{\partial \boldsymbol{K}^{g\theta}}{\partial \boldsymbol{p}_w} \cdot \dot{\boldsymbol{\theta}} \\ \frac{\partial \boldsymbol{K}^{\theta d}}{\partial \boldsymbol{p}_w} \cdot \dot{\boldsymbol{d}} + \frac{\partial \boldsymbol{K}^{\theta g}}{\partial \boldsymbol{p}_w} \cdot \dot{\boldsymbol{p}}_w - \frac{\partial \boldsymbol{K}^{\theta g}}{\partial \boldsymbol{p}_w} \cdot \dot{\boldsymbol{p}}_g + \frac{\partial \boldsymbol{K}^{\theta\theta}}{\partial \boldsymbol{p}_w} \cdot \dot{\boldsymbol{\theta}} \end{bmatrix}$$

$$\begin{bmatrix} \mathbf{0} \\ \frac{\partial \boldsymbol{K}^{wd}}{\partial \boldsymbol{p}_g} \cdot \dot{\boldsymbol{d}} - \frac{\partial \boldsymbol{K}^{wg}}{\partial \boldsymbol{p}_g} \cdot \dot{\boldsymbol{p}}_w + \frac{\partial \boldsymbol{K}^{wg}}{\partial \boldsymbol{p}_g} \cdot \dot{\boldsymbol{p}}_g + \frac{\partial \boldsymbol{K}^{w\theta}}{\partial \boldsymbol{p}_g} \cdot \dot{\boldsymbol{\theta}} \\ \frac{\partial \boldsymbol{K}^{gd}}{\partial \boldsymbol{p}_g} \cdot \dot{\boldsymbol{d}} + \frac{\partial \boldsymbol{K}^{gw}}{\partial \boldsymbol{p}_g} \cdot \dot{\boldsymbol{p}}_w + \frac{\partial \boldsymbol{K}^{gg}}{\partial \boldsymbol{p}_g} \cdot \dot{\boldsymbol{p}}_g + \frac{\partial \boldsymbol{K}^{g\theta}}{\partial \boldsymbol{p}_g} \cdot \dot{\boldsymbol{\theta}} \\ \frac{\partial \boldsymbol{K}^{\theta d}}{\partial \boldsymbol{p}_g} \cdot \dot{\boldsymbol{d}} + \frac{\partial \boldsymbol{K}^{\theta g}}{\partial \boldsymbol{p}_g} \cdot \dot{\boldsymbol{p}}_w - \frac{\partial \boldsymbol{K}^{\theta g}}{\partial \boldsymbol{p}_g} \cdot \dot{\boldsymbol{p}}_g + \frac{\partial \boldsymbol{K}^{\theta\theta}}{\partial \boldsymbol{p}_g} \cdot \dot{\boldsymbol{\theta}} \end{bmatrix}$$

$$\begin{bmatrix} \mathbf{0} \\ \frac{\partial \boldsymbol{K}^{wd}}{\partial \boldsymbol{\theta}} \cdot \dot{\boldsymbol{d}} - \frac{\partial \boldsymbol{K}^{wg}}{\partial \boldsymbol{\theta}} \cdot \dot{\boldsymbol{p}}_w + \frac{\partial \boldsymbol{K}^{wg}}{\partial \boldsymbol{\theta}} \cdot \dot{\boldsymbol{p}}_g + \frac{\partial \boldsymbol{K}^{w\theta}}{\partial \boldsymbol{\theta}} \cdot \dot{\boldsymbol{\theta}} \\ \frac{\partial \boldsymbol{K}^{gd}}{\partial \boldsymbol{\theta}} \cdot \dot{\boldsymbol{d}} + \frac{\partial \boldsymbol{K}^{gw}}{\partial \boldsymbol{\theta}} \cdot \dot{\boldsymbol{p}}_w + \frac{\partial \boldsymbol{K}^{gg}}{\partial \boldsymbol{\theta}} \cdot \dot{\boldsymbol{p}}_g + \frac{\partial \boldsymbol{K}^{g\theta}}{\partial \boldsymbol{\theta}} \cdot \dot{\boldsymbol{\theta}} \\ \frac{\partial \boldsymbol{K}^{\theta d}}{\partial \boldsymbol{\theta}} \cdot \dot{\boldsymbol{d}} + \frac{\partial \boldsymbol{K}^{\theta g}}{\partial \boldsymbol{\theta}} \cdot \dot{\boldsymbol{p}}_w - \frac{\partial \boldsymbol{K}^{\theta g}}{\partial \boldsymbol{\theta}} \cdot \dot{\boldsymbol{p}}_g + \frac{\partial \boldsymbol{K}^{\theta\theta}}{\partial \boldsymbol{\theta}} \cdot \dot{\boldsymbol{\theta}} \end{bmatrix} \tag{4.150}$$

$$\frac{\partial \boldsymbol{F}^{INT}}{\partial \boldsymbol{D}} = \begin{bmatrix} \frac{\partial \boldsymbol{F}^{INT}}{\partial \boldsymbol{d}} & \frac{\partial \boldsymbol{F}^{INT}}{\partial \boldsymbol{p}_w} & \frac{\partial \boldsymbol{F}^{INT}}{\partial \boldsymbol{p}_g} & \frac{\partial \boldsymbol{F}^{INT}}{\partial \boldsymbol{\theta}} \end{bmatrix} \tag{4.151}$$

$$\frac{\partial \boldsymbol{F}^{INT}}{\partial \boldsymbol{d}} = \begin{bmatrix} \frac{\partial \boldsymbol{F}^{d,INT}}{\partial \boldsymbol{d}} \\ -\frac{\partial \boldsymbol{F}^{w1,INT}}{\partial \boldsymbol{d}} - \frac{\partial \boldsymbol{F}^{w2,INT}}{\partial \boldsymbol{d}} \\ -\frac{\partial \boldsymbol{F}^{g,INT}}{\partial \boldsymbol{d}} \\ \frac{\partial \boldsymbol{F}^{\theta 1,INT}}{\partial \boldsymbol{d}} + \frac{\partial \boldsymbol{F}^{\theta 2,INT}}{\partial \boldsymbol{d}} \end{bmatrix}, \quad \frac{\partial \boldsymbol{F}^{INT}}{\partial \boldsymbol{p}_w} = \begin{bmatrix} -\frac{\partial \boldsymbol{F}^{dp,INT}}{\partial \boldsymbol{p}_w} \\ -\frac{\partial \boldsymbol{F}^{w1,INT}}{\partial \boldsymbol{p}_w} - \frac{\partial \boldsymbol{F}^{w2,INT}}{\partial \boldsymbol{p}_w} \\ -\frac{\partial \boldsymbol{F}^{g,INT}}{\partial \boldsymbol{p}_w} \\ \frac{\partial \boldsymbol{F}^{\theta 1,INT}}{\partial \boldsymbol{p}_w} + \frac{\partial \boldsymbol{F}^{\theta 2,INT}}{\partial \boldsymbol{p}_w} \end{bmatrix}$$

$$\frac{\partial \boldsymbol{F}^{INT}}{\partial \boldsymbol{p}_g} = \begin{bmatrix} -\frac{\partial \boldsymbol{F}^{dp,INT}}{\partial \boldsymbol{p}_g} \\ -\frac{\partial \boldsymbol{F}^{w1,INT}}{\partial \boldsymbol{p}_g} - \frac{\partial \boldsymbol{F}^{w2,INT}}{\partial \boldsymbol{p}_g} \\ -\frac{\partial \boldsymbol{F}^{g,INT}}{\partial \boldsymbol{p}_g} \\ \frac{\partial \boldsymbol{F}^{\theta 1,INT}}{\partial \boldsymbol{p}_g} + \frac{\partial \boldsymbol{F}^{\theta 2,INT}}{\partial \boldsymbol{p}_g} \end{bmatrix}, \quad \frac{\partial \boldsymbol{F}^{INT}}{\partial \boldsymbol{\theta}} = \begin{bmatrix} -\frac{\partial \boldsymbol{F}^{d\theta,INT}}{\partial \boldsymbol{\theta}} \\ -\frac{\partial \boldsymbol{F}^{w1,INT}}{\partial \boldsymbol{\theta}} - \frac{\partial \boldsymbol{F}^{w2,INT}}{\partial \boldsymbol{\theta}} \\ -\frac{\partial \boldsymbol{F}^{g,INT}}{\partial \boldsymbol{\theta}} \\ \frac{\partial \boldsymbol{F}^{\theta 1,INT}}{\partial \boldsymbol{\theta}} + \frac{\partial \boldsymbol{F}^{\theta 2,INT}}{\partial \boldsymbol{\theta}} \end{bmatrix}$$

$$\frac{\partial \boldsymbol{F}^{EXT}}{\partial \boldsymbol{D}} = \left[\begin{array}{cccc} \frac{\partial \boldsymbol{F}^{EXT}}{\partial \boldsymbol{d}} & \frac{\partial \boldsymbol{F}^{EXT}}{\partial \boldsymbol{p}_w^e} & \frac{\partial \boldsymbol{F}^{EXT}}{\partial \boldsymbol{p}_g^e} & \frac{\partial \boldsymbol{F}^{EXT}}{\partial \boldsymbol{\theta}} \end{array} \right] \tag{4.152}$$

$$\frac{\partial \boldsymbol{F}^{EXT}}{\partial \boldsymbol{d}} = \left[\begin{array}{c} \frac{\partial \boldsymbol{F}^{df,EXT}}{\partial \boldsymbol{d}} \\ \mathbf{0} \\ \mathbf{0} \\ \frac{\partial \boldsymbol{F}^{\theta 3,EXT}}{\partial \boldsymbol{d}} \end{array} \right], \quad \frac{\partial \boldsymbol{F}^{EXT}}{\partial \boldsymbol{p}_w} = \left[\begin{array}{c} \frac{\partial \boldsymbol{F}^{d,EXT}}{\partial \boldsymbol{p}_w} \\ \frac{\partial \boldsymbol{F}^{w,EXT}}{\partial \boldsymbol{p}_w} \\ \frac{\partial \boldsymbol{F}^{g,EXT}}{\partial \boldsymbol{p}_w} \\ \frac{\partial \boldsymbol{F}^{\theta 3,EXT}}{\partial \boldsymbol{p}_w} \end{array} \right]$$

$$\frac{\partial \boldsymbol{F}^{EXT}}{\partial \boldsymbol{p}_g} = \left[\begin{array}{c} \frac{\partial \boldsymbol{F}^{d,EXT}}{\partial \boldsymbol{p}_g} \\ \frac{\partial \boldsymbol{F}^{w,EXT}}{\partial \boldsymbol{p}_g} \\ \frac{\partial \boldsymbol{F}^{g,EXT}}{\partial \boldsymbol{p}_g} \\ \frac{\partial \boldsymbol{F}^{\theta 3,EXT}}{\partial \boldsymbol{p}_g} \end{array} \right], \quad \frac{\partial \boldsymbol{F}^{EXT}}{\partial \boldsymbol{\theta}} = \left[\begin{array}{c} \frac{\partial \boldsymbol{F}^{d,EXT}}{\partial \boldsymbol{\theta}} \\ \frac{\partial \boldsymbol{F}^{w,EXT}}{\partial \boldsymbol{\theta}} \\ \frac{\partial \boldsymbol{F}^{g,EXT}}{\partial \boldsymbol{\theta}} \\ -\frac{\partial \boldsymbol{F}^{\theta 2,EXT}}{\partial \boldsymbol{\theta}} + \frac{\partial \boldsymbol{F}^{\theta 3,EXT}}{\partial \boldsymbol{\theta}} \end{array} \right]$$

The components in those tangent functions are written as follows:

$$\frac{\partial \boldsymbol{K}^{wd}}{\partial \boldsymbol{d}} \cdot \dot{\boldsymbol{d}} = \mathbf{0} \tag{4.153}$$

$$\frac{\partial \boldsymbol{K}^{gd}}{\partial \boldsymbol{d}} \cdot \dot{\boldsymbol{d}} = \mathbf{0} \tag{4.154}$$

$$\frac{\partial \boldsymbol{K}^{\theta d}}{\partial \boldsymbol{d}} \cdot \dot{\boldsymbol{d}} = \mathbf{0} \tag{4.155}$$

$$\begin{aligned} \frac{\partial \boldsymbol{K}^{wg}}{\partial \boldsymbol{d}} \cdot \dot{\boldsymbol{p}}_w &= \mathop{\mathbf{A}}_{e=1}^{n_{\text{el}}} \frac{\partial \boldsymbol{k}_e^{wg}}{\partial \boldsymbol{d}^e} \cdot \dot{\boldsymbol{p}}_w^e \\ &= \mathop{\mathbf{A}}_{e=1}^{n_{\text{el}}} \int_{\Omega^e} \dot{p}_w \left(S_g \frac{\partial \rho^{gvR}}{\partial s} + (\rho^{wR} - \rho^{gvR}) \frac{\partial S_w}{\partial s} \right) (\boldsymbol{N}^{e,p})^T \otimes \frac{\partial n}{\partial \boldsymbol{d}^e} da \end{aligned} \tag{4.156}$$

$$\begin{aligned} \frac{\partial \boldsymbol{K}^{gw}}{\partial \boldsymbol{d}} \cdot \dot{\boldsymbol{p}}_w &= \mathop{\mathbf{A}}_{e=1}^{n_{\text{el}}} \frac{\partial \boldsymbol{k}_e^{gw}}{\partial \boldsymbol{d}^e} \cdot \dot{\boldsymbol{p}}_w^e \\ &= \mathop{\mathbf{A}}_{e=1}^{n_{\text{el}}} \int_{\Omega^e} \dot{p}_w \left(S_g \frac{\partial \rho^{gaR}}{\partial p_w} + \rho^{gaR} \frac{\partial S_w}{\partial s} \right) (\boldsymbol{N}^{e,p})^T \otimes \frac{\partial n}{\partial \boldsymbol{d}^e} da \end{aligned} \tag{4.157}$$

$$\begin{aligned} \frac{\partial \boldsymbol{K}^{\theta g}}{\partial \boldsymbol{d}} \cdot \dot{\boldsymbol{p}}_w &= \mathop{\mathbf{A}}_{e=1}^{n_{\text{el}}} \frac{\partial \boldsymbol{k}_e^{\theta g}}{\partial \boldsymbol{d}^e} \cdot \dot{\boldsymbol{p}}_w^e \\ &= \mathop{\mathbf{A}}_{e=1}^{n_{\text{el}}} \int_{\Omega^e} \dot{p}_w \left(\rho^{wR} \Delta H_{vap} \right) \frac{\partial S_w}{\partial s} (\boldsymbol{N}^{e,p})^T \otimes \frac{\partial n}{\partial \boldsymbol{d}^e} da \end{aligned} \tag{4.158}$$

$$\frac{\partial \boldsymbol{K}^{wg}}{\partial \boldsymbol{d}} \cdot \dot{\boldsymbol{p}}_g = \mathop{\mathsf{A}}_{e=1}^{n_{\mathrm{el}}} \frac{\partial \boldsymbol{k}_e^{wg}}{\partial \boldsymbol{d}^e} \cdot \dot{\boldsymbol{p}}_g^e$$

$$= \mathop{\mathsf{A}}_{e=1}^{n_{\mathrm{el}}} \int_{\Omega^e} \dot{p}_g \left(S_g \frac{\partial \rho^{gvR}}{\partial s} + (\rho^{wR} - \rho^{gvR}) \frac{\partial S_w}{\partial s} \right) (\boldsymbol{N}^{e,p})^T \otimes \frac{\partial n}{\partial \boldsymbol{d}^e} da \tag{4.159}$$

$$\frac{\partial \boldsymbol{K}^{gg}}{\partial \boldsymbol{d}} \cdot \dot{\boldsymbol{p}}_g = \mathop{\mathsf{A}}_{e=1}^{n_{\mathrm{el}}} \frac{\partial \boldsymbol{k}_e^{gg}}{\partial \boldsymbol{d}^e} \cdot \dot{\boldsymbol{p}}_g^e$$

$$= \mathop{\mathsf{A}}_{e=1}^{n_{\mathrm{el}}} \int_{\Omega^e} \dot{p}_g \left(S_g \frac{\partial \rho^{gaR}}{\partial p_g} - \rho^{gaR} \frac{\partial S_w}{\partial s} \right) (\boldsymbol{N}^{e,p})^T \otimes \frac{\partial n}{\partial \boldsymbol{d}^e} da \tag{4.160}$$

$$\frac{\partial \boldsymbol{K}^{\theta g}}{\partial \boldsymbol{d}} \cdot \dot{\boldsymbol{p}}_g = \mathop{\mathsf{A}}_{e=1}^{n_{\mathrm{el}}} \frac{\partial \boldsymbol{k}_e^{\theta g}}{\partial \boldsymbol{d}^e} \cdot \dot{\boldsymbol{p}}_g^e$$

$$= \mathop{\mathsf{A}}_{e=1}^{n_{\mathrm{el}}} \int_{\Omega^e} \dot{p}_g \left(\rho^{wR} \Delta H_{vap} \right) \frac{\partial S_w}{\partial s} (\boldsymbol{N}^{e,p})^T \otimes \frac{\partial n}{\partial \boldsymbol{d}^e} da \tag{4.161}$$

$$\frac{\partial \boldsymbol{K}^{w\theta}}{\partial \boldsymbol{d}} \cdot \dot{\boldsymbol{\theta}} = \mathop{\mathsf{A}}_{e=1}^{n_{\mathrm{el}}} \frac{\partial \boldsymbol{k}_e^{w\theta}}{\partial \boldsymbol{d}^e} \cdot \dot{\boldsymbol{\theta}}^e$$

$$= \mathop{\mathsf{A}}_{e=1}^{n_{\mathrm{el}}} \int_{\Omega^e} \dot{\theta} (\boldsymbol{N}^{e,p})^T \otimes \left(\frac{\partial n}{\partial \boldsymbol{d}^e} S_g \frac{\partial \rho^{gvR}}{\partial \theta} - \frac{\partial \beta_{swg}}{\partial \boldsymbol{d}^e} \right) da \tag{4.162}$$

$$\frac{\partial \boldsymbol{K}^{g\theta}}{\partial \boldsymbol{d}} \cdot \dot{\boldsymbol{\theta}} = \mathop{\mathsf{A}}_{e=1}^{n_{\mathrm{el}}} \frac{\partial \boldsymbol{k}_e^{g\theta}}{\partial \boldsymbol{d}^e} \cdot \dot{\boldsymbol{\theta}}^e$$

$$= \mathop{\mathsf{A}}_{e=1}^{n_{\mathrm{el}}} \int_{\Omega^e} \dot{\theta} (\boldsymbol{N}^{e,p})^T \otimes \frac{\partial n}{\partial \boldsymbol{d}^e} \left(S_g \frac{\partial \rho^{gaR}}{\partial \theta} + \beta_s \rho^{gaR} S_g \right) da \tag{4.163}$$

$$\frac{\partial \boldsymbol{K}^{\theta\theta}}{\partial \boldsymbol{d}} \cdot \dot{\boldsymbol{\theta}} = \mathop{\mathsf{A}}_{e=1}^{n_{\mathrm{el}}} \frac{\partial \boldsymbol{k}_e^{\theta\theta}}{\partial \boldsymbol{d}^e} \cdot \dot{\boldsymbol{\theta}}^e$$

$$= \mathop{\mathsf{A}}_{e=1}^{n_{\mathrm{el}}} \int_{\Omega^e} \dot{\theta} \left[\frac{\partial (\rho C)_{eff}}{\partial n} + \Delta H_{vap} S_w \rho^{wR} (\beta_w - \beta_s) \right] \cdot (\boldsymbol{N}^{e,\theta})^T \otimes \frac{\partial n}{\partial \boldsymbol{d}^e} da \tag{4.164}$$

$$\frac{\partial \boldsymbol{K}^{wd}}{\partial \boldsymbol{p}_w} \cdot \dot{\boldsymbol{d}} = \mathop{\mathsf{A}}_{e=1}^{n_{\mathrm{el}}} \frac{\partial \boldsymbol{k}_e^{wd}}{\partial \boldsymbol{p}_w^e} \cdot \dot{\boldsymbol{d}}^e$$

$$= \mathop{\mathsf{A}}_{e=1}^{n_{\mathrm{el}}} \int_{\Omega^e} \dot{\epsilon}_v (\boldsymbol{N}^{e,p})^T \cdot \left(\rho^{gvR} \frac{\partial S_w}{\partial s} - \rho^{wR} \frac{\partial S_w}{\partial s} - S_g \frac{\partial \rho^{gvR}}{\partial s} \right) \boldsymbol{N}^{e,p} da \tag{4.165}$$

$$\frac{\partial \boldsymbol{K}^{gd}}{\partial \boldsymbol{p}_w} \cdot \dot{\boldsymbol{d}} = \mathop{\mathsf{A}}_{e=1}^{n_{\mathrm{el}}} \frac{\partial \boldsymbol{k}_e^{gd}}{\partial \boldsymbol{p}_w^e} \cdot \dot{\boldsymbol{d}}^e$$

$$= \mathop{\mathsf{A}}_{e=1}^{n_{\mathrm{el}}} \int_{\Omega^e} \dot{\epsilon}_v (\boldsymbol{N}^{e,p})^T \cdot \left(\rho^{gaR} \frac{\partial S_w}{\partial s} + S_g \frac{\partial \rho^{gaR}}{\partial p_w} \right) \boldsymbol{N}^{e,p} da \tag{4.166}$$

$$\frac{\partial \boldsymbol{K}^{\theta d}}{\partial \boldsymbol{p}_w} \cdot \dot{\boldsymbol{d}} = \mathop{\mathsf{A}}_{e=1}^{n_{\mathrm{el}}} \frac{\partial \boldsymbol{k}_e^{\theta d}}{\partial \boldsymbol{p}_w^e} \cdot \dot{\boldsymbol{d}}^e$$

$$= \mathop{\mathbf{A}}_{e=1}^{n_{\text{el}}} \int_{\Omega^e} \dot{\epsilon}_v (\boldsymbol{N}^{e,\theta})^T \cdot \left(\Delta H_{vap} \rho^{wR} \frac{\partial S_w}{\partial s} \right) \boldsymbol{N}^{e,p} da \tag{4.167}$$

$$\begin{aligned}
\frac{\partial \boldsymbol{K}^{wg}}{\partial \boldsymbol{p}_w} \cdot \dot{\boldsymbol{p}}_w &= \mathop{\mathbf{A}}_{e=1}^{n_{\text{el}}} \frac{\partial \boldsymbol{k}_e^{wg}}{\partial \boldsymbol{p}_w^e} \cdot \dot{\boldsymbol{p}}_w^e \\
&= \mathop{\mathbf{A}}_{e=1}^{n_{\text{el}}} \int_{\Omega^e} \dot{p}_w \cdot \left[2n \frac{\partial \rho^{gvR}}{\partial s} \frac{\partial S_w}{\partial s} - n S_g \frac{\partial^2 \rho^{gvR}}{\partial s^2} - n(\rho^{wR} - \rho^{gvR}) \frac{\partial^2 S_w}{\partial s^2} \right] \\
&\qquad \cdot (\boldsymbol{N}^{e,p})^T \cdot \boldsymbol{N}^{e,p} da
\end{aligned} \tag{4.168}$$

$$\begin{aligned}
\frac{\partial \boldsymbol{K}^{gw}}{\partial \boldsymbol{p}_w} \cdot \dot{\boldsymbol{p}}_w &= \mathop{\mathbf{A}}_{e=1}^{n_{\text{el}}} \frac{\partial \boldsymbol{k}_e^{gw}}{\partial \boldsymbol{p}_w^e} \cdot \dot{\boldsymbol{p}}_w^e \\
&= \mathop{\mathbf{A}}_{e=1}^{n_{\text{el}}} \int_{\Omega^e} \dot{p}_w (\boldsymbol{N}^{e,p})^T \cdot \left(n S_g \frac{\partial^2 \rho^{gaR}}{\partial {p_w}^2} - n \rho^{gaR} \frac{\partial^2 S_w}{\partial s^2} \right) \boldsymbol{N}^{e,p} da
\end{aligned} \tag{4.169}$$

$$\begin{aligned}
\frac{\partial \boldsymbol{K}^{\theta g}}{\partial \boldsymbol{p}_w} \cdot \dot{\boldsymbol{p}}_w &= \mathop{\mathbf{A}}_{e=1}^{n_{\text{el}}} \frac{\partial \boldsymbol{k}_e^{\theta g}}{\partial \boldsymbol{p}_w^e} \cdot \dot{\boldsymbol{p}}_w^e \\
&= \mathop{\mathbf{A}}_{e=1}^{n_{\text{el}}} \int_{\Omega^e} \dot{p}_w \cdot \left(-n \rho^{wR} \Delta H_{vap} \frac{\partial^2 S_w}{\partial s^2} \right) \cdot (\boldsymbol{N}^{e,\theta})^T \cdot \boldsymbol{N}^{e,p} da
\end{aligned} \tag{4.170}$$

$$\begin{aligned}
\frac{\partial \boldsymbol{K}^{wg}}{\partial \boldsymbol{p}_w} \cdot \dot{\boldsymbol{p}}_g &= \mathop{\mathbf{A}}_{e=1}^{n_{\text{el}}} \frac{\partial \boldsymbol{k}_e^{wg}}{\partial \boldsymbol{p}_w^e} \cdot \dot{\boldsymbol{p}}_g^e \\
&= \mathop{\mathbf{A}}_{e=1}^{n_{\text{el}}} \int_{\Omega^e} \dot{p}_g \cdot n \left(2 \frac{\partial \rho^{gvR}}{\partial s} \frac{\partial S_w}{\partial s} - S_g \frac{\partial^2 \rho^{gvR}}{\partial s^2} - (\rho^{wR} - \rho^{gvR}) \frac{\partial^2 S_w}{\partial s^2} \right) \\
&\qquad \cdot (\boldsymbol{N}^{e,p})^T \cdot \boldsymbol{N}^{e,p} da
\end{aligned} \tag{4.171}$$

$$\begin{aligned}
\frac{\partial \boldsymbol{K}^{gg}}{\partial \boldsymbol{p}_w} \cdot \dot{\boldsymbol{p}}_g &= \mathop{\mathbf{A}}_{e=1}^{n_{\text{el}}} \frac{\partial \boldsymbol{k}_e^{gg}}{\partial \boldsymbol{p}_w^e} \cdot \dot{\boldsymbol{p}}_g^e \\
&= \mathop{\mathbf{A}}_{e=1}^{n_{\text{el}}} \int_{\Omega^e} \dot{p}_g \cdot n \left(\left(\frac{\partial \rho^{gaR}}{\partial p_g} - \frac{\partial \rho^{gaR}}{\partial p_w} \right) \frac{\partial S_w}{\partial s} + S_g \frac{\partial^2 \rho^{gaR}}{\partial p_g \partial p_w} + \rho^{gaR} \frac{\partial^2 S_w}{\partial s^2} \right) \\
&\qquad \cdot (\boldsymbol{N}^{e,p})^T \cdot \boldsymbol{N}^{e,p} da
\end{aligned} \tag{4.172}$$

$$\begin{aligned}
\frac{\partial \boldsymbol{K}^{\theta g}}{\partial \boldsymbol{p}_w} \cdot \dot{\boldsymbol{p}}_g &= \mathop{\mathbf{A}}_{e=1}^{n_{\text{el}}} \frac{\partial \boldsymbol{k}_e^{\theta g}}{\partial \boldsymbol{p}_w^e} \cdot \dot{\boldsymbol{p}}_g^e \\
&= \mathop{\mathbf{A}}_{e=1}^{n_{\text{el}}} \int_{\Omega^e} \dot{p}_g \cdot \left(-n \rho^{wR} \Delta H_{vap} \frac{\partial^2 S_w}{\partial s^2} \right) \cdot (\boldsymbol{N}^{e,p})^T \cdot \boldsymbol{N}^{e,p} da
\end{aligned} \tag{4.173}$$

$$\begin{aligned}
\frac{\partial \boldsymbol{K}^{w\theta}}{\partial \boldsymbol{p}_w} \cdot \dot{\boldsymbol{\theta}} &= \mathop{\mathbf{A}}_{e=1}^{n_{\text{el}}} \frac{\partial \boldsymbol{k}_e^{w\theta}}{\partial \boldsymbol{p}_w^e} \cdot \dot{\boldsymbol{\theta}}^e \\
&= \mathop{\mathbf{A}}_{e=1}^{n_{\text{el}}} \int_{\Omega^e} \dot{\theta} (\boldsymbol{N}^{e,p})^T \cdot \left[n \frac{\partial \rho^{gvR}}{\partial \theta} \frac{\partial S_w}{\partial s} - n S_g \frac{\partial^2 \rho^{gvR}}{\partial s \partial \theta} + \frac{\partial \beta_{swg}}{\partial s} \right] \boldsymbol{N}^{e,p} da
\end{aligned} \tag{4.174}$$

$$\frac{\partial \boldsymbol{K}^{g\theta}}{\partial \boldsymbol{p}_w} \cdot \dot{\boldsymbol{\theta}} = \mathop{\mathbf{A}}_{e=1}^{n_{\text{el}}} \frac{\partial \boldsymbol{k}_e^{g\theta}}{\partial \boldsymbol{p}_w^e} \cdot \dot{\boldsymbol{\theta}}^e$$

$$= \mathop{\mathbf{A}}_{e=1}^{n_{\text{el}}} \int_{\Omega^e} \dot{\theta} \cdot \left[n \frac{\partial \rho^{gaR}}{\partial \theta} \frac{\partial S_w}{\partial s} + n S_g \frac{\partial^2 \rho^{gaR}}{\partial p_w \partial \theta} - \beta_s (1-n) S_g \frac{\partial \rho^{gaR}}{\partial p_w} \right.$$
$$\left. - \beta_s (1-n) \rho^{gaR} \frac{\partial S_w}{\partial s} \right] \cdot (\boldsymbol{N}^{e,p})^T \cdot \boldsymbol{N}^{e,p} da \quad (4.175)$$

$$\frac{\partial \boldsymbol{K}^{\theta\theta}}{\partial \boldsymbol{p}_w} \cdot \dot{\boldsymbol{\theta}} = \mathop{\mathbf{A}}_{e=1}^{n_{\text{el}}} \frac{\partial \boldsymbol{k}_e^{\theta\theta}}{\partial \boldsymbol{p}_w^e} \cdot \dot{\boldsymbol{\theta}}^e$$
$$= \mathop{\mathbf{A}}_{e=1}^{n_{\text{el}}} \int_{\Omega^e} \dot{\theta} \cdot \left[\frac{\partial (\rho C)_{eff}}{\partial p_w} - \Delta H_{vap} \rho^{wR} [\beta_w n + \beta_s (1-n)] \frac{\partial S_w}{\partial s} \right]$$
$$\cdot (\boldsymbol{N}^{e,\theta})^T \cdot \boldsymbol{N}^{e,p} da \quad (4.176)$$

$$\frac{\partial \boldsymbol{K}^{wd}}{\partial \boldsymbol{p}_g} \cdot \dot{\boldsymbol{d}} = \mathop{\mathbf{A}}_{e=1}^{n_{\text{el}}} \frac{\partial \boldsymbol{k}_e^{wd}}{\partial \boldsymbol{p}_g^e} \cdot \dot{\boldsymbol{d}}^e$$
$$= \mathop{\mathbf{A}}_{e=1}^{n_{\text{el}}} \int_{\Omega^e} \dot{\epsilon}_v (\boldsymbol{N}^{e,p})^T \cdot \left(\rho^{wR} \frac{\partial S_w}{\partial s} - \rho^{gvR} \frac{\partial S_w}{\partial s} + S_g \frac{\partial \rho^{gvR}}{\partial s} \right) \boldsymbol{N}^{e,p} da \quad (4.177)$$

$$\frac{\partial \boldsymbol{K}^{gd}}{\partial \boldsymbol{p}_g} \cdot \dot{\boldsymbol{d}} = \mathop{\mathbf{A}}_{e=1}^{n_{\text{el}}} \frac{\partial \boldsymbol{k}_e^{gd}}{\partial \boldsymbol{p}_g^e} \cdot \dot{\boldsymbol{d}}^e$$
$$= \mathop{\mathbf{A}}_{e=1}^{n_{\text{el}}} \int_{\Omega^e} \dot{\epsilon}_v (\boldsymbol{N}^{e,p})^T \cdot \left(S_g \frac{\partial \rho^{gaR}}{\partial p_g} - \rho^{gaR} \frac{\partial S_w}{\partial s} \right) \boldsymbol{N}^{e,p} da \quad (4.178)$$

$$\frac{\partial \boldsymbol{K}^{\theta d}}{\partial \boldsymbol{p}_g} \cdot \dot{\boldsymbol{d}} = \mathop{\mathbf{A}}_{e=1}^{n_{\text{el}}} \frac{\partial \boldsymbol{k}_e^{\theta d}}{\partial \boldsymbol{p}_g^e} \cdot \dot{\boldsymbol{d}}^e$$
$$= \mathop{\mathbf{A}}_{e=1}^{n_{\text{el}}} \int_{\Omega^e} \dot{\epsilon}_v (\boldsymbol{N}^{e,\theta})^T \cdot \left(-\Delta H_{vap} \rho^{wR} \frac{\partial S_w}{\partial s} \right) \boldsymbol{N}^{e,p} da \quad (4.179)$$

$$\frac{\partial \boldsymbol{K}^{wg}}{\partial \boldsymbol{p}_g} \cdot \dot{\boldsymbol{p}}_w = \mathop{\mathbf{A}}_{e=1}^{n_{\text{el}}} \frac{\partial \boldsymbol{k}_e^{wg}}{\partial \boldsymbol{p}_g^e} \cdot \dot{\boldsymbol{p}}_w^e$$
$$= \mathop{\mathbf{A}}_{e=1}^{n_{\text{el}}} \int_{\Omega^e} \dot{p}_w \cdot \left(-2n \frac{\partial \rho^{gvR}}{\partial s} \frac{\partial S_w}{\partial s} + n S_g \frac{\partial^2 \rho^{gvR}}{\partial s^2} + n (\rho^{wR} - \rho^{gvR}) \frac{\partial^2 S_w}{\partial s^2} \right)$$
$$\cdot (\boldsymbol{N}^{e,p})^T \cdot \boldsymbol{N}^{e,p} da \quad (4.180)$$

$$\frac{\partial \boldsymbol{K}^{gw}}{\partial \boldsymbol{p}_g} \cdot \dot{\boldsymbol{p}}_w = \mathop{\mathbf{A}}_{e=1}^{n_{\text{el}}} \frac{\partial \boldsymbol{k}_e^{gw}}{\partial \boldsymbol{p}_g^e} \cdot \dot{\boldsymbol{p}}_w^e$$
$$= \mathop{\mathbf{A}}_{e=1}^{n_{\text{el}}} \int_{\Omega^e} \dot{p}_w \cdot n \left[\frac{\partial S_w}{\partial s} \left(\frac{\partial \rho^{gaR}}{\partial p_g} - \frac{\partial \rho^{gaR}}{\partial p_g} \right) + S_g \frac{\partial^2 \rho^{gaR}}{\partial p_w \partial p_g} + \rho^{gaR} \frac{\partial^2 S_w}{\partial s^2} \right]$$
$$\cdot (\boldsymbol{N}^{e,p})^T \cdot \boldsymbol{N}^{e,p} da \quad (4.181)$$

$$\frac{\partial \boldsymbol{K}^{\theta g}}{\partial \boldsymbol{p}_g} \cdot \dot{\boldsymbol{p}}_w = \mathop{\mathbf{A}}_{e=1}^{n_{\text{el}}} \frac{\partial \boldsymbol{k}_e^{\theta g}}{\partial \boldsymbol{p}_g^e} \cdot \dot{\boldsymbol{p}}_w^e$$
$$= \mathop{\mathbf{A}}_{e=1}^{n_{\text{el}}} \int_{\Omega^e} \dot{p}_w \cdot \left(n \rho^{wR} \Delta H_{vap} \frac{\partial^2 S_w}{\partial s^2} \right) \cdot (\boldsymbol{N}^{e,p})^T \cdot \boldsymbol{N}^{e,p} da \quad (4.182)$$

$$\frac{\partial \boldsymbol{K}^{wg}}{\partial \boldsymbol{p}_g}\cdot\dot{\boldsymbol{p}}_g = \mathop{\mathsf{A}}_{e=1}^{n_{\mathrm{el}}}\frac{\partial \boldsymbol{k}_e^{wg}}{\partial \boldsymbol{p}_g^e}\cdot\dot{\boldsymbol{p}}_g^e$$
$$= \mathop{\mathsf{A}}_{e=1}^{n_{\mathrm{el}}}\int_{\Omega^e}\dot{p}_g(\boldsymbol{N}^{e,p})^T\left[-2n\frac{\partial\rho^{gvR}}{\partial s}\frac{\partial S_w}{\partial s}+nS_g\frac{\partial^2\rho^{gvR}}{\partial s^2}+n(\rho^{wR}-\rho^{gvR})\frac{\partial^2 S_w}{\partial s^2}\right]$$
$$\cdot(\boldsymbol{N}^{e,p})^T\cdot\boldsymbol{N}^{e,p}da \qquad (4.183)$$

$$\frac{\partial \boldsymbol{K}^{gg}}{\partial \boldsymbol{p}_g}\cdot\dot{\boldsymbol{p}}_g = \mathop{\mathsf{A}}_{e=1}^{n_{\mathrm{el}}}\frac{\partial \boldsymbol{k}_e^{gg}}{\partial \boldsymbol{p}_g^e}\cdot\dot{\boldsymbol{p}}_g^e$$
$$= \mathop{\mathsf{A}}_{e=1}^{n_{\mathrm{el}}}\int_{\Omega^e}\dot{p}_g\cdot n\left(-2\frac{\partial\rho^{gaR}}{\partial p_g}\frac{\partial S_w}{\partial s}+S_g\frac{\partial^2\rho^{gaR}}{\partial {p_g}^2}-\rho^{gaR}\frac{\partial^2 S_w}{\partial s^2}\right)$$
$$\cdot(\boldsymbol{N}^{e,p})^T\cdot\boldsymbol{N}^{e,p}da \qquad (4.184)$$

$$\frac{\partial \boldsymbol{K}^{\theta g}}{\partial \boldsymbol{p}_g}\cdot\dot{\boldsymbol{p}}_g = \mathop{\mathsf{A}}_{e=1}^{n_{\mathrm{el}}}\frac{\partial \boldsymbol{k}_e^{\theta g}}{\partial \boldsymbol{p}_g^e}\cdot\dot{\boldsymbol{p}}_g^e$$
$$= \mathop{\mathsf{A}}_{e=1}^{n_{\mathrm{el}}}\int_{\Omega^e}\dot{p}_g\cdot\left(n\rho^{wR}\Delta H_{vap}\frac{\partial^2 S_w}{\partial s^2}\right)\cdot(\boldsymbol{N}^{e,p})^T\cdot\boldsymbol{N}^{e,p}da \qquad (4.185)$$

$$\frac{\partial \boldsymbol{K}^{w\theta}}{\partial \boldsymbol{p}_g}\cdot\dot{\boldsymbol{\theta}} = \mathop{\mathsf{A}}_{e=1}^{n_{\mathrm{el}}}\frac{\partial \boldsymbol{k}_e^{w\theta}}{\partial \boldsymbol{p}_g^e}\cdot\dot{\boldsymbol{\theta}}^e$$
$$= \mathop{\mathsf{A}}_{e=1}^{n_{\mathrm{el}}}\int_{\Omega^e}\dot{\theta}\cdot\left[-n\frac{\partial\rho^{gvR}}{\partial\theta}\frac{\partial S_w}{\partial s}+nS_g\frac{\partial^2\rho^{gvR}}{\partial s\partial\theta}-\frac{\partial\beta_{swg}}{\partial s}\right]$$
$$\cdot(\boldsymbol{N}^{e,p})^T\cdot\boldsymbol{N}^{e,p}da \qquad (4.186)$$

$$\frac{\partial \boldsymbol{K}^{g\theta}}{\partial \boldsymbol{p}_g}\cdot\dot{\boldsymbol{\theta}} = \mathop{\mathsf{A}}_{e=1}^{n_{\mathrm{el}}}\frac{\partial \boldsymbol{k}_e^{g\theta}}{\partial \boldsymbol{p}_g^e}\cdot\dot{\boldsymbol{\theta}}^e$$
$$= \mathop{\mathsf{A}}_{e=1}^{n_{\mathrm{el}}}\int_{\Omega^e}\dot{\theta}\cdot\left[-n\frac{\partial\rho^{gaR}}{\partial\theta}\frac{\partial S_w}{\partial s}+nS_g\frac{\partial^2\rho^{gaR}}{\partial p_g\partial\theta}-\beta_s(1-n)S_g\frac{\partial\rho^{gaR}}{\partial p_g}\right.$$
$$\left.+\beta_s(1-n)\rho^{gaR}\frac{\partial S_w}{\partial s}\right]\cdot(\boldsymbol{N}^{e,p})^T\cdot\boldsymbol{N}^{e,p}da \qquad (4.187)$$

$$\frac{\partial \boldsymbol{K}^{\theta\theta}}{\partial \boldsymbol{p}_g}\cdot\dot{\boldsymbol{\theta}} = \mathop{\mathsf{A}}_{e=1}^{n_{\mathrm{el}}}\frac{\partial \boldsymbol{k}_e^{\theta\theta}}{\partial \boldsymbol{p}_g^e}\cdot\dot{\boldsymbol{\theta}}^e$$
$$= \mathop{\mathsf{A}}_{e=1}^{n_{\mathrm{el}}}\int_{\Omega^e}\dot{\theta}\cdot\left\{\frac{\partial(\rho C)_{eff}}{\partial p_g}+\Delta H_{vap}\rho^{wR}[\beta_w n+\beta_s(1-n)]\frac{\partial S_w}{\partial s}\right\}$$
$$\cdot(\boldsymbol{N}^{e,\theta})^T\cdot\boldsymbol{N}^{e,p}da \qquad (4.188)$$

$$\frac{\partial \boldsymbol{K}^{wd}}{\partial \boldsymbol{\theta}}\cdot\dot{\boldsymbol{d}} = \mathop{\mathsf{A}}_{e=1}^{n_{\mathrm{el}}}\frac{\partial \boldsymbol{k}_e^{wd}}{\partial \boldsymbol{\theta}^e}\cdot\dot{\boldsymbol{d}}^e$$
$$= \mathop{\mathsf{A}}_{e=1}^{n_{\mathrm{el}}}\int_{\Omega^e}\dot{\epsilon}_v(\boldsymbol{N}^{e,p})^T\cdot\left(S_w\frac{\partial\rho^{wR}}{\partial\theta}+S_g\frac{\partial\rho^{gvR}}{\partial\theta}\right)\boldsymbol{N}^{e,\theta}da \qquad (4.189)$$

$$\frac{\partial \boldsymbol{K}^{gd}}{\partial \boldsymbol{\theta}} \cdot \dot{\boldsymbol{d}} = \mathop{\mathsf{A}}_{e=1}^{n_{\mathrm{el}}} \frac{\partial \boldsymbol{k}_e^{gd}}{\partial \boldsymbol{\theta}^e} \cdot \dot{\boldsymbol{d}}^e$$

$$= \mathop{\mathsf{A}}_{e=1}^{n_{\mathrm{el}}} \int_{\Omega^e} \dot{\epsilon}_v (\boldsymbol{N}^{e,p})^T \cdot \left(\frac{\partial \rho^{gaR}}{\partial \theta} S_g \right) \boldsymbol{N}^{e,\theta} da \tag{4.190}$$

$$\frac{\partial \boldsymbol{K}^{\theta d}}{\partial \boldsymbol{\theta}} \cdot \dot{\boldsymbol{d}} = \mathop{\mathsf{A}}_{e=1}^{n_{\mathrm{el}}} \frac{\partial \boldsymbol{k}_e^{\theta d}}{\partial \boldsymbol{\theta}^e} \cdot \dot{\boldsymbol{d}}^e$$

$$= \mathop{\mathsf{A}}_{e=1}^{n_{\mathrm{el}}} \int_{\Omega^e} \dot{\epsilon}_v (\boldsymbol{N}^{e,p})^T \cdot \left(-\Delta H_{vap} S_w \frac{\partial \rho^{wR}}{\partial \theta} \right) \boldsymbol{N}^{e,\theta} da \tag{4.191}$$

$$\frac{\partial \boldsymbol{K}^{wg}}{\partial \boldsymbol{\theta}} \cdot \dot{\boldsymbol{p}}_w = \mathop{\mathsf{A}}_{e=1}^{n_{\mathrm{el}}} \frac{\partial \boldsymbol{k}_e^{wg}}{\partial \boldsymbol{\theta}^e} \cdot \dot{\boldsymbol{p}}_w^e$$

$$= \mathop{\mathsf{A}}_{e=1}^{n_{\mathrm{el}}} \int_{\Omega^e} \dot{p}_w (\boldsymbol{N}^{e,p})^T \cdot \left[n S_g \frac{\partial^2 \rho^{gvR}}{\partial s \partial \theta} + n \left(\frac{\partial \rho^{wR}}{\partial \theta} - \frac{\partial \rho^{gvR}}{\partial \theta} \right) \frac{\partial S_w}{\partial s} \right] \cdot (\boldsymbol{N}^{e,p})^T \cdot \boldsymbol{N}^{e,\theta} da \tag{4.192}$$

$$\frac{\partial \boldsymbol{K}^{gw}}{\partial \boldsymbol{\theta}} \cdot \dot{\boldsymbol{p}}_w = \mathop{\mathsf{A}}_{e=1}^{n_{\mathrm{el}}} \frac{\partial \boldsymbol{k}_e^{gw}}{\partial \boldsymbol{\theta}^e} \cdot \dot{\boldsymbol{p}}_w^e$$

$$= \mathop{\mathsf{A}}_{e=1}^{n_{\mathrm{el}}} \int_{\Omega^e} \dot{p}_w (\boldsymbol{N}^{e,p})^T \cdot \left(n S_g \frac{\partial^2 \rho^{gaR}}{\partial p_w \partial \theta} + n \frac{\partial \rho^{gaR}}{\partial \theta} \frac{\partial S_w}{\partial s} \right) \boldsymbol{N}^{e,\theta} da \tag{4.193}$$

$$\frac{\partial \boldsymbol{K}^{\theta g}}{\partial \boldsymbol{\theta}} \cdot \dot{\boldsymbol{p}}_w = \mathop{\mathsf{A}}_{e=1}^{n_{\mathrm{el}}} \frac{\partial \boldsymbol{k}_e^{\theta g}}{\partial \boldsymbol{\theta}^e} \cdot \dot{\boldsymbol{p}}_w^e$$

$$= \mathop{\mathsf{A}}_{e=1}^{n_{\mathrm{el}}} \int_{\Omega^e} \dot{p}_w (\boldsymbol{N}^{e,\theta})^T \cdot \left(n \Delta H_{vap} \frac{\partial \rho^{wR}}{\partial \theta} \frac{\partial S_w}{\partial s} \right) \boldsymbol{N}^{e,\theta} da \tag{4.194}$$

$$\frac{\partial \boldsymbol{K}^{wg}}{\partial \boldsymbol{\theta}} \cdot \dot{\boldsymbol{p}}_g = \mathop{\mathsf{A}}_{e=1}^{n_{\mathrm{el}}} \frac{\partial \boldsymbol{k}_e^{wg}}{\partial \boldsymbol{\theta}^e} \cdot \dot{\boldsymbol{p}}_g^e$$

$$= \mathop{\mathsf{A}}_{e=1}^{n_{\mathrm{el}}} \int_{\Omega^e} \dot{p}_g \cdot \left[n S_g \frac{\partial^2 \rho^{gvR}}{\partial s \partial \theta} + n \left(\frac{\partial \rho^{wR}}{\partial \theta} - \frac{\partial \rho^{gvR}}{\partial \theta} \right) \frac{\partial S_w}{\partial s} \right] \cdot (\boldsymbol{N}^{e,p})^T \cdot \boldsymbol{N}^{e,\theta} da \tag{4.195}$$

$$\frac{\partial \boldsymbol{K}^{gg}}{\partial \boldsymbol{\theta}} \cdot \dot{\boldsymbol{p}}_g = \mathop{\mathsf{A}}_{e=1}^{n_{\mathrm{el}}} \frac{\partial \boldsymbol{k}_e^{gg}}{\partial \boldsymbol{\theta}^e} \cdot \dot{\boldsymbol{p}}_g^e$$

$$= \mathop{\mathsf{A}}_{e=1}^{n_{\mathrm{el}}} \int_{\Omega^e} \dot{p}_g (\boldsymbol{N}^{e,p})^T \cdot \left(n S_g \frac{\partial^2 \rho^{gaR}}{\partial p_g \partial \theta} - n \frac{\partial \rho^{gaR}}{\partial \theta} \frac{\partial S_w}{\partial s} \right) \boldsymbol{N}^{e,\theta} da \tag{4.196}$$

$$\frac{\partial \boldsymbol{K}^{\theta g}}{\partial \boldsymbol{\theta}} \cdot \dot{\boldsymbol{p}}_g = \mathop{\mathsf{A}}_{e=1}^{n_{\mathrm{el}}} \frac{\partial \boldsymbol{k}_e^{\theta g}}{\partial \boldsymbol{\theta}^e} \cdot \dot{\boldsymbol{p}}_g^e$$

$$= \mathop{\mathsf{A}}_{e=1}^{n_{\mathrm{el}}} \int_{\Omega^e} \dot{p}_g (\boldsymbol{N}^{e,\theta})^T \cdot \left(n \Delta H_{vap} \frac{\partial \rho^{wR}}{\partial \theta} \frac{\partial S_w}{\partial s} \right) \boldsymbol{N}^{e,\theta} da \tag{4.197}$$

$$\frac{\partial \boldsymbol{K}^{w\theta}}{\partial \boldsymbol{\theta}} \cdot \dot{\boldsymbol{\theta}} = \mathop{\mathbf{A}}_{e=1}^{n_{\mathrm{el}}} \frac{\partial \boldsymbol{k}_e^{w\theta}}{\partial \boldsymbol{\theta}^e} \cdot \dot{\boldsymbol{\theta}}^e$$

$$= \mathop{\mathbf{A}}_{e=1}^{n_{\mathrm{el}}} \int_{\Omega^e} \dot{\theta}^e (\boldsymbol{N}^{e,p})^T \cdot \left(n S_g \frac{(\partial)^2 \rho^{gvR}}{\partial \theta^2} - \frac{\partial \beta_{swg}}{\partial \theta} \right) \boldsymbol{N}^{e,\theta} da \tag{4.198}$$

$$\frac{\partial \boldsymbol{K}^{g\theta}}{\partial \boldsymbol{\theta}} \cdot \dot{\boldsymbol{\theta}} = \mathop{\mathbf{A}}_{e=1}^{n_{\mathrm{el}}} \frac{\partial \boldsymbol{k}_e^{g\theta}}{\partial \boldsymbol{\theta}^e} \cdot \dot{\boldsymbol{\theta}}^e$$

$$= \mathop{\mathbf{A}}_{e=1}^{n_{\mathrm{el}}} \int_{\Omega^e} \dot{\theta}^e (\boldsymbol{N}^{e,p})^T \cdot \left(n S_g \frac{(\partial)^2 \rho^{gaR}}{\partial \theta^2} - \beta_s (1-n) S_g \frac{\partial \rho^{gaR}}{\partial \theta} \right) \boldsymbol{N}^{e,\theta} da \tag{4.199}$$

$$\frac{\partial \boldsymbol{K}^{\theta\theta}}{\partial \boldsymbol{\theta}} \cdot \dot{\boldsymbol{\theta}} = \mathop{\mathbf{A}}_{e=1}^{n_{\mathrm{el}}} \frac{\partial \boldsymbol{k}_e^{\theta\theta}}{\partial \boldsymbol{\theta}^e} \cdot \dot{\boldsymbol{\theta}}^e$$

$$= \mathop{\mathbf{A}}_{e=1}^{n_{\mathrm{el}}} \int_{\Omega^e} \dot{\theta} \cdot \left[\frac{\partial (\rho C)_{eff}}{\partial \theta} + \Delta H_{vap} S_w [\beta_w n + \beta_s (1-n)] \frac{\partial \rho^{wR}}{\partial \theta} \right] \cdot (\boldsymbol{N}^{e,\theta})^T \cdot \boldsymbol{N}^{e,\theta} da \tag{4.200}$$

$$\frac{\partial \boldsymbol{F}^{d,INT}}{\partial \boldsymbol{d}} = \mathop{\mathbf{A}}_{e=1}^{n_{\mathrm{el}}} \frac{\partial \boldsymbol{f}_e^{d,INT}}{\partial \boldsymbol{d}^e} = \mathop{\mathbf{A}}_{e=1}^{n_{\mathrm{el}}} \int_{\Omega^e} (\boldsymbol{B}^{e,u})^T \frac{\partial \boldsymbol{\sigma}'}{\partial \boldsymbol{\epsilon}} \boldsymbol{B}^{e,u} da \tag{4.201}$$

$$\frac{\partial \boldsymbol{F}^{w1,INT}}{\partial \boldsymbol{d}} = \mathop{\mathbf{A}}_{e=1}^{n_{\mathrm{el}}} \frac{\partial \boldsymbol{f}_e^{w1,INT}}{\partial \boldsymbol{d}^e} = \mathop{\mathbf{A}}_{e=1}^{n_{\mathrm{el}}} \int_{\Omega^e} \rho^{wR} (\boldsymbol{B}^{e,p})^T \frac{\partial \tilde{\boldsymbol{v}}_w^D}{\partial \boldsymbol{d}} da \tag{4.202}$$

$$\frac{\partial \boldsymbol{F}^{w2,INT}}{\partial \boldsymbol{d}} = \mathop{\mathbf{A}}_{e=1}^{n_{\mathrm{el}}} \frac{\partial \boldsymbol{f}_e^{w2,INT}}{\partial \boldsymbol{d}^e} = \mathop{\mathbf{A}}_{e=1}^{n_{\mathrm{el}}} \int_{\Omega^e} \rho^{gvR} (\boldsymbol{B}^{e,p})^T \frac{\partial \tilde{\boldsymbol{v}}_{gv}^D}{\partial \boldsymbol{d}} da \tag{4.203}$$

$$\frac{\partial \boldsymbol{F}^{g,INT}}{\partial \boldsymbol{d}} = \mathop{\mathbf{A}}_{e=1}^{n_{\mathrm{el}}} \frac{\partial \boldsymbol{f}_e^{g,INT}}{\partial \boldsymbol{d}^e} = \mathop{\mathbf{A}}_{e=1}^{n_{\mathrm{el}}} \int_{\Omega^e} \rho^{gaR} (\boldsymbol{B}^{e,p})^T \frac{\partial \tilde{\boldsymbol{v}}_{ga}^D}{\partial \boldsymbol{d}} da \tag{4.204}$$

$$\frac{\partial \boldsymbol{F}^{\theta 1,INT}}{\partial \boldsymbol{d}} = \mathop{\mathbf{A}}_{e=1}^{n_{\mathrm{el}}} \frac{\partial \boldsymbol{f}_e^{\theta 1,INT}}{\partial \boldsymbol{d}^e}$$

$$= \mathop{\mathbf{A}}_{e=1}^{n_{\mathrm{el}}} \int_{\Omega^e} (\boldsymbol{N}^{e,\theta})^T (\boldsymbol{B}^{e,\theta} \boldsymbol{\theta}^e)^T \left(\rho^{wR} C^w \frac{\partial \tilde{\boldsymbol{v}}_w^D}{\partial \boldsymbol{d}} + \rho^{gR} C^g \frac{\partial \tilde{\boldsymbol{v}}_g^D}{\partial \boldsymbol{d}} \right) da \tag{4.205}$$

$$\frac{\partial \boldsymbol{F}^{\theta 2,INT}}{\partial \boldsymbol{d}} = \mathop{\mathbf{A}}_{e=1}^{n_{\mathrm{el}}} \frac{\partial \boldsymbol{f}_e^{\theta 2,INT}}{\partial \boldsymbol{d}^e} = \mathop{\mathbf{A}}_{e=1}^{n_{\mathrm{el}}} \int_{\Omega^e} \Delta H_{vap} \rho^{wR} (\boldsymbol{B}^{e,\theta})^T \frac{\partial \tilde{\boldsymbol{v}}_w^D}{\partial \boldsymbol{d}} da \tag{4.206}$$

$$\frac{\partial \boldsymbol{F}^{dp,INT}}{\partial \boldsymbol{p}_w} = \mathop{\mathbf{A}}_{e=1}^{n_{\mathrm{el}}} \frac{\partial \boldsymbol{f}_e^{dp,INT}}{\partial \boldsymbol{p}_w^e} = \mathop{\mathbf{A}}_{e=1}^{n_{\mathrm{el}}} \int_{\Omega^e} (\tilde{\boldsymbol{B}}^{e,u})^T \boldsymbol{N}^{e,p} \left[(\boldsymbol{p}_g^e - \boldsymbol{p}_w^e) \frac{\partial \chi}{\partial s} \boldsymbol{N}^{e,p} + \chi \mathbf{1} \right] da \tag{4.207}$$

$$\frac{\partial \boldsymbol{F}^{w1,INT}}{\partial \boldsymbol{p}_w} = \mathop{\mathbf{A}}_{e=1}^{n_{\mathrm{el}}} \frac{\partial \boldsymbol{f}_e^{w1,INT}}{\partial \boldsymbol{p}_w^e} = \mathop{\mathbf{A}}_{e=1}^{n_{\mathrm{el}}} \int_{\Omega^e} \rho^{wR} (\boldsymbol{B}^{e,p})^T \frac{\partial \tilde{\boldsymbol{v}}_w^D}{\partial \boldsymbol{p}_w} da \tag{4.208}$$

$$\frac{\partial \boldsymbol{F}^{w2,INT}}{\partial \boldsymbol{p}_w} = \mathop{\mathbf{A}}_{e=1}^{n_{\mathrm{el}}} \frac{\partial \boldsymbol{f}_e^{w2,INT}}{\partial \boldsymbol{p}_w^e} = \mathop{\mathbf{A}}_{e=1}^{n_{\mathrm{el}}} \int_{\Omega^e} (\boldsymbol{B}^{e,p})^T \left(\rho^{gvR} \frac{\partial \tilde{\boldsymbol{v}}_{gv}^D}{\partial \boldsymbol{p}_w} + \tilde{\boldsymbol{v}}_{gv}^D \otimes \frac{\partial \rho^{gvR}}{\partial \boldsymbol{p}_w} \right) da \tag{4.209}$$

$$\frac{\partial \boldsymbol{F}^{g,INT}}{\partial \boldsymbol{p}_w} = \mathop{\mathbf{A}}_{e=1}^{n_{\text{el}}} \frac{\partial \boldsymbol{f}_e^{g,INT}}{\partial \boldsymbol{p}_w^e} = \mathop{\mathbf{A}}_{e=1}^{n_{\text{el}}} \int_{\Omega^e} (\boldsymbol{B}^{e,p})^T \left(\rho^{gaR} \frac{\partial \tilde{\boldsymbol{v}}_{ga}^D}{\partial \boldsymbol{p}_w} + \tilde{\boldsymbol{v}}_{ga}^D \otimes \frac{\partial \rho^{gaR}}{\partial \boldsymbol{p}_w} \right) da \tag{4.210}$$

$$\begin{aligned} \frac{\partial \boldsymbol{F}^{\theta 1,INT}}{\partial \boldsymbol{p}_w} &= \mathop{\mathbf{A}}_{e=1}^{n_{\text{el}}} \frac{\partial \boldsymbol{f}_e^{\theta 1,INT}}{\partial \boldsymbol{p}_w^e} \mathop{\mathbf{A}}_{e=1}^{n_{\text{el}}} \int_{\Omega^e} (\boldsymbol{N}^{e,\theta})^T (\boldsymbol{B}^{e,\theta} \boldsymbol{\theta}^e)^T \\ &= \cdot \left(\rho^{wR} C^w \frac{\partial \tilde{\boldsymbol{v}}_w^D}{\partial \boldsymbol{p}_w} + \rho^{gR} C^g \frac{\partial \tilde{\boldsymbol{v}}_g^D}{\partial \boldsymbol{p}_w} + C^g \tilde{\boldsymbol{v}}_g^D \otimes \frac{\partial \rho^{gR}}{\partial \boldsymbol{p}_w} \right) da \end{aligned} \tag{4.211}$$

$$\frac{\partial \boldsymbol{F}^{\theta 2,INT}}{\partial \boldsymbol{p}_w} = \mathop{\mathbf{A}}_{e=1}^{n_{\text{el}}} \frac{\partial \boldsymbol{f}_e^{\theta 2,INT}}{\partial \boldsymbol{p}_w^e} = \mathop{\mathbf{A}}_{e=1}^{n_{\text{el}}} \int_{\Omega^e} \Delta H_{vap} \rho^{wR} (\boldsymbol{B}^{e,\theta})^T \cdot \frac{\partial \tilde{\boldsymbol{v}}_w^D}{\partial \boldsymbol{p}_w} da \tag{4.212}$$

$$\begin{aligned} \frac{\partial \boldsymbol{F}^{dp,INT}}{\partial \boldsymbol{p}_g} &= \mathop{\mathbf{A}}_{e=1}^{n_{\text{el}}} \frac{\partial \boldsymbol{f}_e^{dp,INT}}{\partial \boldsymbol{p}_g^e} = \mathop{\mathbf{A}}_{e=1}^{n_{\text{el}}} \int_{\Omega^e} (\tilde{\boldsymbol{B}}^{e,u})^T \boldsymbol{N}^{e,p} \\ &\qquad \cdot \left[(\boldsymbol{p}_w^e - \boldsymbol{p}_g^e) \frac{\partial \chi}{\partial s} \boldsymbol{N}^{e,p} + (1-\chi) \mathbf{1} \right] da \end{aligned} \tag{4.213}$$

$$\frac{\partial \boldsymbol{F}^{w1,INT}}{\partial \boldsymbol{p}_g} = \mathop{\mathbf{A}}_{e=1}^{n_{\text{el}}} \frac{\partial \boldsymbol{f}_e^{w1,INT}}{\partial \boldsymbol{p}_g^e} = \mathop{\mathbf{A}}_{e=1}^{n_{\text{el}}} \int_{\Omega^e} \rho^{wR} (\boldsymbol{B}^{e,p})^T \frac{\partial \tilde{\boldsymbol{v}}_w^D}{\partial \boldsymbol{p}_g} da \tag{4.214}$$

$$\frac{\partial \boldsymbol{F}^{w2,INT}}{\partial \boldsymbol{p}_g} = \mathop{\mathbf{A}}_{e=1}^{n_{\text{el}}} \frac{\partial \boldsymbol{f}_e^{w2,INT}}{\partial \boldsymbol{p}_g^e} = \mathop{\mathbf{A}}_{e=1}^{n_{\text{el}}} \int_{\Omega^e} (\boldsymbol{B}^{e,p})^T \left(\rho^{gvR} \frac{\partial \tilde{\boldsymbol{v}}_{gv}^D}{\partial \boldsymbol{p}_g} + \tilde{\boldsymbol{v}}_{gv}^D \otimes \frac{\partial \rho^{gvR}}{\partial \boldsymbol{p}_g} \right) da \tag{4.215}$$

$$\frac{\partial \boldsymbol{F}^{g,INT}}{\partial \boldsymbol{p}_g} = \mathop{\mathbf{A}}_{e=1}^{n_{\text{el}}} \frac{\partial \boldsymbol{f}_e^{g,INT}}{\partial \boldsymbol{p}_g^e} = \mathop{\mathbf{A}}_{e=1}^{n_{\text{el}}} \int_{\Omega^e} (\boldsymbol{B}^{e,p})^T \left(\rho^{gaR} \frac{\partial \tilde{\boldsymbol{v}}_{ga}^D}{\partial \boldsymbol{p}_g} + \tilde{\boldsymbol{v}}_{ga}^D \otimes \frac{\partial \rho^{gaR}}{\partial \boldsymbol{p}_g} \right) da \tag{4.216}$$

$$\begin{aligned} \frac{\partial \boldsymbol{F}^{\theta 1,INT}}{\partial \boldsymbol{p}_g} &= \mathop{\mathbf{A}}_{e=1}^{n_{\text{el}}} \frac{\partial \boldsymbol{f}_e^{\theta 1,INT}}{\partial \boldsymbol{p}_g^e} = \mathop{\mathbf{A}}_{e=1}^{n_{\text{el}}} \int_{\Omega^e} (\boldsymbol{N}^{e,\theta})^T \cdot (\boldsymbol{B}^{e,\theta} \boldsymbol{\theta}^e)^T \\ &\qquad \cdot \left(\rho^{wR} C^w \frac{\partial \tilde{\boldsymbol{v}}_w^D}{\partial \boldsymbol{p}_g} + \rho^{gR} C^g \frac{\partial \tilde{\boldsymbol{v}}_g^D}{\partial \boldsymbol{p}_g} + C^g \tilde{\boldsymbol{v}}_g^D \otimes \frac{\partial \rho^{gR}}{\partial \boldsymbol{p}_g} \right) da \end{aligned} \tag{4.217}$$

$$\frac{\partial \boldsymbol{F}^{\theta 2,INT}}{\partial \boldsymbol{p}_g} = \mathop{\mathbf{A}}_{e=1}^{n_{\text{el}}} \frac{\partial \boldsymbol{f}_e^{\theta 2,INT}}{\partial \boldsymbol{p}_w^e} = \mathop{\mathbf{A}}_{e=1}^{n_{\text{el}}} \int_{\Omega^e} \Delta H_{vap} \rho^{wR} (\boldsymbol{B}^{e,\theta})^T \cdot \frac{\partial \tilde{\boldsymbol{v}}_w^D}{\partial \boldsymbol{p}_g} da \tag{4.218}$$

$$\frac{\partial \boldsymbol{F}^{dp,INT}}{\partial \boldsymbol{\theta}} = \mathop{\mathbf{A}}_{e=1}^{n_{\text{el}}} \frac{\partial \boldsymbol{f}_e^{dp,INT}}{\partial \boldsymbol{\theta}^e} = \mathbf{0} \tag{4.219}$$

$$\frac{\partial \boldsymbol{F}^{d\theta,INT}}{\partial \boldsymbol{\theta}} = \mathop{\mathbf{A}}_{e=1}^{n_{\text{el}}} \frac{\partial \boldsymbol{f}_e^{w1,INT}}{\partial \boldsymbol{\theta}^e} = \mathop{\mathbf{A}}_{e=1}^{n_{\text{el}}} \int_{\Omega^e} 3 K_B \alpha_{skel}^{\theta} (\tilde{\boldsymbol{B}}^{e,u})^T \cdot \boldsymbol{N}^{e,\theta} da \tag{4.220}$$

$$\frac{\partial \boldsymbol{F}^{w1,INT}}{\partial \boldsymbol{\theta}} = \mathop{\mathbf{A}}_{e=1}^{n_{\text{el}}} \frac{\partial \boldsymbol{f}_e^{w1,INT}}{\partial \boldsymbol{\theta}^e} = \mathop{\mathbf{A}}_{e=1}^{n_{\text{el}}} \int_{\Omega^e} (\boldsymbol{B}^{e,p})^T \left(\tilde{\boldsymbol{v}}_w^D \frac{\partial \rho^{wR}}{\partial \boldsymbol{\theta}^e} \boldsymbol{N}^{e,\theta} + \rho^{wR} \frac{\partial \tilde{\boldsymbol{v}}_w^D}{\partial \boldsymbol{\theta}^e} \right) da \tag{4.221}$$

$$\frac{\partial \boldsymbol{F}^{w2,INT}}{\partial \boldsymbol{\theta}} = \mathop{\mathbf{A}}_{e=1}^{n_{\text{el}}} \frac{\partial \boldsymbol{f}_e^{w2,INT}}{\partial \boldsymbol{\theta}^e} = \mathop{\mathbf{A}}_{e=1}^{n_{\text{el}}} \int_{\Omega^e} (\boldsymbol{B}^{e,p})^T \left(\tilde{\boldsymbol{v}}_{gv}^D \frac{\partial \rho^{gvR}}{\partial \boldsymbol{\theta}^e} \boldsymbol{N}^{e,\theta} + \rho^{gvR} \frac{\partial \tilde{\boldsymbol{v}}_{gv}^D}{\partial \boldsymbol{\theta}^e} \right) da \tag{4.222}$$

$$\frac{\partial \boldsymbol{F}^{g,INT}}{\partial \boldsymbol{\theta}} = \mathop{\mathbf{A}}_{e=1}^{n_{\text{el}}} \frac{\partial \boldsymbol{f}_e^{g,INT}}{\partial \boldsymbol{\theta}^e} = \mathop{\mathbf{A}}_{e=1}^{n_{\text{el}}} \int_{\Omega^e} (\boldsymbol{B}^{e,p})^T \left(\tilde{\boldsymbol{v}}_{ga}^D \frac{\partial \rho^{gaR}}{\partial \boldsymbol{\theta}^e} \boldsymbol{N}^{e,\theta} + \rho^{gaR} \frac{\partial \tilde{\boldsymbol{v}}_{ga}^D}{\partial \boldsymbol{\theta}^e} \right) da \tag{4.223}$$

$$\frac{\partial \boldsymbol{F}^{\theta 1,INT}}{\partial \boldsymbol{\theta}} = \mathop{\mathbf{A}}_{e=1}^{n_{\rm el}} \frac{\partial \boldsymbol{f}_e^{\theta 1,INT}}{\partial \boldsymbol{\theta}^e} = \mathop{\mathbf{A}}_{e=1}^{n_{\rm el}} \int_{\Omega^e} \Big\{ (\boldsymbol{N}^{e,\theta})^T (\boldsymbol{B}^{e,\theta} \cdot \boldsymbol{\theta}^e)^T \cdot \left(\rho^{wR} C^w \frac{\partial \tilde{\boldsymbol{v}}_w^D}{\partial \boldsymbol{\theta}^e} + C^w \tilde{\boldsymbol{v}}_w^D \otimes \frac{\partial \rho^{wR}}{\partial \boldsymbol{\theta}^e} + \rho^{gR} C^g \frac{\partial \tilde{\boldsymbol{v}}_g^D}{\partial \boldsymbol{\theta}^e} + C^g \tilde{\boldsymbol{v}}_g^D \otimes \frac{\partial \rho^{gR}}{\partial \boldsymbol{\theta}^e} \right) + \left[(\boldsymbol{N}^{e,\theta})^T \otimes (\rho^{wR} C^w \tilde{\boldsymbol{v}}_w^D + \rho^{gR} C^g \tilde{\boldsymbol{v}}_g^D)^T + K_{eff}^{\theta} (\boldsymbol{B}^{e,\theta})^T \right] \boldsymbol{B}^{e,\theta} \Big\} da \quad (4.224)$$

$$\frac{\partial \boldsymbol{F}^{\theta 2,INT}}{\partial \boldsymbol{\theta}} = \mathop{\mathbf{A}}_{e=1}^{n_{\rm el}} \frac{\partial \boldsymbol{f}_e^{\theta 2,INT}}{\partial \boldsymbol{\theta}^e} = \mathop{\mathbf{A}}_{e=1}^{n_{\rm el}} \int_{\Omega^e} \Delta H_{vap} (\boldsymbol{B}^{e,\theta})^T \cdot \left[\tilde{\boldsymbol{v}}_w^D \frac{\partial \rho^{gR}}{\partial \theta^e} + \rho^{wR} \frac{\partial \tilde{\boldsymbol{v}}_w^D}{\partial \boldsymbol{\theta}^e} \right] da \quad (4.225)$$

where

$$\frac{\partial p_{gv}}{\partial \theta} = p_{gv} \frac{M_w}{R\theta^2} \left(\Delta H_{vap} + \frac{s}{\rho^{wR}} \right) \quad (4.226)$$

$$\frac{\partial p_{gv}}{\partial s} = p_{gv} \left(\frac{-M_w}{R\theta \rho^{wR}} \right) \quad (4.227)$$

$$\frac{\partial^2 p_{gv}}{\partial s^2} = \frac{-M_w}{R\theta \rho^{wR}} \frac{\partial p_{gv}}{\partial s} \quad (4.228)$$

$$\frac{\partial^2 p_{gv}}{\partial s \partial \theta} = -\frac{M_w}{R\theta \rho^{wR}} \frac{\partial p_{gv}}{\partial \theta} + p_{gv} \frac{M_w}{R\theta^2 \rho^{wR}} \quad (4.229)$$

$$\frac{\partial^2 p_{gv}}{\partial \theta^2} = \frac{\partial p_{gv}}{\partial \theta} \left(\frac{M_w \Delta H_{vap}}{R\theta^2} + \frac{M_w s}{R\theta^2 \rho^{wR}} \right) - p_{gv} \left(\frac{2M_w \Delta H_{vap}}{R\theta^3} + \frac{2M_w \Delta s}{R\theta^3 \rho^{wR}} + \frac{\partial \rho^{wR}}{\partial \theta} \frac{M_w s}{R\theta^2 (\rho^{wR})^2} \right) \quad (4.230)$$

$$\frac{\partial \rho^{gvR}}{\partial \theta} = \frac{M_w}{R\theta} \frac{\partial p_{gv}}{\partial \theta} - p_{gv} \frac{M_w}{R\theta^2} \quad (4.231)$$

$$\frac{\partial \rho^{gvR}}{\partial s} = \frac{M_w}{R\theta} \frac{\partial p_{gv}}{\partial s} \quad (4.232)$$

$$\frac{\partial^2 \rho^{gvR}}{\partial s^2} = \frac{M_w}{R\theta} \frac{\partial^2 p_{gv}}{\partial s^2} \quad (4.233)$$

$$\frac{\partial^2 \rho^{gvR}}{\partial s \partial \theta} = \frac{M_w}{R\theta} \left(\frac{1}{\theta} \frac{\partial^2 p_{gv}}{\partial s \partial \theta} - \frac{1}{\theta^2} \frac{\partial p_{gv}}{\partial s} \right) \quad (4.234)$$

$$\frac{\partial^2 \rho_{gvR}}{\partial \theta^2} = \frac{M_w}{R\theta} \left(\frac{\partial^2 p_{gv}}{\partial \theta^2} + \frac{2p_{gv}}{\theta^2} - \frac{2}{\theta} \frac{\partial p_{gv}}{\partial \theta} \right) \quad (4.235)$$

$$p_{ga} = p_g - p_{gv} \quad (4.236)$$

$$\frac{\partial p_{ga}}{\partial p_w} = \frac{\partial p_{gv}}{\partial s} \quad (4.237)$$

$$\frac{\partial p_{ga}}{\partial p_g} = 1 - \frac{\partial p_{gv}}{\partial s} \quad (4.238)$$

$$\frac{\partial p_{ga}}{\partial \theta} = -\frac{\partial p_{gv}}{\partial \theta} \quad (4.239)$$

$$\frac{\partial \rho_{gaR}}{\partial p_w} = \frac{M_a}{R\theta}\frac{\partial p_{gv}}{\partial s}\,, \quad \frac{\partial \rho_{gaR}}{\partial p_g} = \frac{M_w}{R\theta}\left(1 - \frac{\partial p_{gv}}{\partial s}\right) \tag{4.240}$$

$$\frac{\partial \rho^{gaR}}{\partial \theta} = -\frac{M_a}{R\theta}\left(\frac{\partial p_{gv}}{\partial \theta} + \frac{p_{ga}}{\theta}\right) \tag{4.241}$$

$$\frac{\partial^2 \rho^{gaR}}{\partial {p_w}^2} = \frac{\partial^2 \rho_{gaR}}{\partial {p_g}^2} = -\frac{M_a}{R\theta}\frac{\partial^2 p_{gv}}{\partial s^2} \tag{4.242}$$

$$\frac{\partial^2 \rho_{ga}}{\partial \theta^2} = \frac{M_a}{R\theta}\left(\frac{2}{\theta}\frac{\partial p_{gv}}{\partial \theta} + \frac{2p_{ga}}{\theta^2} - \frac{\partial^2 p_{gv}}{\partial \theta^2}\right) \tag{4.243}$$

$$\frac{\partial^2 \rho^{gaR}}{\partial p_w \partial \theta} = \frac{M_a}{R\theta}\left(\frac{\partial^2 p_{gv}}{\partial s \partial \theta} - \frac{1}{\theta}\frac{\partial p_{gv}}{\partial s}\right) \tag{4.244}$$

$$\frac{\partial^2 \rho^{gaR}}{\partial p_g \partial \theta} = -\frac{M_a}{R\theta}\left[\frac{\partial^2 p_{gv}}{\partial s \partial \theta} + \frac{1}{\theta}\left(1 - \frac{\partial p_{gv}}{\partial s}\right)\right] \tag{4.245}$$

$$\frac{\partial^2 \rho^{gaR}}{\partial p_w \partial p_g} = \frac{M_a}{R\theta}\frac{\partial^2 p_{gv}}{\partial s^2} \tag{4.246}$$

$$\frac{\partial \rho_{gR}}{\partial p_w} = \frac{\partial \rho_{gaR}}{\partial p_w} - \frac{\partial \rho_{gvR}}{\partial s} \tag{4.247}$$

$$\frac{\partial \rho_{gR}}{\partial p_g} = \frac{\partial \rho_{gaR}}{\partial p_g} + \frac{\partial \rho_{gvR}}{\partial s} \tag{4.248}$$

$$\frac{\partial \rho_{gR}}{\partial \theta} = \frac{\partial \rho_{gaR}}{\partial \theta} + \frac{\partial \rho_{gvR}}{\partial \theta} \tag{4.249}$$

$$\tilde{\boldsymbol{v}}_w^D = -K_w(\nabla p_w - \rho^{wR}\boldsymbol{g})\,, \quad K_w = \frac{\kappa(n)K_{rw}(S_w)}{\mu_w(\theta)} \tag{4.250}$$

$$\frac{\partial \tilde{\boldsymbol{v}}_w^D}{\partial \boldsymbol{d}^e} = -\frac{\partial K_w}{\partial n}(\nabla p_w - \rho^{wR}\boldsymbol{g}) \otimes \frac{\partial n}{\partial \boldsymbol{d}^e} \tag{4.251}$$

$$\frac{\partial \tilde{\boldsymbol{v}}_w^D}{\partial \boldsymbol{p}_w^e} = \frac{\partial K_w}{\partial S_w}\frac{\partial S_w}{\partial s}(\nabla p_w - \rho^{wR}\boldsymbol{g})\boldsymbol{N}^{e,p} - K_w\boldsymbol{B}^{e,p} \tag{4.252}$$

$$\frac{\partial \tilde{\boldsymbol{v}}_w^D}{\partial \boldsymbol{p}_g^e} = -\frac{\partial K_w}{\partial S_w}\frac{\partial S_w}{\partial s}(\nabla p_w - \rho^{wR}\boldsymbol{g})\boldsymbol{N}^{e,p} \tag{4.253}$$

$$\frac{\partial \tilde{\boldsymbol{v}}_w^D}{\partial \boldsymbol{\theta}^e} = -\frac{\partial K_w}{\partial \theta}(\nabla p_w - \rho^{wR}\boldsymbol{g})\boldsymbol{N}^{e,\theta} + K_w\boldsymbol{g} \otimes \frac{\partial \rho^{wR}}{\partial \theta}bN^{e,\theta} \tag{4.254}$$

$$\tilde{\boldsymbol{v}}_g^D = -K_g(\nabla p_g - \rho^{gR}\boldsymbol{g})\,, \quad K_g = \frac{\kappa(n)K_{rg}(1 - S_w)}{\mu_g(\theta)} \tag{4.255}$$

$$\frac{\partial \tilde{\boldsymbol{v}}_g^D}{\partial \boldsymbol{d}^e} = -\frac{\partial K_g}{\partial n}(\nabla p_g - \rho^{gR}\boldsymbol{g}) \otimes \frac{\partial n}{\partial \boldsymbol{d}^e} \tag{4.256}$$

$$\frac{\partial \tilde{\boldsymbol{v}}_g^D}{\partial \boldsymbol{p}_w^e} = \frac{\partial K_g}{\partial S_w}\frac{\partial S_w}{\partial s}(\nabla p_g - \rho^{gR}\boldsymbol{g})\boldsymbol{N}^{e,p} + K_g\boldsymbol{g} \otimes \frac{\partial \rho^{gR}}{p_w}\boldsymbol{N}^{e,p} \tag{4.257}$$

$$\frac{\partial \tilde{\boldsymbol{v}}_g^D}{\partial \boldsymbol{p}_g^e} = -\frac{\partial K_g}{\partial S_w}\frac{\partial S_w}{\partial s}(\nabla p_g - \rho^{gR}\boldsymbol{g})\boldsymbol{N}^{e,p} - K_g\left(\boldsymbol{B}^{e,p} - \boldsymbol{g}\otimes\frac{\partial \rho^{gR}}{p_g}\boldsymbol{N}^{e,p}\right) \tag{4.258}$$

$$\frac{\partial \tilde{\boldsymbol{v}}_g^D}{\partial \boldsymbol{\theta}^e} = -\frac{\partial K_g}{\partial \theta}(\nabla p_g - \rho^{gR}\boldsymbol{g})\boldsymbol{N}^{e,\theta} + K_g\boldsymbol{g}\otimes\frac{\partial \rho^{gR}}{\partial \theta}\boldsymbol{N}^{e,\theta} \tag{4.259}$$

$$\tilde{\boldsymbol{v}}_{gv}^D = -K_g\nabla p_g - nS_g\tau D_0\frac{p_{atm}}{p_{gv}}\nabla\left(\frac{p_{gv}}{p_g}\right) \tag{4.260}$$

$$\frac{\partial \tilde{\boldsymbol{v}}_{gv}^D}{\partial \boldsymbol{d}^e} = -\frac{\partial K_g}{\partial n}\nabla p_g\otimes\frac{\partial n}{\partial \boldsymbol{d}^e} - S_gD_0\frac{p_{atm}}{p_{gv}}\left(\tau + n\frac{\partial \tau}{\partial n}\right)\nabla\left(\frac{p_{gv}}{p_g}\right)\otimes\frac{\partial n}{\partial \boldsymbol{d}^e} \tag{4.261}$$

$$\frac{\partial \tilde{\boldsymbol{v}}_{gv}^D}{\partial \boldsymbol{p}_w^e} = \frac{\partial K_g}{\partial S_w}\frac{\partial S_w}{\partial s}\nabla p_g\otimes\boldsymbol{N}^{e,p} - nD_0p_{atm}\frac{\partial\left[\frac{S_g\tau\nabla\left(\frac{p_{gv}}{p_g}\right)}{p_{gv}}\right]}{\partial \boldsymbol{p}_w^e} \tag{4.262}$$

$$\frac{\partial \tilde{\boldsymbol{v}}_{gv}^D}{\partial \boldsymbol{p}_g^e} = -\frac{\partial K_g}{\partial S_w}\frac{\partial S_w}{\partial s}\nabla p_g\otimes\boldsymbol{N}^{e,p} - K_g\boldsymbol{B}^{e,p} - nD_0p_{atm}\frac{\partial\left[\frac{S_g\tau\nabla\left(\frac{p_{gv}}{p_g}\right)}{p_{gv}}\right]}{\partial \boldsymbol{p}_g^e} \tag{4.263}$$

$$\frac{\partial \tilde{\boldsymbol{v}}_{gv}^D}{\partial \boldsymbol{\theta}^e} = -\frac{\partial K_g}{\partial \theta}\nabla p_g\otimes\boldsymbol{N}^{e,\theta} - nS_g\tau p_{atm}\frac{\partial\left[\frac{D_0\nabla\left(\frac{p_{gv}}{p_g}\right)}{p_{gv}}\right]}{\partial \boldsymbol{\theta}^e} \tag{4.264}$$

$$\tilde{\boldsymbol{v}}_{ga}^D = -K_g(\nabla p_g + nS_g\tau D_0\frac{p_{atm}}{p_{ga}}\nabla\left(\frac{p_{ga}}{p_g}\right) \tag{4.265}$$

$$\frac{\partial \tilde{\boldsymbol{v}}_{ga}^D}{\partial \boldsymbol{d}^e} = -\frac{\partial K_g}{\partial n}\nabla p_g\otimes\frac{\partial n}{\partial \boldsymbol{d}^e} + S_gD_0\frac{p_{atm}}{p_{ga}}\left(\tau + n\frac{\partial \tau}{\partial n}\right)\nabla\left(\frac{p_{gv}}{p_g}\right)\otimes\frac{\partial n}{\partial \boldsymbol{d}^e} \tag{4.266}$$

$$\frac{\partial \tilde{\boldsymbol{v}}_{ga}^D}{\partial \boldsymbol{p}_w^e} = \frac{\partial K_g}{\partial S_w}\frac{\partial S_w}{\partial s}\nabla p_g\otimes\boldsymbol{N}^{e,p} + nD_0p_{atm}\frac{\partial\left[\frac{S_g\tau\nabla\left(\frac{p_{gv}}{p_g}\right)}{p_{ga}}\right]}{\partial \boldsymbol{p}_w^e} \tag{4.267}$$

$$\frac{\partial \tilde{\boldsymbol{v}}_{ga}^D}{\partial \boldsymbol{p}_g^e} = -\frac{\partial K_g}{\partial S_w}\frac{\partial S_w}{\partial s}\nabla p_g\otimes\boldsymbol{N}^{e,p} - K_g\boldsymbol{B}^{e,p} + nD_0p_{atm}\frac{\partial\left[\frac{S_g\tau\nabla\left(\frac{p_{gv}}{p_g}\right)}{p_{ga}}\right]}{\partial \boldsymbol{p}_g^e} \tag{4.268}$$

$$\frac{\partial \tilde{\boldsymbol{v}}_{ga}^D}{\partial \boldsymbol{\theta}^e} = -\frac{\partial K_g}{\partial \theta}\nabla p_g\otimes\boldsymbol{N}^{e,\theta} + nS_g\tau p_{atm}\frac{\partial\left[\frac{D_0\nabla\left(\frac{p_{gv}}{p_g}\right)}{p_{ga}}\right]}{\partial \boldsymbol{\theta}^e} \tag{4.269}$$

in which,

$$\frac{\partial\left[\frac{S_g\tau\nabla\left(\frac{p_{gv}}{p_g}\right)}{p_{gv}}\right]}{\partial \boldsymbol{p}_w^e} = \frac{1}{p_{gv}}\frac{\partial\left[S_g\tau\nabla\left(\frac{p_{gv}}{p_g}\right)\right]}{\partial \boldsymbol{p}_w^e} + \frac{1}{p_{gv}^2}S_g\tau\nabla\left(\frac{p_{gv}}{p_g}\right)\frac{\partial p_{gv}}{\partial s}\boldsymbol{N}^{e,p} \tag{4.270}$$

$$\frac{\partial\left[S_g\tau\nabla\left(\frac{p_{gv}}{p_g}\right)\right]}{\partial\boldsymbol{p}_w^e}=\frac{\partial S_w}{\partial s}\nabla\left(\frac{p_{gv}}{p_g}\right)\left(\tau+S_g\frac{\partial\tau}{\partial S_g}\right)\boldsymbol{N}^{e,p}+S_g\tau\frac{\partial\left[\nabla\left(\frac{p_{gv}}{p_g}\right)\right]}{\partial\boldsymbol{p}_w^e} \tag{4.271}$$

$$\nabla\left(\frac{p_{gv}}{p_g}\right)=\frac{1}{p_g}\frac{\partial p_{gv}}{\partial s}(\nabla p_g-\nabla p_w)+\frac{1}{p_g}\frac{\partial p_{gv}}{\partial\theta}\nabla\theta-\frac{p_{gv}}{{p_g}^2}\nabla p_g \tag{4.272}$$

$$\begin{aligned}\frac{\partial\left[\nabla\left(\frac{p_{gv}}{p_g}\right)\right]}{\partial\boldsymbol{p}_w^e}=&-\frac{1}{p_g}\frac{\partial^2 p_{gv}}{\partial s^2}(\nabla p_g-\nabla p_w)\boldsymbol{N}^{e,p}-\frac{1}{p_g}\frac{\partial p_{gv}}{\partial s}\boldsymbol{B}^{e,p}\\&-\frac{1}{p_g}\frac{\partial^2 p_{gv}}{\partial s\partial\theta}\nabla\theta\cdot\boldsymbol{N}^{e,p}+\frac{1}{{p_g}^2}\nabla p_g\frac{\partial p_{gv}}{\partial s}\boldsymbol{N}^{e,p}\end{aligned} \tag{4.273}$$

$$\frac{\partial\left[\frac{S_g\tau\nabla\left(\frac{p_{gv}}{p_g}\right)}{p_{gv}}\right]}{\partial\boldsymbol{p}_g^e}=\frac{1}{p_{gv}}\frac{\partial\left[S_g\tau\nabla\left(\frac{p_{gv}}{p_g}\right)\right]}{\partial\boldsymbol{p}_g^e}-\frac{1}{p_{gv}^2}S_g\tau\nabla\left(\frac{p_{gv}}{p_g}\right)\frac{\partial p_{gv}}{\partial s}\boldsymbol{N}^{e,p} \tag{4.274}$$

$$\frac{\partial\left[S_g\tau\nabla\left(\frac{p_{gv}}{p_g}\right)\right]}{\partial\boldsymbol{p}_g^e}=-\frac{\partial S_w}{\partial s}\nabla\left(\frac{p_{gv}}{p_g}\right)\left(\tau+S_g\frac{\partial\tau}{\partial S_g}\right)\boldsymbol{N}^{e,p}+S_g\tau\frac{\partial\left[\nabla\left(\frac{p_{gv}}{p_g}\right)\right]}{\partial\boldsymbol{p}_g^e} \tag{4.275}$$

$$\begin{aligned}\frac{\partial\left[\nabla\left(\frac{p_{gv}}{p_g}\right)\right]}{\partial\boldsymbol{p}_g^e}=&\frac{1}{p_g}\frac{\partial^2 p_{gv}}{\partial s^2}(\nabla p_g-\nabla p_w)\boldsymbol{N}^{e,p}+\frac{1}{p_g}\frac{\partial p_{gv}}{\partial s}\boldsymbol{B}^{e,p}+\frac{1}{p_g}\frac{\partial^2 p_{gv}}{\partial s\partial\theta}\nabla\theta\cdot\boldsymbol{N}^{e,p}\\&-\frac{2}{{p_g}^2}\nabla p_g\frac{\partial p_{gv}}{\partial s}\boldsymbol{N}^{e,p}+\frac{1}{{p_g}^2}\nabla p_w\frac{\partial p_{gv}}{\partial s}\boldsymbol{N}^{e,p}+\frac{2p_{gv}}{{p_g}^3}\nabla p_g\boldsymbol{N}^{e,p}\\&-\frac{p_{gv}}{{p_g}^2}\boldsymbol{B}^{e,p}-\frac{1}{{p_g}^2}\frac{\partial p_{gv}}{\partial\theta}\nabla\theta\boldsymbol{N}^{e,p}\end{aligned} \tag{4.276}$$

$$\begin{aligned}\frac{\partial\left[\frac{D_0\nabla\left(\frac{p_{gv}}{p_g}\right)}{p_{gv}}\right]}{\partial\boldsymbol{\theta}^e}=&\frac{1}{p_{gv}}\left\{\frac{\partial D_0}{\partial\theta}\nabla\left(\frac{p_{gv}}{p_g}\right)\boldsymbol{N}^{e,\theta}+D_0\frac{\partial\left[\nabla\left(\frac{p_{gv}}{p_g}\right)\right]}{\partial\boldsymbol{\theta}^e}\right\}\\&-\frac{1}{{p_{gv}}^2}D_0\nabla\left(\frac{p_{gv}}{p_g}\right)\frac{\partial p_{gv}}{\partial\theta}\boldsymbol{N}^{e,\theta}\end{aligned} \tag{4.277}$$

$$\begin{aligned}\frac{\partial\left[\nabla\left(\frac{p_{gv}}{p_g}\right)\right]}{\partial\boldsymbol{\theta}^e}=&\left[\frac{1}{p_g}\frac{\partial^2 p_{gv}}{\partial s\partial\theta}(\nabla p_g-\nabla p_w)+\frac{1}{p_g}\frac{\partial^2 p_{gv}}{\partial s^2}\nabla\theta\right]\boldsymbol{N}^{e,p}\\&+\frac{1}{p_g}\frac{\partial p_{gv}}{\partial\theta}\boldsymbol{B}^{e,\theta}-\frac{1}{{p_g}^2}\nabla p_g\frac{\partial p_{gv}}{\partial\theta}\boldsymbol{N}^{e,\theta}\end{aligned} \tag{4.278}$$

$$\frac{\partial\left[\frac{S_g\tau\nabla\left(\frac{p_{gv}}{p_g}\right)}{p_{ga}}\right]}{\partial\boldsymbol{p}_w^e}=\frac{1}{p_{ga}}\frac{\partial\left[S_g\tau\nabla\left(\frac{p_{gv}}{p_g}\right)\right]}{\partial\boldsymbol{p}_w^e}+\frac{1}{p_{ga}^2}S_g\tau\nabla\left(\frac{p_{gv}}{p_g}\right)\frac{\partial p_{ga}}{\partial s}\boldsymbol{N}^{e,p} \tag{4.279}$$

$$\frac{\partial\left[\frac{S_g\tau\nabla\left(\frac{p_{gv}}{p_g}\right)}{p_{ga}}\right]}{\partial\boldsymbol{p}_g^e}=\frac{1}{p_{ga}}\frac{\partial\left[S_g\tau\nabla\left(\frac{p_{gv}}{p_g}\right)\right]}{\partial\boldsymbol{p}_g^e}-\frac{1}{p_{ga}^2}S_g\tau\nabla\left(\frac{p_{gv}}{p_g}\right)\frac{\partial p_{ga}}{\partial s}\boldsymbol{N}^{e,p} \tag{4.280}$$

$$\frac{\partial\left[\frac{D_0\nabla\left(\frac{p_{gv}}{p_g}\right)}{p_{ga}}\right]}{\partial\boldsymbol{\theta}^e}=\frac{1}{p_{ga}}\left\{\frac{\partial D_0}{\partial\theta}\nabla\left(\frac{p_{gv}}{p_g}\right)\boldsymbol{N}^{e,\theta}+D_0\frac{\partial\left[\nabla\left(\frac{p_{gv}}{p_g}\right)\right]}{\partial\boldsymbol{\theta}^e}\right\}$$
$$-\frac{1}{{p_{ga}}^2}D_0\nabla\left(\frac{p_{gv}}{p_g}\right)\frac{\partial p_{ga}}{\partial\theta}\boldsymbol{N}^{e,\theta} \tag{4.281}$$

4.3 Numerical example

Comparison to an analytical solution for transient partially saturated flow

In this part, the partially saturated TPM model is reduced to be a partially saturated PM model by setting the temperature to be constant. To verify this reduced model, we take the analytical solution by Srivastava and Yeh (1991) for water flow through a partially saturated soil column with the water table at the bottom. The infiltration seepage S^w happens at the top as shown in the left figure in Figure 4.2. The displacements at the lateral surfaces are fixed in the radial direction, and the bottom is fixed in the vertical direction. All the surfaces are impermeable. The right figure in Figure 4.2 shows the profile of negative pore water pressure head in vadose zone as is provided in the one-dimensional analytical solution (Srivastava and Yeh, 1991). Figure 4.3 shows that a good agreement is obtained from the comparison between the reduced partially saturated TPM model and the analytical solution.

$$
\begin{aligned}
k_w(s) &= \frac{K_s}{\gamma_w}\exp(-\alpha s/\gamma_w) \\
S(s) &= \frac{1}{\Theta}\left[\Theta_r + (\Theta_s - \Theta_r)\exp(\alpha s/\gamma_w)\right]
\end{aligned}
\tag{4.282}
$$

Table 4.1: Parameters used in the comparison to the analytical solution in Srivastava and Yeh (1991)

Soil Parameter	Value	Units	
Saturated permeability	K_s	2.8×10^{-6}	m/s
Saturated volumetric water content	Θ_s	0.45	
Residual volumetric water content	Θ_r	0.2	
Initial infiltration seepage rate	S_0^w	2.8×10^{-7}	m/s
Final infiltration seepage rate	$S^w(t > 0, final)$	$9S_0^w$	m/s

Figure 4.2: (a) Mesh for FEM of partially saturated flow.(b) Analytical solution for partially saturated flow in vadose zone(Figure 1 of Srivastava and Yeh (1991)).

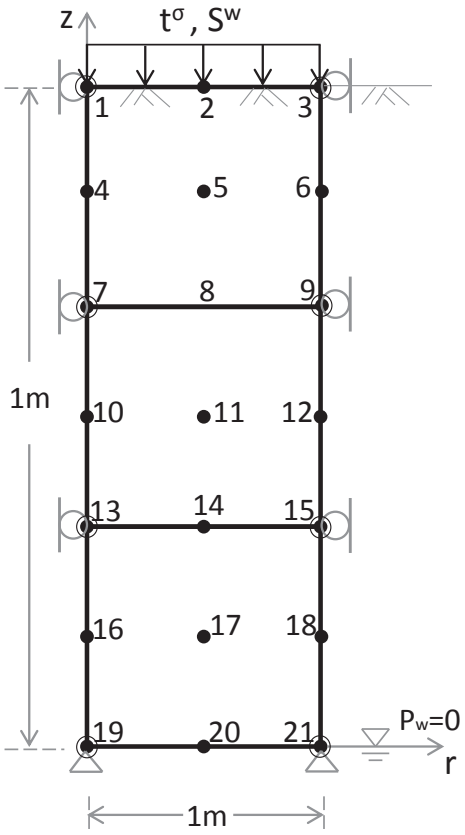

(a)

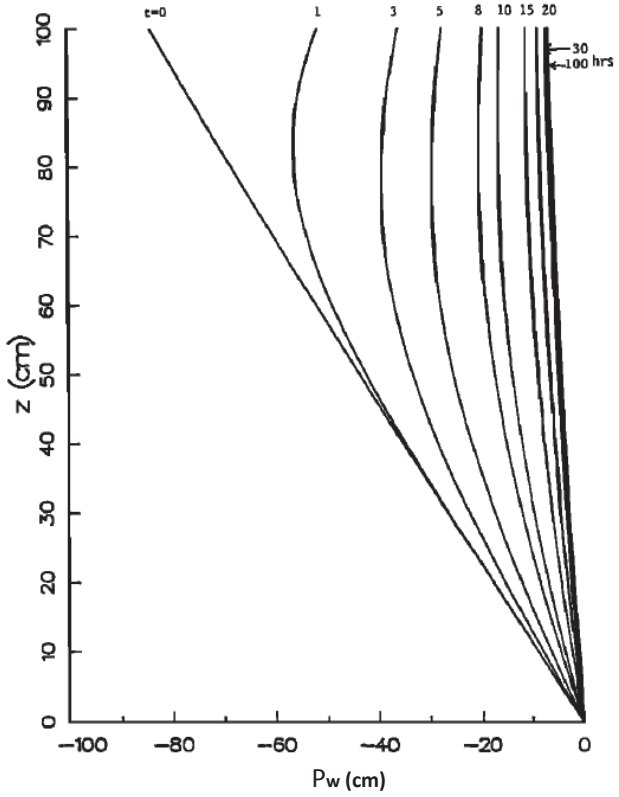

(b)

Figure 4.3: Comparison of the suction in vadose zone.

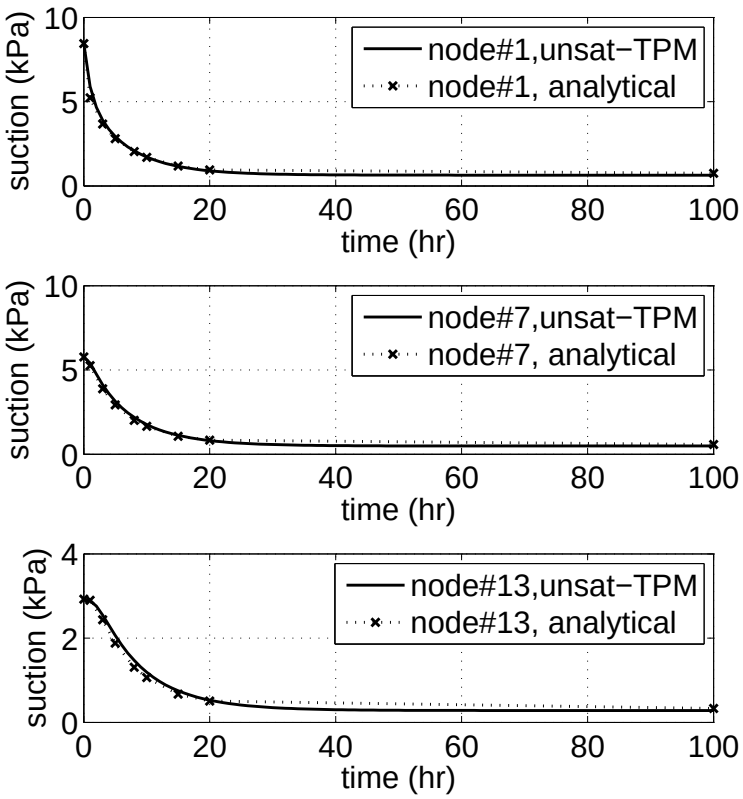

4.4 Thermo-poro-elasto-plasticity for porous media

4.4.1 Nonlinear thermo-elasticity

According to Laloui and Cekerevac (2008a), the total strain rate of the solid skeleton is written as :

$$\boldsymbol{\epsilon} = \boldsymbol{\epsilon}^e + \boldsymbol{\epsilon}^\theta + \boldsymbol{\epsilon}^p \tag{4.283}$$

in which, $\boldsymbol{\epsilon}^e$, $\boldsymbol{\epsilon}^\theta$ and $\boldsymbol{\epsilon}^p$ denote elastic, thermal and plastic components of the total solid skeleton strain, respectively. The reversible thermal strain is $\boldsymbol{\epsilon}^\theta = \beta^\theta_{skel}\mathbf{1}$, where β^θ_{skel} = linear thermal expansion coefficient of the soil skeleton; with vector $\mathbf{1} = [1\,1\,1\,0]$ when expressing $\boldsymbol{\epsilon}^\theta$ in vector form, otherwise, in tensor form, $\epsilon^\theta_{ij} = \beta^\theta_{skel}\,\delta_{ij}$. The rate form of effective Cauchy stress tensor is conventionally written as:

$$\dot{\boldsymbol{\sigma}}' = \boldsymbol{c}^e : \dot{\boldsymbol{\epsilon}}^e; \quad \dot{\boldsymbol{\epsilon}}^e = \dot{\boldsymbol{\epsilon}} - \dot{\boldsymbol{\epsilon}}^\theta - \dot{\boldsymbol{\epsilon}}^p \tag{4.284}$$

where $\boldsymbol{c}^e$ denotes the fourth-order elastic modulus tensor.

In this part, the thesis refers to Borja (2004b); Borja et al. (1997) and research notes by R.A. Regueiro at University of Colorado, Boulder in the formulation of hyperelastic model. Volumetric and deviatoric invariants of the small elastic strain tensor are defined as:

$$\epsilon^e_v = \boldsymbol{\epsilon}^e_{kk}, \quad \epsilon^e_{sh} = \sqrt{\frac{2}{3}} \parallel \boldsymbol{e}^e \parallel,\ e^e_{ij} = \epsilon^e_{ij} - \frac{1}{3}\epsilon^e_v\delta_{ij} \tag{4.285}$$

where, δ_{ij} is Kronecker delta. A class of stored energy function is defined in terms of ϵ^e_v and ϵ^e_{sh}, which are the elastic volumetric strain and elastic shear strain, respectively.

$$\rho^s\,\psi(\epsilon^e_v, \epsilon^e_s) = p'_0\tilde{\kappa}\exp\left(\frac{\epsilon^e_v - \epsilon^e_{v0}}{\tilde{\kappa}}\right) + \frac{3}{2}\mu\epsilon^{e2}_{sh} \tag{4.286}$$

where, ϵ^e_{v0} denotes elastic volumetric strain corresponding to a mean normal stress of p_0; $\tilde{\kappa}$ denotes elastic compressibility index; and $\mu = \mu(\epsilon^e_v)$ is elastic shear modulus defined as

$$\mu = \mu_0 + \alpha(-p'_0)\exp\left(-\frac{\epsilon^e_v - \epsilon^e_{v0}}{\tilde{\kappa}}\right) \tag{4.287}$$

where, μ_0 and α are material constants. The effective Cauchy stress tensor $\boldsymbol{\sigma}'$ and the elastic moduli tensor can be expressed in terms of $\rho^s\,\psi$ as

$$\sigma'_{ij} = \frac{\partial(\rho^s\psi^s)}{\partial\epsilon^e_{ij}} \tag{4.288}$$

$$c^e_{ijkl} = \frac{\partial\sigma'_{ij}}{\partial\epsilon^e_{kl}} = \frac{\partial^2(\rho^s\psi^s)}{\partial\epsilon^e_{ij}\partial\epsilon^e_{kl}} \tag{4.289}$$

With the expression of stored energy function (4.286), then we can use the chain rule to rewrite (4.288) in the form:

$$\sigma'_{ij} = \frac{\partial(\rho^s\psi^s)}{\partial\epsilon^e_v}\frac{\partial\epsilon^e_v}{\partial\epsilon^e_{ij}} + \frac{\partial(\rho^s\psi^s)}{\partial\epsilon^e_s}\frac{\partial\epsilon^e_s}{\partial\epsilon^e_{ij}} \tag{4.290}$$

Let us set

$$p' = \frac{\partial(\rho^s\psi^s)(\epsilon^e_v,\epsilon^e_s)}{\partial\epsilon^e_v},\ q = \frac{\partial(\rho^s\psi^s)(\epsilon^e_v,\epsilon^e_s)}{\partial\epsilon^e_s} \tag{4.291}$$

Then, (4.290) becomes:

$$\boldsymbol{\sigma}'_{ij} = p'\delta_{ij} + \sqrt{\frac{2}{3}}\,q\,\hat{n}_{ij} \tag{4.292}$$

where, $\hat{n}_{ij} = e^e_{ij}/\parallel \boldsymbol{e}^e \parallel = \sqrt{2/3}e^e_{ij}/\epsilon^e_s$; p' and q are the volumetric and deviatoric stress invariants of the effective Cauchy stress tensor $\boldsymbol{\sigma}'$, respectively, and are expressed as

$$p' = \frac{1}{3}\mathbf{tr}(\boldsymbol{\sigma}'),\ q = \sqrt{\frac{3}{2}}\parallel \boldsymbol{s} \parallel,\ \boldsymbol{s} = \boldsymbol{\sigma}' - p'\mathbf{1} \tag{4.293}$$

According to (4.286), one can derive the elastic constitutive equations for p' and q as follows:

$$p' = p'_0\beta\exp\left(-\frac{\epsilon^e_v - \epsilon^e_{v0}}{\tilde{\kappa}}\right) \tag{4.294}$$

$$q = 3\mu\epsilon^e_s \tag{4.295}$$

where, μ is given in (4.287), and

$$\beta = 1 + \frac{3\alpha(\epsilon^e_s)^2}{2\tilde{\kappa}} \tag{4.296}$$

Now let us calculate the elastic moduli in (4.289)

$$\begin{aligned}\frac{\partial\sigma'_{ij}}{\partial\epsilon^e_{kl}} &= \frac{\partial\sigma'_{ij}}{\partial p'}\frac{\partial p'}{\partial\epsilon^e_{kl}} + \frac{\partial\sigma'_{ij}}{\partial q}\frac{\partial q}{\partial\epsilon^e_{kl}} + \frac{\partial\sigma'_{ij}}{\partial\hat{n}_{ij}}\frac{\partial\hat{n}_{ij}}{\partial\epsilon^e_{kl}} \\ &= \delta_{ij}\frac{\partial p'}{\partial\epsilon^e_{kl}} + \sqrt{\frac{2}{3}}\hat{n}_{ij}\frac{\partial q}{\partial\epsilon^e_{kl}} + \sqrt{\frac{2}{3}}\,q\,\frac{\partial\hat{n}_{ij}}{\partial\epsilon^e_{kl}}\end{aligned} \tag{4.297}$$

where

$$\frac{\partial p'}{\partial \epsilon^e_{kl}} = \frac{p'_0}{\tilde{\kappa}} \exp\left(\frac{\epsilon^e_v - \epsilon^e_{v0}}{\tilde{\kappa}}\right)\left(3\alpha\epsilon^e_s \frac{\partial \epsilon^e_s}{\partial \epsilon^e_{kl}} - \beta \frac{\partial \epsilon^e_v}{\partial \epsilon^e_{kl}}\right) \tag{4.298}$$

$$\frac{\partial q}{\partial \epsilon^e_{kl}} = 3\epsilon^e_s \frac{\alpha p'_0}{\tilde{\kappa}} \exp\left(\frac{\epsilon^e_v - \epsilon^e_{v0}}{\tilde{\kappa}}\right) \frac{\partial \epsilon^e_v}{\partial \epsilon^e_{kl}} + 3\mu \frac{\partial \epsilon^e_s}{\partial \epsilon^e_{kl}} \tag{4.299}$$

where according to the definition in (4.285), we obtain

$$\frac{\partial \epsilon^e_v}{\partial \epsilon^e_{kl}} = \frac{\partial \epsilon^e_{ii}}{\partial \epsilon^e_{kl}} = \delta_{ik}\delta_{il} = \delta_{ij} \tag{4.300}$$

$$\frac{\partial e^e_{ab}}{\partial \epsilon^e_{kl}} = \frac{\partial \epsilon^e_{ab}}{\partial \epsilon^e_{kl}} - \frac{1}{3}\delta_{ab}\frac{\partial \epsilon^e_v}{\partial \epsilon^e_{kl}} = \delta_{ak}\delta_{bl} - \frac{1}{3}\delta_{ab}\delta_{kl} \tag{4.301}$$

$$\frac{\partial \epsilon^e_s}{\partial \epsilon^e_{kl}} = \frac{\partial \epsilon^e_s}{\partial e^e_{ab}}\frac{\partial e^e_{ab}}{\partial \epsilon^e_{kl}} = \sqrt{\frac{2}{3}}\hat{n}_{ab}\left(\delta_{ak}\delta_{bl} - \frac{1}{3}\delta_{ab}\delta_{kl}\right) = \sqrt{\frac{2}{3}}\hat{n}_{kl} \tag{4.302}$$

$$\begin{aligned}
\frac{\partial \hat{n}_{ij}}{\partial \epsilon^e_{kl}} &= \frac{1}{\parallel \boldsymbol{e}^e \parallel}\frac{\partial e^e_{ij}}{\partial \epsilon^e_{kl}} + e^e_{ij}\frac{\partial\left[(e^e_{ab}e^e_{ab})^{-\frac{1}{2}}\right]}{\partial \epsilon^e_{kl}} \\
&= \frac{1}{\parallel \boldsymbol{e}^e \parallel}\left(\delta_{ik}\delta_{jl} - \frac{1}{3}\delta_{ij}\delta_{kl}\right) - \frac{1}{2}\left(e^e_{ab}e^e_{ab}\right)^{-\frac{3}{2}}\left(2e^e_{ab}\right)\frac{\partial e^e_{ab}}{\partial \epsilon^e_{kl}} \\
&= \frac{1}{\parallel \boldsymbol{e}^e \parallel}\left(\delta_{ik}\delta_{jl} - \frac{1}{3}\delta_{ij}\delta_{kl}\right) - \frac{e^e_{kl}e^e_{ij}}{\parallel \boldsymbol{e}^e \parallel^3} \\
&= \frac{1}{\parallel \boldsymbol{e}^e \parallel}\left(\delta_{ik}\delta_{jl} - \frac{1}{3}\delta_{ij}\delta_{kl} - \hat{n}_{ij}\hat{n}_{kl}\right)
\end{aligned} \tag{4.303}$$

Then (4.298 and 4.299) become

$$\frac{\partial p'}{\partial \epsilon^e_{kl}} = \frac{p'_0}{\tilde{\kappa}} \exp\left(\frac{\epsilon^e_v - \epsilon^e_{v0}}{\tilde{\kappa}}\right)\left(3\alpha\epsilon^e_s\sqrt{\frac{2}{3}}\hat{n}_{kl} - \beta\delta_{kl}\right) \tag{4.304}$$

$$\frac{\partial q}{\partial \epsilon^e_{kl}} = \frac{3\alpha p'_0}{\tilde{\kappa}}\epsilon^e_s \exp\left(\frac{\epsilon^e_v - \epsilon^e_{v0}}{\tilde{\kappa}}\right)\delta_{kl} + 3\mu\sqrt{\frac{2}{3}}\hat{n}_{kl} \tag{4.305}$$

(4.297) takes the form

$$\begin{aligned}
\frac{\partial \boldsymbol{\sigma}'}{\partial \boldsymbol{\epsilon}^e} &= \left[-\frac{p'_0}{\tilde{\kappa}}\beta\exp\left(\frac{\epsilon^e_v - \epsilon^e_{v0}}{\tilde{\kappa}}\right) - \frac{2q}{9\epsilon^e_s}\right]\mathbf{1}\otimes\mathbf{1} \\
&\quad + \sqrt{\frac{2}{3}}\frac{2\alpha}{\tilde{\kappa}}p'_0\epsilon^e_s\exp\left(\frac{\epsilon^e_v - \epsilon^e_{v0}}{\tilde{\kappa}}\right)(\mathbf{1}\otimes\hat{\boldsymbol{n}} + \hat{\boldsymbol{n}}\otimes\mathbf{1}) \\
&\quad + \left(2\mu - \frac{2q}{3\epsilon^e_s}\right)\hat{\boldsymbol{n}}\otimes\hat{\boldsymbol{n}} + \frac{2q}{3\epsilon^e_s}\boldsymbol{I}
\end{aligned} \tag{4.306}$$

where $\boldsymbol{I}$ is a rank-four identity tensor defined as $I_{ijkl} = (\delta_{ik} + \delta_{jl})/2$

4.4.2 Thermo-plasticity

It is known that the essentials of a plasticity model are a yield function, a flow rule and a hardening law. Many enhanced versions of Cam-clay-type models have been proposed to capture the mechanical behavior (Alonso et al., 1990; Gens and Alonso, 1992; Wheeler and Sivakumar, 1995b; Vaunat et al., 2000; Loret and Khalili, 2002; Gallipoli et al., 2003a) and the thermal-plastic properties of partially saturated soil(Khalili and Loret, 2001; Laloui and Cekerevac, 2003, 2008b; François and Laloui, 2008). We mainly refer to Borja (2004b) and Laloui and Cekerevac (2003), and assume that the the yield function is defined in the effective stress space, and the size of the yield surface is controlled by the effective preconsolidation pressure, suction and temperature.

Generally, the yield function for partially saturated soils is assumed to take the following form:

$$F(p', q, p'_c) = \frac{q^2}{M^2} + (p' - p'_s)(p' - \bar{p}_c) = 0 \tag{4.307}$$

$$\bar{p}_c = -\exp[a(\xi)](-p'_c)^{b(\xi)} \left[1 - \gamma_\theta \log\left(\frac{\theta}{\theta_0}\right)\right] \tag{4.308}$$

$$p'_s = k\, s \tag{4.309}$$

where p' and q are invariants defined in (4.291), M is the slope of critical state line, k is a dimensionless material parameter that is equal to or greater than zero, s is suction, $s = p_g - p_w$; $\bar{p}_c$ is defined as the effective preconsolidation pressure at temperature θ, which is assumed to vary with plastic volume strain ϵ_v^p, suction s and temperature θ, p'_c is the saturated effective preconsolidation pressure at reference temperature θ_0, it can be considered as the plastic stress-like internal state variable of the material model, and it varies solely with the plastic deformation in the form (Borja, 2004b):

$$p'_c = p'_{c,n} \exp\left[\frac{-(\epsilon_v^p - \epsilon_{v,n}^p)}{\tilde{\lambda} - \tilde{\kappa}}\right] \tag{4.310}$$

and refer to (4.318) for the expression of ξ in (4.308). The sign convention of strain and stress is: negative under compaction, positive under dilation. ϵ_v^p and $\epsilon_{v,n}^p$ are plastic volumetric strains at current time step t_{n+1} and previous time step t_n, respectively; $p'_{c,n}$ denotes the effective preconsolidation pressure at time step t_n; $\tilde{\lambda}$ denotes the virgin compression index of the soil. The trial elastic

strain $\boldsymbol{\epsilon}^{e,tr}$ and the elastic strain at $tn+1$ are given respectively as,

$$\boldsymbol{\epsilon}^{e,tr} = \boldsymbol{\epsilon}^{e}_{n} + \Delta\boldsymbol{\epsilon} - \Delta\boldsymbol{\epsilon}^{\theta}, \quad \boldsymbol{\epsilon}^{e}_{n+1} = \boldsymbol{\epsilon}^{e,tr} - \Delta\gamma\frac{\partial F}{\partial \boldsymbol{\sigma'}} \tag{4.311}$$

where, $\Delta\boldsymbol{\epsilon}^{\theta} = \beta^{\theta}_{skel}\Delta\theta$, and $\Delta\theta = \theta_{n+1} - \theta_n$ is the temperature difference between current time step t_{n+1} and previous time step t_n. Thus, the volumetric strains are,

$$\epsilon^{e,tr}_{v} = \epsilon_{v,n} + \Delta\epsilon_v - \epsilon^{\theta}_{v}, \quad \epsilon^{e}_{v,n+1} = \epsilon^{e}_{v,n} + \Delta\epsilon^{e}_{v} \tag{4.312}$$

$$\epsilon^{p}_{v} = \epsilon_v - \epsilon^{e}_{v} - \epsilon^{\theta}_{v} \tag{4.313}$$

$$\epsilon^{p}_{v,n} = \epsilon_{v,n} - \epsilon^{e}_{v,n} - \epsilon^{\theta}_{v,n} \tag{4.314}$$

$$\epsilon^{p}_{v} - \epsilon^{p}_{v,n} = \underbrace{\epsilon_v - \epsilon_{v,n}}_{\Delta\epsilon_v} + \epsilon^{e}_{v,n} - \Delta\epsilon^{\theta}_{v} - \epsilon^{e}_{v} = \epsilon^{e,tr}_{v} - \epsilon^{e}_{v} \tag{4.315}$$

Then, (4.310) can be written in the form

$$p'_c = p'_{c,n}\exp\left[\frac{-(\epsilon^{e,tr}_{v} - \epsilon^{e}_{v})}{\tilde{\lambda} - \tilde{\kappa}}\right] \tag{4.316}$$

For partially saturated condition, $a(\xi)$ and $b(\xi)$ in (4.308) take the form

$$a(\xi) = \frac{N[c(\xi) - 1]}{\tilde{\lambda}c(\xi) - \tilde{\kappa}}, \quad b(\xi) = \frac{\tilde{\lambda} - \tilde{\kappa}}{\tilde{\lambda}c(\xi) - \tilde{\kappa}} \tag{4.317}$$

where N is the reference value of v_{sat} at unit saturated preconsolidation stress; $\xi \geq 0$ is called the "bonding variable", and has a minimum value of zero at saturated condition. It is expressed in terms of the air void fraction $1 - S_w$ and a suction function $f(s)$:

$$\xi = f(s)(1 - S_w), \quad f(s) = 1 + \frac{s/p_{atm}}{10.7 + 2.4(s/p_{atm})} \tag{4.318}$$

where p_{atm} is the atmospheric pressure. The suction function $f(s)$ is a hyperbolic approximation to the curve describing the meniscus-induced interparticle force between two identical spheres (Fisher, 1926). Refer to Borja (2004b) for more details. The degree of water saturation S_w may be expressed as a function of suction s. Here we adopt the relation proposed by van Genuchten (van Genuchten, 1980). $c(\xi)$ is defined as

$$c(\xi) := \frac{v}{v_{sat}} \tag{4.319}$$

where, v denotes the specific volume of the virgin compression curve in the partially saturated state; v_{sat} denotes the corresponding specific volume in the fully saturated state. According to Gallipoli et al. (2003a), $c(\xi)$ takes the following form:

$$c(\xi) = 1 - c_1 \left[1 - \exp(c_2 \xi)\right] \tag{4.320}$$

where c_1 and c_2 are fitting parameters. For a fully saturated condition, $c(\xi) = 1$, $a(\xi) = 0$, and $b(\xi) = 1$. We recall that

$$\dot{\epsilon}_v^p = \mathrm{tr}(\dot{\boldsymbol{\epsilon}}^p) = \dot{\gamma}\, \mathrm{tr}\left(\frac{\partial F}{\partial \boldsymbol{\sigma}'}\right) = \dot{\gamma}(2p' - p'_s - \bar{p}_c) \tag{4.321}$$

Thus the preconsolidation pressure rate gives the plastic hardening relation

$$\dot{p}'_c = \frac{-p'_c}{\tilde{\lambda} - \tilde{\kappa}}\, \mathrm{tr}(\dot{\epsilon}^p) = \underbrace{(2p' - p'_s - \bar{p}_c)(p_c)'_n \exp\left[\frac{-(\epsilon_v^{e,tr} - \epsilon_v^e)}{\tilde{\lambda} - \tilde{\kappa}}\right] \cdot \frac{-1}{\tilde{\lambda} - \tilde{\kappa}}}_{h^{pc}}\, \dot{\gamma} \tag{4.322}$$

Note that $\dot{p}'_c$ and $\mathrm{tr}(\dot{\boldsymbol{\epsilon}}^p)$ share the same sign. According to the sign convention mentioned before, positive (softening) under plastic dilation, i.e., the size of the yield surface decreases, negative (hardening) under plastic compaction, and perfect plasticity at the critical state. Now we come to the plastic flow rule, which defines the direction of the plastic strain rate in the model. Associative plastic flow is assumed, i.e., the plastic potential function $G =$ the yield function F, such that

$$\dot{\boldsymbol{\epsilon}}^p = \dot{\gamma}\frac{\partial G}{\partial \boldsymbol{\sigma}'} = \dot{\gamma}\frac{\partial F}{\partial \boldsymbol{\sigma}'} \tag{4.323}$$

where the non-negative plastic multiplier $\dot{\gamma}$ satisfies Kuhn-Tucker conditions, i.e., $\dot{\gamma} \geq 0$, $F \leq 0$, $\dot{\gamma}F = 0$. Backward Euler is adopted to obtain the plastic strain at time step t_{n+1}:

$$\boldsymbol{\epsilon}_{n+1}^p = \boldsymbol{\epsilon}_n^p + \Delta\gamma \left(\frac{\partial F}{\partial \boldsymbol{\sigma}}\right)_{n+1} \tag{4.324}$$

$$\boldsymbol{\epsilon}_{n+1}^p = \boldsymbol{\epsilon}_{n+1} - \boldsymbol{\epsilon}_{n+1}^e - \boldsymbol{\epsilon}_{n+1}^\theta \tag{4.325}$$

$$\boldsymbol{\epsilon}_n^p = \boldsymbol{\epsilon}_n - \boldsymbol{\epsilon}_n^e - \boldsymbol{\epsilon}_n^\theta \tag{4.326}$$

where $\Delta\gamma = \Delta t\, \dot{\gamma}_{n+1} \geq 0$ is the discrete consistency parameter. Substitute (4.325) and (4.326) into

(4.324) to obtain

$$\begin{aligned}
&\boldsymbol{\epsilon}_{n+1} - \boldsymbol{\epsilon}^e_{n+1} - \boldsymbol{\epsilon}^\theta_{n+1} = \boldsymbol{\epsilon}_n - \boldsymbol{\epsilon}^e_n - \boldsymbol{\epsilon}^\theta_n + \Delta\gamma \left(\frac{\partial F}{\partial \boldsymbol{\sigma}}\right)_{n+1} \\
\Rightarrow \quad &\boldsymbol{\epsilon}^e_{n+1} = \underbrace{\boldsymbol{\epsilon}_{n+1} - \boldsymbol{\epsilon}_n}_{\Delta\boldsymbol{\epsilon}} + \boldsymbol{\epsilon}^e_n - \underbrace{(\boldsymbol{\epsilon}^\theta_{n+1} - \boldsymbol{\epsilon}^\theta_n)}_{\Delta\boldsymbol{\epsilon}^\theta} - \Delta\gamma \left(\frac{\partial F}{\partial \boldsymbol{\sigma}}\right)_{n+1} \\
\Rightarrow \quad &\boldsymbol{\epsilon}^e_{n+1} = \underbrace{\boldsymbol{\epsilon}^e_n + \Delta\boldsymbol{\epsilon}}_{\boldsymbol{\epsilon}^{e,tr}_{n+1}} - \Delta\boldsymbol{\epsilon}^\theta - \Delta\gamma \left(\frac{\partial F}{\partial \boldsymbol{\sigma}}\right)_{n+1}
\end{aligned} \tag{4.327}$$

where $\Delta\boldsymbol{\epsilon}^\theta = \beta^\theta_{skel}(\theta_{n+1} - \theta_n)$. Now we solve $\frac{\partial F}{\partial \boldsymbol{\sigma}'}$ in the plastic strain rate:

$$\frac{\partial F}{\partial \boldsymbol{\sigma}'} = \frac{\partial F}{\partial p'}\frac{\partial p'}{\partial \boldsymbol{\sigma}'} + \frac{\partial F}{\partial q}\frac{\partial q}{\partial \boldsymbol{\sigma}'} \tag{4.328}$$

where

$$\frac{\partial F}{\partial p'} = (2p' - p'_s - \bar{p}_c); \quad \frac{\partial F}{\partial q} = \frac{2q}{M^2} \tag{4.329}$$

$$\left(\frac{\partial p'}{\partial \boldsymbol{\sigma}'}\right)_{ij} = \frac{1}{3}\delta_{ij}; \quad \left(\frac{\partial q}{\partial \boldsymbol{\sigma}'}\right)_{ij} = \sqrt{\frac{3}{2}}\hat{n}_{ij} \tag{4.330}$$

Then,

$$\left(\frac{\partial F}{\partial \boldsymbol{\sigma}'}\right)_{ij} = \frac{1}{3}(2p' - p'_s - \bar{p}_c)\delta_{ij} + \frac{2q}{M^2}\sqrt{\frac{3}{2}}\hat{n}_{ij} \tag{4.331}$$

The elastic strain invariants can be obtained by trial values:

$$\begin{aligned}
\epsilon^e_v &= \epsilon^{e,tr}_v - \Delta\epsilon^\theta_v - \Delta\gamma \mathrm{tr}\left(\frac{\partial F}{\partial \boldsymbol{\sigma}'}\right) \\
&= \epsilon^{e,tr}_v - \Delta\epsilon^\theta_v - \Delta\gamma\frac{\partial F}{\partial p'}
\end{aligned} \tag{4.332}$$

$$\begin{aligned}
\epsilon^e_s &= \sqrt{\frac{2}{3}}\sqrt{e^e_{ab}e^e_{ab}} \\
&= \epsilon^{e,tr}_s - \Delta\gamma\frac{\partial F}{\partial q}
\end{aligned} \tag{4.333}$$

To solve for $\Delta\gamma$, we construct a residual vector $\boldsymbol{R}$ and an unknown vector $\boldsymbol{X}$:

$$\boldsymbol{R}(\boldsymbol{X}) = \begin{bmatrix} R_v \\ R_s \\ R_F \end{bmatrix} = \begin{bmatrix} \epsilon^e_v - \epsilon^{e,tr}_v + \Delta\gamma\frac{\partial F}{\partial p} \\ \epsilon^e_s - \epsilon^{e,tr}_s + \Delta\gamma\frac{\partial F}{\partial q} \\ F \end{bmatrix} \tag{4.334}$$

and,

$$\boldsymbol{X} = \begin{bmatrix} \epsilon_v^e \\ \epsilon_s^e \\ \Delta\gamma \end{bmatrix} \tag{4.335}$$

We adopt Newton-Raphson method to solve:

$$\begin{gathered} \boldsymbol{R}_{n+1}(\boldsymbol{X}_{n+1}) = \boldsymbol{0} \\ \boldsymbol{R}_{n+1}^k + \left(\frac{\partial \boldsymbol{R}}{\partial \boldsymbol{X}}\right)_{n+1}^k \cdot \delta\boldsymbol{X} = \boldsymbol{0} \quad \Rightarrow \quad \delta\boldsymbol{X} = -\left(\frac{\partial \boldsymbol{R}}{\partial \boldsymbol{X}}\right)^{-1} \cdot \boldsymbol{R}^k \\ \boldsymbol{X}^{k+1} = \boldsymbol{X}^k + \delta\boldsymbol{X} \end{gathered} \tag{4.336}$$

The driving forces in this nonlinear problem are the trail elastic strains $\epsilon_v^{e,tr}$ and $\epsilon_s^{e,tr}$, thermal strain ϵ^θ, and the matrix suction s. $\epsilon_v^{e,tr}$ and $\epsilon_s^{e,tr}$ are held fixed at local iteration level; ϵ^θ and s can be calculated at global level. To solve this nonlinear matrix equation by Newton-Raphson method, we need to calculate the consistent tangent operator:

$$\frac{\partial \boldsymbol{R}}{\partial \boldsymbol{X}} = \begin{bmatrix} \frac{\partial R_v}{\partial \epsilon_v^e} & \frac{\partial R_v}{\partial \epsilon_s^e} & \frac{\partial R_v}{\partial \Delta\gamma} \\ \frac{\partial R_s}{\partial \epsilon_v^e} & \frac{\partial R_s}{\partial \epsilon_s^e} & \frac{\partial R_s}{\partial \Delta\gamma} \\ \frac{\partial R_F}{\partial \epsilon_v^e} & \frac{\partial R_F}{\partial \epsilon_s^e} & \frac{\partial R_F}{\partial \Delta\gamma} \end{bmatrix} \tag{4.337}$$

Substituting (4.329) and calculating the derivatives in (4.337) lead to

$$\frac{\partial \boldsymbol{R}}{\partial \boldsymbol{X}} = \begin{bmatrix} 1 + \Delta\gamma\left(2\frac{\partial p'}{\partial \epsilon_v^e} - \frac{\partial \bar{p}_c}{\partial \epsilon_v^e}\right) & 2\Delta\frac{\partial p'}{\partial \epsilon_s^e} & \frac{\partial F}{\partial p'} \\ \Delta\gamma\frac{2}{M^2}\frac{\partial q}{\partial \epsilon_v^e} & 1 + \Delta\gamma\frac{2}{M^2}\frac{\partial q}{\partial \epsilon_s^e} & \frac{\partial F}{\partial q} \\ \frac{\partial F}{\partial p'}\frac{\partial p'}{\partial \epsilon_v^e} + \frac{\partial F}{\partial q}\frac{\partial q}{\partial \epsilon_v^e} + \frac{\partial F}{\partial \bar{p}_c}\frac{\partial \bar{p}_c}{\partial \epsilon_v^e} & \frac{\partial F}{\partial p'}\frac{\partial p'}{\partial \epsilon_s^e} + \frac{\partial F}{\partial q}\frac{\partial q}{\partial \epsilon_s^e} & 0 \end{bmatrix} \tag{4.338}$$

where

$$\frac{\partial p'}{\partial \epsilon_v^e} = -\frac{p'}{\tilde{\kappa}}; \quad \frac{\partial p'}{\partial \epsilon_s^e} = p_0' \exp(\omega)\frac{\partial \beta}{\partial \epsilon_s^e} = \frac{\alpha\epsilon_s^e}{\tilde{\kappa}} p_0' \exp(\omega) \tag{4.339}$$

$$\frac{\partial q}{\partial \epsilon_v^e} = 3\epsilon_s^e\frac{\partial \mu}{\partial \epsilon_v^e} = 3\frac{\alpha\epsilon_s^e}{\tilde{\kappa}} p_0' \exp(\omega) = \frac{\partial p'}{\partial \epsilon_s^e}; \quad \frac{\partial q}{\partial \epsilon_s^e} = 3\mu \tag{4.340}$$

$$\frac{\partial \bar{p}_c}{\partial \epsilon_v^e} = \frac{\partial \bar{p}_c}{\partial p_c'}\frac{p_c'}{\partial \epsilon_v^e} = \frac{\partial \bar{p}_c}{\partial p_c'}\frac{p_c'}{\tilde{\lambda} - \tilde{\kappa}} \tag{4.341}$$

$$\tag{4.342}$$

where $\omega = -\frac{\epsilon_v^e - \epsilon_{v0}^e}{\tilde{\kappa}}$. According to (4.308),

$$\frac{\partial \bar{p}_c}{\partial p'_c} = \frac{b(\xi)\bar{p}_c}{p'_c} \tag{4.343}$$

Instead of solving (4.336) for $\delta \boldsymbol{X}$, we combine terms in (4.337) to construct the following matrices:

$$\boldsymbol{A} = \begin{bmatrix} \frac{\partial R_v}{\partial \epsilon_v^e} & \frac{\partial R_v}{\partial \epsilon_s^e} \\ \frac{\partial R_s}{\partial \epsilon_v^e} & \frac{\partial R_s}{\partial \epsilon_s^e} \end{bmatrix}; \quad \boldsymbol{B} = \begin{bmatrix} \frac{\partial R_v}{\partial \epsilon_v^e} \\ \frac{\partial R_s}{\partial \epsilon_s^e} \end{bmatrix}; \quad \boldsymbol{C} = \begin{bmatrix} \frac{\partial R_F}{\partial \Delta\gamma} & \frac{\partial R_F}{\partial \Delta\gamma} \end{bmatrix} \tag{4.344}$$

Let us rewrite (4.336) and drop the iteration number k

$$\begin{bmatrix} R_v \\ R_s \\ R_F \end{bmatrix} + \begin{bmatrix} \boldsymbol{A} & \boldsymbol{B} \\ \boldsymbol{C} & \boldsymbol{0} \end{bmatrix} \cdot \begin{bmatrix} \delta\epsilon_v^e \\ \delta\epsilon_s^e \\ \delta\Delta\gamma \end{bmatrix} = \begin{bmatrix} 0 \\ 0 \\ 0 \end{bmatrix} \tag{4.345}$$

(4.345) can be split into two equations

$$\begin{bmatrix} R_v \\ R_s \end{bmatrix} + \boldsymbol{A} \begin{bmatrix} \delta\epsilon_v^e \\ \delta\epsilon_s^e \end{bmatrix} + \boldsymbol{B}(\delta\Delta\gamma) = \boldsymbol{0} \tag{4.346}$$

$$R_F + \boldsymbol{C} \begin{bmatrix} \delta\epsilon_v^e \\ \delta\epsilon_s^e \end{bmatrix} = 0 \tag{4.347}$$

We Multiply (4.346) by matrix $\boldsymbol{A}$ and combine with (4.347) to obtain

$$R_F - \boldsymbol{C}\boldsymbol{A}^{-1} \begin{bmatrix} R_v \\ R_s \end{bmatrix} - \boldsymbol{C}\boldsymbol{A}^{-1}\boldsymbol{B}(\delta\Delta\gamma) = 0 \tag{4.348}$$

$$\Rightarrow \delta\Delta\gamma = \frac{R_F - \boldsymbol{C}\boldsymbol{A}^{-1} \begin{bmatrix} R_v \\ R_s \end{bmatrix}}{\boldsymbol{C}\boldsymbol{A}^{-1}\boldsymbol{B}} \tag{4.349}$$

Substituting (4.349) into (4.346) gives the increments of ϵ_v and ϵ_s

$$\begin{bmatrix} \delta\epsilon_v^e \\ \delta\epsilon_s^e \end{bmatrix} = -\boldsymbol{A}^{-1} \left(\begin{bmatrix} R_v \\ R_s \end{bmatrix} + \boldsymbol{B}(\delta\Delta\gamma) \right) \tag{4.350}$$

We update to obtain

$$(\epsilon_v^e)^{k+1} = (\epsilon_v^e)^k + \delta\epsilon_v^e \tag{4.351}$$

$$(\epsilon_s^e)^{k+1} = (\epsilon_s^e)^k + \delta\epsilon_s^e \tag{4.352}$$

$$(\Delta\gamma)^{k+1} = (\Delta\gamma)^k + \delta\Delta\gamma \tag{4.353}$$

Update $\boldsymbol{R}^{k+1}$ and check whether the absolute or (and) relative tolerance is (are) acceptable. If acceptable, exit and calculate the elastic strain $\boldsymbol{\epsilon}^e$ and the effective stress $\boldsymbol{\sigma}'$.

4.4.2.1 Consistent tangent operators

In this section we develop expressions of consistent tangent operators for both saturated and partially saturated conditions. The yield function rate is:

$$\dot{F} = \frac{\partial F}{\partial \boldsymbol{\sigma}'} : \dot{\boldsymbol{\sigma}}' + \frac{\partial F}{\partial s}\,\dot{s} + \frac{\partial F}{\partial p_c'}\,\dot{p}_c' + \frac{\partial F}{\partial \theta}\,\dot{\theta} = 0 \tag{4.354}$$

where,

$$\frac{\partial F}{\partial s} = -(p' - \bar{p}_c)\frac{\partial p_s'}{\partial s} - (p' - p_s')\frac{\partial \bar{p}_c}{\partial s} \tag{4.355}$$

$$\frac{\partial F}{\partial p_c'} = -(p' - p_s')\frac{\partial \bar{p}_c}{\partial p_c'} \tag{4.356}$$

$$\frac{\partial F}{\partial \theta} = -(p' - p_s')\frac{\partial \bar{p}_c}{\partial \theta} \tag{4.357}$$

in (4.355)

$$\frac{\partial p_s'}{\partial s} = k; \quad \frac{\partial \bar{p}_c}{\partial s} = \frac{\partial \bar{p}_c}{\partial \xi}\frac{\partial \xi}{\partial s} \tag{4.358}$$

We recall that $\bar{p}_c = \bar{p}_c(p_c, \xi(s), \theta)$ in (4.308). Differentiating $\bar{p}_c$ with respect to ξ and θ gives

$$\frac{\partial \bar{p}_c}{\partial \xi} = \bar{p}_c\left[a'(\xi) + b'(\xi)\ln(-p_c')\right] \tag{4.359}$$

$$\frac{\partial \bar{p}_c}{\partial \theta} = \frac{\gamma_\theta}{log_{10}\theta}\exp[a(\xi)](-p_c)^{b(\xi)} \tag{4.360}$$

where

$$a'(\xi) = \frac{Nb(\xi)}{\tilde{\lambda}c(\xi) - \tilde{\kappa}}, \quad b'(\xi) = \frac{-\tilde{\lambda}b(\xi)}{\tilde{\lambda}c(\xi) - \tilde{\kappa}}c'(\xi), \quad c'(\xi) = c_1c_2\exp(c_2\xi) \tag{4.361}$$

The derivative of the variable ξ with respect to the suction s is:

$$\xi'(s) = (1 - S_w) f'(s) - f(s) S'_w(s) \tag{4.362}$$

where

$$f'(s) = \frac{10.7/p_{atm}}{\left[10.7 + 2.4(s/p_{atm})\right]^2} \tag{4.363}$$

With the commonly used van Genuchten model (van Genuchten, 1980), the degree of water saturation is written as (see notations in (5.18))

$$\frac{S_w - S_r}{S_s - S_r} = \left[1 + (s/a)^n\right]^{-m} (1 - S_r) + S_r \tag{4.364}$$

then, one can write the derivative of S_w with respect to suction s as

$$S'_w(s) = \frac{\partial S_w}{\partial s} = -(1 - S_r) \left(\frac{mn}{a}\right) \left[1 + \frac{s}{a}\right]^{-(m+1)} \tag{4.365}$$

The effective Cauchy stress tensor rate is written as:

$$\dot{\boldsymbol{\sigma}}' = \boldsymbol{c}^e : \dot{\boldsymbol{\epsilon}}^e = \boldsymbol{c}^e : (\dot{\boldsymbol{\epsilon}} - \dot{\boldsymbol{\epsilon}}^\theta - \dot{\boldsymbol{\epsilon}}^p) \tag{4.366}$$

Substitute (4.331, 4.366, 4.355, 4.356) and (4.357) into (4.354) to obtain

$$\frac{\partial F}{\partial \boldsymbol{\sigma}'} : \boldsymbol{c}^e : \dot{\boldsymbol{\sigma}}' + \left[\frac{\partial F}{\partial \theta} - \frac{\partial F}{\partial \boldsymbol{\sigma}'} : \boldsymbol{c}^e : (\beta^\theta_{skel} \mathbf{1})\right] \dot{\theta} + \frac{\partial F}{\partial s} \dot{s} - \underbrace{\left[\frac{\partial F}{\partial \boldsymbol{\sigma}'} : \boldsymbol{c}^e : \frac{\partial F}{\partial \boldsymbol{\sigma}'} - \frac{\partial F}{\partial p'_c} h^{pc}\right]}_{\chi} \dot{\gamma} = 0 \tag{4.367}$$

Thus, the plastic multiplier takes the form

$$\dot{\gamma} = \frac{1}{\chi} \left\{ \frac{\partial F}{\partial \boldsymbol{\sigma}'} : \boldsymbol{c}^e : \dot{\boldsymbol{\epsilon}} + \frac{\partial F}{\partial s} \dot{s} + \left[\frac{\partial F}{\partial \theta} - \frac{\partial F}{\partial \boldsymbol{\sigma}'} : \boldsymbol{c}^e : (\beta^\theta_s \mathbf{1})\right] \dot{\theta} \right\} \tag{4.368}$$

Finally, the effective constitutive Cauchy stress rate is

$$\begin{aligned} \dot{\boldsymbol{\sigma}}' \;=\; & \underbrace{\left(\boldsymbol{c}^e - \frac{1}{\chi} \boldsymbol{c}^e : \frac{\partial F}{\partial \boldsymbol{\sigma}'} \otimes \frac{\partial F}{\partial \boldsymbol{\sigma}'} : \boldsymbol{c}^e\right)}_{\boldsymbol{c}^{ep}} : \dot{\boldsymbol{\epsilon}} - \frac{1}{\chi} \frac{\partial F}{\partial s} (\boldsymbol{c}^e : \frac{\partial F}{\partial \boldsymbol{\sigma}'}) \dot{s} \\ & - \underbrace{\left\{ \beta^\theta_s \boldsymbol{c}^e : \mathbf{1} + \frac{1}{\chi} \left[\frac{\partial F}{\partial \theta} - \frac{\partial F}{\partial \boldsymbol{\sigma}'} : \boldsymbol{c}^e : \beta^\theta_s \mathbf{1}\right] \otimes (\boldsymbol{c}^e : \frac{\partial F}{\partial \boldsymbol{\sigma}'}) \right\}}_{\boldsymbol{c}^\theta} \dot{\theta} \end{aligned} \tag{4.369}$$

where $\boldsymbol{c}^{ep}$ is called the continuum elastoplastic tangent under partially saturated condition with temperature. Below we list the other continuum tangents

$$\frac{\partial \boldsymbol{\sigma}'}{\partial s} = -\frac{1}{\chi}\frac{\partial F}{\partial s}\left(\boldsymbol{c}^e : \frac{\partial F}{\partial \boldsymbol{\sigma}'}\right) \tag{4.370}$$

$$\frac{\partial \boldsymbol{\sigma}'}{\partial \theta} = \frac{\partial \boldsymbol{\sigma}'}{\partial \boldsymbol{\epsilon}}\frac{\partial \boldsymbol{\epsilon}}{\partial \theta} - \boldsymbol{c}^{\theta} = \boldsymbol{c}^{ep} : (\beta_s^{\theta}\,\mathbf{1}) - \boldsymbol{c}^{\theta} = -\frac{1}{\chi}\frac{\partial F}{\partial \theta}\boldsymbol{c}^e : \frac{\partial F}{\partial \boldsymbol{\sigma}'} \tag{4.371}$$

Note that, generally, the material consistent tangent $(\partial \boldsymbol{\sigma}'/\partial \boldsymbol{\epsilon})_{n+1}$ and the continuum elastoplastic tangent $\boldsymbol{c}^{ep}$ are different. And the advantage of the consistent tangent is that it will allow the Newton-Raphson algorithm to demonstrate quadratic convergence for the global solution iterative scheme, however, the continuum tangent usually gives linear convergence. Now let us derive the material consistent tangent $\frac{\partial \boldsymbol{\sigma}'}{\partial \boldsymbol{\epsilon}}$.

$$\begin{aligned}\frac{\partial \sigma'_{ij}}{\partial \epsilon_{kl}} &= \frac{\partial \sigma'_{ij}}{\partial p'}\frac{\partial p'}{\partial \epsilon_{kl}} + \frac{\partial \sigma'_{ij}}{\partial q}\frac{\partial q}{\partial \epsilon_{kl}} + \frac{\partial \sigma'_{ij}}{\partial \hat{n}_{ij}}\frac{\partial \hat{n}_{ij}}{\partial \epsilon_{kl}} \\ &= \delta_{ij}\frac{\partial p'}{\partial \epsilon_{kl}} + \sqrt{\frac{2}{3}}\hat{n}_{ij}\frac{\partial q}{\partial \epsilon_{kl}} + \sqrt{\frac{2}{3}}\,q\,\frac{\partial \hat{n}_{ij}}{\partial \epsilon_{kl}}\end{aligned} \tag{4.372}$$

where

$$\frac{\partial p'}{\partial \epsilon_{kl}} = \frac{\partial p'}{\partial \epsilon_v^e}\frac{\partial \epsilon_v^e}{\partial \epsilon_{kl}} + \frac{\partial p'}{\partial \epsilon_s^e}\frac{\partial \epsilon_s^e}{\partial \epsilon_{kl}} = \frac{p'_0}{\tilde{\kappa}}\exp\left(\frac{\epsilon_v^e - \epsilon_{v0}^e}{\tilde{\kappa}}\right)\left(\,3\alpha\epsilon_s^e\frac{\partial \epsilon_s^e}{\partial \epsilon_{kl}} - \beta\frac{\partial \epsilon_v^e}{\partial \epsilon_{kl}}\right) \tag{4.373}$$

$$\frac{\partial q}{\partial \epsilon_{kl}} = \frac{\partial q}{\partial \epsilon_v^e}\frac{\partial \epsilon_v^e}{\partial \epsilon_{kl}} + \frac{\partial q}{\partial \epsilon_s^e}\frac{\partial \epsilon_s^e}{\partial \epsilon_{kl}} = 3\epsilon_s^e\frac{\alpha p'_0}{\tilde{\kappa}}\exp\left(\frac{\epsilon_v^e - \epsilon_{v0}^e}{\tilde{\kappa}}\right)\frac{\partial \epsilon_v^e}{\partial \epsilon_{kl}} + 3\mu\frac{\partial \epsilon_s^e}{\partial \epsilon_{kl}} \tag{4.374}$$

We recall (4.327) and drop the $n+1$:

$$\epsilon_{ab}^e = \epsilon_{ab}^{e,tr} - \Delta\gamma\frac{\partial F}{\partial \sigma'_{ab}} \tag{4.375}$$

$$\epsilon_{ab}^{e,tr} = (\epsilon_{ab}^e)_n + \underbrace{\epsilon_{ab} - (\epsilon_{ab})_n}_{\Delta\epsilon_{ab}} - \epsilon_{ab}^{\theta} \tag{4.376}$$

$(\epsilon_{ab}^e)_n$ and $(\epsilon_{ab})_n$ are fixed values at the local level, which can be obtained from previous time step t_n, and ϵ_{ab}^{θ} is also fixed at local level, because it can be obtained from the global solution. Thus, the three terms are not functions of ϵ_{kl}. Then,

$$\frac{\partial \epsilon_{ab}^{e,tr}}{\partial \epsilon_{kl}} = \delta_{ak}\delta_{bl} \tag{4.377}$$

$$\frac{\partial \epsilon^e_{ab}}{\partial \epsilon_{kl}} = \frac{\partial \epsilon^{e,tr}_{ab}}{\partial \epsilon_{kl}} - \frac{\partial \Delta\gamma}{\partial \epsilon_{kl}} \frac{\partial F}{\partial \sigma'_{ab}} - \Delta\gamma \frac{\partial^2 F}{\partial \sigma'_{ab} \partial \epsilon_{kl}} \tag{4.378}$$

Let us assume

$$\hat{\boldsymbol{n}}^{tr} = \hat{\boldsymbol{n}} \tag{4.379}$$

Recall

$$e^{e,tr}_{ab} = \epsilon^{e,tr}_{ab} - \frac{1}{3}\epsilon^{e,tr}_{v}\delta_{ab} \tag{4.380}$$

The derivative is written as

$$\frac{\partial e^{e,tr}_{ab}}{\partial \epsilon_{kl}} = \frac{\partial(\epsilon^{e,tr}_{ab} - \frac{1}{3}\epsilon^{e,tr}_{v}\delta_{ab})}{\partial \epsilon_{kl}} = \delta_{ak}\delta_{bl} - \frac{1}{3}\delta_{kl}\delta_{ab} \tag{4.381}$$

$$\begin{aligned}
\frac{\partial \hat{n}^{tr}_{ij}}{\partial \epsilon_{kl}} &= \frac{1}{\parallel \boldsymbol{e}^{e,tr} \parallel} \frac{\partial e^{e,tr}_{ij}}{\partial \epsilon_{kl}} + e^{e,tr}_{ij} \frac{\partial \left[(e^{e,tr}_{ab} e^{e,tr}_{ab})^{-\frac{1}{2}} \right]}{\partial \epsilon_{kl}} \\
&= \frac{1}{\parallel \boldsymbol{e}^{e,tr} \parallel} \left(\delta_{ak}\delta_{bl} - \frac{1}{3}\delta_{kl}\delta_{ab} \right) - \frac{1}{2} \left(e^{e,tr}_{ab} e^{e,tr}_{ab} \right)^{-\frac{3}{2}} (2e^{e,tr}_{ab}) \frac{\partial e^{e,tr}_{ab}}{\partial \epsilon_{kl}} \\
&= \frac{1}{\parallel \boldsymbol{e}^{e,tr} \parallel} \left(\delta_{ak}\delta_{bl} - \frac{1}{3}\delta_{kl}\delta_{ab} - \hat{n}^{tr}_{ij}\hat{n}^{tr}_{kl} \right)
\end{aligned} \tag{4.382}$$

We need to construct three equations to solve for $\frac{\partial \epsilon^e_v}{\partial \boldsymbol{\epsilon}}$, $\frac{\partial \epsilon^e_s}{\partial \boldsymbol{\epsilon}}$, $\frac{\partial(\Delta\gamma)}{\partial \boldsymbol{\epsilon}}$. According to (4.331) and (4.377), one can write

$$\epsilon^e_v = \epsilon^{e,tr}_v - \Delta\gamma \frac{\partial F}{\partial \sigma'_{kk}} \tag{4.383}$$

$$\frac{\partial \epsilon^{e,tr}_v}{\partial \epsilon_{kl}} = \delta_{kl} \tag{4.384}$$

$$\frac{\partial F}{\partial \sigma'_{kk}} = \frac{\partial F}{\partial p'} = 2p' - p'_s - \bar{p}_c \tag{4.385}$$

Then,

$$\frac{\partial \epsilon^e_v}{\partial \epsilon_{kl}} = \delta_{kl} - (2p' - p'_s - \bar{p}_c) \frac{\partial \Delta\gamma}{\partial \epsilon_{kl}} - \Delta\gamma \left(2\frac{\partial p'}{\partial \epsilon_{kl}} - \frac{\partial \bar{p}_c}{\partial \epsilon_{kl}} \right) \tag{4.386}$$

where,

$$\frac{\partial \bar{p}_c}{\partial \epsilon_{kl}} = \frac{\partial \bar{p}_c}{\partial p_c} \left(\frac{\partial p_c}{\partial \epsilon^{e,tr}_v} \frac{\partial \epsilon^{e,tr}_v}{\partial \epsilon_{kl}} + \frac{\partial p_c}{\partial \epsilon^e_v} \frac{\partial \epsilon^e_v}{\partial \epsilon_{kl}} \right) \tag{4.387}$$

where,

$$\frac{\partial p_c}{\partial \epsilon_v^{e,tr}} = \frac{-1}{\tilde{\lambda}-\tilde{\kappa}} p_c \tag{4.388}$$

$$\frac{\partial p_c}{\partial \epsilon_v^{e}} = \frac{1}{\tilde{\lambda}-\tilde{\kappa}} p_c \tag{4.389}$$

Substituting (4.373, 4.387, 4.389) into (4.386) gives

$$\left[1+\Delta\gamma\left(2\frac{\partial p'}{\partial \epsilon_v^e}-\frac{\bar{p}_c}{\partial p_c}\frac{\partial p_c}{\partial \epsilon_v^e}\right)\right]\frac{\partial \epsilon_v^e}{\partial \boldsymbol{\epsilon}}+\left(2\Delta\gamma\frac{\partial p'}{\partial \epsilon_s^e}\right)\frac{\partial \epsilon_s^e}{\partial \boldsymbol{\epsilon}}+\frac{\partial F}{\partial p'}\frac{\partial \Delta\gamma}{\partial \boldsymbol{\epsilon}}=\left(1+\Delta\gamma\frac{\partial \bar{p}_c}{\partial p_c}\frac{\partial p_c}{\partial \epsilon_v^{e,tr}}\right)\mathbf{1} \tag{4.390}$$

where, $\mathbf{1}$ is 6×1 vector, and is given as

$$\mathbf{1}=\begin{bmatrix} 1 & 1 & 1 & 0 & 0 & 0 \end{bmatrix}^T \tag{4.391}$$

(4.333) becomes

$$\epsilon_s^e = \epsilon_s^{e,tr} - \Delta\gamma\frac{\partial F}{\partial q} \tag{4.392}$$

then,

$$\frac{\partial \epsilon_s^e}{\partial \epsilon_{kl}} = \frac{\partial \epsilon_s^{e,tr}}{\partial \epsilon_{kl}} - \frac{\partial \Delta\gamma}{\partial \epsilon_{kl}}\frac{\partial F}{\partial q} - \Delta\gamma\frac{\left(\frac{\partial F}{\partial q}\right)}{\partial \epsilon_{kl}} \tag{4.393}$$

where,

$$\frac{\left(\frac{\partial F}{\partial q}\right)}{\partial \epsilon_{kl}} = \frac{2}{M^2}\frac{\partial q}{\partial \epsilon_{kl}} = \frac{2}{M^2}\left(\frac{\partial q}{\partial \epsilon_s^e}\frac{\partial \epsilon_s^e}{\partial \epsilon_{kl}}+\frac{\partial q}{\partial \epsilon_v^e}\frac{\partial \epsilon_v^e}{\partial \epsilon_{kl}}\right) \tag{4.394}$$

With (4.381), we derive

$$\begin{aligned}
\frac{\partial \epsilon_s^e}{\partial \epsilon_{kl}} &= \sqrt{\frac{2}{3}}\times\frac{1}{2}\left(e_{ab}^{e,tr}\cdot e_{ab}^{e,tr}\right)^{-\frac{1}{2}}(2e_{ab}^{e,tr})\frac{\partial e_{ab}^{e,tr}}{\partial \epsilon_{kl}} \\
&= \sqrt{\frac{2}{3}}\frac{e_{ab}^{e,tr}}{\parallel \boldsymbol{e}^{e,tr}\parallel}\left(\delta_{ak}\delta_{bl}-\frac{1}{3}\delta_{ab}\delta_{kl}\right) \\
&= \sqrt{\frac{2}{3}}\frac{e_{kl}^{e,tr}}{\parallel \boldsymbol{e}^{e,tr}\parallel} = \sqrt{\frac{2}{3}}\hat{\boldsymbol{n}}^{tr}
\end{aligned} \tag{4.395}$$

Thus (4.393) becomes

$$\left(1+\frac{2\Delta\gamma}{M^2}\frac{\partial q}{\partial \epsilon_s^e}\right)\frac{\partial \epsilon_s^e}{\partial \boldsymbol{\epsilon}}+\left(\frac{2\Delta\gamma}{M^2}\frac{\partial q}{\partial \epsilon_v^e}\right)\frac{\partial \epsilon_v^e}{\partial \boldsymbol{\epsilon}}+\frac{\partial F}{\partial q}\frac{\partial \Delta\gamma}{\partial \boldsymbol{\epsilon}}=\sqrt{\frac{2}{3}}\hat{\boldsymbol{n}}^{tr} \tag{4.396}$$

Let us assume

$$\frac{\partial F}{\partial \epsilon_{kl}} = 0 \tag{4.397}$$

$$\begin{aligned}\frac{\partial F}{\partial \boldsymbol{\epsilon}} &= \frac{\partial F}{\partial p'}\frac{\partial p'}{\partial \boldsymbol{\epsilon}} + \frac{\partial F}{\partial q}\frac{\partial q}{\partial \boldsymbol{\epsilon}} + \frac{\partial F}{\partial \bar{p}_c}\frac{\partial \bar{p}_c}{\partial p'_c}\frac{\partial p'_c}{\partial \boldsymbol{\epsilon}} \\ &= \frac{\partial F}{\partial p'}\left(\frac{\partial p'}{\partial \epsilon_v^e}\frac{\partial \epsilon_v^e}{\partial \boldsymbol{\epsilon}} + \frac{\partial p'}{\partial \epsilon_s^e}\frac{\partial \epsilon_s^e}{\partial \boldsymbol{\epsilon}}\right) + \frac{\partial F}{\partial q}\left(\frac{\partial q}{\partial \epsilon_v^e}\frac{\partial \epsilon_v^e}{\partial \boldsymbol{\epsilon}} + \frac{\partial q}{\partial \epsilon_s^e}\frac{\partial \epsilon_s^e}{\partial \boldsymbol{\epsilon}}\right) \\ &\quad + \frac{\partial F}{\partial \bar{p}_c}\frac{\partial \bar{p}_c}{\partial p'_c}\left(\frac{\partial p'_c}{\partial \epsilon_v^{e,tr}}\frac{\partial \epsilon_v^{e,tr}}{\partial \boldsymbol{\epsilon}} + \frac{\partial p'_c}{\partial \epsilon_v^e}\frac{\partial \epsilon_v^e}{\partial \boldsymbol{\epsilon}}\right) \end{aligned} \tag{4.398}$$

We Group terms to obtain

$$\underbrace{\left(\frac{\partial F}{\partial p'}\frac{\partial p'}{\partial \epsilon_v^e} + \frac{\partial F}{\partial q}\frac{\partial q}{\partial \epsilon_v^e} + \frac{\partial F}{\partial \bar{p}_c}\frac{\partial \bar{p}_c}{\partial p'_c}\frac{\partial p'_c}{\partial \epsilon_v^e}\right)}_{A}\frac{\partial \epsilon_v^e}{\partial \boldsymbol{\epsilon}} + \underbrace{\left(\frac{\partial F}{\partial p'}\frac{\partial p'}{\partial \epsilon_s^e} + \frac{\partial F}{\partial q}\frac{\partial q}{\partial \epsilon_s^e}\right)}_{B}\frac{\partial \epsilon_s^e}{\partial \boldsymbol{\epsilon}} = -\frac{\partial F}{\partial \bar{p}_c}\frac{\partial \bar{p}_c}{\partial p'_c}\frac{\partial p'_c}{\partial \epsilon_v^{e,tr}}\mathbf{1} \tag{4.399}$$

Combine (4.390), (4.396) and (4.399) to obtain the matrix equation

$$\underbrace{\begin{bmatrix} \left[1 + \Delta\gamma\left(2\frac{\partial p'}{\partial \epsilon_v^e} - \frac{\bar{p}_c}{\partial p_c}\frac{\partial p_c}{\partial \epsilon_v^e}\right)\right]\boldsymbol{I} & \left(\frac{2\Delta\gamma}{M^2}\frac{\partial q}{\partial \epsilon_v^e}\right)\boldsymbol{I} & \frac{\partial F}{\partial p'}\boldsymbol{I} \\ \left(2\Delta\gamma\frac{\partial p'}{\partial \epsilon_s^e}\right)\boldsymbol{I} & \left(1 + \frac{2\Delta\gamma}{M^2}\frac{\partial q}{\partial \epsilon_s^e}\right)\boldsymbol{I} & \frac{\partial F}{\partial q}\boldsymbol{I} \\ A\boldsymbol{I} & B\boldsymbol{I} & \mathbf{0} \end{bmatrix}}_{18\times 18} \cdot \underbrace{\begin{bmatrix} \frac{\partial \epsilon_v^e}{\partial \boldsymbol{\epsilon}} \\ \frac{\partial \epsilon_s^e}{\partial \boldsymbol{\epsilon}} \\ \frac{\partial \Delta\gamma}{\partial \boldsymbol{\epsilon}} \end{bmatrix}}_{18\times 1} = \underbrace{\begin{bmatrix} \left(1 + \Delta\gamma\frac{\partial \bar{p}_c}{\partial p'_c}\frac{\partial p'_c}{\partial \epsilon_v^{e,tr}}\right)\mathbf{1} \\ \sqrt{\frac{2}{3}}\hat{\boldsymbol{n}}^{tr} \\ \left(-\frac{\partial F}{\partial \bar{p}_c}\frac{\partial \bar{p}_c}{\partial p'_c}\frac{\partial p'_c}{\partial \epsilon_v^{e,tr}}\right)\mathbf{1} \end{bmatrix}}_{18\times 1} \tag{4.400}$$

Note that, $\boldsymbol{I}$ is 6×6 unit tensor, and should not be confused with $\mathbf{1}$, which is 6×1 vector as mentioned before. Set

$$\boldsymbol{M} = \underbrace{\begin{bmatrix} \left[1 + \Delta\gamma\left(2\frac{\partial p'}{\partial \epsilon_v^e} - \frac{\bar{p}_c}{\partial p'_c}\frac{\partial p'_c}{\partial \epsilon_v^e}\right)\right]\boldsymbol{I} & \left(\frac{2\Delta\gamma}{M^2}\frac{\partial q}{\partial \epsilon_v^e}\right)\boldsymbol{I} \\ \left(2\Delta\gamma\frac{\partial p'}{\partial \epsilon_s^e}\right)\boldsymbol{I} & \left(1 + \frac{2\Delta\gamma}{M^2}\frac{\partial q}{\partial \epsilon_s^e}\right)\boldsymbol{I} \end{bmatrix}}_{12\times 12} \tag{4.401}$$

Then, (4.400) can be decomposed into

$$\underbrace{\boldsymbol{M}\begin{bmatrix} \frac{\partial \epsilon_v^e}{\partial \boldsymbol{\epsilon}} \\ \frac{\partial \epsilon_s^e}{\partial \boldsymbol{\epsilon}} \end{bmatrix}}_{12\times 1} + \underbrace{\begin{bmatrix} \frac{\partial F}{\partial p'}\boldsymbol{I} \\ \frac{\partial F}{\partial q}\boldsymbol{I} \end{bmatrix}}_{12\times 6} \cdot \underbrace{\frac{\partial \Delta\gamma}{\partial \boldsymbol{\epsilon}}}_{6\times 1} = \underbrace{\begin{bmatrix} \left(1 + \Delta\gamma\frac{\partial \bar{p}_c}{\partial p'_c}\frac{\partial p'_c}{\partial \epsilon_v^{e,tr}}\right)\mathbf{1} \\ \sqrt{\frac{2}{3}}\hat{\boldsymbol{n}}^{tr} \end{bmatrix}}_{12\times 1} \tag{4.402}$$

$$\underbrace{\begin{bmatrix} A\boldsymbol{I} & B\boldsymbol{I} \end{bmatrix}}_{6\times 12}\underbrace{\begin{bmatrix} \frac{\partial \epsilon_v^e}{\partial \boldsymbol{\epsilon}} \\ \frac{\partial \epsilon_s^e}{\partial \boldsymbol{\epsilon}} \end{bmatrix}}_{12\times 1} = \underbrace{\left(-\frac{\partial F}{\partial \bar{p}_c}\frac{\partial \bar{p}_c}{\partial p'_c}\frac{\partial p'_c}{\partial \epsilon_v^{e,tr}}\right)\mathbf{1}}_{6\times 1} \tag{4.403}$$

We pre-multiple (4.402) by $[A\boldsymbol{I} \quad B\boldsymbol{I}]\ \boldsymbol{M}^{-1}$ to get

$$\underbrace{\left[\begin{array}{cc} A\boldsymbol{I} & B\boldsymbol{I} \end{array}\right]\left[\begin{array}{c} \frac{\partial \epsilon_v^e}{\partial \boldsymbol{\epsilon}} \\ \frac{\partial \epsilon_s^e}{\partial \boldsymbol{\epsilon}} \end{array}\right]}_{\boldsymbol{C}_{(6\times 1)}} + \underbrace{\left[\begin{array}{cc} A\boldsymbol{I} & B\boldsymbol{I} \end{array}\right] \cdot \boldsymbol{M}^{-1} \cdot \left[\begin{array}{c} \frac{\partial F}{\partial p'}\boldsymbol{I} \\ \frac{\partial F}{\partial q}\boldsymbol{I} \end{array}\right]}_{\boldsymbol{D}_{(6\times 6)}} \cdot \frac{\partial \Delta\gamma}{\partial \boldsymbol{\epsilon}}$$

$$= \underbrace{\left[\begin{array}{cc} A\boldsymbol{I} & B\boldsymbol{I} \end{array}\right] \cdot \boldsymbol{M}^{-1} \cdot \left[\begin{array}{c} \left(1 + \Delta\gamma \frac{\partial \bar{p}_c}{\partial p'_c} \frac{\partial p'_c}{\partial \epsilon_v^{e,tr}}\right)\mathbf{1} \\ \sqrt{\frac{2}{3}}\hat{\boldsymbol{n}}^{tr} \end{array}\right]}_{6\times 1} \tag{4.404}$$

Combine with (4.403) to obtain

$$\frac{\partial \Delta\gamma}{\partial \boldsymbol{\epsilon}} = \boldsymbol{D}^{-1}\left(\left[\begin{array}{cc} A\boldsymbol{I} & B\boldsymbol{I} \end{array}\right] \cdot \boldsymbol{M}^{-1} \cdot \left[\begin{array}{c} \left(1 + \Delta\gamma \frac{\partial \bar{p}_c}{\partial p'_c} \frac{\partial p'_c}{\partial \epsilon_v^{e,tr}}\right)\mathbf{1} \\ \sqrt{\frac{2}{3}}\hat{\boldsymbol{n}}^{tr} \end{array}\right] + \frac{\partial F}{\partial \bar{p}_c}\frac{\partial \bar{p}_c}{\partial p'_c}\frac{\partial p'_c}{\partial \epsilon_v^{e,tr}}\mathbf{1}\right) \tag{4.405}$$

$$\left[\begin{array}{c} \frac{\partial \epsilon_v^e}{\partial \boldsymbol{\epsilon}} \\ \frac{\partial \epsilon_s^e}{\partial \boldsymbol{\epsilon}} \end{array}\right] = \boldsymbol{M}^{-1}\left(\left[\begin{array}{c} \left(1 + \Delta\gamma \frac{\partial \bar{p}_c}{\partial p'_c} \frac{\partial p'_c}{\partial \epsilon_v^{e,tr}}\right)\mathbf{1} \\ \sqrt{\frac{2}{3}}\hat{\boldsymbol{n}}^{tr} \end{array}\right] - \left[\begin{array}{c} \frac{\partial F}{\partial p'}\boldsymbol{I} \\ \frac{\partial F}{\partial q}\boldsymbol{I} \end{array}\right] \cdot \frac{\partial \Delta\gamma}{\partial \boldsymbol{\epsilon}}\right) \tag{4.406}$$

Chapter 5

Finite element analysis of the energy foundations experiments

5.1 Introduction to the energy foundations experiments

This chapter presents an axisymmetric, small strain, fully-coupled thermo-poro-mechanical (TPM) finite element analysis (FEA) of soil-structure interaction (SSI) between energy foundations and partially saturated silt. The simulations involve two types of energy foundations: semi-implicit foundation and end-bearing foundation. A series of centrifuge-scale tests were performed on the two types of foundations at the University of Colorado at Boulder. Numerical results are compared with experimental observations (Stewart, 2012; Stewart and McCartney, 2013; Goode, 2013; Goode and McCartney, 2014). Good agreement is obtained between the experimental and modeling results. Thermally-induced liquid water and water vapor flow inside the soil were found to have an impact on soil-structure interaction. With further improvements (including interface elements at the foundation-soil interface), FEA with the validated thermo-poro-mechanical model can be used to predict performance and soil-structure interaction mechanisms for energy foundations.

5.2 Constitutive equations

In this section, we introduce the constitutive equations adopted in thermo-poro-mechanical model, and show how the material parameters are fitted with the experimental data.

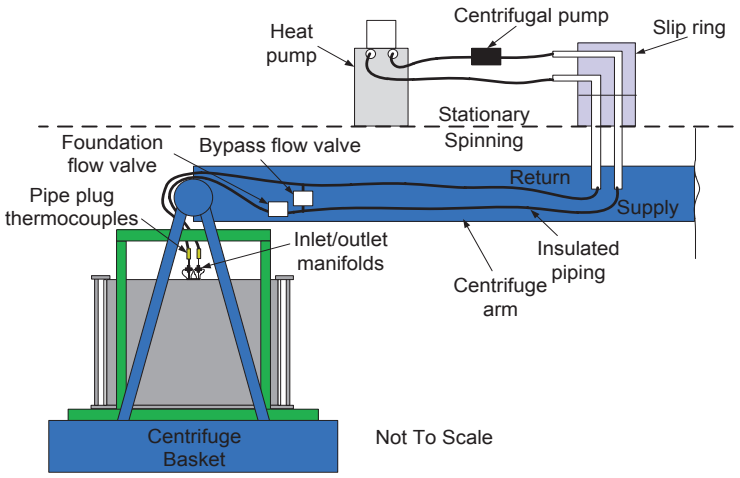

Figure 5.1: Schematic of overall temperature control system, including heat pump, auxiliary pump and fluid transition into experimental setup (Stewart, 2012)

Figure 5.2: a single energy foundation SSI experiment mounted on a 400 g-ton centrifuge bucket.

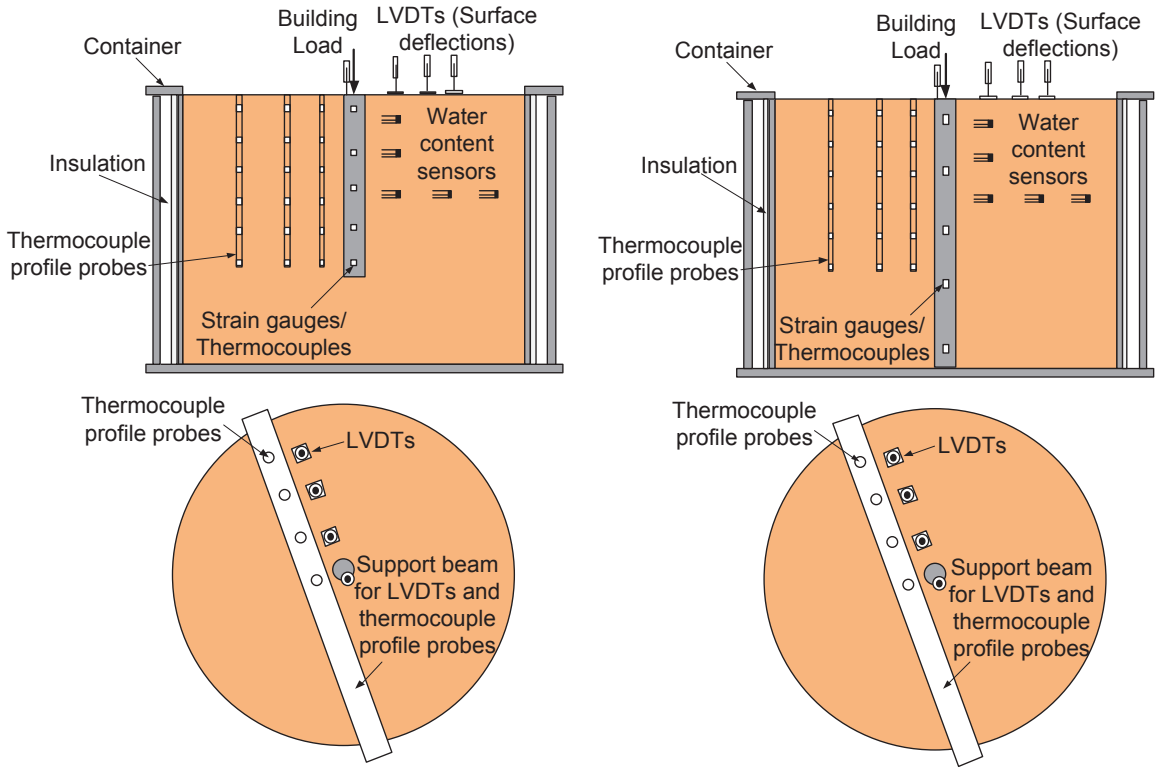

Figure 5.3: Schematic showing approximate locations of instrumentation, left: semi-floating foundation, right: end-bearing foundation (Stewart, 2012)

Table 5.1: Centrifuge scaling rules are summarized according to (Ko, 1988).

Quantity	**Prototype**	**Model**
Length	1	$1/N$
Force	1	$1/N^2$
Stress	1	1
Strain	1	1
Elastic modulus	1	1
Acceleration	1	N
Temperature	1	1
Displacement	1	$1/N$
Time (diffusive flow processes)	1	$1/N^2$

5.2.1 Mechanical properties

5.2.1.1 Effective stress equations

For saturated porous media, the expression of the effective stress is proposed by Terzaghi (1943):

$$\boldsymbol{\sigma}' = \boldsymbol{\sigma} + p_w \mathbf{1} \tag{5.1}$$

where, $\boldsymbol{\sigma}'$ and $\boldsymbol{\sigma}$ are the effective and total stress tensors, respectively. To be consistent, the sign convention in mechanics is used, i.e., $\boldsymbol{\sigma}'$ and $\boldsymbol{\sigma}$ are positive in tension. p_w is the pore water pressure.

For partially saturated porous media, Terzaghi's classic effective stress equation have been extended to account for the negative pore water pressures in various forms (Bishop, 1959; Khalili et al., 2004; Lu et al., 2010; Borja and White, 2010). For example, a commonly used form proposed by Bishop (1959) is expressed as:

$$\boldsymbol{\sigma}' = (\boldsymbol{\sigma} + p_g \mathbf{1}) - \chi(p_g - p_w)\mathbf{1} \tag{5.2}$$

where, p_g is the pore gas pressure, $p_g - p_w$ denotes the matric suction s is positive for partially saturated soils, χ is a material property referred to as the effective stress parameter, which depends on the degree of saturation or matric suction. In (5.2), $\boldsymbol{\sigma} + p_g \mathbf{1}$ represents the net stress, and $\chi(p_g - p_w)\mathbf{1}$ represents the suction stress. 5.2 will reduce to the classic effective stress equation by setting $\chi = 0$ for perfectly dry soils, or $\chi = 1$ for saturated soils. Borja and White (2010); Lewis and Schrefler (1998) use $\chi = S_w$, where S_w is the degree of saturation. In our code we will use the same relationship.

5.2.1.2 Densities

Water density

Fernandez (1972) proposed an equation for compressibility of water in the form:

$$\rho^{wR} = \rho^{wR0} \exp\left[-\beta_w^{\theta}(\theta - \theta_0) + \frac{1}{K^w}(p_w - p_{w0})\right] \tag{5.3}$$

where $\beta_w^\theta = 4.0 \times 10^{-4}\, K^{-1}$ (Khalili et al., 2010) is the volumetric thermal expansion coefficient of water; θ and θ_0 are respectively the current and reference temperatures; p_w and ρ^{wR} are respectively the pore water pressure and the water real mass density at current temperature θ; p_{w0} and ρ^{wR0} are respectively the pore pressure and water density at reference temperature θ_0; K^w is the bulk modulus of water.

Lewis and Schrefler (1998) proposed a simpler form for the compressible water phase by retaining the first-order terms of the series expansion of (5.3) as follows

$$\rho^{wR} = \rho^{wR0}\left[1 - \beta_w^\theta(\theta - \theta_0) + \frac{1}{K_w}(p_w - p_{w0})\right] \tag{5.4}$$

With the assumption in this thesis that water is mechanically incompressible, i.e., K_w is large enough that $\frac{1}{K_w}$ goes to zero, we rewrite the real mass density equation of water in the form (Lewis and Schrefler, 1998):

$$\rho^{wR} = \rho^{wR0}\left[1 - \beta_w^\theta(\theta - \theta_0)\right] \tag{5.5}$$

and the material time derivative of water real mass density is given as,

$$\frac{D^w \rho^{wR}}{D\,t} = -\rho^{wR0}\beta_w^\theta \frac{D^w \theta}{D\,t} \tag{5.6}$$

Solid density

Using the same procedure as we did for water density, the real mass density for a compressible solid phase can be expressed in the form

$$\rho^{sR} = \rho^{sR0}\left[1 - \beta_s^\theta(\theta - \theta_0) + \frac{1}{K_s}(p_s - p_{s0})\right] \tag{5.7}$$

where K^s is the bulk modulus of the solid phase; β_s^θ is the volumetric thermal expansion coefficient of solid grains (with an estimate $\beta_s^\theta = 3.5 \times 10^{-5}\, K^{-1}$ for the solid grains of silt is obtained by Khalili et al. (2010) via a drained heating-cooling test), p_s and ρ^{sR} are respectively the solid phase pressure (not the solid skeleton mean effective stress p') and the solid real mass density at current temperature θ; p_{s0} and ρ^{sR0} are respectively the solid phase pressure and solid real mass density at reference temperature θ_0. For a mechanically incompressible solid phase, the material time

derivative of the solid phase is simplified to be:

$$\frac{D^s\,\rho^{sR}}{D\,t} = -\rho^{sR0}\beta_s^{\theta}\frac{D^s\,\theta}{D\,t} \tag{5.8}$$

Gas densities

The gas phase is assumed to be a mixture of water vapor(gv) and dry air (ga). The ideal gas law is applied to the gas and its components, such that the real mass densities can be expressed as:

$$\rho^{gv} = \frac{p_{gv}M_w}{\theta R} \tag{5.9}$$

$$\rho^{ga} = \frac{p_{ga}M_a}{\theta R} \tag{5.10}$$

where p_{gv} and p_{ga} are respectively the pressure of water vapor and dry air of the gas phase, M_w and M_a are molar mass of constituent water and air, respectively, and R is the universal gas constant. According to Dalton's law of additivity of partial pressures, we write the real mass density and the pressure of gas phase as,

$$\rho^{g} = \rho^{gv} + \rho^{ga} \tag{5.11}$$

$$p_g = p_{gv} + p_{ga} \tag{5.12}$$

where saturated vapor pressure $p_{\mathrm{gvs}}(\theta)$ and relative humidity RH (according to Kelvin's law) are given as follows,

$$p_{\mathrm{gvs}}(\theta) = p_{\mathrm{gvso}}\exp\left[-\frac{M_{\mathrm{w}}\triangle H_{\mathrm{vap}}}{R}\left(\frac{1}{\theta}-\frac{1}{\theta_o}\right)\right] \tag{5.13}$$

$$\mathrm{RH} = \exp\left(\frac{-s\,M_{\mathrm{w}}}{R\theta\rho^{\mathrm{wR}}}\right) \tag{5.14}$$

5.2.1.3 Kelvin's law and Clausius-Clapeyron equation

For water vapor, the relative humidity RH is employed to relate the vapor pressure p_{gv} to the saturated vapor pressure p_{gvs} as follows,

$$\mathrm{RH} = \frac{p_{gv}}{p_{gvs}(\theta)} \tag{5.15}$$

where $p_{gvs}(\theta)$ only depends on temperature. The saturated vapor pressure p_{gvs}, which depends only on temperature θ, is predicted by the Clausius-Clapeyron equation:

$$p_{gvs}(\theta) = p_{gvs0} \exp\left[-\frac{M_w \triangle H_{vap}}{R}\left(\frac{1}{\theta} - \frac{1}{\theta_0}\right)\right] \tag{5.16}$$

where p_{gvs0} is the saturated vapor pressure at reference temperature θ_0, $\triangle H_{vap}$ is the latent heat of vaporization, M_w the molar mass of water, R the universal gas constant. Kelvin's law is applied to relate the relative humidity to the suction or capillary pressure in the pores ($s = p_g - p_w$) as

$$\mathrm{RH} = \exp\left(\frac{-s\, M_w}{R\, \theta \rho^{wR}}\right) \tag{5.17}$$

In the model, the vapor pressure under certain temperature and suction conditions can be obtained with (5.15)-(5.17), therefore, the air pressure can be calculated by the difference of gas pressure and vapor pressure. Thus the real mass densities of vapor, air and gas will be obtained with ideal gas law.

5.2.2 Hydraulic properties

5.2.2.1 Soil-water retention curve (SWRC)

A most frequently used SWRC equation presented by van Genuchten (1980) relates the degree of saturation to the suction of the soil in the form

$$S_e = \frac{S_w - S_r}{S_s - S_r} = \left[\frac{1}{1 + (s/a)^n}\right]^m \tag{5.18}$$

where S_e is the effective degree of saturation; S_w is the degree of saturation; S_r and $S_s = 1$ are relatively the residual and saturated degree of saturations; n and m are van Genuchten model parameters, and $m = 1 - 1/n$, $s = p_g - p_w$ is the suction, α, m and other parameters are obtained from the curves. The fitted parameters for drying curve are chosen in the numerical modeling, as shown in Table 5.3.

5.2.2.2 Darcy's Law

The porous media is filled with a wetting fluid (water) and a non-wetting fluid (gas). Darcy's law is extended to the partially saturated case to obtain the Darcy's velocities of water and gas: Darcy's law is applied to the partially saturated porous media to get Darcy's velocity (or apparent velocity) of water and gas respectively (Section 6.5.2 of Coussy (2004)):

$$\widetilde{\boldsymbol{v}}_w^D = -\frac{\kappa(n)K_{rw}(S_w)}{\mu_w(\theta)}(\nabla p_w - \rho^{wR}\boldsymbol{g}) \tag{5.19}$$

$$\widetilde{\boldsymbol{v}}_g^D = -\frac{\kappa(n)K_{rg}(S_w)}{\mu_g(\theta)}(\nabla p_g - \rho^{gR}\boldsymbol{g}) \tag{5.20}$$

where $K_{rw}(S_e)$ and $K_{rg}(S_e)$ are the relative permeabilities related to respectively water and gas. They both are functions of the effective degree of saturation (S_e). Here n is the porosity of the porous media, and $n = n^w + n^g$. The Darcy's velocities of water and gas are defined in the form:

$$\widetilde{\boldsymbol{v}}_w^D = n_w\widetilde{\boldsymbol{v}}_w = n\,S_w(\boldsymbol{v}_w - \boldsymbol{v}_s) \tag{5.21}$$

$$\widetilde{\boldsymbol{v}}_g^D = n_g\widetilde{\boldsymbol{v}}_g = n\,S_g(\boldsymbol{v}_g - \boldsymbol{v}_s) \tag{5.22}$$

where $\boldsymbol{v}_w$, $\boldsymbol{v}_g$, $\boldsymbol{v}_s$ are the real velocities of water, gas and solid phases, respectively; $\widetilde{\boldsymbol{v}}_w$ and $\widetilde{\boldsymbol{v}}_g$ are the relative velocities of water and gas phase, respectively. $S_g = 1 - S_w$. The material porosity $\kappa = l^2\delta(n)$ is also called the intrinsic permeability of the skeleton due to its dependency solely on the porous network geometry. l is assumed to characterize the porous network geometry as far as the porous media is saturated with one fluid for simple geometries. Among various expressions of $\delta(n)$ derived in the literature, a frequently used form by Kozeny-Carman's equation (Carman, 1956) is given as

$$\delta(n) = \frac{n^3}{1-n^2} \tag{5.23}$$

Experimental determination of the intrinsic permeability κ will be necessary for more complex geometries (Coussy, 2004). For partially saturated soils, the expression frequently used in association with the expression (5.18), the relative permeability depends on the effective degree of saturation

S_e (van Genuchten, 1980),

$$K_{rw}(S_e) = \sqrt{S_e}\left[1-(1-S_e^{\frac{1}{m}})^m\right]^2 \tag{5.24}$$

$$K_{rg}(S_e) = \sqrt{1-S_e}\left(1-S_e^{\frac{1}{m}}\right)^{2m} \tag{5.25}$$

For saturated soils, the permeability k_s is then identified as:

$$k_s = \frac{\kappa(n)}{\mu_w(\theta)} = \frac{l^2}{\mu_w}\delta(n) \tag{5.26}$$

where, l^2, $\mu_w(\theta)$ and $\delta(n)$ are already defined in (5.19).

5.2.2.3 Fick's Law

As a vapor-air mixture, the apparent velocity of gas can be defined in the form:

$$\tilde{\boldsymbol{v}}_g^D = \frac{p_{gv}}{p_g}\tilde{\boldsymbol{v}}_{gv}^D + \frac{p_{ga}}{p_g}\tilde{\boldsymbol{v}}_{ga}^D \tag{5.27}$$

where $\tilde{\boldsymbol{v}}_{gv}^D$ and $\tilde{\boldsymbol{v}}_{ga}^D$ are respectively the apparent relative velocities of vapor and air. Vapor is transported both by advection which is governed by Darcy's law, and molecular diffusion through the gas, which is governed by Fick's law. An explicit form of the velocity of vapor and air is given by combining Darcy's and Fick's laws (Coussy, 2004):

$$\widetilde{\boldsymbol{v}}_{gv}^D = nS_g(\boldsymbol{v}_{gv}-\boldsymbol{v}_s) = -\frac{\kappa(n)K_{rg}}{\mu_g(\theta)}\nabla p_g - D\,\nabla\left[\ln\left(\frac{p_{gv}}{p_g}\right)\right] \tag{5.28}$$

$$\widetilde{\boldsymbol{v}}_{ga}^D = nS_g(\boldsymbol{v}_{ga}-\boldsymbol{v}_s) = -\frac{\kappa(n)K_{rg}}{\mu_g(\theta)}\nabla p_g - D\,\nabla\left[\ln\left(\frac{p_{ga}}{p_g}\right)\right] \tag{5.29}$$

where $n = n_g + n_w$ is the overall porosity, S_g is degree of gas saturation. p_g, p_{gv}, and p_{ga} are gas, water vapor and dry air pressures, repsepectively. The diffusion coefficient D involved in Fick's law is expressed in Coussy (2004):

$$D = (n_g \times \tau)D_0\left(\frac{p_{atm}}{p_g}\right), \quad D_0 = \delta_0\left(\frac{\theta}{\theta_0}\right)^{1.88} \tag{5.30}$$

where the parameters involved are obtained through experiments (De Vries and Kruger, 1966): $\delta_0 = 2.17\times10^{-5}m^2s$ at $\theta_0 = 273K$, and $p_{atm} = 101325Pa$. τ is the so-called tortuosity, and a usual expression of τ (Millington, 1959) shows its dependence on n and S_g as,

$$\tau(n, S_g) = n^{1/3}S_g^{7/3} \tag{5.31}$$

5.2.3 Thermal properties

5.2.3.1 Fourier's law and thermal conductivity

A generalized Fourier's law is assumed for heat conduction in the TPM model,

$$\boldsymbol{q} = -\boldsymbol{K}^{\theta}_{eff} \mathrm{grad}\, \theta \tag{5.32}$$

where, $\boldsymbol{K}^{\theta}_{eff}$ is referred to as the effective thermal conductivity tensor for the soil mixuture, and $\boldsymbol{q}$ is the heat flux of the porous media, which is the sum of the partial heat fluxes of each phase $\boldsymbol{q}^{\alpha}$. For isotropic porous media, we then have

$$\boldsymbol{K}^{\theta}_{eff} = K^{\theta}_{eff} \mathbf{1} \tag{5.33}$$

where K^{θ}_{eff} denotes the effective thermal conductivity, and is assumed to be constant inside the homogeneous porous media. The effective thermal conductivity can either be predicted with a linear mixture relationship (5.34) or determined experimentally.

$$K^{\theta}_{eff} = n^s\, K^{\theta}_s + n^w\, K^{\theta}_w + n^g\, K^{\theta}_g \tag{5.34}$$

where n^s, n^w and n^g are, respectively the volumetric fractions of solid, water and gas. Accordingly, K^{θ}_s, K^{θ}_w and K^{θ}_g are, respectively, the thermal conductivities of solid, water and gas.

Figure 5.4 gives the thermal conductivity of Bonny silt as a function of solid porosity (Stewart, 2012). During the experiments, the thermal conductivity of a cylindrical Bonny silt specimen is measured after isotropic consolidation to different void ratios. The linear regression equation to represent the dependence of thermal conductivity of Bonny silt on solid volumetric fraction is given in the form:

$$K^{\theta}_{eff} = 2.039\, n^s + 0.1 \tag{5.35}$$

In the model, quadratic equations of the thermal conductivities of water and gas (K^{θ}_w and K^{θ}_g) are used (Campbell et al., 1994):

$$K^{\theta}_w = 0.554 + 2.24 \times 10^{-3} \times (\theta - 273.15) - 9.87 \times \times 10^{-6} \times (\theta - 273.15)^2 \tag{5.36}$$

$$K^{\theta}_g = 0.024 + 7.73 \times 10^{-5} \times (\theta - 273.15) - 2.6 \times \times 10^{-8} \times (\theta - 273.15)^2 \tag{5.37}$$

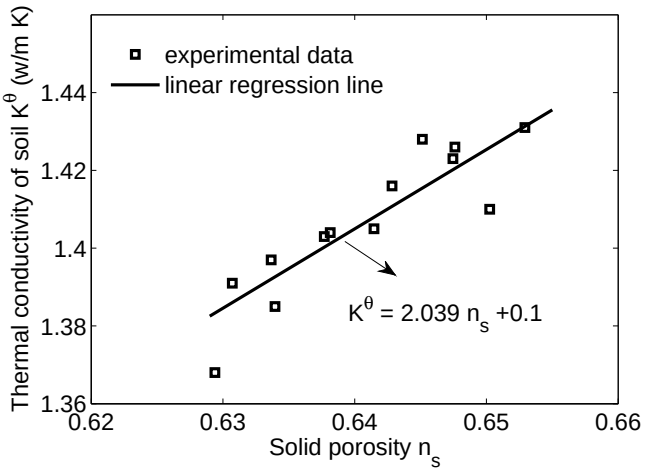

Figure 5.4: Thermal conductivity of Bonny silt.

where $\theta - 273.15$ denotes the conversion from Kelvin to Celsius temperature unites. The parameters are curve fitted parameters. The thermal conductivity of the mineral fraction is assumed to be constant. With (5.36), (5.37) and (5.35), we choose $2.04 W/(m \cdot K)$ as the thermal conductivity of solid K_s^θ in the model, so that the thermal conductivity of Bonny silt calculated by (5.34) will be within the range of experimental results (see Figure 5.4).

5.3 Coupled TPM FEA of centrifuge experiments

5.3.1 Semi-floating energy foundation centrifuge experiment

5.3.1.1 Centrifuge Physical Model

A series of centrifuge-scale tests were performed on semi-floating energy foundations in partially saturated silt by Goode (2013). A scale-model energy foundation having a diameter of 63.5 mm and a length of 342.9 mm was fabricated to study the impact of mechanical loading and heating on the internal strain distribution in energy foundations. A centrifuge acceleration of 24g was used throughout this study, so the corresponding prototype-scale foundation length is 8.2 m with a diameter of 1.5 m. However, the FEA in this study was performed in model scale to avoid issues related to the scaling of temperature and diffusive heat transfer in the centrifuge as recommended by Stewart and McCartney (2013).

Seven strain gages and thermocouples were embedded within the foundation to characterize the strain response and temperature distribution within the foundation at the depths shown in the schematic in Figure 5.5. Three loops of Perfluoroalkoxy (PFA) tubing with an inside diameter of 3.175 mm were used to circulate heated fluid through the foundation. The loops were affixed to the inside of the reinforcing cage so that the inlet and outlet tubes were on the opposite sides of the foundation and so that they did not cross the bottom of the cage. The foundation has a larger diameter than that of Stewart and McCartney (2013) to provide more space around embedded instrumentation and to incorporate a larger fraction and size of coarse aggregates into the concrete mix design. Although drilled shafts are typically cast-in-place, the model foundation was precast in a cardboard mold with a reinforcement cage having an opening size of 12.7 mm to ensure quality construction considering the extensive instrumentation. This approach also allows for characterization of the mechanical and thermal properties of the foundation. The larger fraction of coarse aggregates led to a Young's modulus of reinforced concrete of 30 GPa that was closer to that of drilled shaft foundations in the field than that of Stewart and McCartney (2013). The measured coefficient of thermal expansion of the scale-model energy foundation was $16\mu\epsilon/^oC$, which is

greater than that of reinforced concrete in full-scale drilled shaft foundations (typically between 10 and $12\mu\epsilon/^oC$). Details of the instrumentation calibration are provided by Goode and McCartney (2014).

A cross-sectional profile schematic and a top-view plan schematic of the container used in the centrifuge-scale tests is shown in Figure 5.6. The container is an aluminum cylinder with an inside diameter of 605 mm, wall thickness of 13 mm, and an inside height of 533.4 mm. The foundation is tested in a soil layer having a thickness of 533.4 mm, so its tip will rest on a layer of compacted silt leading to a semi-floating end restraint boundary condition. The schematics in Figure 5.6 show the positions of the embedded strain gauges and thermocouples within the foundations, linearly-variable differential transformers (LVDTs) used to measure vertical displacements of the foundation and soil, dielectric sensors used to monitor the volumetric water content and temperature of the surrounding soil, and thermocouple profile probes for measuring the temperature of the soil. A 13 mm-thick insulation sheet is wrapped around the container to minimize heat transfer through the sides of the cylinder, which corresponds with an adiabatic boundary condition on the container surface. The bottom of the container is not insulated in order to provide a stiff platform during mechanical loading. Although a slight heat loss will likely occur from both the top and the bottom of the container, these boundary are assumed to be adiabatic in the FEA for simplicity. Heat convection at the boundaries will be included in future work to provide a more accurate simulation. The top of the container is covered using plastic wrap to minimize loss of fluid and to reduce convective heat transfer at the soil surface. Thus, no water flux at the top of the soil is assumed in the analysis. In the experiment, the temperature of the energy foundation is controlled by circulating fluid with a known temperature through the heat exchanger tubes attached to the inside of the reinforcement cage at r = 24.25mm, but a constant temperature was applied to this radial location in the FEA.

In the centrifuge-scale experiments, the same scale-model foundation was used in different tests. The tests were performed with identical conditions, except that different temperature changes were applied to the foundation in the different tests. The test procedures involve application of a seating load (600N) in load-control conditions (i.e., zero head stiffness), followed by heating of the

foundation to reach a desired temperature. After the head displacements, internal axial strains, and temperature of the foundation stabilized under each change in temperature, the foundation was loaded to failure to define the load-settlement curve. After reaching a load of 3265 N in model scale, the foundation was unloaded. A general schematic of the experimental procedures is shown in Figure 5.7, and a list of the testing phases is shown in Table 5.2.

To simulate SSI of an energy foundation in partially saturated silt under thermal, hydraulic, and mechanical loads in the centrifuge experiments, a simplified axisymmetric FE mesh contains 81 elements, 9 elements in radial r direction and 9 elements in axial z direction, as shown in Figure 5.8. The partially saturated soil is modeled as an overconsolidated soil layer with thermo-elasto-plastic behavior. The geometry of the FE model (Figure 5.8) is the same as the experimental samples. The heights of the semi-floating foundation and the container are $342.9mm$ and $533.4mm$, respectively.

Boundary conditions and initial conditions are simplified according to knowledge of the experimental conditions. The initial conditions are shown in Table 5.4. As for boundary conditions, due to the axisymmetry of the problem, and assumed rigidity of the bucket, nodal displacements on the z axis ($r = 0$) and right edge ($r = R$) are $u_r = 0$, and nodal displacements on the bottom ($z = -H$) are $u_z = 0$. An unreinforced concrete energy foundation is assumed to be impermeable in this analysis. For now, on the top of the soil, we assume zero water flux $S^w = 0$, and the pore gas pressure being kept to be atmospheric pressure $p_g = p_{atm}$. We notice that the assumption of undrained boundary condition for pore water pressure and drained boundary condition for pore gas pressure at the top may not be justified, but it will be improved in future work when we consider soil-atmosphere interaction to account for evaporation fluxes. To mimic the heating condition of the circulating fluid through the "U" shape heat exchanger tubes, we assume that temperature is prescribed along the z axis at $r = 24.25mm$ for simplicity. However, technically, a 3-D model including a computational fluid dynamics (CFD) analysis of the heated fluid flow through the tubes would be a more accurate estimate of the thermal boundary condition. During circulation of heated fluid through the heat exchange elements in the foundation, energy foundations typically reach a relatively constant temperature with depth. This has been observed in several previous laboratory

studies (Stewart and McCartney, 2013). The constant temperature conditions were selected in the study to evaluate the thermo-mechanical soil-structure interaction behavior of the foundation, not to evaluate the transient heat transfer processes, which we believe would be better simulated with a heat flux boundary condition. The temperature at the top of the soil is held constant at room temperature (20 °C, 293 K), and the other surfaces are adiabatic as indicated in Figure 5.8. Corresponding to the seating load ($600N$), a corresponding effective solid-skeleton traction $\boldsymbol{t}^{\sigma'} = [0\ -t^{\sigma'}]$, $t^{\sigma'} = 189kPa$, is applied on the top of the energy foundation. During Phase 5, a load of $3645N$ was applied to simulate the load to fail the foundation (Goode, 2013). The parameters of the reinforced concrete energy foundation (F) and soil (Table 5.3) are determined from experimental measurements (Goode, 2013). Fluid parameters are assumed for water. In addition, the paper refers to Borja (2004b) for certain elasto-plastic parameters of the soil that are not tested in the experiment.

The simulation of the centrifuge experiments is part of the validation process of the TPM model. After the model is further improved and validated, FEA can be combined with the centrifuge experiments to obtain a comprehensive understanding of the fundamental soil mechanics phenomena involved in energy foundations. With this knowledge, we may assess the potential issues, evaluate the long-term performance and sustainability, thereby providing practical design guidance for energy foundations.

Table 5.2: Experimental and FE simulation procedure shown in Figure 5.7.

Phase 1	Consolidation under g-level N =1 in simulation, representing compaction of soil
Phase 2	Spin up centrifuge to a g-level of $N = 24$, wait for equilibration
Phase 3	Apply a seating load at the foundation top, wait for equilibrium
Phase 4	Heating the foundations to different temperatures
Phase 5	Load the foundations to failure, and then unload under different temperatures

Table 5.3: Parameters used in the FEA.

Parameter	Symbol	Value	Unit
Linear thermal expansion coefficient of energy foundation	β_F^θ	16×10^{-6}	$/K$
Linear thermal expansion coefficient of solid skeleton	β_{skel}^θ	8.7×10^{-6}	$/K$
Linear thermal expansion coefficient of solid	β_s^θ	1.17×10^{-5}	$/K$
Linear thermal expansion coefficient of water	β_w^θ	6.9×10^{-5}	$/K$
Specific heat capacity of energy foundation	C_F	855	$J/(K \cdot kg)$
Specific heat capacity of solid	C_s	1000	$J/(K \cdot kg)$
Specific heat capacity of water	C_w	4180	$J/(K \cdot kg)$
Mass density of energy foundation	ρ_F	2564	kg/m^3
Specific gravity of soil solids	G_s	2.6	
Thermal conductivity of reinforced concrete	K_F^θ	1.978	$W/(m \cdot K)$
Thermal conductivity of soil mixture	K_s^θ	1.24	$W/(m \cdot K)$
Young's modulus of reinforced concrete	E_F	30×10^9	Pa
Poisson's ratio of energy foundation	ν_F	0.18	m/m
van Genutchen model parameter	a	19.4×10^3	Pa
van Genutchen model parameter	n	1.8	
Intrinsic permeability of soil mixture	κ	1.22×10^{-14}	m^2
Initial mean effective preconsolidation pressure	p_c'	100×10^3	Pa
Initial mean effective pressure	p_0'	70×10^3	Pa
Elastoplastic parameter (slope of critical state line)	M	1.305	
Elastoplastic parameter (slope of isotropic normal compression line)	$\tilde{\lambda}$	0.14	
Elastoplastic parameter (slope of isotropic recompression line)	$\tilde{\kappa}$	0.034	
Thermoplastic parameter	γ^θ	0.04	

Table 5.4: Initial conditions for soil used in FEA.

Porosity	0.4
Volumetric water content	0.226
Suction	$30\,kPa$
Gas pressure	$101\,kPa$
Temperature	$20\,^oC(293K)$

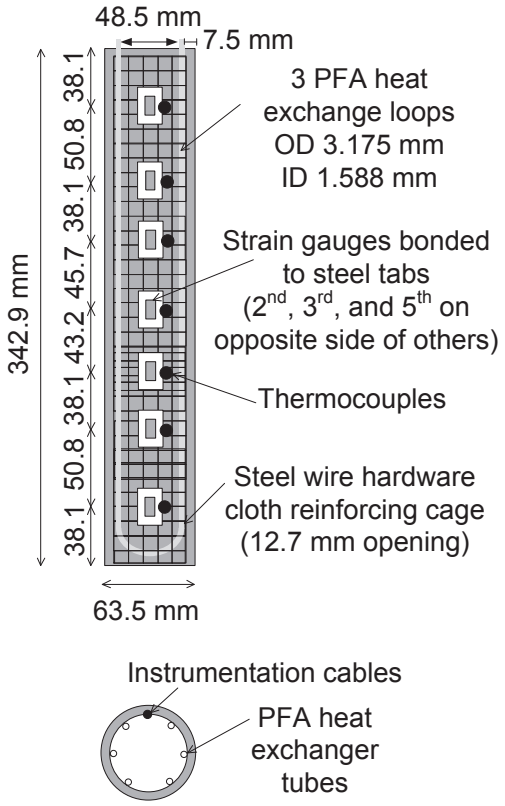

Figure 5.5: Cross-sections of the scale-model energy foundation (Goode and McCartney, 2014).

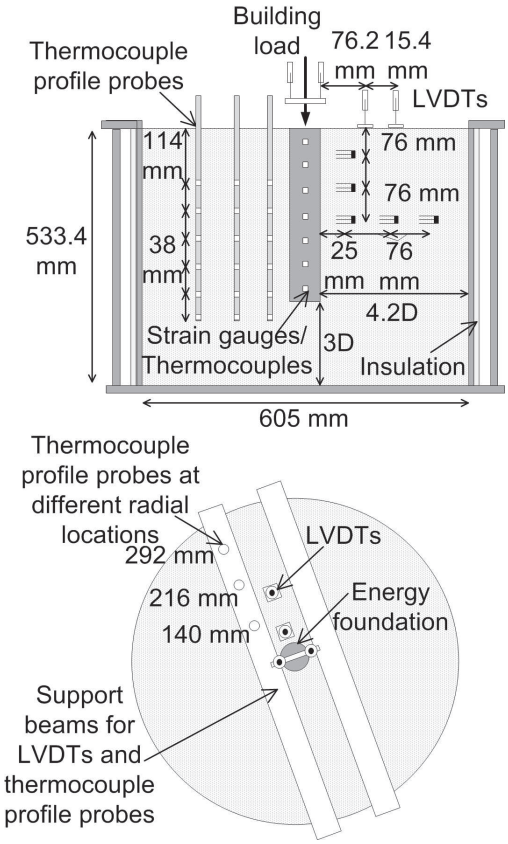

Figure 5.6: Experimental setup and instrumentation plan (Goode and McCartney, 2014).

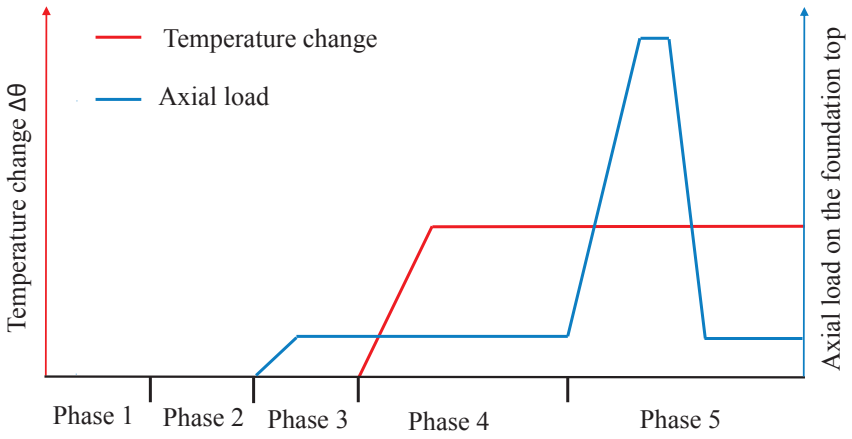

Figure 5.7: Schematic of general testing procedures for energy foundation centrifuge experiment.

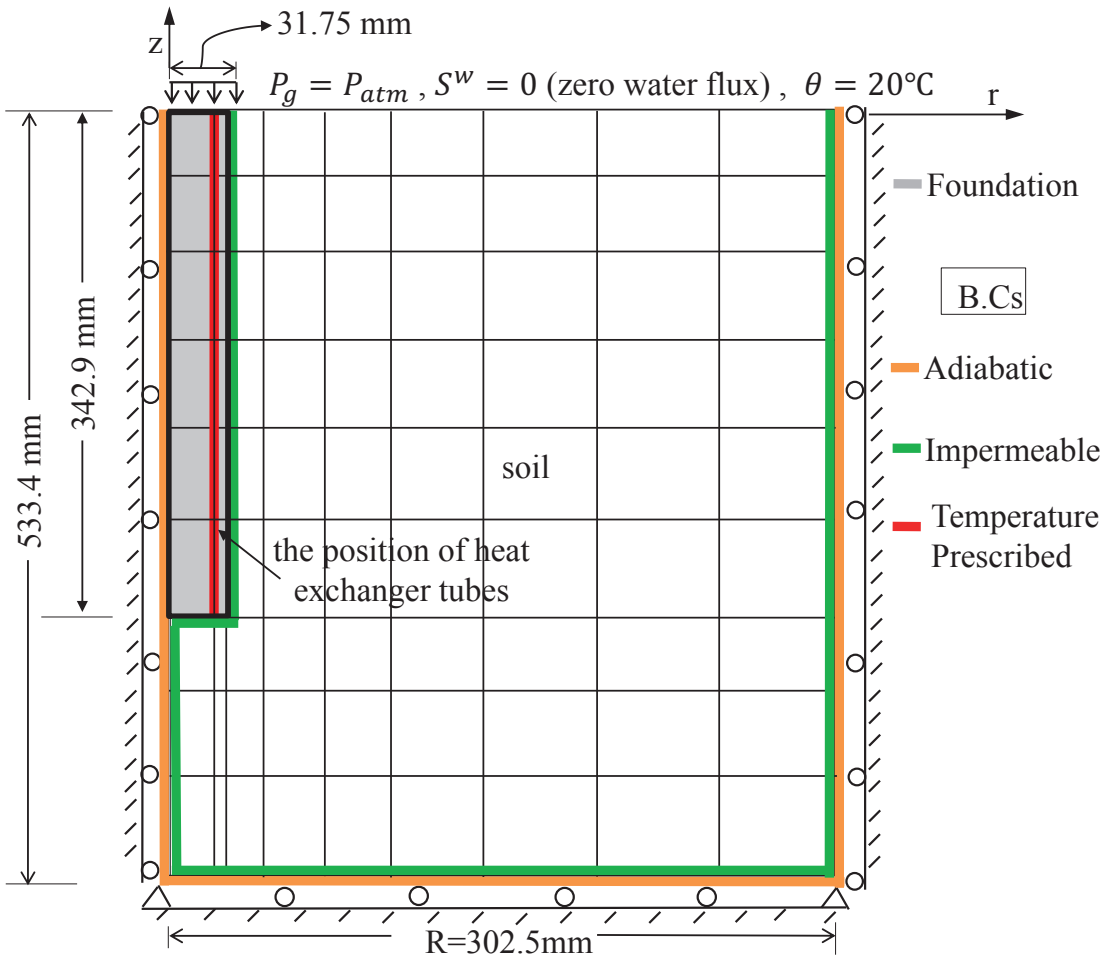

Figure 5.8: Axisymmetric FE mesh and geometry for simulating semi-floating energy foundation centrifuge experiment. Boundary conditions are included.

5.3.1.2 TPM FEA Results

Contour plots show various results on the deformed mesh with displacement magnification factor equal to 100. Temperature contours (Figures 5.9, 5.11, and 5.13) indicate that although the foundation reaches steady-state temperature at the end of each test, the soil is not necessarily at steady-state temperature, for example, soil mixture temperature remains near the initial value $\theta_0 = 20^oC(293K)$ at further radial distance in the soil. This means that the system response is representative of transient heating, meaning the soil mixture temperature is still evolving. The modeling results of thermal axial strains ϵ_{zz}^{θ} within the foundation are compared with experimental data collected by the strain gauges in Figure 5.21. Good agreement is observed in the comparison throughout the energy foundation. Note that, different from the sign conventions used by Stewart and McCartney (2013) and Goode (2013), positive strains are used to denote elongation of a foundation or soil element (e.g., due to application of tension or due to thermal expansion), the coefficient of thermal expansion is defined as a positive value, and a positive settlement is defined as an upward heave. Here, the so-called "thermal axial strain" should not be confused with the term we usually use, which is defined as $\epsilon^{\theta} = \beta^{\theta}\Delta\theta$. In the thesis particularly, the thermal axial strain ϵ_{zz}^{θ} is the total vertical strain at the end of temperature increase ϵ_{zz} zeroed out by subtracting the total vertical strain caused by mechanical effects ϵ_{zz}^{mech} including the gravity and building load, i.e., $\epsilon_{zz}^{\theta} = \epsilon_{zz} - \epsilon_{zz}^{mech}$. The energy foundation achieves almost uniform thermal axial strain distribution except at the bottom where much smaller thermal strain is observed. It is understandable because the thermal expansion of the foundation bottom is partially constrained by the soil resistance underneath. Also, as shown in the temperature contours, the temperature at the foundation bottom is always relatively lower than the upper region due to the contact with the underneath soil. While, for the foundation top, we can conclude that it almost expands freely under thermal loading, based on the fact that the strain values are approximately equal to the calculation by free thermal expansion $\epsilon^{\theta} = \beta^{\theta}\,\Delta\theta$. Figures 5.10, 5.12 and 5.14 show that thermal axial strains inside the soil vary more noticeably. Temperature increases cause expansion of the soil near the foundation-soil

interface ($31.75mm < r < 132.75mm$). Negligible positive expansive axial strains are observed at further radial distance. The negative compressive axial strains within the soil underneath the foundation imply that the compression due to the building load on the top of the foundation is dominant, compared to the thermal expansion.

Figures 5.15 and 5.16 indicate significant changes in suction and volumetric water content respectively near the soil-foundation interface. For example, volumetric water content decreases from an initial value of 0.226 to approximately 0.18 near the foundation-soil interface ($r = 31.75mm$), and a small rise occurs in the soil at $r = 56.75mm$. Volumetric water contents increase slightly in the region of $56.75mm < r < 92mm$, however, no significant variation is observed beyond $r = 92mm$. Figure 5.17 indicates that a net rate of evaporation is produced within the soil due to rapidly increasing temperatures. A sharp rise of water vapor pressure (from initial value of $2.5kPa$ to around $6.5kPa$) happens near the soil-foundation interface ($r = 31.75mm$), and a smaller rise occurs further from the interface. The formed density gradients drive vapor from the hotter region (soil-foundation interface) to the cooler region. Arrows in Figure 5.19 show the direction of water vapor flow inside the soil. Also, higher vapor velocity is observed under larger temperature gradients. This diffusion process is governed by many factors including hydraulic and thermal properties of soil, which require further research. Condensation occurs when the hotter vapor migrates to the region of lower temperature, and hence leads to a rise in volumetric water content, as shown in Figure 5.16 at $56.75mm < r < 92mm$. As the soil near the soil-foundation interface becomes drier ($p_w \approx 60kPa$ at $r = 31.75mm$) compared to the soil further from the interface (p_w approaches $75kPa$ at $56.75mm$), pore water pressure gradients are formed, which force liquid water to flow from the wetter region to the drier region, as shown in Figure 5.18. The movement of pore water is illustrated by the direction of water flow inside the soil in Figure 5.20. In the soil at further radial distance, gravity mainly induces downward pore water flow. The pore liquid water flow is in the direction of the soil-foundation interface near the interface. The trend of thermally-induced fluid flow will be more obvious as the tests run longer or under higher thermal load (Wang et al., 2014). Variations of volumetric water content are compared vertically and horizontally between

the modeling and experimental results in Figure 5.22. Similar trends are observed though the experimental results exhibit slightly higher values. Volumetric water contents are very close at the same radius ($r = 58mm$). While the temperature increases within soil, volumetric water contents rise higher in the region closer to the foundation-soil surface ($r = 58mm$) than in the further region ($r = 101mm$). In the further region ($r = 177mm$), much lower increase of the volumetric water content is observed at the end of Phase 4. But the thermally driven moisture movement might change the distribution of volumetric water content as the temperature gradients become lower within the soil. Further research involving higher temperature gradients and longer-term observations are necessary to investigate the thermally-induced fluid (liquid water and water vapor) flow. Figure 5.23 presents the average temperature variations of the foundation center and the different positions in the soil during Phase 4. The temperature trend at the foundation center depends on how the prescribed temperature is applied at $r = 24.25mm$. In the simulation, the prescribed temperature linearly ramps up from room temperature (20^oC) to 39^oC during the first 1.35 hours, and then is kept constant for the rest of Phase 4. According to the temperature comparison, the simplified assumption of the thermal boundary condition does not capture the transient trend at the foundation center exactly, but after a certain time (3 hours in this case), the difference becomes negligible when the foundation arrives at the steady-state temperature. The temperature within the soil ($r = 106, 155, 216, 293mm$) changes relatively slow, compared to the foundation.

In an attempt to simulate the failure process during Phase 5 in the centrifuge experiment, the model uses a failure load of $3645N$ estimated from the experimental observations (Goode, 2013) as the ultimate load on the top of the foundation. Figure 5.24 shows that the settlements corresponding to the ultimate capacity in the experiment are much larger than those from the modeling results. Load-settlement curves from the modeling results imply that plasticity is not reached in the soil continuum under the estimated ultimate load, even though the nonlinear thermo-elasto-plastic constitutive model is applied to the soil continuum. Because of the assumption of a perfect bond at the foundation-soil interface, the model failed to capture the side-shear failure that induced the slippage at the interface and meanwhile contributed to the large settlements in the experiment.

We believe that with the interface elements implemented along the foundation-soil interface, the model can provide more accurate simulation of the failure mechanism. This will be investigated in Section 7.3.3.

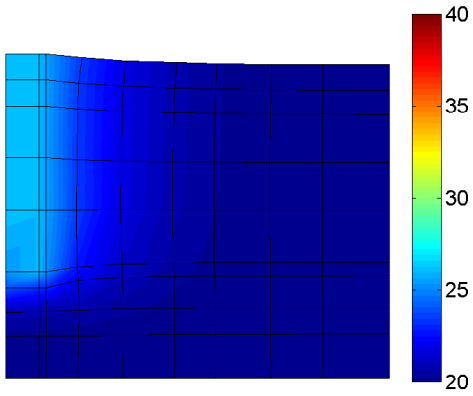

Figure 5.9: Temperature (^oC) contours at the end of Phase 4 under $\Delta\theta = 6^oC$.

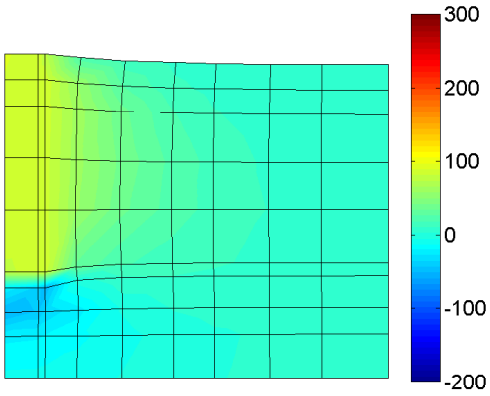

Figure 5.10: Thermal axial strain $\epsilon_{zz}(\mu\epsilon)$ contours at the end of Phase 4 under $\Delta\theta = 6^oC$.

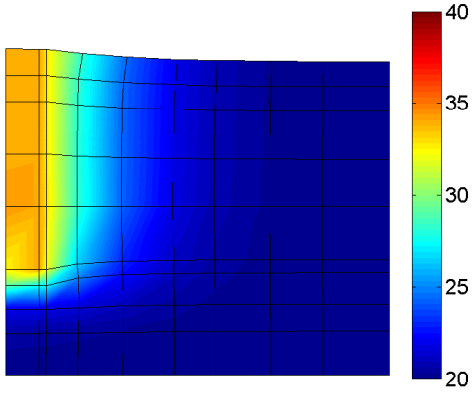

Figure 5.11: Temperature (^oC) contours at the end of Phase 4 under $\Delta\theta = 14^oC$.

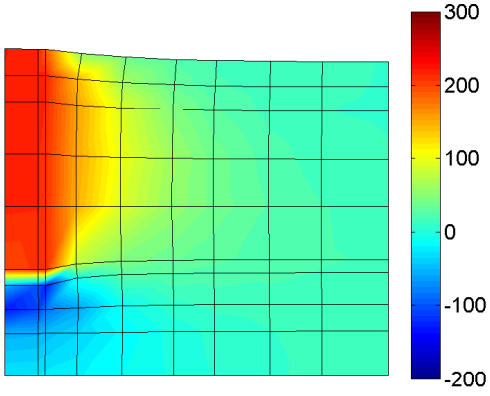

Figure 5.12: Thermal axial strain $\epsilon_{zz}(\mu\epsilon)$ contours at the end of Phase 4 under $\Delta\theta = 14^oC$.

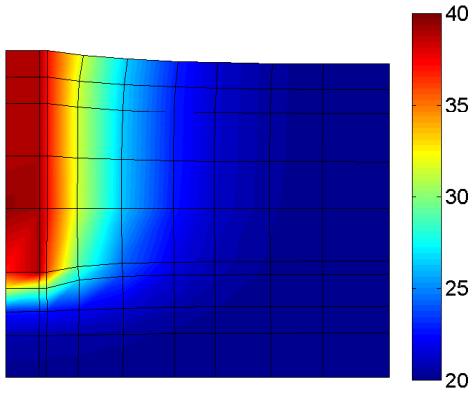

Figure 5.13: Temperature (^oC) contours at the end of Phase 4 under $\Delta\theta = 19^oC$.

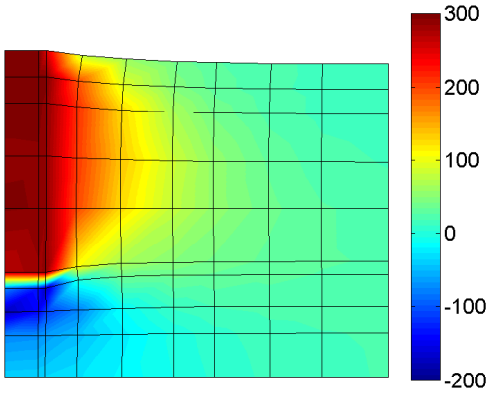

Figure 5.14: Thermal axial strain $\epsilon_{zz}(\mu\epsilon)$ contours at the end of Phase 4 under $\Delta\theta = 19^oC$.

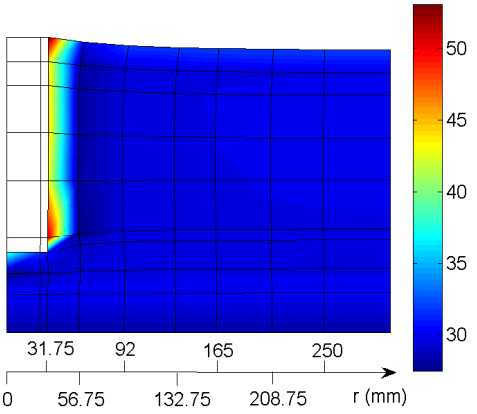

Figure 5.15: Contours of suction (kPa) in soil at the end of Phase 4 under $\Delta\theta = 19^oC$.

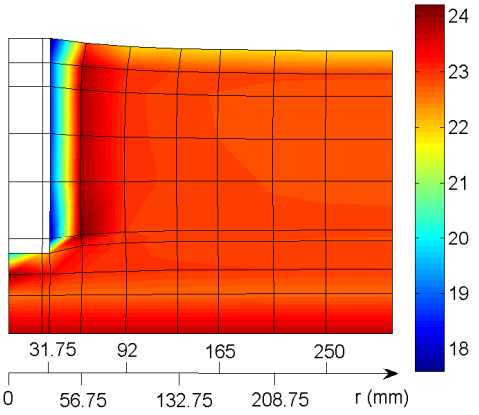

Figure 5.16: Volumetric water content (%) (100 n^w) contours in soil at the end of Phase 4 under $\Delta\theta = 19^oC$.

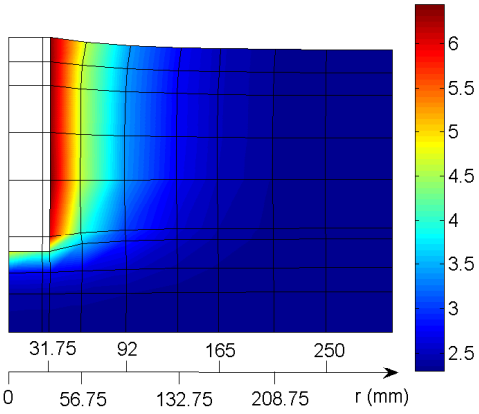

Figure 5.17: Contours of absolute pore water vapor pressure (kPa) in soil at the end of Phase 4 under $\Delta\theta = 19^oC$.

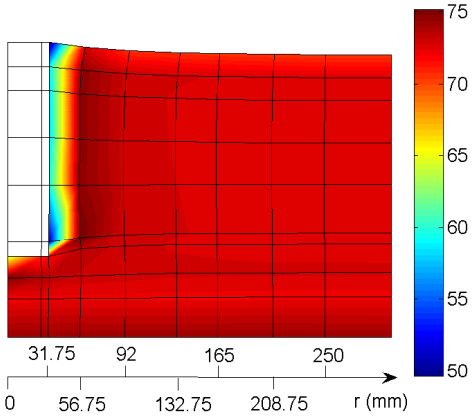

Figure 5.18: Contours of pore water liquid pressure (kPa) in soil at the end of Phase 4 under $\Delta\theta = 19^oC$.

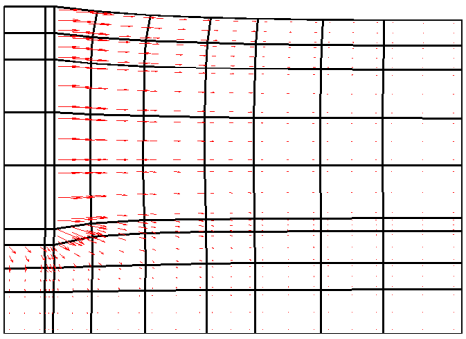

Figure 5.19: Pore water vapor flow vectors in soil at the end of Phase 4 under $\Delta\theta = 19^oC$.

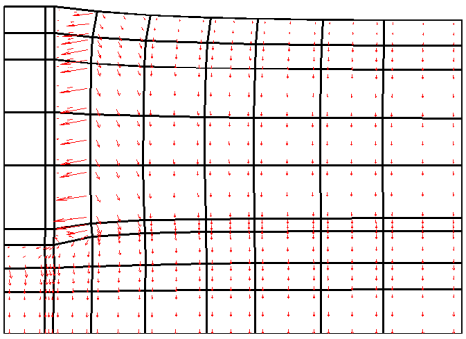

Figure 5.20: Pore water liquid flow vectors in soil at the end of Phase 4 under $\Delta\theta = 19^oC$.

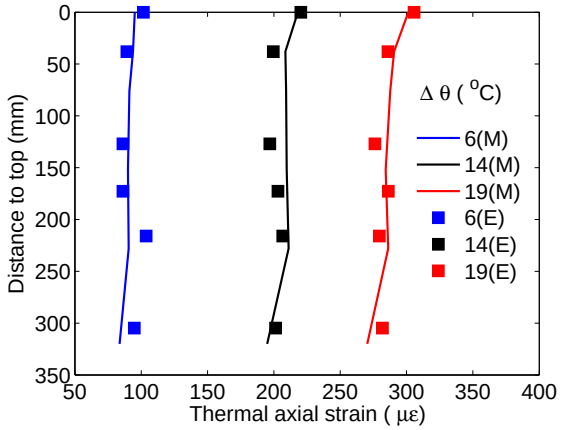

Figure 5.21: Comparison of thermal axial strain ϵ^{θ}_{zz} within the energy foundations at the end of Phase 4 under different temperature changes between model (M) predictions and experimental (E) data from Goode (2013).

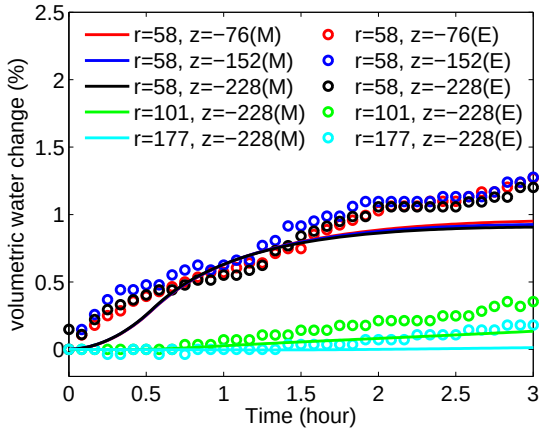

Figure 5.22: Comparison of volumetric water content within soil during Phase 4 under $\Delta\theta = 19^oC$ at different positions (mm) between model (M) predictions and experimental (E) data from Goode (2013).

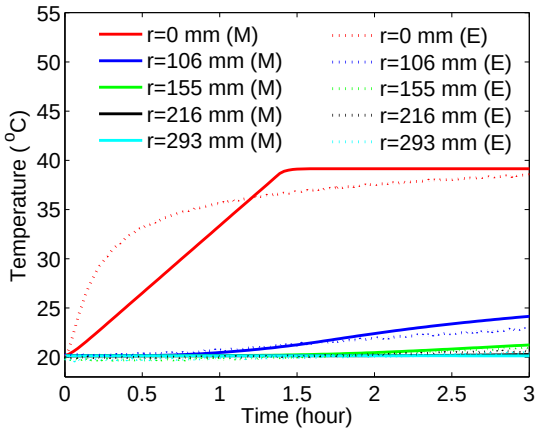

Figure 5.23: Comparison of temperature variation at the center of the energy foundation ($r = 0mm$) and different radii inside the surrounding soil during Phase 4 under $\Delta\theta = 19^oC$ between model (M) predictions and experimental (E) data from Goode (2013).

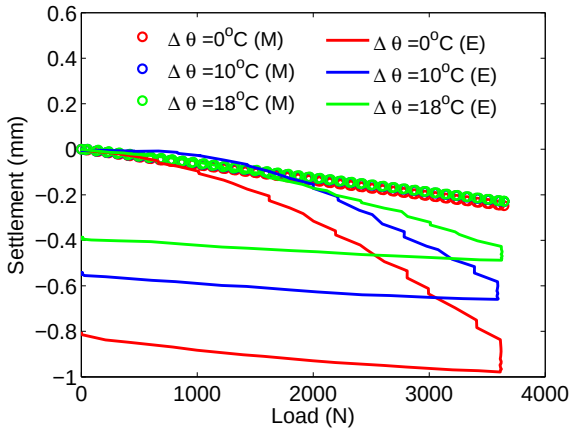

Figure 5.24: Comparison of load-settlement curves between model (M) predictions and experimental (E) data within soil during Phase 5 from Goode (2013).

5.3.2 End-bearing energy foundation centrifuge test

A simplified axisymmetric FE mesh containing 30 elements (Figure 5.25) is created to simulate SSI of an end-bearing energy foundation under thermal, hydraulic, and mechanical loads in the centrifuge experiment with centrifugation to an acceleration of 24 times gravity (N=24). In the experiment, the foundation is heated in stages over a range of temperatures expected in the field through P4-P7 as shown in Figure 5.26. The partially saturated soil is modeled as an overconsolidated soil layer with linear thermo-elastic behavior. Elastic, hydraulic, and thermal parameters are applied for Bonny silt. Fluid parameters are assumed for water. The geometry of the FE model is the same as that in the experiments. The height of the energy foundation is $H = 0.537m$. The radius of the energy foundation is $a = 0.025m$, and the radius of the centrifuge bucket is $R = 0.3025m$.

Initial conditions and boundary conditions are simplified according to knowledge of the experimental conditions. The initial conditions include: porosity $n_0 = 0.425$; volumetric water content $w_0 = 26\%$; suction $s_0 = 32kPa$; gas pressure $p_{g0} = 101kPa$; temperature $\theta_0 = 20^oC$. As for boundary conditions, due to the axisymmetry of the problem, and assumed rigidity of the bucket, nodal displacements on the z axis ($r = 0$) and right edge ($r = R$) are $u_r = 0$, and nodal displacements on the bottom ($z = -H$) are $u_z = 0$. An unreinforced concrete energy foundation is assumed to be impermeable in this analysis. There is reinforcement in the actual experiment, but since failure of the foundation is unlikely, linear thermoelastic assumption for the concrete is reasonable, with or without reinforcement. Also zero water flux $S^w = 0$ at the top of soil is assumed, since plastic sheeting is placed on the top surface to minimize evaporation. The pore gas pressure p_g on the top is held to be atmospheric pressure $p_g = p_{atm}$ at $z = 0$. In the experiment or the field, the temperature of the energy foundation is actually controlled by circulating fluid with a known temperature through a series of three equally spaced "U" shape heat exchanger tubes attached to the inside of the reinforcement cage at $r = 0.02m$. Technically, a 3-D model including a CFD analysis of the heated fluid flow through the tubes would be a more accurate estimate of the thermal boundary

condition. However, for simplicity, we assume that temperature is prescribed along the z axis at $r = 0.02m$. During circulation of heated fluid through the heat exchange elements in the foundation, energy foundations typically reach a relatively constant temperature with depth. This has been observed in several previous laboratory studies (Stewart and McCartney, 2013). The constant temperature conditions were selected in the study to evaluate the thermo-mechanical soil-structure interaction behavior of the foundation, not to evaluate the transient heat transfer processes, which we agree would be better simulated with a heat flux boundary condition. The temperature at the top of the soil is held constant at room temperature (20 °C), and the other surfaces are adiabatic as indicated in Figure 5.25. Axial load is exerted on the top of the energy foundation instantaneously, and is kept constant during the test. Effective solid-skeleton traction $\boldsymbol{t}^{\sigma'} = [0 \ -t^{\sigma'}]$, $t^{\sigma'} = 384kPa$, is applied on the top of the energy foundation. The parameters of the unreinforced concrete energy foundation (c) and soil (Table 5.5) are determined from experimental measurements.

TPM FEA Results for the end-bearing foundation centrifuge experiment:

Figure 5.27 - Figure 5.38 are plotted contours of various results on the deformed mesh with displacement magnification factor equal to 100. Temperature contours (Figure 5.27 - Figure 5.30) indicate that although the foundation reaches steady temperatures after each stage, the soil is not necessarily at steady-state temperature, for example, soil mixture temperature remains near the initial value $\theta_0 = 20^oC$ at further radial distance in the soil. This means that the system response is representative of transient heating. About 10 hours after the end of phase 7 (phase 7 ends at about 2.64 hr), higher temperature is observed inside the soil near the foundation, as shown in Figure 5.31. Variation of the pore gas pressure is negligible during the heating process as shown in Figure 5.32. Figure 5.33 and Figure 5.34 indicate significant changes in suction and volumetric water content respectively near the soil-foundation interface. For example, suction increases from an initial value of $32kPa$ to nearly $60kPa$ near the interface ($r = 0.025m$), and smaller rise occurs in the soil at $r = 0.05m$. Suction drops slightly in the region of $0.05m < r < 0.14m$, however, no significant variation of suction is observed beyond $r = 0.14m$. A corresponding trend is detected regarding volumetric water content distribution in Figure 5.34. Figure 5.35 indicates that a net rate

of evaporation is produced within the soil due to rapidly increasing temperatures. A sharp rise of water vapor pressure (from initial value of $2.5kPa$ to around $7kPa$) happens near the soil-foundation interface ($r = 0.025m$), and a smaller rise occurs further from the interface. The formed density gradients drive vapor from the hotter region (soil-foundation interface) to the cooler region. Arrows in Figure 5.37 show the direction of water vapor flow inside the soil. Also, higher vapor velocity is observed under larger temperature gradients. This diffusion process is governed by many factors including hydraulic and thermal properties of soil, which require further research. Condensation occurs when the hotter vapor migrates to the region of lower temperature, and hence leads to a rise in volumetric water content, as shown in Figure 5.34 at $0.05m < r < 0.14m$. As the soil near the soil-foundation interface becomes drier ($p_w \approx 45kPa$ at $r = 0.025m$) compared to the soil further from the interface ($p_w \approx 70kPa$ at $r = 0.05m$), pore water pressure gradients are formed, which force liquid water to flow from the wetter region to the drier region, as shown in Figure 5.36. The movement of pore water is illustrated by the direction of water flow inside the soil in Figure 5.38. In the soil at further radial distance, gravity mainly induces downward pore water flow. The pore liquid water flow is in the direction of the soil-foundation interface near the interface. The comparison of thermal strain between FEA and experimental results in Figure 5.39 shows good agreement at the foundation top, with similar trend observed for the rest of the foundation. One of the possible reasons for the difference is the assumption of perfect bond at the soil-foundation interface in the model, therefore, side shear resistance along the length of the foundation is not well represented. Implementation of interface elements at the soil-foundation interface will likely allow closer representation of the SSI conditions. Figure 5.40 indicates that both experimental and modeling results show smaller thermally induced stress at the top of the foundation as compared to the bottom. Figure 5.41 shows good agreement of displacement at the foundation top in the temperature range of 20^oCto30^oC, but in the range 30^oCto40^oC, the linear elastic solid skeleton constitutive behavior and function of temperature needs to be modified. The thermal expansion coefficient of the energy foundation estimated from Figure 5.41 is $\approx 6.8 \times 10^{-6}/K$. This value is slightly smaller than the given parameter $\beta_c^\theta = 7.5 \times 10^{-6}/K$ due to the assumption of perfect

bond at the soil-foundation interface in the FEA model. This assumption will be relaxed when the interface element is implemented. The top displacements of foundation and soil are shown in Figure 5.42 with respect to radial coordinate r and phase loading. The deformation of soil is a combination of thermal expansion and solid skeleton consolidation due to gravity level increases in centrifuge experiments.

Table 5.5: Parameters used in the FEA.

Parameter	Symbol	Value	Unit
Linear thermal expansion coefficient of concrete	β_c^θ	7.5×10^{-6}	$/K$
Linear thermal expansion coefficient of solid skeleton	β_{skel}^θ	8.7×10^{-6}	$/K$
Linear thermal expansion coefficient of soil solid	β_s^θ	1.17×10^{-5}	$/K$
Specific heat capacity of concrete	C_c	855	$J/(K \cdot kg)$
Specific heat capacity of soil solid	C_s	1000	$J/(K \cdot kg)$
Specific gravity of soil solid	G_s	2.6	
Thermal conductivity of concrete	K_c^θ	2.6	$W/(m \cdot K)$
Thermal conductivity of solid	K_s^θ	1.24	$W/(m \cdot K)$
Young's modulus of concrete foundation	E_c	7.17×10^9	Pa
Poisson's ratio of concrete foundation	ν_c	0.18	m/m
Lamé parameter of soil solid skeleton	λ_{skel}	2.9×10^7	Pa
Lamé parameter of soil solid skeleton	μ_{skel}	4.7×10^7	Pa
van Genutchen model parameter	α	0.357×10^{-4}	Pa^{-1}
van Genutchen model parameter	n	1.8	
Hydraulic conductivity of saturated soil	k_{sat}	1.3×10^{-7}	m/s

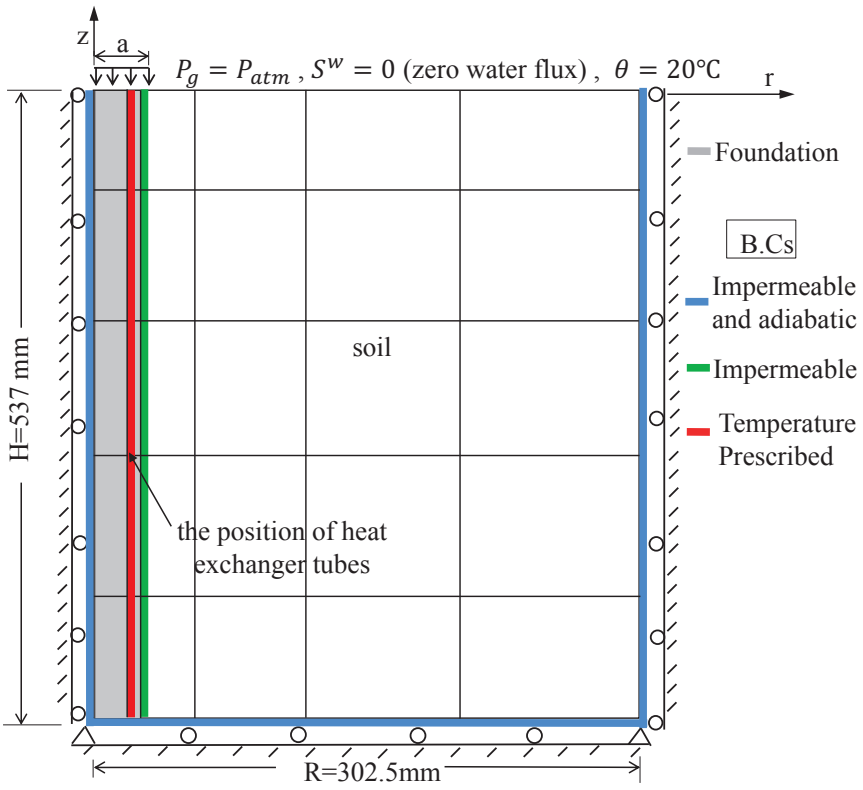

Figure 5.25: Axisymmetric FE mesh and geometry for simulating end-bearing energy foundation centrifuge experiment. Boundary conditions are included.

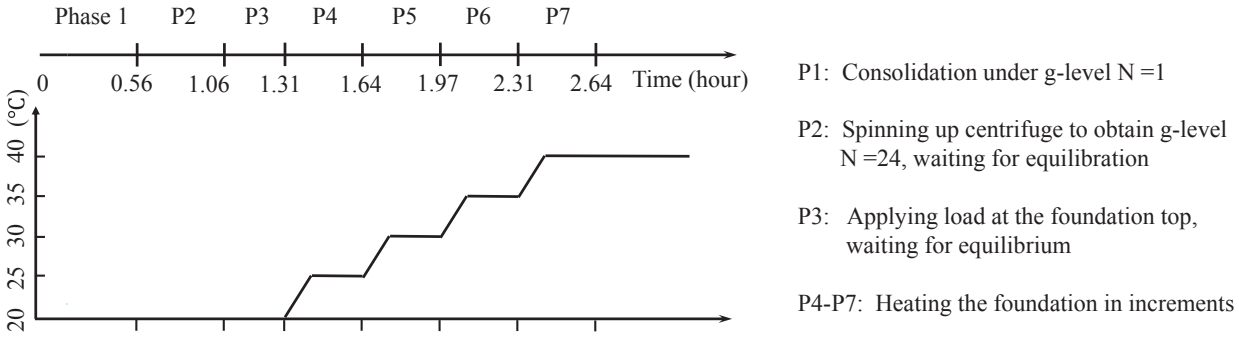

Figure 5.26: Schematic of testing procedure for energy foundation centrifuge experiment (P:Phase).

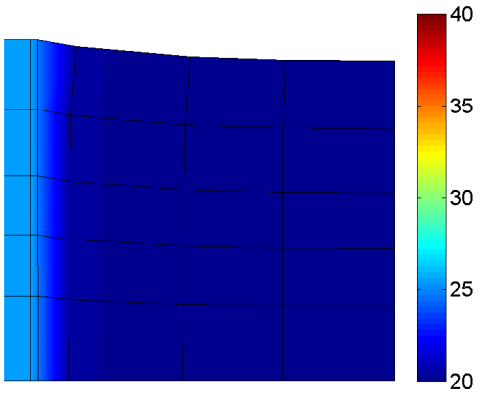

Figure 5.27: Temperature (^oC) contour at $\Delta\theta = 5^oC$ (the end of phase 4).

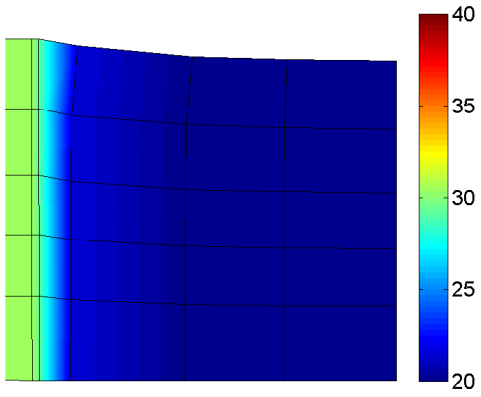

Figure 5.28: Temperature (^oC) contour at $\Delta\theta = 10^oC$ (the end of phase 5).

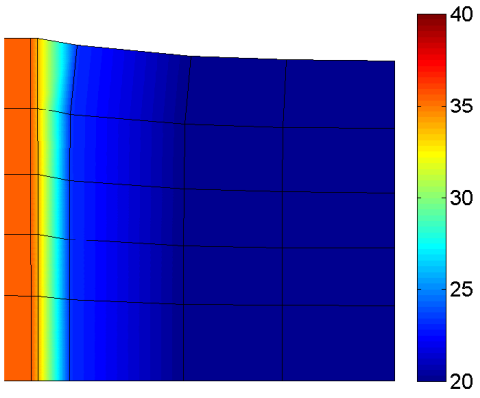

Figure 5.29: Temperature (^oC) contour at $\Delta\theta = 15^oC$ (the end of phase 6).

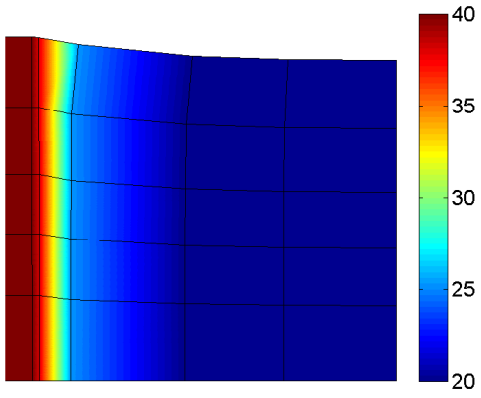

Figure 5.30: Temperature (^oC) contour at $\Delta\theta = 20^oC$ (the end of phase 7).

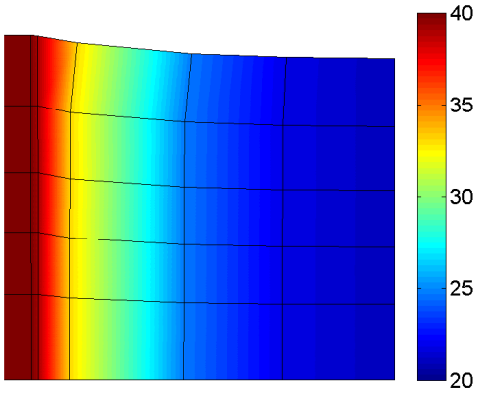

Figure 5.31: Temperature (^oC) contour at 10 hours after the last thermal loading phase.

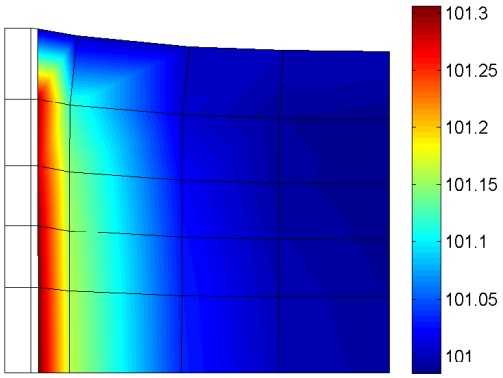

Figure 5.32: Contour of pore gas pressure (kPa) in soil at 10 hours after the last thermal loading phase.

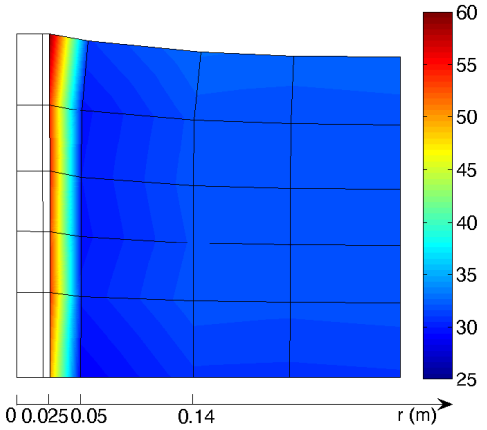

Figure 5.33: Contour of suction (kPa) in soil at 10 hours after the last thermal loading phase.

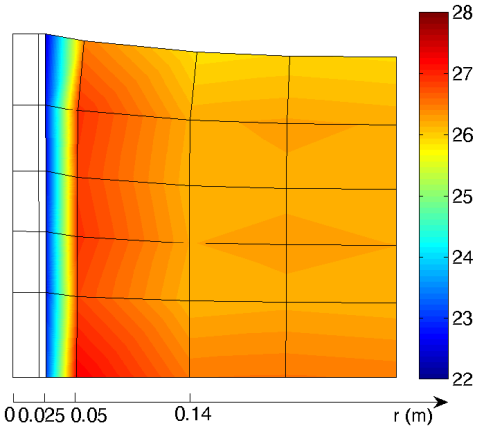

Figure 5.34: Volumetric water content (%) ($100n^w$) contour in soil at 10 hours after the last thermal loading phase.

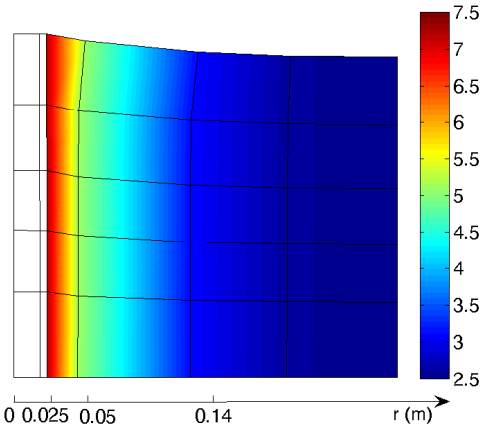

Figure 5.35: Contour of pore water vapor pressure (kPa) in soil at 10 hours after the last thermal loading phase hours.

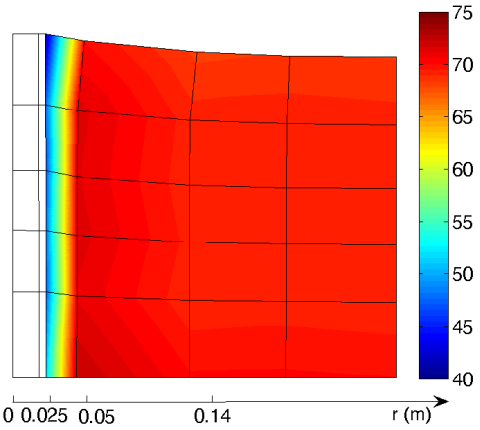

Figure 5.36: Contour of pore water pressure (kPa) in soil at 10 hours after the last thermal loading phase.

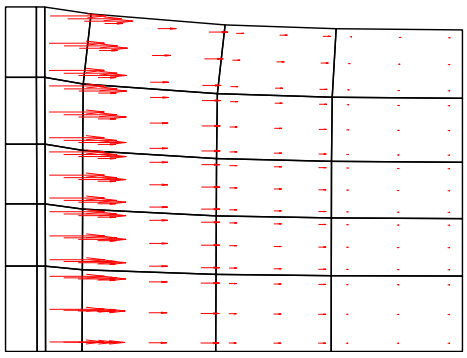

Figure 5.37: Pore water vapor flow vectors in soil at 10 hours after the last thermal loading phase.

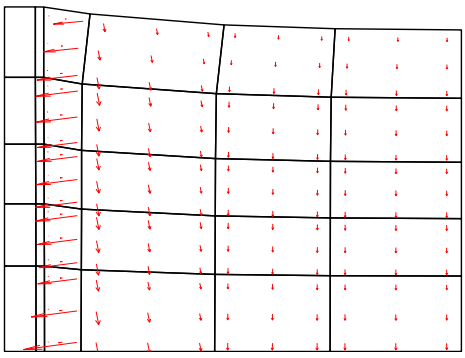

Figure 5.38: Pore water flow vectors in soil at 10 hours after the last thermal loading phase.

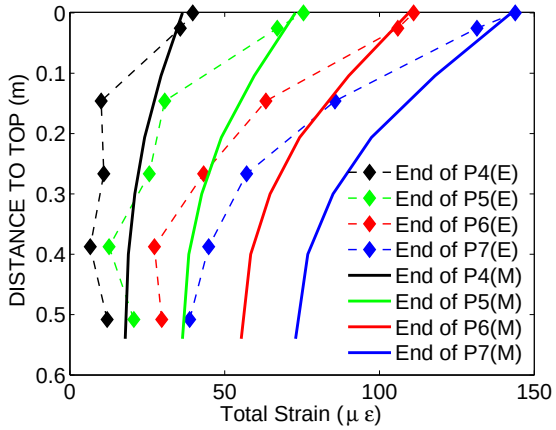

Figure 5.39: Comparison of total vertical strain ϵ_{zz} between experimental (E) data (Stewart, 2012) and model (M) predictions inside the energy foundation.

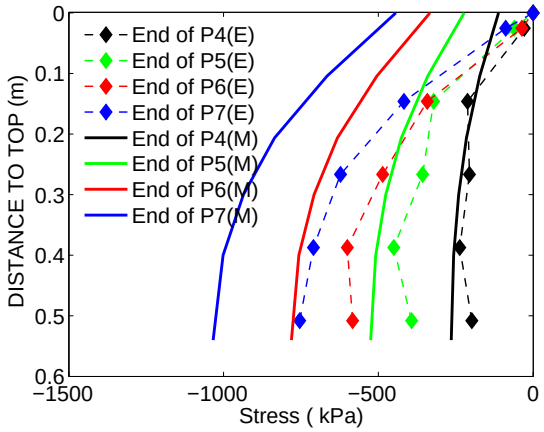

Figure 5.40: Comparison of stress σ_{zz} between experimental (E) calculations (Stewart, 2012) and model (M) predictions inside the energy foundation.

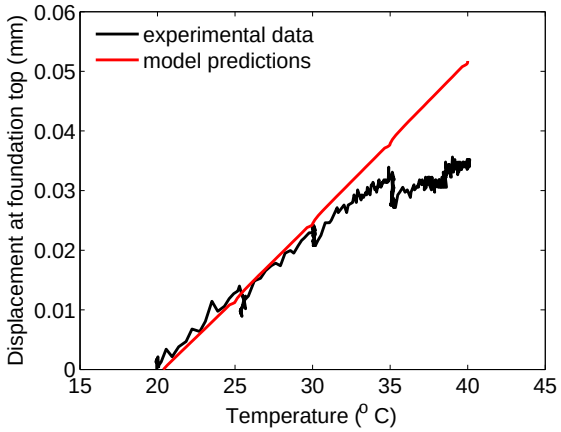

Figure 5.41: Comparison of vertical displacement versus temperature at the center of the foundation top between experimental (Stewart, 2012) and model results.

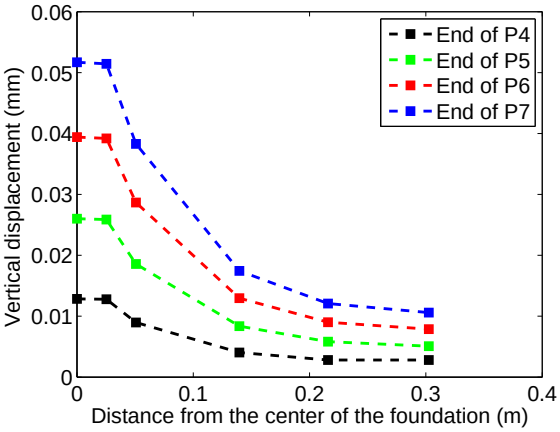

Figure 5.42: Vertical displacement d_z of the top of the energy foundation and soil surface as a function of r at different Phases.

Chapter 6

Fully and partially saturated poro-mechanical (PM) cohesive interface element (CIE) models implemented within TPM FE framework

6.1 Fully saturated PM CIE model

This part we introduce the formulation of interface element under isothermal and saturated conditions. This discussion follows R.A.Regueiro's notes at the University of Colorado, Boulder.

6.1.1 Governing equations

Balance equations are derived for the continuum and the crack separately, and then are combined to obtain the governing equations for the fractured porous media.

6.1.1.1 Balance of linear momentum

The balance of linear momentum equation for continuum and discontinuity is written as:

$$\begin{cases} \frac{\partial \sigma_{ij}}{\partial x_j} + \rho b_i = 0 & x_i \in \Omega / S \\ u_i = g_i^u & x_i \in \Gamma_g \\ \sigma'_{ij} \nu_j = t_i^{\sigma'} & x_i \in \Gamma_t \\ \sigma'^{+}_{ij} n_j^+ = T_i'^{+} & x_i \in S^+ \\ \sigma'^{+}_{ij} n_j^- = T_i'^{-} & x_i \in S^- \end{cases} \tag{6.1}$$

where $\boldsymbol{n}$, $\boldsymbol{n}^+$ and $\boldsymbol{n}^-$ are respectively the normal vectors of surface S, S^+ and S^-; $\boldsymbol{\nu}$ is the normal vector of surface of continuum (see Figures 6.1 and 6.2). The assumptions are: for small rotation, $\boldsymbol{n} = \boldsymbol{n}^+ = -\boldsymbol{n}^-$, and for large rotation of S, $\boldsymbol{n} = \frac{1}{2}(\boldsymbol{n}^+ - \boldsymbol{n}^-)$. $\boldsymbol{T}'^{+}$ and $\boldsymbol{T}'^{-}$ are respectively the

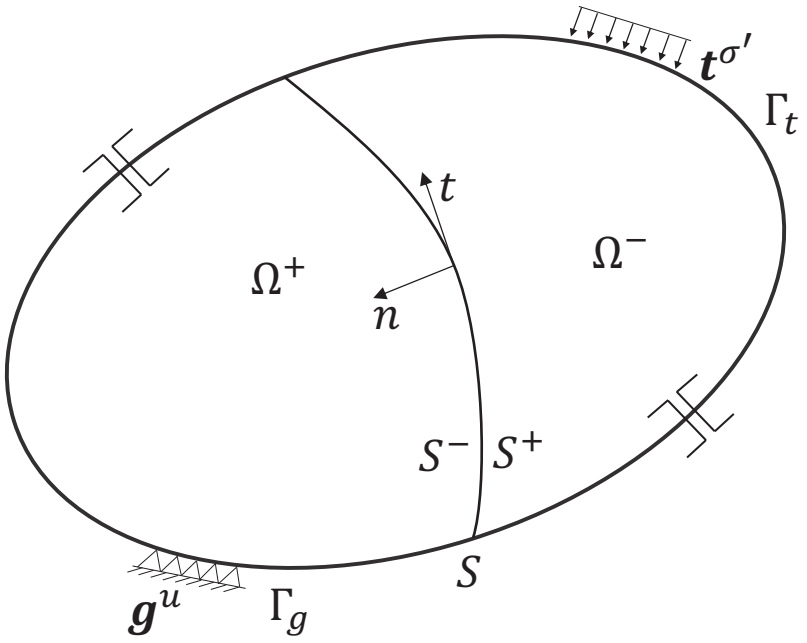

Figure 6.1: Sketch of continuum with discontinuity.

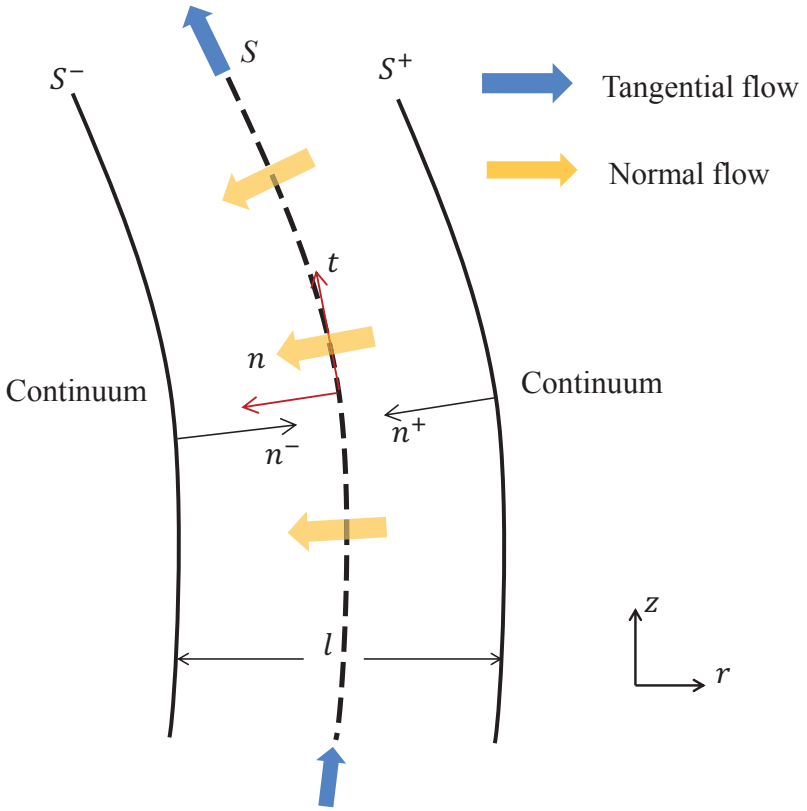

Figure 6.2: Sketch of 2D zero-thickness interface element with fluid flow in tangential and normal directions.

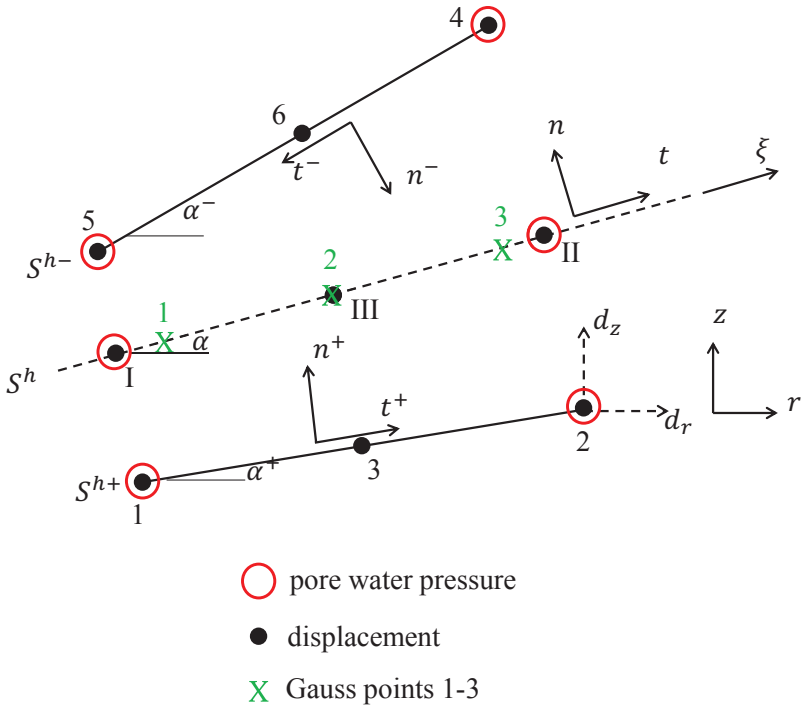

Figure 6.3: Schematic of mixed Q6P4 saturated PM cohesive surface element, indicating local node numbering of the six nodes 1-6, the three virtual interface nodes I-III on the virtual surface S, and the three Gauss points 1-3 (in green) on natural coordinate ξ.

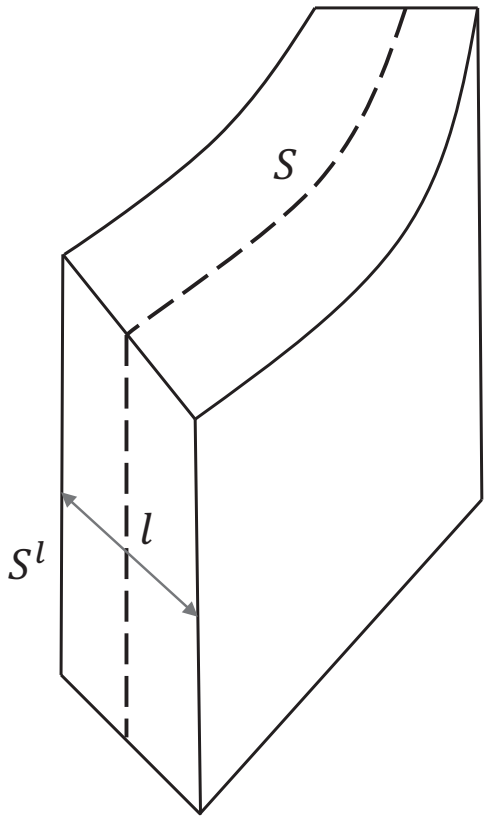

Figure 6.4: Schematic of the crack S^l with a width of l.

effective traction on surface S^+ and surface S^-. We define an effective traction T_i' on the virtual surface S (see Figure 6.2), which can be expressed by a constitutive equation. Furthermore, we assume effective traction continuity across S, such that

$$T_i' = T_i'^{+} = -T_i'^{-} \tag{6.2}$$

In the code, $\boldsymbol{T}' = [T_r'\,;\, T_z']$ in the global coordinate system is calculated through the following equation:

$$\boldsymbol{T}' = \boldsymbol{\Lambda}^{-1}\tilde{\boldsymbol{T}}' \tag{6.3}$$

where, $\tilde{\boldsymbol{T}}' = [T_t'; T_n']$ is the effective traction on S in the local coordinate system (Figure 6.1). We apply weighted function $w_i = \delta u_i$ to formulate the weak form of balance of linear momentum

$$\int_\Omega w_i \left(\frac{\partial \sigma_{ij}}{\partial x_j} + \rho b_i \right) dv = 0 \tag{6.4}$$

Using the chain rule, one can write

$$\int_\Omega w_i \frac{\partial \sigma_{ij}}{\partial x_j} dv = \int_\Omega \frac{\partial (w_i \sigma_{ij})}{\partial x_j} dv - \int_\Omega \frac{\partial w_i}{\partial x_j} \sigma_{ij} dv \tag{6.5}$$

We apply the divergence theorem to obtain

$$\int_\Omega \frac{\partial (w_i \sigma_{ij})}{\partial x_j} dv = \int_\Gamma w_i \sigma_{ij} \tilde{n}_j da \tag{6.6}$$

where $\tilde{n}_j$ is a generic normal vector to surface Γ, and $\Gamma = \Gamma_t + \Gamma_g + S^- + S^+$; thus we rewrite

$$\int_\Gamma w_i \sigma_{ij} \tilde{n}_j da = \int_{\Gamma_t} w_i \sigma_{ij} \nu_j da + \underbrace{\int_{\Gamma_g} w_i \sigma_{ij} \nu_j da}_{w_i = 0 on \Gamma_g} + \int_{S^+} w_i^+ \sigma_{ij}^+ n_j^+ da + \int_{S^-} w_i^- \sigma_{ij}^- n_j^- da \tag{6.7}$$

where we apply the effective stress principle to obtain,

$$\sigma_{ij} = \sigma_{ij}' - p_f \delta_{ij} \tag{6.8}$$

$$\sigma_{ij}^+ = \sigma_{ij}'^{+} - p_f^+ \delta_{ij} \tag{6.9}$$

$$\sigma_{ij}^- = \sigma_{ij}'^{-} - p_f^- \delta_{ij} \tag{6.10}$$

where p_f is the pore fluid pressure in the continuum; p_f^+ and p_f^- are respectively the pore fluid pressures on surfaces S^+ and S^-, positive in compression.

We substitute the effective stress expressions into (6.7):

$$\begin{aligned}\int_{\Gamma_t} w_i \sigma_{ij} \nu_j da &= \int_{\Gamma_t} w_i \left(\sigma'_{ij} - p_f \delta_{ij}\right) \nu_j da \\ &= \int_{\Gamma_t} w_i \sigma'_{ij} \nu_j da - \int_{\Gamma_t} w_i p_f \delta_{ij} \nu_j da \\ &= \int_{\Gamma_t} w_i t_i^{\sigma'} da - \int_{\Gamma_t} w_i p_f \nu_i da \end{aligned} \tag{6.11}$$

With 6.2, and assuming an average pore fluid pressure p_f^S associated with the virtual surface S, we can write

$$\begin{aligned}\int_{S^+} w_i^+ \sigma_{ij}^+ n_j^+ da &= \int_{S^+} w_i^+ T_i'^+ da - \int_{S^+} w_i^+ p_f^+ n_i^+ da \\ &= \int_S w_i^+ T_i' da - \int_S w_i^+ p_f^S n_i da \end{aligned} \tag{6.12}$$

where $p_f^S = \frac{1}{2}(p_f^+ + p_f^-)$. Similarly,

$$\begin{aligned}\int_{S^-} w_i^- \sigma_{ij}^- n_j^- da &= \int_{S^-} w_i^- T_i'^- da - \int_{S^-} w_i^- p_f^- n_i^- da \\ &= \int_S w_i^- \left(-T_i'\right) da - \int_S w_i^- p_f^S \left(-n_i\right) da \end{aligned} \tag{6.13}$$

We substitute (6.11), (6.12) and (6.13) into (6.7) to obtain

$$\begin{aligned}\int_\Gamma w_i \sigma_{ij} \tilde{n}_j da &= \int_{\Gamma_t} w_i t_i^{\sigma'} da - \int_{\Gamma_t} w_i p_f \nu_i da \\ &\quad + \int_S \left(w_i^+ - w_i^-\right) T_i' da + \int_S \left(w_i^- - w_i^+\right) p_f^S \, n_i \, da \end{aligned} \tag{6.14}$$

Let us introduce the definition of jump displacement vector and jump weighting function vector across S as,

$$[[\boldsymbol{u}]] := \boldsymbol{u}^{S^-} - \boldsymbol{u}^{S^+}; \quad [[\boldsymbol{w}]] := \boldsymbol{w}^{S^-} - \boldsymbol{w}^{S^+} \tag{6.15}$$

where the superscripts + and − denotes the surface S^+ and S^-; $\boldsymbol{u}^{S^-}$ and $\boldsymbol{u}^{S^+}$ are the displacement vectors on S^- and S^+, respectively; $[[\boldsymbol{u}]] = [u_t\,;\, u_n]$, where u_t and u_n denote tangential and normal

displacement jumps, respectively. Use (6.8) to write the 2nd term on the R.H.S. of (6.5) in the bulk continuum as

$$\int_\Omega \frac{\partial w_i}{\partial x_j}\sigma_{ij}dv = \int_\Omega \frac{\partial w_i}{\partial x_j}\sigma'_{ij}dv - \int_\Omega p_f \frac{\partial w_i}{\partial x_i}dv \tag{6.16}$$

Substitute (6.14) into (6.5) to obtain

$$\begin{aligned}&\int_\Omega \frac{\partial w_i}{\partial x_j}\sigma'_{ij}dv - \int_\Omega p_f \frac{\partial w_i}{\partial x_i}dv + \int_{\Gamma_t} w_i p_f \nu_i da \\ &+ \int_S [[w_i]]T'_i da - \int_S [[w_i]]p_f^S\, n_i\, da = \int_\Omega w_i \rho b_i dv + \int_{\Gamma_t} w_i t_i^{\sigma'} da\end{aligned} \tag{6.17}$$

The discrete Galerkin form of the variables are written as, $\boldsymbol{u}^h$, $[[\boldsymbol{u}^h]]$, p_f^h, $(p_f^S)^h$, $[[p_f^h]]$; the Galerkin form of the corresponding weighting functions are: $\boldsymbol{w}^h$, $[[\boldsymbol{w}^h]]$, ζ^h, $(\zeta^S)^h$ and $[[\zeta^h]]$. The local node order of the zero-thickness interface element is shown in Figure 6.3.

(1) Displacement

The Galerkin form of the displacement vector of the continuum FE is (using Q9P4 for bulk continuum FE discretization):

$$\begin{aligned}\boldsymbol{u}^h(\boldsymbol{\xi},t) &= \sum_{a=1}^{9} N_a^u(\boldsymbol{\xi})\,\boldsymbol{d}_a^e(t) = \boldsymbol{N}^{e,u}\cdot\boldsymbol{d}^e \\ &= \underbrace{\begin{bmatrix} \boldsymbol{N}_1^u & \dots & \boldsymbol{N}_9^u \end{bmatrix}}_{\boldsymbol{N}^{e,u}{}_{(2\times 18)}} \begin{bmatrix} \boldsymbol{d}_1^e \\ \vdots \\ \boldsymbol{d}_9^e \end{bmatrix}\end{aligned} \tag{6.18}$$

for $a = 1, 2, ..., 9$,

$$\boldsymbol{N}_a^u = \begin{bmatrix} N_a^u & 0 \\ 0 & N_a^u \end{bmatrix}, \quad \boldsymbol{d}_a^e = \begin{bmatrix} d_{r(a)}^e \\ d_{z(a)}^e \end{bmatrix} \tag{6.19}$$

$$\boldsymbol{w}^h(\boldsymbol{\xi}) = \boldsymbol{N}^{e,u}\cdot\boldsymbol{c}^e \tag{6.20}$$

Next, let us write the Galerkin form of displacement vector of zero-thickness interface element (see Figure 6.3:

$$\boldsymbol{u}^{S^-,h} = \begin{bmatrix} \frac{\xi(1+\xi)}{2} & -\frac{\xi(1-\xi)}{2} & (1-\xi)(1+\xi) \end{bmatrix} \cdot \begin{Bmatrix} \boldsymbol{d}_4^{cse} \\ \boldsymbol{d}_5^{cse} \\ \boldsymbol{d}_6^{cse} \end{Bmatrix} \tag{6.21}$$

$$\boldsymbol{u}^{S^+,h} = \left[\begin{array}{ccc} -\frac{\xi(1-\xi)}{2} & \frac{\xi(1+\xi)}{2} & (1-\xi)(1+\xi) \end{array} \right] \cdot \left\{ \begin{array}{c} \boldsymbol{d}_1^{cse} \\ \boldsymbol{d}_2^{cse} \\ \boldsymbol{d}_3^{cse} \end{array} \right\} \tag{6.22}$$

Thus, the jump displacement vector is written as

$$\begin{aligned} [[u^h]] &= \boldsymbol{u}^{S^-,h} - \boldsymbol{u}^{S^+,h} \\ &= \underbrace{\left[\begin{array}{cccccc} -\boldsymbol{N}_1^{cse,u} & -\boldsymbol{N}_2^{cse,u} & -\boldsymbol{N}_3^{cse,u} & \boldsymbol{N}_4^{cse,u} & \boldsymbol{N}_5^{cse,u} & \boldsymbol{N}_6^{cse,u} \end{array} \right]}_{\boldsymbol{N}^{cse,u}{}_{(2\times 12)}} \cdot \underbrace{\left\{ \begin{array}{c} \boldsymbol{d}_1^{cse} \\ \boldsymbol{d}_2^{cse} \\ \boldsymbol{d}_3^{cse} \\ \boldsymbol{d}_4^{cse} \\ \boldsymbol{d}_5^{cse} \\ \boldsymbol{d}_6^{cse} \end{array} \right\}}_{\boldsymbol{d}^{cse}{}_{(12\times 1)}} \end{aligned} \tag{6.23}$$

where, for $a = 1, 2..., 6$

$$\boldsymbol{N}_a^{cse,u} = \left[\begin{array}{cc} N_a^{cse,u} & 0 \\ 0 & N_a^{cse,u} \end{array} \right] \tag{6.24}$$

The shape functions for cohesive element are:

$$N_1^{cse,u} = N_5^{cse,u} = -\frac{\xi(1-\xi)}{2} \tag{6.25}$$

$$N_2^{cse,u} = N_4^{cse,u} = \frac{\xi(1+\xi)}{2} \tag{6.26}$$

$$N_3^{cse,u} = N_6^{cse,u} = (1-\xi)(1+\xi) \tag{6.27}$$

(2) Pore fluid pressure

The Galerkin form of pore fluid pressure in the bulk porous continuum:

$$\begin{aligned} p_f^h(\boldsymbol{\xi},t) &= \sum_{a=1}^{4} N_a^p(\boldsymbol{\xi})\, p_{f,a}^e = \boldsymbol{N}^{e,p}\cdot \boldsymbol{p}_f^e \\ &= \underbrace{\begin{bmatrix} N_1^p & N_2^p & N_3^p & N_4^p \end{bmatrix}}_{\boldsymbol{N}^{e,p}{}_{(1\times 4)}} \begin{bmatrix} p_{f,1}^e \\ p_{f,2}^e \\ p_{f,3}^e \\ p_{f,4}^e \end{bmatrix} \end{aligned} \tag{6.28}$$

$$\zeta^h(\boldsymbol{\xi},t) = \boldsymbol{N}^{e,p}(\boldsymbol{\xi})\cdot \boldsymbol{\alpha}^e \tag{6.29}$$

where, $\boldsymbol{\xi} = [\xi, \eta]$ denotes parent coordinates. The nodal shape functions for bilinear quadrilateral are,

$$\begin{aligned} N_1^p &= \tfrac{1}{4}(1-\xi)(1-\eta) \\ N_2^p &= \tfrac{1}{4}(1+\xi)(1-\eta) \\ N_3^p &= \tfrac{1}{4}(1+\xi)(1+\eta) \\ N_4^p &= \tfrac{1}{4}(1-\xi)(1+\eta) \end{aligned} \tag{6.30}$$

On the cohesive surface element: (1) The pore fluid pressure on surface S is denoted by p_f^S, and $p_f^S = \frac{1}{2}\left(p_f^+ + p_f^-\right)$, then,

$$p_f^{Sh} = \underbrace{\frac{1}{2}\begin{bmatrix} N_1^{cse1,p} & N_2^{cse1,p} & N_4^{cse1,p} & N_5^{cse1,p} \end{bmatrix}}_{\boldsymbol{N}^{cse1,p}{}_{(1\times 4)}} \cdot \underbrace{\begin{Bmatrix} p_{f,1}^{cse} \\ p_{f,2}^{cse} \\ p_{f,3}^{cse} \\ p_{f,4}^{cse} \end{Bmatrix}}_{\boldsymbol{p}_f^{cse}{}_{(4\times 1)}} \tag{6.31}$$

where, the shape functions $N_a^{cse1,p}, a = 1, 2, 4, 5$ are:

$$\begin{aligned} N_1^{cse1,p} &= N_5^{cse1,p} = \tfrac{1}{2}(1-\xi) \\ N_1^{cse2,p} &= N_4^{cse1,p} = \tfrac{1}{2}(1+\xi) \end{aligned} \tag{6.32}$$

The weighting function of p_f^S is denoted by ζ^S; the Galerkin form is:

$$\zeta^{Sh} = \boldsymbol{N}^{cse1,p}\cdot \boldsymbol{\alpha}^{cse} \tag{6.33}$$

(2) The weighting function of jump pore fluid pressure on the cohesive surface element is denoted by $[[\zeta]]$; the Galerkin form is written as:

$$[[\zeta^h]] = \underbrace{\begin{bmatrix} -N_1^{cse1,p} & -N_2^{cse1,p} & N_4^{cse1,p} & N_5^{cse1,p} \end{bmatrix}}_{\boldsymbol{N}^{cse2,p}} \cdot \boldsymbol{\alpha}^{cse} \tag{6.34}$$

where, the shape functions $N_a^{cse1,p}, a = 1, 2, 4, 5$ are the same as those defined in (6.32). The jump pore fluid pressure is written as

$$[[p_f^h]] = \boldsymbol{N}^{cse2,p} \cdot \boldsymbol{p}_f^{cse} \tag{6.35}$$

6.1.1.2 Balance of mass

In this part, we will write balance of mass for discontinuity (or cohesive interface element) and continuum (or bulk element) separately. Then combine the two equations to obtain one balance of mass equation for discontinuity and continuum together. The balance of mass in discontinuity S^l (with changing aperture l) is:

$$\frac{\partial \dot{u}_i}{\partial x_i} + \frac{\partial (\tilde{v}_f^{D,S})_i}{\partial x_i} = 0, \quad x_i \in S^l, \quad i = t, n \tag{6.36}$$

where u_i is the displacement component in the discontinuity; t and n denote "tangential" and "normal", respectively . $\tilde{\boldsymbol{v}}_f^{D,S} = [\tilde{v}_t^{D,S}; \tilde{v}_n^{D,S}]$ is Darcy's velocity of the fluid in discontinuity. The aperture of the discontinuity (or crack) S^l is denoted by $l = l_0 + u_n$, where, l_0 is the initial width of the discontinuity, and u_n is the displacement jump normal to S between S^+ and S^- due to the development of the crack. A Heaviside step function is assumed to express the displacement (or velocity) in the discontinuity:

$$\dot{u}_i = [[\dot{u}_i(\boldsymbol{x})]] H_S(\boldsymbol{x}), \quad \boldsymbol{x} \in S^l \tag{6.37}$$

where H_S is a heaviside step function on S. The divergence of $\dot{\boldsymbol{u}}$ is then,

$$\frac{\partial \dot{u}_i}{\partial x_i} = \frac{\partial [[\dot{u}_i(\boldsymbol{x})]]}{\partial x_i} H_S(\boldsymbol{x}) + [[\dot{u}_i(\boldsymbol{x})]] n_i \delta_S \tag{6.38}$$

where $\boldsymbol{n}$ is the normal vector of surface S, therefore we have $[[\dot{u}_i(\boldsymbol{x})]]n_i = [[\dot{u}_n(\boldsymbol{x})]]$; δ_S is the Dirac delta function on S. We ignore the first term on the R.H.S of (6.38) for now to obtain

$$\frac{\partial \dot{u}_i}{\partial x_i} = [[\dot{u}_n(\boldsymbol{x})]]\delta_S \tag{6.39}$$

In 2D, we define the nodal displacement vector of an oriented cohesive interface element (see Figure 6.3) in the local coordinate system $\boldsymbol{t} = (t, n)$ as:

$$\tilde{\boldsymbol{d}}_a^e = \left\{ \begin{array}{c} (d_t^e)_a \\ (d_n^e)_a \end{array} \right\} \tag{6.40}$$

As shown in Figure 6.3, an averaged angle α of S with respect to global coordinate frame $r - z$ is defined as:

$$\alpha = \frac{1}{2}(\alpha^+ + \alpha^-) \tag{6.41}$$

To establish a geometrical relationship between the nodal displacement vector in the local coordinate system and that in the global coordinate system $\boldsymbol{r} = (r, z)$, we construct a matrix $\boldsymbol{\Lambda}^e$, such that

$$\left\{ \begin{array}{c} (d_t^e)_a \\ (d_n^e)_a \end{array} \right\} = \underbrace{\left[\begin{array}{cc} cos\alpha & sin\alpha \\ -sin\alpha & cos\alpha \end{array} \right]}_{\boldsymbol{\Lambda}^e} \cdot \left\{ \begin{array}{c} (d_r^e)_a) \\ (d_z^e)_a \end{array} \right\} \tag{6.42}$$

Thus, the Galerkin form of element displacement jump can be written as

$$[[\tilde{\boldsymbol{u}}^e(\boldsymbol{t})]] = \left[\begin{array}{c} u_t^e \\ u_n^e \end{array} \right] = \boldsymbol{\Lambda}^e \cdot [[\boldsymbol{u}^e(\boldsymbol{r})]] = \boldsymbol{\Lambda}^e \cdot \boldsymbol{N}^{cse,u} \cdot \boldsymbol{d}^{cse} \tag{6.43}$$

If we write

$$\boldsymbol{\Lambda}^e = \left[\begin{array}{c} \boldsymbol{\Lambda}_1^e \\ \boldsymbol{\Lambda}_2^e \end{array} \right] \tag{6.44}$$

note,

$$\boldsymbol{\Lambda}_1^e = \left[\begin{array}{cc} cos\alpha & sin\alpha \end{array} \right] = \boldsymbol{t}^T; \quad \boldsymbol{\Lambda}_2^e = \left[\begin{array}{cc} -sin\alpha & cos\alpha \end{array} \right] = \boldsymbol{n}^T \tag{6.45}$$

The displacement jump in normal and tangential directions are given as

$$u_n = \boldsymbol{n}^T[[\boldsymbol{u}(\boldsymbol{r})]]; \quad u_t = \boldsymbol{t}^T[[\boldsymbol{u}(\boldsymbol{r})]] \tag{6.46}$$

Thus, $u_n > 0$ implies that the crack is opening; $u_n < 0$ implies that the crack is closing. Let us derive the divergence of $(\tilde{\boldsymbol{v}}_f^{D,S})$, the superficial velocity of the pore fluid in the crack S^l.

$$\frac{\partial(\tilde{v}_f^{D,S})_i}{\partial x_i} = \frac{\partial \tilde{v}_n^{D,S}}{\partial x_n} + \frac{\partial \tilde{v}_t^{D,S}}{\partial x_t} \tag{6.47}$$

where $\tilde{v}_n^{D,S}$ and $\tilde{v}_t^{D,S}$ are respectively the velocities in normal and tangential directions within the crack volume S^l (see Figure 6.4).

We apply weighting function ζ and integrate (6.36) over the volume of the discontinuity S^l to obtain

$$\int_{S^l} \zeta \dot{u}_n \delta_S \, dv + \int_{S^l} \zeta \frac{\partial(\tilde{v}_f^{D,S})_i}{\partial x_i} dv = 0 \tag{6.48}$$

According to the nature of the Dirac delta step function, the volumetric integration over S^l can be converted to area integration over S in the following form:

$$\int_{S^l} \zeta \dot{u}_n \delta_S \, dv = \int_S \zeta^S \dot{u}_n da \tag{6.49}$$

Let us derive the second term in (6.48). We use chain rule again to obtain

$$\int_{S^l} \zeta \frac{\partial(\tilde{v}_f^{D,S})_i}{\partial x_i} dv = \int_{S^l} \frac{\partial(\zeta \tilde{v}_f^{D,S})_i}{\partial x_i} dv - \int_{S^l} \frac{\partial \zeta}{\partial x_i} (\tilde{v}_f^{D,S})_i dv \tag{6.50}$$

We apply the divergence theorem to obtain

$$\int_{S^l} \frac{\partial(\zeta \tilde{v}_f^{D,S})_i}{\partial x_i} dv = \int_{S^+} \zeta^+ (\tilde{v}_f^{S^+,D})_i \, n_i^+ \, da + \int_{S^-} \zeta^- (\tilde{v}_f^{S^-,D})_i \, n_i^- \, da + \int_{\Gamma_S} \zeta (\tilde{v}_f^{D,S})_i \, \nu_i da \tag{6.51}$$

where Γ_S is the end boundary of the crack, with $\boldsymbol{\nu}$ being the normal vector.

$$\int_{\Gamma_S} \zeta (\tilde{v}_f^{D,S})_i \, \nu_i da = \int_{\Gamma_S} \zeta (-S^{w,S}) da \tag{6.52}$$

where $S^{w,S}$ is the flux at the ends of the boundaries of the crack domain S^l. We define the flux into the crack to be positive, thus

$$(\tilde{v}_f^{D,S^+})_i \, n_i^+ = \tilde{v}_n^{D,S^+} = \tilde{v}_n^{D,S} \tag{6.53}$$

$$(\tilde{v}_f^{D,S^-})_i \, n_i^- = \tilde{v}_n^{D,S^-} = -\tilde{v}_n^{D,S} \tag{6.54}$$

Therefore, substituting the upper equations and using the definition of jump weighting function $[[\zeta^S]]$ on surface S gives:

$$\begin{aligned}\int_{S^+} \zeta^+ (\tilde{v}_f^{D,S^+})_i \, n_i^+ da + \int_{S^-} \zeta^- (\tilde{v}_f^{D,S^-})_i \, n_i^- da &= \int_{S^+} \zeta^+ \tilde{v}_n^{D,S} da - \int_{S^-} \zeta^- \tilde{v}_n^{D,S} da \\ &= \int_S (\zeta^+ - \zeta^-) \tilde{v}_n^{D,S} da \\ &= \int_S -[[\zeta^S]] \tilde{v}_n^{D,S} da \end{aligned} \tag{6.55}$$

Substituting (6.52) and (6.55) into (6.50) yields

$$\int_{S^l} \zeta \frac{\partial (\tilde{v}_f^{D,S})_i}{\partial x_i} dv = -\int_S [[\zeta^S]] \, \tilde{v}_n^{D,S} da - \int_{\Gamma_S} \zeta S^{w,S} da - \int_{S^l} \frac{\partial \zeta}{\partial x_i} (\tilde{v}_f^{D,S})_i dv \tag{6.56}$$

where, the last term can be written as

$$\int_{S^l} \frac{\partial \zeta}{\partial x_i} (\tilde{v}_f^{D,S})_i dv = \int_{S^l} \frac{\partial \zeta}{\partial x_t} \tilde{v}_t^{D,S} dv + \int_{S^l} \frac{\partial \zeta}{\partial x_n} \tilde{v}_n^{D,S} dv \tag{6.57}$$

We assume the derivative of ζ with respect to x_n takes the form:

$$\frac{\partial \zeta}{\partial x_n} = [[\zeta^S]] \, \delta_S \tag{6.58}$$

where δ_S is δ function as in (6.38), such that

$$\int_{S^l} \frac{\partial \zeta}{\partial x_n} \tilde{v}_n^{D,S} dv = \int_S [[\zeta^S]] \, \tilde{v}_n^{D,S} \, da \approx 2\pi r_0 \int_S [[\zeta^S]] \, \tilde{v}_n^{D,S} \, ds \tag{6.59}$$

where $\tilde{v}_n^{D,S}$ denotes the normal velocity of fluid on the crack surface S, and can be expressed with a constitutive equation. Combining (6.59), (6.57), (6.56) and (6.48) allows us to write the balance of mass equation of the discontinuity as follows

$$\int_S \zeta^S \dot{u}_n \, da - \int_S [[\zeta^S]] \tilde{v}_n^{D,S} da - \int_{\Gamma_S} \zeta S_f da - \int_S [[\zeta]] \, \tilde{v}_n^{D,S} \, da - \int_{S^l} \frac{\partial \zeta}{\partial x_t} \tilde{v}_t^{D,S} dv = 0 \tag{6.60}$$

Now let us add the balance of mass equations of bulk and discontinuity together

$$\begin{aligned}&\int_\Omega \zeta \frac{\partial \dot{u}_i}{\partial x_i} \, dv - \int_\Omega \frac{\partial \zeta}{\partial x_i} \, (\tilde{v}_f^D)_i \, dv + \int_S \zeta^S \dot{u}_n da - 2 \int_S [[\zeta^S]] \, \tilde{v}_n^{D,S} da \\ &- \int_{S^l} \frac{\partial \zeta}{\partial x_t} \, \tilde{v}_t^{D,S} \, dv = \int_{\Gamma_s} \zeta S^w da + \int_{\Gamma_S} \zeta S^{w,S} da \end{aligned} \tag{6.61}$$

where S^w is the fluid flux at the continuum boundary Γ_s; $\boldsymbol{u}$ is the displacement of the solid skeleton; $\tilde{\boldsymbol{v}}_f^D$ is the Darcy's velocity of pore fluid in the continuum. The element of volume dv for an axisymmetric solid can be expressed as (assuming independence with respect to angle θ)

$$dv = r\, d\theta\, da = 2\pi r da \tag{6.62}$$

where $da = drdz$ is the element of area in the generating cross section of $r - z$ in the bulk. The volume integration is then written as

$$\int_\Omega (\bullet) dv = 2\pi \int_A (\bullet) r da \tag{6.63}$$

For the crack, however, we have:

$$\int_{S^l} (\bullet) dv = 2\pi \int_S (\bullet) l r ds \tag{6.64}$$

$$\text{for} S^l, dv = l\, r\, d\theta ds = 2\pi l\, r\, ds \tag{6.65}$$

where ds is the differential arc length element of the discontinuity S. Then, the area integration of fluid flux at the end of the discontinuity (z faces) is:

$$\int_{\Gamma_S} \zeta S^{w,S}\, da = \left(2\pi l\, r\, \zeta S^{w,S}\right)_{0,L} \tag{6.66}$$

where 0 and L denote the two ends of the crack S^L, respectively.

$$\int_{S^l} \frac{\partial \zeta}{\partial x_t} \tilde{v}_t^{D,S} dv = 2\pi \int_S \frac{\partial \zeta}{\partial x_t}\, \tilde{v}_t^{D,S}\, l\, r\, ds \tag{6.67}$$

We use the upper relation in (6.60) and cancel 2π to arrive at

$$\int_S \zeta^S \dot{u}_n r ds - 2\int_S [[\zeta^S]]\, \tilde{v}_n^{D,S} r ds - \left[l_0 r_0 \zeta_0 S_0^{w,S} + l_L r_L \zeta_L S_L^{w,S}\right] - \int_S \frac{\partial \zeta}{\partial x_t}\, \tilde{v}_t^{D,S}\, lr\, ds = 0 \tag{6.68}$$

For quadratic CSE, ds can be related to the global coordinate vector $\boldsymbol{r} = [r, z]^T$ as follows:

$$ds = \sqrt{dr^2 + dz^2} = f(\xi) d\xi = \sqrt{\left(\frac{dr}{d\xi}\right)^2 + \left(\frac{dz}{d\xi}\right)^2}\, d\xi \tag{6.69}$$

where

$$\frac{dr}{d\xi} = \frac{\partial \left[\begin{array}{ccc} -\frac{1}{2}\xi(1-\xi) & \frac{1}{2}\xi(1+\xi) & (1-\xi)(1+\xi) \end{array} \right]}{\partial \xi} \cdot \left\{ \begin{array}{c} \frac{1}{2}(r_1+r_5) \\ \frac{1}{2}(r_2+r_4) \\ \frac{1}{2}(r_3+r_6) \end{array} \right\}$$

$$= \left[\begin{array}{ccc} \xi-0.5 & \xi+0.5 & -2\xi \end{array} \right] \cdot \left\{ \begin{array}{c} \frac{1}{2}(r_1+r_5) \\ \frac{1}{2}(r_2+r_4) \\ \frac{1}{2}(r_3+r_6) \end{array} \right\} \tag{6.70}$$

similarly,

$$\frac{dz}{d\xi} = \left[\begin{array}{ccc} \xi-0.5 & \xi+0.5 & -2\xi \end{array} \right] \cdot \left\{ \begin{array}{c} \frac{1}{2}(z_1+z_5) \\ \frac{1}{2}(z_2+z_4) \\ \frac{1}{2}(z_3+z_6) \end{array} \right\} \tag{6.71}$$

where, r_a and z_a are the coordinates of node a, and the order of numbering is in accordance with that in Figure 6.3, thus, by chain rule,

$$\frac{\partial(\bullet)}{\partial s} = \frac{\partial(\bullet)}{\partial \xi}\frac{1}{f(\xi)} \tag{6.72}$$

Note that for CSE element specifically, $ds = dx_t$, i.e., $\frac{\partial(\bullet)}{\partial x_t} = \frac{\partial(\bullet)}{\partial s}$.

For an axisymmetric problem, the volume and surface integrations can be respectively reduced to surface and line integrations:

$$\int_{S^l}(\bullet)dv = \int_0^{2\pi}\int_S\int_0^l(\bullet)dx_n ds r d\theta = 2\pi\int_S(\bullet)lrds \tag{6.73}$$

$$\int_S(\bullet)da = \int_0^{2\pi}\int_S(\bullet)dsrd\theta = 2\pi\int_S(\bullet)rda \tag{6.74}$$

where $(\bullet)$ is assumed constant in direction of x_n (normal to the virtual crack surface S).

6.1.2 Constitutive relations for saturated interface element

The normal velocity in the crack is expressed as Segura and Carol (2008):

$$\tilde{v}_n^{D,S} = \hat{k}_n(p_f^+ - p_f^-) = -\hat{k}_n[[p_f^S]] \tag{6.75}$$

where $\hat{k}_n = \kappa/(\mu_f\, l)$ is the normal permeability, κ = intrinsic normal permeability with the unit of m^2; μ_f = dynamic viscosity of fluid, with the unit of $Pa \cdot s$; l denotes the aperture, with the unit of m. The tangential velocity in the crack takes the following formSegura and Carol (2008):

$$\tilde{v}_t^{D,S} = -\hat{k}_t \left(\frac{\partial p_f^S}{\partial x_t} - \rho^{fR} \boldsymbol{g} \frac{\partial z^S}{\partial x_t} \right) \tag{6.76}$$

where $\hat{k}_t$ = tangential permeability of the crack with the unit of $m^2/(Pa \cdot s)$, and is given as

$$\hat{k}_t = \frac{l^2}{12\mu_f} \tag{6.77}$$

where $l = u_n + l_0$ is the changing width of the crack, where $u_n = \boldsymbol{n}^T \cdot [[\boldsymbol{u}(\boldsymbol{r})]]$, l_0 is the initial width of the crack; μ_f = the dynamic viscosity of fluid; z = elevation of crack center. $\boldsymbol{g} = [0; -g]$, where $g = 9.81N/m^2$. Let us derive for the finite element formulation:

$$\frac{\partial p_f^S}{\partial x_t} = \frac{\partial p_f^S}{\partial s} \approx \frac{\partial p_f^{S^h}}{\partial \xi} \frac{\partial \xi}{\partial s} = \frac{\partial \boldsymbol{N}^{cse1,p}}{\partial \xi} \cdot \boldsymbol{p}_f^{cse} \cdot \frac{1}{f(\xi)} = \boldsymbol{B}^{cse1,p} \cdot \boldsymbol{p}_f^{cse} \tag{6.78}$$

where

$$\boldsymbol{B}^{cse1,p} = \frac{1}{f(\xi)} \begin{bmatrix} -\frac{1}{4} & \frac{1}{4} & \frac{1}{4} & -\frac{1}{4} \end{bmatrix} \tag{6.79}$$

$$\frac{\partial z^S}{\partial x_t} = \frac{\partial z^S}{\partial s} = \frac{\partial z^S}{\partial \xi} \frac{\partial \xi}{\partial s} = \frac{\partial z^S}{\partial \xi} \frac{1}{f(\xi)} \tag{6.80}$$

where, the Galerkin form of z^S in CSE is obtained from

$$z_{cse}^{S^h} = \underbrace{\begin{bmatrix} -\frac{1}{2}\xi(1-\xi) & \frac{1}{2}\xi(1+\xi) & (1-\xi)(1+\xi) \end{bmatrix}}_{\boldsymbol{N}^{case,S}} \cdot \underbrace{\begin{Bmatrix} z_{cse,I}^S \\ z_{cse,II}^S \\ z_{cse,III}^S \end{Bmatrix}}_{\boldsymbol{z}_{cse}^S} \tag{6.81}$$

where,

$$\boldsymbol{z}_{cse}^S = \begin{Bmatrix} \frac{1}{2}(z_1 + z_5) \\ \frac{1}{2}(z_2 + z_4) \\ \frac{1}{2}(z_3 + z_6) \end{Bmatrix} \tag{6.82}$$

thus, the derivative in CSE is:

$$\frac{\partial z^S_{cse}}{\partial \xi} = \underbrace{\begin{bmatrix} \xi - 0.5 & \xi + 0.5 & -2\xi \end{bmatrix}}_{\boldsymbol{B}^{cse,S}} \cdot \boldsymbol{z}^S_{cse} \tag{6.83}$$

6.1.3 Finite element formulation

The finite element form of balance of linear momentum equation (6.17) is written as

$$\begin{aligned} &\mathop{\mathbf{A}}_{e=1}^{n_{\text{bel}}} (\boldsymbol{c}^e)^T \cdot \Bigg[\underbrace{\int_{\Omega^e} (\boldsymbol{B}^{e,u})^T \cdot \boldsymbol{\sigma}' dv}_{\boldsymbol{f}^{d,int}_e(\boldsymbol{d}^e)} - \underbrace{\int_{\Omega^e} \left(\tilde{\boldsymbol{B}}^{e,u}\right)^T \cdot \boldsymbol{N}^{e,p} dv}_{\boldsymbol{k}^{dp1}_e} \cdot \boldsymbol{p}^e_f \\ &- \underbrace{\int_{\Omega^e} \rho \, (\boldsymbol{N}^{e,u})^T \cdot \boldsymbol{b} \, dv}_{\boldsymbol{f}^{df,ext}_e(\boldsymbol{d}^e)} - \underbrace{\int_{\Gamma^e_t} (\boldsymbol{N}^{e,u})^T \, \boldsymbol{t}^{\sigma'} da}_{\boldsymbol{f}^{dt,ext}_e} + \underbrace{\int_{\Gamma^e_t} (\boldsymbol{N}^{e,u})^T \cdot \boldsymbol{\nu} \cdot \boldsymbol{N}^{e,p} da}_{\boldsymbol{k}^{dp2}_e} \cdot \boldsymbol{p}^e_f \Bigg] \\ &= \mathop{\mathbf{A}}_{e=1}^{n_{\text{cel}}} (\boldsymbol{c}^{cse})^T \left[- \underbrace{\int_{S^e} (\boldsymbol{N}^{cse,u})^T \cdot \boldsymbol{T}' da}_{\boldsymbol{f}^{d,int}_{cse}(\boldsymbol{d}^{cse})} + \underbrace{\int_{S^e} (\boldsymbol{N}^{cse,u})^T \cdot \boldsymbol{n} \cdot \boldsymbol{N}^{cse1,p} da}_{\boldsymbol{k}^{dp}_{cse}} \cdot \boldsymbol{p}^{cse}_f \right] \end{aligned} \tag{6.84}$$

where, n_{bel} denotes the number of bulk elements; correspondingly, n_{cel} denotes the number of cohesive elements.

The finite element form of balance of mass equation (6.61) is:

$$\begin{aligned}
&\mathop{\mathbf{A}}_{e=1}^{n_{\text{bel}}}(\boldsymbol{\alpha}^e)^T\cdot\Bigg[\underbrace{\int_{\Omega^e}(\boldsymbol{N}^{e,p})^T\cdot\tilde{\boldsymbol{B}}^{e,u}dv}_{\left(\boldsymbol{k}_e^{dp1}\right)^T}\cdot\dot{\boldsymbol{d}}^e-\underbrace{\int_{\Omega^e}(\boldsymbol{B}^{e,p})^T\cdot\tilde{\boldsymbol{v}}_f^D dv}_{\boldsymbol{f}_e^{p,int}(\boldsymbol{d}^e,\boldsymbol{p}_f^e)}-\underbrace{\int_{\Gamma_s^e}(\boldsymbol{N}^{e,p})^T\,S^w dv}_{\boldsymbol{f}_e^{p,ext}}\Bigg]\\
&+\mathop{\mathbf{A}}_{e=1}^{n_{\text{cel}}}(\boldsymbol{\alpha}^{cse})^T\cdot\Bigg[\underbrace{\int_{S^e}\left(\boldsymbol{N}^{cse1,p}\right)^T\boldsymbol{n}^T\cdot\boldsymbol{N}^{cse,u}da}_{\left(\boldsymbol{k}_{cse}^{dp}\right)^T}\cdot\dot{\boldsymbol{d}}^{cse}-\underbrace{\int_{S^e}\left(\boldsymbol{N}^{cse2,p}\right)^T\cdot(2\tilde{v}_n^{D,S})da}_{\boldsymbol{f}_{cse}^{p1,int}(\boldsymbol{d}^{cse},\boldsymbol{p}_f^{cse})}\\
&-\underbrace{\int_{S^{l^e}}\left(\boldsymbol{B}^{cse1,p}\right)^T\cdot\tilde{v}_t^{D,S}\,dv}_{\boldsymbol{f}_{cse}^{p2,int}(\boldsymbol{d}^{cse},\boldsymbol{p}_f^{cse})}-\int_{\Gamma_S^e}\left(\boldsymbol{N}^{cse1,p}\right)^T S^{w,S}da\Bigg]=\boldsymbol{0}
\end{aligned}\tag{6.85}$$

In the local degree of freedom matrix, the order of nodes in cohesive surface element follows the order in Figure 6.3. $\boldsymbol{d}^e$ and $\boldsymbol{d}^{cse}$ are respectively the nodal displacement vectors of bulk element and cohesive interface element. After assembly, we can write the coupled two governing equations in the matrix vector form:

$$\boldsymbol{C}(\boldsymbol{D})\cdot\dot{\boldsymbol{D}}+\boldsymbol{F}^{INT}(\boldsymbol{D})=\boldsymbol{F}^{EXT}(\boldsymbol{D})\tag{6.86}$$

where

$$\begin{aligned}
\boldsymbol{C}(\boldsymbol{D}) &= \begin{bmatrix}\boldsymbol{0} & \boldsymbol{0}\\ (\boldsymbol{K}^{dp1})^T+\left(\boldsymbol{K}_{cse}^{dp}\right)^T & \boldsymbol{0}\end{bmatrix}\\
&= \mathop{\mathbf{A}}_{e=1}^{n_{\text{bel}}}\begin{bmatrix}\underbrace{\boldsymbol{0}}_{18\times18} & \underbrace{\boldsymbol{0}}_{18\times4}\\ \underbrace{\left(\boldsymbol{k}_e^{dp1}\right)^T}_{4\times18} & \underbrace{\boldsymbol{0}}_{4\times4}\end{bmatrix}+\mathop{\mathbf{A}}_{e=1}^{n_{\text{cel}}}\begin{bmatrix}\underbrace{\boldsymbol{0}}_{18\times18} & \underbrace{\boldsymbol{0}}_{18\times4}\\ \underbrace{\left(\boldsymbol{k}_{cse}^{dp}\right)^T}_{4\times12} & \underbrace{\boldsymbol{0}}_{4\times10}\end{bmatrix}
\end{aligned}\tag{6.87}$$

The global degrees of freedom $\boldsymbol{D}$ and the rate form $\dot{\boldsymbol{D}}$ are:

$$\boldsymbol{D}=\begin{bmatrix}\boldsymbol{d}\\ \boldsymbol{p}_f\end{bmatrix};\quad \dot{\boldsymbol{D}}=\begin{bmatrix}\dot{\boldsymbol{d}}\\ \dot{\boldsymbol{p}}_f\end{bmatrix}\tag{6.88}$$

The internal force $\boldsymbol{F}^{INT}$ assembled from bulk elements and cohesive surface elements is given as

$$\begin{aligned}
\boldsymbol{F}^{INT} &= \begin{bmatrix} \boldsymbol{F}^{d,INT} + \boldsymbol{F}_{cse}^{d,INT} + \left(\boldsymbol{K}^{dp2} - \boldsymbol{K}^{dp1} - \boldsymbol{K}_{cse}^{dp}\right) \cdot \boldsymbol{p}_f \\ -\boldsymbol{F}^{p,INT} - \boldsymbol{F}_{cse}^{p1,INT} - \boldsymbol{F}_{cse}^{p2,INT} \end{bmatrix} \\
&= \mathop{\mathsf{A}}_{e=1}^{n_{\text{bel}}} \begin{bmatrix} \underbrace{\boldsymbol{f}_e^{d,int}}_{18\times1} + \underbrace{\left(\boldsymbol{k}_e^{dp2} - \boldsymbol{k}_e^{dp1}\right)}_{18\times4} \cdot \underbrace{\boldsymbol{p}_f^e}_{4\times1} \\ -\underbrace{\boldsymbol{f}_e^{p,int}}_{4\times1} \end{bmatrix} + \mathop{\mathsf{A}}_{e=1}^{n_{\text{cel}}} \begin{bmatrix} \underbrace{\boldsymbol{f}_{cse}^{d,int}}_{12\times1} - \underbrace{\boldsymbol{k}_{cse}^{dp}}_{12\times4} \cdot \underbrace{\boldsymbol{p}_f^{cse}}_{4\times1} \\ \underbrace{\boldsymbol{0}}_{6\times1} \\ -\underbrace{\boldsymbol{f}_{cse}^{p1,int}}_{4\times1} - \underbrace{\boldsymbol{f}_{cse}^{p2,int}}_{4\times1} \end{bmatrix}
\end{aligned} \tag{6.89}$$

The external force $\boldsymbol{F}^{EXT}$ assembled from bulk elements and cohesive surface elements is given as

$$\begin{aligned}
\boldsymbol{F}^{EXT} &= \begin{bmatrix} \boldsymbol{F}^{df,EXT} + \boldsymbol{F}^{dt,EXT} \\ \boldsymbol{F}^{p,EXT} + \boldsymbol{F}_{cse}^{p0,EXT} + \boldsymbol{F}_{cse}^{pL,EXT} \end{bmatrix} \\
&= \mathop{\mathsf{A}}_{e=1}^{n_{\text{bel}}} \begin{bmatrix} \underbrace{\boldsymbol{f}_e^{df,ext}}_{18\times1} + \underbrace{\boldsymbol{f}_e^{dt,ext}}_{18\times1} \\ \underbrace{\boldsymbol{f}_e^{p,ext}}_{4\times1} \end{bmatrix} + \mathop{\mathsf{A}}_{e=1}^{n_{\text{cel}}} \begin{bmatrix} \underbrace{\boldsymbol{0}}_{18\times1} \\ \underbrace{\boldsymbol{f}_{cse}^{p0,ext}}_{4\times1} + \underbrace{\boldsymbol{f}_{cse}^{pL,ext}}_{4\times1} \end{bmatrix}
\end{aligned} \tag{6.90}$$

Recall the generalized trapezoidal rule and construct the consistent tangent:

$$\boldsymbol{C}(\boldsymbol{D}_{n+1}) \cdot \boldsymbol{V}_{n+1} + \boldsymbol{F}^{INT}(\boldsymbol{D}_{n+1}) = \boldsymbol{F}^{EXT}(\boldsymbol{D}_{n+1}) \tag{6.91}$$

where $\boldsymbol{V} = \dot{\boldsymbol{D}}$. The subscript $n+1$ denotes the current time step; and the subscript n denotes the previous converged time step. α is the time integration parameter, and typically, $\alpha = 0$ for forward Euler; $\alpha = 0.5$ for trapezoidal rule; $\alpha = 1$ for backward Euler, which will be used here.

$$\boldsymbol{D}_{n+1} = \tilde{\boldsymbol{D}}_{n+1} + \alpha\Delta t \boldsymbol{V}_{n+1},\ \tilde{\boldsymbol{D}}_{n+1} = \boldsymbol{D}_n + \Delta t(1-\alpha)\boldsymbol{V}_n \tag{6.92}$$

The Newton-Raphson iteration algorithm is used to solve for $\boldsymbol{V}_{n+1}^{k+1}$, where the superscript $k+1$

denotes the iteration number in one time step.

$$\begin{aligned}
\boldsymbol{R}(\boldsymbol{V}_{n+1}^{k+1}) &= \boldsymbol{C}(\boldsymbol{D}_{n+1}^{k+1}) \cdot \boldsymbol{V}_{n+1}^{k+1} + \boldsymbol{F}^{INT}(\boldsymbol{D}_{n+1}^{k+1}) - \boldsymbol{F}^{EXT}(\boldsymbol{D}_{n+1}^{k+1}) = \boldsymbol{0} \\
&= \boldsymbol{R}^k + \frac{\partial \boldsymbol{R}^k}{\partial \boldsymbol{V}} \cdot \delta \boldsymbol{V} \\
\Longrightarrow \delta \boldsymbol{V} &= -\left(\frac{\partial \boldsymbol{R}^k}{\partial \boldsymbol{V}}\right)^{-1} \cdot \boldsymbol{R}^k \\
\boldsymbol{V}_{n+1}^{k+1} &= \boldsymbol{V}_{n+1}^{k} + \delta \boldsymbol{V} \\
\boldsymbol{D}_{n+1}^{k+1} &= \tilde{\boldsymbol{D}}_{n+1} + \alpha \Delta t \boldsymbol{V}_{n+1}^{k+1}
\end{aligned} \tag{6.93}$$

Generally, the consistent tangent is written as:

$$\frac{\partial \boldsymbol{R}}{\partial \boldsymbol{V}} = \left(\frac{\partial \boldsymbol{C}}{\partial \boldsymbol{D}} \cdot \frac{\partial \boldsymbol{D}}{\partial \boldsymbol{V}}\right) \cdot \boldsymbol{V} + \boldsymbol{C} + \frac{\partial \boldsymbol{F}^{INT}}{\partial \boldsymbol{D}} \cdot \frac{\partial \boldsymbol{D}}{\partial \boldsymbol{V}} - \frac{\partial \boldsymbol{F}^{EXT}}{\partial \boldsymbol{D}} \cdot \frac{\partial \boldsymbol{D}}{\partial \boldsymbol{V}} \tag{6.94}$$

where

$$\frac{\partial \boldsymbol{D}}{\partial \boldsymbol{V}} = \alpha \Delta t\,; \quad \frac{\partial \boldsymbol{C}}{\partial \boldsymbol{D}} = 0 \tag{6.95}$$

therefore,

$$\frac{\partial \boldsymbol{R}}{\partial \boldsymbol{V}} = \boldsymbol{C} + \left(\frac{\partial \boldsymbol{F}^{INT}}{\partial \boldsymbol{D}} - \frac{\partial \boldsymbol{F}^{EXT}}{\partial \boldsymbol{D}}\right) \cdot \frac{\partial \boldsymbol{D}}{\partial \boldsymbol{V}} \tag{6.96}$$

where

$$\begin{aligned}
\frac{\partial \boldsymbol{F}^{INT}}{\partial \boldsymbol{D}} &= \left[\begin{array}{cc} \frac{\partial \boldsymbol{F}^{INT}}{\partial \boldsymbol{d}} & \frac{\partial \boldsymbol{F}^{INT}}{\partial \boldsymbol{p}_f} \end{array}\right] \\
&= \mathop{\mathbf{A}}_{e=1}^{n_{\text{bel}}} \left[\begin{array}{cc} \underbrace{\frac{\partial \boldsymbol{f}_e^{d,int}}{\partial \boldsymbol{d}^e}}_{18\times 18} & \left(\underbrace{\boldsymbol{k}_e^{dp2}}_{18\times 4} - \underbrace{\boldsymbol{k}_e^{dp1}}_{18\times 4}\right) \\ -\underbrace{\frac{\partial \boldsymbol{f}_e^{p,int}}{\partial \boldsymbol{d}^e}}_{4\times 18} & -\underbrace{\frac{\partial \boldsymbol{f}_e^{p,int}}{\partial \boldsymbol{p}_f^e}}_{4\times 4} \end{array}\right] \\
&+ \mathop{\mathbf{A}}_{e=1}^{n_{\text{cel}}} \left[\begin{array}{ccc} \underbrace{\frac{\partial \boldsymbol{f}_{cse}^{d,int}}{\partial \boldsymbol{d}^{cse}}}_{12\times 12} & \underbrace{\boldsymbol{0}}_{12\times 6} & -\underbrace{\boldsymbol{k}_{cse}^{dp}}_{12\times 4} \\ \underbrace{\boldsymbol{0}}_{6\times 12} & \underbrace{\boldsymbol{0}}_{6\times 6} & \underbrace{\boldsymbol{0}}_{6\times 4} \\ \left(-\underbrace{\frac{\partial \boldsymbol{f}_{cse}^{p1,int}}{\partial \boldsymbol{d}^{cse}}}_{4\times 12} - \underbrace{\frac{\partial \boldsymbol{f}_{cse}^{p2,int}}{\partial \boldsymbol{d}^{cse}}}_{4\times 12}\right) & \underbrace{\boldsymbol{0}}_{4\times 6} & \left(-\underbrace{\frac{\partial \boldsymbol{f}_{cse}^{p1,int}}{\partial \boldsymbol{p}_f^{cse}}}_{4\times 4} - \underbrace{\frac{\partial \boldsymbol{f}_{cse}^{p2,int}}{\partial \boldsymbol{p}_f^{cse}}}_{4\times 4}\right) \end{array}\right]
\end{aligned} \tag{6.97}$$

$$\frac{\partial \boldsymbol{F}^{EXT}}{\partial \boldsymbol{D}} = \left[\begin{array}{cc} \frac{\partial \boldsymbol{F}^{EXT}}{\partial \boldsymbol{d}} & \frac{\partial \boldsymbol{F}^{EXT}}{\partial \boldsymbol{p}_f} \end{array} \right]$$

$$= \mathop{\mathbf{A}}_{e=1}^{n_{\text{bel}}} \left[\begin{array}{cc} \underbrace{\frac{\partial \boldsymbol{f}^{df,ext}}{\partial \boldsymbol{d}^e}}_{18\times 18} & \underbrace{\mathbf{0}}_{18\times 4} \\ \underbrace{\mathbf{0}}_{4\times 18} & \underbrace{\mathbf{0}}_{4\times 4} \end{array} \right] + \mathop{\mathbf{A}}_{e=1}^{n_{\text{cel}}} \left[\begin{array}{cc} \underbrace{\mathbf{0}}_{18\times 18} & \underbrace{\mathbf{0}}_{18\times 4} \\ \left(\underbrace{\frac{\partial \boldsymbol{f}_{cse}^{p0,ext}}{\partial \boldsymbol{d}^{cse}}}_{4\times 12} + \underbrace{\frac{\partial \boldsymbol{f}_{cse}^{pL,ext}}{\partial \boldsymbol{d}^{cse}}}_{4\times 12} \right) & \underbrace{\mathbf{0}}_{4\times 10} \end{array} \right] \tag{6.98}$$

The details of the derivatives are shown as follows:

$$\frac{\partial \boldsymbol{f}_e^{d,int}}{\partial \boldsymbol{d}^e} = \int_{\Omega^e} (\boldsymbol{B}^{e,u})^T \cdot \frac{\partial \boldsymbol{\sigma}'}{\partial \boldsymbol{\epsilon}} \cdot \boldsymbol{B}^{e,u}\, dv \tag{6.99}$$

$$\frac{\partial \boldsymbol{f}_e^{p,int}}{\partial \boldsymbol{d}^e} = \int_{\Omega_e} (\boldsymbol{B}^{e,p})^T \cdot \frac{\partial \tilde{\boldsymbol{v}}_f^D}{\partial \boldsymbol{d}^e}\, dv = \int_{\Omega_e} -(\boldsymbol{B}^{e,p})^T \cdot \frac{\partial k_f}{\partial n} (\nabla p_f - \rho^{fR} \boldsymbol{g}) \otimes \frac{\partial n}{\partial \boldsymbol{d}^e}\, dv \tag{6.100}$$

$$\frac{\partial \boldsymbol{f}_e^{p,int}}{\partial \boldsymbol{p}_f^e} = \int_{\Omega_e} (\boldsymbol{B}^{e,p})^T \cdot \frac{\partial \tilde{\boldsymbol{v}}_f^D}{\partial \boldsymbol{p}_f^e}\, dv = \int_{\Omega_e} -k_f\ (\boldsymbol{B}^{e,p})^T \cdot \boldsymbol{B}^{e,p} \tag{6.101}$$

where, $\frac{\partial \boldsymbol{\sigma}'}{\partial \boldsymbol{\epsilon}}$ is consistent tangent from constitutive model of solid skeleton; k_f denotes the saturated permeability given as $k_f = \frac{\kappa(n)}{\mu_f}$, where $\kappa(n)$ = intrinsic permeability, μ_f = dynamic viscosity of fluid.

$$\begin{aligned} \frac{\partial \boldsymbol{f}_{cse}^{d,int}}{\partial \boldsymbol{d}^{cse}} &= \int_{S^e} (\boldsymbol{N}^{cse,u})^T \cdot \frac{\partial \boldsymbol{T}'^{,h}(\boldsymbol{d}^{cse})}{\partial \boldsymbol{d}^{cse}} da \\ &= \int_{S^e} (\boldsymbol{N}^{cse,u})^T \cdot (\boldsymbol{\Lambda}^e)^T \cdot \frac{\partial \widetilde{\boldsymbol{T}}'^{,h}(\boldsymbol{d}^{cse})}{\partial [[\tilde{\boldsymbol{u}}^h]]} \cdot \frac{\partial [[\tilde{\boldsymbol{u}}^h]]}{\partial [[\boldsymbol{u}^h]]} \cdot \frac{\partial [[\boldsymbol{u}^h]]}{\partial \boldsymbol{d}^{cse}} da \\ &= \int_{S^e} (\boldsymbol{N}^{cse,u})^T \cdot (\boldsymbol{\Lambda}^e)^T \cdot \frac{\partial \widetilde{\boldsymbol{T}}'^{,h}(\boldsymbol{d}^{cse})}{\partial [[\tilde{\boldsymbol{u}}^h]]} \cdot \boldsymbol{\Lambda}^e \cdot \boldsymbol{N}^{cse,u}\, da \end{aligned} \tag{6.102}$$

where, $\boldsymbol{T}'^{,h}$ and $\widetilde{\boldsymbol{T}}'^{,h}$ are Galerkin forms of the cohesive traction at the crack surface $\boldsymbol{T}'$ and $\widetilde{\boldsymbol{T}}'$, which are respectively written as,

$$\boldsymbol{T}' = \left[\begin{array}{c} T_r' \\ \\ T_z' \end{array} \right]; \quad \widetilde{\boldsymbol{T}}' = \left[\begin{array}{c} \widetilde{T}_t' \\ \\ \widetilde{T}_n' \end{array} \right] \tag{6.103}$$

$$\widetilde{\boldsymbol{T}}' = \boldsymbol{\Lambda} \cdot \boldsymbol{T}' \Rightarrow \boldsymbol{T}'^{,h} = (\boldsymbol{\Lambda}^e)^{-1} \cdot \widetilde{\boldsymbol{T}}'^{,h} = (\boldsymbol{\Lambda}^e)^T \cdot \widetilde{\boldsymbol{T}}'^{,h} \tag{6.104}$$

and, $\widetilde{\boldsymbol{T}}'^{,h}(\boldsymbol{d}^{cse})$ is obtained from a nonlinear function of CIE displacement $\boldsymbol{d}^{cse}$; $\frac{\partial \widetilde{\boldsymbol{T}}'^{,h}}{\partial [[\tilde{\boldsymbol{u}}^h]]}$ is called the elasto-plastic consistent tangent in the local frame of CSE, assuming there is elasticity associated with the crack material.

Furthermore,

$$\frac{\partial \boldsymbol{f}_{cse}^{p1,int}}{\partial \boldsymbol{d}^{cse}} = \int_{S^e} \left(\boldsymbol{N}^{cse2,p}\right)^T \cdot \left(2\frac{\partial \tilde{v}_n^{D,S}}{\partial \boldsymbol{d}^{cse}}\right) da \tag{6.105}$$

$$\frac{\partial \boldsymbol{f}_{cse}^{p1,int}}{\partial \boldsymbol{p}_f^{cse}} = \int_{S^e} \left(\boldsymbol{N}^{cse2,p}\right)^T \cdot \left(2\frac{\partial \tilde{v}_n^{D,S}}{\partial \boldsymbol{p}_f^{cse}}\right) da \tag{6.106}$$

$$\frac{\partial \boldsymbol{f}_{cse}^{p2,int}}{\partial \boldsymbol{d}^{cse}} = \int_{S^e} \left(\boldsymbol{B}^{cse1,p}\right)^T \cdot \frac{\partial(\tilde{v}_t^{D,S}\, l)}{\partial \boldsymbol{d}^{cse}}\, da \tag{6.107}$$

$$\frac{\partial \boldsymbol{f}_{cse}^{p2,int}}{\partial \boldsymbol{p}_f^{cse}} = \int_{S^e} \left(\boldsymbol{B}^{cse1,p}\right)^T \cdot \frac{\partial(\tilde{v}_t^{D,S}\, l)}{\partial \boldsymbol{p}_f^{cse}}\, da \tag{6.108}$$

with the expression $\tilde{v}_t^{D,S}$ in (6.76) and (6.77), we can derive the derivatives w.r.t. $\boldsymbol{d}^{cse}$ and $\boldsymbol{p}_f^{cse}$, assuming fluid is incompressible, i.e., ρ^{fR} is constant.

$$\begin{aligned}\frac{\partial(\tilde{v}_t^{D,S}\, l)}{\partial \boldsymbol{d}^{cse}} &= \frac{\partial(\hat{k}_t\, l)}{\partial \boldsymbol{d}^{cse}}\left(\frac{\partial\, p_f}{\partial\, x_t} - \rho^{fR}\boldsymbol{g}\,\frac{\partial\, z^S}{\partial\, x_t}\right) \\ &= \frac{3l^2}{12\mu_f}\frac{\partial l}{\partial \boldsymbol{d}^{cse}}\left(\frac{\partial\, p_f}{\partial\, x_t} - \rho^{fR}\boldsymbol{g}\,\frac{\partial\, z^S}{\partial\, x_t}\right) \\ &= \frac{l^2}{4\mu_f}\boldsymbol{n}^T \cdot \boldsymbol{N}^{cse,u}\left(\frac{\partial\, p_f}{\partial\, x_t} - \rho^{fR}\boldsymbol{g}\,\frac{\partial\, z^S}{\partial\, x_t}\right)\end{aligned} \tag{6.109}$$

$$\frac{\partial(\tilde{v}_t^{D,S} l)}{\partial \boldsymbol{p}_f^{cse}} = \hat{k}_t l\left(\boldsymbol{B}^{cse1,p} \cdot \frac{1}{f(\xi)}\right) \tag{6.110}$$

$$\frac{\partial \tilde{v}_n^{D,S}}{\partial \boldsymbol{d}^{cse}} = -\frac{\partial \hat{k}_n}{\partial \boldsymbol{d}^{cse}}[[p_f^S]] = \frac{\partial \hat{k}_n}{\partial l}\boldsymbol{n}^T \cdot \boldsymbol{N}^{cse,u}[[p_f^S]] \tag{6.111}$$

$$\frac{\partial \tilde{v}_n^{D,S}}{\partial \boldsymbol{p}_f^{cse}} = -\hat{k}_n\frac{\partial [[p_f^S]]}{\partial \boldsymbol{p}_f^{cse}} = -\hat{k}_n \boldsymbol{N}^{csp2,p} \tag{6.112}$$

6.2 Biphasic partially saturated PM CIE model

The fracture is characterized by very high permeability and very low storage capacity, in contrast, the porous continuum is characterized by low permeability and high storage capacity.

6.2.1 Governing equations

6.2.1.1 Balance of linear momentum

The balance of linear momentum equation for the partially saturated continuum with discontinuity is written as

$$\begin{cases} \frac{\partial \sigma_{ij}}{\partial x_j} + \rho b_i = 0 & x_i \in \Omega \\ u_i = g_i^u & x_i \in \Gamma_g \\ \sigma_{ij}\nu_j = t_i^\sigma & x_i \in \Gamma_t \\ \sigma_{ij}'^{+} n_j^+ = T_i'^{+} & x_i \in S^+ \\ \sigma_{ij}'^{+} n_j^- = T_i'^{-} & x_i \in S^- \end{cases} \tag{6.113}$$

Apply weighting function w_i to the balance equation to get

$$\int_\Omega w_i \left(\frac{\partial \sigma_{ij}}{\partial x_j} + \rho b_i \right) dv = 0 \tag{6.114}$$

Use chain rule and apply divergence theorem to the 1st term of (6.114), then we have

$$\begin{aligned} \int_\Omega w_i \frac{\partial \sigma_{ij}}{\partial x_j} dv &= \int_\Omega \frac{\partial (w_i \sigma_{ij})}{\partial x_j} dv - \int_\Omega \frac{\partial w_i}{\partial x_j} \sigma_{ij} dv \\ &= \int_\Gamma w_i \sigma_{ij} \tilde{n}_j da - \int_\Omega \frac{\partial w_i}{\partial x_j} \sigma_{ij} dv \end{aligned} \tag{6.115}$$

where the boundary $\Gamma = \Gamma_t + \Gamma_g + S^+ + S^-$, thus,

$$\int_\Gamma w_i \sigma_{ij} \tilde{n}_j da = \int_{\Gamma_t} w_i \sigma_{ij} \nu_j da + \int_{\Gamma_g} w_i \sigma_{ij} \nu_j da + \int_{S^+} w_i^+ \sigma_{ij}^+ n_j^+ da + \int_{S^-} w_i^- \sigma_{ij}^- n_j^- da \tag{6.116}$$

the integral over the prescribed displacement boundary Γ_g, i.e. the 2nd term in (6.116) is equal to zero. For partially saturated biphasic mixture, Bishop's expression of the total stress tensor is

given as

$$\sigma_{ij} = \sigma'_{ij} + \chi s \delta_{ij} \tag{6.117}$$

$$\sigma^{+}_{ij} = \sigma'^{+}_{ij} + \chi^{+} s^{+} \delta_{ij} \tag{6.118}$$

$$\sigma^{-}_{ij} = \sigma'^{-}_{ij} + \chi^{-} s^{-} \delta_{ij} \tag{6.119}$$

where σ'_{ij}, σ'^{+}_{ij}, and σ'^{-}_{ij} are respectively the effective stress tensors on the continuum elements and interfaces S^{+} and S^{-}; χ, χ^{+}, and χ^{-} are respectively the material properties referred to as the effective stress parameters, which depend on the suction. s, s^{+}, and s^{-} are respectively the suctions of the continuum elements, S^{+} and S^{-}, and the suctions are defined as

$$s = p_g - p_w; \quad s^{+} = p^{+}_g - p^{+}_w; \quad s^{-} = p^{-}_g - p^{-}_w \tag{6.120}$$

where p_g, p^{+}_g, and p^{-}_g are pore gas pressures of bulk, S^{+} and S^{-}, and are assumed to be zero for partially saturated biphasic mixture, thus

$$s = -p_w; \quad s^{+} = -p^{+}_w; \quad s^{-} = -p^{-}_w \tag{6.121}$$

We define a averaged pore pressure on the interface element S as

$$p^{S}_w = \frac{1}{2}(p^{+}_w + p^{-}_w) \tag{6.122}$$

and a pore water pressure jump in the discontinuity

$$[[p_w]] = p^{-}_w - p^{+}_w \tag{6.123}$$

thus, for the biphasic formulation, we have

$$s^{S} = -p^{S}_w; \quad [[s]] = s^{-} - s^{+} = -[[p_w]] \tag{6.124}$$

Given p^{S}_w and $[[p_w]]$, p^{+}_w and p^{-}_w can be calculated as follows:

$$p^{+}_w = -\frac{1}{2}[[p_w]] + p^{S}_w; \quad p^{-}_w = \frac{1}{2}[[p_w]] + p^{S}_w; \tag{6.125}$$

correspondingly, the suctions on S^+ and S^- are written as

$$s^+ = -p_w^+ = \frac{1}{2}[[p_w]] - p_w^S; \quad s^- = -p_w^- = -\frac{1}{2}[[p_w]] - p_w^S \tag{6.126}$$

We make the following assumptions

$$\chi^+ = \chi^- = \chi^S = \frac{1}{2}(\chi^+ + \chi^-) \tag{6.127}$$

$$n_i^+ = -n_i^- = n_i \tag{6.128}$$

$$T_i'^{,+} = -T_i'^{,-} = T_i' \tag{6.129}$$

where the effective stress tensor on interface element T_i' is calculated through a constitutive model. then we can rewrite the surface integrals in (6.116)

$$\begin{aligned}
\int_{\Gamma_t} w_i \sigma_{ij} \nu_j da &= \int_{\Gamma_t} w_i \left(\sigma'_{ij} + \chi s \delta_{ij}\right) \nu_j da \\
&= \int_{\Gamma_t} w_i \sigma'_{ij} \nu_j da + \int_{\Gamma_t} \chi s w_i \delta_{ij} \nu_j da \\
&= \int_{\Gamma_t} w_i t_i^{\sigma'} da + \int_{\Gamma_t} \chi s w_i \nu_i da \qquad (6.130) \\
\int_{S^+} w_i^+ \sigma_{ij}^+ n_j^+ da &= \int_{S^+} w_i^+ T_i'^+ da + \int_{S^+} \chi^+ s^+ w_i^+ n_i^+ da \\
&= \int_S w_i^+ T_i' da + \int_S \chi^S s^{S,+} w_i^+ n_i da \qquad (6.131) \\
\int_{S^-} w_i^- \sigma_{ij}^- n_j^- da &= \int_{S^-} w_i^- T_i'^- da + \int_{S^-} \chi^- s^- w_i^- n_i^- da \\
&= \int_S -w_i^- T_i' da + \int_S \chi^S s^{S,-} w_i^- (-n_i) da \qquad (6.132)
\end{aligned}$$

Substituting (6.130), (6.131), and (6.132), and (6.126) into (6.116) yields

$$\begin{aligned}
\int_\Gamma w_i \sigma_{ij} \tilde{n}_j da &= \int_{\Gamma_t} w_i t_i^{\sigma'} da + \int_{\Gamma_t} \chi s w_i \delta_{ij} \nu_j da + \int_S \left(w_i^+ - w_i^-\right) T_i' da \\
&\quad + \int_S w_i^+ \chi^S \left(\frac{1}{2}[[p_w]] - p_w^S\right) n_i da + \int_S w_i^- \chi^S \left(-\frac{1}{2}[[p_w]] - p_w^S\right) (-n_i) da \\
&= \int_{\Gamma_t} w_i t_i^{\sigma'} da - \int_{\Gamma_t} \chi p_w w_i \nu_i da - \int_S [[w_i]] T_i' da \\
&\quad + \int_S \chi^S n_i [[p_w^S]] \frac{1}{2} \left(w_i^+ + w_i^-\right) da + \int_S \chi^S p_w^S n_i \underbrace{\left(w_i^- - w_i^+\right)}_{[[w_i]]} da \qquad (6.133)
\end{aligned}$$

The 2nd term on the R.H.S. of (6.115) can be written as

$$\int_\Omega \frac{\partial w_i}{\partial x_j} \sigma_{ij} dv = \int_\Omega \frac{\partial w_i}{\partial x_j} \sigma'_{ij} dv - \int_\Omega \chi p_w \frac{\partial w_i}{\partial x_i} dv \tag{6.134}$$

where the effective stress tensor of the continuum σ'_{ij} will be calculate from the elastic or elasto-plastic constitutive model. Substitute (6.133) and (6.134) into (6.114) to obtain the balance of linear momentum of the continuum with discontinuity:

$$\int_\Omega \frac{\partial w_i}{\partial x_j}\sigma'_{ij}dv - \int_\Omega (\chi p_w)\frac{\partial w_i}{\partial x_i}dv + \int_{\Gamma_t}(\chi p_w)w_i\nu_i da + \int_S [[w_i]]T'_i da - \int_S (\chi^S p_w^S)[[w_i]]n_i da$$
$$\underbrace{-\int_S \frac{1}{2}\chi^S[[p_w]](w_i^+ + w_i^-)n_i da}_{Term1} = \int_\Omega \rho w_i b_i dv + \int_{\Gamma_t} w_i t_i^{\sigma'} da \tag{6.135}$$

(6.135) is similar to the balance of linear momentum equation of saturated condition, but note p_w is negative for the biphasic partially saturated mixture. "Term 1" needs to check further.

6.2.1.2 Balance of mass

The balance of mass equations for the discontinuity and bulk element are derived separately, assuming the discontinuity is also biphasic partially saturated mixture. Adding the two equations to obtain the balance of mass equation of the whole system. First, let us write the balance of mass for the continuum Ω,

$$S_w\frac{\partial \dot{u}_i}{\partial x_i} + n\frac{D^s S_w}{Dt} + \frac{\partial\left(\tilde{v}_w^D\right)_i}{\partial x_i} = 0 \quad (x_i \in \Omega) \tag{6.136}$$

Apply the weighting function ζ and integrate over the continuum domain Ω, the weak form is:

$$\int_\Omega \zeta S_w\frac{\partial \dot{u}_i}{\partial x_i}dv + \int_\Omega \zeta n\frac{\partial S_w}{\partial s}\frac{D^s s}{Dt}dv + \int_\Omega \zeta\frac{\partial\left(\tilde{v}_w^D\right)_i}{\partial x_i}dv = 0 \tag{6.137}$$

Apply the chain rule and divergence theorem to the last term of the left-hand side of (6.137),

$$\begin{aligned}\int_\Omega \zeta\frac{\partial\left(\tilde{v}_w^s\right)_i}{\partial x_i}dv &= \int_\Omega \frac{\partial\left(\zeta\tilde{v}_w^D\right)_i}{\partial x_i}dv - \int_\Omega \frac{\partial\zeta}{\partial x_i}\left(\tilde{v}_w^D\right)_i dv \\ &= \int_{\partial\Omega}\zeta\left(\tilde{v}_w^s\right)_i n_i da - \int_\Omega \frac{\partial\zeta}{\partial x_i}\left(\tilde{v}_w^D\right)_i dv\end{aligned} \tag{6.138}$$

where the boundary of the continuum is: $\partial\Omega = \Gamma_t + \Gamma_g$, thus

$$\int_{\partial\Omega}\zeta\left(\tilde{v}_w^D\right)_i n_i da = \int_{\Gamma_s}\zeta\left(\tilde{v}_w^D\right)_i n_i da + \int_{\Gamma_r}\zeta\left(\tilde{v}_w^D\right)_i n_i da \tag{6.139}$$

in which, Γ_s is the water flux boundary where $\left(\tilde{v}_w^D\right)_i n_i = -S^w$. On boundary Γ_r pore water pressure is prescribed, and $\zeta = 0$ on Γ_r.

Similar to (6.136), the balance equation for discontinuity S^l with the width of l is

$$S_w^S \frac{\partial \dot{u}_i}{\partial x_i} + n^S \frac{D^s S_w^S}{Dt} + \frac{\partial \tilde{v}_i^{D,S}}{\partial x_i} = 0, \quad x_i \in S^l \tag{6.140}$$

where S_w^S = degree of saturation of the crack, and n^S = porosity of the crack. $\tilde{v}_i^{D,S}$ $(i = t, n)$ is the tangential (t) or normal (n) component of superficial velocity of pore water flow in the crack. Here van-Genuchten model is adopted to relate the degree of saturation S_w^S and the suction s^S in the crack. Extended Darcy's velocity is applied to the tangential velocity of pore water flow in the crack,

$$\tilde{v}_t^{D,S} = \hat{k}_{rw}\, \hat{k}_t \left(\frac{\partial p_f^S}{\partial x_t} - \rho^{fR} \boldsymbol{g} \frac{\partial z^S}{\partial x_t} \right) \tag{6.141}$$

where $\hat{k}_{rw}$ and $\hat{k}_t$ are respectively relative permeability and absolute permeability of the crack in the tangential direction to the crack. The assumptions made here include: the absolute permeability of the crack domain S^l is higher than that of the continuum porous media domain Ω; the air entry value in the crack is lower than that in the continuum porous media; cubic law is used to estimate the absolute permeability of the crack in the tangential direction as follows:

$$\hat{k}_t = \frac{l^2}{12\mu_w} \tag{6.142}$$

where l = width of the crack; μ_w = dynamic viscosity of water with the unit of $Pa \cdot s$. The material time derivative of degree of saturation in (6.140) can be written as

$$\frac{D^s S_w^S}{Dt} = \frac{D^s S_w^S}{Ds^S} \frac{D^s s^S}{Dt} \tag{6.143}$$

The divergence of displacement in the crack is defined as (see (6.37)-(6.38)

$$\frac{\partial \dot{u}_i}{\partial x_i} = [[\dot{u}_n(\boldsymbol{x})]] \delta_S \tag{6.144}$$

and the divergence of velocity of water flow in the crack:

$$\frac{\partial \tilde{v}_i^{D,S}}{\partial x_i} = \frac{\partial \tilde{v}_n^{D,S}}{\partial x_n} + \frac{\partial \tilde{v}_t^{D,S}}{\partial x_t} \tag{6.145}$$

Apply weighting function ζ to (6.140) and integrate over the crack domain S^l, then we have

$$\int_{S^l} \zeta S_w^S [[\dot{u}_n]] \delta_S dv + \int_{S^l} \zeta n^S \frac{\partial S_w^S}{\partial s^S} \dot{s^S} dv + \int_{S^l} \zeta \frac{\partial \tilde{v}_i^{D,S}}{\partial x_i} dv = 0 \tag{6.146}$$

The first term on L.H.S. is:

$$\int_{S^l} \zeta S_w^S [[\dot{u}_n]] \delta_S dv = \int_S \zeta S_w^S [[\dot{u}_n]] da \tag{6.147}$$

Apply the divergence theorem:

$$\begin{aligned} \int_{S^l} \zeta \frac{\partial \tilde{v}_i^{D,S}}{\partial x_i} dv &= \int_{S^l} \frac{\partial \left(\zeta \tilde{v}_i^{D,S}\right)}{\partial x_i} dv - \int_{S^l} \frac{\partial \zeta}{\partial x_i} \tilde{v}_i^{D,S} dv \\ &= \int_{\partial S^l} \zeta \tilde{v}_i^{D,S} n_i da - \int_{S^l} \frac{\partial \zeta}{\partial x_i} \tilde{v}_i^{D,S} dv \end{aligned} \tag{6.148}$$

where the boundary of the crack S^l is $\partial S^l = S^+ + S^- + \Gamma_S$, and Γ_S is the end boundary which is perpendicular to S (see figure 6.4), and the outward normal vector of Γ_s is denoted as $\boldsymbol{\nu}$, and the water flux at $S_S^w = -\tilde{v}_i^{D,S} \nu_i$. S_S^w should not be confused with the degree of saturation of the crack S_w^S. Water flux at interfaces S^+ and S^- are respectively $\tilde{v}_n^{D,S^+} = \tilde{v}_i^{D,S} n_i^+$ and $\tilde{v}_n^{D,S-} = \tilde{v}_i^{D,S} n_i^-$. $\tilde{v}_n^{D,S} = \tilde{v}_n^{D,S^+} = -\tilde{v}_n^{D,S^-}$, and is defined as

$$\tilde{v}_n^{D,S} = \hat{k}_{rw} \hat{k}_n \left(p_w^+ - p_w^-\right) = -\hat{k}_{rw} \hat{k}_n [[p_w]] \tag{6.149}$$

where $\hat{k}_{rw}$ and $\hat{k}_n$ are respectively the relative and absolute permeability in the normal direction of the crack (or across the crack). Thus the 1st term in (6.148) is

$$\begin{aligned} \int_{\partial S^l} \zeta \tilde{v}_i^{D,S} n_i da &= \int_{S^+} \zeta^+ \tilde{v}_i^{D,S} n_i^+ da + \int_{S^-} \zeta^- \tilde{v}_i^{D,S} n_i^- da + \int_{\Gamma_S} \zeta \tilde{v}_i^{D,S} \nu_i da \\ &= \int_{S^+} \zeta^+ \tilde{v}_n^{D,S,+} da + \int_{S^-} \zeta^+ \tilde{v}_n^{D,S,-} da - \int_{\Gamma_S} \zeta S^{w,S} da \\ &= \int_S (\zeta^+ - \zeta^-) \tilde{v}_n^{D,S} da - \int_{\Gamma_S} \zeta S_S^w da \\ &= \int_S -[[\zeta]] \tilde{v}_n^{D,S} da - \int_{\Gamma_S} \zeta S_S^w da \end{aligned} \tag{6.150}$$

The 2nd term on the right-hand side of (6.148) is:

$$\int_{S^l} \frac{\partial \zeta}{\partial x_i} \tilde{v}_i^{D,S} dv = \int_{S^l} \frac{\partial \zeta}{\partial x_t} \tilde{v}_t^{D,S} dv + \int_{S^l} \frac{\partial \zeta}{\partial x_n} \tilde{v}_n^{D,S} dv \tag{6.151}$$

We assume:

$$\frac{\partial \zeta}{\partial x_n} = [[\zeta]] \delta_S \tag{6.152}$$

then the integral over S^l is converted to the integral over the interface surface S

$$\int_{S^l} \frac{\partial \zeta}{\partial x_n} \tilde{v}_n^{D,S} dv = \int_S [[\zeta]] \tilde{v}_n^{D,S} da \tag{6.153}$$

Substitute into (6.146) to obtain

$$\begin{aligned} &\int_S \zeta S_w^S [[\dot{u}_n]] da + \int_{S^l} \zeta n^S \dot{s}^S \frac{\partial S_w^S}{\partial s^S} dv - \int_S [[\zeta]] \tilde{v}_n^{D,S} da \\ &- \int_{\Gamma_S} \zeta S_S^w da - \int_{S^l} \frac{\partial \zeta}{\partial x_t} \tilde{v}_t^{D,S} dv - \int_S [[\zeta]] \tilde{v}_n^{D,S} da = 0 \end{aligned} \tag{6.154}$$

Combine with the weighted residual form of balance of mass equation of bulk, we obtain

$$\begin{aligned} &\int_S \zeta S_w^S [[\dot{u}_n]] da + \int_{S^l} \zeta n \dot{s}^S \frac{\partial S_w^S}{\partial s^S} dv - \int_{\Gamma_S} \zeta S^{w,S} da - \int_{S^l} \frac{\partial \zeta}{\partial x_t} \tilde{v}_t^{D,S} dv - 2 \int_S [[\zeta]] \tilde{v}_n^{D,S} da \\ &+ \int_\Omega \zeta S_w \frac{\partial \dot{u}_i}{\partial x_i} dv + \int_\Omega \zeta n \frac{\partial S_w}{\partial s} \frac{D^s s}{Dt} dv - \int_{\Gamma_s} \zeta S^w da - \int_\Omega \frac{\partial \zeta}{\partial x_i} \left(\tilde{v}_w^D \right)_i dv = 0 \end{aligned} \tag{6.155}$$

6.2.2 Finite element formulations

The finite element form of balance of linear momentum equation (6.135) is written as

$$\begin{aligned} &\mathop{\mathbf{A}}_{e=1}^{n_{\text{bel}}} (\boldsymbol{c}^e)^T \cdot \Bigg[\underbrace{\int_{\Omega^e} (\boldsymbol{B}^{e,u})^T \cdot \boldsymbol{\sigma}' dv}_{\boldsymbol{f}_e^{d,int}(\boldsymbol{d}^e)} - \underbrace{\int_{\Omega^e} \chi \left(\tilde{\boldsymbol{B}}^{e,u} \right)^T \cdot \boldsymbol{N}^{e,p} dv}_{\boldsymbol{k}_e^{dp1}(\boldsymbol{p}_w^e)} \cdot \boldsymbol{p}_w^e \\ &- \underbrace{\int_{\Omega^e} \rho \left(\boldsymbol{N}^{e,u} \right)^T \cdot \boldsymbol{b} \, dv}_{\boldsymbol{f}_e^{df,ext}(\boldsymbol{d}^e)} - \underbrace{\int_{\Gamma_t^e} (\boldsymbol{N}^{e,u})^T \, \boldsymbol{t}^{\sigma'} da}_{\boldsymbol{f}_e^{dt,ext}} + \underbrace{\int_{\Gamma_t^e} \chi \left(\boldsymbol{N}^{e,u} \right)^T \cdot \boldsymbol{\nu} \cdot \boldsymbol{N}^{e,p} da}_{\boldsymbol{k}_e^{dp2}(\boldsymbol{p}_w^e)} \cdot \boldsymbol{p}_w^e \Bigg] \\ &+ \mathop{\mathbf{A}}_{e=1}^{n_{\text{cel}}} (\boldsymbol{c}^{cse})^T \left[\underbrace{\int_{S^e} (\boldsymbol{N}^{cse,u})^T \cdot \boldsymbol{T}' da}_{\boldsymbol{f}_{cse}^{d,int}(\boldsymbol{d}^{cse})} - \underbrace{\int_{S^e} \chi^S \left(\boldsymbol{N}^{cse,u} \right)^T \cdot \boldsymbol{n} \cdot \boldsymbol{N}^{cse1,p} da}_{\boldsymbol{k}_{cse}^{dp}(\boldsymbol{p}_w^{cse})} \cdot \boldsymbol{p}_w^{cse} \right] = \boldsymbol{0} \end{aligned} \tag{6.156}$$

where n_{bel} denotes the number of bulk element; correspondingly, n_{cel} denotes the number of cohesive element. For now, the term "Term 1" is ignored; it needs to check that if it should be considered.

The finite element form of balance of mass equation (6.155) is:

$$\begin{aligned}
&\mathop{\mathbf{A}}_{e=1}^{n_{\text{bel}}}(\boldsymbol{\alpha}^e)^T\cdot\Bigg[\underbrace{\int_{\Omega^e}S_w\left(\boldsymbol{N}^{e,p}\right)^T\cdot\tilde{\boldsymbol{B}}^{e,u}dv}_{\boldsymbol{k}_e^{pd}}\cdot\dot{\boldsymbol{d}}^e-\underbrace{\int_{\Omega^e}\left(\boldsymbol{N}^{e,p}\right)^T n\frac{\partial S_w}{\partial s}\boldsymbol{N}^{e,p}dv}_{\boldsymbol{k}_e^{pp}(\boldsymbol{d}^e,\boldsymbol{p}_w^e)}\cdot\dot{\boldsymbol{p}_w}^e\\
&\qquad-\underbrace{\int_{\Omega^e}\left(\boldsymbol{B}^{e,p}\right)^T\cdot\tilde{\boldsymbol{v}}_w^D dv}_{\boldsymbol{f}_e^{p,int}(\boldsymbol{d}^e,\boldsymbol{p}_w^e)}-\underbrace{\int_{\Gamma_s^e}\left(\boldsymbol{N}^{e,p}\right)^T S^w dv}_{\boldsymbol{f}_e^{p,ext}}\Bigg]\\
+&\mathop{\mathbf{A}}_{e=1}^{n_{\text{cel}}}(\boldsymbol{\alpha}^{cse})^T\cdot\Bigg[\underbrace{\int_{S^e}S_w^S\left(\boldsymbol{N}^{cse1,p}\right)^T\boldsymbol{n}^T\cdot\boldsymbol{N}^{cse,u}da}_{\boldsymbol{k}_{cse}^{pd}}\cdot\dot{\boldsymbol{d}}^{cse}-\underbrace{\int_{S^e}\left(\boldsymbol{N}^{cse2,p}\right)^T\cdot(2\tilde{v}_n^{D,S})da}_{\boldsymbol{f}_{cse}^{p1,int}(\boldsymbol{d}^{cse},\boldsymbol{p}_f^{cse})}\\
&\qquad-\underbrace{\int_{S^{l,e}}\left(\boldsymbol{N}^{cse1,p}\right)^T n^S\frac{\partial S_w^S}{\partial s^S}\boldsymbol{N}^{cse1,p}dv}_{\boldsymbol{k}_{cse}^{pp}(\boldsymbol{d}^{cse},\boldsymbol{p}_w^{cse})}\cdot\dot{\boldsymbol{p}_w}^{cse}-\underbrace{\int_{S^{l,e}}\left(\boldsymbol{B}^{cse1,p}\right)^T\cdot\tilde{v}_t^{D,S}\,dv}_{\boldsymbol{f}_{cse}^{p2,int}(\boldsymbol{d}^{cse},\boldsymbol{p}_w^{cse})}\\
&\qquad-\int_{\Gamma_S^e}S^{w,S}da\Bigg]=\boldsymbol{0}
\end{aligned}\tag{6.157}$$

If we choose $\chi = S_w$ and $\chi^S = S_w^S$ respectively for the continuum and the discontinuity, then we have $\boldsymbol{k}_e^{dp1} = \left(\boldsymbol{k}_e^{pd}\right)^T$, and $\boldsymbol{k}_{cse}^{dp} = \left(\boldsymbol{k}_{cse}^{pd}\right)^T$. The surface integrals over the element of the crack surface S^e and the two end surfaces perpendicular to the crack Γ_S^e, as well as the volumetric integral over the crack volume S^l are implemented with axisymmetric formulations.

6.3 Elasto-plastic cohesive interface element (CIE) model

So far, the normal/shear constitutive model Carol et al. (1997) used for the poro-mechanical or thermo-poro-mechanical interface element does not include suction or temperature effects explicitly, i.e. F=F($\tilde{\boldsymbol{T}}'$,$\boldsymbol{q}$), G=G($\tilde{\boldsymbol{T}}'$,$\boldsymbol{q}$). We should further consider certain constitutive model to make F and G dependent on suction s^S and temperature θ^S of the discontinuity.

6.3.1 Traction-displacement model for geomaterials

The yield function F and potential function G that model post-bifurcation softening along the virtual discontinuity surface S is given as Carol et al. (1997) (we use f and g for the yield function and potential function respectively for the continuum.)

$$F = \sqrt{T_t'^2 + (c - \chi \tan\phi)^2} - (c - T_n' \tan\phi) \tag{6.158}$$

$$G = \sqrt{T_t'^2 + (c - \chi \tan\psi)^2} - (c - T_n' \tan\psi) \tag{6.159}$$

where

$$\chi = \chi_r + (\chi_p - \chi_r) \exp\left[-\alpha_\chi(\epsilon_n^p + \epsilon_s^p)\right] \tag{6.160}$$

$$c = c_r + (c_p - c_r) \exp\left[-\alpha_c(\epsilon_n^p + \epsilon_s^p)\right] \tag{6.161}$$

$$\tan\phi = \tan\phi_r + (\tan\phi_p - \tan\phi_r)\exp(-\alpha_\phi \epsilon_s^p) \tag{6.162}$$

$$\tan\psi = (\tan\psi_p)\exp(-\alpha_\psi \epsilon_s^p) \tag{6.163}$$

where

$$\epsilon_s^p = \int_0^t \dot{\epsilon}_s^p \, dt \tag{6.164}$$

$$\epsilon_n^p = \int_0^t \dot{\epsilon}_n^p \, dt \tag{6.165}$$

$$\dot{\epsilon}_s^p = \frac{sign(T_t')}{G_f^{II}} \langle |T_t'| - |T_n'^{,*} \tan\phi| \rangle \dot{u}_t^p \tag{6.166}$$

$$\dot{\epsilon}_n^p = \frac{1}{G_f^I} \langle T_n' \rangle \dot{u}_n^p \tag{6.167}$$

Where the local effective traction vector is $\tilde{\boldsymbol{T}}' = [T_t' \,;\, T_n']$. The rate of local plastic jump displacement vector $[[\dot{\tilde{\boldsymbol{u}}}^p]] = [\dot{u}_t^p \,;\, \dot{u}_n^p]$; χ = tensile strength; c = cohesion; ϕ = friction angle, ψ = dilation angle; G_f^I = the fracture energy when cracks occur under pure tension (Mode I); G_f^{II} = the fracture energy when cracks occur under shear and very high compression with no dilation allowed (asymptotic Mode II); and

$$\langle T_n' \rangle = \frac{T_n' + |T_n'|}{2}; \quad T_n'^{,*} = \frac{T_n' - |T_n'|}{2} \tag{6.168}$$

where $\langle T_n' \rangle \geq 0$ for tensile normal effective traction, and $\langle T_n' \rangle \leq 0$ for compressive normal effective traction We define the internal state variable vector as:

$$\boldsymbol{q} = [\chi, c, \tan\phi, \tan\psi]^T \tag{6.169}$$

and, $\alpha_\chi, \alpha_c, \alpha_\phi$ and α_ψ are material parameters that control the rate of softening of internal variables;

6.3.2 Implementation of elasto-plastic CIE model

For plastic loading of the interface $\dot{\gamma}_\delta > 0$, the rate forms employed in the elasto-plastic CIE model are presented as

$$\dot{\widetilde{\boldsymbol{T}}}' = \boldsymbol{K}^e \cdot [[\dot{\tilde{\boldsymbol{u}}}^e]] = \boldsymbol{K}^e \cdot \left([[\dot{\tilde{\boldsymbol{u}}}]] - [[\dot{\tilde{\boldsymbol{u}}}^p]] \right) \tag{6.170}$$

$$[[\dot{\tilde{\boldsymbol{u}}}^p]] = \dot{\gamma}_\delta \frac{\partial G(\widetilde{\boldsymbol{T}}', \boldsymbol{q})}{\partial \widetilde{\boldsymbol{T}}'} \tag{6.171}$$

$$\dot{\boldsymbol{q}} = \dot{\gamma}_\delta \boldsymbol{h}^q \tag{6.172}$$

$$\dot{F}(\widetilde{\boldsymbol{T}}', \boldsymbol{q}) = 0 \tag{6.173}$$

where $\boldsymbol{K}^e$ is the elastic modulus of the crack, and note the e denotes "elastic" instead of "element"; K_t and K_n are the tangential and normal stiffnesses, respectively, of the crack; $[[\tilde{\boldsymbol{u}}]] = [u_t \; u_n]^{\mathrm{T}}$ is the local jump displacement vector; $[[\tilde{\boldsymbol{u}}^e]] = [u_t^e \,;\, u_n^e]$ and $[[\tilde{\boldsymbol{u}}^p]] = [u_t^p \,;\, u_n^p]$ are respectively the local elastic and plastic jump displacement vectors; $\dot{\gamma}_\delta$ is the rate of plastic multiplier along the crack; F and G are yield and plastic potential functions, respectively; $\boldsymbol{q}$ is the internal state variable vector;

$\boldsymbol{h}^q$ is the softening function vector; and the elastic stiffness matrix of the crack takes the following form:

$$\boldsymbol{K}^e = \begin{bmatrix} K_t & 0 \\ 0 & K_n \end{bmatrix} \tag{6.174}$$

Integrating (6.170-6.171) by applying Backward Euler time integration gives

$$\Delta\widetilde{\boldsymbol{T}} = \boldsymbol{K}^e \cdot (\Delta[[\tilde{\boldsymbol{u}}]] - \Delta[[\tilde{\boldsymbol{u}}^p]]) \tag{6.175}$$

$$\Delta[[\tilde{\boldsymbol{u}}^p]] = \Delta\gamma_\delta \left(\partial G_{\widetilde{\mathrm{T}}'}\right)_{n+1} \tag{6.176}$$

$$\Delta\boldsymbol{q} = \Delta\gamma_\delta \boldsymbol{h}^q_{n+1} \tag{6.177}$$

$$F_{n+1} = 0 \tag{6.178}$$

where, the subscript $n+1$ denotes the current time step designator, and subscript n will be used as the previous time step designator in the following equations, such that

$$\Delta\widetilde{\boldsymbol{T}} = \widetilde{\boldsymbol{T}}_{n+1} - \widetilde{\boldsymbol{T}}_n \tag{6.179}$$

$$\Delta\boldsymbol{q} = \boldsymbol{q}_{n+1} - \boldsymbol{q}_n \tag{6.180}$$

and, $\Delta[[\tilde{\boldsymbol{u}}]]$ is calculated from global iteration for the CIE nodal displacements, and is kept constant during local iteration, i.e., $\delta(\Delta[[\tilde{\boldsymbol{u}}]]) = 0$, $\delta(\bullet) = (\bullet)^{k+1} - (\bullet)^k$ is the local Newton-Raphson increment, with $k+1$ the current iteration.

If we write (6.175-6.178) in residual form and leave off the current time step designator $n+1$, we will obtain

$$\boldsymbol{R} = \begin{bmatrix} \boldsymbol{R}_{\widetilde{\mathrm{T}}'} \\ \boldsymbol{R}_q \\ R_{\mathrm{F}} \end{bmatrix} = \begin{bmatrix} \Delta\widetilde{\boldsymbol{T}}' - \boldsymbol{K}^e \cdot \Delta[[\tilde{\boldsymbol{u}}]] + \Delta\gamma_\delta \boldsymbol{K}^e \cdot \partial G_{\widetilde{\boldsymbol{T}}'} \\ -\Delta\boldsymbol{q} + \Delta\gamma_\delta \boldsymbol{h}^q \\ F \end{bmatrix} = \boldsymbol{0} \tag{6.181}$$

We construct an unknown vector $\boldsymbol{X}$ and rewrite (6.181) in the following form

$$\boldsymbol{R}(\boldsymbol{X}) = \boldsymbol{0}; \quad \boldsymbol{X} = \begin{bmatrix} \widetilde{\boldsymbol{T}}' \\ \boldsymbol{q} \\ \Delta\gamma_\delta \end{bmatrix} \tag{6.182}$$

Recall (4.336) and calculate the consistent tangent operator:

$$\begin{aligned}\frac{\partial \boldsymbol{R}}{\partial \boldsymbol{X}} &= \begin{bmatrix} \frac{\partial \boldsymbol{R}_{\widetilde{\mathrm{T}}'}}{\partial \widetilde{\boldsymbol{T}}'} & \frac{\partial \boldsymbol{R}_{\widetilde{\mathrm{T}}'}}{\partial \boldsymbol{q}} & \frac{\partial \boldsymbol{R}_{\widetilde{\mathrm{T}}'}}{\partial \Delta\gamma_\delta} \\ \frac{\partial \boldsymbol{R}_q}{\partial \widetilde{\boldsymbol{T}}'} & \frac{\partial \boldsymbol{R}_q}{\partial \boldsymbol{q}} & \frac{\partial \boldsymbol{R}_q}{\partial \Delta\gamma_\delta} \\ \frac{\partial R_{\mathrm{F}}}{\partial \widetilde{\boldsymbol{T}}'} & \frac{\partial R_{\mathrm{F}}}{\partial \boldsymbol{q}} & \frac{\partial R_{\mathrm{F}}}{\partial \Delta\gamma_\delta} \end{bmatrix} \\ &= \begin{bmatrix} \mathbf{1} + \Delta\gamma_\delta \boldsymbol{K}^e \cdot \partial G_{\widetilde{\boldsymbol{T}}'\widetilde{\boldsymbol{T}}'} & \Delta\gamma_\delta \boldsymbol{K}^e \cdot \partial G_{\widetilde{\boldsymbol{T}}'\boldsymbol{q}} & \boldsymbol{K}^e \cdot \partial G_{\widetilde{\boldsymbol{T}}'} \\ \Delta\gamma_\delta \cdot \partial \boldsymbol{h}^q_{\widetilde{\boldsymbol{T}}'} & -\boldsymbol{I} + \Delta\gamma_\delta \cdot \partial \boldsymbol{h}^q_{\boldsymbol{q}} & \boldsymbol{h}^q \\ \partial F_{\widetilde{\boldsymbol{T}}'} & \partial F_{\boldsymbol{q}} & 0 \end{bmatrix} \end{aligned} \tag{6.183}$$

where,

$$\mathbf{1} = \begin{bmatrix} 1 & 0 \\ 0 & 1 \end{bmatrix}; \quad \boldsymbol{I} = \begin{bmatrix} 1 & 0 & 0 & 0 \\ 0 & 1 & 0 & 0 \\ 0 & 0 & 1 & 0 \\ 0 & 0 & 0 & 1 \end{bmatrix} \tag{6.184}$$

Applying the same approach used in (4.344) and (4.345) allows us to write

$$\begin{bmatrix} \boldsymbol{R}_{\widetilde{T}'} \\ \boldsymbol{R}_q \\ R_F \end{bmatrix} + \begin{bmatrix} \boldsymbol{A} & \boldsymbol{B} \\ \boldsymbol{C} & \mathbf{0} \end{bmatrix} \cdot \begin{bmatrix} \delta\widetilde{\boldsymbol{T}}' \\ \delta \boldsymbol{q} \\ \delta(\Delta\gamma_\delta) \end{bmatrix} = \begin{bmatrix} \mathbf{0} \\ \mathbf{0} \\ 0 \end{bmatrix} \tag{6.185}$$

where,

$$\boldsymbol{A} = \begin{bmatrix} \frac{\partial \boldsymbol{R}_{\widetilde{T}'}}{\partial \widetilde{\boldsymbol{T}}'} & \frac{\partial \boldsymbol{R}_{\widetilde{T}'}}{\partial \boldsymbol{q}} \\ \frac{\partial \boldsymbol{R}_q}{\partial \widetilde{\boldsymbol{T}}'} & \frac{\partial \boldsymbol{R}_q}{\partial \boldsymbol{q}} \end{bmatrix} = \begin{bmatrix} \mathbf{1} + \Delta\gamma_\delta \boldsymbol{K}^e \cdot \partial G_{\widetilde{\boldsymbol{T}}'\widetilde{\boldsymbol{T}}'} & \Delta\gamma_\delta \boldsymbol{K}^e \cdot \partial G_{\widetilde{\boldsymbol{T}}'\boldsymbol{q}} \\ \Delta\gamma_\delta \cdot \partial \boldsymbol{h}^q_{\widetilde{\boldsymbol{T}}'} & -\boldsymbol{I} + \Delta\gamma_\delta \cdot \partial \boldsymbol{h}^q_{\boldsymbol{q}} \end{bmatrix} \tag{6.186}$$

$$\boldsymbol{B} = \begin{bmatrix} \frac{\partial \boldsymbol{R}_{\widetilde{T}'}}{\partial \Delta\gamma} \\ \frac{\partial \boldsymbol{R}_q}{\partial \Delta\gamma} \end{bmatrix} = \begin{bmatrix} \boldsymbol{K}^e \cdot \partial G_{\widetilde{\boldsymbol{T}}'} \\ \boldsymbol{h}^q \end{bmatrix} \tag{6.187}$$

$$\boldsymbol{C} = \begin{bmatrix} \frac{\partial \boldsymbol{R}_F}{\partial \widetilde{\boldsymbol{T}}'} & \frac{\partial \boldsymbol{R}_F}{\partial \boldsymbol{q}} \end{bmatrix} = \begin{bmatrix} \partial F_{\widetilde{\boldsymbol{T}}'} & \partial F_{\boldsymbol{q}} \end{bmatrix} \tag{6.188}$$

The details of the derivatives are shown in Section 6.3.2.3. We can write the following results by following the same procedure through (4.346) to (4.350):

$$\delta(\Delta\gamma_\delta) = \frac{R_F - \boldsymbol{C} \cdot \boldsymbol{A}^{-1} \cdot \begin{bmatrix} \boldsymbol{R}_{\widetilde{T}'} \\ \boldsymbol{R}_q \end{bmatrix}}{\boldsymbol{C} \cdot \boldsymbol{A}^{-1} \cdot \boldsymbol{B}} \tag{6.189}$$

$$\begin{bmatrix} \delta\widetilde{\boldsymbol{T}}' \\ \delta\boldsymbol{q} \end{bmatrix} = -\boldsymbol{A}^{-1}\left(\begin{bmatrix} \boldsymbol{R}_{\widetilde{\mathrm{T}}'} \\ \boldsymbol{R}_q \end{bmatrix} + \delta(\Delta\gamma_\delta)\cdot\boldsymbol{B}\right) \tag{6.190}$$

With the solution of $\delta\boldsymbol{X}$, we can update $\boldsymbol{X}^k$ to obtain $\boldsymbol{X}^{k+1}$, then check if the convergence is satisfied, if not, go through the procedure again till convergence is satisfied.

$$(\widetilde{\boldsymbol{T}}')^{k+1} = (\widetilde{\boldsymbol{T}}')^k + \delta\widetilde{\boldsymbol{T}}' \tag{6.191}$$

$$(\boldsymbol{q})^{k+1} = (\boldsymbol{q})^k + \delta\boldsymbol{q} \tag{6.192}$$

$$(\Delta\gamma_\delta)^{k+1} = (\Delta\gamma_\delta)^k + \delta(\Delta\gamma_\delta) \tag{6.193}$$

where, k denotes the local iteration number designator.

6.3.2.1 Formulation of softening function $\boldsymbol{h}^q$

Let us formulate the expression for the softening function $\boldsymbol{h}^q$. According to (6.169), (6.171) and (6.172), we can write

$$\dot{\boldsymbol{q}} = \frac{\partial\boldsymbol{q}}{\partial\tilde{\boldsymbol{\epsilon}}^p}\frac{\partial\tilde{\boldsymbol{\epsilon}}^p}{\partial[[\tilde{\boldsymbol{u}}^p]]}[[\dot{\tilde{\boldsymbol{u}}}^p]] = \dot{\gamma}_\delta\frac{\partial\boldsymbol{q}}{\partial\tilde{\boldsymbol{\epsilon}}^p}\frac{\partial\tilde{\boldsymbol{\epsilon}}^p}{\partial[[\tilde{\boldsymbol{u}}^p]]}\frac{\partial G}{\partial\widetilde{\boldsymbol{T}}'} \tag{6.194}$$

$$\text{and, } \boldsymbol{h}^q = \frac{\partial\boldsymbol{q}}{\partial\tilde{\boldsymbol{\epsilon}}^p}\frac{\partial\tilde{\boldsymbol{\epsilon}}^p}{\partial[[\tilde{\boldsymbol{u}}^p]]}\partial G_{\tilde{\boldsymbol{T}}'} \tag{6.195}$$

where,

$$\tilde{\boldsymbol{\epsilon}}^p = \begin{bmatrix} \epsilon_s^p \\ \epsilon_n^p \end{bmatrix};\quad [[\tilde{\boldsymbol{u}}^p]] = \begin{bmatrix} u_t^p \\ u_n^p \end{bmatrix};\quad \partial G_{\tilde{\boldsymbol{T}}'} = \begin{bmatrix} \frac{\partial G}{\partial T_t'} \\ \frac{\partial G}{\partial T_n'} \end{bmatrix} \tag{6.196}$$

Thus, we can write the derivatives in (6.195) as

$$\frac{\partial\boldsymbol{q}}{\partial\tilde{\boldsymbol{\epsilon}}^p} = \begin{bmatrix} A_1 & A_2 \\ A_3 & A_4 \\ A_5 & A_6 \\ A_7 & A_8 \end{bmatrix} = \begin{bmatrix} \frac{\partial\chi}{\partial\epsilon_s^p} & \frac{\partial\chi}{\partial\epsilon_n^p} \\ \frac{\partial c}{\partial\epsilon_s^p} & \frac{\partial c}{\partial\epsilon_n^p} \\ \frac{\partial\tan\phi}{\partial\epsilon_s^p} & \frac{\partial\tan\phi}{\partial\epsilon_n^p} \\ \frac{\partial\tan\psi}{\partial\epsilon_s^p} & \frac{\partial\tan\psi}{\partial\epsilon_n^p} \end{bmatrix} \tag{6.197}$$

$$\frac{\partial\tilde{\boldsymbol{\epsilon}}^p}{\partial[[\tilde{\boldsymbol{u}}^p]]} = \begin{bmatrix} B_1 & B_2 \\ B_3 & B_4 \end{bmatrix} = \begin{bmatrix} \frac{\partial\epsilon_s^p}{\partial u_t} & \frac{\partial\epsilon_s^p}{\partial u_n} \\ \frac{\partial\epsilon_n^p}{\partial u_t} & \frac{\partial\epsilon_n^p}{\partial u_n} \end{bmatrix} \tag{6.198}$$

where according to (6.160)- (6.167), we can derive

$$A_1 = A_2 = (\chi_p - \chi_r)\exp\left[-\alpha_\chi(\epsilon_n^p + \epsilon_s^p)\right]\cdot(-\alpha_\chi) = -\alpha_\chi(\chi - \chi_r)$$

$$A_3 = A_4 = (c_p - c_r)\exp\left[-\alpha_c(\epsilon_n^p + \epsilon_s^p)\right]\cdot(-\alpha_c) = -\alpha_c(c - c_r)$$

$$A_5 = (\tan\phi_p - \tan\phi_r)\exp(-\alpha_\phi\epsilon_s^p)\cdot(-\alpha_\phi) = -\alpha_\phi(\tan\phi - \tan\phi_r)$$

$$A_6 = 0$$

$$A_7 = (\tan\psi_p)\exp(-\alpha_\psi\epsilon_s^p)\cdot(-\alpha_\psi) = -\alpha_\psi\tan\psi$$

$$A_8 = 0$$

$$B_1 = \frac{\partial\epsilon_s^p}{\partial u_t} = \frac{sign(T_t')}{G_f^{\mathrm{II}}}\langle|T_t'| - |T_n'^*\tan\phi|\rangle$$

$$B_2 = \frac{\partial\epsilon_s^p}{\partial u_n} = 0$$

$$B_3 = \frac{\partial\epsilon_n^p}{\partial u_t} = 0$$

$$B_4 = \frac{\partial\epsilon_n^p}{\partial u_n} = \frac{1}{G_f^{\mathrm{I}}}\langle T_n'\rangle$$

and $\boldsymbol{h}^q$ can be written as

$$\boldsymbol{h}^q = \begin{bmatrix} h^q(1) \\ h^q(2) \\ h^q(3) \\ h^q(4) \end{bmatrix} = \begin{bmatrix} A_1 & A_2 \\ A_3 & A_4 \\ A_5 & A_6 \\ A_7 & A_8 \end{bmatrix} \cdot \begin{bmatrix} B_1 & B_2 \\ B_3 & B_4 \end{bmatrix} \cdot \begin{bmatrix} \frac{\partial G}{\partial T_t'} \\ \frac{\partial G}{\partial T_n'} \end{bmatrix} \tag{6.199}$$

where

$$h^q(1) = A_1B_1\frac{\partial G}{\partial T_t'} + A_2B_4\frac{\partial G}{\partial T_n'}$$

$$h^q(2) = A_3B_1\frac{\partial G}{\partial T_t'} + A_4B_4\frac{\partial G}{\partial T_n'}$$

$$h^q(3) = A_5B_1\frac{\partial G}{\partial T_t'}$$

$$h^q(4) = A_7B_1\frac{\partial G}{\partial T_t'}$$

6.3.2.2 Consistent tangents of elasto-plastic interface element model

Write (6.181) using Backward Euler time integration method:

$$\boldsymbol{R}_{n+1} = \begin{bmatrix} \widetilde{\boldsymbol{T}}'_{n+1} - \widetilde{\boldsymbol{T}}'_{n} - \boldsymbol{K}^e \cdot [[\tilde{\boldsymbol{u}}]]_{n+1} + \boldsymbol{K}^e \cdot [[\tilde{\boldsymbol{u}}]]_n + \Delta\gamma_\delta \boldsymbol{K}^e \cdot (\partial G_{\widetilde{\boldsymbol{T}}'})_{n+1} \\ -\Delta\boldsymbol{q} + \Delta\gamma_\delta \boldsymbol{h}^q \\ F \end{bmatrix} = \boldsymbol{0} \tag{6.200}$$

Take the derivatives of $\boldsymbol{R}_{n+1}$ w.r.t. $[[\tilde{\boldsymbol{u}}]]_{n+1}$ and Multiply the first equation in (6.200) by $(\boldsymbol{K}^e)^{-1}$:

$$\begin{bmatrix} (\boldsymbol{K}^e)^{-1} \cdot \frac{\partial \widetilde{\boldsymbol{T}}'_{n+1}}{\partial [[\tilde{\boldsymbol{u}}]]_{n+1}} - \boldsymbol{1} + \frac{\partial G}{\partial \widetilde{\boldsymbol{T}}'_{n+1}} \otimes \frac{\partial \Delta\gamma_\delta}{\partial [[\tilde{\boldsymbol{u}}]]_{n+1}} + \Delta\gamma_\delta \left(\frac{\partial^2 G}{\partial \widetilde{\boldsymbol{T}}'^2_{n+1}} \frac{\partial \widetilde{\boldsymbol{T}}'_{n+1}}{\partial [[\tilde{\boldsymbol{u}}]]_{n+1}} + \frac{\partial^2 G}{\partial \widetilde{\boldsymbol{T}}'_{n+1} \partial \boldsymbol{q}_{n+1}} \frac{\partial \boldsymbol{q}_{n+1}}{\partial [[\tilde{\boldsymbol{u}}]]_{n+1}} \right) \\ \frac{\partial \boldsymbol{q}_{n+1}}{\partial [[\tilde{\boldsymbol{u}}]]_{n+1}} + \boldsymbol{h}^q_{n+1} \otimes \frac{\partial \Delta\gamma_\delta}{\partial [[\tilde{\boldsymbol{u}}]]_{n+1}} + \Delta\gamma_\delta \left(\frac{\partial \boldsymbol{h}^q_{n+1}}{\partial \widetilde{\boldsymbol{T}}'_{n+1}} \frac{\partial \widetilde{\boldsymbol{T}}'_{n+1}}{\partial [[\tilde{\boldsymbol{u}}]]_{n+1}} + \frac{\partial \boldsymbol{h}^q_{n+1}}{\partial \boldsymbol{q}_{n+1}} \frac{\partial \boldsymbol{q}_{n+1}}{\partial [[\tilde{\boldsymbol{u}}]]_{n+1}} \right) \\ \frac{\partial F}{\partial \widetilde{\boldsymbol{T}}'_{n+1}} \frac{\partial \widetilde{\boldsymbol{T}}'_{n+1}}{\partial [[\tilde{\boldsymbol{u}}]]_{n+1}} + \frac{\partial F}{\partial \boldsymbol{q}_{n+1}} \frac{\partial \boldsymbol{q}_{n+1}}{\partial [[\tilde{\boldsymbol{u}}]]_{n+1}} \end{bmatrix} = \boldsymbol{0}$$

Leave off the subscript $n+1$ and rewrite the above equation in the following form

$$\begin{bmatrix} (\boldsymbol{K}^e)^{-1} + \Delta\gamma_\delta \partial G_{\tilde{\boldsymbol{T}}'\tilde{\boldsymbol{T}}'} & \Delta\gamma_\delta \partial G_{\tilde{\boldsymbol{T}}'\boldsymbol{q}} & (\partial G_{\tilde{\boldsymbol{T}}'})^T \\ \Delta\gamma_\delta \partial \boldsymbol{h}^q_{\tilde{\boldsymbol{T}}'} & \boldsymbol{I} + \Delta\gamma_\delta \partial \boldsymbol{h}^q_{\boldsymbol{q}} & \boldsymbol{h}^q \\ \partial F_{\tilde{\boldsymbol{T}}'} & \partial F_{\boldsymbol{q}} & 0 \end{bmatrix} \cdot \begin{bmatrix} \frac{\partial \widetilde{\boldsymbol{T}}'}{\partial [[\tilde{\boldsymbol{u}}]]} \\ \frac{\partial \boldsymbol{q}}{\partial [[\tilde{\boldsymbol{u}}]]} \\ \frac{\partial \Delta\gamma_\delta}{\partial [[\tilde{\boldsymbol{u}}]]} \end{bmatrix} = \begin{bmatrix} \boldsymbol{1} \\ \boldsymbol{0}_4 \\ \boldsymbol{0}_1 \end{bmatrix} \tag{6.201}$$

where, $\boldsymbol{1}$ and $\boldsymbol{I}$ are the same as those in (6.184), and

$$\boldsymbol{0}_4 = \begin{bmatrix} 0 & 0 \\ 0 & 0 \\ 0 & 0 \\ 0 & 0 \end{bmatrix}; \quad \boldsymbol{0}_1 = \begin{bmatrix} 0 & 0 \end{bmatrix}$$

Note

$$\frac{\partial \widetilde{\boldsymbol{T}}'}{\partial [[\tilde{\boldsymbol{u}}]]} = \begin{bmatrix} \frac{\partial T'_t}{\partial u_t} & \frac{\partial T'_t}{\partial u_n} \\ \frac{\partial T'_n}{\partial u_t} & \frac{\partial T'_n}{\partial u_n} \end{bmatrix} \tag{6.202}$$

$$\frac{\partial \boldsymbol{q}}{\partial [[\tilde{\boldsymbol{u}}]]} = \begin{bmatrix} \frac{\partial \chi}{\partial u_t} & \frac{\partial \chi}{\partial u_n} \\ \frac{\partial c}{\partial u_t} & \frac{\partial c}{\partial u_n} \\ \frac{\partial \tan\phi}{\partial u_t} & \frac{\partial \tan\phi}{\partial u_n} \\ \frac{\partial \tan\psi}{\partial u_t} & \frac{\partial \tan\psi}{\partial u_n} \end{bmatrix} \tag{6.203}$$

$$\frac{\partial \Delta\gamma_\delta}{\partial[[\tilde{\boldsymbol{u}}]]} = \begin{bmatrix} \frac{\partial(\Delta\gamma_\delta)}{\partial u_t} & \frac{\partial(\Delta\gamma_\delta)}{\partial u_n} \end{bmatrix} \tag{6.204}$$

Using a similar approach as in Section 4.4.2, we set

$$\boldsymbol{A} = \begin{bmatrix} (\boldsymbol{K}^e)^{-1} + \Delta\gamma_\delta \partial G_{\widetilde{\boldsymbol{T}}'\widetilde{\boldsymbol{T}}'} & \Delta\gamma_\delta \partial G_{\widetilde{\boldsymbol{T}}'\boldsymbol{q}} \\ \Delta\gamma_\delta \partial \boldsymbol{h}^q_{\widetilde{\boldsymbol{T}}'} & \boldsymbol{I} + \Delta\gamma_\delta \partial \boldsymbol{h}^q_{\boldsymbol{q}} \end{bmatrix} \tag{6.205}$$

$$\boldsymbol{B} = \begin{bmatrix} (\partial G_{\widetilde{\boldsymbol{T}}'})^T \\ \boldsymbol{h}^q \end{bmatrix}; \quad \boldsymbol{C} = \begin{bmatrix} \partial F_{\widetilde{\boldsymbol{T}}'} & \partial F_{\boldsymbol{q}} \end{bmatrix} \tag{6.206}$$

The solution can then be written as

$$\frac{\partial(\Delta\gamma_\delta)}{\partial[[\tilde{\boldsymbol{u}}]]} = \frac{\boldsymbol{C}\cdot\boldsymbol{A}^{-1}\cdot\begin{bmatrix}\mathbf{1}\\ \mathbf{0}\end{bmatrix}}{\boldsymbol{C}\cdot\boldsymbol{A}^{-1}\cdot\boldsymbol{B}} \tag{6.207}$$

$$\begin{bmatrix} \frac{\partial \widetilde{\boldsymbol{T}}'}{\partial[[\tilde{\boldsymbol{u}}]]} \\ \frac{\partial \boldsymbol{q}}{\partial[[\tilde{\boldsymbol{u}}]]} \end{bmatrix} = \boldsymbol{A}^{-1}\left(\begin{bmatrix}\mathbf{1}\\ \mathbf{0}\end{bmatrix} - \boldsymbol{B}\cdot\frac{\partial \widetilde{\boldsymbol{T}}'}{\partial[[\tilde{\boldsymbol{u}}]]}\right) \tag{6.208}$$

where $\frac{\partial \widetilde{\boldsymbol{T}}'}{\partial[[\tilde{\boldsymbol{u}}]]}$ is the material interface consistent tangent used in (6.102).

6.3.2.3 Derivatives in elasto-plastic interface element model

Now let us formulate the derivatives. Set $Q_F = T_t'^2 + (c - \chi\tan\phi)^2$, and the derivatives of yield function F w.r.t $\widetilde{\boldsymbol{T}}'$ and $\boldsymbol{q}$ denoted by $\partial F_{\widetilde{\boldsymbol{T}}'}$ and $\partial F_{\boldsymbol{q}}$ are written as

$$\partial F_{\widetilde{\boldsymbol{T}}'} = \frac{\partial F}{\partial \widetilde{\boldsymbol{T}}'} = \begin{bmatrix} \frac{\partial F}{\partial T_t'} & \frac{\partial F}{\partial T_n'} \end{bmatrix} \tag{6.209}$$

$$\partial F_{\boldsymbol{q}} = \frac{\partial F}{\partial \boldsymbol{q}} = \begin{bmatrix} \frac{\partial F}{\partial \chi} & \frac{\partial F}{\partial c} & \frac{\partial F}{\partial \tan\phi} & \frac{\partial F}{\partial \tan\psi} \end{bmatrix} \tag{6.210}$$

$$\partial \boldsymbol{h}^q_{\boldsymbol{q}} = \frac{\partial \boldsymbol{h}^q}{\partial \boldsymbol{q}} = \begin{bmatrix} \frac{\partial h^q(1)}{\partial \chi} & \frac{\partial h^q(1)}{\partial c} & \frac{\partial h^q(1)}{\partial \tan\phi} & \frac{\partial h^q(1)}{\partial \tan\psi} \\ \frac{\partial h^q(2)}{\partial \chi} & \frac{\partial h^q(2)}{\partial c} & \frac{\partial h^q(2)}{\partial \tan\phi} & \frac{\partial h^q(2)}{\partial \tan\psi} \\ \frac{\partial h^q(3)}{\partial \chi} & \frac{\partial h^q(3)}{\partial c} & \frac{\partial h^q(3)}{\partial \tan\phi} & \frac{\partial h^q(3)}{\partial \tan\psi} \\ \frac{\partial h^q(4)}{\partial \chi} & \frac{\partial h^q(4)}{\partial c} & \frac{\partial h^q(4)}{\partial \tan\phi} & \frac{\partial h^q(4)}{\partial \tan\psi} \end{bmatrix} \tag{6.211}$$

$$\partial \boldsymbol{h}^q_{\widetilde{\boldsymbol{T}}'} = \frac{\partial \boldsymbol{h}^q}{\partial \widetilde{\boldsymbol{T}}'} = \begin{bmatrix} \frac{\partial h^q(1)}{\partial \partial T'_t} & \frac{\partial h^q(1)}{\partial \partial T'_n} \\ \frac{\partial h^q(2)}{\partial \partial T'_t} & \frac{\partial h^q(2)}{\partial \partial T'_n} \\ \frac{\partial h^q(3)}{\partial \partial T'_t} & \frac{\partial h^q(3)}{\partial \partial T'_n} \\ \frac{\partial h^q(4)}{\partial \partial T'_t} & \frac{\partial h^q(4)}{\partial \partial T'_n} \end{bmatrix} \tag{6.212}$$

$$\partial G_{\widetilde{\boldsymbol{T}}'} = \frac{\partial G}{\partial \widetilde{\boldsymbol{T}}'} = \begin{bmatrix} \frac{\partial G}{\partial T'_t} & \frac{\partial G}{\partial T'_n} \end{bmatrix} \tag{6.213}$$

$$\partial G_{\widetilde{\boldsymbol{T}}'\widetilde{\boldsymbol{T}}'} = \frac{\partial^2 G}{\partial \boldsymbol{T}' \partial \boldsymbol{T}'} = \begin{bmatrix} \frac{\partial^2 G}{\partial {T'_t}^2} & \frac{\partial^2 G}{\partial T'_t \partial T'_n} \\ \frac{\partial^2 G}{\partial T'_n \partial T'_t} & \frac{\partial^2 G}{\partial {T'_n}^2} \end{bmatrix} \tag{6.214}$$

$$\partial G_{\widetilde{\boldsymbol{T}}'\boldsymbol{q}} = \frac{\partial^2 G}{\partial \boldsymbol{T}' \partial \boldsymbol{q}} = \begin{bmatrix} \frac{\partial^2 G}{\partial T'_t \partial \chi} & \frac{\partial^2 G}{\partial T'_t \partial c} & \frac{\partial^2 G}{\partial T'_t \partial (\tan\phi)} & \frac{\partial^2 G}{\partial T'_t \partial (\tan\psi)} \\ \frac{\partial^2 G}{\partial T'_n \partial \chi} & \frac{\partial^2 G}{\partial T'_n \partial c} & \frac{\partial^2 G}{\partial T'_n \partial (\tan\phi)} & \frac{\partial^2 G}{\partial T'_n \partial (\tan\psi)} \end{bmatrix} \tag{6.215}$$

where,

$$\frac{\partial F}{\partial T'_t} = T'_t \cdot (Q_F)^{-0.5} \tag{6.216}$$

$$\frac{\partial F}{\partial T'_n} = \tan\phi \tag{6.217}$$

$$\frac{\partial F}{\partial \chi} = (c - \chi \tan\phi) \cdot (-\tan\phi) \cdot (Q_F)^{-0.5} \tag{6.218}$$

$$\frac{\partial F}{\partial c} = (c - \chi \tan\phi) \cdot (Q_F)^{-0.5} - 1 \tag{6.219}$$

$$\frac{\partial F}{\partial (\tan\phi)} = T'_n - (c - \chi \tan\phi) \cdot \chi \cdot (Q_F)^{-0.5} \tag{6.220}$$

$$\frac{\partial F}{\partial (\tan\psi)} = 0 \tag{6.221}$$

set $Q_G = {T'_t}^2 + (c - \chi \tan\psi)^2$, and the details are given as

$$\frac{\partial G}{\partial T'_t} = T'_t \cdot {Q_G}^{-0.5} \tag{6.222}$$

$$\frac{\partial G}{\partial T'_n} = \tan\psi \tag{6.223}$$

$$\frac{\partial^2 G}{\partial {T'_t}^2} = (c - \chi \tan\psi)^2 \cdot (Q_G)^{-1.5} \tag{6.224}$$

$$\frac{\partial^2 G}{\partial {T'_n}^2} = 0 \tag{6.225}$$

$$\frac{\partial^2 G}{\partial T'_t \partial T'_n} = \frac{\partial^2 G}{\partial T'_n \partial T'_t} = 0 \tag{6.226}$$

$$\frac{\partial^2 G}{\partial T'_t \partial \chi} = T'_t \cdot \tan\psi \cdot (c - \chi \tan\psi) \cdot (Q_G)^{-1.5} \tag{6.227}$$

$$\frac{\partial^2 G}{\partial T_t' \partial c} = -T_t' \cdot (c - \chi \tan\psi) \cdot (Q_G)^{-1.5} \tag{6.228}$$

$$\frac{\partial^2 G}{\partial T_t' \partial (\tan\phi)} = 0 \tag{6.229}$$

$$\frac{\partial^2 G}{\partial T_t' \partial (\tan\psi)} = T_t' \cdot \chi \cdot (c - \chi \tan\psi) \cdot (Q_G)^{-1.5} \tag{6.230}$$

$$\frac{\partial^2 G}{\partial T_n' \partial \chi} = \frac{\partial^2 G}{\partial T_n' \partial c} = \frac{\partial^2 G}{\partial T_n' \partial (\tan\phi)} = 0 \tag{6.231}$$

$$\frac{\partial^2 G}{\partial T_n' \partial (\tan\psi)} = 1 \tag{6.232}$$

Let us take the derivatives of $\boldsymbol{q}$ w.r.t T_t' and T_n'. Note that $A_1 - A_8$ are only functions of $\boldsymbol{q}$ not $\widetilde{\boldsymbol{T}}'$, i.e., $\frac{\partial A_a}{\partial \widetilde{\boldsymbol{T}}'} = \mathbf{0}$, where, $a = 1, \ldots, 8$. Also note $\frac{\partial B_4}{\partial T_t'} = 0$, thus

$$\frac{\partial q(1)}{\partial T_t'} = A_1 \frac{\partial B_1}{\partial T_t'} \frac{\partial G}{\partial T_t'} + A_1 B_1 \frac{\partial^2 G}{\partial T_t'^2} \tag{6.233}$$

$$\frac{\partial q(1)}{\partial T_n'} = A_1 \frac{\partial B_1}{\partial T_n'} \frac{\partial G}{\partial T_t'} + A_2 \frac{\partial B_4}{\partial T_n'} \frac{\partial G}{\partial T_n'} \tag{6.234}$$

$$\frac{\partial q(2)}{\partial T_t'} = A_3 \frac{\partial B_1}{\partial T_t'} \frac{\partial G}{\partial T_t'} + A_3 B_1 \frac{\partial^2 G}{\partial T_t'^2} \tag{6.235}$$

$$\frac{\partial q(2)}{\partial T_n'} = A_3 \frac{\partial B_1}{\partial T_n'} \frac{\partial G}{\partial T_t'} + A_4 \frac{\partial B_4}{\partial T_n'} \frac{\partial G}{\partial T_n'} \tag{6.236}$$

$$\frac{\partial q(3)}{\partial T_t'} = A_5 \frac{\partial B_1}{\partial T_t'} \frac{\partial G}{\partial T_t'} + A_5 B_1 \frac{\partial^2 G}{\partial T_t'^2} \tag{6.237}$$

$$\frac{\partial q(3)}{\partial T_n'} = A_5 \frac{\partial B_1}{\partial T_n'} \frac{\partial G}{\partial T_t'} \tag{6.238}$$

$$\frac{\partial q(4)}{\partial T_t'} = A_7 \frac{\partial B_1}{\partial T_t'} \frac{\partial G}{\partial T_t'} + A_7 B_1 \frac{\partial^2 G}{\partial T_t'^2} \tag{6.239}$$

$$\frac{\partial q(4)}{\partial T_n'} = A_7 \frac{\partial B_1}{\partial T_n'} \frac{\partial G}{\partial T_t'} \tag{6.240}$$

recall

$$|T_n'| = \text{sign}(T_n') T_n'$$

$$\langle T_n' \rangle = \frac{T_n' + |T_n'|}{2}$$

$$T_n'^* = \frac{T_n' - |T_n'|}{2} = \frac{1}{2}[1 - \text{sign}(T_n')] T_n'$$

$$\frac{\partial \langle T_n' \rangle}{\partial T_n'} = \frac{1}{2}[1 + \text{sign}(T_n')]$$

$$\frac{\partial T_n'^*}{\partial T_n'} = \frac{1}{2}[1 - \text{sign}(T_n')]$$

$$
\begin{aligned}
\text{set,} \quad & R = |T_t'| - |T_n'^{*} \tan\phi| \\
\text{thus,} \quad & \frac{\partial\langle R\rangle}{\partial R} = \frac{1}{2}[1+\text{sign}(R)] \\
& \frac{\partial R}{\partial T_t'} = \text{sign}(T_t'); \quad \frac{\partial R}{\partial T_n'} = -\text{sign}(T_n'^{*}\tan\phi)\cdot\tan\phi\cdot\frac{\partial T_n'^{*}}{\partial T_n'} \\
& \frac{\partial\langle R\rangle}{\partial T_t'} = \frac{1}{2}[1+\text{sign}(R)]\,\text{sign}(T_t') \\
& \frac{\partial\langle R\rangle}{\partial T_n'} = -\frac{1}{2}[1+\text{sign}(R)]\,\text{sign}(T_n'^{*}\tan\phi)\cdot\tan\phi\cdot\frac{\partial T_n'^{*}}{\partial T_n'}
\end{aligned}
$$

Then, we can write

$$
\begin{aligned}
\frac{\partial B_1}{\partial T_t'} &= \frac{\text{sign}(T_t')}{G_f^{\text{II}}}\frac{\partial\langle R\rangle}{\partial T_t'} = \frac{1}{2G_f^{\text{II}}}[1+\text{sign}(R)] \\
\frac{\partial B_1}{\partial T_n'} &= \frac{\text{sign}(T_t')}{G_f^{\text{II}}}\frac{\partial\langle R\rangle}{\partial T_n'} = -\frac{\text{sign}(T_t')}{4G_f^{\text{II}}}\cdot\tan\phi\cdot\text{sign}(T_n'^{*}\tan\phi)\cdot[1+\text{sign}(R)]\cdot[1-\text{sign}(T_n')] \\
\frac{\partial B_4}{\partial T_n'} &= \frac{1}{2G_f^{\text{I}}}(1+\text{sign}[T_n')]
\end{aligned}
$$

Now let us take the derivatives of $\boldsymbol{h}^q$ w.r.t $\boldsymbol{q}$. First we write down the nonzero derivatives of $A_1 \ldots A_8$ and $B_1 \ldots B_4$ w.r.t. $\boldsymbol{q}$:

$$\frac{\partial A_1}{\partial\chi} = \frac{\partial A_2}{\partial\chi} = -\alpha_\chi \tag{6.241}$$

$$\frac{\partial A_3}{\partial c} = \frac{\partial A_4}{\partial c} = -\alpha_c \tag{6.242}$$

$$\frac{\partial A_5}{\partial(\tan\phi)} = -\alpha_\phi \tag{6.243}$$

$$\frac{\partial A_7}{\partial(\tan\psi)} = -\alpha_\psi \tag{6.244}$$

$$\frac{\partial B_1}{\partial(\tan\phi)} = \frac{\text{sign}(T_t')}{G_f^{\text{II}}}\cdot\frac{\partial\langle R\rangle}{\partial R}\cdot\text{sign}(T_n'^{*}\tan\phi)\cdot T_n'^{*} \tag{6.245}$$

Thus,

$$
\begin{aligned}
\frac{\partial h^q(1)}{\partial\chi} =& \frac{\partial A_1}{\partial\chi}B_1\frac{\partial G}{\partial T_t'} + A_1\cancel{\frac{\partial B_1}{\partial\chi}}\frac{\partial G}{\partial T_t'} + A_1B_1\frac{\partial^2 G}{\partial T_t'\partial\chi} \\
&+ \frac{\partial A_2}{\partial\chi}B_4\frac{\partial G}{\partial T_n'} + A_2\cancel{\frac{\partial B_4}{\partial\chi}}\frac{\partial G}{\partial T_n'} + A_2B_4\cancel{\frac{\partial^2 G}{\partial T_n'\partial\chi}} \\
=& \frac{\partial A_1}{\partial\chi}B_1\frac{\partial G}{\partial T_t'} + A_1B_1\frac{\partial^2 G}{\partial T_t'\partial\chi} + \frac{\partial A_2}{\partial\chi}B_4\frac{\partial G}{\partial T_n'}
\end{aligned} \tag{6.246}
$$

$$\begin{aligned}\frac{\partial h^q(1)}{\partial c} =&\cancel{\frac{\partial A_1}{\partial c}}B_1\frac{\partial G}{\partial T_t'} + A_1\cancel{\frac{\partial B_1}{\partial c}}\frac{\partial G}{\partial T_t'} + A_1B_1\frac{\partial^2 G}{\partial T_t'\partial c}\\ &+\cancel{\frac{\partial A_2}{\partial c}}B_4\frac{\partial G}{\partial T_n'} + A_2\cancel{\frac{\partial B_4}{\partial c}}\frac{\partial G}{\partial T_n'} + A_2B_4\cancel{\frac{\partial^2 G}{\partial T_n'\partial c}}\\ =&A_1B_1\frac{\partial^2 G}{\partial T_t'\partial c}\end{aligned} \tag{6.247}$$

$$\begin{aligned}\frac{\partial h^q(1)}{\partial \tan\phi} =&\cancel{\frac{\partial A_1}{\partial(\tan\phi)}}B_1\frac{\partial G}{\partial T_t'} + A_1\frac{\partial B_1}{\partial(\tan\phi)}\frac{\partial G}{\partial T_t'} + A_1B_1\cancel{\frac{\partial^2 G}{\partial T_t'\partial(\tan\phi)}}\\ &+\cancel{\frac{\partial A_2}{\partial(\tan\phi)}}B_4\frac{\partial G}{\partial T_n'} + A_2\cancel{\frac{\partial B_4}{\partial(\tan\phi)}}\frac{\partial G}{\partial T_n'} + A_2B_4\cancel{\frac{\partial^2 G}{\partial T_n'\partial(\tan\phi)}}\\ =&A_1\frac{\partial B_1}{\partial(\tan\phi)}\frac{\partial G}{\partial T_t'}\end{aligned} \tag{6.248}$$

$$\begin{aligned}\frac{\partial h^q(1)}{\partial \tan\psi} =&\cancel{\frac{\partial A_1}{\partial(\tan\psi)}}B_1\frac{\partial G}{\partial T_t'} + A_1\cancel{\frac{\partial B_1}{\partial(\tan\psi)}}\frac{\partial G}{\partial T_t'} + A_1B_1\frac{\partial^2 G}{\partial T_t'\partial(\tan\psi)}\\ &+\cancel{\frac{\partial A_2}{\partial(\tan\psi)}}B_4\frac{\partial G}{\partial T_n'} + A_2\cancel{\frac{\partial B_4}{\partial(\tan\psi)}}\frac{\partial G}{\partial T_n'} + A_2B_4\frac{\partial^2 G}{\partial T_n'\partial(\tan\psi)}\\ =&A_1B_1\frac{\partial^2 G}{\partial T_t'\partial(\tan\psi)} + A_2B_4\frac{\partial^2 G}{\partial T_n'\partial(\tan\psi)}\end{aligned} \tag{6.249}$$

$$\begin{aligned}\frac{\partial h^q(2)}{\partial \chi} =&\cancel{\frac{\partial A_3}{\partial \chi}}B_1\frac{\partial G}{\partial T_t'} + A_3\cancel{\frac{\partial B_1}{\partial \chi}}\frac{\partial G}{\partial T_t'} + A_3B_1\frac{\partial^2 G}{\partial T_t'\partial \chi}\\ &+\cancel{\frac{\partial A_4}{\partial \chi}}B_4\frac{\partial G}{\partial T_n'} + A_4\cancel{\frac{\partial B_4}{\partial \chi}}\frac{\partial G}{\partial T_n'} + A_4B_4\cancel{\frac{\partial^2 G}{\partial T_n'\partial \chi}}\\ =&A_3B_1\frac{\partial^2 G}{\partial T_t'\partial \chi}\end{aligned} \tag{6.250}$$

$$\begin{aligned}\frac{\partial h^q(2)}{\partial c} =&\frac{\partial A_3}{\partial c}B_1\frac{\partial G}{\partial T_t'} + A_3\cancel{\frac{\partial B_1}{\partial c}}\frac{\partial G}{\partial T_t'} + A_3B_1\frac{\partial^2 G}{\partial T_t'\partial c}\\ &+\frac{\partial A_4}{\partial c}B_4\frac{\partial G}{\partial T_n'} + A_4\cancel{\frac{\partial B_4}{\partial c}}\frac{\partial G}{\partial T_n'} + A_4B_4\cancel{\frac{\partial^2 G}{\partial T_n'\partial c}}\\ =&\frac{\partial A_3}{\partial c}B_1\frac{\partial G}{\partial T_t'} + A_3B_1\frac{\partial^2 G}{\partial T_t'\partial c} + \frac{\partial A_4}{\partial c}B_4\frac{\partial G}{\partial T_n'}\end{aligned} \tag{6.251}$$

$$\begin{aligned}\frac{\partial h^q(2)}{\partial \tan\phi} =&\cancel{\frac{\partial A_3}{\partial(\tan\phi)}}B_1\frac{\partial G}{\partial T_t'} + A_3\frac{\partial B_1}{\partial(\tan\phi)}\frac{\partial G}{\partial T_t'} + A_3B_1\cancel{\frac{\partial^2 G}{\partial T_t'\partial(\tan\phi)}}\\ &+\cancel{\frac{\partial A_4}{\partial(\tan\phi)}}B_4\frac{\partial G}{\partial T_n'} + A_4\cancel{\frac{\partial B_4}{\partial(\tan\phi)}}\frac{\partial G}{\partial T_n'} + A_4B_4\cancel{\frac{\partial^2 G}{\partial T_n'\partial(\tan\phi)}}\\ =&A_3\frac{\partial B_1}{\partial(\tan\phi)}\frac{\partial G}{\partial T_t'}\end{aligned} \tag{6.252}$$

$$\begin{aligned}\frac{\partial h^q(2)}{\partial \tan\psi} =&\cancel{\frac{\partial A_3}{\partial(\tan\psi)}}B_1\frac{\partial G}{\partial T_t'} + A_3\cancel{\frac{\partial B_1}{\partial(\tan\psi)}}\frac{\partial G}{\partial T_t'} + A_3B_1\frac{\partial^2 G}{\partial T_t'\partial(\tan\psi)}\\ &+\cancel{\frac{\partial A_4}{\partial(\tan\psi)}}B_4\frac{\partial G}{\partial T_n'} + A_4\cancel{\frac{\partial B_4}{\partial(\tan\psi)}}\frac{\partial G}{\partial T_n'} + A_4B_4\frac{\partial^2 G}{\partial T_n'\partial(\tan\psi)}\\ =&A_3B_1\frac{\partial^2 G}{\partial T_t'\partial(\tan\psi)} + A_4B_4\frac{\partial^2 G}{\partial T_n'\partial(\tan\psi)} \qquad (6.253)\\ \frac{\partial h^q(3)}{\partial \chi} =&\cancel{\frac{\partial A_5}{\partial \chi}}B_1\frac{\partial G}{\partial T_t'} + A_5\cancel{\frac{\partial B_1}{\partial \chi}}\frac{\partial G}{\partial T_t'} + A_5B_1\frac{\partial^2 G}{\partial T_t'\partial \chi}\\ =&A_5B_1\frac{\partial^2 G}{\partial T_t'\partial \chi} \qquad (6.254)\\ \frac{\partial q(3)}{\partial c} =&\cancel{\frac{\partial A_5}{\partial c}}B_1\frac{\partial G}{\partial T_t'} + A_5\cancel{\frac{\partial B_1}{\partial c}}\frac{\partial G}{\partial T_t'} + A_5B_1\frac{\partial^2 G}{\partial T_t'\partial c}\\ =&A_5B_1\frac{\partial^2 G}{\partial T_t'\partial c} \qquad (6.255)\\ \frac{\partial h^q(3)}{\partial(\tan\phi)} =&\frac{\partial A_5}{\partial(\tan\phi)}B_1\frac{\partial G}{\partial T_t'} + A_5\frac{\partial B_1}{\partial(\tan\phi)}\frac{\partial G}{\partial T_t'} + A_5B_1\cancel{\frac{\partial^2 G}{\partial T_t'\partial(\tan\phi)}}\\ =&\frac{\partial A_5}{\partial(\tan\phi)}B_1\frac{\partial G}{\partial T_t'} + A_5\frac{\partial B_1}{\partial(\tan\phi)}\frac{\partial G}{\partial T_t'} \qquad (6.256)\\ \frac{\partial h^q(3)}{\partial(\tan\psi)} =&\cancel{\frac{\partial A_5}{\partial(\tan\psi)}}B_1\frac{\partial G}{\partial T_t'} + A_5\cancel{\frac{\partial B_1}{\partial(\tan\psi)}}\frac{\partial G}{\partial T_t'} + A_5B_1\frac{\partial^2 G}{\partial T_t'\partial(\tan\psi)}\\ =&A_5B_1\frac{\partial^2 G}{\partial T_t'\partial(\tan\psi)} \qquad (6.257)\\ \frac{\partial h^q(4)}{\partial \chi} =&\cancel{\frac{\partial A_7}{\partial \chi}}B_1\frac{\partial G}{\partial T_t'} + A_7\cancel{\frac{\partial B_1}{\partial \chi}}\frac{\partial G}{\partial T_t'} + A_7B_1\frac{\partial^2 G}{\partial T_t'\partial \chi}\\ =&A_7B_1\frac{\partial^2 G}{\partial T_t'\partial \chi} \qquad (6.258)\\ \frac{\partial h^q(4)}{\partial c} =&\cancel{\frac{\partial A_7}{\partial c}}B_1\frac{\partial G}{\partial T_t'} + A_7\cancel{\frac{\partial B_1}{\partial c}}\frac{\partial G}{\partial T_t'} + A_7B_1\frac{\partial^2 G}{\partial T_t'\partial c}\\ =&A_7B_1\frac{\partial^2 G}{\partial T_t'\partial c} \qquad (6.259)\\ \frac{\partial h^q(4)}{\partial(\tan\phi)} =&\cancel{\frac{\partial A_7}{\partial(\tan\phi)}}B_1\frac{\partial G}{\partial T_t'} + A_7\frac{\partial B_1}{\partial(\tan\phi)}\frac{\partial G}{\partial T_t'} + A_7B_1\cancel{\frac{\partial^2 G}{\partial T_t'\partial(\tan\phi)}}\\ =&A_7\frac{\partial B_1}{\partial(\tan\phi)}\frac{\partial G}{\partial T_t'} \qquad (6.260)\\ \frac{\partial h^q(4)}{\partial(\tan\psi)} =& \frac{\partial A_7}{\partial(\tan\psi)}B_1\frac{\partial G}{\partial T_t'} + A_7\cancel{\frac{\partial B_1}{\partial(\tan\psi)}}\frac{\partial G}{\partial T_t'} + A_7B_1\frac{\partial^2 G}{\partial T_t'\partial(\tan\psi)}\\ =&\frac{\partial A_7}{\partial(\tan\psi)}B_1\frac{\partial G}{\partial T_t'} + A_7B_1\frac{\partial^2 G}{\partial T_t'\partial(\tan\psi)} \qquad (6.261)\end{aligned}$$

6.4 Numerical example

Three numerical examples are set up in this section. The first two examples are designed to test the hydraulic (pore water pressure generation) and mechanical (elastic and plastic) performance of the fully saturated poro-mechanical CIE model, and the third one is designed to analyze liquid flow in a fractured partially saturated porous media. Linear isotropic elastic constitutive model is used for the bulk elements.

6.4.1 Case study of fully saturated poro-mechanical CIE

Two examples are set up to test the performance of the saturated poro-mechanical CIE model under compression and tension respectively.

6.4.1.1 Fully saturated PM CIE under compression

The dimensions and boundary conditions are indicated in Figure 6.5: two matrix blocks, each has a column of two bulk elements; initial vertical aperture $l_0 = 1cm$, and is represented by two cohesive interface elements, i.e. element 5 and element 6. The bottom and side surface are fixed in normal displacement, and are impermeable. Due to the axisymmetry, the axis boundary is fixed in r direction, and is impermeable. Water table is set at the top $z = 1m$ to represent a fully saturated condition. Effective traction $\boldsymbol{t}^{\sigma'} = 10kPa$ is applied on the top of the matrix ($\boldsymbol{t}^{\sigma} = \boldsymbol{t}^{\sigma'}$) at $z = 1m$ since $p_f = 0$ at $z = 1m$. Pore water pressure generation due to the gravity and traction in the matrix and the fracture are analyzed. The closing of the fracture under compression is observed.

Results: Figure 6.6 illustrates the changes of pore water pressure at different depths in the matrix and the fracture, i.e. $z = 0$ and $z = 0.5m$ at various radial distances $r = 0to1 + l$. In the matrix (node 13, 18, 25, and 30), pore water pressure builds up due to successive applications of gravity and traction, then dissipates with time, and eventually reaches hydrostatic steady state. While with the initial aperture $l_0 = 1cm$, the fracture behaves like an open channel saturated with water, therefore, the generation of pore water pressure is negligible within the crack (see the curves

for nodes 15, 16, 27, and 28). Figure 6.7 shows the vertical displacement change at different depths, i.e. $z = 1cm$ and $z = 0.5m$. Same displacements are observed within the matrix and the fracture at the same level, which implies no displacement jump in the tangential direction within the fracture, i,e, $u_t \approx 0$ (see Figure 6.8). Correspondingly, the tangential stress is almost zero as shown in Figure 6.9. Under the gravity and traction and with the horizontally fixed boundaries, the two compressed matrix blocks tend to push against each other, thus the closing of the crack, i.e. $u_n < 0$ in Figure 6.8. Correspondingly, the fracture is under compression state, i.e. $T_n < 0$ as shown in Figure 6.9. Figure 6.10 illustrates the evolution of the yield surface during the compression-dominated process. Yield surface does not change because only compressive elasticity occurs along the interface.

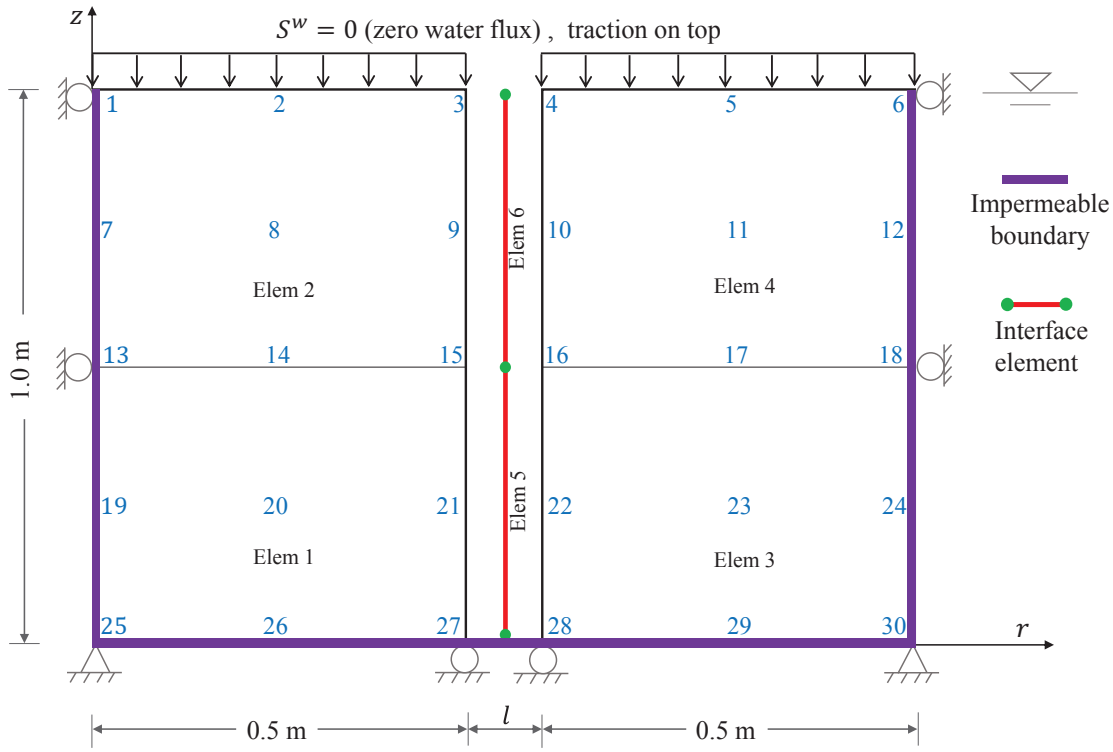

Figure 6.5: Axisymmetric finite element mesh for a fully saturated soil column with vertical fracture with initial aperture $l_0 = 1cm$: 30 nodes, four saturated Q9P4 PM bulk elements (Elem1-Elem4) and two Q6P4 PM CIEs (Elem5-Elem6). Gravity load is applied, and effective traction $\boldsymbol{t}^{\sigma'} = 10kPa$ is exerted on top.

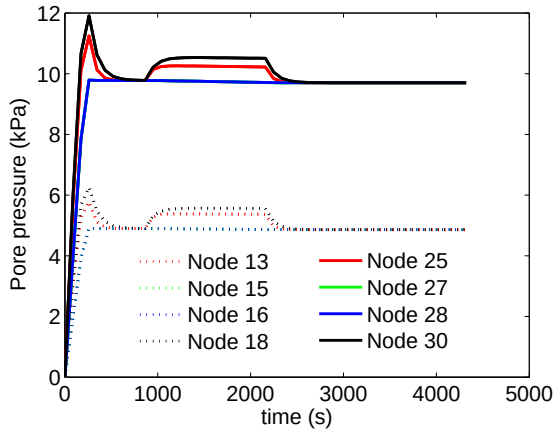

Figure 6.6: Pore water pressure.

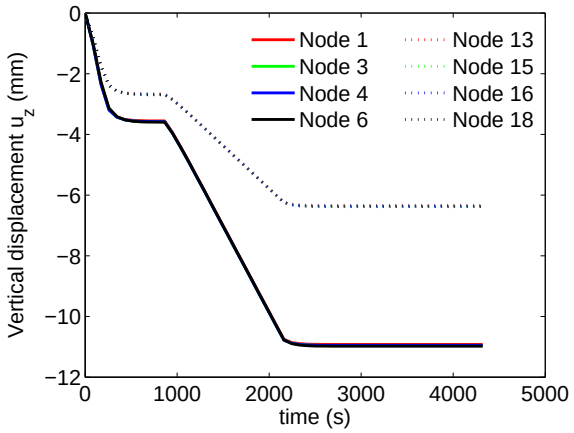

Figure 6.7: Vertical displacement.

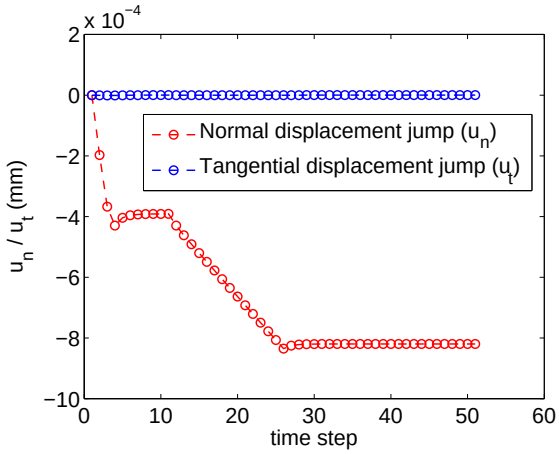

Figure 6.8: Variation of normal and tangential displacement jumps, i.e. u_n and u_t at the first (or lower) Gauss point of element 5 (CIE).

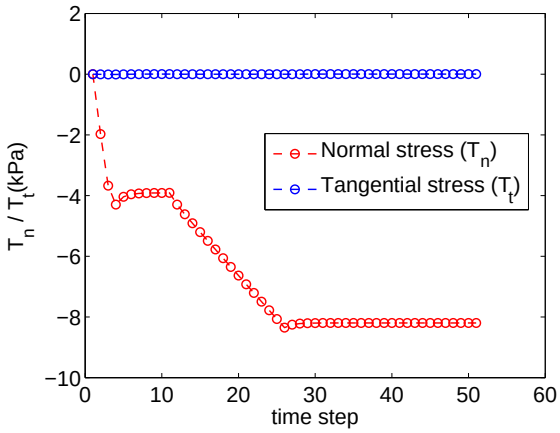

Figure 6.9: Variation of normal stress T_n and tangential stress T_t at the first (or lower) Gauss point of element 5 (CIE).

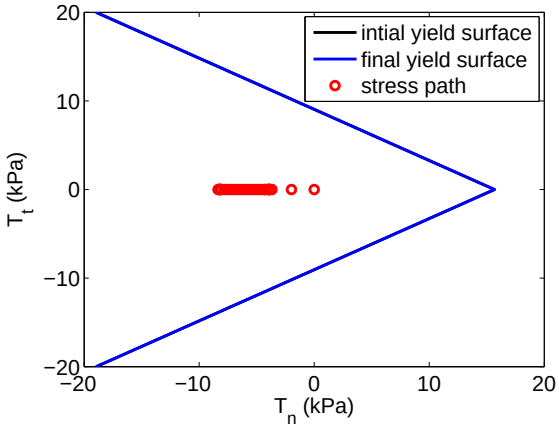

Figure 6.10: Stress path and yield surface evolution at the first (or lower) Gauss point of element 5 (CIE).

6.4.1.2 Fully saturated poro-mechanical CIEs under tension

The following example is set up to test the plastic performance of fully saturated poro-mechanical CIEs under tension. The elasto-plastic parameters for the cohesive interface element model are listed in Table 6.1. Different from the previous example, gravity and traction are not applied, the top is fixed vertically, and the side surface is prescribed with horizontal displacement $u_r = 1cm$ as shown in figure 6.11.

Results: Figure 6.12 shows negligible pore water pressure is observed during the opening of the crack. Figure 6.13 illustrates the horizontal displacements of the two FE facets at the bottom of the crack. At $t = 5hour$, the horizontal displacement difference starts to increase dramatically, which corresponds to the rise of the plastic normal displacement jump u_n^p as shown in Figure 6.14. In this tension-dominated process, the tangential displacement jump u_t is negligible in figure 6.14. In Figure 6.15, the normal effective stress T_n' increases with the normal displacement jump u_n inside the crack, and eventually reaches $\chi_p(Pa) = 3.464 \times 10^3$ (see Table 6.1) and triggers plasticity of the cohesive interface element. After that T_n' starts to decrease as the cohesive interface element softens which is illustrated by the shrinking of the yield surface in Figure 6.15.

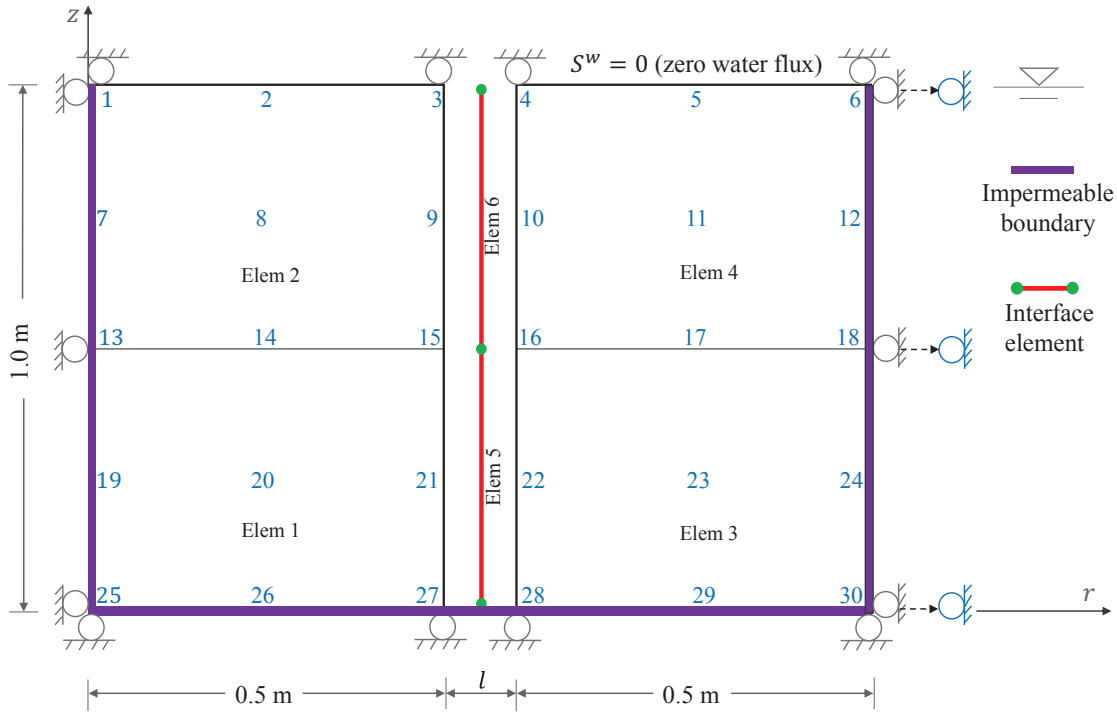

Figure 6.11: Axisymmetric finite element mesh for fully saturated fracture soil column with four saturated Q9P4 bulk poromechanical elements and two Q6P4 poromechanical CIEs. Initial vertical aperture $l_0 = 1 \times 10^{-5} m$, and prescribed horizontal displacement $u_r = 1cm$ is applied on the side surface at $r = 1 + l$.

Table 6.1: Parameters for elasto-plastic CIE model depicted in Figure 6.11.

Symbol(unit)	Value
$K_n(Pa/m)$	1×10^7
$K_t(Pa/m)$	1×10^7
$G_f^I(Pa \cdot m)$	1×10^4
$G_f^{II}(Pa \cdot m)$	1×10^4
$\chi_p(Pa)$	$c_p/tan(\phi_p) = 3.464 \times 10^3$
$\chi_r(Pa)$	0
$c_p(Pa)$	2000
$c_r(Pa)$	0
$\phi_p(rad)$	0.5236
$\phi_r(rad)$	0
$\psi_p(rad)$	0.087
α_χ	200
α_c	200
α_ϕ	900
α_ψ	900

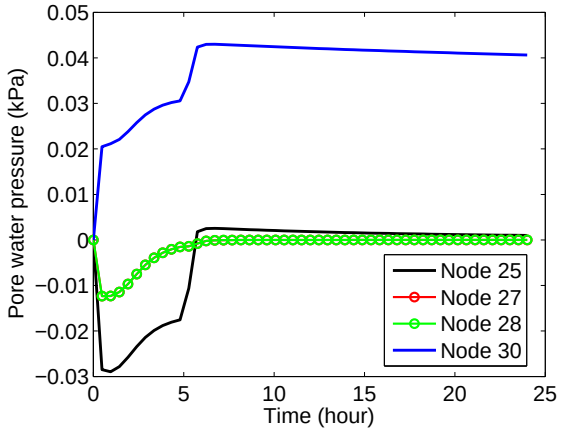

Figure 6.12: Variation of pore water pressure at the bottom, with gravity equal to zero.

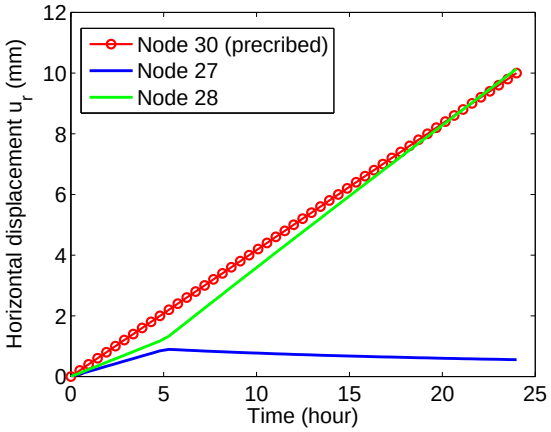

Figure 6.13: Variation of horizontal displacement at the bottom of the crack (node 27 or 28).

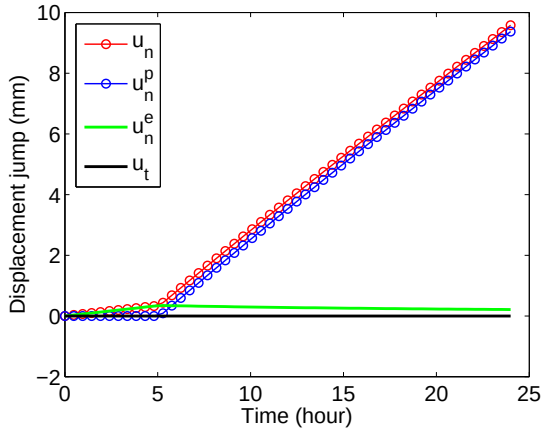

Figure 6.14: Plot of total normal, plastic normal, elastic normal, and total tangential displacement jumps, i.e. u_n, u_n^p, u_n^e, and u_t, at the first (or lower) Gauss point of element 5.

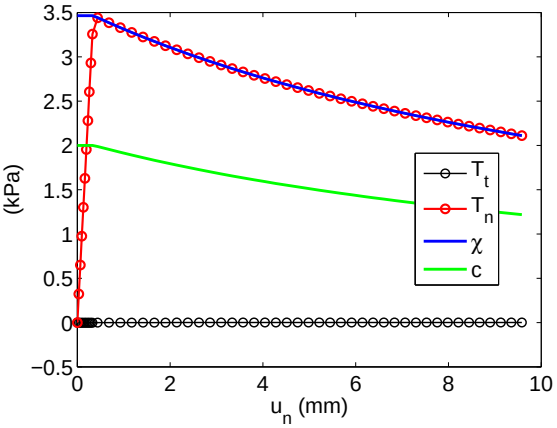

Figure 6.15: Plot of tangential effective stress T_t', normal effective stress T_n', and the plastic parameters χ and c in CIE model at the first (or lower) Gauss point of element 5.

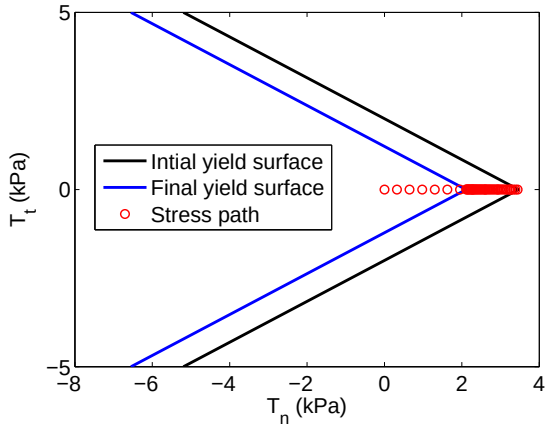

Figure 6.16: Stress path and yield surface evolution at the first (or lower) Gauss point of element 5.

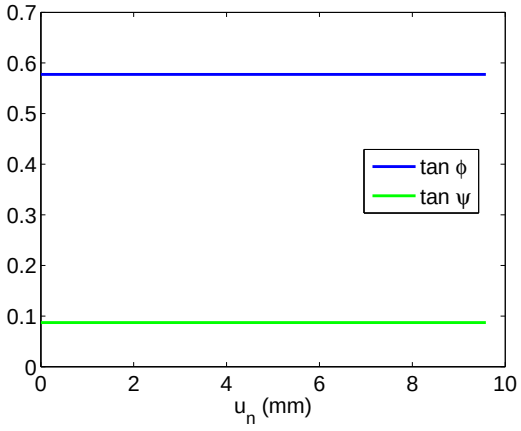

Figure 6.17: Variations of plastic variables $tan\phi$ and $tan\psi$ at the first (or lower) Gauss point of element 5.

6.4.1.3 Fluid injection into horizontal crack with crack opening

In this example, we consider a single horizontal crack with initial aperture $l_0 = 1mm$ in the middle of a saturated soil column. The axis, bottom, and side surface are fixed in normal displacement, and are impermeable. Water table is set at the top $z = 1.001m$, i.e., $p_w = 0$. At the beginning of the simulation, gravity $g = 9.8m/s^2$ is applied instantaneously, and fluid is injected from the surface as shown in Figure 6.18. The fluid injection lasts for 2 minutes with the rate $S^{w,S} = 18m/hour$. External traction is not applied, and the top is free to move under the gravity load and the fluid injection. we use the same parameters in Table 6.1. Figure 6.18 shows that 306 nodes and 72 elements in total are used in the FEA.

Results: In Figure 6.19, uniform positive normal displacement jump u_n within the horizontal crack implies that the crack opens evenly due to the fluid injection. The displacement jump in tangential direction is negligible. According to Figure 6.20, with the free top boundary, a rigid body movement is indicated for the top bulk elements, and no vertical movement is observed within the bottom bulk elements due to the fluid injection. Figure 6.21 shows that at a time of $\approx 0.52min$, softening elastoplasticity is enabled, thus, the tensile strength χ and cohesion c start to degrade as shown in Figure 6.27. Figure 6.23 shows that two-minute fluid injection induces an approximate increase of $7.5kPa$ in pore water within the crack, compared to the hydrostatic state.

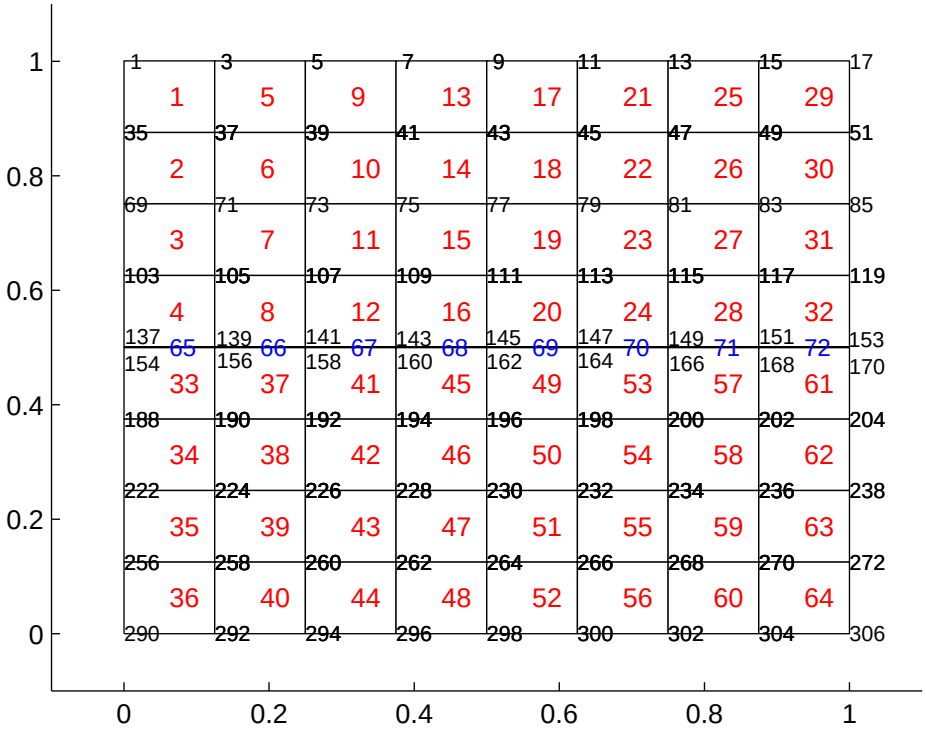

Figure 6.18: Axisymmetric FE mesh for saturated porous medium with a single horizontal crack. Sixty-four saturated Q9P4 bulk poromechanical elements (element 1-element 64) and eight Q6P4 poromechanical CIEs (element 65-element 72). Initial vertical aperture $l_0 = 1mm$. Gravity load is applied, and fluid is injected at the surface $r = 1m$ (nodes 153 and 170) with the rate $S^{w,S} = 18m/hour$.

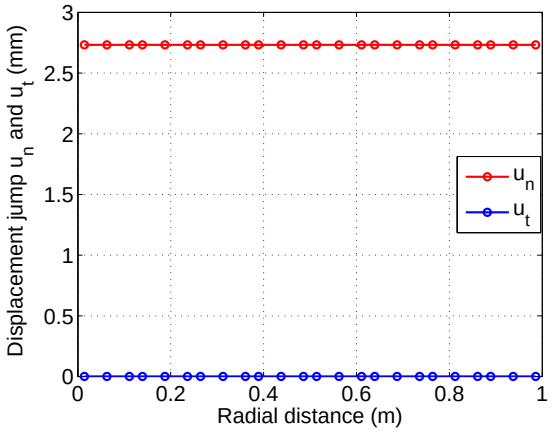

Figure 6.19: Normal and tangential displacement jumps (u_n and u_t) within the horizontal crack.

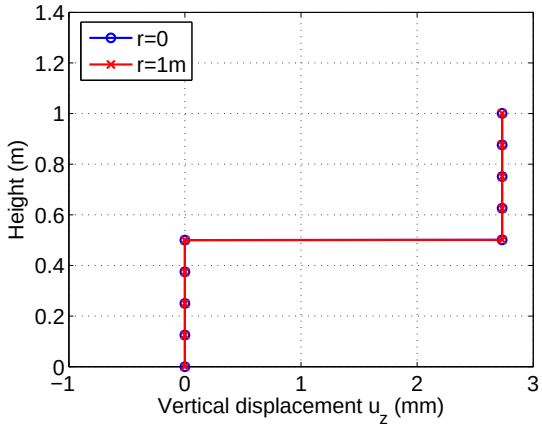

Figure 6.20: Variations of vertical displacement u_z along the axis $r = 0$ and the side surface $r = 1m$ at $t = 2min$.

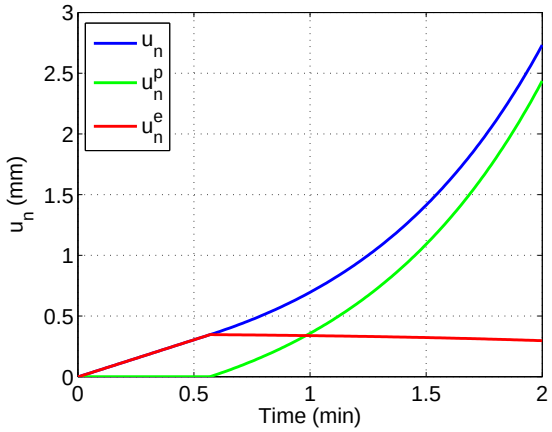

Figure 6.21: Variations of the normal displacement jump u_n as well as its plastic and elastic components (u_n^p and u_n^e) at the third Gauss point of element 72 (CIE).

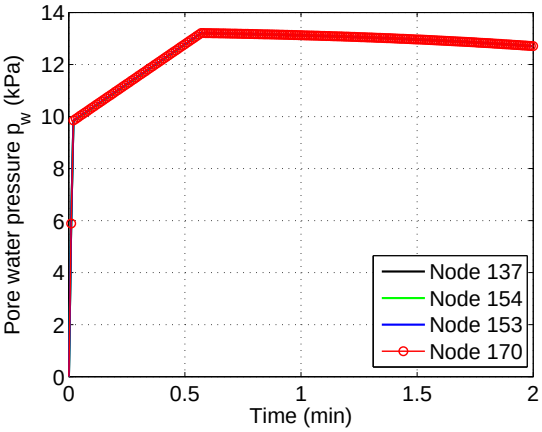

Figure 6.22: Variations of pore water pressure at the top (nodes 137 and 153) and the bottom (nodes 154 and 170) of the crack at $r = 0$ and $r = 1m$.

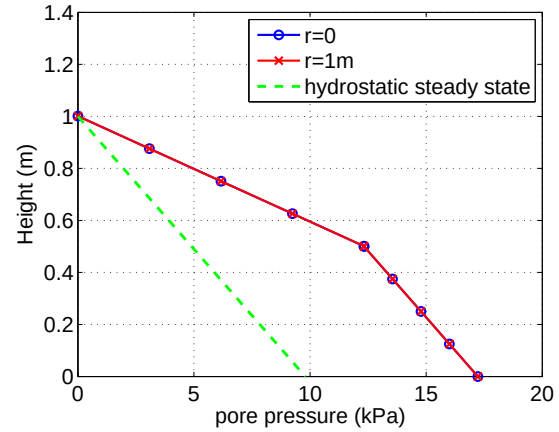

Figure 6.23: Variations of pore water pressure along the axis ($r = 0$) and the side surface $r = 1m$ at $t = 2min$, compared to the distribution under hydrostatic state .

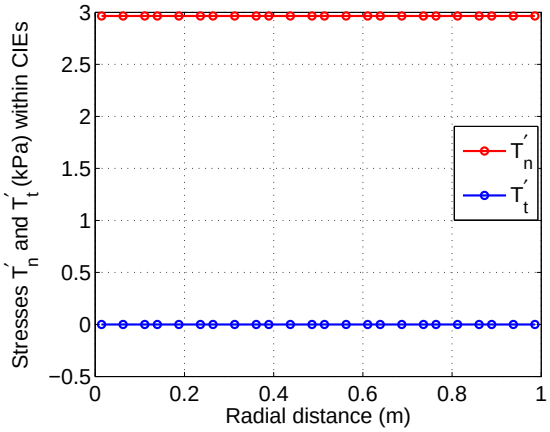

Figure 6.24: Effective normal and tangential stresses (T_n' and T_t') within the horizontal crack.

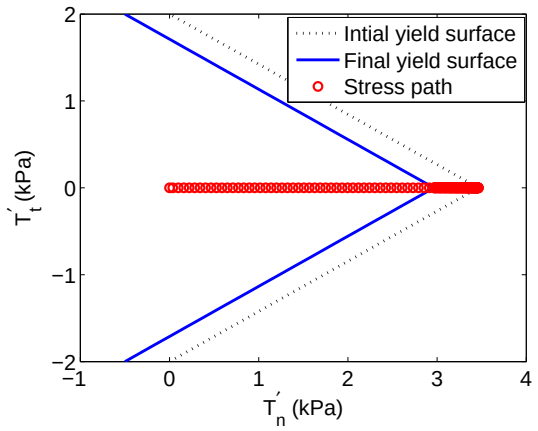

Figure 6.25: Stress path and yield surface evolution at the third Gauss point of element 72 (CIE).

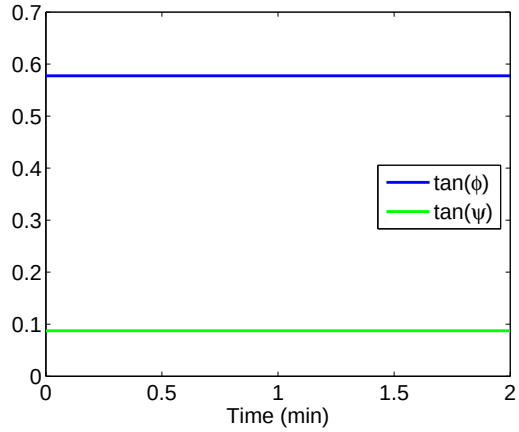

Figure 6.26: Variations of plastic variables $tan(\phi)$ and $tan(\psi)$ at the third Gauss point of element 72 (CIE).

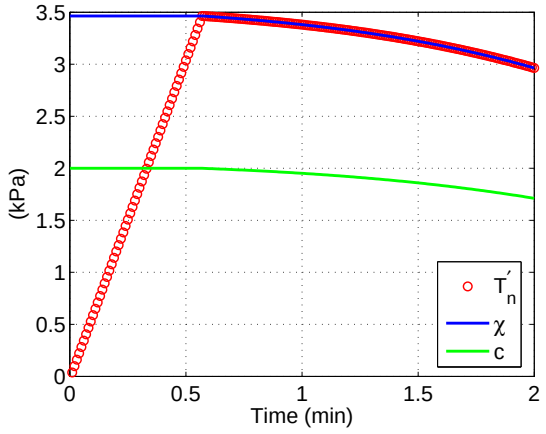

Figure 6.27: Variations of plastic variables χ and c at the third Gauss point of element 72 (CIE).

6.4.2 Case study of partially saturated poro-mechanical CIE

Assumptions: Certain assumptions imposed on the zero-thickness CIE model for partially saturated fractured porous media can be summarized as follows:

(1) The partially saturated fracture may be open or partly filled, and a constant porosity n^c which is larger than the porosity of the matrix is used during the evolution. The porosity of the porous matrix can change with the volumetric deformation of the solid skeleton. If the fracture is blocked, e.g., filled up with a different material, then our model can still handle it by treating the fracture also as porous medium, and assigning different material parameters.

(2) For longitudinal (or tangential) fluid flow in the fracture, a laminar flow is valid, thus cubic law is applied to saturated permeability, and Darcy's law is adopted for fluid flow.

(3) For hydraulic properties, van Genuchten model and relative permeability function (6.263) are applied to both the matrix and the fracture. The parameters for the fracture depend on the aperture of the fracture $l = l_0 + u_n$. But generally, the air entry value for the fracture is smaller than that for the matrix; the residual degree of saturation S_r is smaller than that of the matrix; the absolute permeability of the fracture is larger than that of the matrix. We might also consider that the parameter m in (6.263) for the fracture to be larger than that of the matrix in that m represents the slope as degree of saturation decreases with suction (see Figure 6.30), i.e. larger m corresponds to a steeper slope. It means that as the suction increases in the fractured porous media, the drying process in the fracture is faster than that in the matrix (solid skeleton porous medium).

6.4.2.1 Liquid flow in partially saturated fractured porous media

The geometry and boundary conditions of the test case are shown in Figure 6.33. A single horizontal aperture with a width of l lies in the middle of a porous medium. As indicated in Figure 6.34, two Q6P4 interface elements 17 and 18 and sixteen Q9P4 bulk elements are used to discretize the partially saturated single fractured soil column under an axisymmetric condition. An

instantaneous increase of suction is imposed on the bottom at $z = 0$. Due to axisymmetry of the problem, the axis $r = 0$ is impermeable and fixed in r direction. The top and side surfaces are also impermeable boundaries. The bottom and side surfaces are fixed respectively in the normal directions of z and r. An initially linear suction profile is assumed, as indicated by the black curve in Figure 6.36, and suction at the bottom is 10 kPa. A summary of parameters for the matrix and the fracture is given in Table 6.2. Linear elastic model is used for the bulk elements of the matrix, and an elasto-plastic model as described in Section 6.3.2.2 is used for the interface elements of the fracture, with the same parameters in Table 6.1. In the simulation, gravity load is ramped up to $9.8m/s^2$ for the first 10 days, and is kept constant during the following time span of 9610 days.

$$S_e = \frac{S_w - S_r}{S_s - S_r} = \left[\frac{1}{1 + (s/a)^n}\right]^m \tag{6.262}$$

$$K_{rw}(S_e) = \sqrt{S_e}\left[1 - (1 - S_e^{\frac{1}{m}})^m\right]^2 \tag{6.263}$$

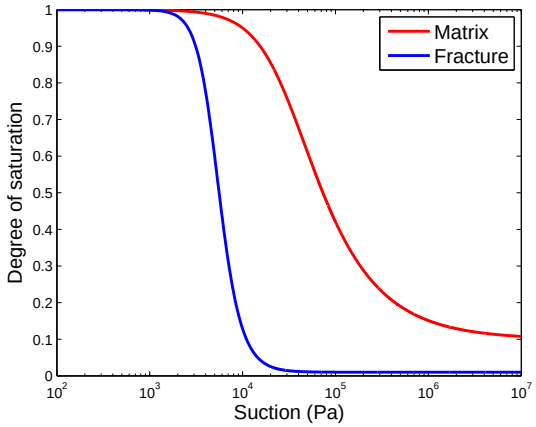

Figure 6.28: SWRCs of fracture and matrix with parameters in Table 6.2.

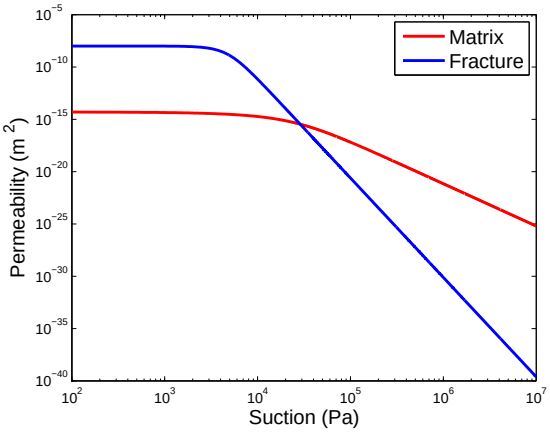

Figure 6.29: Permeabilities of partially saturated matrix and fracture with parameters in Table 6.2.

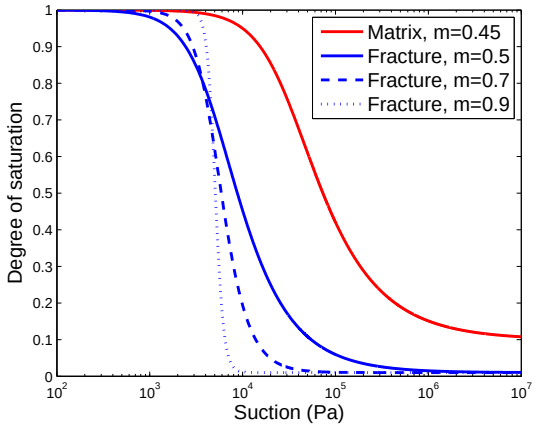

Figure 6.30: Comparison of SWRCs of fracture using different values of m.

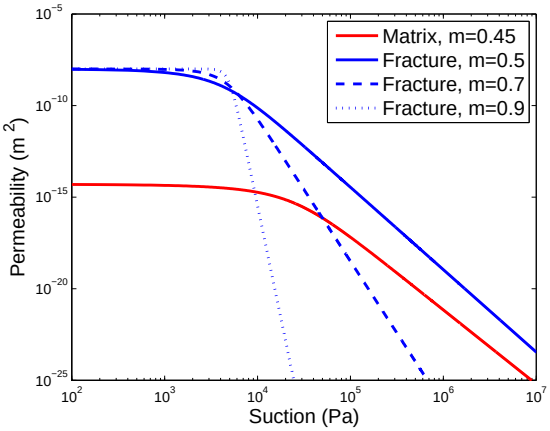

Figure 6.31: Comparison of Apparent permeability using different values of m.

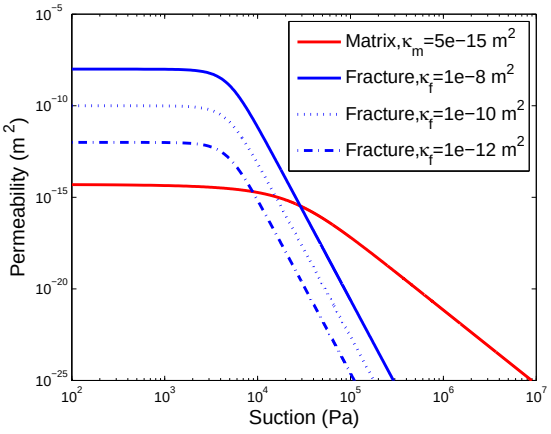

Figure 6.32: Apparent permeability versus suction for partially saturated matrix and fracture with different saturated permeabilities.

Table 6.2: Parameters for the partially saturated fracture and matrix.

Parameter	Symbol	Value
Matrix		
Initial porosity	n_0	0.42
Traction	$\boldsymbol{t}^{\sigma'}$	0 Pa
Young's modulus	E	$1 \times 10^6 Pa$
Poisson's ratio	ν	0.3
Specific gravity of soil particle	G_s	2.7
Saturated degree of saturation	S_s	1
Residual degree of saturation	S_r	0.1
van Genuchten parameter	a	30 kPa
van Genuchten parameter	n	1.818
van Genuchten parameter	$m = 1 - 1/n$	0.45
Saturated permeability	κ	$5 \times 10^{-15} m^2$
Fracture		
Porosity	n^S	0.75
Saturated degree of saturation	S_s^S	1
Residual degree of saturation	S_r^S	0.01
van Genuchten parameter	a_{van}^S	5 kPa
van Genuchten parameter	n_{van}^S	4
van Genuchten parameter	$m_{van}^S = 1 - 1/n_{van}^c$	0.75
Intrinsic permeability	κ^S	$1 \times 10^{-8} m^2$

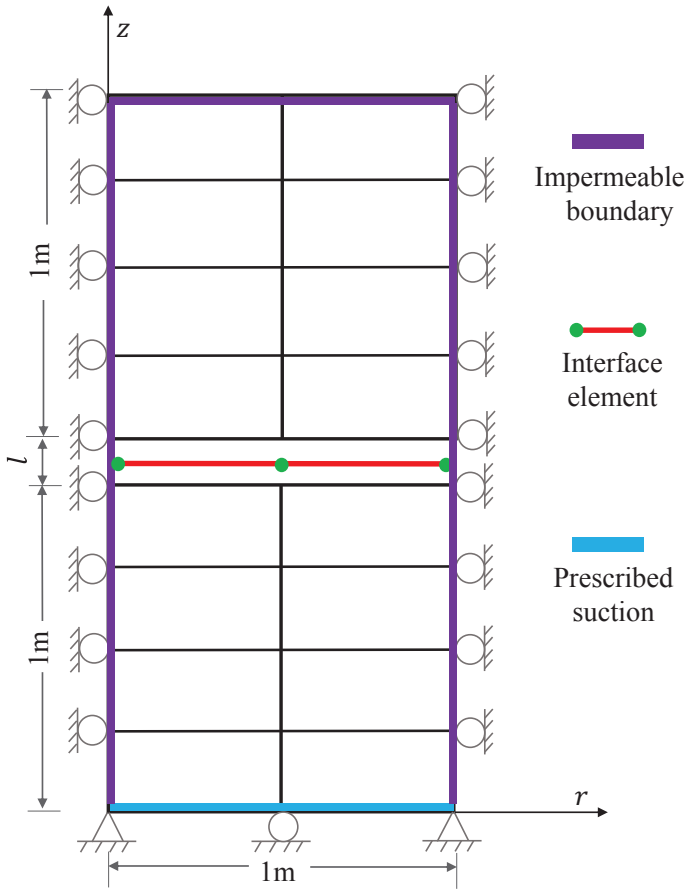

Figure 6.33: Sixteen partially saturated Q9P4 bulk poromechanical elements and two Q6P4 poromechanical interface elements for axisymmetric finite element mesh of horizontal crack with gravity load, and zero traction at the top surface.

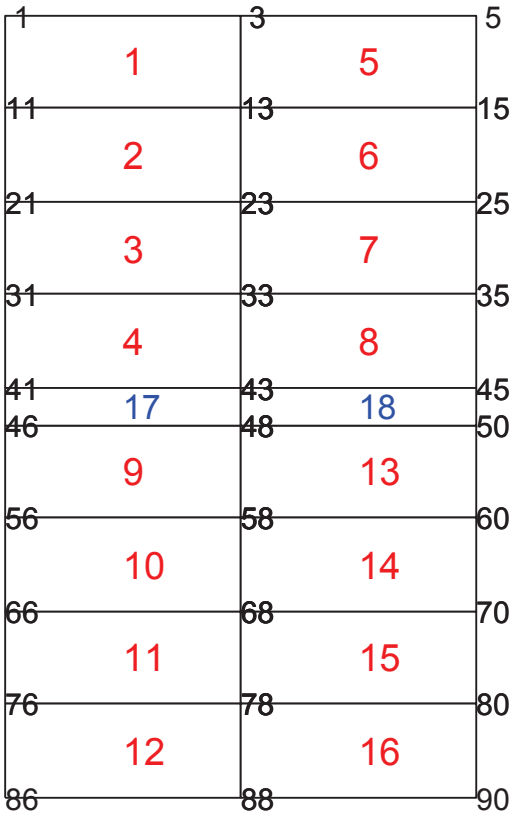

Figure 6.34: Finite element mesh with 16 bulk elements and 2 interface elements.

Results: Figures 6.35 and 6.36 show the influence of the aperture width on suction of the matrix and the fracture. Three different apertures are analyzed, i.e. $l_0 = 0.1cm$, $l_0 = 1cm$, and $l_0 = 10cm$. Although it is axisymmetric condition, the case is actually a one-dimensional problem. Thus the two columns of elements should behave exactly the same. Figure 6.35 plots suction at the top and the bottom of interface element 17, i.e. node 41 and node 46 (see Figure 6.34). Under the suction boundary condition at the bottom of the matrix, suction increases faster in the matrix below the fracture than the matrix above the fracture. The suction at the bottom of the crack will eventually arrive at the same steady sate value with the three different aperture widths. However, larger initial aperture width leads to a lower suction at the top of the crack. To explore the reason for this phenomena, we should know that the initially unsaturated fracture with larger aperture tends to desaturate faster as suction increases in the fracture. And as the fracture drains, air pockets will form along the surface of the fracture, thereby impeding the liquid flow between the adjacent matrix elements across the fracture and reducing the effective permeability for liquid flow normal to the fracture surface. The suctions are consistent within the fracture at the beginning of the drainage, i.e. no suction jump across the fracture. As the fracture becomes drier, it eventually loses the ability to transmit liquid flow, i.e. the matrix regions above and below the fracture are separated by the crack, and become independent of each other with respect to liquid flow, hence a suction jump between the top and the bottom of the fracture. For larger aperture, the foregoing process happens earlier, therefore, lower suction is kept in the matrix above the fracture. After the two matrix regions are separated by the fracture between them, a linear suction distribution with respect to height is reached within each of the matrix regions at the end of the simulation, with higher suction at higher elevation. Note that the same suction distribution is obtained within the matrix region below the fracture independent of the aperture width.

In Figure 6.37 and 6.36, we use fracture continuum intrinsic permeability κ^c with different magnitudes, i.e. $10^{-8}m^2$, $10^{-10}m^2$, and $10^{-12}m^2$, and keep the other parameters to simulate the same problem with the aperture equal to $1mm$. Lower κ^c corresponds to a lower ability to transmit the

liquid flow across the fracture, therefore, the suction jump between the top and the bottom of the fracture occurs earlier, and the matrix regions above and below the fracture become independent of each other thereafter. The other hydraulic parameters can also influence the flow field to a certain degree, which makes the sensitivity analysis necessary when knowledge of the hydraulic properties is incomplete.

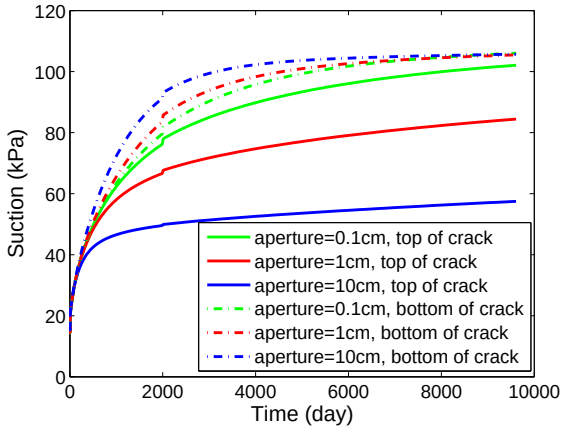

Figure 6.35: Variations of suction for partially saturated single fractured porous media with different initial apertures at the end of simulation.

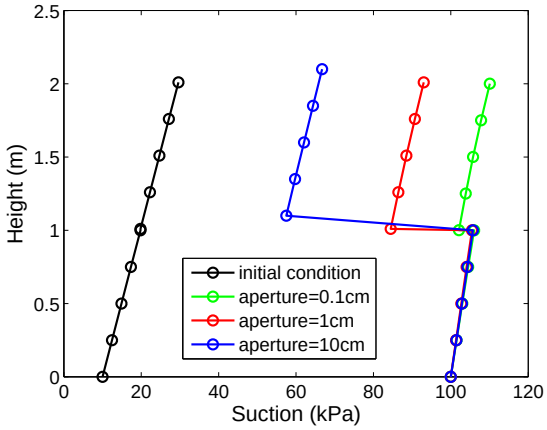

Figure 6.36: Variations of suction profiles for partially saturated single fractured porous media with different initial apertures.

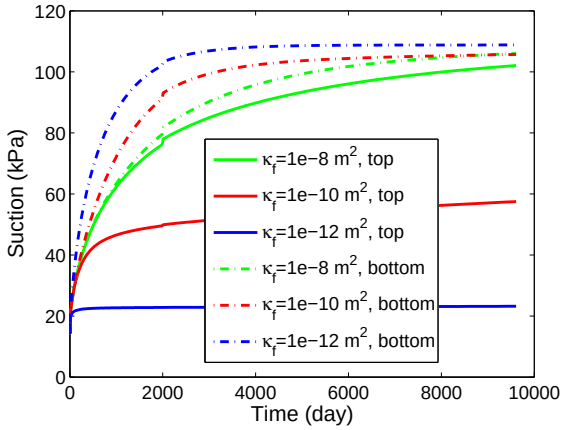

Figure 6.37: Variations of suction versus time for partially saturated single fractured porous media using different intrinsic permeabilities of the fracture.

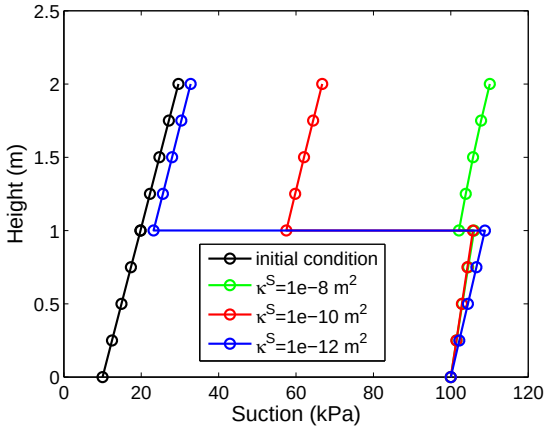

Figure 6.38: Comparisons of suction profiles for partially saturated single fractured porous media using different intrinsic permeabilities of fracture at the end of simulation.

Chapter 7

Fully and partially saturated thermo-poro-mechanical (TPM) cohesive interface element (CIE) models

7.1 Fully saturated thermo-poro-mechanical (TPM) interface element model

7.1.1 Governing equations for TPM CIE model

7.1.1.1 Balance of linear momentum

The weak form of balance of linear momentum equation for the continuum with discontinuity under nonisothermal condition is the same as the one under isothermal condition, except that the constitutive model for the effective stress tensor $\boldsymbol{\sigma}'$ is different due to the thermal effects.

7.1.1.2 Balance of mass

We first write the balance of mass equation for the discontinuity (of (3.24) for continuum):

$$\nabla \cdot \boldsymbol{v}^S + \nabla \cdot \tilde{\boldsymbol{v}}_f^{D,S} - \left[\beta_s^\theta (1 - n^S) + \beta_f^\theta n^S\right] \dot{\theta^S} - \beta_f^\theta \tilde{\boldsymbol{v}}_f^{D,S} \cdot (\nabla \theta^S) = 0 \,, \boldsymbol{x} \in S^l \tag{7.1}$$

where $\boldsymbol{v}^S$ is the velocity of solid skeleton in the discontinuity, n^S is the porosity of the fracture, and can be expressed as

$$\boldsymbol{v}^S = \dot{\boldsymbol{u}}^S(\boldsymbol{x}, t) = [[\dot{\boldsymbol{u}}(t)]] \, H_S(\boldsymbol{x}) \tag{7.2}$$

where t denotes time, instead of "tangential", and $[[\boldsymbol{u}]] := \boldsymbol{u}^{S^-} - \boldsymbol{u}^{S^+}$ is the jump in displacement across the discontinuity surface S, and it is possible for $[[\boldsymbol{u}]]$ to vary along S. But here it is assumed

to be constant with respect to $\boldsymbol{x}$ of a material point. And the Heaviside function is defined as

$$H_s = \begin{cases} 0 & \text{if} \boldsymbol{x} \in \Omega^- \\ 1 & \text{if} \boldsymbol{x} \in \Omega^+ \end{cases} \tag{7.3}$$

According to Regueiro (1998), the gradient of Heaviside $\nabla H_S = \boldsymbol{n}\delta_S$, where δ_S is the Dirac-delta function on S. The divergence of $\boldsymbol{v}$ can then be written as

$$\nabla \cdot \boldsymbol{v}^S = [[\dot{\boldsymbol{u}}(t)]]\boldsymbol{n}\,\delta_S \tag{7.4}$$

where n denotes the normal vector, which should not be confused with the porosity of the discontinuity n^S. $\tilde{\boldsymbol{v}}_f^{D,S}$ is Darcy's velocity of fluid flow in the discontinuity S, and its two components in the tangential and normal directions are respectively $\tilde{v}_t^{D,S}$ and $\tilde{v}_n^{D,S}$. Applying the weighting function ζ^S to (7.1), and integrating over the volume of crack S^l, we have

$$\int_{S^l} \zeta^S [[\dot{\boldsymbol{u}}]]\boldsymbol{n}\delta_S dv + \int_{S^l} \zeta^S \nabla\cdot\tilde{\boldsymbol{v}}_f^{D,S} dv - \int_{S^l} \zeta^S \left[\beta_s^\theta(1-n^S) + \beta_f^\theta n^S\right]\dot{\theta^S} dv - \int_{S^l} \zeta^S \beta_f^\theta \tilde{\boldsymbol{v}}_f^{D,S}\cdot(\nabla\theta^S) dv = 0 \tag{7.5}$$

Excluding the signs, let us derive the terms on the left hand side of (7.5)

$$\text{the 1st term} = \int_S \zeta^S \dot{u}_n da \tag{7.6}$$

$$\begin{aligned} \text{the 2nd term} &= \int_{S^l} \nabla\cdot(\zeta^S\tilde{\boldsymbol{v}}_f^{D,S}) dv - \int_{S^l} \tilde{\boldsymbol{v}}_f^{D,S}\cdot(\nabla\zeta^S) dv \\ &= \int_{\partial S^l} \zeta^S \tilde{\boldsymbol{v}}_f^{D,S}\cdot\tilde{\boldsymbol{n}} da - \int_{S^l}\left(\tilde{v}_t^{D,S}\frac{\partial\zeta^S}{\partial x_t} + \tilde{v}_n^{D,S}\frac{\partial\zeta^S}{\partial x_n}\right) dv \end{aligned} \tag{7.7}$$

$$\text{the 4th term} = \int_{S^l} \zeta^S \beta_f^\theta \left(\tilde{v}_t^{D,S}\frac{\partial\theta^S}{\partial x_t} + \tilde{v}_n^{D,S}\frac{\partial\theta^S}{\partial x_n}\right) dv \tag{7.8}$$

where $\tilde{n}_j$ is a generic normal vector to surface Γ, and $\Gamma = \Gamma_t + \Gamma_g + S^- + S^+$. Substitute into (7.5) to get the balance of mass equation for the discontinuity:

$$\begin{aligned} &\int_S \zeta^S [[\dot{u}_n]] da - 2\int_S [[\zeta]]\tilde{v}_n^{D,S} da - \int_{S^l} \zeta^S \left[\beta_s^\theta(1-n^S) + \beta_f^\theta n^S\right]\dot{\theta}^S dv - \int_{S^l} \zeta^S \beta_f^\theta \tilde{v}_t^{D,S}\frac{\partial\theta^S}{\partial x_t} dv \\ &- \int_S \zeta^S \beta_f^\theta \tilde{v}_n^{D,S}[[\theta]] da - \int_{S^l} \tilde{v}_t^{D,S}\frac{\partial\zeta^S}{\partial x_t} dv = \int_{\Gamma_S} \zeta^S S_{w,S} da \end{aligned} \tag{7.9}$$

Take ζ^S as an example, and we derive its gradient and apply the same rule to θ^S, φ^S, and p_f^S

$$\frac{\partial\zeta^S}{\partial x_t} = \frac{\partial\zeta^S}{\partial s} = \frac{\partial\zeta^S}{\partial\xi}\frac{\partial\xi}{\partial s} = \boldsymbol{B}^{cse1,p}\cdot\{\boldsymbol{\theta}^{cse}\} \tag{7.10}$$

$$\frac{\partial\zeta^S}{\partial x_n} = [[\zeta]]\delta_S \tag{7.11}$$

where, $\boldsymbol{\beta}^{cse}$ is nodal value vector of weighting function ζ^S. We can also write,

$$\dot{\theta}^S = \boldsymbol{N}^{cse1,p} \cdot \left\{ \dot{\boldsymbol{\theta}}^{cse} \right\} \tag{7.12}$$

$$[[\theta]] = \boldsymbol{N}^{cse2,p} \cdot \{\boldsymbol{\theta}^{cse}\} \tag{7.13}$$

$$[[\zeta]] = \boldsymbol{N}^{cse2,p} \cdot \{\boldsymbol{\beta}^{cse}\} \tag{7.14}$$

$$\frac{\partial \theta^S}{\partial x_t} = \boldsymbol{B}^{cse1,p} \cdot \{\boldsymbol{\theta}^{cse}\} \tag{7.15}$$

$$\frac{\partial \theta^S}{\partial x_n} = \boldsymbol{N}^{cse2,p} \cdot \{\boldsymbol{\theta}^{cse}\} \tag{7.16}$$

Recall the dimensionality reduction for axisymmetric condition,

$$\int_{S^l} (\bullet) dv = 2\pi \int_S (\bullet) lr ds \tag{7.17}$$

$$\int_S (\bullet) da = 2\pi \int_S (\bullet) r ds \tag{7.18}$$

$$\int_\Omega (\bullet) dv = 2\pi \int_A (\bullet) r dr dz \tag{7.19}$$

The finite element formulation of the balance of mass equation for the discontinuity is then written as

$$\begin{aligned}
\mathop{\mathbf{A}}_{e=1}^{n_{\text{cel}}} (\boldsymbol{\alpha}^{cse})^T \cdot \Bigg[& \underbrace{\int_{S^e} (\boldsymbol{N}^{cse1,p})^T \cdot \boldsymbol{n}^T \cdot \boldsymbol{N}^{cse,u} \, da}_{\boldsymbol{k}_{cse}^{pd}} \left\{ \dot{\boldsymbol{d}}^{cse} \right\} \\
& - \underbrace{\int_{S^e} \left[\beta_s^\theta (1 - n^S) + \beta_f^\theta n^S \right] \, l \, (\boldsymbol{N}^{cse1,p})^T \cdot \boldsymbol{N}^{cse1,p} \, da}_{\boldsymbol{k}_{cse}^{p\theta}(\boldsymbol{d}^{cse})} \left\{ \dot{\boldsymbol{\theta}}^{cse} \right\} \\
& - \underbrace{\int_{S^e} (\boldsymbol{N}^{cse2,p})^T \, (2 \tilde{v}_n^{D,S}) \, da}_{\boldsymbol{f}_{cse}^{p1,int}(\boldsymbol{d}^{cse}, \boldsymbol{p}_f^{cse})} - \underbrace{\int_{S^e} (\boldsymbol{B}^{cse1,p})^T \, \tilde{v}_t^{D,S} \, l \, da}_{\boldsymbol{f}_{cse}^{p2,int}(\boldsymbol{d}^{cse}, \boldsymbol{p}_f^{cse})} \\
& - \underbrace{\int_{S^e} \beta_f^\theta \, \tilde{v}_n^{D,S} \, (\boldsymbol{N}^{cse1,p})^T \cdot \boldsymbol{N}^{cse2,p} \cdot \{\boldsymbol{\theta}^{cse}\} \, da}_{\boldsymbol{f}_{cse}^{p4,int}(\boldsymbol{d}^{cse}, \boldsymbol{p}_f^{cse}, \boldsymbol{\theta}^{cse})} \\
& - \underbrace{\int_{S^e} \beta_f^\theta \, \tilde{v}_t^{D,S} \, l \, (\boldsymbol{N}^{cse1,p})^T \cdot \boldsymbol{B}^{cse1,p} \cdot \{\boldsymbol{\theta}^{cse}\} \, da}_{\boldsymbol{f}_{cse}^{p3,int}(\boldsymbol{d}^{cse}, \boldsymbol{p}_f^{cse}, \boldsymbol{\theta}^{cse})} = \underbrace{\int_{\Gamma_S} (\boldsymbol{N}^{cse1,p})^T S^{w,S} \, da}_{\boldsymbol{f}_{cse}^{p,ext}} \Bigg]
\end{aligned} \tag{7.20}$$

7.1.1.3 Balance of energy

Similar to the continuum in (3.94), the balance of energy equation for discontinuity is written as

$$\begin{aligned}&(\rho C)^S\dot{\theta^S} + \rho^{fR}C_f\tilde{\boldsymbol{v}}_f^S\cdot\nabla\theta^S + \alpha_{skel}^{\theta,S}\theta^S\,\mathrm{tr}(\dot{\boldsymbol{\sigma}}) - \tilde{\boldsymbol{v}}_f^{D,S}\cdot(-\nabla p_f^S + \rho^{fR}\boldsymbol{g})\\&+\nabla\cdot\boldsymbol{q}^S - (\rho\, r)^S - \left[\beta_s^{\theta,S}(1-n^S) + \beta_f^{\theta,S}n^S\right]\dot{p_f^S} - \beta_f^{\theta}\tilde{\boldsymbol{v}}_f^{D,S}\cdot\nabla p_f^S = 0\end{aligned} \tag{7.21}$$

where the superscript or subscript "S" indicates the properties of the crack. For example, $(\rho C)^S$ = heat capacity per unit volume of the crack; K_b^S= bulk modulus of the solid skeleton of the crack; $\alpha_{skel}^{\theta,S}$ = linear thermal expansion coefficient of the crack solid skeleton. $\beta_f^{\theta,S}$ and $\beta_s^{\theta,S}$ are respectively the volumetric thermal expansion coefficient of fluid (or water here) and solid phases in the crack. In the future, we need to derive directly the thermodynamics for the discontinuity to check the energy conservation equation and the constitutive relation forms. Applying weighting function φ^S to (7.21), and integrate over S^l:

$$\begin{aligned}\int_{S^l}\varphi(\nabla\cdot\boldsymbol{q}^S)dv &= \int_{S^l}\left[\nabla\cdot(\varphi^S\boldsymbol{q}^S) - (\nabla\varphi^S)\cdot\boldsymbol{q}^S\right]dv\\&= \int_{\partial S^l}\varphi^S\boldsymbol{q}^S\cdot\tilde{\boldsymbol{n}}da - \int_{S^l}\left(\frac{\partial\varphi^S}{\partial x_n}q_n^S + \frac{\partial\varphi^S}{\partial x_t}q_t^S\right)dv\end{aligned} \tag{7.22}$$

where $\partial S^l = S^+\cup S^-\cup\Gamma_S$. Then

$$\begin{aligned}\int_{\partial S^l}\varphi^S\boldsymbol{q}^S\cdot\tilde{\boldsymbol{n}}da &= \int_{S^+}(\varphi^+\boldsymbol{q}^+\boldsymbol{n}^+)da + \int_{S^-}(\varphi^-\boldsymbol{q}^-\boldsymbol{n}^-)da + \int_{\Gamma_S}\varphi^S\boldsymbol{q}^S\boldsymbol{\nu}da\\&= \int_{S^+}(\varphi^+q_n^{S,+})da + \int_{S^-}(\varphi^-q_n^{S,-})da + \int_{\Gamma_S}\varphi^S(-q^{end})da\\&= \int_S -[[\varphi]]q_n^S da - \int_{\Gamma_S}\varphi q^{end}da\end{aligned} \tag{7.23}$$

assuming $\frac{\partial\varphi^S}{\partial x_n} = [[\varphi^S]]\,\delta_S$, (7.22) becomes

$$\begin{aligned}\int_{S^l}\varphi(\nabla\cdot\boldsymbol{q})dv &= -\int_S[[\varphi]]q_n^S da - \int_{\Gamma_S}\varphi q^{end}da - \int_S[[\varphi]]q_n^S da - \int_{S^l}\frac{\partial\varphi^S}{\partial x_t}q_t^S dv\\&= -2\int_S[[\varphi]]q_n^S da - \int_{\Gamma_S}\varphi q^{end}da - \int_{S^l}\frac{\partial\varphi^S}{\partial x_t}q_t^S dv\end{aligned} \tag{7.24}$$

where $[[\varphi]] = \varphi^- - \varphi^+$. Assuming $q_n^S = q_n^{S,+} = -q_n^{S,-}$, the heat flux across the discontinuity q^S is expressed as

$$q_n^S = \hat{K}_n^\theta(\theta^+ - \theta^-) = -\hat{K}_n^\theta[[\theta]] = -\hat{K}_n^\theta \boldsymbol{N}^{cse2,p} \cdot \{\boldsymbol{\theta}^{cse}\} \tag{7.25}$$

$$q_t^S = -\hat{K}_t^\theta \frac{\partial \theta^S}{\partial x_t} = -\hat{K}_t^\theta \boldsymbol{B}^{cse1,p} \cdot \{\boldsymbol{\theta}^{cse}\} \tag{7.26}$$

and where $\hat{K}_n^\theta$ and $\hat{K}_t^\theta$ are respectively the thermal conductivities at normal n and tangential t directions of the crack; q^{end} denotes the heat flux at the ends of the crack Γ_S.

Apply the weighting function φ^S, and write the finite element formulation of the energy conservation equation for the discontinuity

$$\begin{aligned}
&\mathop{\mathsf{A}}_{e=1}^{n_{\text{cel}}} (\boldsymbol{\beta}^{cse})^T \cdot \Bigg[\underbrace{\int_{S^e} 3K_b^S \alpha_{skel}^{\theta,S} \theta^S (\boldsymbol{N}^{cse1,p})^T \cdot \boldsymbol{n}^T \cdot \boldsymbol{N}^{cse,u}\, da}_{\boldsymbol{k}_{cse}^{\theta d}(\boldsymbol{\theta}^{cse})} \left\{\dot{\boldsymbol{d}}^{cse}\right\} \\
&- \underbrace{\int_{S^e} \left(\beta_s^{\theta,S}(1-n^S) + \beta_f^{\theta,S} n^S\right) l\, (\boldsymbol{N}^{cse1,p})^T \cdot \boldsymbol{N}^{cse1,p}\, da}_{\boldsymbol{k}_{cse}^{\theta p}(\boldsymbol{d}^{cse})} \left\{\dot{\boldsymbol{p}}_f^{cse}\right\} \\
&+ \underbrace{\int_{S^e} \left[(\rho C)^S - 9K_b^S(\alpha_S^\theta)^2 \theta^S\right] l\, (\boldsymbol{N}^{cse1,p})^T \cdot \boldsymbol{N}^{cse1,p}\, da}_{\boldsymbol{k}_{cse}^{\theta\theta}(\boldsymbol{\theta}^{cse})} \left\{\dot{\boldsymbol{\theta}}^{cse}\right\} \\
&+ \underbrace{\int_{S^e} (\rho^{fR} C_f)^S \tilde{v}_n^{D,S}\, (\boldsymbol{N}^{cse1,p})^T \cdot \boldsymbol{N}^{cse2,p} \cdot \{\boldsymbol{\theta}^{cse}\}\, da}_{\boldsymbol{f}_{cse}^{\theta 1,int}(\boldsymbol{d}^{cse},\boldsymbol{p}_f^{cse},\boldsymbol{\theta}^{cse})} + \underbrace{\int_{S^e} (\rho^{fR} C_f)^S\, \tilde{v}_t^{D,S}\, l\, (\boldsymbol{N}^{cse1,p})^T \cdot \boldsymbol{B}^{cse1,p} \cdot \{\boldsymbol{\theta}^{cse}\}\, da}_{\boldsymbol{f}_{cse}^{\theta 2,int}(\boldsymbol{d}^{cse},\boldsymbol{p}_f^{cse},\boldsymbol{\theta}^{cse})} \\
&+ \underbrace{\int_{S^e} 2\hat{K}_n^\theta \boldsymbol{N}^{cse2,p} \cdot \{\boldsymbol{\theta}^{cse}\}\, (\boldsymbol{N}^{cse2,p})^T\, da}_{\boldsymbol{f}_{cse}^{\theta 3,int}(\boldsymbol{d}^{cse},\boldsymbol{\theta}^{cse})} + \underbrace{\int_{S^e} \hat{K}_t^\theta \boldsymbol{B}^{cse1,p} \cdot \{\boldsymbol{\theta}^{cse}\}\, l\, (\boldsymbol{B}^{cse1,p})^T\, da}_{\boldsymbol{f}_{cse}^{\theta 4,int}(\boldsymbol{d}^{cse},\boldsymbol{\theta}^{cse})} \\
&- \underbrace{\int_{S^e} \beta_f^{\theta,S} \tilde{v}_n^{D,S}\, (\boldsymbol{N}^{cse1,p})^T \cdot \boldsymbol{N}^{cse2,p} \cdot \left\{\boldsymbol{p}_f^{cse}\right\}\, da}_{\boldsymbol{f}_{cse}^{\theta 5,int}(\boldsymbol{d}^{cse},\boldsymbol{p}_f^{cse})} - \underbrace{\int_{S^e} \beta_f^{\theta,S} \tilde{v}_t^{D,S}\, l\, (\boldsymbol{N}^{cse1,p})^T \cdot \boldsymbol{B}^{cse1,p} \cdot \left\{\boldsymbol{p}_f^{cse}\right\}\, da}_{\boldsymbol{f}_{cse}^{\theta 6,int}(\boldsymbol{d}^{cse},\boldsymbol{p}_f^{cse})} \\
&= \underbrace{\int_{\Gamma_S} (\boldsymbol{N}^{cse1,p})^T q^{end}\, da}_{\boldsymbol{f}_{cse}^{\theta q,ext}} + \underbrace{\int_{S^l} (\boldsymbol{N}^{cse1,p})^T (\rho r)^S\, dv}_{\boldsymbol{f}_{cse}^{\theta r,ext}} \Bigg]
\end{aligned} \tag{7.27}$$

where $\boldsymbol{f}_{cse}^{\theta r,ext}$ is the heat source within the discontinuity, and will be ignored here.

7.1.2 Finite element formulations

We combine with the finite element equations for the matrix, i.e. (3.105), (3.107), and (3.108) and those for the interface element, to write the following equations for TPM model of saturated fractured porous media.

(1) Balance of linear momentum:

$$\begin{aligned}
&\mathop{\mathbf{A}}_{e=1}^{n_{\mathrm{bel}}}(\boldsymbol{c}^e)^T\cdot\Bigg[\underbrace{\int_{\Omega^e}(\boldsymbol{B}^{e,u})^T\cdot\boldsymbol{\sigma}'dv}_{\boldsymbol{f}_e^{d,int}(\boldsymbol{d}^e)}-\underbrace{\int_{\Omega^e}\left(\tilde{\boldsymbol{B}}^{e,u}\right)^T\cdot\boldsymbol{N}^{e,p}dv}_{\boldsymbol{k}_e^{dp1}}\cdot\boldsymbol{p}_f^e\\
&-\underbrace{\int_{\Omega^e}\rho\,(\boldsymbol{N}^{e,u})^T\cdot\boldsymbol{b}\,dv}_{\boldsymbol{f}_e^{df,ext}(\boldsymbol{d}^e)}-\underbrace{\int_{\Gamma^e}(\boldsymbol{N}^{e,u})^T\,\boldsymbol{t}^{\sigma'}da}_{\boldsymbol{f}_e^{dt,ext}}+\underbrace{\int_{\Gamma^e}(\boldsymbol{N}^{e,u})^T\cdot\boldsymbol{\nu}\cdot\boldsymbol{N}^{e,p}da}_{\boldsymbol{k}_e^{dp2}}\cdot\boldsymbol{p}_f^e\Bigg]\\
&+\mathop{\mathbf{A}}_{e=1}^{n_{\mathrm{cel}}}(\boldsymbol{c}^{cse})^T\left[\underbrace{\int_{S^e}(\boldsymbol{N}^{cse,u})^T\cdot\boldsymbol{T}'da}_{\boldsymbol{f}_{cse}^{d,int}(\boldsymbol{d}^{cse})}-\underbrace{\int_{S^e}(\boldsymbol{N}^{cse,u})^T\cdot\boldsymbol{n}\cdot\boldsymbol{N}^{cse1,p}da}_{\boldsymbol{k}_{cse}^{dp}}\cdot\boldsymbol{p}_f^{cse}\right]=0
\end{aligned}\tag{7.28}$$

Note although it has the same format with (6.84), $\boldsymbol{\sigma}'$ and $\boldsymbol{T}'$ are calculated from elastic deformation of the matrix and the fracture, which are obtained by deducting the thermal strain from the total strain.

(2) Balance of mass:

$$\begin{aligned}
&\mathop{\mathbf{A}}_{e=1}^{n_{\mathrm{el}}}(\boldsymbol{\alpha}^e)^T\cdot\Bigg[\underbrace{\left(\int_{\Omega_{\mathrm{f}}^e}(\boldsymbol{N}^{e,\theta})^T\cdot\tilde{\boldsymbol{B}}^{e,u}dv\right)}_{\boldsymbol{k}_e^{pd}}\cdot\dot{\boldsymbol{d}}^e-\underbrace{\left[\int_{\Omega_{\mathrm{f}}^e}(\beta_s^\theta\,n^s+\beta_f^\theta\,n^f)(\boldsymbol{N}^{e,\theta})^T\cdot\boldsymbol{N}^{e,\theta}\,dv\right]}_{\boldsymbol{k}_e^{p\theta}}\cdot\dot{\boldsymbol{\theta}}^e\\
&-\underbrace{\int_{\Omega_{\mathrm{f}}^e}(\boldsymbol{B}^{e,\theta})^T\cdot\tilde{\boldsymbol{v}}_f^D\,dv}_{\boldsymbol{f}_e^{pp,int}}-\underbrace{\int_{\Omega_{\mathrm{f}}^e}\beta_f^\theta(\boldsymbol{N}^{e,\theta})^T\cdot\left[(\tilde{\boldsymbol{v}}_f^D)^T\cdot\boldsymbol{B}^{e,\theta}\cdot\boldsymbol{\theta}^e\right]dv}_{\boldsymbol{f}_e^{p\theta,int}}-\underbrace{\int_{\Gamma_s^e}(\boldsymbol{N}^{e,\theta})^T S^w\,da}_{\boldsymbol{f}_e^{p,ext}}\Bigg]
\end{aligned}$$

$$
\begin{aligned}
&+\mathop{\mathbf{A}}_{e=1}^{n_{\text{cel}}}(\boldsymbol{\alpha}^{cse})^T\cdot\Bigg[\underbrace{\int_{S^e}(\boldsymbol{N}^{cse1,p})^T\cdot\boldsymbol{n}^T\cdot\boldsymbol{N}^{cse,u}\,da}_{\boldsymbol{k}_{cse}^{pd}=(\boldsymbol{k}_{cse}^{dp})^T}\left\{\dot{\boldsymbol{d}}^{cse}\right\}\\
&-\underbrace{\int_{S^e}\left[\beta_s^{\theta,S}(1-n^S)+\beta_f^{\theta,S}n^S\right]\,l\,(\boldsymbol{N}^{cse1,p})^T\cdot\boldsymbol{N}^{cse1,p}\,da}_{\boldsymbol{k}_{cse}^{p\theta}(\boldsymbol{d}^{cse})}\left\{\dot{\boldsymbol{\theta}}^{cse}\right\}\\
&-\underbrace{\int_{S^e}(\boldsymbol{N}^{cse2,p})^T\,(2\tilde{\boldsymbol{v}}_n^{D,S})\,da}_{\boldsymbol{f}_{cse}^{p1,int}(\boldsymbol{d}^{cse},\boldsymbol{p}_f^{cse})}-\underbrace{\int_{S^e}(\boldsymbol{B}^{cse1,p})^T\,\tilde{v}_t^{D,S}\,l\,da}_{\boldsymbol{f}_{cse}^{p2,int}(\boldsymbol{d}^{cse},\boldsymbol{p}_f^{cse})}\\
&-\underbrace{\int_{S^e}\beta_f^{\theta,S}\,\tilde{v}_n^{D,S}\,(\boldsymbol{N}^{cse1,p})^T\cdot\boldsymbol{N}^{cse2,p}\cdot\{\boldsymbol{\theta}^{cse}\}\,da}_{\boldsymbol{f}_{cse}^{p3,int}(\boldsymbol{d}^{cse},\boldsymbol{p}_f^{cse},\boldsymbol{\theta}^{cse})}-\underbrace{\int_{S^e}\beta_f^{\theta,S}\,\tilde{v}_t^{D,S}\,l\,(\boldsymbol{N}^{cse1,p})^T\cdot\boldsymbol{B}^{cse1,p}\cdot\{\boldsymbol{\theta}^{cse}\}\,da}_{\boldsymbol{f}_{cse}^{p4,int}(\boldsymbol{d}^{cse},\boldsymbol{p}_f^{cse},\boldsymbol{\theta}^{cse})}\\
&-\underbrace{\int_{\Gamma_S}(\boldsymbol{N}^{cse1,p})^T S^{w,S}\,da}_{\boldsymbol{f}_{cse}^{p,ext}}=0\Bigg]
\end{aligned}
\tag{7.29}
$$

(3) Balance of energy:

$$
\begin{aligned}
&\mathop{\mathbf{A}}_{e=1}^{n_{\text{el}}}(\boldsymbol{\beta}^e)^T\cdot\Bigg[\underbrace{\left(\int_{\Omega^e}\left((\rho C)_m-9K^{skel}(\alpha_{skel}^{\theta})^2(\boldsymbol{N}^{e,\theta}\cdot\boldsymbol{\theta}^e)\right)(\boldsymbol{N}^{e,\theta})^T\cdot\boldsymbol{N}^{e,\theta}dv\right)}_{\boldsymbol{k}_e^{\theta\theta}}\cdot\dot{\boldsymbol{\theta}}^e+\\
&\underbrace{\left(\int_{\Omega^e}3K^{skel}\alpha_{skel}^{\theta}(\boldsymbol{N}^{e,\theta})^T(\boldsymbol{N}^{e,\theta}\boldsymbol{\theta}^e)\cdot\tilde{\boldsymbol{B}}^{e,u}dv\right)}_{\boldsymbol{k}_e^{\theta d}}\cdot\dot{\boldsymbol{d}}^e-\underbrace{\left(\int_{\Omega^e}(\beta_s^{\theta}\,n^s+\beta_f^{\theta}\,n^f)(\boldsymbol{N}^{e,\theta})^T\boldsymbol{N}^{e,\theta}\,dv\right)}_{\boldsymbol{k}_e^{\theta p}}\cdot\dot{\boldsymbol{p}}_f^e\\
&+\underbrace{\int_{\Omega^e}(\boldsymbol{B}^{e,\theta})^T\cdot\boldsymbol{K}_\theta\cdot\boldsymbol{B}^{e,\theta}\cdot\boldsymbol{\theta}^e dv}_{\boldsymbol{f}_e^{\theta 1,int}}+\underbrace{\int_{\Omega^e}\rho^{fR}C^f(\boldsymbol{N}^{e,\theta})^T\,(\tilde{\boldsymbol{v}}_f^D)^T\cdot\boldsymbol{B}^{e,\theta}\cdot\boldsymbol{\theta}^e\,dv}_{\boldsymbol{f}_e^{\theta 2,int}}\\
&-\underbrace{\int_{\Omega^e}(\boldsymbol{N}^{e,\theta})^T\cdot(\tilde{\boldsymbol{v}}_f^D)^T\cdot(-\boldsymbol{B}^{e,\theta}\cdot\boldsymbol{p}_f^e+\rho^{fR}\boldsymbol{g})\,dv}_{\boldsymbol{f}_e^{\theta 3,int}}-\underbrace{\int_{\Omega^e}\beta_f^{\theta}(\boldsymbol{N}^{e,\theta})^T\cdot(\tilde{\boldsymbol{v}}_f^D)^T\cdot(\boldsymbol{B}^{e,\theta}\cdot\boldsymbol{p}_f^e)\,dv}_{\boldsymbol{f}_e^{\theta 4,int}}\\
&-\underbrace{\int_{\Omega^e}\rho(\boldsymbol{N}^{e,\theta})^T r\,dv}_{\boldsymbol{f}_e^{\theta r,ext}}-\underbrace{\int_{\Gamma_q^e}(\boldsymbol{N}^{e,\theta})^T q\,da}_{\boldsymbol{f}_e^{\theta q,ext}}\Bigg]
\end{aligned}
$$

$$
\begin{aligned}
&+\mathop{\mathbf{A}}_{e=1}^{n_{\text{cel}}}(\boldsymbol{\beta}^{cse})^T\cdot\Bigg[\underbrace{\int_{S^e}3K_b^S\alpha_{skel}^{\theta,S}\theta^S(\boldsymbol{N}^{cse1,p})^T\cdot\boldsymbol{n}^T\cdot\boldsymbol{N}^{cse,u}\,da}_{\boldsymbol{k}_{cse}^{\theta d}(\boldsymbol{\theta}^{cse})}\left\{\dot{\boldsymbol{d}}^{cse}\right\}\\
&-\underbrace{\int_{S^e}\left(\beta_s^{\theta,S}(1-n^S)+\beta_f^{\theta,S}n\right)l\,(\boldsymbol{N}^{cse1,p})^T\cdot\boldsymbol{N}^{cse1,p}\,da}_{\boldsymbol{k}_{cse}^{\theta p}(\boldsymbol{d}^{cse})=k_{cse}^{p\theta}}\left\{\dot{\boldsymbol{p}}_f^{cse}\right\}\\
&+\underbrace{\int_{S^e}\left[(\rho C)^S-9K_b^S(\alpha_c^\theta)^2\theta^S\right]l\,(\boldsymbol{N}^{cse1,p})^T\cdot\boldsymbol{N}^{cse1,p}\,da}_{\boldsymbol{k}_{cse}^{\theta\theta}(\boldsymbol{\theta}^{cse})}\left\{\dot{\boldsymbol{\theta}}^{cse}\right\}\\
&+\underbrace{\int_{S^e}(\rho^{fR}C_f)^S\tilde{v}_n^{D,S}\,(\boldsymbol{N}^{cse1,p})^T\cdot\boldsymbol{N}^{cse2,p}\cdot\{\boldsymbol{\theta}^{cse}\}\,da}_{\boldsymbol{f}_{cse}^{\theta1,int}(\boldsymbol{d}^{cse},\boldsymbol{p}_f^{cse},\boldsymbol{\theta}^{cse})}+\underbrace{\int_{S^e}(\rho^{fR}C_f)^S\,\tilde{v}_t^{D,S}\,l\,(\boldsymbol{N}^{cse1,p})^T\cdot\boldsymbol{B}^{cse1,p}\cdot\{\boldsymbol{\theta}^{cse}\}\,da}_{\boldsymbol{f}_{cse}^{\theta2,int}(\boldsymbol{d}^{cse},\boldsymbol{p}_f^{cse},\boldsymbol{\theta}^{cse})}\\
&+\underbrace{\int_{S^e}2\hat{K}_n^\theta\boldsymbol{N}^{cse2,p}\cdot\{\boldsymbol{\theta}^{cse}\}\,(\boldsymbol{N}^{cse2,p})^T\,da}_{\boldsymbol{f}_{cse}^{\theta3,int}(\boldsymbol{d}^{cse},\boldsymbol{\theta}^{cse})}+\underbrace{\int_{S^e}\hat{K}_t^\theta\,l\,\boldsymbol{B}^{cse1,p}\cdot\{\boldsymbol{\theta}^{cse}\}\cdot(\boldsymbol{B}^{cse1,p})^T\,da}_{\boldsymbol{f}_{cse}^{\theta4,int}(\boldsymbol{d}^{cse},\boldsymbol{\theta}^{cse})}\\
&-\underbrace{\int_{S^e}\beta_f^{\theta,S}\tilde{v}_n^{D,S}\,(\boldsymbol{N}^{cse1,p})^T\cdot\boldsymbol{N}^{cse2,p}\cdot\left\{\boldsymbol{p}_f^{cse}\right\}\,da}_{\boldsymbol{f}_{cse}^{\theta5,int}(\boldsymbol{d}^{cse},\boldsymbol{p}_f^{cse})}-\underbrace{\int_{S^e}\beta_f^{\theta,S}\tilde{v}_t^{D,S}\,l\,(\boldsymbol{N}^{cse1,p})^T\cdot\boldsymbol{B}^{cse1,p}\cdot\left\{\boldsymbol{p}_f^{cse}\right\}\,da}_{\boldsymbol{f}_{cse}^{\theta6,int}(\boldsymbol{d}^{cse},\boldsymbol{p}_f^{cse})}\\
&-\underbrace{\int_{\Gamma_S}(\boldsymbol{N}^{cse1,p})^Tq^{end}\,da}_{\boldsymbol{f}_{cse}^{\theta q,ext}}-\underbrace{\int_{S^l}(\boldsymbol{N}^{cse1,p})^T(\rho r)^S\,dv}_{\boldsymbol{f}_{cse}^{\theta r,ext}}=0\Bigg]
\end{aligned}
\tag{7.30}
$$

(7.28), (7.29), and (7.30) may be written in one matrix equation as follows:

$$
\boldsymbol{C}(\boldsymbol{D})\cdot\dot{\boldsymbol{D}}+\boldsymbol{F}^{INT}(\boldsymbol{D})=\boldsymbol{F}^{EXT}(\boldsymbol{D}) \tag{7.31}
$$

such that,

$$
\boldsymbol{C}(\boldsymbol{D})=\begin{bmatrix}\mathbf{0} & \mathbf{0} & \mathbf{0}\\ \boldsymbol{K}^{pd}+\boldsymbol{K}_{cse}^{pd} & \mathbf{0} & -\left(\boldsymbol{K}^{p\theta}+\boldsymbol{K}_{cse}^{p\theta}\right)\\ \boldsymbol{K}^{\theta d}+\boldsymbol{K}_{cse}^{\theta d} & -\left(\boldsymbol{K}^{\theta p}+\boldsymbol{K}_{cse}^{\theta p}\right) & \boldsymbol{K}^{\theta\theta}+\boldsymbol{K}_{cse}^{\theta\theta}\end{bmatrix} \tag{7.32}
$$

The global degree of freedom vector and its rate form are:

$$
\boldsymbol{D}=\begin{bmatrix}\boldsymbol{d}\\ \boldsymbol{p}_f\\ \boldsymbol{\theta}\end{bmatrix};\quad \dot{\boldsymbol{D}}=\begin{bmatrix}\dot{\boldsymbol{d}}\\ \dot{\boldsymbol{p}}_f\\ \dot{\boldsymbol{\theta}}\end{bmatrix} \tag{7.33}
$$

The assembled $\boldsymbol{F}^{INT}$ and $\boldsymbol{F}^{EXT}$ are:

$$\boldsymbol{F}^{INT} = \begin{bmatrix} \boldsymbol{F}^{d,INT} + \boldsymbol{F}^{d,INT}_{cse} + \left(\boldsymbol{K}^{dp2} - \boldsymbol{K}^{dp1} - \boldsymbol{K}^{dp}_{cse}\right) \cdot \boldsymbol{p}_f \\ -\boldsymbol{F}^{pp,INT} - \boldsymbol{F}^{p\theta,INT}_{cse} - \boldsymbol{F}^{p1,INT}_{cse} - \boldsymbol{F}^{p2,INT}_{cse} - \boldsymbol{F}^{p3,INT}_{cse} - \boldsymbol{F}^{p4,INT}_{cse} \\ \boldsymbol{F}^{\theta,INT} + \boldsymbol{F}^{\theta,INT}_{cse} \end{bmatrix} \tag{7.34}$$

where

$$\boldsymbol{F}^{\theta,INT} = \boldsymbol{F}^{\theta 1,INT} + \boldsymbol{F}^{\theta 2,INT} - \boldsymbol{F}^{\theta 3,INT} - \boldsymbol{F}^{\theta 4,INT}$$

$$\boldsymbol{F}^{\theta,INT}_{cse} = \boldsymbol{F}^{\theta,INT}_{cse} + \boldsymbol{F}^{\theta 2,INT}_{cse} + \boldsymbol{F}^{\theta 3,INT}_{cse} + \boldsymbol{F}^{\theta 4,INT}_{cse} - \boldsymbol{F}^{\theta 5,INT}_{cse} - \boldsymbol{F}^{\theta 6,INT}_{cse}$$

$$\boldsymbol{F}^{EXT} = \begin{bmatrix} \boldsymbol{F}^{df,EXT} + \boldsymbol{F}^{dt,EXT} \\ \boldsymbol{F}^{p,EXT} + \boldsymbol{F}^{p,EXT}_{cse} \\ \boldsymbol{F}^{\theta r,EXT} + \boldsymbol{F}^{\theta q,EXT} + \boldsymbol{F}^{\theta r,EXT}_{cse} + \boldsymbol{F}^{\theta q,EXT}_{cse} \end{bmatrix} \tag{7.35}$$

For simplicity, we assume the linear thermal expansion coefficient of the fracture (or crack) $\alpha^{\theta,S}_{skel}$ is negligible. And also we can assume that the solid partial volumetric thermal expansion coefficient of the fracture is equal to that of the matrix, i.e. $\beta^{\theta,S}_s = \beta^{\theta}_s$. Since $\beta^{\theta,S}_f$ is approximately 10 times larger than $\beta^{\theta,S}_s$, therefore it is reasonable to assume that $\beta^{\theta,S}_s n^S$ is negligible compared to $\beta^{\theta,S}_f n_f$ in $\boldsymbol{K}^{\theta p}$. These assumptions can be relaxed later, and adding these terms is straightforward.

The derivatives of $\boldsymbol{k}'_{cse}s$ and $\boldsymbol{f}'_{cse}s$ with respect to $\boldsymbol{d}^{cse}$, $\boldsymbol{p}^{cse}_f$, and $\boldsymbol{\theta}^{cse}$ may be written as

$$\begin{aligned}
\frac{\partial \boldsymbol{f}^{d,int}_{cse}}{\partial \boldsymbol{d}^{cse}} &= \int_{S^e} (\boldsymbol{N}^{cse,u})^T \cdot \frac{\partial \boldsymbol{T}'(\boldsymbol{d}^{cse})}{\partial \boldsymbol{d}^{cse}} da \\
&= \int_{S^e} (\boldsymbol{N}^{cse,u})^T \cdot \frac{\partial \boldsymbol{T}'}{\partial \widetilde{\boldsymbol{T}}'} \cdot \frac{\partial \widetilde{\boldsymbol{T}}'}{\partial [[\tilde{\boldsymbol{u}}]]} \cdot \frac{\partial [[\tilde{\boldsymbol{u}}]]}{\partial \boldsymbol{d}^{cse}} \, da \\
&= \int_{S^e} (\boldsymbol{N}^{cse,u})^T \cdot (\boldsymbol{\Lambda}^e)^T \cdot \frac{\partial \widetilde{\boldsymbol{T}}'}{\partial [[\tilde{\boldsymbol{u}}]]} \cdot \boldsymbol{\Lambda}^e \cdot \boldsymbol{N}^{cse,u} \, da \\
&\quad \text{where,} \frac{\partial \widetilde{\boldsymbol{T}}'}{\partial [[\tilde{\boldsymbol{u}}]]} \text{ can be calculated from the constitutive model.} \\
\frac{\partial \boldsymbol{k}^{p\theta}_{cse}}{\partial \boldsymbol{d}^{cse}} &= \frac{\partial \boldsymbol{k}^{\theta p}_{cse}}{\partial \boldsymbol{d}^{cse}} = \int_{S^e} \left[\beta^{\theta,S}_s (1-n) + \beta^{\theta,S}_f n\right] (\boldsymbol{N}^{cse1,p})^T \cdot \boldsymbol{N}^{cse1,p} \cdot \frac{\partial l}{\partial \boldsymbol{d}^{cse}} \\
\frac{\partial \boldsymbol{f}^{p1,int}_{cse}}{\partial \boldsymbol{d}^{cse}} &= \int_{S^e} 2 \left(\boldsymbol{N}^{cse2,p}\right)^T \cdot \frac{\partial \tilde{v}^{D,S}_n}{\partial \boldsymbol{d}^{cse}} \, da
\end{aligned}$$

$$
\begin{aligned}
\frac{\partial \boldsymbol{f}_{cse}^{p1,int}}{\partial \boldsymbol{p}_f^{cse}} &= \int_{S^e} 2\left(\boldsymbol{N}^{cse2,p}\right)^T \cdot \frac{\partial \tilde{v}_n^{D,S}}{\partial \boldsymbol{p}_f^{cse}}\, da \\
\frac{\partial \boldsymbol{f}_{cse}^{p2,int}}{\partial \boldsymbol{d}^{cse}} &= \int_{S^e} \left(\boldsymbol{B}^{cse1,p}\right)^T \cdot \frac{\partial (\tilde{v}_t^{D,S}\, l)}{\partial \boldsymbol{d}^{cse}}\, da \\
\frac{\partial \boldsymbol{f}_{cse}^{p2,int}}{\partial \boldsymbol{p}_f^{cse}} &= \int_{S^e} \left(\boldsymbol{B}^{cse1,p}\right)^T \cdot l \cdot \frac{\partial \tilde{v}_t^{D,S}}{\partial \boldsymbol{p}_f^{cse}}\, da \\
\frac{\partial \boldsymbol{f}_{cse}^{p3,int}}{\partial \boldsymbol{d}^{cse}} &= \int_{S^e} \beta_f^{\theta,S}\, \left(\boldsymbol{N}^{cse1,p}\right)^T \cdot \boldsymbol{N}^{cse2,p} \cdot \{\boldsymbol{\theta}^{cse}\} \cdot \frac{\partial \tilde{v}_n^{D,S}}{\partial \boldsymbol{d}^{cse}}\, da \\
\frac{\partial \boldsymbol{f}_{cse}^{p3,int}}{\partial \boldsymbol{p}_f^{cse}} &= \int_{S^e} \beta_f^{\theta,S}\, \left(\boldsymbol{N}^{cse1,p}\right)^T \cdot \boldsymbol{N}^{cse2,p} \cdot \{\boldsymbol{\theta}^{cse}\} \frac{\partial \tilde{v}_n^{D,S}}{\partial \boldsymbol{p}_f^{cse}}\, da \\
\frac{\partial \boldsymbol{f}_{cse}^{p3,int}}{\partial \boldsymbol{\theta}^{cse}} &= \int_{S^e} \beta_f^{\theta,S}\, \tilde{v}_n^{D,S}\, \left(\boldsymbol{N}^{cse1,p}\right)^T \cdot \boldsymbol{N}^{cse2,p} \\
\frac{\partial \boldsymbol{f}_{cse}^{p4,int}}{\partial \boldsymbol{d}^{cse}} &= \int_{S^e} \beta_f^{\theta,S}\, \left(\boldsymbol{N}^{cse1,p}\right)^T \cdot \left(\boldsymbol{B}^{cse1,p}\right)^T \cdot \{\boldsymbol{\theta}^{cse}\} \cdot \frac{\partial (\tilde{v}_t^{D,S}\, l)}{\partial \boldsymbol{d}^{cse}}\, da \\
\frac{\partial \boldsymbol{f}_{cse}^{p4,int}}{\partial \boldsymbol{p}_f^{cse}} &= \int_{S^e} \beta_f^{\theta,S}\, l\, \left(\boldsymbol{N}^{cse1,p}\right)^T \cdot \left(\boldsymbol{B}^{cse1,p}\right)^T \cdot \{\boldsymbol{\theta}^{cse}\} \cdot \frac{\partial \tilde{v}_t^{D,S}}{\partial \boldsymbol{p}_f^{cse}}\, da \\
\frac{\partial \boldsymbol{f}_{cse}^{p4,int}}{\partial \boldsymbol{\theta}^{cse}} &= \int_{S^e} \beta_f^{\theta,S}\, \tilde{v}_t^{D,S}\, l\, \left(\boldsymbol{N}^{cse1,p}\right)^T \cdot \left(\boldsymbol{B}^{cse1,p}\right)^T\, da \\
\frac{\partial \boldsymbol{f}_{cse}^{\theta 1,int}}{\partial \boldsymbol{d}^{cse}} &= \int_{S^e} (\rho^{fR} C_f)^S\, \left(\boldsymbol{N}^{cse1,p}\right)^T \cdot \boldsymbol{N}^{cse2,p} \cdot \{\boldsymbol{\theta}^{cse}\} \cdot \frac{\partial \tilde{v}_n^{D,S}}{\partial \boldsymbol{d}^{cse}}\, da \\
\frac{\partial \boldsymbol{f}_{cse}^{\theta 1,int}}{\partial \boldsymbol{p}_f^{cse}} &= \int_{S^e} (\rho^{fR} C_f)^S\, \left(\boldsymbol{N}^{cse1,p}\right)^T \cdot \boldsymbol{N}^{cse2,p} \cdot \{\boldsymbol{\theta}^{cse}\} \cdot \frac{\partial \tilde{v}_n^{D,S}}{\partial \boldsymbol{p}_f^{cse}}\, da \\
\frac{\partial \boldsymbol{f}_{cse}^{\theta 1,int}}{\partial \boldsymbol{\theta}^{cse}} &= \int_{S^e} (\rho^{fR} C_f)^S\, \tilde{v}_n^c\, \left(\boldsymbol{N}^{cse1,p}\right)^T \cdot \boldsymbol{N}^{cse2,p}\, da \\
\frac{\partial \boldsymbol{f}_{cse}^{\theta 2,int}}{\partial \boldsymbol{d}^{cse}} &= \int_{S^e} (\rho^{fR} C_f)^S\, \left(\boldsymbol{N}^{cse1,p}\right)^T \cdot \boldsymbol{B}^{cse1,p} \cdot \{\boldsymbol{\theta}^{cse}\} \cdot \frac{\partial (\tilde{v}_t^{D,S}\, l)}{\partial \boldsymbol{d}^{cse}}\, da \\
\frac{\partial \boldsymbol{f}_{cse}^{\theta 2,int}}{\partial \boldsymbol{p}_f^{cse}} &= \int_{S^e} (\rho^{fR} C_f)^S\, l\, \left(\boldsymbol{N}^{cse1,p}\right)^T \cdot \boldsymbol{B}^{cse1,p} \cdot \{\boldsymbol{\theta}^{cse}\} \cdot \frac{\partial \tilde{v}_t^{D,S}}{\partial \boldsymbol{p}_f^{cse}}\, da \\
\frac{\partial \boldsymbol{f}_{cse}^{\theta 2,int}}{\partial \boldsymbol{\theta}^{cse}} &= \int_{S^e} (\rho^{fR} C_f)^S\, \tilde{v}_t^{D,S}\, l\, \left(\boldsymbol{N}^{cse1,p}\right)^T \cdot \boldsymbol{B}^{cse1,p}\, da \\
\frac{\partial \boldsymbol{f}_{cse}^{\theta 3,int}}{\partial \boldsymbol{d}^{cse}} &= \int_{S^e} 2\boldsymbol{N}^{cse2,p} \cdot \{\boldsymbol{\theta}^{cse}\} (\boldsymbol{N}^{cse2,p})^T \frac{\partial \hat{K}_n^{\theta}}{\partial l} \frac{\partial l}{\partial \boldsymbol{d}^{cse}}\, da \\
\frac{\partial \boldsymbol{f}_{cse}^{\theta 3,int}}{\partial \boldsymbol{\theta}^{cse}} &= \int_{S^e} 2\hat{K}_n^{\theta} (\boldsymbol{N}^{cse2,p})^T \cdot \boldsymbol{N}^{cse2,p}\, da \\
\frac{\partial \boldsymbol{f}_{cse}^{\theta 4,int}}{\partial \boldsymbol{d}^{cse}} &= \int_{S^e} \hat{K}_t^{\theta} \boldsymbol{B}^{cse1,p} \cdot \{\boldsymbol{\theta}^{cse}\}\, (\boldsymbol{B}^{cse1,p})^T \cdot \frac{\partial l}{\partial \boldsymbol{d}^{cse}}\, da \\
\frac{\partial \boldsymbol{f}_{cse}^{\theta 4,int}}{\partial \boldsymbol{\theta}^{cse}} &= \int_{S^e} \hat{K}_t^{\theta}\, l\, (\boldsymbol{B}^{cse1,p})^T \cdot \boldsymbol{B}^{cse1,p}\, da \\
\frac{\partial \boldsymbol{f}_{cse}^{\theta 5,int}}{\partial \boldsymbol{d}^{cse}} &= \int_{S^e} \beta_f^{\theta,S}\, \left(\boldsymbol{N}^{cse1,p}\right)^T \cdot \boldsymbol{N}^{cse2,p} \cdot \left\{\boldsymbol{p}_f^{cse}\right\} \cdot \frac{\partial \tilde{v}_n^{D,S}}{\partial \boldsymbol{d}^{cse}}\, da
\end{aligned}
$$

$$\frac{\partial \boldsymbol{f}_{cse}^{\theta 5,int}}{\partial \boldsymbol{p}_f^{cse}} = \int_{S^e} \left[\beta_f^{\theta,S}\, \tilde{v}_n^{D,S}\, \left(\boldsymbol{N}^{cse1,p}\right)^T \cdot \boldsymbol{N}^{cse2,p} + \beta_f^{\theta}\, \left(\boldsymbol{N}^{cse1,p}\right)^T \cdot \boldsymbol{N}^{cse2,p} \cdot \left\{\boldsymbol{p}_f^{cse}\right\} \cdot \frac{\partial \tilde{v}_n^{D,S}}{\partial \boldsymbol{p}_f^{cse}} \right] da$$

$$\frac{\partial \boldsymbol{f}_{cse}^{\theta 6,int}}{\partial \boldsymbol{d}^{cse}} = \int_{S^e} \beta_f^{\theta,S}\, \left(\boldsymbol{N}^{cse1,p}\right)^T \cdot \boldsymbol{B}^{cse1,p} \cdot \left\{\boldsymbol{p}_f^{cse}\right\} \cdot \frac{\partial (\tilde{v}_t^{D,S}\, l)}{\partial \boldsymbol{d}^{cse}}\, da$$

$$\frac{\partial \boldsymbol{f}_{cse}^{\theta 6,int}}{\partial \boldsymbol{p}_f^{cse}} = \int_{S^e} \left[\beta_f^{\theta,S}\, \tilde{v}_t^{D,S}\, l\, \left(\boldsymbol{N}^{cse1,p}\right)^T \cdot \boldsymbol{B}^{cse1,p} + \beta_f^{\theta,S}\, l\, \left(\boldsymbol{N}^{cse1,p}\right)^T \cdot \boldsymbol{B}^{cse1,p} \cdot \left\{\boldsymbol{p}_f^{cse}\right\} \cdot \frac{\partial \tilde{v}_t^{D,S}}{\partial \boldsymbol{p}_f^{cse}} \right] da$$

7.2 Partially saturated TPM CIE model

7.2.1 Governing equations and finite element formulations

The governing equations are obtained by extending the saturated TPM CIE, and details are omitted here.

7.2.1.1 Balance of linear momentum for matrix and fracture

The finite element form of balance of linear momentum equation is written as

$$\begin{aligned}
&\mathop{\mathbf{A}}_{e=1}^{n_{\text{bel}}} (\boldsymbol{c}^e)^T \cdot \Bigg[\underbrace{\int_{\Omega^e} (\boldsymbol{B}^{e,u})^T \cdot \boldsymbol{\sigma}' dv}_{\boldsymbol{f}_e^{d,int}} - \underbrace{\int_{\Omega^e} (\tilde{\boldsymbol{B}}^{e,u})^T \cdot \boldsymbol{N}^{e,p} \cdot \left[\chi \boldsymbol{p}_w^e + (1-\chi)\boldsymbol{p}_g^e\right] dv}_{\boldsymbol{f}_e^{dp,int}} \\
&- \underbrace{\int_{\Omega^e} \rho \left(\boldsymbol{N}^{e,u}\right)^T \cdot \boldsymbol{b}\, dv}_{\boldsymbol{f}_e^{df,ext}} - \underbrace{\int_{\Gamma_t^e} \left(\boldsymbol{N}^{e,u}\right)^T \boldsymbol{t}^{\sigma'} da}_{\boldsymbol{f}_e^{dt,ext}} + \underbrace{\int_{\Gamma_t^e} \chi \left(\boldsymbol{N}^{e,u}\right)^T \cdot \boldsymbol{\nu} \cdot \boldsymbol{N}^{e,p}\, da}_{\boldsymbol{k}_e^{dp2}} \cdot \boldsymbol{p}_w^e \Bigg] \\
&+ \mathop{\mathbf{A}}_{e=1}^{n_{\text{cel}}} (\boldsymbol{c}^{cse})^T \left[\underbrace{\int_{S^e} (\boldsymbol{N}^{cse,u})^T \cdot \boldsymbol{T}' da}_{\boldsymbol{f}_{cse}^{d,int}} - \underbrace{\int_{S^e} (\boldsymbol{N}^{cse,u})^T \cdot \boldsymbol{n} \cdot \boldsymbol{N}^{cse1,p} \left[\chi^S \boldsymbol{p}_w^e + (1-\chi^S)\boldsymbol{p}_g^e\right] da}_{\boldsymbol{f}_{cse}^{dp,int}} \right] = \boldsymbol{0}
\end{aligned} \tag{7.36}$$

where, n_{bel} denotes the number of bulk element; correspondingly, n_{cel} denotes the number of cohesive element.

7.2.1.2 Balance of mass for water species in discontinuity

$$\mathop{\mathbf{A}}_{e=1}^{n_{\text{cel}}} (\boldsymbol{\alpha}^{cse})^T \cdot \quad \Bigg[\underbrace{\int_{S^e} (\rho^{wR} S_w^S + \rho^{gvR} S_g^S)(\boldsymbol{N}^{cse1,p})^T \cdot \boldsymbol{n}^T \cdot \boldsymbol{N}^{cse,u}\, da}_{\boldsymbol{k}_{cse}^{wd}} \left\{ \dot{\boldsymbol{d}}^{cse} \right\}$$

$$
\begin{aligned}
&+ \underbrace{\int_{S^e} \left[n^S (\rho^{wR} - \rho^{gvR}) \frac{\partial S_w^S}{\partial s} + n^S S_g^S \frac{\partial \rho^{gvR}}{\partial s} \right] l \, (\boldsymbol{N}^{cse1,p})^T \cdot \boldsymbol{N}^{cse1,p} \, da}_{\boldsymbol{k}_{cse}^{wg}} \{\dot{\boldsymbol{p}}_g^{cse}\} \\
&- \underbrace{\int_{S^e} \left[n (\rho^{wR} - \rho^{gvR}) \frac{\partial S_w^S}{\partial s} + n^S S_g^S \frac{\partial \rho^{gvR}}{\partial s} \right] l \, (\boldsymbol{N}^{cse1,p})^T \cdot \boldsymbol{N}^{cse1,p} \, da}_{\boldsymbol{k}_{cse}^{wg}} \{\dot{\boldsymbol{p}}_w^{cse}\} \\
&+ \underbrace{\int_{S^e} \left(n^S S_g^S \frac{\partial \rho^{gvR}}{\partial \theta} - \beta_{swg}^S \right) l \, (\boldsymbol{N}^{cse1,p})^T \, \boldsymbol{N}^{cse1,p} \, da}_{\boldsymbol{k}_{cse}^{w\theta}} \left\{ \dot{\boldsymbol{\theta}}^{cse} \right\} \\
&- \underbrace{\int_{S^e} (\boldsymbol{N}^{cse2,p})^T \, 2 \rho^{wR} (\tilde{v}_w^{D,S})_n \, da}_{\boldsymbol{f}_{cse}^{w1,int}} - \underbrace{\int_{S^e} (\boldsymbol{B}^{cse1,p})^T \, \rho^{wR} (\tilde{v}_w^{D,S})_t \, l \, da}_{\boldsymbol{f}_{cse}^{w2,int}} \\
&- \underbrace{\int_{S^e} (\boldsymbol{N}^{cse2,p})^T \, 2 \rho^{gvR} (\tilde{v}_{gv}^{D,S})_n \, da}_{\boldsymbol{f}_{cse}^{w3,int}} - \underbrace{\int_{S^e} (\boldsymbol{B}^{cse1,p})^T \, \rho^{gvR} (\tilde{v}_{gv}^{D,S})_t \, l \, da}_{\boldsymbol{f}_{cse}^{w4,int}} \\
&= \underbrace{\int_{\Gamma_S} (\boldsymbol{N}^{cse1,p})^T \left(S^{w,S} + S^{gv,S} \right) \, da}_{\boldsymbol{f}_{cse}^{w,ext}} \Bigg]
\end{aligned}
\tag{7.37}
$$

7.2.1.3 Balance of mass for dry air in discontinuity

$$
\begin{aligned}
\sum_{e=1}^{n_{\text{cel}}} \mathbf{A} (\boldsymbol{\beta}^{cse})^T \cdot \Bigg[& \underbrace{\int_{S^e} \rho^{gaR} S_g^S (\boldsymbol{N}^{cse1,p})^T \cdot \boldsymbol{n}^T \cdot \boldsymbol{N}^{cse,u} \, da}_{\boldsymbol{k}_{cse}^{gd}} \left\{ \dot{\boldsymbol{d}}^{cse} \right\} \\
&+ \underbrace{\int_{S^e} \left[n^S S_g^S \frac{\partial \rho^{gaR}}{\partial p_w} + n \rho^{gaR} \frac{S_w^S}{\partial s} \right] l \, (\boldsymbol{N}^{cse1,p})^T \cdot \boldsymbol{N}^{cse1,p} \, da}_{\boldsymbol{k}_{cse}^{gw}} \{\dot{\boldsymbol{p}}_w^{cse}\} \\
&+ \underbrace{\int_{S^e} \left[n^S S_g^S \frac{\partial \rho^{gaR}}{\partial p_g} - n^S \rho^{gaR} \frac{S_w^S}{\partial s} \right] l \, (\boldsymbol{N}^{cse1,p})^T \cdot \boldsymbol{N}^{cse1,p} \, da}_{\boldsymbol{k}_{cse}^{gg}} \{\dot{\boldsymbol{p}}_g^{cse}\} \\
&+ \underbrace{\int_{S^e} \left(n^S S_g^S \frac{\partial \rho^{gaR}}{\partial \theta} - \beta_s^{\theta,S} (1 - n^S) \rho^{gaR} S_g^S \right) l \, (\boldsymbol{N}^{cse1,p})^T \, \boldsymbol{N}^{cse1,p} \, da}_{\boldsymbol{k}_{cse}^{g\theta}} \left\{ \dot{\boldsymbol{\theta}}^{cse} \right\}
\end{aligned}
$$

$$
\begin{aligned}
&- \underbrace{\int_{S^e} (\boldsymbol{N}^{cse2,p})^T \, 2\rho^{gaR} (\tilde{v}_{ga}^{D,S})_n \, da}_{\boldsymbol{f}_{cse}^{g1,int}} - \underbrace{\int_{S^e} (\boldsymbol{B}^{cse1,p})^T \, \rho^{gaR} (\tilde{v}_{ga}^{D,S})_t \, l \, da}_{\boldsymbol{f}_{cse}^{g2,int}} \\
&= \underbrace{\int_{\Gamma_S} (\boldsymbol{N}^{cse1,p})^T S^{ga,S} \, da}_{\boldsymbol{f}_{cse}^{g,ext}} \Bigg] \qquad (7.38)
\end{aligned}
$$

7.2.1.4 Energy conservation for mixture in discontinuity

$$
\begin{aligned}
\overset{n_{\text{cel}}}{\underset{e=1}{\mathbf{A}}} \quad & (\boldsymbol{\beta}^{cse})^T \cdot \Bigg[\underbrace{\int_{S^e} -\Delta H_{vap} \rho^{wR} S_w^S (\boldsymbol{N}^{cse1,p})^T \cdot \boldsymbol{n}^T \cdot \boldsymbol{N}^{cse,u} \, da}_{\boldsymbol{k}_{cse}^{\theta d}} \left\{ \dot{\boldsymbol{d}}^{cse} \right\} \\
& + \underbrace{\int_{S^e} n^S \rho^{wR} \Delta H_{vap} \left(\frac{\partial S_w^S}{\partial s} \right) l \, (\boldsymbol{N}^{cse1,p})^T \cdot \boldsymbol{N}^{cse1,p} \, da}_{\boldsymbol{k}_{cse}^{\theta w}} \{ \dot{\boldsymbol{p}}_w^{cse} \} \\
& - \underbrace{\int_{S^e} n \rho^{wR} \Delta H_{vap} \left(\frac{\partial S_w^S}{\partial s} \right) l \, (\boldsymbol{N}^{cse1,p})^T \cdot \boldsymbol{N}^{cse1,p} \, da}_{\boldsymbol{k}_{cse}^{\theta w}} \{ \dot{\boldsymbol{p}}_g^{cse} \} \\
& + \underbrace{\int_{S^e} \left\{ (\rho C)^S + \Delta H_{vap} S_w^S \rho^{wR} \left[\beta_s^{\theta,S} (1 - n^S) + \beta_w^{\theta,S} \right] \right\} l \, (\boldsymbol{N}^{cse1,p})^T \cdot \boldsymbol{N}^{cse1,p} \, da}_{\boldsymbol{k}_{cse}^{\theta\theta}} \left\{ \dot{\boldsymbol{\theta}}^{cse} \right\} \\
& + \underbrace{\int_{S^e} \left(\rho^{wR} C_w (\tilde{v}_w^{D,S})_n + \rho^{gR} C_g (\tilde{v}_g^{D,S})_n \right) \, (\boldsymbol{N}^{cse1,p})^T \cdot \boldsymbol{N}^{cse2,p} \cdot \{ \boldsymbol{\theta}^{cse} \} \, da}_{\boldsymbol{f}_{cse}^{\theta 1,int}} \\
& + \underbrace{\int_{S^e} \left(\rho^{wR} C_w \, (\tilde{v}_w^{D,S})_t + \rho^{gR} C_g \, (\tilde{v}_g^{D,S})_t \right) \, l \, (\boldsymbol{N}^{cse1,p})^T \cdot \boldsymbol{B}^{cse1,p} \cdot \{ \boldsymbol{\theta}^{cse} \} \, da}_{\boldsymbol{f}_{cse}^{\theta 2,int}} \\
& + \underbrace{\int_{S^e} 2 \hat{K}_n^{\theta} \boldsymbol{N}^{cse2,p} \cdot \{ \boldsymbol{\theta}^{cse} \} \, (\boldsymbol{N}^{cse2,p})^T \, da}_{\boldsymbol{f}_{cse}^{\theta 3,int}(\boldsymbol{d}^{cse}, \boldsymbol{\theta}^{cse})} + \underbrace{\int_{S^e} \hat{K}_t^{\theta} \boldsymbol{B}^{cse1,p} \cdot \{ \boldsymbol{\theta}^{cse} \} \, l \, (\boldsymbol{B}^{cse1,p})^T \, da}_{\boldsymbol{f}_{cse}^{\theta 4,int}} \\
& + \underbrace{\int_{S^e} \Delta H_{vap} \left(\rho^{wR} (\tilde{v}_w^{D,S})_n - \rho^{gvR} (\tilde{v}_{gv}^{D,S})_n \right) (\boldsymbol{N}^{cse2,p})^T \, da}_{\boldsymbol{f}_{cse}^{\theta 5,int}}
\end{aligned}
$$

$$+\underbrace{\int_{S^e}\Delta H_{vap}\left(\rho^{wR}(\tilde{v}_w^{D,S})_t-\rho^{gvR}(\tilde{v}_{gv}^{D,S})_t\right)\,l\,(\boldsymbol{B}^{cse1,p})^T\,da}_{\boldsymbol{f}_{cse}^{\theta 6,int}}$$

$$=\underbrace{\int_{\Gamma_S}(\boldsymbol{N}^{cse1,p})^T q^{end}\,da+\int_{S^l}(\boldsymbol{N}^{cse1,p})^T(\rho r)^S\,dv-\int_{\Gamma_S}(\boldsymbol{N}^{cse1,p})^T\Delta H_{vap}\rho^{wR}S^{w,S}\,da}_{\boldsymbol{f}_{cse}^{\theta,ext}}\Bigg] \tag{7.39}$$

The finite element matrix equation for thermo-poro-mechanical interface element model is written as

$$\boldsymbol{C}_{cse}(\boldsymbol{D}^{cse})\cdot\dot{\boldsymbol{D}^{cse}}+\boldsymbol{F}_{cse}^{INT}(\boldsymbol{D}^{cse})=\boldsymbol{F}_{cse}^{EXT}(\boldsymbol{D}^{cse}) \tag{7.40}$$

where

$$\dot{\boldsymbol{D}^{cse}}=\begin{bmatrix}\dot{\boldsymbol{d}}^{cse}\\ \dot{\boldsymbol{p}}_w^{cse}\\ \dot{\boldsymbol{p}}_g^{cse}\\ \dot{\boldsymbol{\theta}^{cse}}\end{bmatrix},\quad \boldsymbol{D}^{cse}=\begin{bmatrix}\boldsymbol{d}^{cse}\\ \boldsymbol{p}_w^{cse}\\ \boldsymbol{p}_g^{cse}\\ \boldsymbol{\theta}^{cse}\end{bmatrix},\quad \boldsymbol{C}=\begin{bmatrix}\boldsymbol{0} & \boldsymbol{0} & \boldsymbol{0} & \boldsymbol{0}\\ \boldsymbol{K}_{cse}^{wd} & -\boldsymbol{K}_{cse}^{wg} & \boldsymbol{K}_{cse}^{wg} & \boldsymbol{K}_{cse}^{w\theta}\\ \boldsymbol{K}_{cse}^{gd} & \boldsymbol{K}_{cse}^{gw} & \boldsymbol{K}_{cse}^{gg} & \boldsymbol{K}_{cse}^{g\theta}\\ \boldsymbol{K}_{cse}^{\theta d} & \boldsymbol{K}_{cse}^{\theta g} & -\boldsymbol{K}_{cse}^{\theta g} & \boldsymbol{K}_{cse}^{\theta\theta}\end{bmatrix}$$

and,

$$\boldsymbol{F}_{cse}^{INT}=\begin{bmatrix}\boldsymbol{F}_{cse}^{d,INT}-\boldsymbol{F}_{cse}^{dp,INT}\\ -\boldsymbol{F}_{cse}^{w1,INT}-\boldsymbol{F}_{cse}^{w2,INT}-\boldsymbol{F}_{cse}^{w3,INT}-\boldsymbol{F}_{cse}^{w4,INT}\\ -\boldsymbol{F}_{cse}^{g1,INT}-\boldsymbol{F}_{cse}^{g2,INT}\\ \boldsymbol{F}_{cse}^{\theta 1,INT}+\boldsymbol{F}_{cse}^{\theta 2,INT}+\boldsymbol{F}_{cse}^{\theta 3,INT}+\boldsymbol{F}_{cse}^{\theta 4,INT}+\boldsymbol{F}_{cse}^{\theta 5,INT}+\boldsymbol{F}_{cse}^{\theta 6,INT}\end{bmatrix}$$

$$\boldsymbol{F}_{cse}^{EXT}=\begin{bmatrix}\boldsymbol{F}_{cse}^{df,EXT}+\boldsymbol{F}_{cse}^{dt,EXT}\\ \boldsymbol{F}_{cse}^{w,EXT}\\ \boldsymbol{F}_{cse}^{g,EXT}\\ \boldsymbol{F}_{cse}^{\theta,EXT}\end{bmatrix}$$

7.3 Numerical examples

In this section, we will test the performance of the fully and partially saturated TPM interface element models.

7.3.1 Case study of fully saturated TPM CIE

To test the fully saturated saturated TPM cohesive interface element (CIE) model, first we set up two examples under axisymmetric condition (see Figures 7.1 and 7.11). For both examples, a linear isotropic elastic constitutive model is adopted for the solid skeleton of the matrix (or bulk elements), and zero-thickness TPM cohesive interface element (CIE) model is used for the fully liquid saturated fracture. The water table is at the top, i.e. $p_w = 0$ respectively at $z = 1.6m$ in Figure 7.1 and $z = 1m$ in Figure 7.11.

7.3.1.1 Fully saturated TPM CIE example 1

An axisymmetric saturated soil column has a depth of 1.6 m and a radius of $2 + l$ m. The vertical fracture with a uniform aperture of l exists between two matrix (or bulk) elements as shown in Figure 7.1. To represent a fully saturated condition, the water table is at the top of the soil domain, which corresponds to a drained boundary $p_w = 0$ at $z = 1.6m$. Also, no heat flux is allowed from the top. The bottom and surface are fixed respectively in vertical and horizontal directions, and are both treated as impermeable and adiabatic boundaries. Due to axisymmetry, the axis is fixed horizontally, and is considered as impermeable and adiabatic boundary. The initial conditions include uniform temperature $\theta = 20^oC$ and a linear distribution of the pore water pressure. The test procedure is depicted in Figure 7.2. Gravity is considered, and zero traction is applied on the top. A prescribed temperature change of $\Delta\theta = 20^oC$ is applied along the axis $r = 0$. Different initial apertures are used, which are $l_0 = 0$, $l_0 = 1cm$, and $l_0 = 10cm$.

Results: The variations of pore water pressure at the bottom of the matrix and the fracture are shown in Figures 7.3, 7.4, and 7.5, respectively. With zero initial aperture, we obtain the

same results as for an uncracked porous medium, i.e. same pore water pressure builds up due to application of gravity, and dissipates afterward till it arrives at hydrostatic state afterward. With initial aperture $l_0 = 1cm$, smaller pore water pressure generation is observed within the crack than that in the matrix (node 73 and node 162). While for even greater aperture $l_0 = 10cm$, the fracture acts like an open channel, thus very small pore water pressure is generated within the crack as shown in Figure 7.5. Figures 7.7-7.9 indicate that temperature jumps inside the crack change with apertures. With aperture smaller than $l_0 = 1cm$, temperature jumps due to the fracture is negligible. With $l_0 = 10cm$, small temperature jump is observed as shown in Figure 7.9. With zero thermal conductivity for the crack, heat transfer does not happen from one matrix to the other, thus a large temperature jump appears as shown in Figure 7.6. Generally, the heat and liquid flow from one matrix into the fracture and through the fracture into another matrix may be affected by thermal, hydraulic and mechanical parameters of the fracture. Further work is necessary with respect to sensitivity analysis of the relevant parameters.

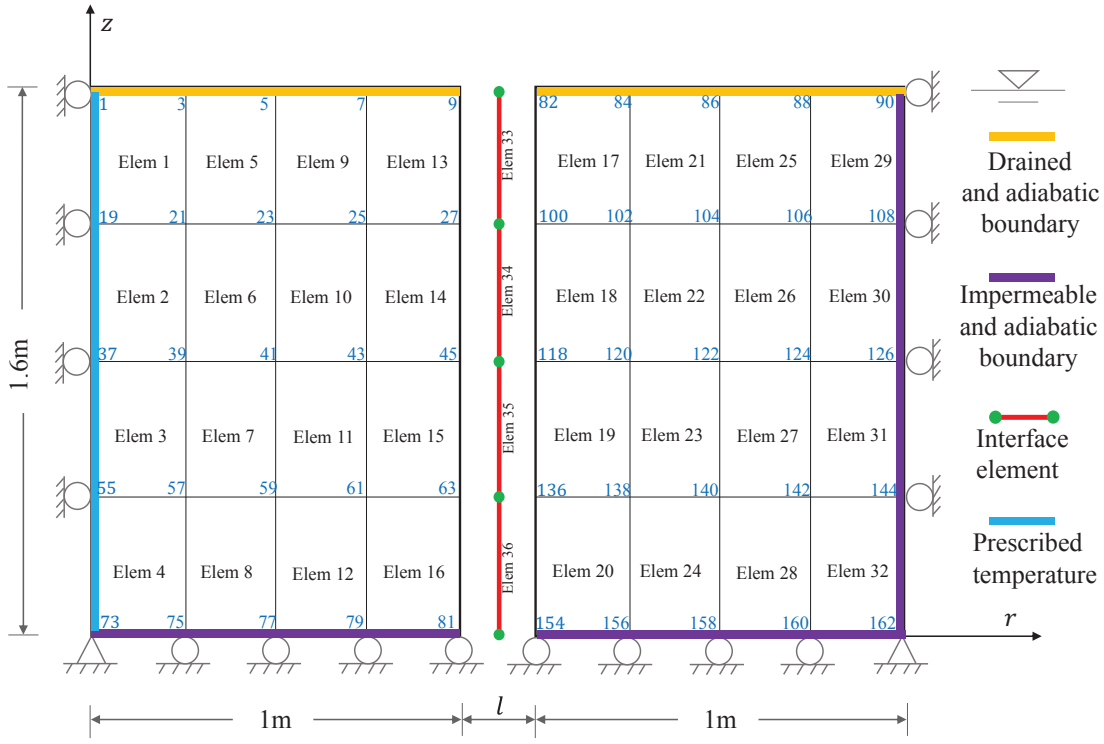

Figure 7.1: Axisymmetric finite element mesh for fully saturated porous media with vertical fracture with aperture l: 162 nodes, thirty-two saturated Q9P4 TPM bulk elements (Elem1-Elem32) and four Q6P4 TPM CIEs (Elem33-Elem36). Gravity load is applied, and zero traction at the top.

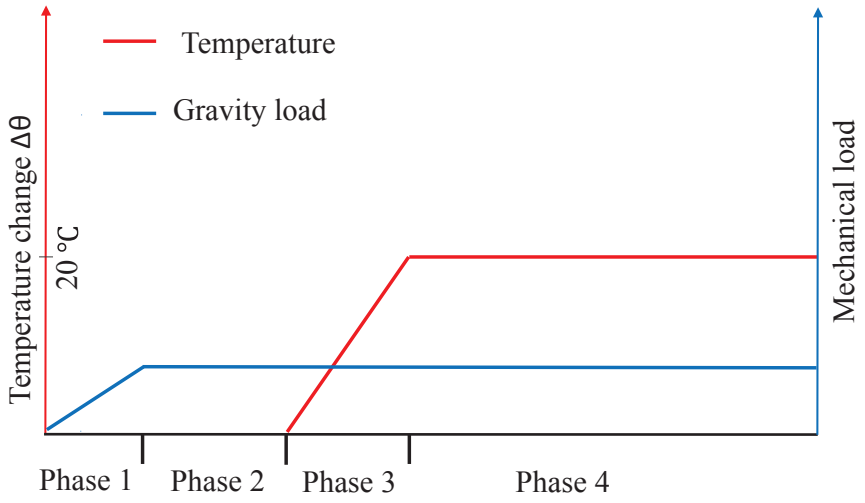

Figure 7.2: Test procedure of the example in Section 7.3.1.1.

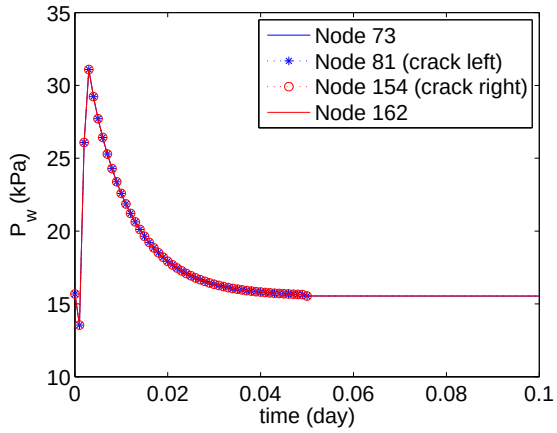

Figure 7.3: Variations of pore water pressure with initial aperture $l_0 = 0$.

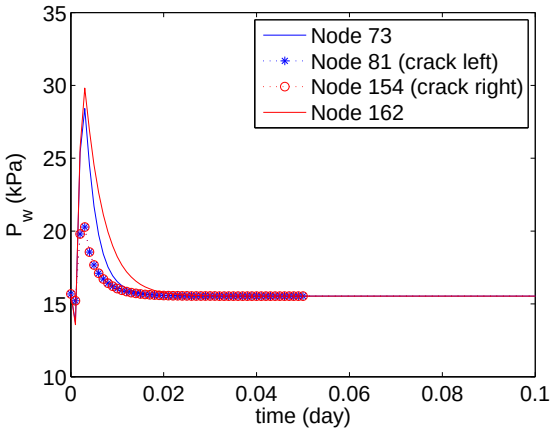

Figure 7.4: Variations of temperature with initial aperture $l_0 = 1cm$.

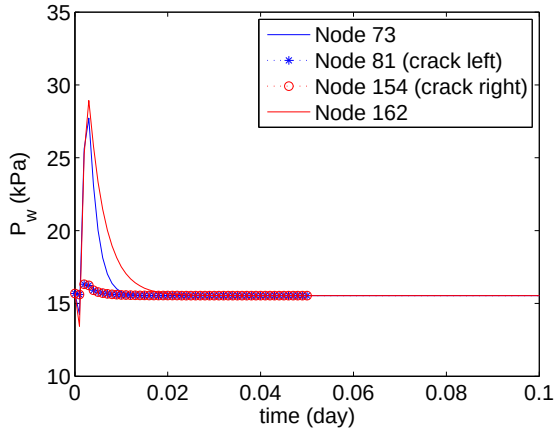

Figure 7.5: Variations of pore water pressure with initial aperture $l_0 = 10cm$.

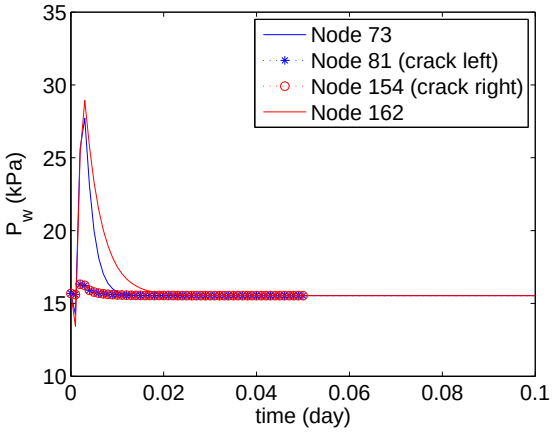

Figure 7.6: Variations of pore water pressure with initial aperture $l_0 = 10cm$, and $K_f^\theta = 0W/(Km)$.

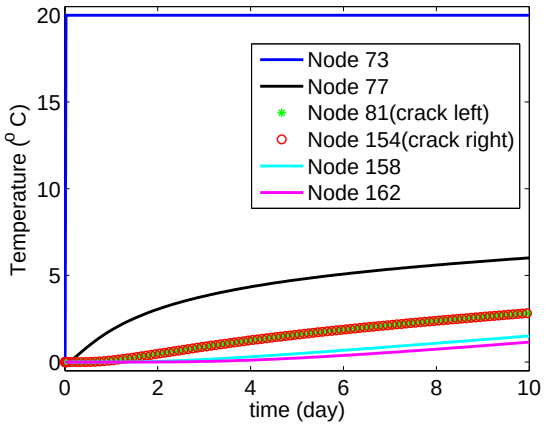

Figure 7.7: Variations of temperature with initial aperture $l_0 = 0$.

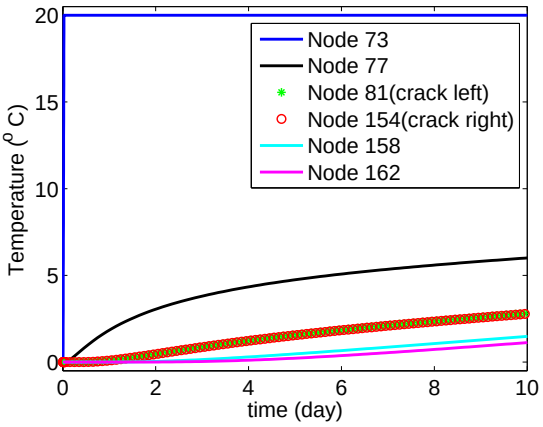

Figure 7.8: Variations of temperature with initial aperture $l_0 = 1cm$.

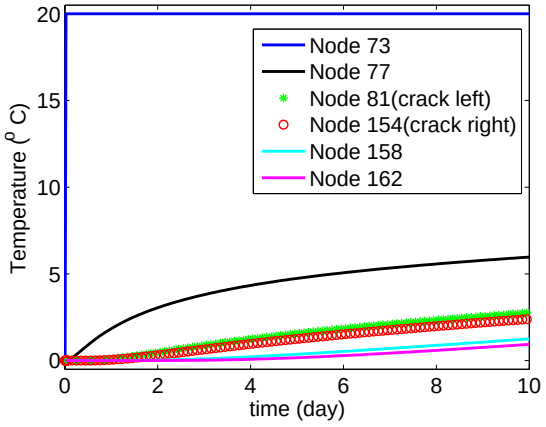

Figure 7.9: Variations of temperature with initial aperture $l_0 = 10cm$.

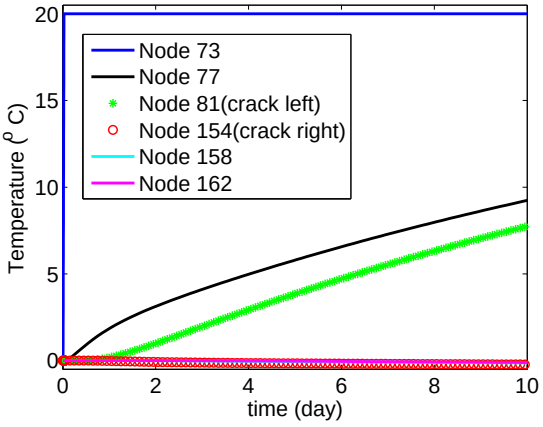

Figure 7.10: Variations of pore water pressure with initial aperture $l_0 = 10cm$, and $K_f^\theta = 0W/(Km)$.

7.3.1.2 Fully saturated thermo-poro-mechanical CIE example 2

We set up the following example to test the plastic performance of the fully saturated thermo-poro-mechanical cohesive interface element. As depicted in Figure 7.11, the axis and side surface are fixed in the horizontal direction; the top and the bottom of the matrix on the right of the crack are fixed vertically. The bottom and the side surface are impermeable and adiabatic; the top boundary is drained and adiabatic. No liquid flux is allowed along the axis $r = 0$ due to the axisymmetry. Water table is set at the top $z = 1m$ to represent a fully saturated condition. To simulate a pull-out test, the bottom of the matrix on the left of the crack is free to move vertically, and a final prescribed vertical displacement $u_z = 5mm$ is ramped up with small enough time step at the top and kept constant after $t = 1day$ to assure the stability during the development of shear plasticity. Also, the gravity is ignored here. During the prescribed vertical displacement is applied, a final prescribed temperature increase of 20^oC is applied with the same ramp function as used for prescribed displacement along the axis (refer to the curve with the legend of Node 73 in Figure 7.13). One column of 6 equal height bulk elements is used for each of the matrix blocks adjacent to the crack. Another 6 equal length zero-thickness CIEs are used for the crack with the initial aperture $l_0 = 1cm$. A total of 78 nodes and 18 elements are shown in Figure 7.11. The same initial conditions are used as the previous example, i.e. uniform temperature $\theta = 20^oC$ and a linear distribution of the pore water pressure.

Results: Figure 7.12 shows the vertical displacement versus the height of the crack at the end of the simulation. Due to the prescribed upward displacement, the left matrix block moves upwards compared to the right matrix block, and the largest vertical displacement difference Δu_z is reached near the top. In this example specifically, the magnitude of Δu_z is the same as that of the total tangential displacement jump u_t, and positive u_t implies that the left virtual surface experiences a larger vertical displacement than the right virtual surface. Figures 7.14-7.17 are plotted at the third Gauss point (closest to the top) of element 13 (CIE). Figure 7.14 shows u_t as well as the its plastic and elastic components, i.e. u_t^p and u_t^e, respectively. It indicates that shear

plasticity is triggered along the virtual surface S^h of CIE at this position at a small value of u_t, and the plastic part u_t^p dominates the total tangential displacement jump u_t after $t \approx 0.26day$. In Figure 7.15, a much smaller positive normal displacement jump u_n is developed compared to u_t during the shear-dominaated process, which implied the crack is slightly under tension as shown in Figure 7.16. The variations of normal stress T_n and tangential stress T_t, which are respectively related to u_n^e and u_t^e, are plotted versus u_t in Figure 7.16. Figure 7.17 shows the stress path (T_n versus T_t) and the yield surface evolution. Combining Figures 7.16 and 7.17, we observe that the tangential stress T_t starts to decrease once plasticity is triggered, hence the shrinking of the yield surface, which is refered to as the stress-softening phenomena.

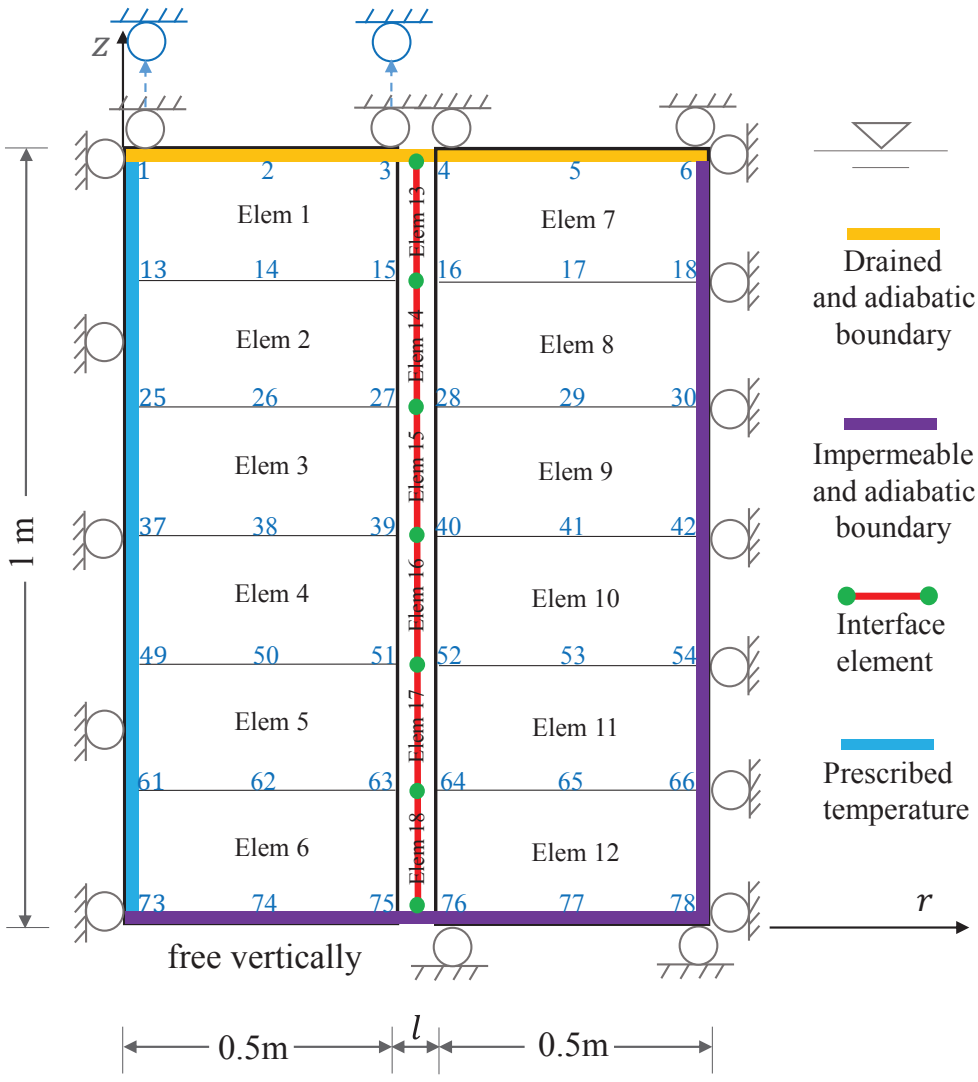

Figure 7.11: Axisymmetric finite element mesh for fully saturated porous media with initial vertical fracture $l_0 = 1cm$: 78 nodes, 12 saturated Q9P4 TPM bulk elements (Elem1-Elem12) and 6 Q6P4 TPM CIEs (Elem13-Elem18). Gravity load is ignored, and zero traction at the top.

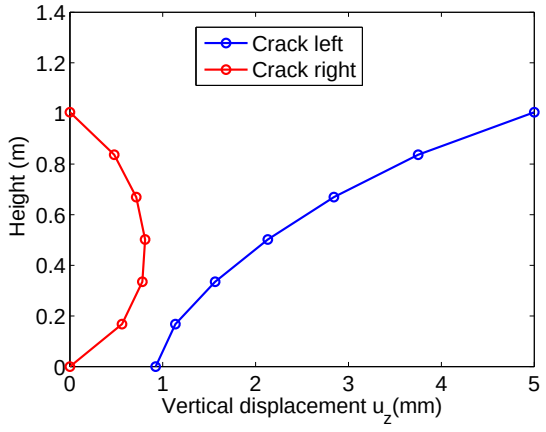

Figure 7.12: Vertical displacement profiles for the two surfaces (S^+ and S^-) of the crack.

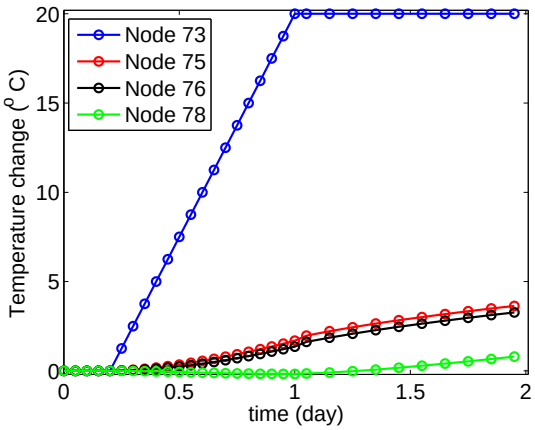

Figure 7.13: Variations of temperature at the bottom nodes.

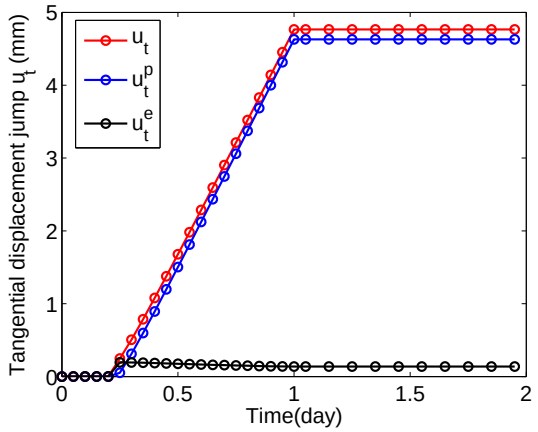

Figure 7.14: Total tangential displacement jump u_t, and its plastic and elastic components u_t^p and u_t^e at the third (or upper) Gauss point of element 13.

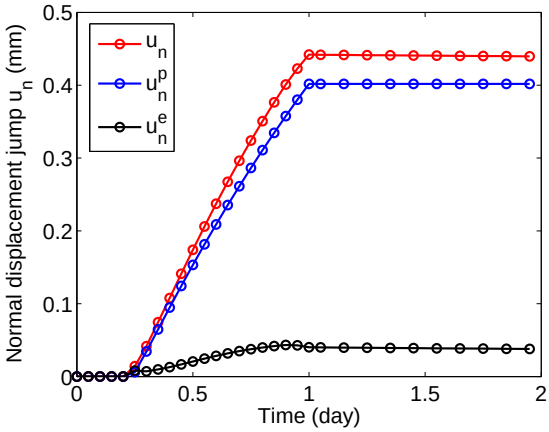

Figure 7.15: Total normal displacement jump u_n, and its plastic and elastic components u_n^p and u_n^e at the third (or upper) Gauss point of element 13.

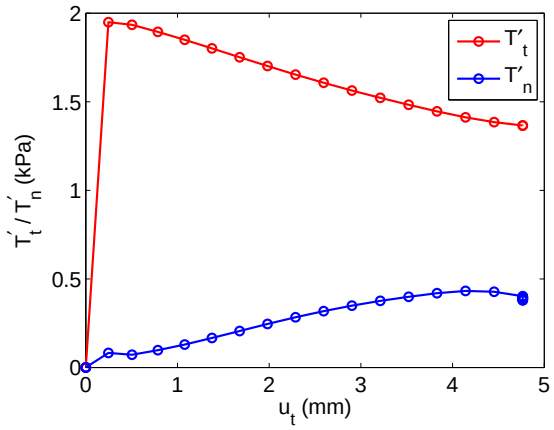

Figure 7.16: Tangential stress T_t and normal stress T_n versus tangential displacement jump at the third (or upper) Gauss point of element 13.

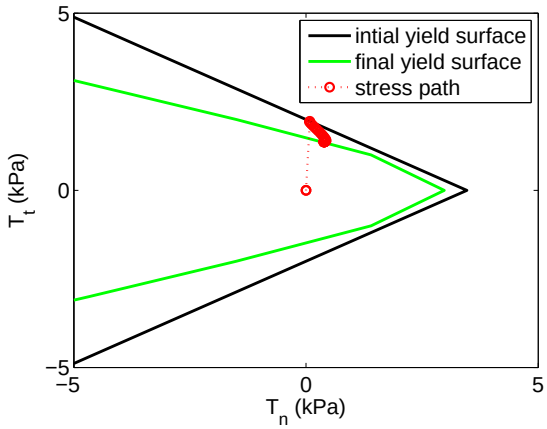

Figure 7.17: Stress path and yield surface evolution at the third (or upper) Gauss point of element 13.

7.3.2 Case study of partially saturated TPM CIE

We set up the following example to test the plastic performance of the partially saturated thermo-poro-mechanical cohesive interface element. The dimensions and boundary conditions are indicated in Figure 7.18. The bottom and side surface are fixed in normal displacement, and are impermeable and adiabatic boundaries. Due to the axisymmetry, the axis boundary is fixed in r direction, and is impermeable. An uniform traction $\boldsymbol{t}^{\sigma'} = 10kPa$ is applied upwards at the top of the left matrix block. An increase temperature of $\Delta\theta = 20^oC$ is prescribed along the axis after the traction is exerted. The test procedure is shown in Figure 7.19.

Results: Figure 7.20 shows that with the traction applied on the left matrix block, a vertical displacement jump Δu_z occurs between the two virtual surfaces of the crack above the height of 0.5m approximately. The largest $\Delta u_z \approx 2.75mm$ is reached at the top. Temperature increase results in the thermal expansion of the crack, which leads to a small but noticeable upward vertical displacement at the top of the crack as shown in Figure 7.20. With small initial aperture $l_0 = 1mm$, temperature difference is negligible within the crack according to curves for node 51 and node 52 in Figure 7.21. Therefore, no significant vertical displacement jump induced by thermal expansion is observed shown by Figure 7.20. Figures 7.22-7.25 are plotted at the third Gauss point (closest to the top) of element 9 (CIE). Figure 7.22 shows the tangential displacement jump u_t as well as the its plastic and elastic components, i.e. u_t^p and u_t^e, respectively. It indicates that shear plasticity is triggered in the cohesive interface element at this position, and the plastic part u_t^p dominates after the step number $n = 12$. Figure 7.23 indicates that a very small positive normal displacement jump u_n is developed compared to u_t, which implied the crack is under tension as shown in Figure 7.24. A softening phenomenon is observed from shrinking of the yield surface in Figure 7.25. The stress path T_n versus T_t in Figure 7.25 and the stress variations in Figure 7.24 indicate that the tangential stress T_t starts to decrease from the second step when plasticity is triggered, along with a small increase of the normal stress T_n.

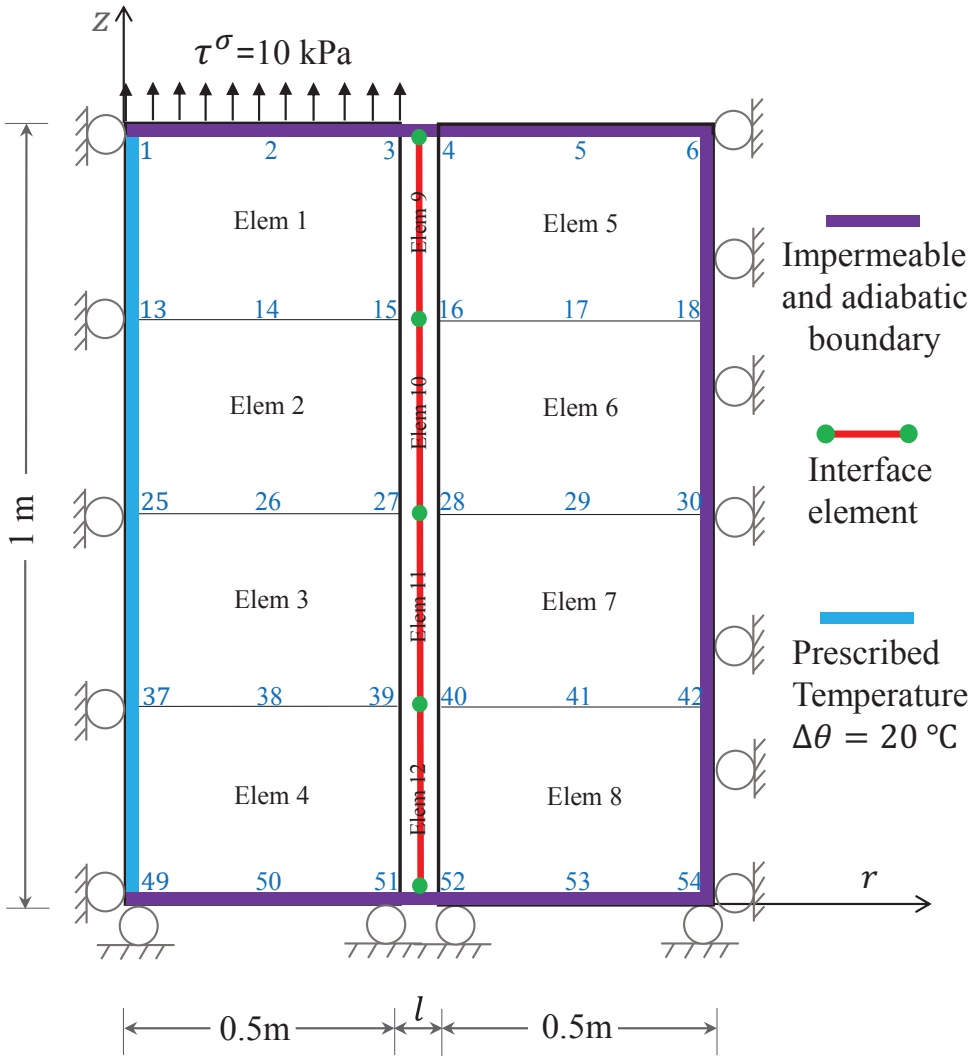

Figure 7.18: Axisymmetric finite element mesh for fully saturated porous media with initial vertical fracture $l_0 = 1mm$: 54 nodes, 8 unsaturated Q9P4 TPM bulk elements (Elem1-Elem8) and 4 Q6P4 TPM CIEs (Elem8-Elem12). Gravity load is applied, and upward traction of $10kPa$ is exerted on top.

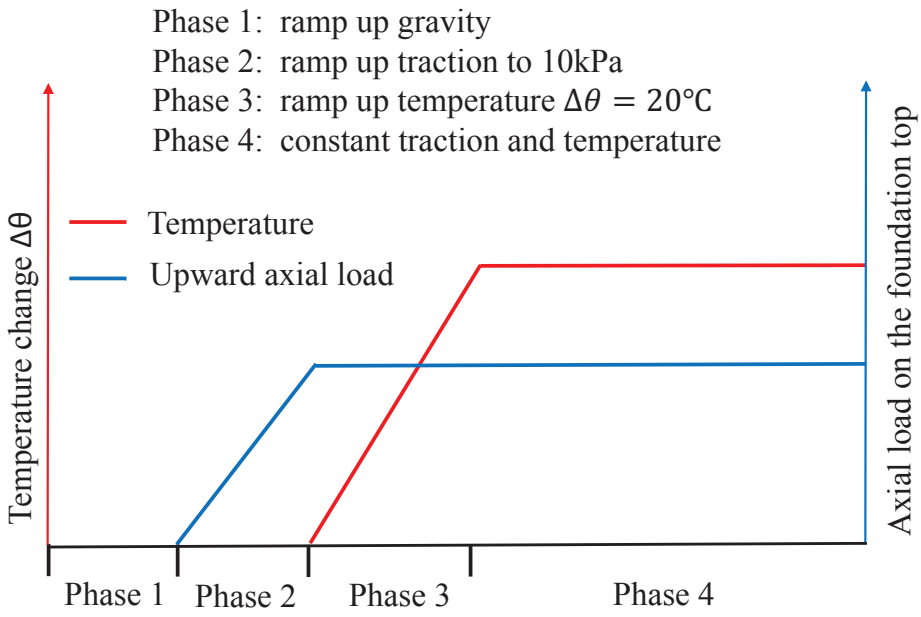

Figure 7.19: Test procedure for example in Section 7.3.2.

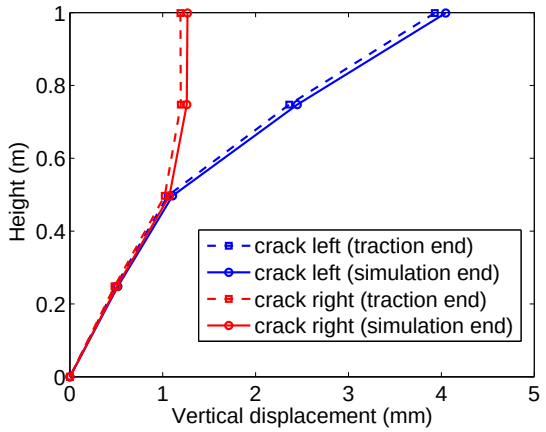

Figure 7.20: Vertical displacement profiles for the two surfaces of the CIEs at the end of phase 2 and phase 4.

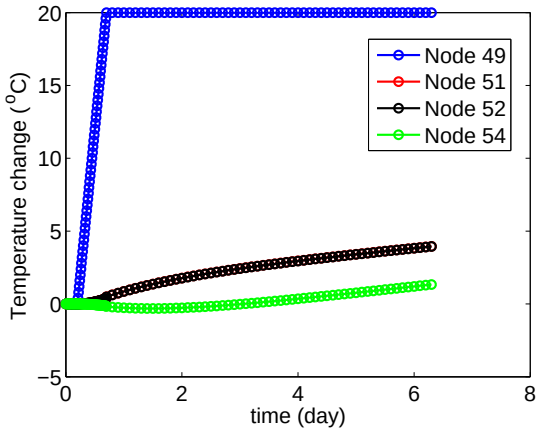

Figure 7.21: Variations of temperature at the bottom nodes.

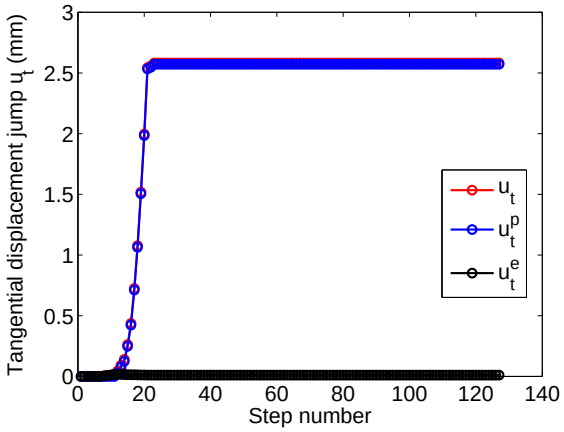

Figure 7.22: Total tangential displacement jump u_t, and its plastic and elastic components u_t^p and u_t^e at the third (or upper) Gauss point of element 9.

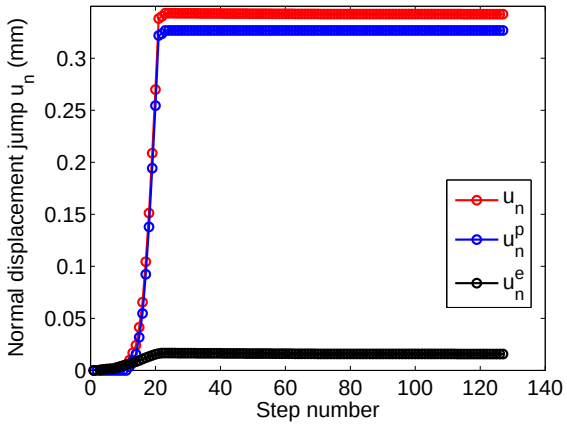

Figure 7.23: Total normal displacement jump u_n, and its plastic and elastic components u_n^p and u_n^e at the third (or upper) Gauss point of element 9.

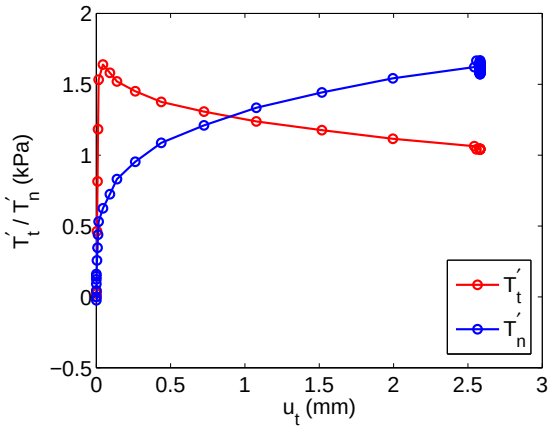

Figure 7.24: Tangential stress T_t and normal stress T_n versus tangential displacement jump at the third (or upper) Gauss point of element 9.

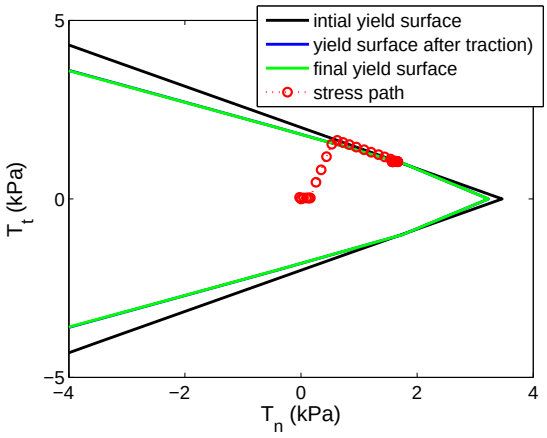

Figure 7.25: Stress path and yield surface evolution at the third (or upper) Gauss point of element 9.

7.3.3 Revisit the energy foundation centrifuge tests

In this part, let us revisit the energy foundation centrifuge test by Goode (2013), and implement the TPM CIEs along the soil-foundation interface. For now, without further information regarding the failure mechanism, e.g. the position of failure plane in the soil beneath the foundation, let us simply implement the CIEs vertically along the height of the soil as shown in Figure 7.26. Six CIEs are used in total, four of which are implemented at the soil-foundation interface, and the other two CIEs are implemented at the soil-soil interface. The CIEs are numbered CIE 1,...CIE 6 from top to bottom. In the future, we can consider the shear failure mechanism and implement CIEs along an inclined failure plane in the soil or consider a random pattern of CIEs, or an extended discontinuity FE implementation that would be insensitive to mesh alignment and refinement. The initial aperture is set to be $l_0 = 1 \times 10^{-5} m$. The plastic parameters for CIEs are listed in Table 7.1, and the other parameters are the same as those of the soil bulk elements. The nonlinear thermo-elasto-plastic constitutive model is applied to the soil continuum.

Table 7.1: Parameters for elasto-plastic CIE model.

Symbol(unit)	Value
$K_n(Pa/m)$	1×10^9
$K_t(Pa/m)$	1×10^8
$G_f^I(Pa \cdot m)$	1×10^4
$G_f^{II}(Pa \cdot m)$	1×10^4
$\chi_p(Pa)$	$c_p/tan(\phi_p)$
$\chi_r(Pa)$	0
$c_p(Pa)$	9500
$c_r(Pa)$	0
$\phi_p(rad)$	0.5236
$\phi_r(rad)$	0
$\psi_p(rad)$	0.087
α_χ	200
α_c	200
α_ϕ	900
α_ψ	900

In order to fit the settlement-load curve obtained from the experiment, different plastic

parameters are tried for the CIE model, and here we present model predictions with the best-fit parameters. However, with more experimental data available, we will be able to improve the predictive capability of the model by calibrating the parameters.

Figure 7.27(a) shows that without implementing TPM CIEs, a perfect bond has to be imposed at the foundation-soil interface. Consequently, the model fails to capture the side-shear failure due to the slippage along the interface. In contrast, the model is greatly improved after implementing TPM CIEs along the interface, i.e. the ultimate load $\approx 3410N$, and the corresponding settlement $\approx 0.85mm$, which are comparable with the experimental observation. When a higher load is applied, the model will not reach a converged state due to softening failure of certain CIE(s). After the unloading process, a smaller residual settlement remained compared to the experimental result. Nonlinearity and linearity are respectively observed in the loading and unloading processes from both the experimental and modeling results. An exploratory sensitivity analysis is conducted to inspect the effect of elastic tangential stiffness K_t on the settlement-loading curve during loading process. In Figure 7.27(c), K_t is incrementaly increased from $5e7Pa/m$ to $1e9Pa/m$, and the other parameters are fixed. For $K_t = 1e8Pa/m$ and $K_t = 5e7Pa/m$, a similar ultimate load is obtained while a larger slope (absolute value) or settlement is observed with lower K_t. The slopes with $K_t = 5e8Pa/m$ and $K_t = 1e9Pa/m$ are similar. While, for both cases ($K_t = 5e8Pa/m$ and $K_r = 1e9Pa/m$), the interface element failure happened at much smaller loads compared to the other two cases. Obviously, K_t is not the only parameter that affects the settlement-loading curve, thus requiring comprehensive sensitive analysis involving more parameters. Figure 7.27(b) indicates that 20^oC temperature increase has negligible effect on the settlement-load curve.

Next, let us inspect the displacement jump within the CIEs. Figures 7.28(a)-(c) show the vertical displacement u_z at the corner nodes of quadrilateral bulk elements adjacent to the left and right surfaces of the CIEs along the height at three different times respectively, i.e., the equilibration of centrifuge spin-up to a g-level of $N = 24$, the end of loading process, and the end of unloading process. In other words, we will analyze the relative vertical movements between the bulk elements on the left and right of the interface. The analysis will be focused on the CIEs along foundation-soil

interface, i.e. from the foundation top ($H = 0.5334m$) to the foundation bottom ($0.195m$). Figure 7.28(a) indicates vertical displacement jump occurs along the foundation-soil interface due to the centrifuge spin-up. Larger downward displacements are observed near the top and the bottom, implying a downward slippage of the foundation relative to the adjoining soil. While an opposite trend is observed in the region near the center of the foundation-soil interface. When the foundation is loaded to the ultimate load, settlement is observed for both the foundation and the soil along the interface, and larger slippage relative to Figure 7.28(a) is indicated by Figure 7.28(b), especially at the top and the bottom. Approximately equal vertical movements at the top and the bottom of the foundation confirms the rigidity of the foundation. Also, various slips happened at the soil-soil interface underneath the foundation during the loading process. In Figure 7.28(c), after the unloading process, the system did not entirely recover to the condition before loading. An alternative way to analyze the relative movement is through the tangential displacement jump u_t at the Gauss points of the CIEs. Note that in the specific case, positive u_t of the CIE denotes an upward movement of the left surface relative to the right surface. From Figure 7.28(d), it is straightforward to see that the largest slippage along the interface happened near the foundation bottom at both the end of loading and the end of unloading sequences. The total tangential displacement jump u_t can be decomposed into elastic and plastic components, namely u_t^e and u_t^p. And according to the formulation of the elasto-plastic CIE model, u_t^e is directly related to the tangential stress developed during shearing of CIE, while u_t^p mainly contributes to the continuous increase of relative slippage after plasticity is triggered. From Figure 7.28(e), the variation of u_t^p of CIEs along the height indicates plasticity mainly occurs within the range of $0.15m < H < 0.35m$. And the largest u_t^p appears at the first (or the lower) Gauss point of CIE 4, which is close to the bottom of the foundation-soil interface at $H \approx 0.2m$. The variations of four plastic variables (χ, c, $tan\phi$, and $tan\psi$) at this point are illustrated in Figures 7.29(a)-(b).

In addition to the displacement jump, we can also explore the failure mechanism by analyzing the stress state of the CIEs. Figures 7.29(c)-(d) show the tangential and normal stresses generated within the CIEs at ends of loading and unloading sequences. Figures 7.30-7.32 show the yield

surface evolution and stress path at all three Gauss points of each CIE. The results further confirm the foregoing conclusion regarding the range of plasticity. Figure 7.30(e) indicates that the CIE close to the top experiences high compression-shear, and maintains elasticity during the loading process. In contrast, Figures 7.31(b),(d), and (f) show that significant softening occurs in CIE 4, which is illustrated by the shrinkage of the yield surface. During unloading, elastic behavior is observed for all the CIEs.

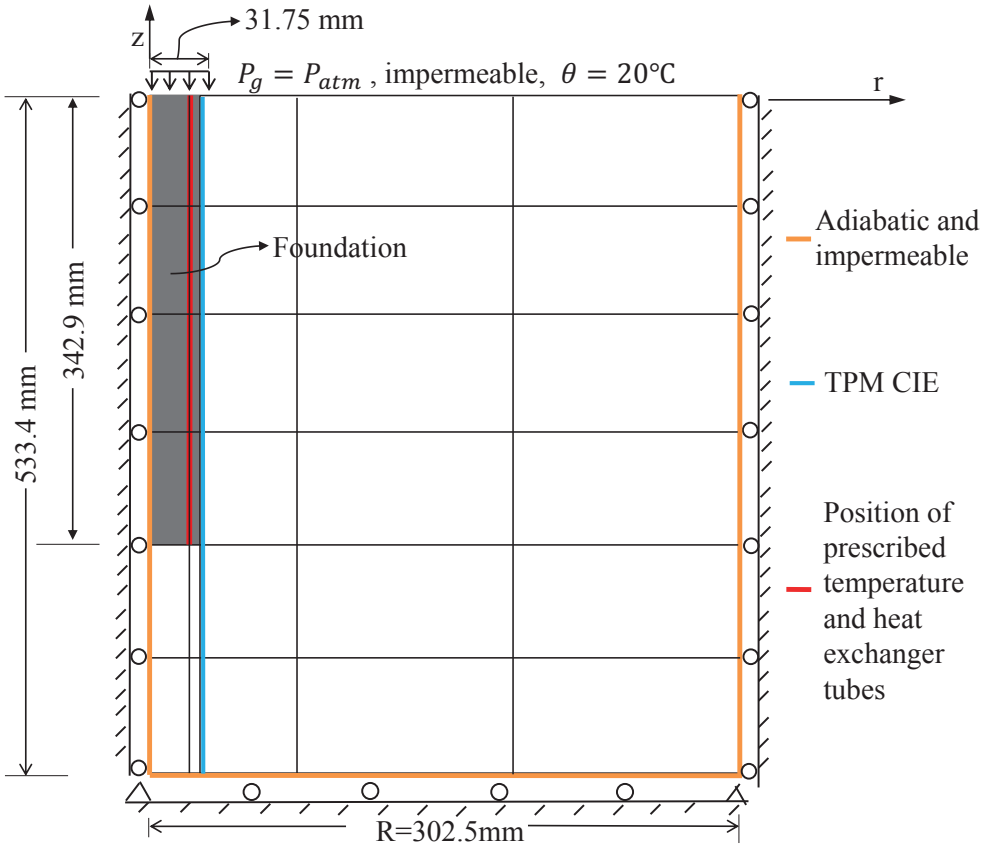

Figure 7.26: Axisymmetric finite element mesh with 6 TPM CIEs for semi-floating energy foundation.

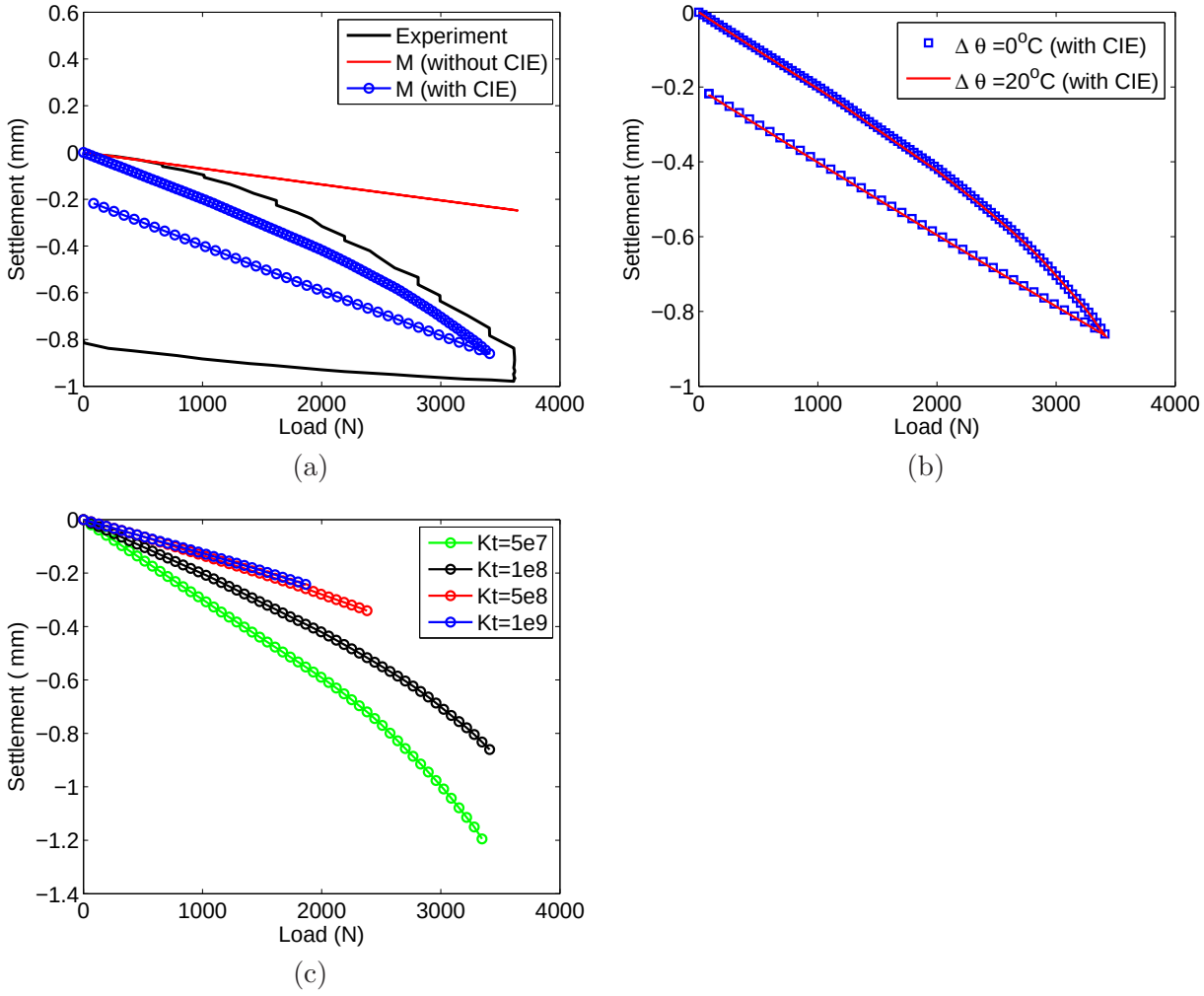

Figure 7.27: Comparisons of settlement-load curves between (a) experimental results, model prediction with and without CIE using parameters in Table 7.1; (b) isothermal ($\Delta\theta = 0^oC$) and nonisothermal ($\Delta\theta = 20^oC$) conditions by model predictions with CIE using parameters in Table 7.1; (c) using different elastic tangential stiffness K_t in TPM CIE model.

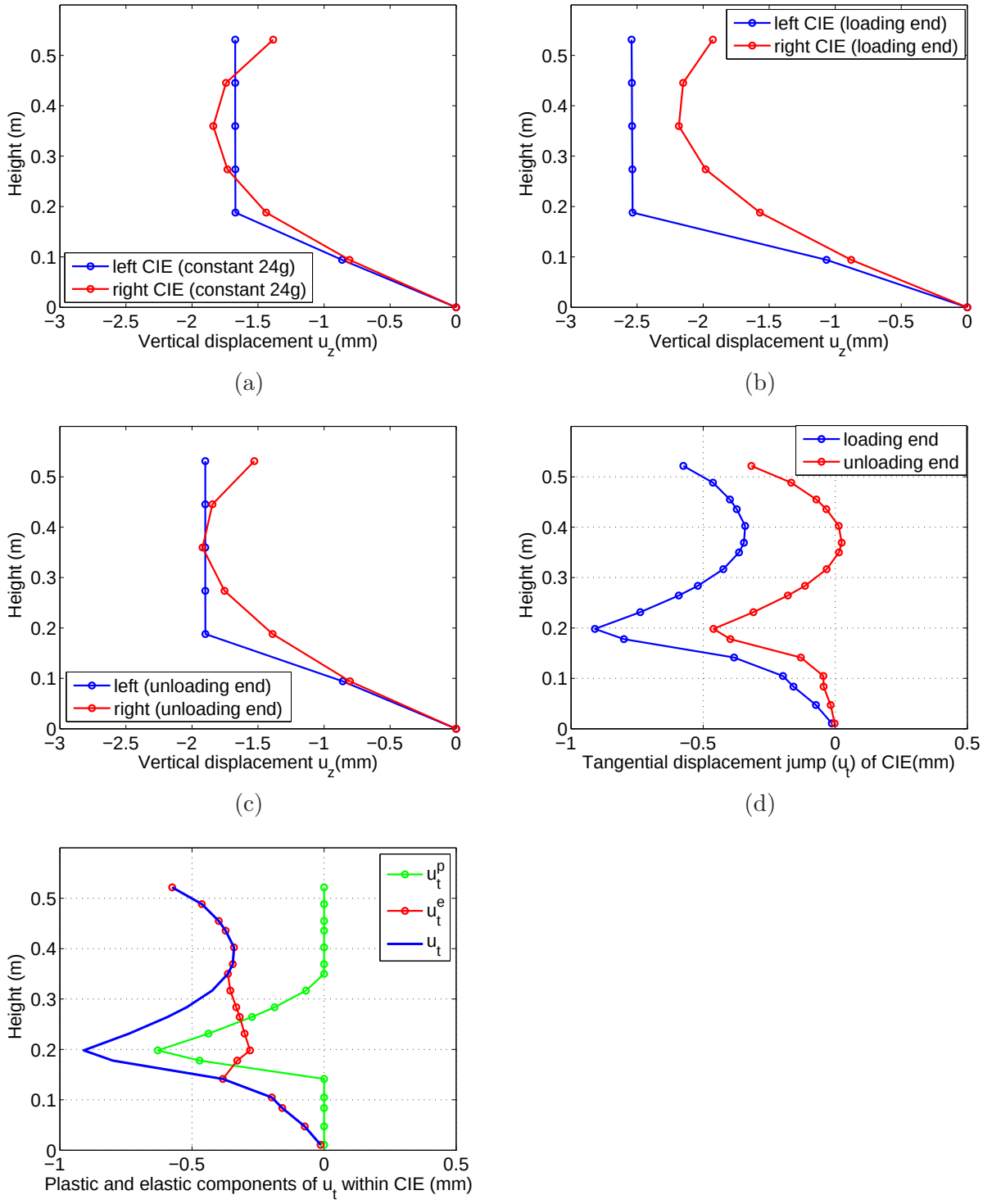

Figure 7.28: Vertical displacement (u_z) versus height within the CIE at (a) the equilibration of centrifuge spin-up; (b) the end of failure load; (c) the end of unloading. (d) Tangential displacement jump u_t within the CIE at the end of loading and unloading. (e) Elastic and plastic components of tangential displacement jump.

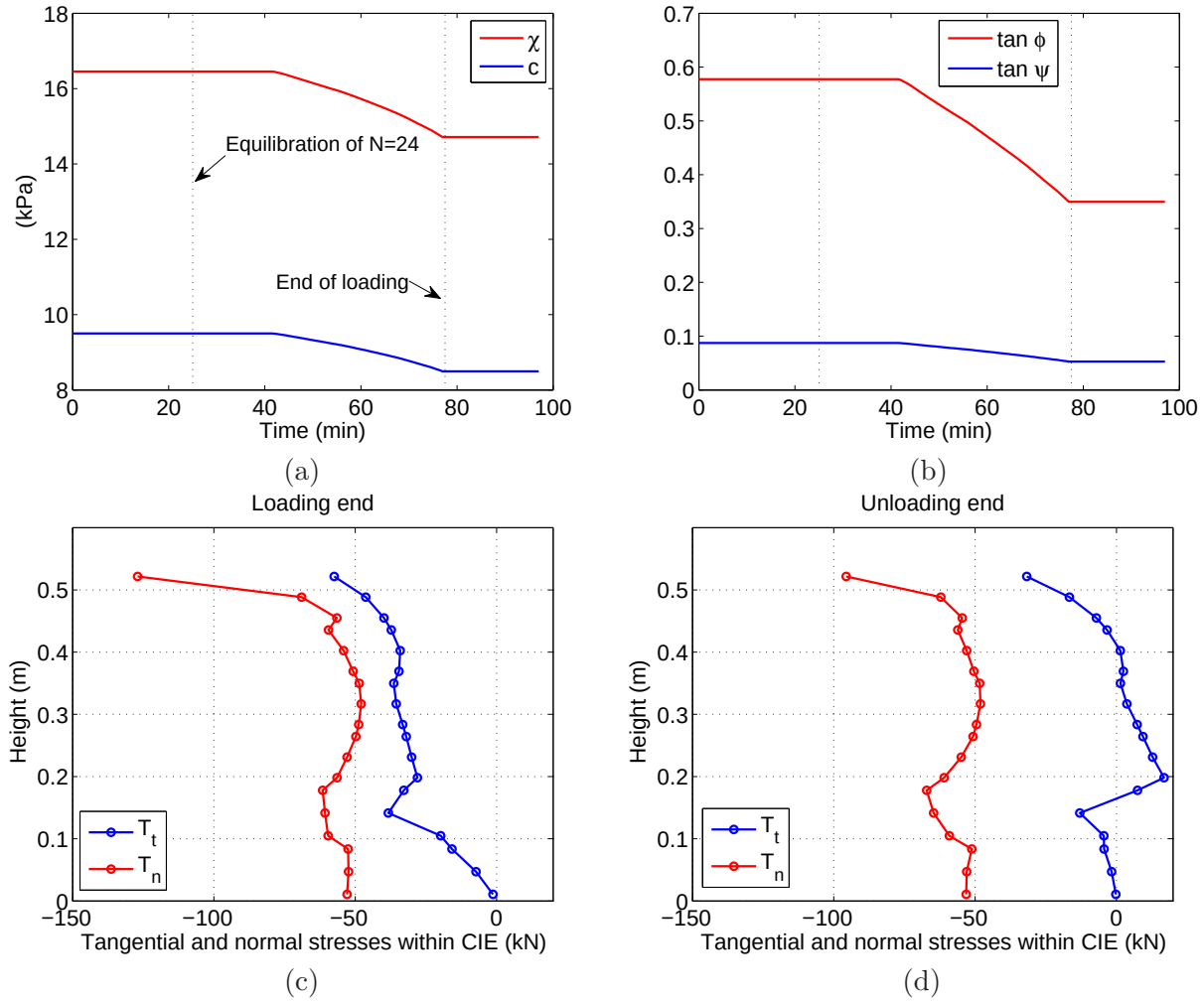

Figure 7.29: (a) Variation of plastic variables χ and c of CIE model. (b) Variation of plastic variables $tan\phi$ and $tan\psi$ of CIE model. (c) T_t'/T_n' versus height at the end of loading. (d) T_t'/T_n' versus height at the end of unloading.

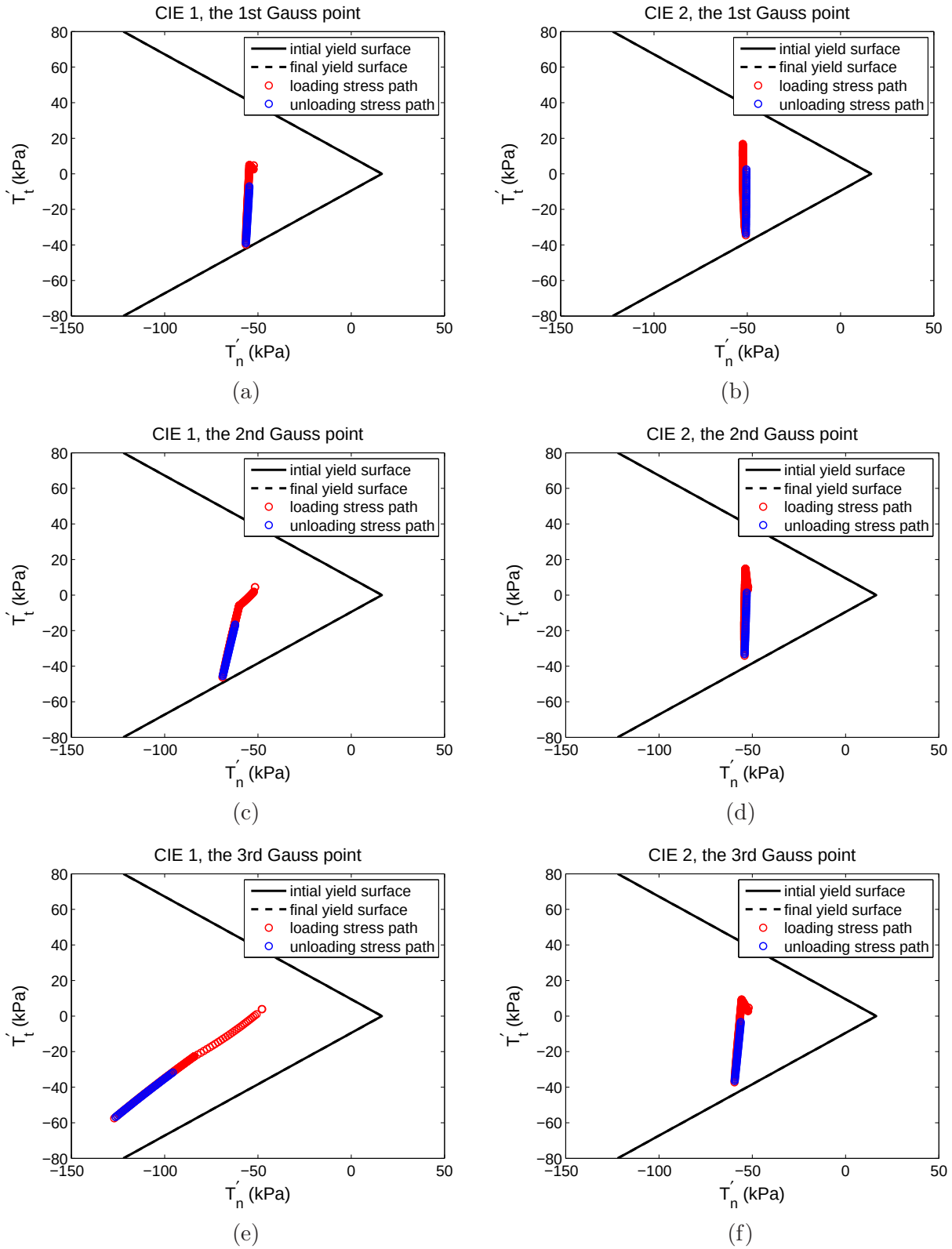

Figure 7.30: Stress path and yield surface evolution at the three Gauss points of CIE 1 and CIE 2.

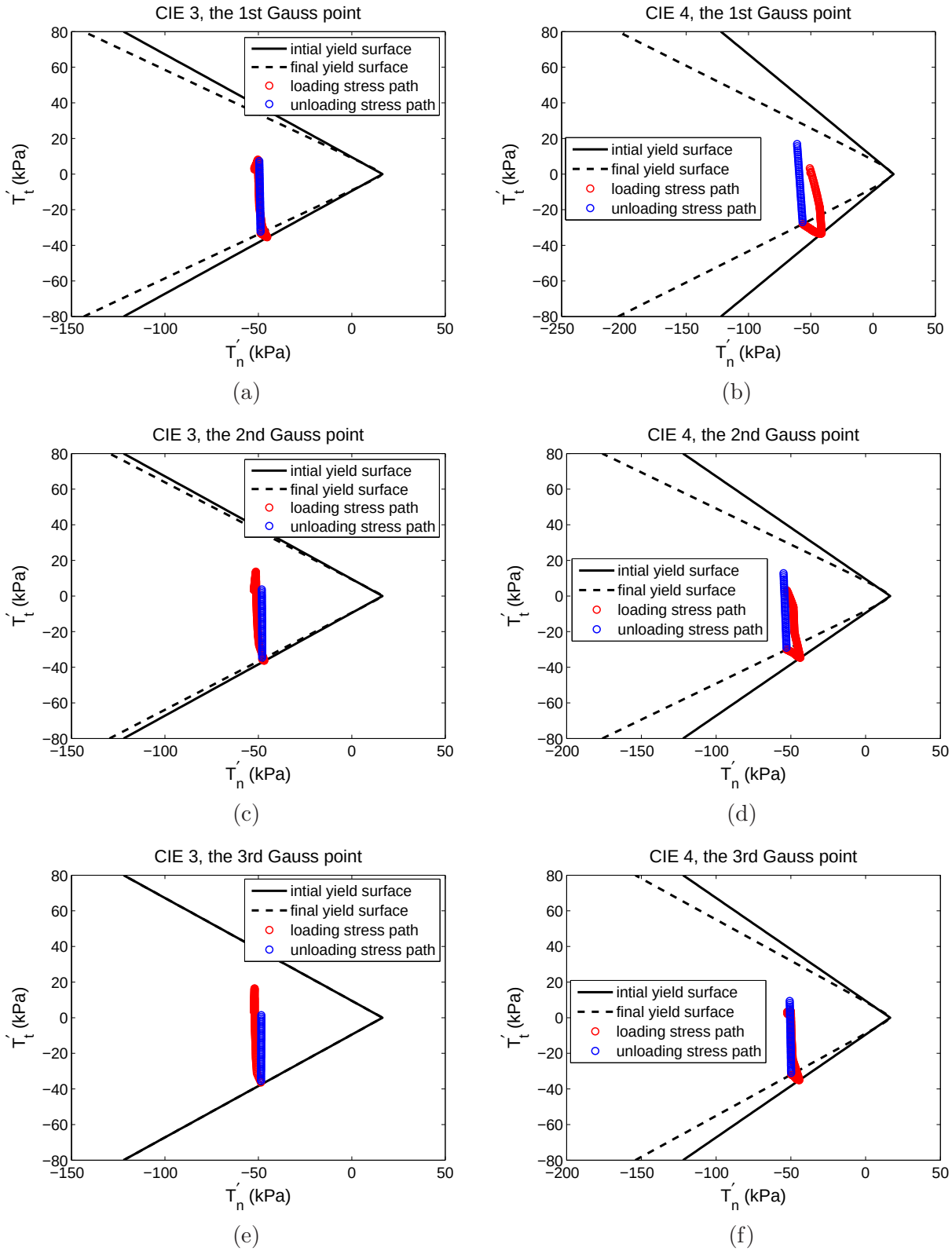

Figure 7.31: Stress path and yield surface evolution at the three Gauss points of CIE 3 and CIE 4.

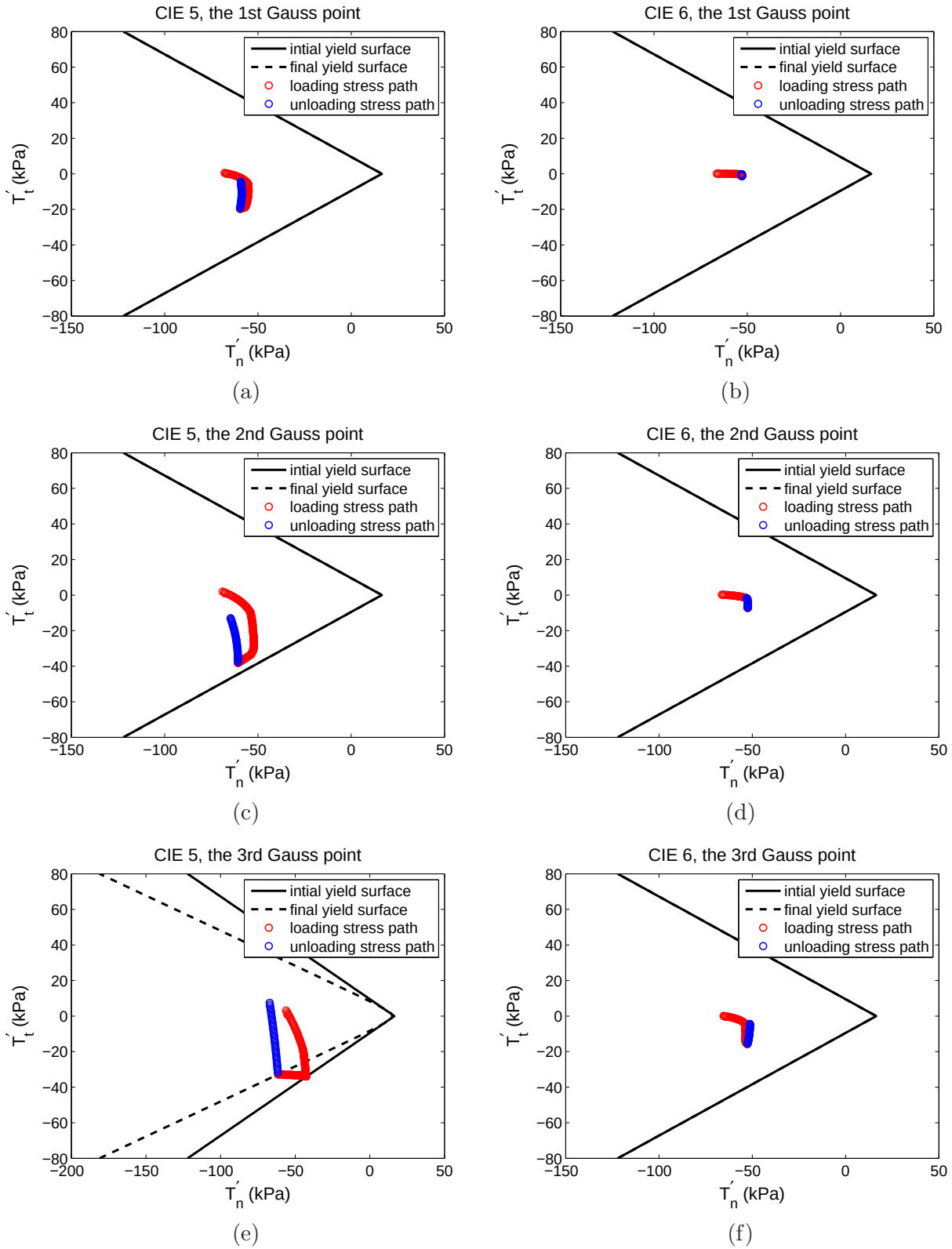

Figure 7.32: Stress path and yield surface evolution at the three Gauss points of CIE 5 and CIE 6.

Chapter 8

Conclusions and Future work

8.1 Thesis summary

The thesis develops fully coupled thermo-poro-mechanical (TPM) models for saturated and partially saturated unfractured geomaterials based on the mixture theory of porous media. Both nonlinear elastic model, and a temperature and suction dependent elasto-plastic Cam-Clay model are implemented for solid skeleton of porous media. The coupled processes involve mechanical response, multiphase fluid flow, and heat flow under both saturated and partially saturated conditions. The finite element method is used to implement the fully coupled models at small strain under quasi-static condition. And the saturated TPM model is verified by comparing with available analytical solutions for various conditions.

Although there are already some published codes, such as TOUGH2 Pruess et al. (1999), CODE_BRIGHT Olivella et al. (1996) to simulate the multiphase flow process, it is necessary to build our own code for the following reasons: to understand how the coupled physics fit together in a monolithically coupled framework, to flexibly insert our own constitutive models for certain soils, and to further develop a coupled TPM cohesive interface element (CIE).

Furthermore, the thesis develops fully coupled TPM cohesive interface element (CIE) models to analyze the coupled thermo-poro-mechanical response and multiphase flow within the geomaterials with either pre-existing or developing fractures for soil-structure interfaces, such as energy foundations, the main motivation for the thesis research. The performance of the CIE is tested by several examples in different aspects, i.e. compression, tensile plasticity, shear plasticity, liquid

flow, and heat flow.

Finally, the partially saturated TPM model is employed to explore the soil-structure interaction by simulating a series of energy foundation centrifuge experiments with Bonny silt Stewart (2012); Stewart and McCartney (2013); Goode (2013); Goode and McCartney (2014). Good agreement is obtained between numerical modeling results and centrifuge modeling observations with respect to temperature, displacement, strain, and volumetric water content. With the implementation of the zero-thickness CIE at the soil-foundation interface, we can relax the assumption of perfect bond by allowing the differences with respect to displacement, pore pressure, and temperature to happen at the interface. Therefore, the model is able to capture the plastic failure process of energy foundations due to the loss of side shear resistance.

Finite element analysis can be combined with the centrifuge experiments to obtain a comprehensive understanding of the fundamental soil mechanics phenomena involved in energy foundations. With this knowledge, we may assess the potential issues, evaluate the long-term performance and sustainability, thereby providing practical design guidance for energy foundations. For example, from both modeling predictions and experimental observations, we found that under temperature increase, the foundation top experienced almost free thermal expansion for both end-bearing and semi-floating energy foundations. The thermally-induced strain arrived at the highest value at the top. For the semi-floating foundation, when failure load was applied and then removed, a permanent plastic deformation remained. Therefore, if the mechanical system is not designed with sufficient capacity, deformation and thermal expansion of energy foundations may cause a loss of foundation-soil friction and affect building performance. In addition, temperature of the soil near the foundation changed during the heating process of the foundation, thus inducing multiphase flow in the nearby soil. The change of thermal storage properties of the underground soil should be considered in order to accurately estimate the heating and cooling capacity of energy foundation systems.

8.2 Future work

In order to improve the predictive capability of the model, future work should involve the following

(1) The simulation of the centrifuge experiments in the thesis has partially validated the TPM model. However, extensive validation is necessary to examine to what extent the assumptions and the constitutive relations in the model can reflect the physical phenomena in a variety of applications. With the validated model, FEA can be combined with the centrifuge experiments to obtain a comprehensive understanding of the fundamental soil mechanics phenomena involved in energy foundations. This will assist us to assess the potential issues, evaluate the long-term performance and sustainability, thereby providing practical design guidance for energy foundations.

(2) Preliminary results indicate certain parameters have an impact on the results. Extension of the current will focus on systematic uncertainty quantification and sensitivity analysis with respect to the thermal, mechanical, and hydraulic parameters. For the sensitive parameters, available physical experiments will be used in model calibration to provide refined estimates. For example, pull-out foundation tests at 1g and more compression tests are suggested to calibrate interface parameters. With the parameters calibrated, the consistency between simulated and experimental results will be further enhanced.

(3) From a modeling perspective, the following extensions will be considered in the future: (a) extension to embedded TPM partially saturated discontinuity models via Extended Finite Element Method (X-FEM), and Assumed Enhanced Strain (AES) method; (b) extension to include coupling with chemistry; (c) extension to finite strain; (d) extension to multiscale fracture, such as for hydraulic fracturing, and reservoir mechanics studies; (e) extension to include inertia terms.

Bibliography

Aagaard, B. T., Knepley, M. G., and Williams, C. A. (2013). A domain decomposition approach to implementing fault slip in finite-element models of quasi-static and dynamic crustal deformation. Journal of Geophysical Research: Solid Earth, 118(6):3059–3079.

Aboustit, B., Advani, S., and Lee, J. (1985a). Variational principles and finite element simulations for thermo-elastic consolidation. International Journal for Numerical and Analytical Methods in Geomechanics, 9(1):49 – 69.

Aboustit, B., Advani, S., and Lee, J. (1985b). Variational principles and finite element simulations for thermo-elastic consolidation. International journal for numerical and analytical methods in geomechanics, 9(1):49–69.

Alfano, G. (2006). On the influence of the shape of the interface law on the application of cohesive-zone models. Composites Science and Technology, 66(6):723–730.

Alonso, E. E., Gens, A., and Josa, A. (1990). A constitutive model for partially saturated soils. Geotechnique, 40(3):405 – 430.

Aymerich, F., Dore, F., and Priolo, P. (2008). Prediction of impact-induced delamination in cross-ply composite laminates using cohesive interface elements. Composites science and technology, 68(12):2383–2390.

Aymerich, F., Dore, F., and Priolo, P. (2009). Simulation of multiple delaminations in impacted cross-ply laminates using a finite element model based on cohesive interface elements. Composites Science and Technology, 69(11):1699–1709.

Bachmann, J. and van der Ploeg, R. R. (2002). A review on recent developments in soil water retention theory: interfacial tension and temperature effects. Plant Nutr. Soil Sci., 165(4):468–478.

Bai, M. and Abousleiman, Y. (1997). Thermoporoelastic coupling with application to consolidation. International Journal for Numerical and Analytical Methods in Geomechanics, 21(2):121 – 132.

Balzani, C. and Wagner, W. (2008). An interface element for the simulation of delamination in unidirectional fiber-reinforced composite laminates. Engineering Fracture Mechanics, 75(9):2597–2615.

Barton, I. (1979). A parameterization of the evaporation from nonsaturated surfaces. Journal of Applied Meteorology, 18(1):43 – 47.

Bear, J. and Bachmat, Y. (1990). Introduction to modeling of transport phenomena in porous media, volume 4. Springer.

Bear, J., Bensabat, J., and Nir, A. (1991). Heat and mass transfer in unsaturated porous media at a hot boundary. i. one-dimensional analytical model. Transport in Porous Media, 6(3):281 – 298.

Beer, G. (1985). An isoparametric joint/interface element for finite element analysis. International Journal for Numerical Methods in Engineering, 21(4):585 – 600. isoparametric joint element;2-D;3-D;shell to shell interfaces;stress analysis;interface element;finite element analysis;solid finite elements;shell finite elements;joint element stiffness;nonlinear joint behaviour;shell-to-solid interfaces;.

Biot, M. (1956). Thermoelasticity and irreversible thermodynamics. Journal of Applied Physics, 27(3):240 – 253.

Biot, M. A. (1941). General theory of three-dimensional consolidation. Journal of applied physics, 12(2):155–164.

Bishop, A. (1959). The principle of effective stress. Teknisk Ukeblad, 106(39):859 – 863.

Bishop, A. and Blight, G. (1963). Some aspects of effective stress in saturated and partly saturated soils. Geotechnique, 13(3):177 – 197.

Bishop, A. and Donald, I. (1961). The exprimental study of partly saturated soil in triaxial apparatus. In Proceedings of the 5th International Conference on SMFE,Dunod,Paris, volume 1, pages 13 – 21.

Blatz, J. and Graham, J. (2003). Elastic-plastic modelling of unsaturated soil using results from a new triaxial test with controlled suction. Geotechnique, 53(1):113 – 122.

Bluhm, J. (2002). Modelling of saturated thermo-elastic porous solids with different phase temperatures. In Porous Media, pages 87–118. Springer.

Blunt, M. J., Jackson, M. D., Piri, M., and Valvatne, P. H. (2002). Detailed physics, predictive capabilities and macroscopic consequences for pore-network models of multiphase flow. Advances in Water Resources, 25(8):1069–1089.

Bolzon, G., Schrefler, B. A., and Zienkiewicz, O. C. (1996). Elastoplastic soil constitutive laws generalized to partially saturated states. Geotechnique, 46(2):279 – 289.

Booker, J. and Savvidou, C. (1985). Consolidation around a point heat source. International Journal for Numerical and Analytical Methods in Geomechanics, 9(2):173 – 184.

Borja, R., Tamagnini, C., and Amorosi, A. (1997). Coupling plasticity and energy-conserving elasticity models for clays. Journal of Geotechnical and Geoenvironmental Engineering, 123(10):948 – 957.

Borja, R. and White, J. (2010). Continuum deformation and stability analyses of a steep hillside slope under rainfall infiltration. Acta Geotechnica, 5(1):1 – 14.

Borja, R. I. (1991). Cam-clay plasticity, part ii: Implicit integration of constitutive equation based on a nonlinear elastic stress predictor. Computer Methods in Applied Mechanics and Engineering, 88(2):225–240.

Borja, R. I. (2004a). Cam-clay plasticity. part v: A mathematical framework for three-phase deformation and strain localization analyses of partially saturated porous media. Computer Methods in Applied Mechanics and Engineering, 193(48-51):5301 – 5338.

Borja, R. I. (2004b). Cam-clay plasticity. part v: A mathematical framework for three-phase deformation and strain localization analyses of partially saturated porous media. Computer Methods in Applied Mechanics and Engineering, 193(48):5301–5338.

Borja, R. I. and Tamagnini, C. (1998). Cam-clay plasticity part iii: Extension of the infinitesimal model to include finite strains. Computer Methods in Applied Mechanics and Engineering, 155(1):73–95.

Bowen, R. (1980). Incompressible porous media models by use of the theory of mixtures. International Journal of Engineering Science, 18(9):1129 – 48.

Bowen, R. (1982). Compressible porous media models by use of the theory of mixtures. International Journal of Engineering Science, 20(6):697 – 735.

Brandl, H. (2006). Energy foundations and other thermo-active ground structures. Geotechnique, 56(2):81 – 122.

Brochard, L., Vandamme, M., and Pellenq, R.-M. (2012). Poromechanics of microporous media. Journal of the Mechanics and Physics of Solids, 60(4):606–622.

Brooks, R. and Corey, A. (1964). Hydraulic properties of porous media. American Society of Agricultural Engineers – Transactions, 7(1):26 – 28.

Burghignoli, A., Desideri, A., and Miliziano, S. (2000). A laboratory study on the thermomechanical behaviour of clayey soils. Canadian Geotechnical Journal, 37(4):764 – 780.

Cai, Y., Gould, P., and Desai, C. (2000). Nonlinear analysis of 3d seismic interaction of soil–pile–structure systems and application. Engineering Structures, 22(2):191–199.

Campanella, R. and Mitchell, J. (1968). Influence of temperature variations on soil behavior. American Society of Civil Engineers Proceedings, Journal of the Soil Mechanics and Foundations Division, 94(SM3):709 – 734.

Campbell, G., Jungbauer, J., Bidlake, W., and Hungerford, R. (1994). Predicting the effect of temperature on soil thermal conductivity. Soil science, 158(5):307–313.

Cappa, F. and Rutqvist, J. (2011a). Impact of co2 geological sequestration on the nucleation of earthquakes. Geophysical Research Letters, 38(17).

Cappa, F. and Rutqvist, J. (2011b). Modeling of coupled deformation and permeability evolution during fault reactivation induced by deep underground injection of co¡ sub¿ 2¡/sub¿. international journal of Greenhouse Gas Control, 5(2):336–346.

Carman, P. C. (1956). Flow of gases through porous media. Butterworths Scientific Publications London.

Carol, I., Prat, P. C., and López, C. M. (1997). Normal/shear cracking model: application to discrete crack analysis. Journal of engineering mechanics, 123(8):765–773.

Cekerevac, C. and Laloui, L. (2004). Experimental study of thermal effects on the mechanical behaviour of a clay. International Journal for Numerical and Analytical Methods in Geomechanics, 28(3):209 – 228.

Cho, W., Lee, J., and Chun, K. (1999). The temperature effects on hydraulic conductivity of compacted bentonite. Applied clay science, 14(1):47–58.

Coleman, B. D. and Noll, W. (1963). The thermodynamics of elastic materials with heat conduction and viscosity. Archive for rational mechanics and analysis, 13(1):168 – 178.

Coleman, J. (1962). Stress-strain relations for partially saturated soils. Geotechnique, 12(4):348–350.

Corigliano, A. and Ricci, M. (2001). Rate-dependent interface models: formulation and numerical applications. International Journal of Solids and Structures, 38(4):547–576.

Coussy, O. (1989). A general theory of thermoporoelatoplasticity for saturated porous materials. Transport in porous media, 4(3):281–293.

Coussy, O. (2004). Poromechanics. Wiley, 2 edition.

Cui, Y. and Delage, P. (1996). Yielding and plastic behaviour of an unsaturated compacted silt. Geotechnique, 46(2):291 – 311.

Cui, Y., Sultan, N., and Delage, P. (2000). A thermomechanical model for saturated clays. Canadian Geotechnical Journal, 37(3):607 – 620.

Day, R. and Potts, D. (1994). Zero thickness interface elementsnumerical stability and application. International Journal for numerical and analytical methods in geomechanics, 18(10):689–708.

de Boer, R. (2005). Trends in continuum mechanics of porous media. Dordrecht ; Norwell, MA : Springer, 1 edition.

De Moel, M., Bach, P. M., Bouazza, A., Singh, R. M., and Sun, J. O. (2010). Technological advances and applications of geothermal energy pile foundations and their feasibility in australia. Renewable and Sustainable Energy Reviews, 14(9):2683–2696.

de Vries, D. (1958). Simultaneous transfer of heat and moisture in porous media. Transactions, American Geophysical Union, 39(5):909 – 915.

De Vries, D. and Kruger, A. (1966). On the value of the diffusion coefficient of water vapour in air. In Proc. Of Colloque Int. Du CNRS, number 160, page 61u72.

Delage, P., Sultan, N., and Cui, Y. (2000). On the thermal consolidation of boom clay. Canadian Geotechnical Journal, 37(2):343 – 354.

Desai, C., Zaman, M., Lightner, J., and Siriwardane, H. (1984). Thin-layer element for interfaces and joints. International Journal for Numerical and Analytical Methods in Geomechanics, 8(1):19–43.

Doherty, P., Al-Huthaili, S., Riffat, S., and Abodahab, N. (2004). Ground source heat pump-description and preliminary results of the eco house system. Applied thermal engineering, 24(17):2627–2641.

Dolbow, J. and Belytschko, T. (1999). A finite element method for crack growth without remeshing. Int. J. Numer. Meth. Engng, 46(1):131–150.

Dormieux, L., Kondo, D., and Ulm, F.-J. (2006). Microporomechanics. John Wiley & Sons.

Dumont, M., Taibi, S., Fleureau, J.-M., Abou-Bekr, N., and Saouab, A. (2011). A thermo-hydro-mechanical model for unsaturated soils based on the effective stress concept. International Journal for Numerical and Analytical Methods in Geomechanics, 35(12):1299 – 1317.

Fang, Y., Nguyen, B. N., Carroll, K., Xu, Z., Yabusaki, S. B., Scheibe, T. D., and Bonneville, A. (2013). Development of a coupled thermo-hydro-mechanical model in discontinuous media for carbon sequestration. International Journal of Rock Mechanics and Mining Sciences, 62:138–147.

Felippa, C. A. (2010). Advanced finite element methods. Course materials (University of Colorado, Boulder).

Fernandez, R. (1972). Natural convection from cylinders buried in porous media. PhD thesis, University of California.

Fisher, R. (1926). On the capillary forces in an ideal soil; correction of formulae given by wb haines. The Journal of Agricultural Science, 16(03):492–505.

François, B. and Laloui, L. (2008). Acmeg-ts: A constitutive model for unsaturated soils under non-isothermal conditions. International journal for numerical and analytical methods in geomechanics, 32(16):1955–1988.

Fredlund, D. and Xing, A. (1994). Equations for the soil-water characteristic curve. Canadian geotechnical journal, 31(4):521 – 532.

Fredlund, D. G. and Morgenstern, N. R. (1977). Stress state variables for unsaturated soils. American Society of Civil Engineers, Journal of the Geotechnical Engineering Division, 103(5):447 – 466.

Gallipoli, D., Gens, A., Sharma, R., and Vaunat, J. (2003a). An elasto-plastic model for unsaturated soil incorporating the effects of suction and degree of saturation on mechanical behaviour. Géotechnique., 53(1):123–136.

Gallipoli, D., Gens, A., Sharma, R. S., and Vaunat, J. (2003b). An elasto-plastic model for unsaturated soil incorporating the effects of suction and degree of saturation on mechanical behaviour. Geotechnique, 53(1):123 – 135.

Gatmiri, B., Maghoul, P., and Duhamel, D. (2010). Two-dimensional transient thermo-hydro-mechanical fundamental solutions of multiphase porous media in frequency and time domains. International Journal of Solids and Structures, 47(5):595 – 610.

Gawin, D., Schrefler, B. A., and Galindo, M. (1996). Thermo-hydro-mechanical analysis of partially saturated porous materials. Engineering Computations, 13(7):113–143.

Ge, S. (1997). A governing equation for fluid flow in rough fractures. Water Resources Research, 33(1):53–61.

Gelet, R., Loret, B., and Khalili, N. (2012). A thermo-hydro-mechanical coupled model in local thermal non-equilibrium for fractured hdr reservoir with double porosity. Journal of Geophysical Research: Solid Earth (1978–2012), 117(B7).

Gens, A. and Alonso, E. E. (1992). A framework for the behaviour of unsaturated expansive clays. Canadian Geotechnical Journal = Revue Canadienne de Geotechnique, 29(6):1013 – 1032.

Gens, A., Carol, I., and Alonso, E. (1989). An interface element formulation for the analysis of soil-reinforcement interaction. Computers and Geotechnics, 7(1):133–151.

Ghabezloo, S. and Sulem, J. (2009). Stress dependent thermal pressurization of a fluid-saturated rock. Rock Mechanics and Rock Engineering, 42(1):1–24.

Goode, J. (2013). Centrifuge modeling of the thermo-mechanical response of energy foundations. Master's thesis, University of Colorado, Boulder, U.S.

Goode, J. and McCartney, J. (2014). Centrifuge modeling of energy foundations in sand. In 8th International Conference on Physical Modelling in Geotechnics, in press.

Goodman, M. and Cowin, S. (1972). A continuum theory for granular materials. Archive for Rational Mechanics and Analysis, 44(4):249 – 266.

Goodman, R. E., Taylor, R. L., and Brekke, T. L. (1968). A model for the mechanics of jointed rock. Journal of Soil Mechanics & Foundations Div.

Graham, J., Alfaro, M., and Ferris, G. (2004). Compression and strength of dense sand at high pressures and elevated temperatures. Canadian Geotechnical Journal, 41(6):1206 – 1212.

Graham, J., Tanaka, N., Crilly, T., and Alfaro, M. (2001). Modified cam-clay modelling of temperature effects in clays. Canadian Geotechnical Journal = Revue Canadienne de Geotechnique, 38(3):608 – 621.

Granger, R. J. (1989). An examination of the concept of potential evaporation. Journal of Hydrology, 111(1-4):9 – 19.

Grant, S. A. and Salehzadeh, A. (1996). Calculation of temperature effects on wetting coefficients of porous solids and their capillary pressure functions. Water Resources Research, 32(2):261–270.

Gray, D. (1970). Handbook on the principles of hydrology. Canadian National Committee for the International Hydrological Decade,National Research Council of Canada,Ottawa.

Gray, W. G. and Hassanizadeh, S. M. (1991). Unsaturated flow theory including interfacial phenomena. Water Resources Research, 27(8):1855–1863.

Gray, W. G. and Schrefler, B. A. (2001). Thermodynamic approach to effective stress in partially saturated porous media. European Journal of Mechanics-A/Solids, 20(4):521–538.

Griffiths, D. (1985). Numerical modelling of interfaces using conventional finite elements. volume 2, pages 837 – 844, Nagoya, Jpn. ADHESIVE SLIDING;EIGHT-NODED QUADRILATERAL ELEMENTS;FRICTIONAL SLIDING;INTERFACE MODELING;.

Hamada, Y., Saitoh, H., Nakamura, M., Kubota, H., and Ochifuji, K. (2007). Field performance of an energy pile system for space heating. Energy and Buildings, 39(5):517 – 24.

Hammel, J., Papendick, R., and Campbell, G. (1981). Fallow tillage effects on evaporation and seedzone water content in a dry summer climate. Soil Science Society of America Journal, 45(6):1016 – 1022.

Haridasan, M. and Jensen, R. (1972). Effect of temperature on pressure head-water content relationship and conductivity of two soils. Soil Science Society of America Journal, 36(5):703–708.

Hassanizadeh, M. and Gray, W. G. (1980). General conservation equations for multi-phase systems: 3. constitutive theory for porous media flow. Advances in Water Resources, 3(1):25–40.

Hassanizadeh, S. M. and Gray, W. (1990). Mechanics and thermodynamics of multiphase flow in porous media including interface boundaries. Advances in Water Resources, 13(4):169 – 86.

Hepbasli, A. (2002). Performance evaluation of a vertical ground-source heat pump system in izmir, turkey. International Journal of Energy Research, 26(13):1121 – 1139.

Hepbasli, A. (2003). Current status of geothermal energy applications in turkey. Energy Sources, 25(7):667–677.

Hepbasli, A., Akdemir, O., and Hancioglu, E. (2003). Experimental study of a closed loop vertical ground source heat pump system. Energy Conversion and Management, 44(4):527 – 548.

Hillel, D. (1980). Application of soil physics. Academic Press, New York.

Holmes, R. (1961). Estimation of soil moisture content using evaporation data. In Proceedings of Hydrology Symposium,No.2 Evaporation, pages 184–196. Queen's Printer,Ottawa.

Hopmans, J. and Dane, J. (1986). Temperature dependence of soil hydraulic properties. Soil Science Society of America Journal, 50(1):4–9.

Hou, Z., Gou, Y., Taron, J., Gorke, U. J., and Kolditz, O. (2012). Thermo-hydro-mechanical modeling of carbon dioxide injection for enhanced gas-recovery (co2-egr): a benchmarking study for code comparison. Environmental Earth Sciences, 67(2):549–561.

Houlsby, G. (1997). The work input to an unsaturated granular material. Geotechnique, 47(1):193 – 196.

Hu, L. and Pu, J. (2004). Testing and modeling of soil-structure interface. Journal of Geotechnical and Geoenvironmental Engineering, 130(8):851–860.

Hueckel, T. and Baldi, G. (1990). Thermoplasticity of saturated clays; experimental constitutive study. Journal of Geotechnical Engineering, 116(12):1778 – 1796.

Hueckel, T. and Borsetto, M. (1990). Thermoplasticity of saturated soils and shales. constitutive equations. Journal of geotechnical engineering, 116(12):1765 – 1777.

Hueckel, T. and Pellegrini, R. (1989). Modeling of thermal failure of saturated clays. In Pietruszczak, S.;Pande, G. N., editor, Numerical Models in Geomechanics, pages 81 – 90.

Hughes, T. J. (2000). The finite element method. Dover Publications, INC. Mineola, New York.

Jabbari, E. and Gatmiri, B. (2007). Thermo-poro-elastostatic green's functions for unsaturated soils. CMES - Computer Modeling in Engineering and Sciences, 18(1):31 – 43.

Jiang, F., Luo, L., and Chen, J. (2013). A novel three-dimensional transient model for subsurface heat exchange in enhanced geothermal systems. International Communications in Heat and Mass Transfer, 41:57–62.

Katona, M. G. (1983). Simple contact-friction interface element with applications to buried culverts. International Journal for Numerical and Analytical Methods in Geomechanics, 7(3):371 – 384.

Khalili, N., Geiser, F., and Blight, G. (2004). Effective stress in unsaturated soils: Review with new evidence. International Journal of Geomechanics, 4(2):115 – 126.

Khalili, N., Habte, M., and Zargarbashi, S. (2008). A fully coupled flow deformation model for cyclic analysis of unsaturated soils including hydraulic and mechanical hystereses. Computers and Geotechnics, 35(6):872 – 89.

Khalili, N. and Khabbaz, M. H. (1998). A unique relationship for x for the determination of the shear strength of unsaturated soils. Geotechnique, 48(5):681 – 687.

Khalili, N. and Loret, B. (2001). An elasto-plastic model for non-isothermal analysis of flow and deformation in unsaturated porous media: formulation. International Journal of Solids and Structures, 38(46-47):8305 – 30.

Khalili, N., Uchaipichat, A., and Javadi, A. (2010). Skeletal thermal expansion coefficient and thermo-hydro-mechanical constitutive relations for saturated homogeneous porous media. Mechanics of materials, 42(6):593–598.

Ko, H. (1988). Summary of the state-of-the-art in centrifuge model testing. Centrifuges in soil mechanics, pages 11–18.

Kohgo, Y., Nakano, M., and Miyazaki, T. (1993). Theoretical aspects of constitutive modelling for unsaturated soils. Soils and Foundations, 33(4):49 – 63.

Kolditz, O., Bauer, S., Bilke, L., Böttcher, N., Delfs, J., Fischer, T., Görke, U., Kalbacher, T., Kosakowski, G., McDermott, C., et al. (2012). Opengeosys: an open-source initiative for numerical simulation of thermo-hydro-mechanical/chemical (thm/c) processes in porous media. Environmental Earth Sciences, 67(2):589–599.

Korsawe, J., Starke, G., Wang, W., and Kolditz, O. (2006). Finite element analysis of poro-elastic consolidation in porous media: Standard and mixed approaches. Computer Methods in Applied Mechanics and Engineering, 195(9):1096–1115.

Kuntiwattanakul, P., Towhata, I., Ohishi, K., and Seko, I. (1995). Temperature effects on undrained shear characteristics of clay. Soils and Foundations, 35(1):147 – 147.

Laloui, L. and Cekerevac, C. (2003). Thermo-plasticity of clays: An isotropic yield mechanism. Computers and Geotechnics, 30(8):649 – 660.

Laloui, L. and Cekerevac, C. (2008a). Non-isothermal plasticity model for cyclic behaviour of soils. International journal for numerical and analytical methods in geomechanics, 32(5):437–460.

Laloui, L. and Cekerevac, C. (2008b). Non-isothermal plasticity model for cyclic behaviour of soils. International Journal for Numerical and Analytical Methods in Geomechanics, 32(5):437 – 460.

Lee, S. and Ghassemi, A. (2010). A three-dimensional thermo-poro-mechanical finite element analysis of a wellbore on damage evolution. pages American Rock Mechanics Association –.

Lee, S. and Ghassemi, A. (2011). Three-dimensional thermo-poro-mechanical modeling of well stimulation and induced microseismicity. 45th US Rock Mechanics / Geomechanics Symposium, pages American Rock Mechanics Association (ARMA) –.

Lewis, R., Majorana, C., and Schrefler, B. (1986). Coupled finite element model for the consolidation of nonisothermal elastoplastic porous media. Transport in Porous Media, 1(2):155 – 178.

Lewis, R. W. and Schrefler, B. A. (1998). The finite element method in the static and dynamic deformation and consolidation of porous media. John Wiley.

Longuemare, P., Mainguy, M., Lemonnier, P., Onaisi, A., Gérard, C., and Koutsabeloulis, N. (2002). Geomechanics in reservoir simulation: overview of coupling methods and field case study. Oil & Gas Science and Technology, 57(5):471–483.

Loret, B. and Khalili, N. (2000). A three-phase model for unsaturated soils. International Journal for Numerical and Analytical Methods in Geomechanics, 24(11):893 – 927.

Loret, B. and Khalili, N. (2002). An effective stress elastic-plastic model for unsaturated porous media. Mechanics of Materials, 34(2):97–116.

Lu, N., Godt, J., and Wu, D. (2010). A closed-form equation for effective stress in unsaturated soil. Water Resources Research, 46:W05515.

Lu, N. and Likos, W. J. (2006). Suction stress characteristic curve for unsaturated soil. Journal of Geotechnical and Geoenvironmental Engineering, 132(2):131 – 142.

Maatouk, A., Leroueil, S., and La Rochelle, P. (1995). Yielding and critical state of a collapsible unsaturated silty soil. Geotechnique, 45(3):465 – 477.

Maghoul, P., Gatmiri, B., and Duhamel, D. (2010). Three-dimensional transient thermo-hydro-mechanical fundamental solutions of unsaturated soils. International Journal for Numerical and Analytical Methods in Geomechanics, 34(3):297 – 329.

McKee, C. and Bumb, A. (1987). Flow-testing coalbed methane production wells in the presence of water and gas. SPE Formation Evaluation, 2(4):599 – 608.

Melenk, J. M. and Babuška, I. (1996). The partition of unity finite element method: basic theory and applications. Computer methods in applied mechanics and engineering, 139(1):289–314.

Miller, C. T., Christakos, G., Imhoff, P. T., McBride, J. F., Pedit, J. A., and Trangenstein, J. A. (1998). Multiphase flow and transport modeling in heterogeneous porous media: challenges and approaches. Advances in Water Resources, 21(2):77–120.

Millington, R. (1959). Gas diffusion in porous media. Science, 130:100 – 102.

Milly, P. (1982). Moisture and heat transport in hysteretic, inhomogeneous porous media: a matrix head-based formulation and a numerical model. Water Resources Research, 18(3):489 – 98.

Modaressi, H. and Laloui, L. (1997). A thermo-viscoplastic constitutive model for clays. International journal for numerical and analytical methods in geomechanics, 21(5):313–335.

Niessner, J. and Hassanizadeh, S. M. (2009). Non-equilibrium interphase heat and mass transfer during two-phase flow in porous media-theoretical considerations and modeling. Advances in Water Resources, 32(12):1756 – 1766.

Noorishad, J., Ayatollahi, M., and Witherspoon, P. (1982). A finite-element method for coupled stress and fluid flow analysis in fractured rock masses. In International Journal of Rock Mechanics and Mining Sciences & Geomechanics Abstracts, volume 19, pages 185–193. Elsevier.

Noorishad, J., Tsang, C., and Witherspoon, P. (1984). Coupled thermal-hydraulic-mechanical phenomena in saturated fractured porous rocks: Numerical approach. Journal of Geophysical Research: Solid Earth (1978-2012), 89(B12):10365–10373.

Oka, F., Higo, Y., Kim, Y., Imura, Y., and Kimoto, S. (2004). Thermo-hydro-mechanically coupled finite element analysis of clay by an elasto-thermo-viscoplastic model. COMPUTATIONAL MECHANICS, WCCM VI in conjunction with APCOM, 4:5–10.

Olivella, S. and Gens, A. (2000). Vapour transport in low permeability unsaturated soils with capillary effects. Transport in Porous Media, 40(2):219 – 241.

Olivella, S., Gens, A., Carrera, J., and Alonso, E. (1996). Numerical formulation for a simulator (code_bright) for the coupled analysis of saline media. Engineering computations, 13(7):87–112.

Omer, A. (2008). Ground-source heat pumps systems and applications. Renewable and Sustainable Energy Reviews, 12(2):344 – 371.

Paaswell, R. E. (1967). Temperature effects on clay soil consolidation. Proceedings of the American Society of Civil Engineers, 93.

Pahud, D. and Matthey, B. (2001). Comparison of the thermal performance of double u-pipe borehole heat exchangers measured in situ. Energy and buildings, 33(5):503–507.

Palciauskas, V. and Domenico, P. (1982). Characterization of drained and undrained response of thermally loaded repository rocks. Water Resources Research, 18(2):281 – 290.

Pande, G. and Sharma, K. (1979). On joint/interface elements and associated problems of numerical ill-conditioning. International Journal for Numerical and Analytical Methods in Geomechanics, 3(3):293–300.

Pao, W. K., Lewis, R. W., and Masters, I. (2001). A fully coupled hydro-thermo-poro-mechanical model for black oil reservoir simulation. International journal for numerical and analytical methods in geomechanics, 25(12):1229–1256.

Papadopoulos, P. and Taylor, R. L. (1992). A mixed formulation for the finite element solution of contact problems. Computer Methods in Applied Mechanics and Engineering, 94(3):373–389.

Penman, H. (1948). Natural evapotranspiration from open water, bare soil and grass. In Proceedings of the Royal Society of London, number 193 in Series A, pages 120–145.

Persoff, P. and Pruess, K. (1995). Two-phase flow visualization and relative permeability measurement in natural rough-walled rock fractures. Water Resources Research, 31(5):1175–1186.

Philip, J. and de Vries, D. (1957). Moisture movement in porous materials under temperature gradients. Transactions, American Geophysical Union, 38(2):222 – 232.

Plum, R. L. and Esrig, M. I. (1969). Some temperature effects on soil compressibility and pore water pressure. Highway Research Board Special Report, (103).

Preene, M. and Powrie, W. (2009). Ground energy systems: from analysis to geotechnical design. Geotechnique, 59(3):261 –271.

Pruess, K. (1991). Tough2: A general-purpose numerical simulator for multiphase fluid and heat flow. NASA STI/Recon Technical Report N, 92:14316.

Pruess, K., Oldenburg, C., and Moridis, G. (1999). Tough2 user's guide version 2.

Pruess, K. and Tsang, Y. (1990). On two-phase relative permeability and capillary pressure of rough-walled rock fractures. Water Resources Research, 26(9):1915–1926.

Pruess, K., Wang, J., and Tsang, Y. (1990). On thermohydrologic conditions near high-level nuclear wastes emplaced in partially saturated fractured tuff: 2. effective continuum approximation. Water Resources Research, 26(6):1249–1261.

Rees, S., Adjali, M., Zhou, Z., Davies, M., and Thomas, H. (2000). Ground heat transfer effects on the thermal performance of earth-contact structures. Sustainable Energy Reviews, 4(3):213 – 65.

Regueiro, R. (1998). Finite element analysis of strain localization in geomaterials taking a strong discontinuity approach. PhD thesis, Stanford University.

Remmers, J., de Borst, R., and Needleman, A. (2003). A cohesive segments method for the simulation of crack growth. Computational mechanics, 31(1-2):69–77.

Rice, J. R. (2006). Heating and weakening of faults during earthquake slip. Journal of Geophysical Research: Solid Earth (1978–2012), 111(B5).

Romero, E., Gens, A., and Lloret, A. (2001). Temperature effects on the hydraulic behaviour of an unsaturated clay. Geotechnical and Geological Engineering, 19(3-4):311 – 332.

Rutqvist, J., Birkholzer, J., Cappa, F., and Tsang, C.-F. (2007). Estimating maximum sustainable injection pressure during geological sequestration of co¡ sub¿ 2¡/sub¿ using coupled fluid flow and geomechanical fault-slip analysis. Energy Conversion and Management, 48(6):1798–1807.

Rutqvist, J., Birkholzer, J., and Tsang, C.-F. (2008). Coupled reservoir–geomechanical analysis of the potential for tensile and shear failure associated with co¡ sub¿ 2¡/sub¿ injection in multilayered reservoir–caprock systems. International Journal of Rock Mechanics and Mining Sciences, 45(2):132–143.

Rutqvist, J., Borgesson, L., Chijimatsu, M., Kobayashi, A., Jing, L., Nguyen, T., Noorishad, J., and Tsang, C.-F. (2001). Thermohydromechanics of partially saturated geological media: Governing equations and formulation of four finite element models. International Journal of Rock Mechanics and Mining Sciences, 38(1):105 – 127.

Rutqvist, J., Vasco, D. W., and Myer, L. (2010). Coupled reservoir-geomechanical analysis of co¡ sub¿ 2¡/sub¿ injection and ground deformations at in salah, algeria. International Journal of Greenhouse Gas Control, 4(2):225–230.

Rutqvist, J., Wu, Y.-S., Tsang, C.-F., and Bodvarsson, G. (2002). A modeling approach for analysis of coupled multiphase fluid flow, heat transfer, and deformation in fractured porous rock. International Journal of Rock Mechanics and Mining Sciences, 39(4):429–442.

Rutqvist, J., Zheng, L., Chen, F., Liu, H.-H., and Birkholzer, J. (2014). Modeling of coupled thermo-hydro-mechanical processes with links to geochemistry associated with bentonite-backfilled repository tunnels in clay formations. Rock Mechanics and Rock Engineering, 47(1):167–186.

Schrefler, B. (2002). Mechanics and thermodynamics of saturated/unsaturated porous materials and quantitative solutions*. Applied Mechanics Reviews, 55(4):351–388.

Schrefler, B., Zhan, X., and Simoni, L. (1995). A coupled model for water flow, airflow and heat flow in deformable porous media. Int. J. Numer. Methods Heat Fluid Flow (UK), 5(6):531 – 547.

Segura, J. and Carol, I. (2004). On zero-thickness interface elements for diffusion problems. International Journal for Numerical and Analytical Methods in Geomechanics, 28(9):947 – 962.

Segura, J. and Carol, I. (2007a). Coupled hm analysis using zero-thickness interface elements with double nodes. part i. theoretical model. International Journal for Numerical and Analytical Methods in Geomechanics, 32(18):2083 – 101.

Segura, J. and Carol, I. (2007b). Coupled hm analysis using zero-thickness interface elements with double nodes. part ii. verification and application. International Journal for Numerical and Analytical Methods in Geomechanics, 32(18):35 – 55.

Segura, J. and Carol, I. (2008). Coupled hm analysis using zero-thickness interface elements with double nodes. part i: Theoretical model. International journal for numerical and analytical methods in geomechanics, 32(18):2083–2101.

Segura, J. and Carol, I. (2010). Numerical modelling of pressurized fracture evolution in concrete using zero-thickness interface elements. Engineering Fracture Mechanics, 77(9):1386 – 99. numerical modelling;pressurized fracture evolution;concrete;zero-thickness interface elements;geotechnical;finite element method;hydro-mechanical behaviour;fracture mechanics-based constitutive model;wedge splitting tests;propagating crack;crack mouth opening displacement;.

Sharma, K. and Desai, C. (1992). Analysis and implementation of thin-layer element for interfaces and joints. Journal of Engineering Mechanics, 118(12):2442–2462.

Shin, S. and Juric, D. (2002). Modeling three-dimensional multiphase flow using a level contour reconstruction method for front tracking without connectivity. Journal of Computational Physics, 180(2):427–470.

Skempton, A. (1984). Effective stress in soils, concrete, and rocks. Selected papers on soil mechanics, pages 4–16.

Soltanzadeh, H. and Jafari, A. (2013). Thermo-poro-mechanical analysis of the effects of low-temperature co 2 injection on caprock integrity. volume 2, pages 1470 – 1479.

Spalding, D. (1980). Numerical computation of multi-phase fluid flow and heat transfer. Recent advances in numerical methods in fluids, 1:139–167.

Srivastava, R. and Yeh, T.-C. J. (1991). Analytical solutions for one-dimensional, transient infiltration toward the water table in homogeneous and layered soils. Water Resources Research, 27(5):753–762.

Stewart, M. A. (2012). Centrifuge modeling of strain distributions in energy foundations. Master's thesis, University of Colorado,Boulder.

Stewart, M. A. and McCartney, J. S. (2013). Centrifuge modeling of soil-structure interaction in energy foundations. ASCE Journal of Geotechnical and Geoenvironmental Engineering, in press.

Sukumar, N. and Belytschko, T. (2000). Arbitrary branched and intersecting cracks with the extended finite element method. Int. J. Numer. Meth. Engng, 48:1741–1760.

Sulem, J., Lazar, P., and Vardoulakis, I. (2007). Thermo-poro-mechanical properties of clayey gouge and application to rapid fault shearing. International journal for numerical and analytical methods in geomechanics, 31(3):523–540.

Sulem, J., Vardoulakis, I., Ouffroukh, H., Boulon, M., and Hans, J. (2004). Experimental characterization of the thermo-poro-mechanical properties of the aegion fault gouge. Comptes Rendus Geoscience, 336(4):455–466.

Tamagnini, R. (2004). An extended cam-clay model for unsaturated soils with hydraulic hysteresis. Geotechnique, 54(3):223 – 228.

Terzaghi, K. (1936). The shearing resistance of saturated soils and the angle between the planes of shear. In In Proceedings of the 1st Conference on Soil Mechanics, volume 1, pages 54–56.

Terzaghi, K. (1943). "Theoretical soil mechanics". John Wiley and Sons, New York, NY.

Therrien, R. and Sudicky, E. (1996). Three-dimensional analysis of variably-saturated flow and solute transport in discretely-fractured porous media. Journal of Contaminant Hydrology, 23(1):1–44.

Thomas, H. and He, Y. (1995). Analysis of coupled heat, moisture and air transfer in a deformable unsaturated soil. Geotechnique, 45(4):677 – 689.

Thomas, H. and He, Y. (1997). A coupled heat-moisture transfer theory for deformable unsaturated soil and its algorithmic implementation. International Journal for Numerical Methods in Engineering, 40(18):3421 – 3441.

Thomas, H. and Missoum, H. (1999). Three-dimensional coupled heat, moisture, and air transfer in a deformable unsaturated soil. International Journal for Numerical Methods in Engineering, 44(7):919 – 43.

Thomas, H. and Rees, S. (2009). Measured and simulated heat transfer to foundation soils. Geotechnique (UK), 59(4):365 – 375.

Thomas, H. R. and King, S. D. (1991). Coupled temperature/capillary potential variations in unsaturated soil. Journal of Engineering Mechanics, 117(11):2475 – 2491.

Tidfors, M. and Sallfors, G. (1989). Temperature effect on preconsolidation pressure. Geotechnical Testing Journal, 12(1):93 – 97.

Toll, D. (1990). A framework for unsaturated soil behaviour. Géotechnique, 40(1):31–44.

Tong, F., Jing, L., and Bin, T. (2012). A water retention curve model for the simulation of coupled thermo-hydro-mechanical processes in geological porous media. Transport in Porous Media, 91(2):509 – 530.

Tong, F., Jing, L., and Zimmerman, R. W. (2009). An effective thermal conductivity model of geological porous media for coupled thermo-hydro-mechanical systems with multiphase flow. International Journal of Rock Mechanics and Mining Sciences, 46(8):1358 – 1369.

Towhata, I., Kuntiwattanaku, P., Seko, I., and Ohishi, K. (1993). Volume change of clays induced by heating as observed in consolidation tests. Soils and Foundations, 33(4):170 – 183.

Tryggvason, G., Bunner, B., Esmaeeli, A., Juric, D., Al-Rawahi, N., Tauber, W., Han, J., Nas, S., and Jan, Y.-J. (2001). A front-tracking method for the computations of multiphase flow. Journal of Computational Physics, 169(2):708–759.

Tsang, C.-F., Barnichon, J., Birkholzer, J., Li, X. L., Liu, H., and Sillen, X. (2012). Coupled thermo-hydro-mechanical processes in the near field of a high-level radioactive waste repository in clay formations. International Journal of Rock Mechanics and Mining Sciences, 49:31–44.

Uchaipichat, A. and Khalili, N. (2009). Experimental investigation of thermo-hydro-mechanical behaviour of an unsaturated silt. Geotechnique, 59(4):339 – 353.

van Genuchten, M. T. (1980). A closed-form equation for predicting the hydraulic conductivity of unsaturated soils. Soil Science Society of America Journal, 44(5):892 – 898.

Vardoulakis, I. (2002). Dynamic thermo-poro-mechanical analysis of catastrophic landslides. Geotechnique, 52(3):157–171.

Vaunat, J., Cante, J., Ledesma, A., and Gens, A. (2000). A stress point algorithm for an elasto-plastic model in unsaturated soils. International Journal of Plasticity, 16(2):121–141.

Volckaert, G., Bernier, F., Alonso, E., Gens, A., Samper, J., Villar, M., Martin-Martin, P., Cuevas, J., Campos, R., Thomas, H., et al. (1996). Thermal-hydraulic-mechanical and geochemical behaviour of the clay barrier in radioactive waste repositories(model development and validation). EUR(Luxembourg).

Walsh, J. (1973). Theoretical bounds for thermal expansion, specific heat, and strain energy due to internal stress. Journal of Geophysical Research, 78(32):7637 – 7646.

Wang, W., Regueiro, R., and McCartney, J. (2014). Coupled thermo-poro-mechanical finite element analysis of an energy foundation centrifuge experiment in partially saturated silt. In 8th International Conference on Physical Modelling in Geotechnics, in press.

Wang, W., Regueiro, R., Stewart, M., and McCartney, J. (2012). Coupled thermo-poro-mechanical finite element analysis of an energy foundation centrifuge experiment in saturated silt. pages 4406 – 15.

Wells, G. and Sluys, L. (2001). A new method for modelling cohesive cracks using finite elements. International Journal for Numerical Methods in Engineering, 50(12):2667–2682.

Wheeler, S. (1996). Inclusion of specific water volume within an elasto-plastic model for unsaturated soil. Canadian Geotechnical Journal, 33(1):42 – 57.

Wheeler, S. and Sivakumar, V. (1995a). Elasto-plastic critical state framework for unsaturated soil. Geotechnique, 45(1):35 – 53.

Wheeler, S. and Sivakumar, V. (1995b). An elasto-plastic critical state framework for unsaturated soil. Geotechnique, 45(1):35–53.

Wheeler, S. J., Sharma, R. S., and Buisson, M. S. R. (2003). Coupling of hydraulic hysteresis and stress-strain behaviour in unsaturated soils. Geotechnique, 53(1):41 – 54.

Wilson, G., Fredlund, D., and Barbour, S. (1994). Coupled soil-atmosphere modelling for soil evaporation. Canadian geotechnical journal, 31(2):151 – 161.

Wilson, G. W., Fredlund, D. G., and Barbour, S. L. (1997). The effect of soil suction on evaporative fluxes from soil surfaces. Canadian Geotechnical Journal = Revue Canadienne de Geotechnique, 34(1):145 – 155.

Wu, W., Li, X., Charlier, R., and Collin, F. (2004). A thermo-hydro-mechanical constitutive model and its numerical modelling for unsaturated soils. Computers and Geotechnics, 31(2):155 – 167.

Xie, D. and Waas, A. M. (2006). Discrete cohesive zone model for mixed-mode fracture using finite element analysis. Engineering Fracture Mechanics, 73(13):1783–1796.

Xu, T. and Pruess, K. (2001). Modeling multiphase non-isothermal fluid flow and reactive geochemical transport in variably saturated fractured rocks: 1. methodology. American Journal of Science, 301(1):16–33.

Yanful, E. K., Bell, A., and Woyshner, M. R. (1993). Design of a composite soil cover for an experimental waste rock pile near newcastle, new brunswick, canada. Canadian geotechnical journal, 30(4):578 – 587.

Yang, D., Rahardjo, H., Leong, E., and Choa, V. (1998). Coupled model for heat, moisture, air flow, and deformation problems in unsaturated soils. Journal of Engineering Mechanics, 124(12):1331 – 1338.

Yari, M. and Javani, N. (2007). Performance assessment of a horizontal-coil geothermal heat pump. International journal of energy research, 31(3):288–299.

Zhai, Z., Zaki, K., Marinello, S., and Abou-Sayed, A. (2009). Coupled thermo-poro-mechanical effects on borehole stability. volume 1, pages 216 – 224.

Zhou, Y., Rajapakse, R., and Graham, J. (1998). Coupled heat-moisture-air transfer in deformable unsaturated media. Journal of Engineering Mechanics, 124(10):1090 – 1099.

Zong-Ze, Y., Hong, Z., and Guo-Hua, X. (1995). A study of deformation in the interface between soil and concrete. Computers and Geotechnics, 17(1):75–92.

Appendix A

Appendix A

Notations	Definitions	Units
$\boldsymbol{\epsilon}$	Total strain	m/m
$\boldsymbol{\epsilon}^e$	Elastic strain	m/m
$\boldsymbol{\epsilon}^\theta$	Thermal strain	m/m
$\boldsymbol{\epsilon}^{skel,e}$	Elastic strain of solid skeleton	
$\mathbf{l}$	2nd order identity matrix $\mathbf{l}_{ij} = \delta_{ij}$	
$\boldsymbol{I}$	4th order identity tensor $I_{ijkl} = \frac{1}{2}(\delta_{ik}\delta jl + \delta_{il}\delta_{jk})$	
α_h	Linear thermal expansion coefficient	$1/K$
C	Specific heat capacity of mixture	$J/(K \cdot kg)$
C^α	Specific heat capacity of α phase	$J/(K \cdot kg)$
θ	Absolute temperature	K
θ^α	Absolute temperature of constituent α	K
κ	Intrinsic permeability	m^2
K_{rw}	Relative permeability with respect to water phase in the continuum	-
K_{rg}	Relative permeability with respect to gas phase in the continuum	-
θ_0	Initial temperature	K
K_B	Bulk modulus	Pa
$\boldsymbol{c}^e$	Elastic modulus tensor	
$\boldsymbol{b}$	Body force	N/kg

$\boldsymbol{g}$	Gravity	m/s^2
e	Specific internal energy	J/kg
ρ	Density (of the porous media)	kg/m^3
ρ^α	Partial density of α phase	kg/m^3
$\rho^{\alpha R}$	Real density of α phase	kg/m^3
$\hat{\rho}^\alpha$	Mass supply per volume element	$kg/(m^3 \cdot s)$
r	Internal source per unit of mass	W/kg
q	Heat flux	W/m^2
φ	Specific Helmholtz free energy	J/kg
η	Specific entropy	$J/(K \cdot kg)$
h_f	Specific enthalpy of fluid phase	J/kg
$\boldsymbol{\sigma}$	Total stress	N/m^2
$\boldsymbol{\sigma'}$	Effective stress	N/m^2
$\boldsymbol{\sigma}^\alpha$	Partial stress of α phase,$\boldsymbol{\sigma}^\alpha = n^\alpha \boldsymbol{\sigma}$	N/m^2
$\boldsymbol{k}^\theta$	Thermal conductivity tensor of mixture	$W/(m \cdot K)$
$\boldsymbol{k}_\alpha^\theta$	Thermal conductivity tensor of α phase	$W/(m \cdot K)$
$\boldsymbol{v}^\alpha$	Velocity of α phase	m/s
$\widetilde{\boldsymbol{v}}_f$	Relative velocity of fluid	m/s
$\widetilde{\boldsymbol{v}}_f^s$	Superficial (Darcy's) velocity	m/s
n^α	Volume fraction of α phase	
V^f	Reference volume of fluid	m^3
V^s	Reference volume of solid	m^3
$\hat{\boldsymbol{h}}^\alpha$	Interaction body forces per unit volume	N/m^3
$\boldsymbol{a}^\alpha$	Acceleration of α phase	m/s^2
$\tilde{\boldsymbol{v}}_f^D$	Darcy's velocity of pore fluid in the continuum	m/s
$\tilde{\boldsymbol{v}}_w^D$	Darcy's velocity of pore water in the continuum	m/s
$\tilde{\boldsymbol{v}}_g^D$	Darcy's velocity of pore gas in the continuum	m/s

$\tilde{\boldsymbol{v}}_{gv}^{D}$	Darcy's velocity of pore water vapor in the continuum	m/s
$\tilde{\boldsymbol{v}}_{ga}^{D}$	Darcy's velocity of pore dry air in the continuum	m/s
$\tilde{\boldsymbol{v}}_{f}^{D,S}$	Darcy's velocity of pore fluid in saturated crack (or discontinuity) S	m/s
$(\tilde{v}_{f}^{D,S})_n$	Normal component of $\tilde{\boldsymbol{v}}_{f}^{S,D}$	m/s
$(\tilde{v}_{f}^{D,S})_t$	Tangential component of $\tilde{\boldsymbol{v}}_{f}^{S,D}$	m/s
$\tilde{\boldsymbol{v}}_{gv}^{D,S}$	Darcy's velocity of pore water in partially saturated crack (or discontinuity) S	m/s
$(\tilde{v}_{gv}^{D,S})_n$	Normal component of $\tilde{\boldsymbol{v}}_{gv}^{S,D}$	m/s
$(\tilde{v}_{gv}^{D,S})_t$	Tangential component of $\tilde{\boldsymbol{v}}_{gv}^{S,D}$	m/s
$\tilde{\boldsymbol{v}}_{ga}^{D,S}$	Darcy's velocity of pore water in partially saturated crack (or discontinuity) S	m/s
$(\tilde{v}_{ga}^{D,S})_n$	Normal component of $\tilde{\boldsymbol{v}}_{ga}^{S,D}$	m/s
$(\tilde{v}_{ga}^{D,S})_t$	Tangential component of $\tilde{\boldsymbol{v}}_{ga}^{S,D}$	m/s
S_w^S	Degree of saturation of the crack S	-
S_w	Degree of saturation of the continuum	-
$S_{w,S}$	Water flux on the crack boundaries	-
S_w	Water flux on the continuum boundaries	-
s^S	Suction in the crack S	kPa
s	Suction of the continuum	kPa
$\hat{k}_t$	Tangential permeability of the crack	$m^2/(Pa \cdot s)$
$\hat{k}_n$	Normal permeability of the crack	$m^2/(Pa \cdot s)$
$[[\boldsymbol{u}]]$	Displacement jump within the crack in global coordinate	m
$[[\tilde{\boldsymbol{u}}]]$	Displacement jump within the crack in local coordinate	m
u_n	Normal displacement jump within the crack	m
u_t	Tangential displacement jump within the crack	m
$\boldsymbol{n}$	Normal vector of the crack	-
$\boldsymbol{t}$	Tangential vector of the crack	-
S^l	Crack volume with the width of l	
S	Crack surface	

k_f	Saturated permeability of the continuum under isotropic condition	$m/(Pa \cdot s)$
$\hat{k}_n$	Saturated permeability of the crack in normal direction	$m/(Pa \cdot s)$
$\hat{k}_t$	Saturated permeability of the crack in tangential direction	$m^2/(Pa \cdot s)$
$\hat{K}_{rw}$	Relative permeability with respect to water phase in the crack	-
$\hat{K}_{rg}$	Relative permeability with respect to gas phase in the crack	-
l	Width of the crack S	m
l_0	Initial width of the crack S	m
$\boldsymbol{T}'$	Effective stress tensor on the crack in global coordinate $[r; z]$	kPa
$\widetilde{\boldsymbol{T}}'$	Effective stress tensor on the crack in local coordinate $[t; n]$	kPa
$\boldsymbol{K}^e$	Elastic stiffness matrix of the discontinuity	Pa/m
K_t	Tangential elastic stiffness of the discontinuity	Pa/m
K_n	Normal elastic stiffness of the discontinuity	Pa/m
$[[\tilde{\boldsymbol{u}}^p]]$	Plastic component of displacement jump in the crack	m/s
$[[\tilde{\boldsymbol{u}}^e]]$	Elastic component of displacement jump in the crack	m/s
$\boldsymbol{q}$	Internal state variable vector	-
ϵ_s^p	Plastic shear strain	-
ϵ_n^p	Plastic normal strain	-
$\hat{K}^\theta$	Thermal conductivity of the crack	$W/(m \cdot K)$
H_s	Heaviside function	-
$\tilde{\boldsymbol{n}}$	Generic normal vector of fractured porous media	-
p_f^S	Averaged pore fluid pressure on the crack S	Pa
$[[p_f]]$	Pore fluid pressure jump across the crack	Pa
θ^S	Averaged temperature on the crack S	K
$[[\theta]]$	Temperature jump across the crack	K
n^S	Porosity of the crack	-
$\alpha_{skel}^{\theta,S}$	Linear thermal expansion coefficient of crack solid skeleton	$1/K$
$\beta_s^{\theta,S}$	Volumetric thermal expansion coefficient of the crack solid phase	$1/K$

$\beta_f^{\theta,S}$	Volumetric thermal expansion coefficient of the crack fluid phase	$1/K$